ALMA MATER STUDIORUM
UNIVERSITÀ DI BOLOGNA

DOTTORATO DI RICERCA IN

CHIMICA

Ciclo 37

Settore Concorsuale: 03/C1 - CHIMICA ORGANICA

Settore Scientifico Disciplinare: CHIM/06 – CHIMICA ORGANICA

NOVEL CATALYTIC TRANSFORMATIONS MEDIATED BY DUAL PHOTOREDOX AND EARTH ABUNDANT TRANSITION METALS

Presentata da: Emanuele Pinosa

Coordinatore Dottorato

Luca Prodi

Supervisore

Pier Giorgio Cozzi

Co-Supervisore

Andrea Gualandi

Esame finale anno 2025

A nonna Gabriella (Bela)

Abstract

The use of photoredox catalysis has emerged as a highly effective approach for accessing radical intermediates. The ability to transform visible light into chemical energy, predominantly through single electron transfer (SET) processes, facilitates the investigation of novel and challenging chemical transformations and unconventional disconnections, thus circumventing the need for traditional radical initiators or stoichiometric metal reagents.

Our research group has been engaged in the development of novel metallaphotoredox methodologies for several years. These combine photoredox- and transition metal-catalytic cycles, with the aim of generating transient nucleophilic organometallic reagents capable of reacting with suitable electrophiles, such as aldehydes, ketones, or imines.

In this context, during my doctoral studies, I primarily focused on the development of innovative catalytic methodologies which combine photocatalysis with earth-abundant transition metals, including cobalt, vanadium, nickel, and titanium. The results were published in international peer-reviewed journals. More in detail, my research group and I published the following results:

1. *A dual cobalt- and photoredox allylation of aldehydes using a TADF-emitter photocatalyst derived from the degradation of the commercially available 3DPAFIPN.*
2. *A dual vanadium- and photoredox diastereoselective pinacol coupling of aromatic aldehydes.*
3. *A dual nickel- and photoredox allylation of aldehydes using Morita-Baylis-Hillman acetates as pronucleophiles. (the manuscript is in preparation)*
4. *A dual titanium- and photoredox allylation of aldehydes for the direct access to α-vinyl-β-hydroxy esters.*

1. Light-induced access to a novel TADF photocatalyst for a dual photoredox- and cobalt-catalyzed allylation of aldehydes

Thermally Activated Delayed Fluorescence (TADF) is a process exhibited by certain molecules that have a small energy gap (generally less than 0.2 eV) between the two lowest excited states, S_1 and T_1. In these molecules, a reverse intersystem crossing (rISC) from T_1 back to S_1 takes place at room temperature, resulting in the so-called delayed fluorescence. These molecules exhibit longer fluorescence lifetimes (ζ_{FLUO}) and higher fluorescence quantum yields (Φ_{FLUO}) compared to other chromophores. In a seminal work, Adachi reported a new organic TADF emitter: 4CzIPN (1,2,3,5-tetrakis(carbazol-9-yl)-4,6-dicyanobenzene). Several other TADF emitters (e.g. 3DPAFIPN, 2,4,6-tris(diphenylamino)-5-fluoroisophthalonitrile) have been reported and are widely used in OLED technologies and photoredox catalysis. The photostability of TADF emitters was investigated by the König group in the photopromoted benzylation of 4CzIPN. 3DPAFIPN dye is commonly used as photocatalyst and it is reported to be stable under standard operating conditions. We discovered that under 456 nm irradiation in the absence of a quencher, it undergoes a photoinduced reaction, where the fluorine atom is substituted by the phenyl ring of the amine moiety.

This new compound, namely 2DPAPhCzDCN (2,4-bis(diphenylamino)-9-phenyl-9H-carbazole-1,3-dicarbonitrile) has been isolated and fully characterized. After a detailed photophysical investigation it was found that 2DPAPhCzDCN itself is a TADF emitter with a higher reduction potential than 3DPAFIPN. This new dye was used in the allylation of aldehydes mediated by $CoBr_2$ as a commercial Co(II) source, dtbpy as the ligand, Hantzsch ester as the sacrificial stoichiometric reductant, THF/H_2O as the solvent mixture under irradiation with a 456 nm lamp. The key aspect of this reaction is that 3DPAFIPN and 4CzIPN failed to promote the cobalt-mediated allylation.

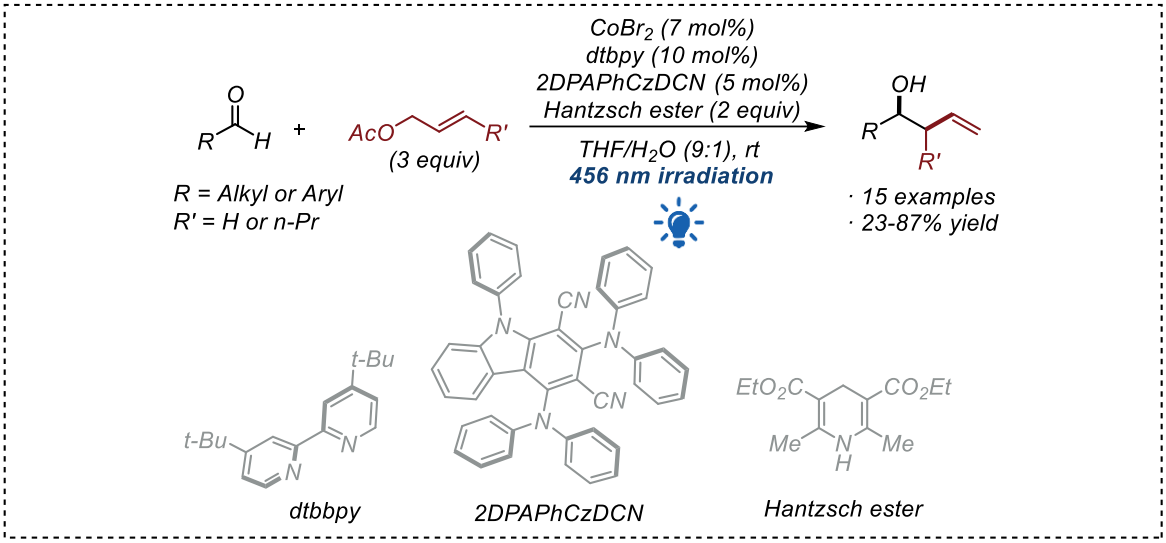

2. Get access to vanadium in low oxidation state: a diastereoselective pinacol coupling

The venerable pinacol coupling reaction is one of the oldest, most studied and most developed organic reactions to obtain access to 1,2-diols from two carbonyl groups. It has been reported with a variety of transition metals (e.g. Ti, V, Sm, Cr) in a low-oxidation state. The mechanism involves the reduction of the metal to a lower oxidation state in a single-electron transfer (SET) step in the presence of a reducing agent, usually another metal (e.g. Zn(0) or Mn(0)), which triggers its redox activity towards the carbonyl. The subsequent SET between the reduced metal and the carbonyl leads to the formation of a ketyl radical that dimerizes in a metal-assisted step leading to the diol. Metallaphotoredox catalysis offers a way to replace the reductive behavior of the stoichiometric metal reductant with a photoredox catalytic cycle. With this idea in mind, recently our group reported a diastereo- and enantioselective version of the pinacol coupling of aromatic aldehydes promoted by titanium complexes. To extend our portfolio, we wanted to study the reactivity of vanadium in a lower oxidation state in the same transformation. After the seminal work of Pedersen in 1989, which used VCl_3·3THF and Zn dust as stoichiometric reductant to generate in situ the dimeric species $[V_2(THF)_6Cl_3]^+[Zn_2Cl_6]^-$ known as the "Pedersen reagent", further developments were made in the following years. After a thorough study we developed a highly diastereoselective protocol using VCl_3·3THF as vanadium(III) precursor, 6,6'-dMe-bipyridine as the ligand, $[n\text{-PrDMQA}^+]$ $[BF_4^-]$ as the photocatalyst, Hantzsch ester as the sacrificial stoichiometric reductant, DCM as the solvent under irradiation with a 590 nm lamp.

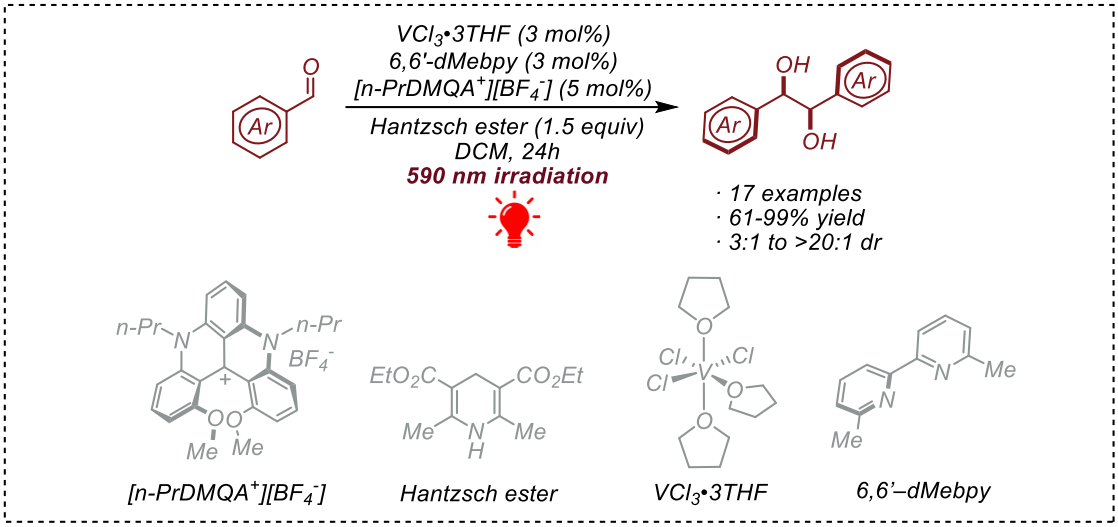

3. *A dual photoredox- and nickel-catalyzed diastereoselective allylation of aldehydes with Morita-Baylis-Hillman adducts*

Nickel is an abundant and inexpensive transition metal and, despite some problems related to health hazards, its industrial, technological and academic applications are growing rapidly. Apart from its abundance and lower cost, nickel derivatives display some useful properties in catalysis, such as the formation of highly reactive organometallic intermediates, the ready availability of many contiguous oxidation states (from -1 to +4), easy homolytic bond cleavage, and the ability to react with unsaturated systems and activate multiple bonds by coordination. These properties are similar to those of the more expensive palladium, e.g. in cross-coupling reactions involving oxidative addition-reductive elimination steps, and can be used in a variety of different transformations such as cross-couplings and C-H activation, even with unreactive substrates, under different modes of activation, e.g. photocatalysis, electrocatalysis or metal reduction. Among this wide range of useful transformations, the application of nickel catalysis in allylation methodologies is particularly relevant. Transition metal-catalyzed allylations are considered among the most important tools for the formation of new C-C bonds and many metals can be used in this transformation. Allylation reactions have been reported with various nucleophilic organometallic allylic species, either stable or generated in situ from suitable precursors. In particular, in recent years our group has reported several new metallaphotoredox allylation protocols. In order to further expand our portfolio, we have developed a new nickel-mediated photoredox allylation reaction using Morita-Baylis-Hillman (MBH) acetates as an unprecedented pronucleophile source producing homoallylic alcohols with greater structural complexity and high regio- and diastereocontrol using $NiCl_2$·glyme as a commercially available Ni(II) source, o-phenanthroline as the ligand, 3DPAFIPN as the photocatalyst, Hantzsch ester as the sacrificial stoichiometric reductant, THF as the solvent under irradiation with a 456 nm lamp. The usefulness of the protocol has also been demonstrated with some post-functionalization of the products.

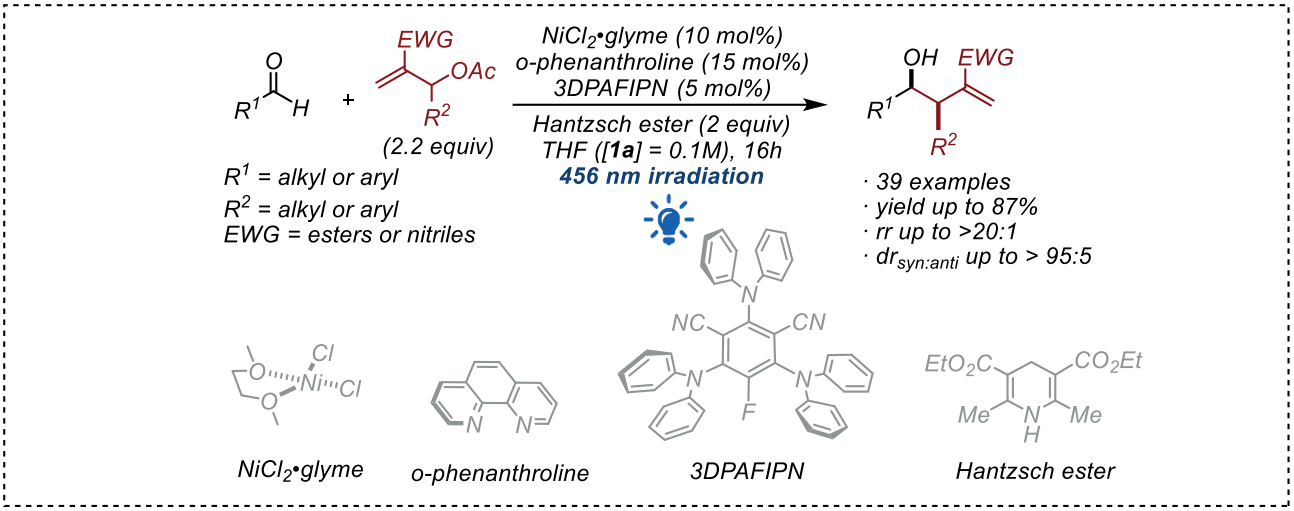

4. A dual photoredox- and titanium-catalyzed approach for the direct access to α-vinyl-β-hydroxy esters

Titanium is one of the most abundant transition metals on earth and has attracted particular attention because it is considered non-toxic and biocompatible, inexpensive and environmentally friendly. In the literature it is widely reported in many in C–C, C–O and C–N bond-forming protocols. Of particular relevance, the high versatility of titanium in low oxidation state has also been extensively reported in allylation reactions. Typically, allyl-titanium species are generated in situ starting from suitable allyl precursors and Cp_2TiCl, previously synthesized from Cp_2TiCl_2, or also generated in situ in the presence of metal reductants. This one-step strategy, known as "Barbier-type reaction", has been widely studied, but the need for stoichiometric amounts of metal reductants, as well as stoichiometric Ti-complexes remains the main drawback of these reactions. Photoredox catalysis offers the possibility of replacing the reductive behavior of metals with milder photocatalytic cycles. With this in mind, our group has recently developed a dual photoredox- and titanium-catalyzed allylation of aldehydes using catalytic Cp_2TiCl_2 as Ti(IV) source. To expand these findings we wanted to introduce a multi-decorated allyl moiety such as 4-bromocrotonates, to achieve a catalytic α-selective vinylogous Reformatsky-type reaction for the synthesis of α-vinyl-β-hydroxy esters, which has been mainly reported using stoichiometric amounts of pre-formed organometallic complexes. Using Cp_2TiCl_2 as a commercially available Ti(IV) source, 3DPAFIPN as the photocatalyst, Hantzsch ester as the sacrificial stoichiometric reductant, THF as the solvent under irradiation with a 456 nm lamp we were able to get access to α-vinyl-β-hydroxy esters in a fast, straightforward, highly regioselective and moderately diastereoselective manner. The presence of multiple functional groups has been exploited with some post-functionalization.

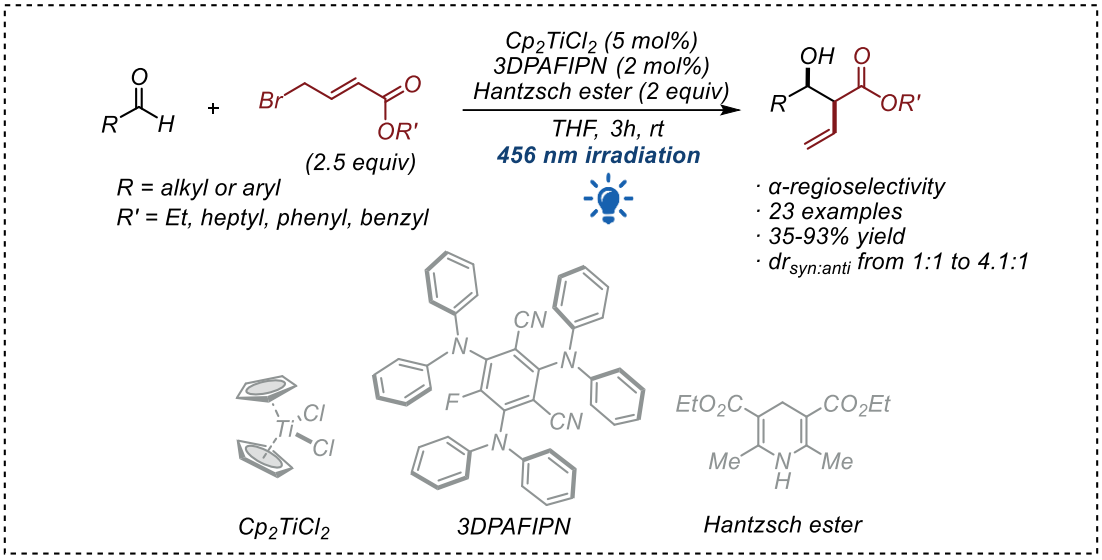
Cp2TiCl2 (5 mol%)
3DPAFIPN (2 mol%)
Hantzsch ester (2 equiv)
THF, 3h, rt
456 nm irradiation
(2.5 equiv)
R = alkyl or aryl
R' = Et, heptyl, phenyl, benzyl
· α-regioselectivity
· 23 examples
· 35-93% yield
· dr syn:anti from 1:1 to 4.1:1
Cp2TiCl2
3DPAFIPN
Hantzsch ester

TABLE OF CONTENTS

Chapter 1. Introduction

1.1 Photocatalysis: concepts and background

Photochemistry is the branch of chemistry concerned with chemical reactions initiated by the absorption of light radiation.[1] The most common light sources are in the range of visible or near-UV region and the energy associated with this radiation is of the same order of magnitude as the energy required to dissociate chemical bonds.[2] The additional energy introduced into the reaction medium is responsible for the observed reactivity, whereas for a non-light-mediated process the same transformation would require an external heating.

In particular, three different types of light-absorbing species can be defined, depending on their fate during the process:[1]

Photocatalyst: a species that catalyzes a reaction upon absorption of a photon and is then regenerated.
Intermediate: a transient species formed either in a catalytic or stoichiometric amount.
Substrate: the light-absorbing species is the substrate itself, which undergoes the chemical transformation.

Consequently, if the substrate or a reaction intermediate is the light-absorbing species the process is defined as *direct photochemistry*, whereas if the light is not absorbed directly by the reactants or their intermediate, but an external photocatalyst is required, the process is defined as *photocatalysis*.

The light-driven reaction is based on the absorption of light, and the energy of the photon is converted into internal energy of the species. Normally, the energy associated with this light promotes electronic transitions from the electronic ground state, usually a closed-shell singlet state S_0, to an excited state. The excited species have different 3-dimensional structures, electronic densities, bond strengths, redox properties and, therefore, different reactivities. An excited molecule must therefore be considered as a different species from the ground state one.

Figure 1.1 shows a Jablonsky diagram, that summarizes all the possible events that can take place through the absorption of a photon, from the excitation to the final fate of the excited state, called deactivation. To understand the basic principles of photocatalysis, it is convenient to treat the physics of the absorption of the photon and the possible deactivation processes into two different sections.

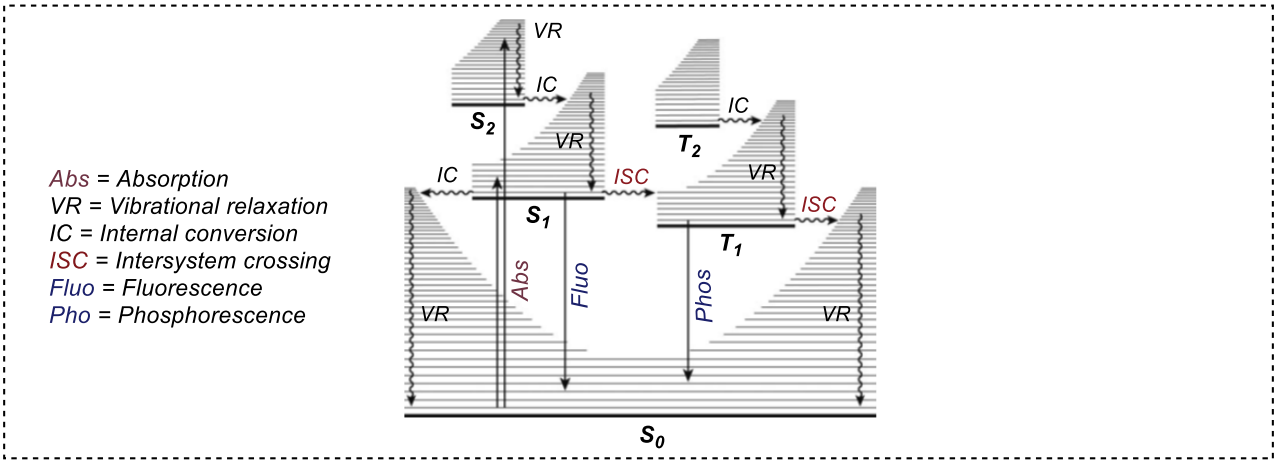

Figure 1.1 Typical Jablonsky diagram. Adapted from reference.[2]

1.1.1 The absorption of light

The absorption of light by the matter can be measured by common spectroscopic techniques and can be represented in a spectrum. Three parameters well describe an absorption band: 1. the wavelength associated with the transition, 2. the shape of the band and 3. its intensity.

The energy associated with the transition must follow the Bohr equation (1):

$$E = Ef - Ei = \frac{hc}{\lambda} \quad (1)$$

Which means that the energy of the incident photon must be equal to the energy gap between the final excited state (Ef) and the initial ground state (Ei) to be absorbed.

The shape and the intensity of the transition can be interpreted and predicted with a detailed quantum-mechanical treatment considering the vibronic transitions, i.e. considering the vibrational states associated with the two electronic states, from the lowest vibrational state v = 0 of the electronic ground state (S_0) to different excited states. Without going into the details of the mathematical derivation, the probability of the transition is proportional to the square of the transition moment. The transition moment depends on three factors, that determine whether a transition can take place.

1. *Electronic transition moment*. It depends on the symmetry and the amount of spatial overlap between the initial and the final orbitals. This requirement is called the *symmetry selection rule*. Therefore, transitions such as $\pi^* \rightarrow \pi$ or $\sigma \rightarrow \sigma^*$ are defined as *symmetry-allowed*, while transitions such as $n \rightarrow \pi^*$ are defined as *symmetry-forbidden*.
2. *Spin transition moment*. It depends on the multiplicity of the two states and strongly influences the intensity of a transition. The moment vanishes when there is a change in the multiplicity. Consequently, transitions involving a change in the multiplicity, e.g. $S_0 \rightarrow T_1$, are defined as *spin-forbidden*, while transitions involving no change in the multiplicity, e.g. $S_0 \rightarrow S_1$, are defined as *spin-allowed*. Typically, electronic transitions in organic molecules are dominated by spin-allowed transitions, e.g. $S_0 \rightarrow S_1$, while spin-forbidden ones are almost unobservable. The rule is not valid in the presence of heavy atoms: the *heavy atom effect* is important in phosphoresce phenomena.
3. *The vibrational overlap integral*, also known as Frank-Condon principle, which influences the shape of a transition. It is related to the overlap between the vibrational state v (at room temperature v = 0, v_0) of the ground state and each vibrational state of the excited states.

1.1.2 The fates of the excited state

When a molecular species is excited, it gains an extra energy amount which makes it more reactive than the surrounding species and it will therefore tend to dissipate this energy to return to its ground state. Three types of deactivation can occur: radiative processes (*r*), non-radiative processes (*nr*) and chemical reactions (*p*). Each of these can be associated with a kinetic rate constant: respectively k_r, k_{nr}, and k_p. Since these three processes can simultaneously occur after the irradiation of a molecule (A) and they are responsible for the decay of its excited state (*A), it is possible to calculate the *lifetime* of the excited species $\tau(^*A)$ according to the equation (2):

$$\tau(^*A) = \frac{1}{k_r + k_{nr} + k_p} = \frac{1}{\sum_j k_j} \quad (2)$$

The probability of each deactivation process can be related to its kinetic constant, and taking this into account, the *efficiency* η_i is defined as:

$$\eta_i = \frac{k_i}{\sum_j k_j} = k_i \tau(^*A) \tag{3}$$

From equation (3), the efficiency of each process can be related to the lifetime of the excited state and its kinetic constant.

Another important parameter to describe photoinduced process is the *quantum yield* Φ. Any physical event that could deactivate or make $\tau(^*A)$ disappear, as well as every product formed in a photochemical of photocatalytic reaction is defined as a *primary process*. The quantum yield of a primary process -*i* is defined[3] as:

$$\Phi_i = \frac{Number\ of\ molecules\ undergoing\ process{-}i}{Number\ of\ photons\ absorbed} \tag{4}$$

Considering the Jablonsky diagram in *Figure 1.1*, upon absorption of a photon an organic molecule in its singlet ground state S_0 populates the different vibrational states of the first excited singlet state S_1 according to the Frank-Condon principle. The first event that takes place is an intermolecular non-radiative vibrational deactivation (VR) to the lowest vibrational level of S_1. The collisions with the surrounding environment allow the dissipation of the extra energy by heat exchange. Since this process occurs on a picosecond scale, all further deactivation events will take place after the complete vibrational relaxation. From this thermally-equilibrated excited state, 1. a non-radiative intramolecular transition between isoenergetic vibrational levels of different electronic states can take place, i.e. *internal conversion* (IC). After the IC step a non-radiative vibrational relaxation to the thermally-equilibrated ground state occurs. 2. alternatively, a radiative deactivation $S_1 \rightarrow S_0$ can take place by emission of a photon which is called *fluorescence*. The emission from the lowest excited state of any multiplicity, as in the case of fluorescence, is referred as Kasha rule.[4] Since a fraction of the photon energy is lost as heat in non-radiative relaxation events, the energy of the emitted light is lower. The energy difference between the absorbed and emitted light is called the *Stokes shift*.

The vibrational structure of the electronic transition can be observed in the case of rigid species, i.e. rigid planar aromatic compounds, or by lowering the temperature, and it generally follows the Franck-Condon principles. Otherwise only a broad, convoluted band is observed. Looking at the absorption and emission spectra, the frequencies that the emission and absorption spectra have in common correspond to the energy difference between the lower vibrational level v_0 of S_1 and the lower vibrational level v_0 of S_0. This energy value is called E_{00} and it is important for calculating the redox potentials of the excited state.

Alternatively, 3. non-radiative transition can take place between S_1 and the excited triplet state T_1. This transition is called *intersystem crossing* (ISC) and, since it involves a change in the spin multiplicity, i.e. it is spin-forbidden, it occurs in species with a strong spin-orbit coupling. Special cases are organic molecules that exhibit the TADF phenomenon, which will be discussed in more detail in section 1.5.2. From T_1, after an internal conversion to the lowest vibrational level, both vibrational relaxation and radiative emission $T_1 \rightarrow S_0$, called *phosphorescence,* can take place. In this case, since the transition is spin-forbidden, the lifetime of the excited state before the deactivation is longer.

The third fate of a thermally-equilibrated excited state is a bimolecular reaction, i.e. a reaction with a substrate. The encounter of the excited species with a reactant and its deactivation is usually referred to as “quenching of the photocatalyst”. Considering the excited S_1, in order to favour the encounter of

the excited photosensitizer with the reactant and allow the quenching, it is important that non-radiative deactivation pathways are not competitive with the emissive decay. If this condition is satisfied, the lifetime of S_1 can be approximated as $\tau_f = \tau_{S1}$ meaning that, if non-radiative pathways are not competitive, the longer lifetime of the excited state can favour the encounter between the reactant species. It is assumed that a fluorophore with τ_{S1}< 1 ns cannot participate in a bimolecular process since its rate decay is of the same order as the rate constant diffusion $k_{diffusion}$ ~ 1-2 x10^{10} s^{-1}. The fluorescence quantum yield Φ_f can also indicate whether the excited state is able to undergo a bimolecular quenching, since higher Φ_f implies that the excited photosensitizer is not high susceptible to other deactivation pathways on the time scale in which the bimolecular quenching occurs.[5]

In *Figure 1.2* three common bimolecular modes of interaction are summarized: energy transfer (EnT), electron transfer (ET) and atom transfer (AT).

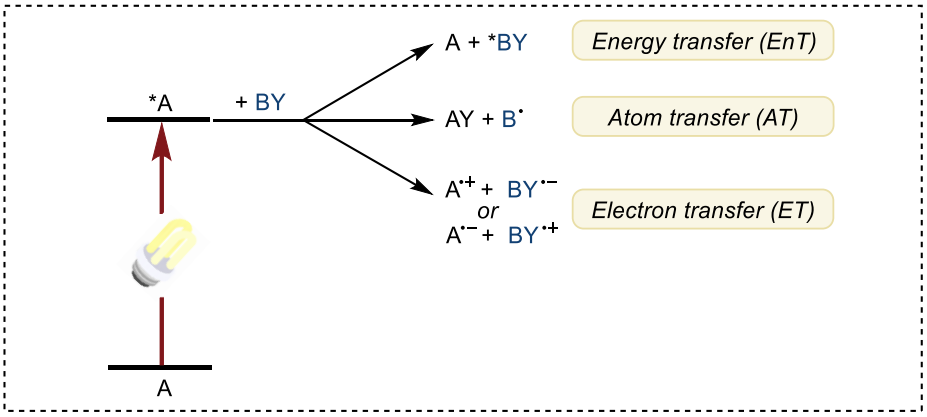

Figure 1.2 Bimolecular modes of interaction of the photoexcited photocatalyst.

1.1.3 Energy transfer process

The energy transfer (EnT) process involves the deactivation of the excited state of a molecular entity (the donor *D, also defined as the *sensitizer*) by transferring energy to a lower-lying state of a second molecular entity (the acceptor A), which is then raised to an higher excited state (*A)[6] as shown in *Figure 1.3*. The thermodynamic ability of the excited state to transfer energy to an acceptor is related to the E_{00} value and it is required that the energy associated with the excited state of the sensitizer is higher than that of the excited state of the acceptor.

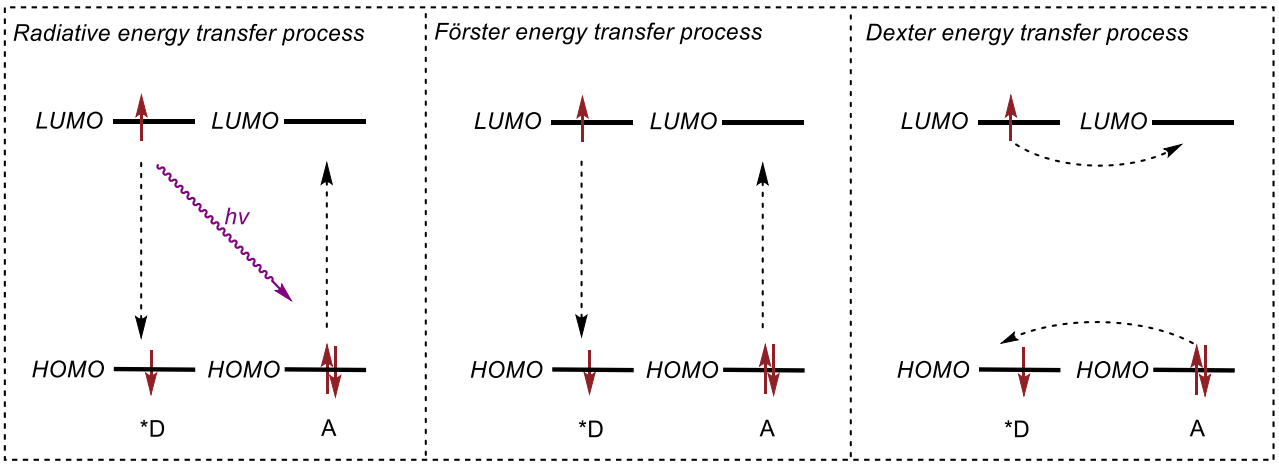

Figure 1.3 Schematic representation of radiative and non-radiative energy transfer processes.

EnT can occur involving both radiative and non-radiative mechanisms. A detailed discussion of the mechanisms is beyond the scope of this introduction. Therefore, only basic concepts will be presented.

The radiative mechanism involves the deactivation of *D by the emission of a photon that is reabsorbed by A. This mechanism does not depend on the distance between *D and A, while it does depend on the concentration of A. The lifetime of the excited state of *D is not affected by the presence of A, while the emission spectra of D and the absorption spectra of A are affected.

Non-radiative mechanisms involve the transfer of energy without the emission of radiation. The process depends on the distance between *D and A and can be treated using a Marcus-type kinetic approach taking into account the E_{00} value:

$$\Delta G^0 = E_{00}(^*A/A) - E_{00}(^*B/B) \quad (5)$$

From the quantum-mechanic treatment, which is not reported, the non-radiative energy transfer process depends on two terms: a coulombic and an exchange term. In the case where the first term is predominant, the process is defined as *Förster-type* energy transfer. It is based on a long range (<10 nm) dipole-dipole interactions between the two species.[7] When the second term is dominant the process is defined as *Dexter-type* energy transfer.[8] It can be described as a double electron transfer: one electron is transferred from the LUMO of *D to the LUMO of A, while the other electron is transferred from the HOMO of A to the HOMO of *D.

1.1.4 Atom transfer process

The atom transfer (AT) process involves the bimolecular quenching of an excited species by the abstraction of an atom to another species. Hydrogen atoms are commonly abstracted, and the process is referred to as Hydrogen-Atom-Transfer (HAT). The process has been reviewed few years ago.[9] The photoexcited photocatalyst *PC induces the homolytic C-H cleavage in Sub-H species resulting in a radical reactant Sub$^\bullet$ and a reduced PC-H species. To use the photoactive species in a catalytic amount, the catalytic cycle must be restored by a sacrificial oxidant or other reactants. The more commonly used photoexcited HAT reagents belong to the polyoxometalates family, and it can be represented by tetrakis(tetrabutylammonium) decatungstate ($[n\text{-}Bu_4N]_4^+[W_{10}O_{32}]^{4-}$ or TBADT) (*Figure 1.4*).

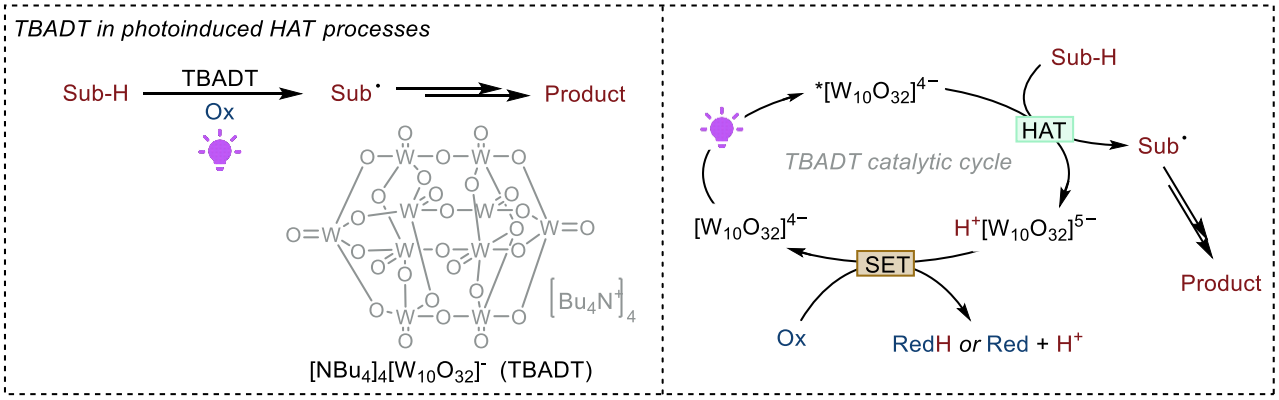

Figure 1.4 Schematic representation of a photoredox HAT processes mediated by TBADT.

This colorless polyanion complex exhibits a strong absorption in the near-UV region. Its photophysical properties have been studied experimentally and computationally in the last decades.[10] Upon excitation, it reaches a singlet excited state that rapidly decays to a putative triplet state with a radical character localized on an oxygen. This explains the reactivity of TBADT in the C-H homolytic cleavage leading to the reduced species $H^+[W_{10}O_{32}]^{5-}$.[11] Various strategies to restore the catalytic cycle have

been developed and different protocols are reported in the literature. Of particular relevance is the possibility to activate inert C(sp^3)-H bonds to enable useful transformations.[12,13]

1.1.5 Electron transfer process

The third bimolecular process that can occur in the presence of a photoexcited species is the electron transfer (ET). The photoexcited species can either accept or transfer an electron acting as an oxidant or a reductant, respectively. Since one electron is involved in this process, the event is usually defined as *single electron transfer* (SET). In particular, the overall process of excitation and the redox event is usually referred to as *photoinduced electron transfer* (PET). Most of the processes reported in the literature are based on PET processes and they have been extensively reviewed in the recent years.[5] In this section, general theoretical aspects of the electron transfer will be briefly discussed, as well as the different modes in which electron transfer can take place.

The first aspect to consider is that an excited species is both a better reductant and oxidant compared to it in its ground state. The reason is illustrated in *Figure 1.5*: if we consider a general organic molecule with a closed-shell ground state and we compare it to an open-shell excited state in which an electron is promoted to an antibonding orbital, it is intuitive that this electron can be more easily removed, which means that the excited state has a lower ionization potential and can act as a better reductant than the ground state. At the same time, the vacancy in a bonding orbital makes more easily to accept an additional electron, which means that the excited state has a higher electron affinity and can act as a better oxidant than the ground state.[2]

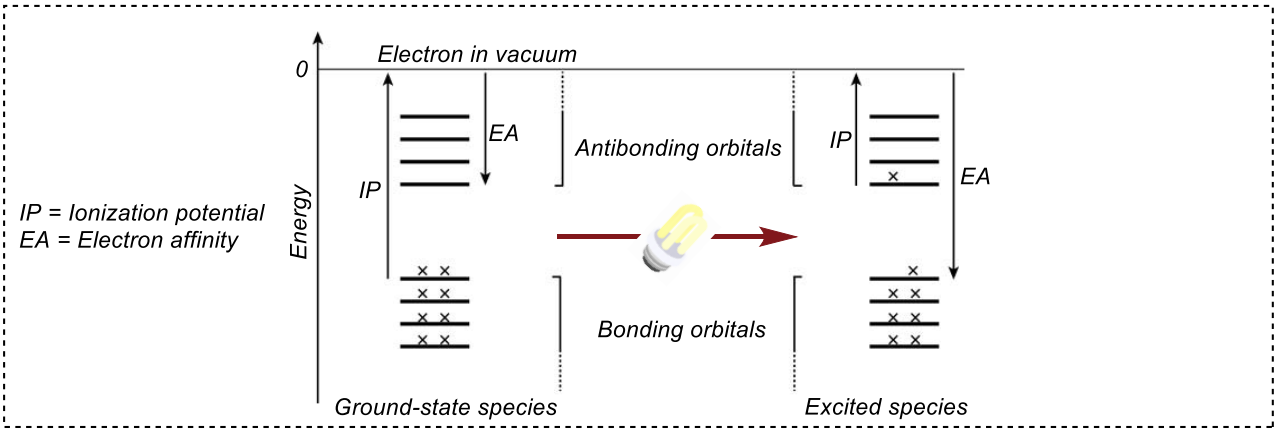

Figure 1.5 Orbital scheme of a ground- and excited state and the respectively different redox properties.

Because of the enhanced redox properties of the excited photocatalyst, two possible pathways of deactivation can occur involving a SET event with another species, i.e. the *quencher* (*Figure 1.6*). If the photocatalyst gains an electron, the deactivation is defined as *reductive quenching*, otherwise, if the photocatalyst loses an electron, the deactivation is defined as *oxidative quenching*. After the quenching event, a stoichiometric agent, even generated *in situ*, must restore the original oxidation state of the photocatalyst in an opposite SET process, i. e. after a reductive quenching a stoichiometric oxidant must be present in the reaction media, otherwise, after an oxidative quenching, a stoichiometric reductant must be present to restore the catalytic cycle. Catalysis involving a photocatalytic cycle in which SET events occur is defined as *photoredox catalysis*.

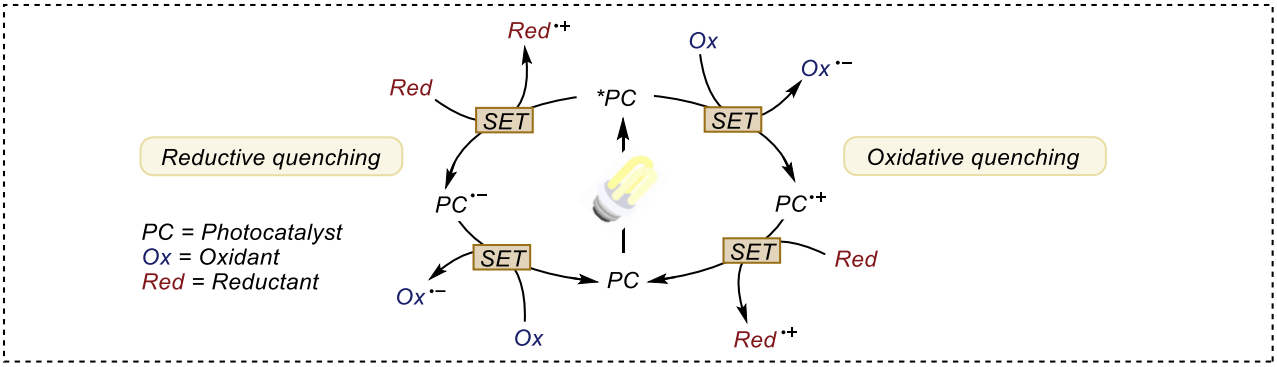

Figure 1.6 General scheme for the oxidative and reductive quenching of a photocatalyst.

Let's consider a general reaction between two substrates A and B in the presence of a photocatalyst PC, where A can be directly involved in a SET oxidation and B that can be directly involved in a SET reduction with the photocatalytic cycle. This reaction can be classified according to three redox outcomes (*Figure 1.7*): net oxidative, net reductive, and net redox neutral. In net oxidative reactions an external oxidant must be added to ensure the photocatalytic turnover. The oxidation event can occur either in the quenching step or as a back oxidation after a reductive quenching (*Figure 1.7 A*). In net reductive reactions an external reducing agent must be added to ensure the photocatalytic turnover. The reduction event can occur either in the quenching step or as a back reduction after an oxidative quenching (*Figure 1.7 B*). Finally, net redox neutral reactions do not require external oxidants or reductants, since an *in situ* generated intermediate is responsible for the turnover of the catalytic cycle (*Figure 1.7 C)*. The figure considers all the possible sequences of events.

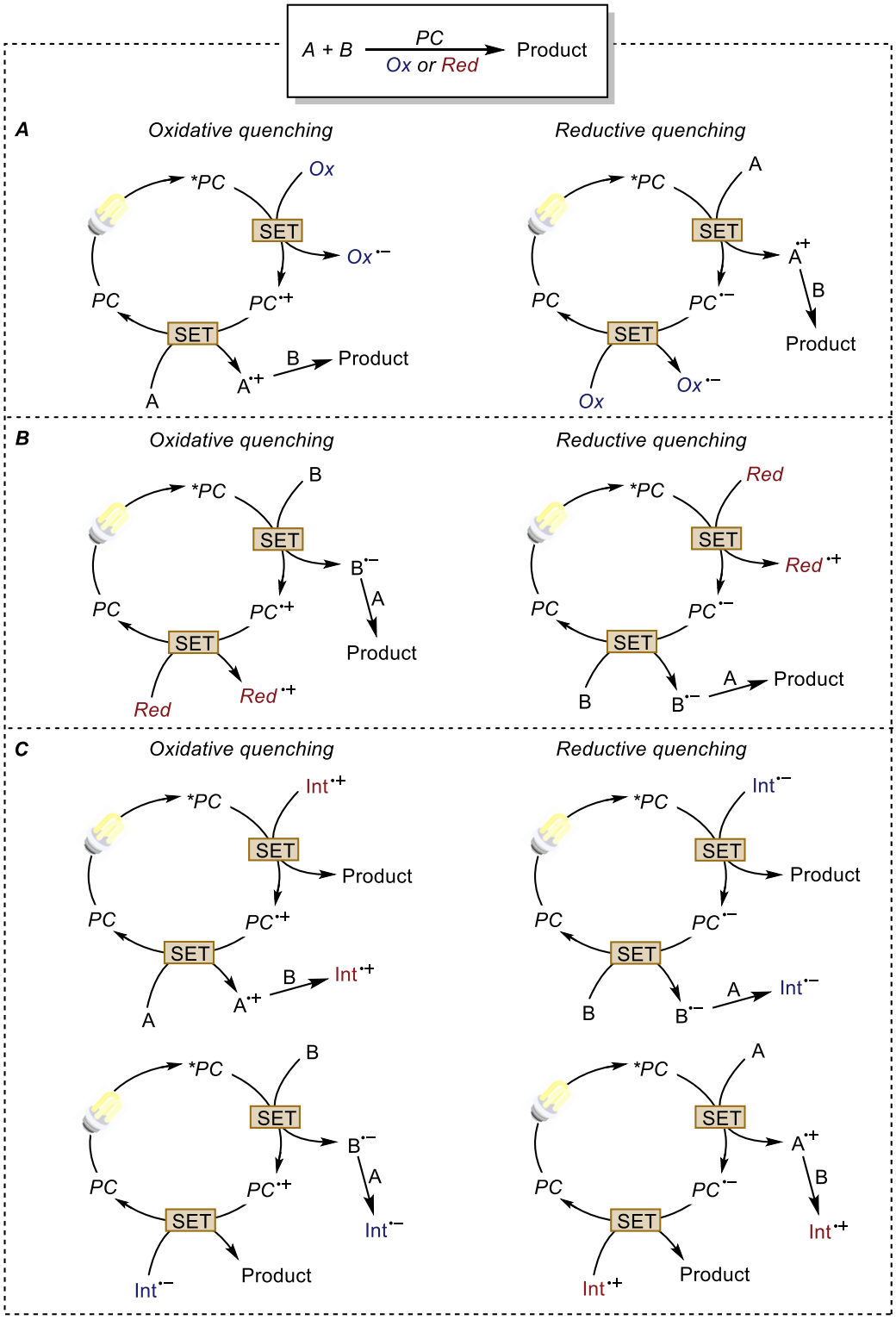

Figure 1.7 Schematic representation of all possible net oxidative (**A**), net reductive (**B**), and net redox-neutral processes (**C**).

Let's consider a general reversible PET process between the photocatalyst (PC) and a substrate (sub). When the SET involves the reduction of the excited photocatalyst *PC to $PC^{\bullet-}$ and the oxidation of the substrate sub to $sub^{\bullet+}$, the equation of the Gibbs free-energy (6) can be written[5] as:

$$\Delta G_{PET} = -\mathcal{F}({}^{*}E_{red}({}^{*}PC/PC^{\bullet-}) - E_{ox}(sub^{\bullet+}/sub)) \quad (6)$$

On the contrary, when the SET involves the oxidation of the excited photocatalyst *PC to $PC^{\cdot+}$ and the reduction of the substrate sub to $sub^{\cdot-}$, the equation of the Gibbs free-energy (7) can be written as:

$$\Delta G_{PET} = -\mathcal{F}(E_{red}(sub/sub^{\cdot-}) - {}^{*}E_{ox}(PC^{\cdot+}/{}^{*}PC)) \quad (7)$$

where $\mathcal{F}$ is the Faraday constant (23.061 kcal V−1 mol−1), E_{ox} and E_{red} are the ground state redox potentials, experimentally obtained from cyclovoltammetry experiments in the oxidation and reduction processes respectively, and $^{*}E_{ox}$ and $^{*}E_{red}$ are the excited state redox potentials. These values can be calculated considering the equations (8) and (9):

$${}^{*}E_{ox}(PC^{\cdot+}/{}^{*}PC) = E_{ox}(PC^{\cdot+}/PC) - E_{00} \quad (8)$$

$${}^{*}E_{red}({}^{*}PC/PC^{\cdot-}) = E_{red}(PC/PC^{\cdot-}) + E_{00} \quad (9)$$

It is important to note that the *PC can be referred either to a singlet S_1 or a triplet T_1 state, depending on the nature of the excited state which is involved in the SET process. The E_{00} is the energy difference between the zero-zero vibrational levels of the ground and excited state, and this corresponds to the electronic spectroscopy energy. As mentioned above, the E_{00} value is fundamental for predicting the thermodynamic feasibility of a SET electron transfer, and can therefore provide important information for describing the reaction mechanism of a reaction and for rational design of a new process.[1] The value can be obtained spectroscopically (*Figure 1.8*) and the vibrational structure of the spectrum is useful for this purpose: E_{00} can be calculated by locating the energy associated with a specific vibrational level v_n of both the S_1 and S_0. In the absence of vibrational structures, E_{00} can be roughly estimated from the absorption profile: 1. from the position of the long wavelength tail (λ_{tail}) (*Figure 1.8 A*),[2] 2. from the λ value at the intersection of the tangent passing through the y-coordinate (ε_{abs}), where ε_{abs}= 10% ε_{max}, with the x-coordinate (*Figure 1.8 B*) or 3. from the λ value at the intersection between the absorption and emission profile of that species (*Figure 1.8 C*). Additionally, 4. computational methods can be also employed.[1] The conversion between λ and E_{00} can be calculated using the Bohr equation (1).

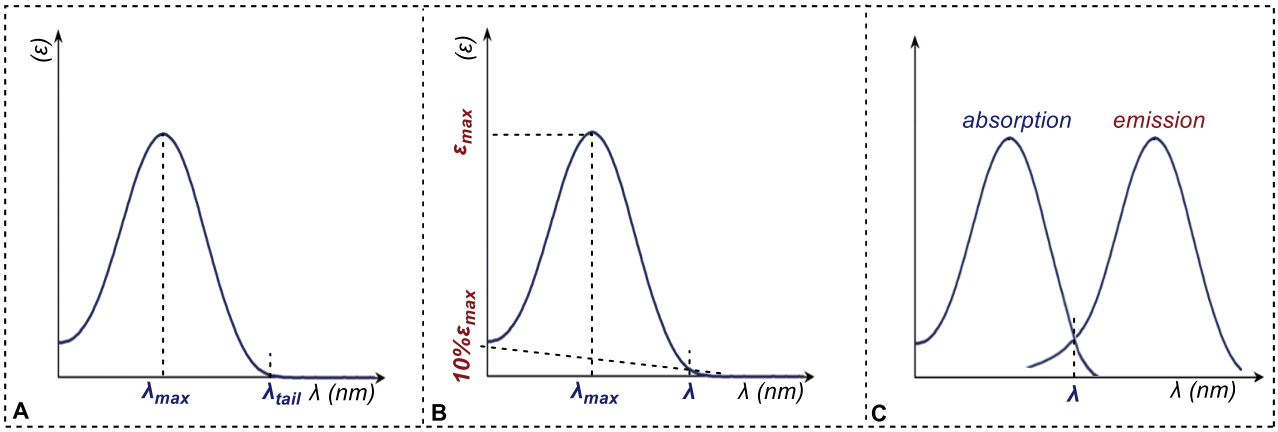

Figure 1.8 Different modes for the spectroscopic determination of the E_{00} value.

As a final practical consideration, in order to present a plausible mechanism for a photoredox transformation, several aspects and experimental tests can be performed. In order to prove or justify each primary process it is necessary 1. to take into account the redox potentials of each possible partner involved in this primary process to evaluate from the ΔG_{ET} whether the process is thermodynamically favoured. 2. in the case of the quenching event, the species(s) responsible for the decay of the excited state can be determined by the *Stern-Volmer* quenching experiment.

The Stern-Volmer quenching experiment is routinely performed to determine the species involved in the decay of the excited photocatalyst. The experiment is based on the reduction of the lifetime of the excited species as a function of a variable amount of a quencher Q. This relationship, known as the Stern-Volmer equation (10) is:

$$\frac{\tau^0}{\tau} = 1 + \tau^0 k_q[Q] \tag{10}$$

where τ^0 is the lifetime of the excited state in the absence of the quencher Q, $\tau\ is$ the lifetime of the excited state in the presence of a given amount of the quencher [Q] and k_q is the quenching constant. The equation can be derived considering the four main competitive deactivation processes, each of which is described by a kinetic constant: non-radiative (*nr*) (k_{nr}), radiative (*r*) (k_r), intramolecular photochemical processes (*p*) (k_p) and intermolecular quenching (*q*) (k_q).

Let's consider first the intramolecular deactivation pathways (*nr*, *r*, *p*). The decay of the excited state can be described by a first-order kinetic law of the variation of its concentration as a function of time (11):

$$-\frac{d[^*PC]_{intra}}{dt} = \left(k_{nr} + k_r + k_p\right)[^*PC] = \frac{1}{\tau^0}[^*PC] \tag{11}$$

In the presence of a quencher Q, the decay of the excited state can be described by a second-order kinetic law of the variation of its concentration as a function of time (12):

$$-\frac{d[^*PC]_{inter}}{dt} = k_q[^*PC][Q] \tag{12}$$

The overall deactivation process is the sum of the intramolecular and intermolecular deactivation pathways (13):

$$-\frac{d[^*PC]}{dt} = -\frac{d[^*PC]_{intra}}{dt} - \frac{d[^*PC]_{inter}}{dt} = \left(k_{nr} + k_r + k_p + k_q[Q]\right)[^*PC] \tag{13}$$

Solving the equation (13) gives equation (14):

$$[^*PC]\ (t) = [^*PC]_0 \exp\left[-\left(k_{nr} + k_r + k_p + k_q[Q]\right)t\right] \tag{14}$$

where $[^*PC]_0$ is the concentration of the excited photocatalyst in the absence of the quencher.

Considering that the lifetime of *PC in the presence of the quencher is given by the equation (15):

$$\tau = \frac{1}{k_{nr} + k_r + k_p + k_q[Q]} \tag{15}$$

And considering τ_0 as the lifetime of *PC in the absence of the quencher (16):

$$\tau_0 = \frac{1}{k_{nr} + k_r + k_p} \tag{16}$$

Combining equation (15) and (16) and considering the ratio τ_0/τ gives the aforementioned equation (10):

$$\frac{\tau_0}{\tau} = \frac{\frac{1}{k_{nr}+k_r+k_p}}{\frac{1}{k_{nr}+k_r+k_p+k_q[Q]}} = \frac{k_{nr}+k_r+k_p+k_q[Q]}{k_{nr}+k_r+k_p} = 1 + \frac{1}{k_{nr}+k_r+k_p}k_q[Q] = 1 + \tau^0 k_q[Q] = 1 + k_{SV}[Q]$$

Equation (10) can be experimentally used since different $\frac{\tau_0}{\tau}$ ratios of the photoexcited species can be measured and plotted as a function of different concentrations of the quencher $[Q]$ with a linear correlation (*Figure 1.9*). The slope of the line, i.e. $\tau^0 k_q$, is defined as the Stern-Volmer quenching constant k_{SV} and it is a useful parameter to determine which species is the most responsible for the quenching process.

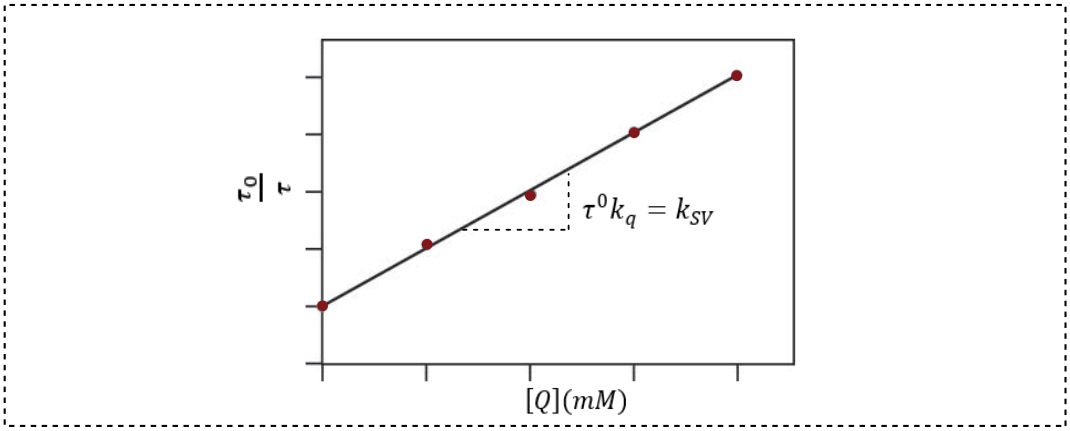

Figure 1.9 Representative Stern-Volmer plot.

Finally, equation (17) is particularly useful for determining the most responsible species for the quenching process is the quenching efficiency of the *i*-species η_q^i which considers its quenching constant k_q^i and its concentration $[Q]^i$:

$$\eta_q^i = \frac{k_q^i \cdot [Q]^i}{k_{nr} + k_r + \sum_0^n k_q^n \cdot [Q]^n} \cdot 100 \qquad (17)$$

1.2 Photoredox catalysis: the beginning

Once the main aspects for understanding photoredox catalysis have been described, in the following section some examples will be given. The aim of these sections is to highlight some cornerstone applications of photoredox catalysis, showing how it is possible to use light to activate small molecules in the formation of new C-C bonds, as well as C-heteroatom bonds, and how modern photocatalytic methodologies are not only of academic interest, but they can be used in the synthesis of complex scaffolds, and are also widely used in industry.

The first example of light-mediated activation of small molecules was reported in 1978 by the Kellog group, who observed that the reduction of sulfonium ions to the corresponding alkanes and thioethers could be enhanced under light irradiation in the presence of a catalytic amount of $[Ru(bpy)_3]Cl_2$ and a stoichiometric amount of the *N*-methyl Hantzsch ester. (*Figure 1.10*).[14,15] The mechanism has been investigated by the authors and involves the reductive quenching of the excited photocatalyst by the 1,4-dihydropyridyl radical of the Hantzsch ester producing a Ru(I) species and a 1,4-dihydropyridyl cation. The reduced Ru(I) can reduce the sulfonium ions leading to the corresponding thioether and a α-carbonyl radical. The latter can abstract a proton to the *N*-methyl Hantzsch ester forming the desired product and the 1,4-dihydropyridyl radical, the effective quencher of the excited photocatalyst.

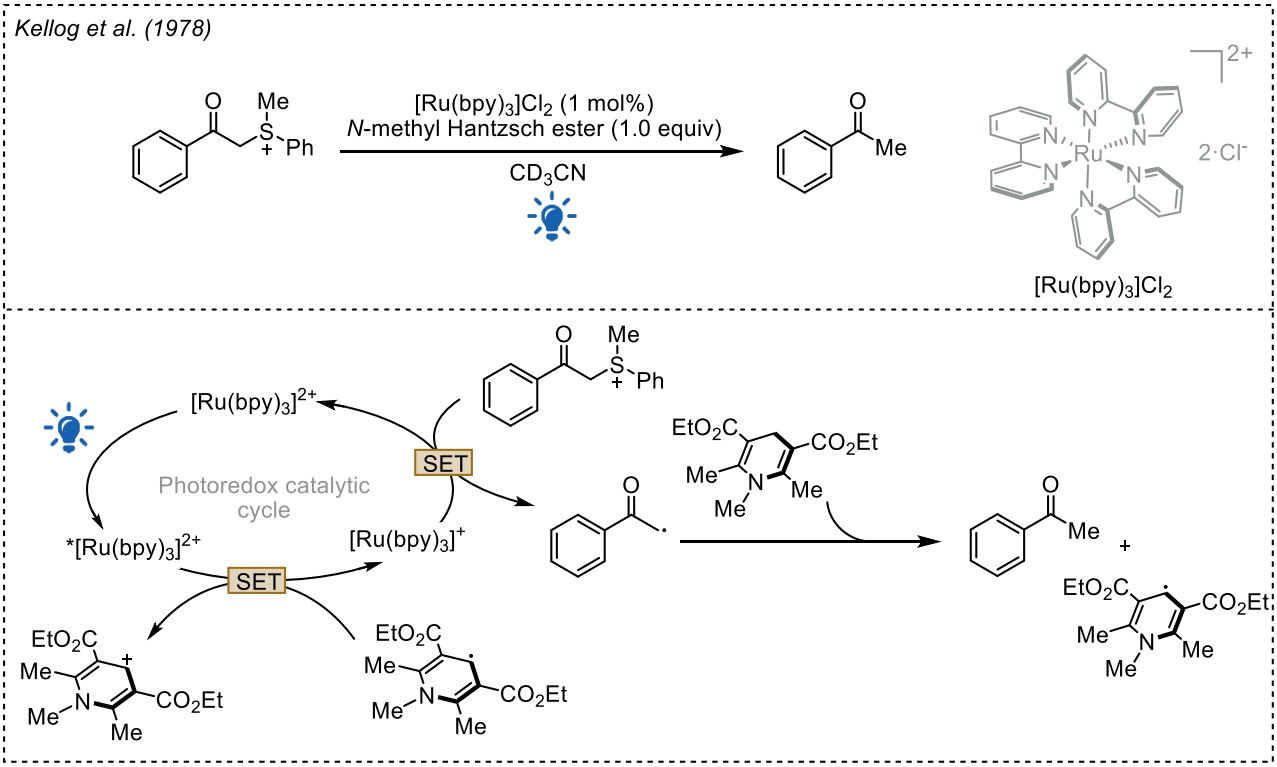

Figure 1.10 Photoredox reduction of sulfonium ions reported by the Kellog group.

In the following years, other authors reported the use of similar strategies using $[Ru(bpy)_3]Cl^{2-}$ dihydropyridine catalyst systems in the reduction of organic substrates including electron-deficient olefins[16–18] and aromatic[19,20] or benzylic[21,22] carbonyls.

Despite the enormous potential of photocatalysis, it was not until the late 2000's that the field attracted widespread community interest, with three seminal papers from the groups of Yoon, Mac Millan and Stephenson, giving rise to a fast-growing field.

In 2008, the Yoon group published a photoredox intramolecular [2+2] enone cycloaddition reaction promoted by $[Ru(bpy)_3]Cl_2$ under white light irradiation (275W CFL lamp) in the presence of $LiBF_4$ as the Lewis acid and DIPEA as the stoichiometric organic reductant (*Figure 1.11*).[23] The presence of a Lewis acid additive was found to be beneficial in modulating the reactivity of the carbonyl moieties facilitating the SET step and the formation of the Y-carbonyl radical. The mechanism involves the reductive quenching of the photoexcited photocatalyst by the DIPEA generating $DIPEA^{\cdot+}$ and a Ru(I) species, capable of reducing a carbonyl group of the bis(enone) activated by the Lewis acid, forming the Y-carbonyl radical . [2+2] radical cyclization takes place, leading to the desired product in high yield and with a moderate *dr* in favour of the *meso* diastereoisomer. As suggested by the authors, the presence of both a negative charge and an unpaired electron in the enone radical anion intermediate is required for the formation of the cyclobutane ring.[24]

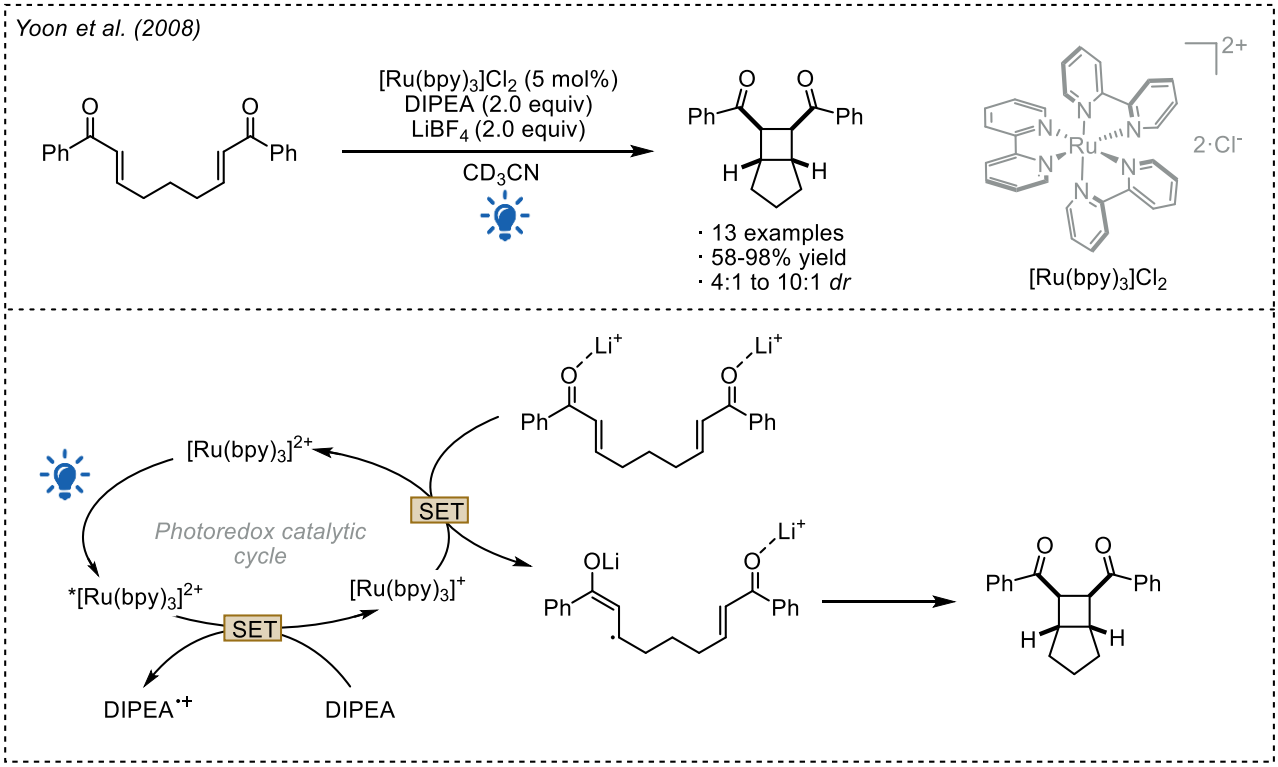

Figure 1.11 Photoredox intramolecular [2+2] enone cycloaddition reported by the Yoon group.

Similar reductive conditions were reported by Stephenson in 2009 in a tin-free dehalogenation protocol for benzylic and α-acyl halides (*Figure 1.12*).[25] The protocol uses the same Ru(II) photocatalyst in the presence of both DIPEA (2 equiv.) and Hantzsch ester (2 equiv.). The proposed mechanism is similar to the previous one and involves the reductive quenching of the excited photocatalyst by DIPEA generating an amine radical cation $DIPEA^{\bullet+}$ and a Ru(I) species, capable of reducing the C-halogen bond. Protonation of the radical yields the desired de-halogenated product. Because of the reduction potential of Ru(I) ($E_{red}(Ru^{II}/Ru^{I})$ = −1.28 V *vs* SCE), benzylic bromides and chloride could be reduced, as they have a reduction potential of around −0.7 V (*vs* SCE), while extending the protocol to less activated halogen derivatives was unsuccessfully.

By replacing $[Ru(bpy)_3]Cl_2$ with the stronger photoreductant *fac*-$Ir(ppy)_3$ ($^*E_{ox}(Ir^{IV}/^*Ir^{III})$ = −1.73 V *vs* SCE) the group was able, years later, to reduce non activated alkyl iodides, which require a stronger reduction power to be reduced (E_{red}(alkyl-I/alkyl$^\bullet$) ~ −1.6 V *vs* SCE).[26]

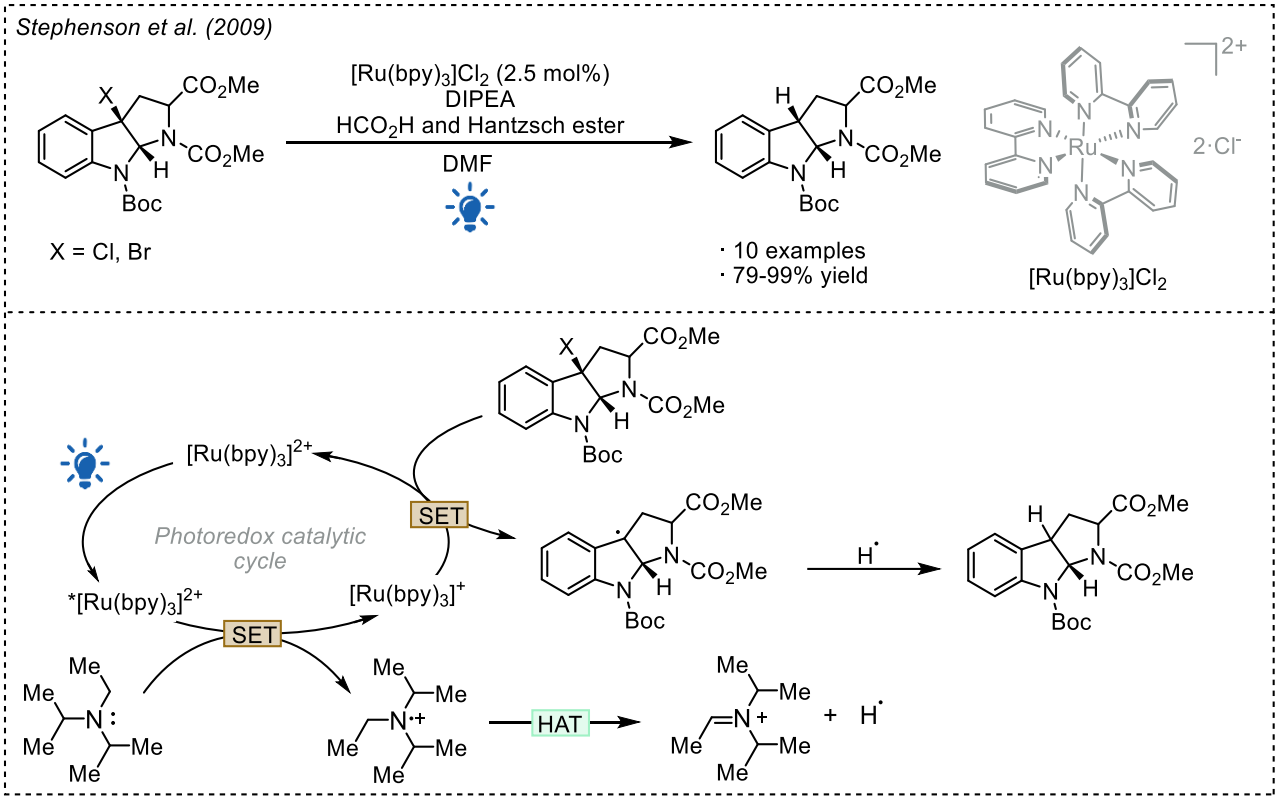

Figure 1.12 Photoredox dehalogenation protocol reported by the Stephenson group.

Finally, in 2008, Nicewicz and MacMillan reported the first protocol combining photoredox catalysis and organocatalysis in the enantioselective α-alkylation of aldehydes (*Figure 1.13*).[27] This is the first example of a dual photoredox catalytic platform and a cornerstone for the next development in the field. Mechanistic details are reported in section 1.6.1, which is dedicated to the dual photoredox organocatalysis.

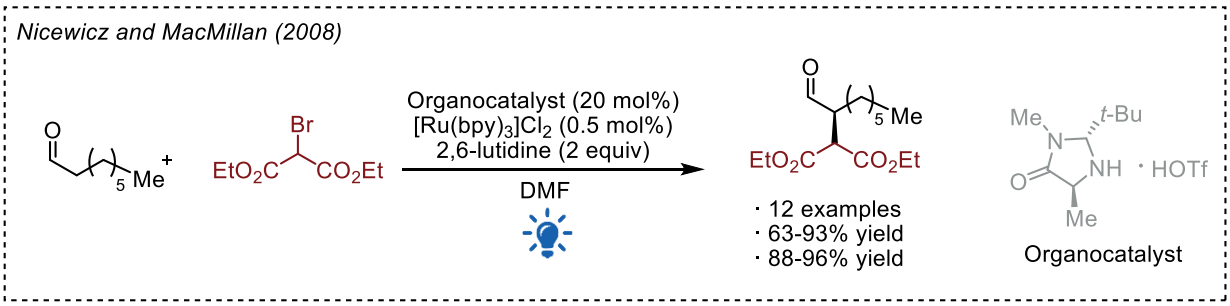

Figure 1.13 Dual photoredox organocatalytic enantioselective α-alkylation of aldehydes reported by Nicewicz and MacMillan.

1.3 Photoredox catalysis: forging new valuable bonds

The three seminal papers reported in the previous paragraphs represent the starting point of a field that has experienced an exponential increase in both the number of publications and in the number of different applications that share the use of light as energy source. Although a significant proportion of the publications concern the formation of new C-C bonds, several groups have reported the formation of useful and valuable carbon-heteroatom bonds. In the following paragraphs some methodologies for the installation of C-C and C-heteroatom bonds will be presented. In particular, the case study of the α-functionalization of amines and the formation of C-X (X = halogen), C-B and C-S bonds will be described.

1.3.1 Forging new C-C bonds: the case study of amine functionalization

Nitrogen heterocycles are an important motif in natural products and biologically active compounds,[28] and as such, the development of new protocols for their synthesis and functionalization is a topic of great interest.

In this context, two general modes of activation can be distinguished, as shown in *Figure 1.14* and they exploit the ability of amines to quench the excited state of the photocatalyst. In the first one after the reductive quenching of the photocatalyst, a *N*-centered radical cation is formed, making the α-amino C-H bond more acidic, so that it can be easily removed in a polar reaction by a weak base generating an α-amino radical.[29] This radical can be oxidized to an iminium ion in another SET event by a suitable terminal oxidant. The second mechanism involves, as before, the formation of an amine radical cation, generated in the reductive quenching of the photocatalyst, which undergoes α-amino C-H abstraction by a radical anion generated *in situ* by the reduction of a suitable oxidant introduced to restore the photocatalytic cycle. In both the cases an iminium ion is formed which is electrophilic towards many different nucleophiles.

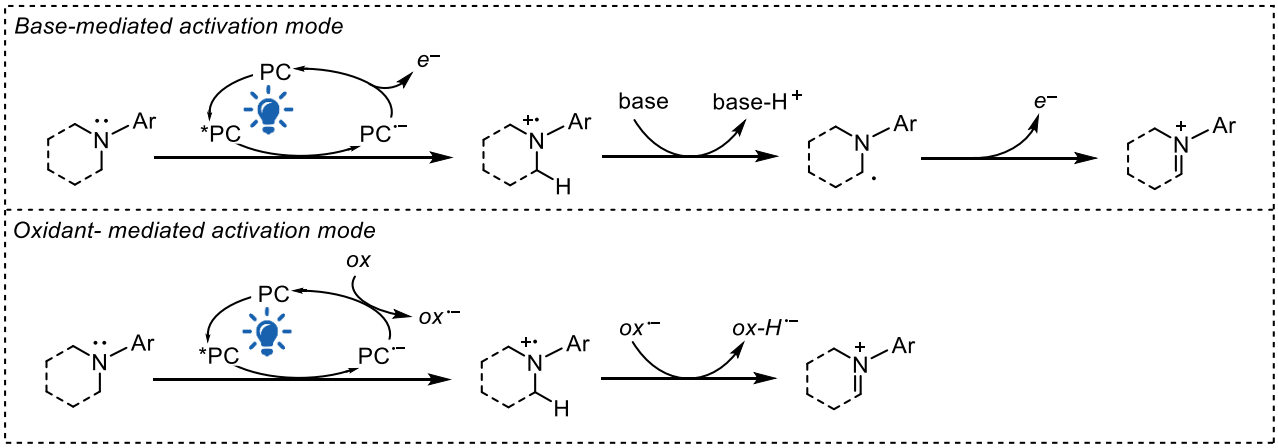

Figure 1.14 Different photoredox-mediated activation modes for the α-functionalization of amines.

An example of the first activation mode was reported by the MacMillan group in 2011 in the α-amino arylation (*Figure 1.15*).[30] Using $Ir(ppy)_3$ as the photocatalyst under irradiation with a CFL lamp, a persistent aryl radical is formed upon the reductive quenching of the photocatalyst by the cyanoarene. A suitable *N*-arylamine can restore the photocatalytic cycle in a reductive step, generating an *N*-radical cation. α-deprotonation with a base, i.e. NaOAc, generates a transient α-amino radical. Radical coupling between the amine radical and the electron deficient arene, followed by the rearomatization of the aromatic ring leads to the desired α-arylamine.

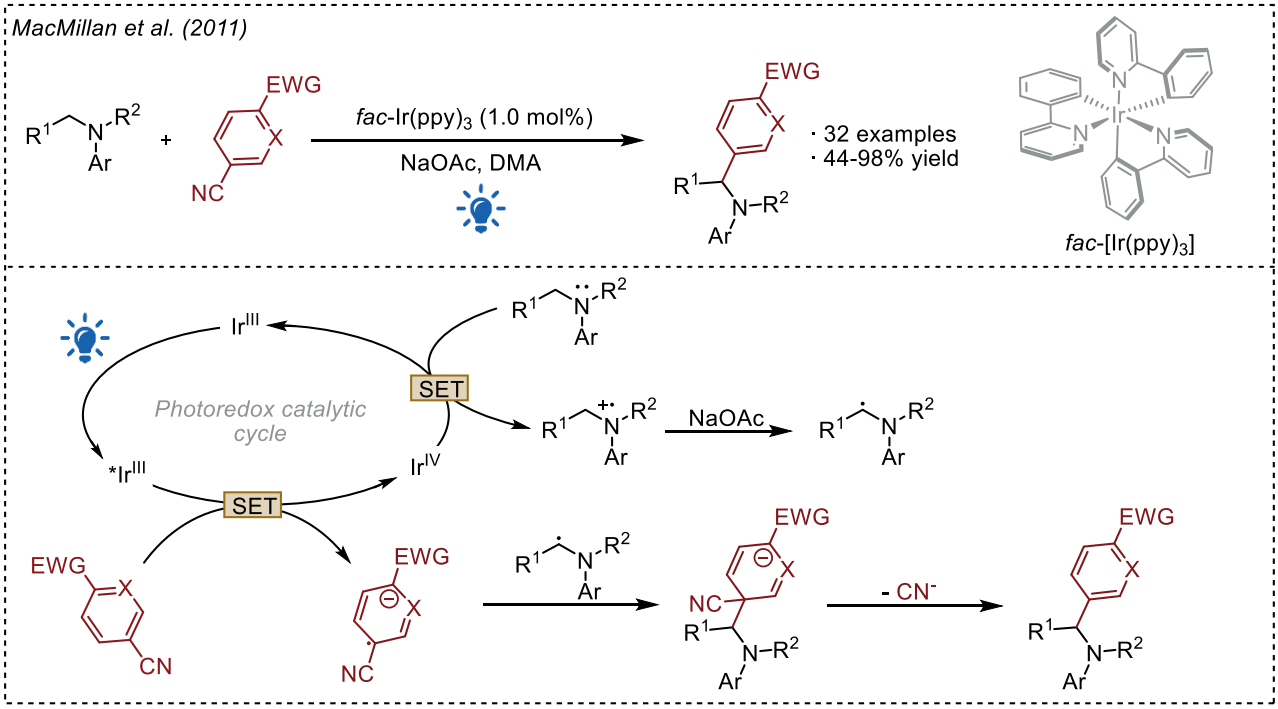

Figure 1.15 Photoredox α-amino arylation protocol reported by the MacMillan group.

As an example of the second activation mode, the Stephenson group reported the first photoredox Aza-Henry reaction in 2010 (*Figure 1.16*).[31] Using $[Ir(ppy)_2(dtbpy)](PF_6)$ as the photocatalyst under irradiation with a CFL lamp, a transient electrophilic iminium ion is formed upon the reductive quenching of the photocatalyst and the C-H abstraction. The iminium can scavenge the nitroalkane derivatives, yielding the corresponding α-functionalized products. When the reaction was tested under an inert atmosphere, the authors observed the formation of the desired product, but the time required to achieve a full conversion was longer. The result suggested that oxygen, as well as the nitroalkane, could act as the oxidants to restore the photocatalytic cycle.

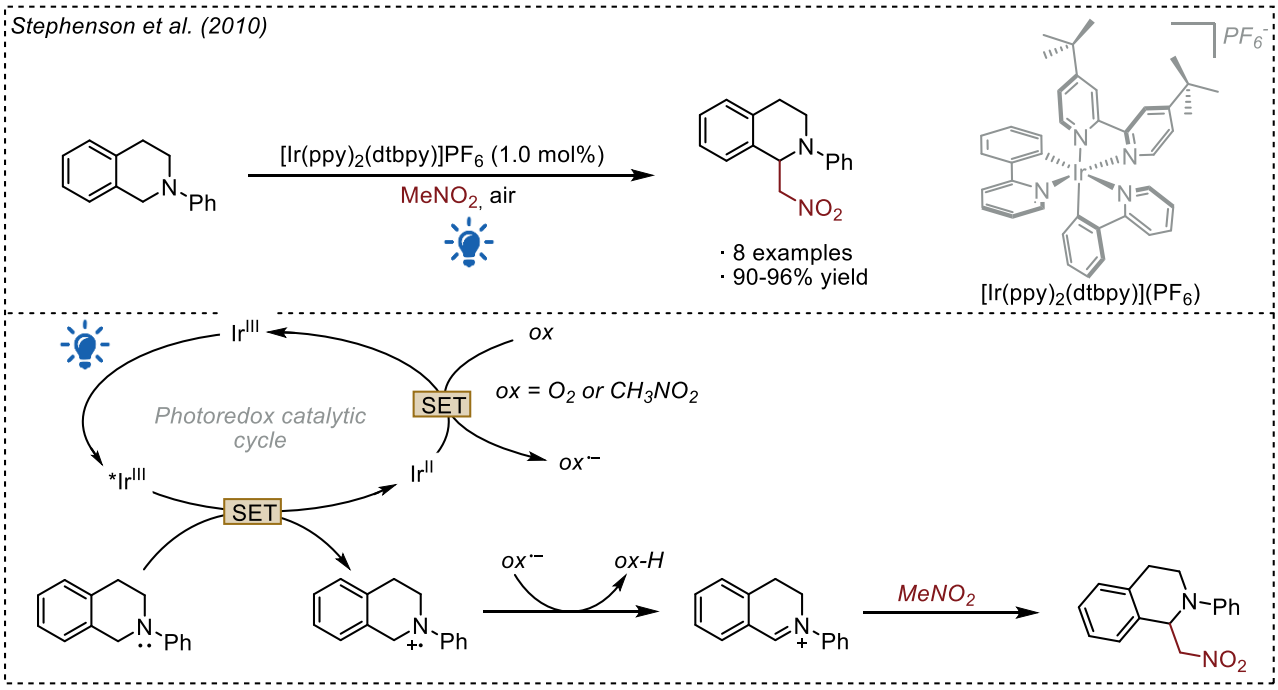

Figure 1.16 Photoredox Aza-Henry reaction reported by the Stephenson group.

1.3.2 Forging new C-X, C-B and C-S bonds: the case study of photoredox decarboxylation

The introduction of carbon-halogen (C-X), carbon-boron (C-B) and carbon-sulphur (C-S) bonds into organic frameworks represents an outstanding source of reactivities: halogenated compounds are widespread in nature[32] and represent an important market share in the pharmaceutical and agrochemical industries, as well as in the materials science.[33] Carbon-sulphur bonds are also ubiquitous, in particular thioethers are important structural motifs in many pharmaceutically drug molecules, in agrochemical products and materials.[34] Carbon-boron bonds are very useful synthetic intermediates because they can be introduced under several stereoselective, reliable and reproducible protocols[35] and then they can be converted into a wide range of functional groups[36] or used in the construction of complex scaffolds.[37] Photoredox catalysis offers several strategies to gain access to C-X, C-B and C-S bonds under mild conditions. The availability of the starting materials is particularly relevant and must be taken into account. Carboxylic acids are widely available in nature and are easily accessible from other functional groups.[38] Carboxylic acid derivatives are known to undergo decarboxylation under various photoredox conditions, either when converted into activated-esters and as free acids.[39] In this context, the activation of carboxylic moieties as redox-active esters (RAE) is a versatile tool towards single electron transfer events, e.g. under photoredox or electrochemical conditions,[40] which induces their decomposition and the concomitant formation of a C-centered radical.[41] As depicted in *Figure 1.17*, a carboxylic acid is first converted into the RAE derivative by the reaction with *N*-hydroxyphtalimide (NHPI), then the intermediate is subjected to a single electron-transfer reduction. The radical anion undergoes a fast reductive fragmentation leading to the phthalimidyl anion ($Npht^{-}$), the corresponding alkyl radical with the extrusion of CO_2.

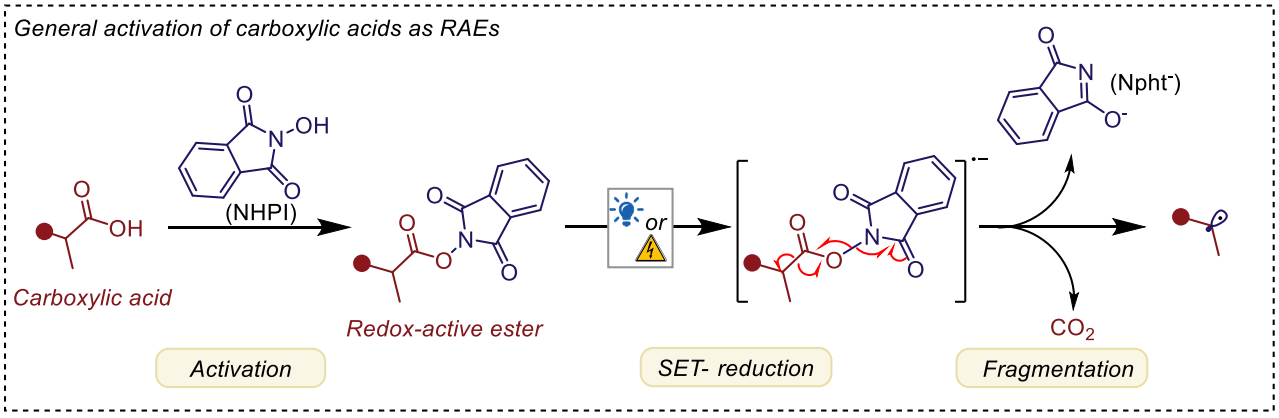

Figure 1.17 Schematic activation of carboxylic acids as RAEs for the formation of C-centered radicals.

In this section two examples by Noble and Aggarwal for the formation of C-B, C-X and C-S bonds under photoredox decarboxylation conditions of RAEs are reported.

The first example was reported in 2017. Using B_2cat_2 as a commercial, inexpensive and air-stable boron source in dimethylacetamide (DMAc) as the solvent under blue light irradiation, the group reported the installation of C-B bonds on primary, secondary and tertiary carboxylic acids (*Figure 1.18*).[42]

The mechanism was investigated using ^{11}B NMR analysis, experimental tests and with UV/Vis measurements. The key aspect of the protocol is the formation of a photoactive species ***II*** by the coordination of the boron/solvent complex ***I*** to both the solvent and the NHPI oxygen. This complex can be irradiated at 450 nm to generate a diradical species (not shown in figure) which decomposes into the intermediates ***III*** and ***V***. The subsequent decomposition of ***V*** liberates CO_2, the Bcat-Npht complex ***VI*** and the C-centered radical, which participates in a catalytic cycle in which different boron

intermediates (***III***, ***VI***, ***VII***) are formed and which ensure the reaction outcome. Finally, the radical can be trapped by the solvent-activated B_2cat_2 ***I*** leading to the B_2cat intermediate ***VIII***. These intermediates are not stable under silica chromatography, so they are usually converted to the Bpin derivatives by simple transesterification with pinacol and triethylamine.

The reaction carried out in the dark showed a much slower rate, whereas the reaction under simpler bulb light was equally effective. This observation can be explained by a radical chain that can be promoted by both irradiation, and thermal input (conversion of ***IV*** into ***III***). Nevertheless, the reaction is faster under irradiation.

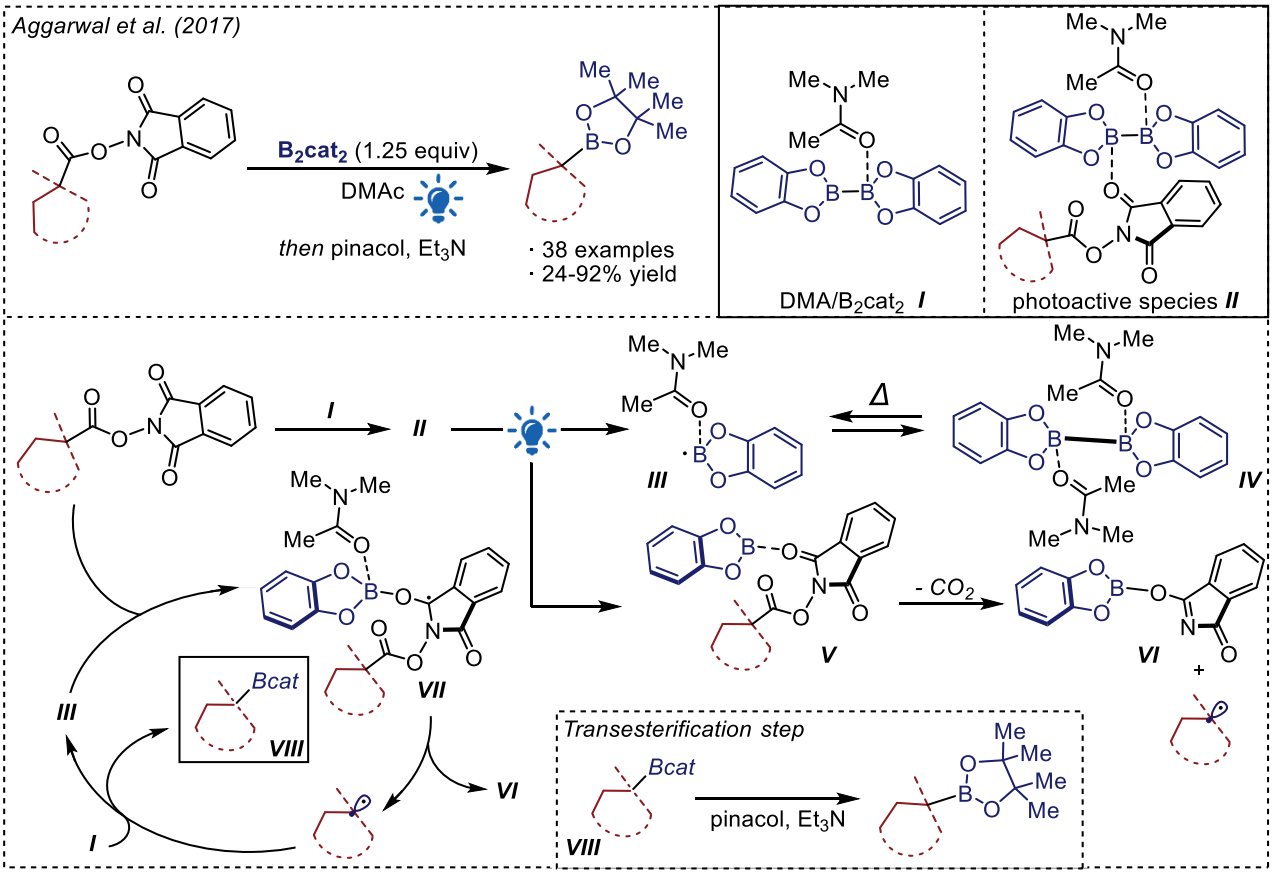

Figure 1.18 Photoredox decarboxylative borylation of carboxylic acids reported by the Aggarwal group.

The second paper discussed was reported in 2023. The group reported a photoredox decarboxylative halogenation using 4CzIPN as the photocatalyst under blue light irradiation and various inorganic salts and additives to install new carbon-halogen bonds (*Figure 1.19*).[43] The decarboxylative bromination proceeds under simple transition-metal-free conditions using 4CzIPN as the organic photoredox catalyst and lithium bromide as the bromide source. No other additives are required. The mechanism, proposed on a thermodynamic basis, involves the reductive quenching of the excited 4CzIPN ($^*E_{red}$(*4CzIPN/4CzIPN$^{\bullet-}$) = +1.35 V *vs* SCE in MeCN) by a bromine anion (E_{ox}(Br$^{\bullet-}$/ Br$^-$) = +0.80 V *vs* SCE in DME). The photocatalytic cycle is restored by a SET event between the reduced 4CzIPN$^{\bullet-}$ (E_{red}(4CzIPN/4CzIPN$^{\bullet-}$) = −1.21 V *vs* SCE) and the RAE, which fragments into CO_2, phtalimidate anion and the alkyl radical. The latter is trapped by $Br_2^{\bullet-}$ generated in a bromide catalytic cycle.

This mild protocol was applied to primary, secondary and tertiary RAE derivatives, and in the functionalization of complex and biological relevant molecules.

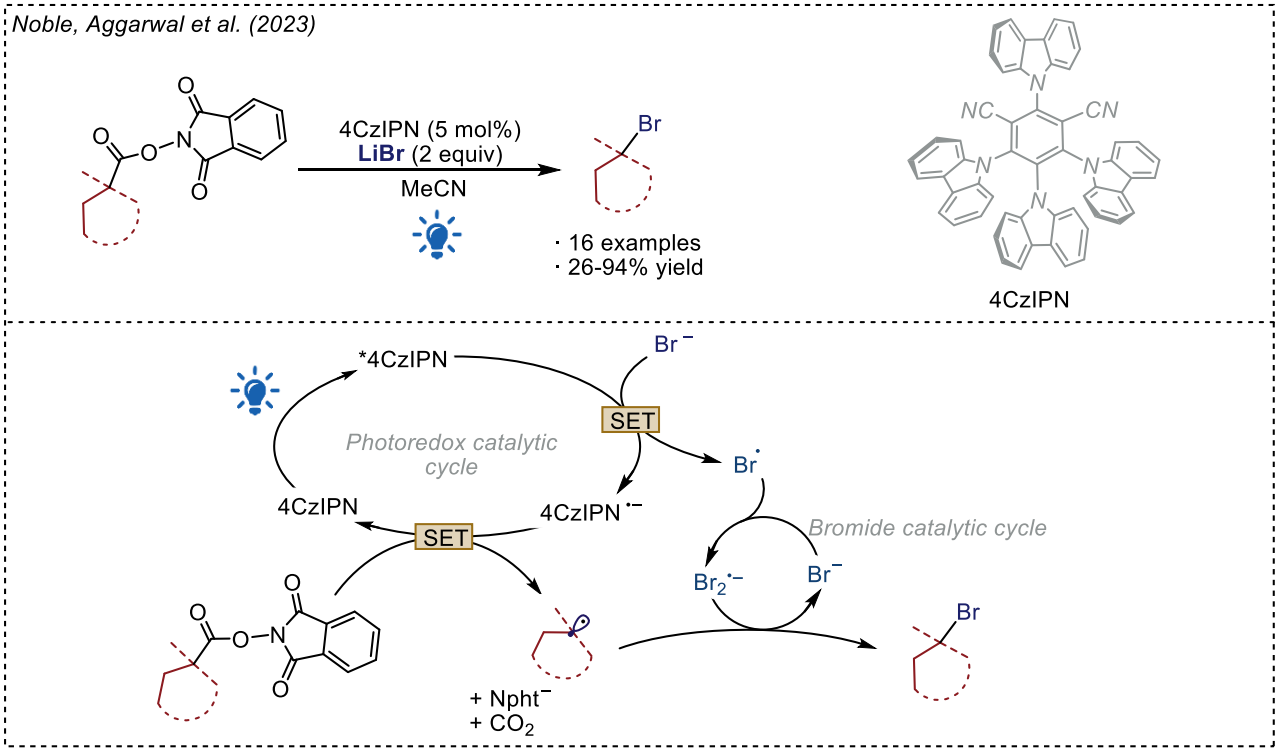

Figure 1.19 Photoredox decarboxylative bromination of carboxylic acids reported by Noble and Aggarwal.

Altough the bromination does not require any additive except the photocatalyst and the halogen source, in the case of the decarboxylative chlorination and thiocyanation, under the same conditions, a non-negligible amount of hydrodecarboxylated (alkane) and dehydrodecarboxylated (alkene) side-products were observed. It was found out that the addition of a catalytic amount of a copper salt, i.e. $CuCl_2$ and CuSCN for the chlorination and thiocyanation respectively, and a suitable ligand, could suppress these two competitive processes. The protocol was reoptimized, replacing 4CzIPN with $[Ir\{dF(CF_3)ppy\}_2(dtbpy)](PF_6)$ as the photocatalyst, and MeCN with acetone as the solvent in the case of the thiocyanation (*Figure 1.20*). In the latter two cases, the photoredox catalytic cycle is similar to the previous one and it involves first the reductive quenching of the excited photocatalyst in the presence of a copper catalytic cycle. The photocatalytic cycle is restored by the reduction of the RAE, which upon fragmentation releases CO_2, the phtalimidate anion and the alkyl radical. The latter is trapped in a Cu(I)/Cu(II) catalytic cycle, leading to the formation of the desired product.

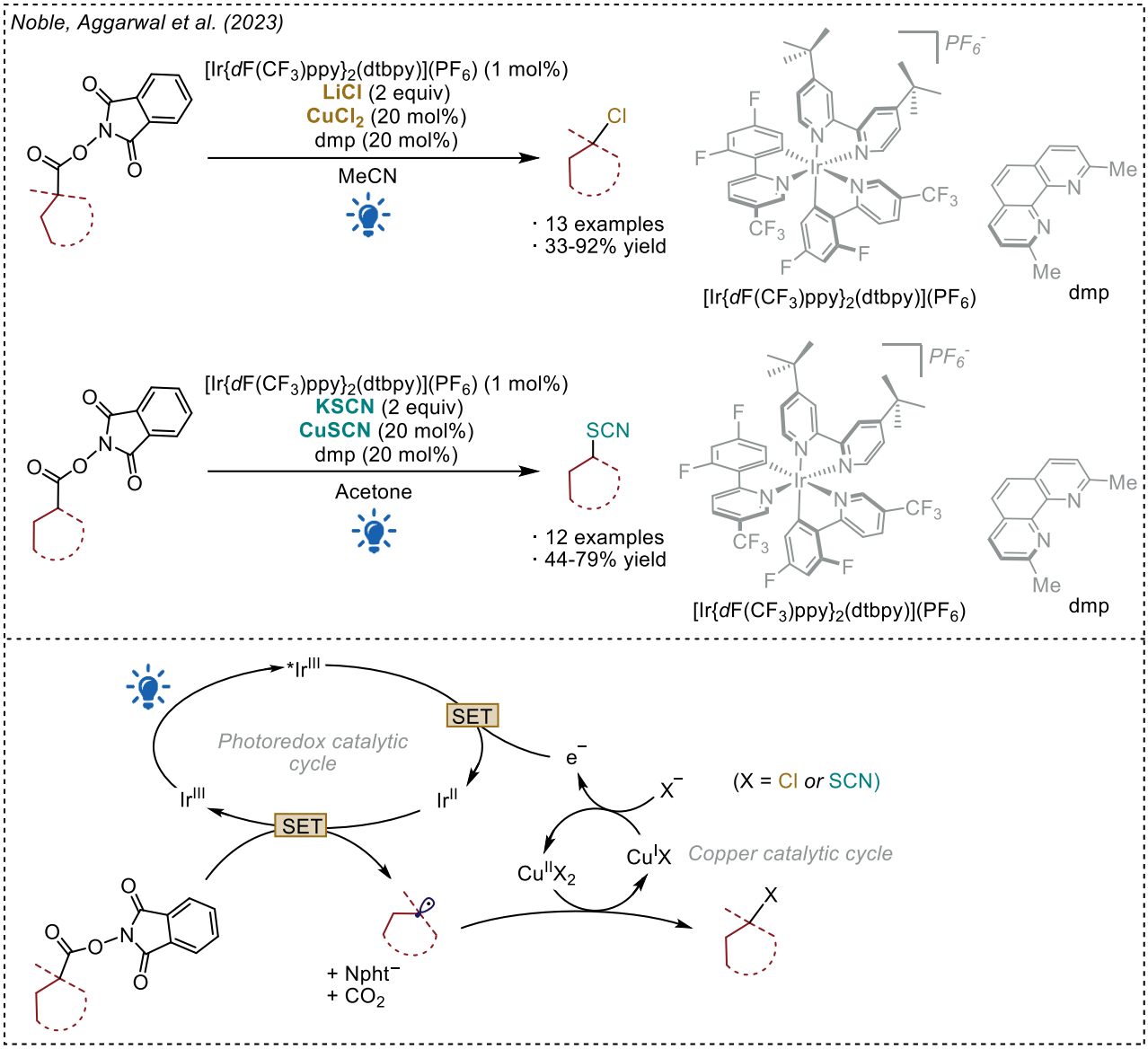

Figure 1.20 Photoredox decarboxylative chlorination and thiocyanation of carboxylic acids reported by Noble and Aggarwal.

Finally, these two examples demonstrate how photoredox catalysis can be successfully applied to the conversion of feedstock carboxylic acids activated as RAEs into valuable products under mild conditions. Although several methods using free carboxylic acids have been reported in the literature,[39,44–46] the activation of the acids as RAEs under straightforward conditions allows the use of milder, simpler and functional group tolerant conditions.

1.3.3 Forging complex frameworks under photoredox conditions

In the previous section some representative examples of how photoredox catalysis can be used to functionalize small molecules were described. However, these protocols can be extended from small and relatively simple molecules to the synthesis of more complex and structurally diversified scaffolds.[47] The successful outcome of these protocols lies in the functional group tolerance and in the mild, regio- and stereoselective conditions. As a taste of the enormous potential, in the following section two examples of the manipulation of complex molecular scaffolds under photoredox conditions are reported.

The first work was reported by the Li group in 2013. The group, among other natural products, notably achieved the total synthesis of Drimentine F and Indotertine A by exploiting the photoredox dehalogenation of the bromobenzyl position of the bromopyrrolindoline derivative ***II***, following the strategy reported by Stephenson in 2009 and discussed in section 1.2,[25] and coupling it with the α,β-unsaturated fragment ***I*** in a Giese reaction (*Figure 1.21*).[48]

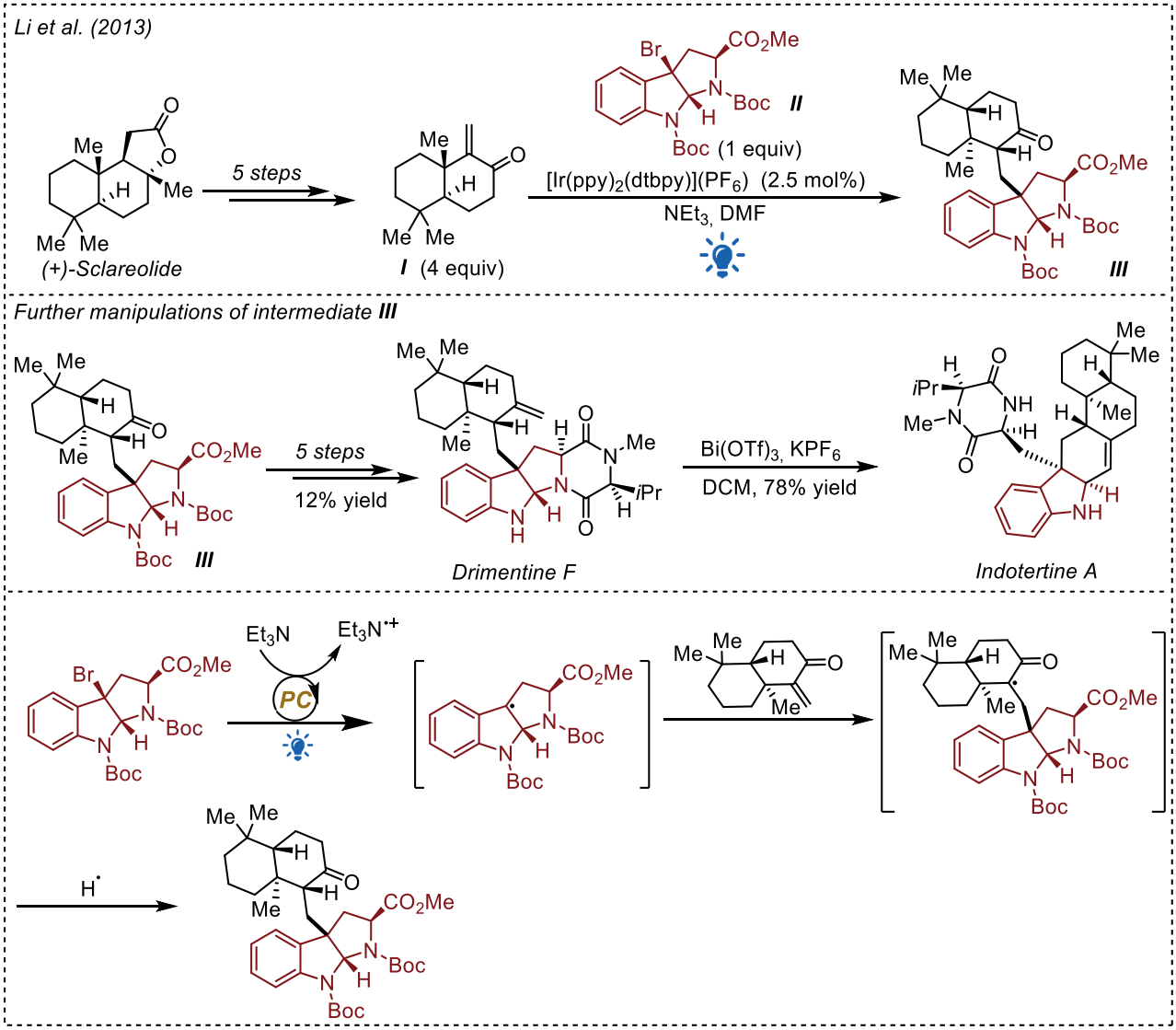

Figure 1.21 Photoredox dehalogenation/Giese coupling step in the total synthesis of Drimentine F and Indotertine A.

The α, β -unsaturated fragment ***I*** was obtained in 5 steps from the natural product (+)-Sclareolide, while the bromopyrrolindoline derivative ***II*** was readily available from *(S)*-di-Boc-tryptophan. After several attempts to connect the two fragments using a radical Giese coupling, i.e. using *n*-Bu_3SnH and standard free radical initiators, the authors found that a slow tertiary radical formation was critical, so they found it convenient to use photoredox debromination conditions. The protocol uses $[Ir(ppy)_2(dtbpy)](PF_6)$ as the photocatalyst in the presence of triethylamine under blue light irradiation. The alkyl radical thus formed undergoes conjugate addition to the α, β -unsaturated fragment ***I*** followed by protonation of the desired intermediate by the triethylamine radical cation, generated after the back-reduction of the photocatalyst. The reaction was carried out with high degree of stereocontrol and a good yield (87%). The key intermediate ***III*** was finally manipulated to obtain the natural product Drimentine F in five steps. A further synthetic step was required to obtain Indotertine A.

The second work was reported by the Overman group on the total synthesis of (−)-Chromodorolide B (*Figure 1.22*).[49] Starting from the acetonide derivative shown in the figure and using the strategy previously described for the decarboxylation of RAEs, in the presence of 4CzIPN as the photocatalyst and Hantzsch ester as the final stoichiometric reductant, the group reported the stereoselective bimolecular radical addition/cyclization/fragmentation (ACF) cascade that led to the formation of the pentacycle moiety of the Chromodorolides with four defined contiguous stereocenters in a single step. The use of 3-chlorobutenolide in the radical coupling step was found to be advantageous, as already observed in previous work by the same group,[50] since 1. the 3-Cl substituent provides a stronger activation of the electrophile butanolide increasing the yields of the radical step, and 2. the chloride can be removed immediately after the coupling in a photoredox-catalyzed step in the presence of a tertiary amine (i.e. Bu_3N).

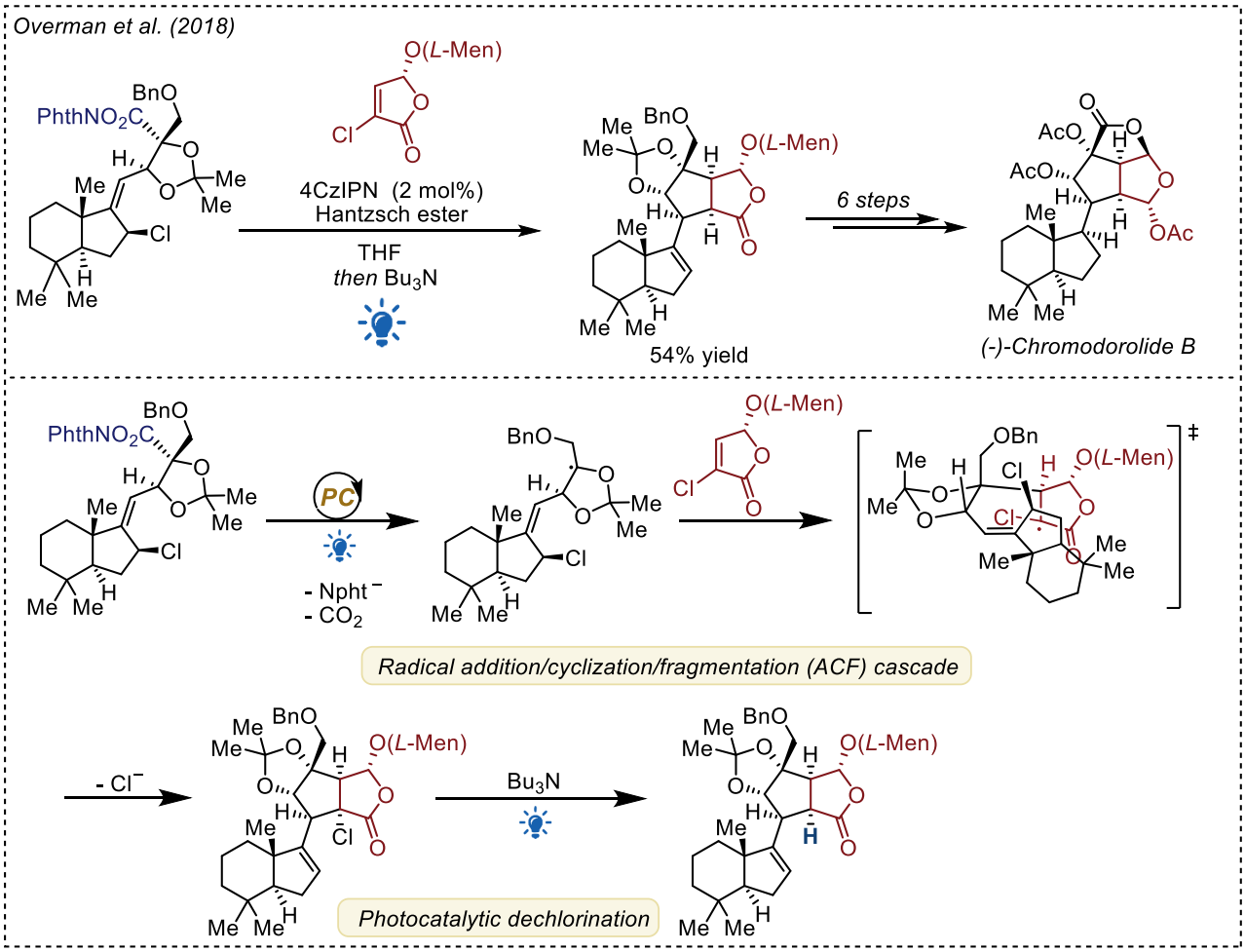

Figure 1.22 Photoredox decarboxylation of RAE-intermediate in the total synthesis of (-)-Chromodorolide B.

1.3.4 Photocatalysis beyond the academia: an industrial application

Several applications of photoredox catalysis have been described in the previous section. In all cases, these conditions are applied on a small scale, usually below the mmol scale. This section aims to show that photoredox conditions can be applied to large scale transformations. Indeed, in recent years there has been a growing interest in the application of photocatalysis on an industrial scale[51,52] although the technological leap between laboratory and industrial scale can be challenging in order to obtain reproducible results.[53] As an example, Sanofi plant in Garessio (Italy) has implemented a photocatalytic process for the production of semi-synthetic artemisinin.[54,55] Artemisinin is a

therapeutically-active compound found in the *Artemisia annua L.*. More specifically, artemisinin is a sesquiterpenoid lactone with a peroxy group and it is an essential drug in the treatment of malaria, but it also exhibits an anti-parasitic as well as an immunosuppressive activity. The demand for artemisinin is growing[55] and methods based on its extraction from natural sources are environmentally, geopolitically and industrially unsustainable. In recent years, Sanofi has implemented a semi-synthetic pathway combining synthetic biology, homogeneous catalysis and photochemistry to achieve efficient, large-scale production of artemisinin at a competitive price (*Figure 1.23*).

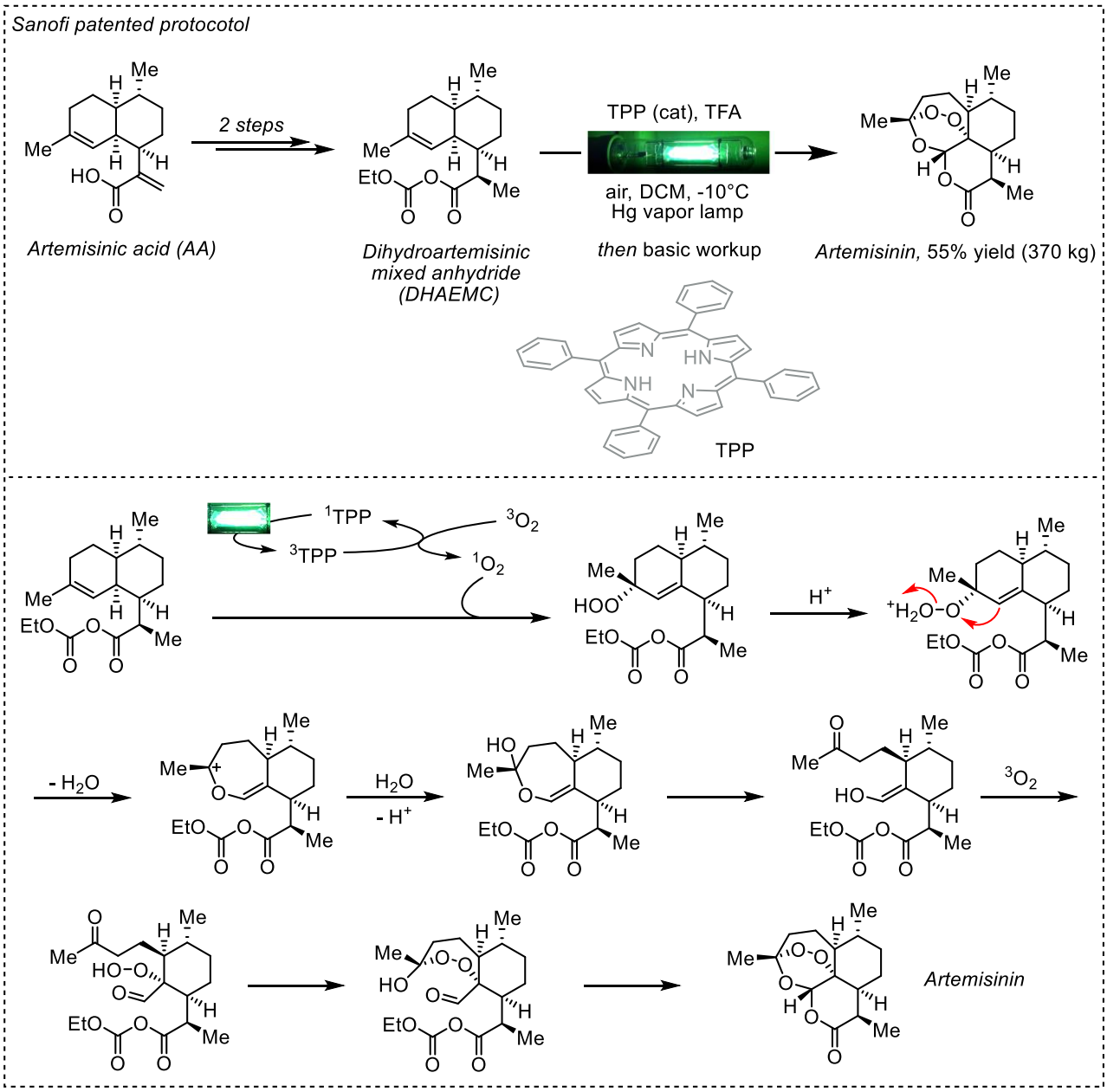

Figure 1.23 Sanofi's implemented photosynthetic protocol for the synthesis of artemisinin and mechanism for the photooxidative cyclization.

Artemisinic acid (AA), an advanced precursor of artemisinin, is produced in yeast and then is converted to the key intermediate dihydroartemisinic mixed anhydride (DHAEMC) in two steps. The final stage of the synthesis of artemisinin involves the conversion of DHAEMC to an hydroperoxide intermediate under photooxidation conditions, followed by a complex rearrangement under acidic conditions. The photooxidation step, named Schenk ene reaction, first involves the stereocontrolled addition of singlet

oxygen to the alkene to form a linear allylic hydroperoxide. The singlet oxygen can be generated by triplet energy transfer in the presence of a catalytic amount of a sensitizer. The authors found it convenient the use of tetraphenylporphyrin (TPP) as the sensitizer under irradiation with a mercury vapor lamp. The oxygen is supplied by bubbling ambient air at about −10 to −15 °C. The hydroperoxide thus formed undergoes an acid-catalyzed Hock cleavage in the presence of trifluoroacetic acid, which leads to artemisinin after a complex rearrangement in the presence of oxygen. The key aspect, from an industrial point of view, is that the hydroperoxide cannot be accumulated on an industrial scale, as an intrinsic hazard is related to its exergonic decomposition. The ability to perform the photooxidation and the acid-promoted fragmentation/cyclization in *one pot* without its accumulation makes the scale-up of the protocol (average batch of 370 kg) feasible and safe.

Finally, the Sanofi protocol for the production of semi-synthetic artemisinin is a remarkable example of the use of photocatalytic conditions for the synthesis of complex, high-value active molecules in the industrial world. Despite the relatively advanced equipment required to carry out photocatalytic protocols, photocatalysis can be applied on small laboratory scale as well as on an industrial reactor scale.

1.4 Metal-based dyes

Metal polypyridyl complexes have played an important role in materials science and photocatalysis.[56] In particular, Ru(II) and Ir(III) complexes, which exhibit visible charge-transfer absorption features, have been extensively studied at both the photophysical and photochemical levels[57] and in a wide range of synthetic transformations.[58–60] Prototypes of Ru- and Ir-based photocatalysts, with their photophysical properties are shown in *Figure 1.24*.

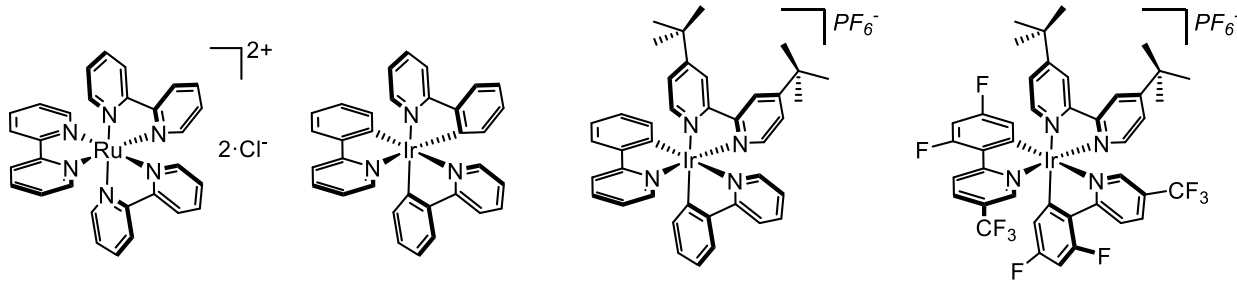

$[Ru(bpy)_3]Cl_2$	fac-$[Ir(ppy)_3]$	$[Ir(ppy)_2(dtbpy)](PF_6)$	$[Ir\{dF(CF_3)ppy\}_2(dtbpy)](PF_6)$
$^*E_{ox}$ = -0.81 V	$^*E_{ox}$ = -1.73 V	$^*E_{ox}$ = -0.96 V	$^*E_{ox}$ = -0.89 V
$^*E_{red}$ = +0.84 V	$^*E_{red}$ = +0.31 V	$^*E_{red}$ = +0.66 V	$^*E_{red}$ = +1.21 V
τ = 1.1 ms	τ = 1.9 μs	τ = 0.56 μs	τ = 2.3 μs
λ_{abs} = 452 nm	λ_{abs} = 375 nm	λ_{abs} = 410 nm	λ_{abs} = 380 nm
λ_{em} = 652 nm	λ_{em} = 518 nm	λ_{em} = 581 nm	λ_{em} = 470 nm
Φ_{em} = 0.095	Φ_{em} = 0.38	Φ_{em} = 0.094	Φ_{em} = 0.68

Figure 1.24 Most common Ru- and Ir-based photocatalysts and some of their photophysical properties. Redox potentials are reported with respect to the SCE.

The photophysics of the metal polypyridyl complexes ML_3^{n+} with octahedral geometry, can be described to a good approximation by considering localized, both metal- and ligand-, molecular orbital configurations. *Figure 1.25* shows the different transitions that can take place upon absorption of light.[61]

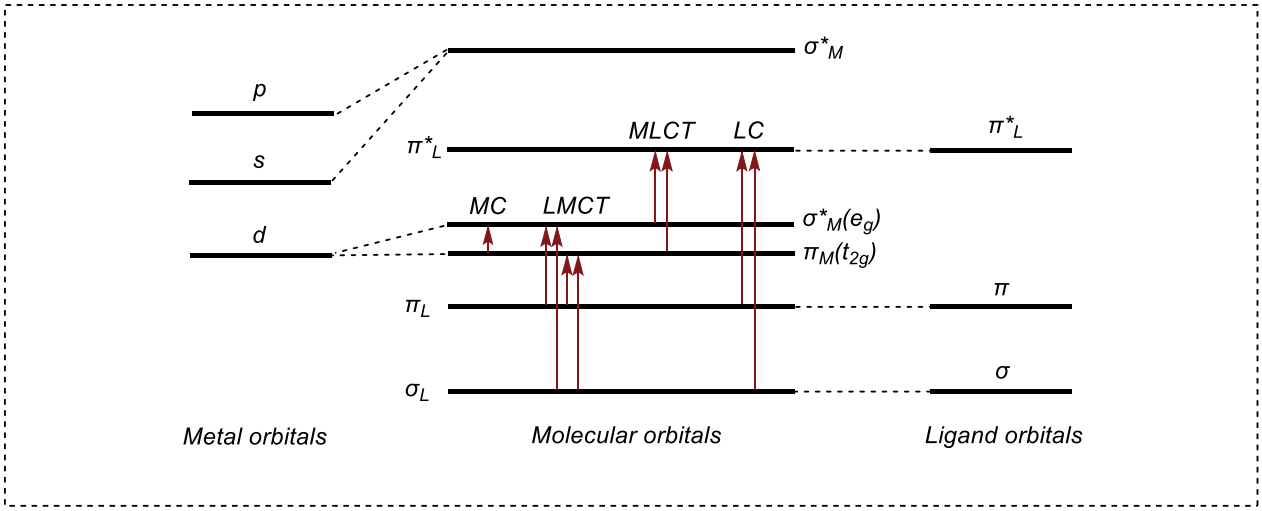

Figure 1.25 Diagram of the electronic transitions in an octahedral complex. Adapted from reference.[61]

Looking at the diagram, four possible types of transitions can take place upon absorption of a photon: ligand-centered (LC), metal-centered (MC), metal-to-ligand charge transfer (MLCT) and ligand-to-metal charge transfer (LMCT).

Transitions involving electrons located in ligand-localized molecular bonding or non-bonding orbitals are called ligand-centered (LC) transitions, and in the case of $[Ru(bpy)_3]^{2+}$ this transition is detected by a strong band in the UV (*Figure 1.26*).[61] The most important transition for photoredox applications is the promotion of an electron in a metal-centered t_{2g} orbital with non-bonding character to a ligand-centered π* orbital ($S_0 \rightarrow S_1$). This transition is defined as metal-to-ligand charge transfer (MLCT). The fast and efficient intersystem crossing (ISC) $S_1 \rightarrow T_1$ leads to a long-lived triplet excited state (^{3}MLCT).[56] The interconversion between the excited singlet state S_1 and the excited triplet state T_1, which is formally forbidden because it involves a spin multiplicity transition, is favoured by spin-orbit coupling with the heavy metal center.

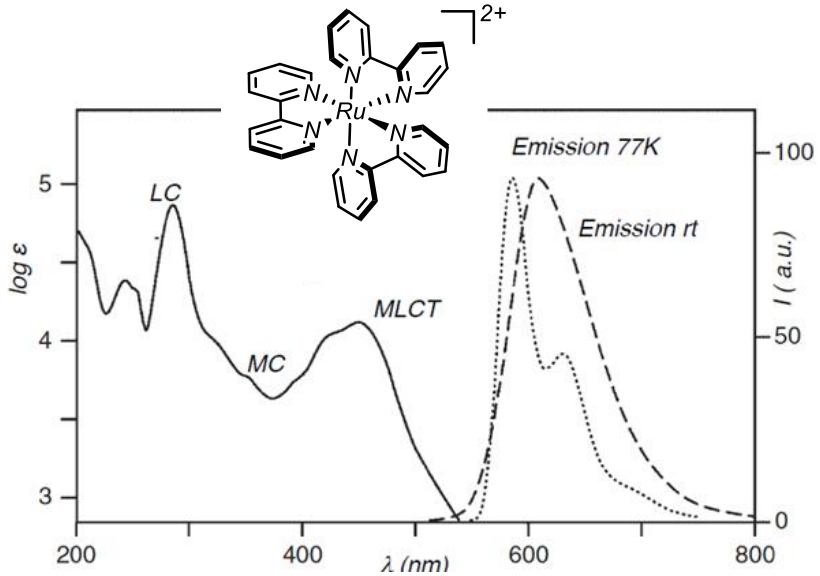

Figure 1.26 Absorption spectrum of $[Ru(bpy)_3]^{2+}$ in MeOH at room temperature (full line), emission spectrum in at room temperature (dashed line) and at 77 K (dotted line). Adapted from reference.[2]

Considering the case of $[Ru(bpy)_3]^{2+}$, the absorption band associated with the MLCT transition is centered at 452 nm in MeOH. Upon absorption of a blue photon, an electron is promoted to a singlet

^{1}MLCT state. This short-lived state is not long enough to interact with other reactants, as it relaxes within 100 fs to a triplet ^{3}MLCT by ISC with a unitary efficiency (Φ_{ISC} ~1) due to the heavy-atom effect. The triplet excited state has a lifetime of 930 ± 40 ns (in deoxygenated ACN)[62] and it is highly dependent on the presence of oxygen, as expected for a triplet excited state. From the ^{3}MLCT it is possible to observe the emission of the complex, centered at 620 nm. The lifetime is long enough to allow the interaction with other reactants and to induce an energy-transfer or electron transfer event. Taking into account the E_{00} = 2.12 eV it possible to calculate the redox potentials at the excited state (*vs* SCE): $^*E_{ox}(Ru^{III}/^*Ru^{II})$ = −0.86 V and $^*E_{red}(^*Ru^{II}/Ru^{I})$ = +0.84 V (*Figure 1.27*).

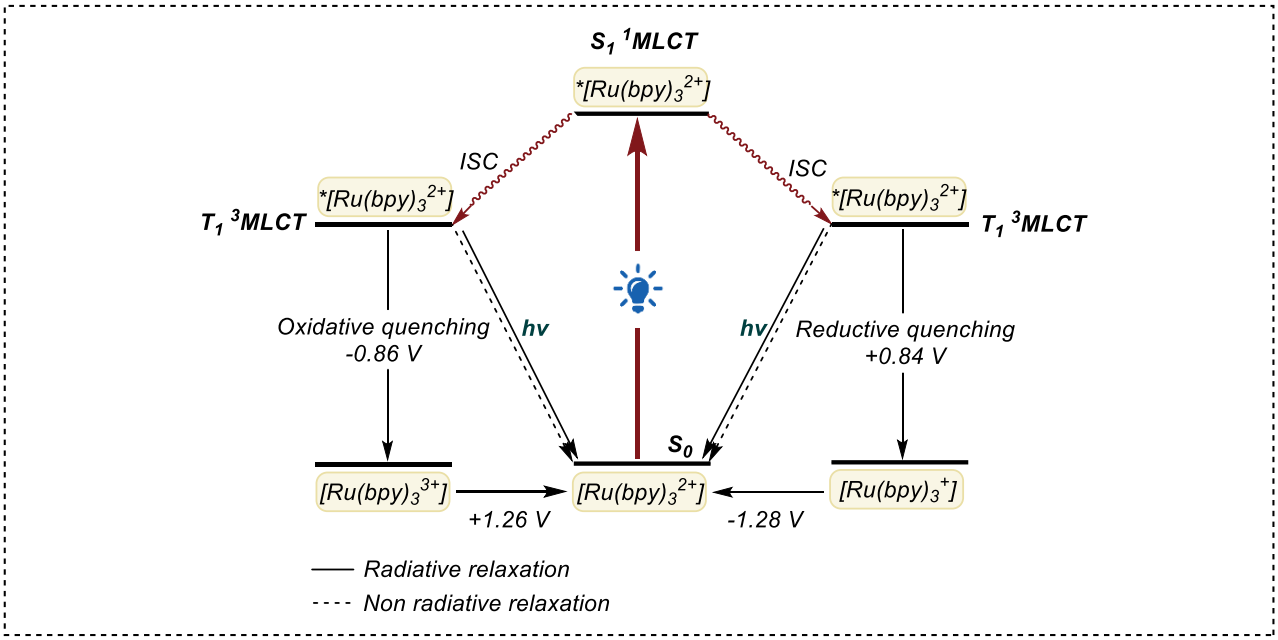

Figure 1.27 Redox potentials of $[Ru(bpy)_3]^{2+}$ at the ground state and in its excited state.

Iridium-based photocatalysts have undergone a rapid development in recent years.[59] In particular, the use of cyclometalated ligands, e.g. phenylpyridine (ppy), and auxiliary ligands, e.g. bipyridine (bpy), gives to Ir-complexes some peculiar and suitable properties for applications in photocatalysis.

Let's consider an iridium heteroleptic complex with the general structure $Ir(C^{\wedge}N)_2(N^{\wedge}N)^+$, of which $[Ir(ppy)_2(dtbpy)]^+$ is the simplest example. Like the Ru-based complexes previously described, this class of Ir(III) complexes exhibits phosphorescence emission that can derive from an excited state localized on both the neutral ancillary N^N ligand and on the cyclometalated C^N ligand.[63] In particular, the emitting excited states of these complexes are a combination of triplet metal-to-ligand charge transfer states (^{3}MLCT), from the metal to the N^N ligands ($t_{2g} \longrightarrow \pi^*_{N\wedge N}$) and triplet ligand-to-ligand charge transfer states (^{3}LLCT) between the phenyl rings of the C^N ligands and the N^N ligands.[63] The interconversion from a singlet MLCT state (^{1}MLCT) to a triplet state (^{3}MLCT) is favoured by the heavy atom effect, as in case of ruthenium complexes (*Figure 1.28*).

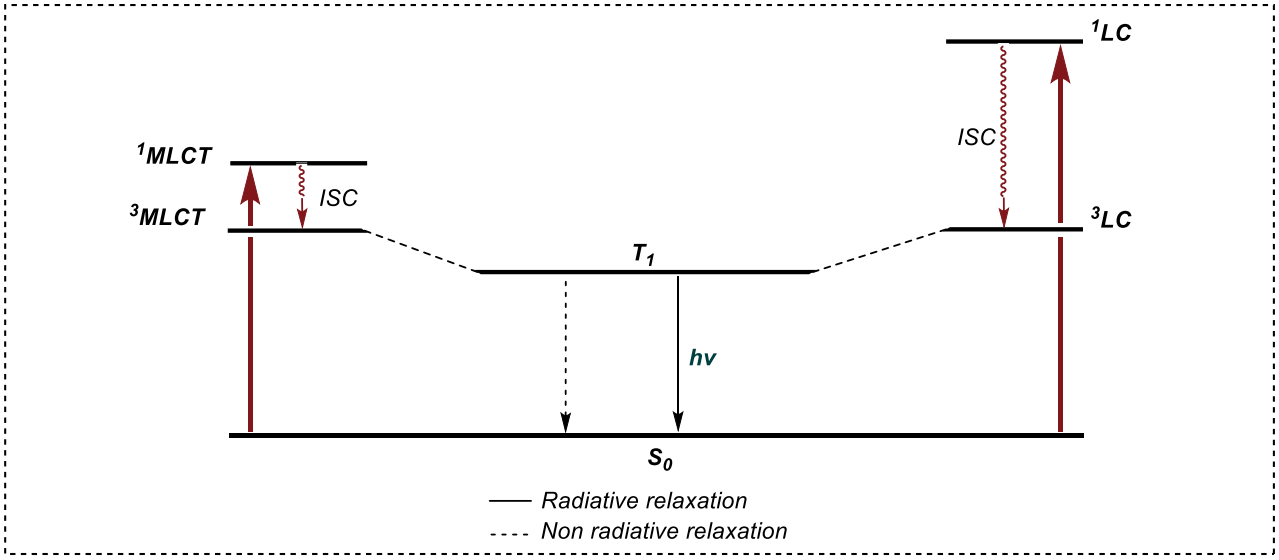

Figure 1.28 Nature of the emissive excited state of Ir(C^N)$_2$(N^N)$^+$complexes as a combination of ^{3}MLCT and ^{3}LLCT states. Adapted from reference.[64]

Regarding the localization of the frontier molecular orbitals (FMOs), in [Ir(ppy)$_2$(bpy)]$^+$ several experimental and computational studies have described the HOMO to be localized on the metal center and the π system of the phenyl group of the ppy, and the LUMO to be localized on the ancillary N^N ligand as shown in *Figure 1.29*.[64]

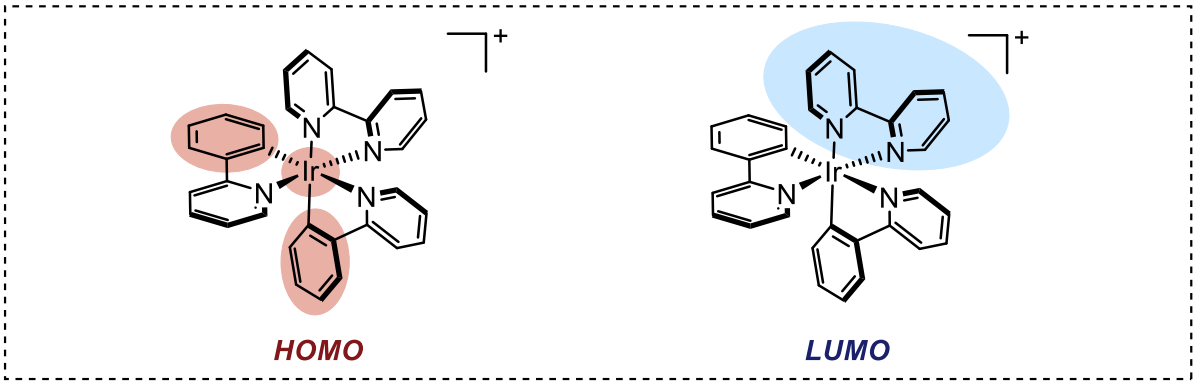

Figure 1.29 Localization of the frontier molecular orbitals in [Ir(ppy)$_2$(bpy)]$^+$.

Considering the localization of the HOMO and the LUMO, it is possible to alter the energy level of the boundary orbitals, thus the HOMO-LUMO gap energy, in a predictable way by functional group modifications on both C^N and N^N ligands.[65] The possibility of multistep synthesis allows each modification to be introduced in a different step.[64,66]

The first consideration is the introduction of electron-withdrawing groups on the anionic cyclometalated ligand, i.e. introducing fluoride- and trifluoromethyl groups as in the case of *d*F(CF$_3$)ppy. Firstly, their introduction tends to stabilize the HOMO by removing electronic density from the metal, while the LUMO is not affected. The resulting complex [Ir{*d*F(CF$_3$)ppy}$_2$(dtbpy)]$^+$ has a higher energy MLCT state and a stronger oxidation potential (*vs* SCE) compared to [Ir(ppy)$_2$(dtbpy)]$^+$: $E_{ox}(Ir^{IV}/Ir^{III})$ = +1.69 V *vs* $E_{ox}(Ir^{IV}/Ir^{III})$ = +1.21 V, respectively.[60]

Finally, by adjusting the substituents and their steric requirements on both the cyclometalated ligand and the ancillary ligand it is possible to fine tune the photophysical and electrochemical properties of the resulting complexes. A library of Ir-based dyes is available in the literature, and now commercially.

1.5 Organic dyes

Ruthenium- and iridium-based photocatalysts have been extensively studied as photocatalysts for decades demonstrating high versatility and reactivity in many transformations and making them a fundamental tool in the field of photocatalysis. The possibility of fine-tuning the photophysical properties of these complexes by modifying the chemical environment around the metal center with different ligands is an advantage of this class of photocatalysts.

Despite these advantages, the low terrestrial abundance of these precious metals, the resulting high cost of the raw metals and the associated environmental impacts for their exploitation make their use increasingly less sustainable.[67,68]

There are two main options to overcome this problem: 1) the use of more abundant metal-based photocatalysts, or 2) the use of organic dyes.

Earth abundant metal-based photocatalysts are well known from the recent literature: Fe,[69] Cu,[70] Cr,[71] Al[72] and other metal-based[65] complexes have been reported as valid alternatives in various photoredox transformations.[56]

The use of fully organic photocatalysts is an interesting alternative since no metals are required at all and with few synthetic steps it is possible to get access to an enormous variety of structures and different photophysical properties, as reviewed by the Nicewicz group in a recent and comprehensive work.[5] Due to the enormous number of different molecules used as organic photosensitizers, a comprehensive and exhaustive overview is impossible.

For the purpose of this introduction, in the following sections two classes of photocatalysts will be described. The first section will cover the photochemical properties of cationic helicene photocatalysts, while in the second section cyanoarene-based dyes will be discussed.

1.5.1 Cationic helicene photocatalysts

Cationic helicene ions are a special class of C-centered cation photocatalysts derived from *ortho*-fused aromatic rings.[73] The term *helicenes* refers to the 3-dimensional arrangement of the fused aromatic rings that resembles a helix. The geometry results in two enantiomeric helixes (*Figure 1.30*) which can be separated by a highly reliable process exploiting a Pummerer-like chemistry.[74,75]

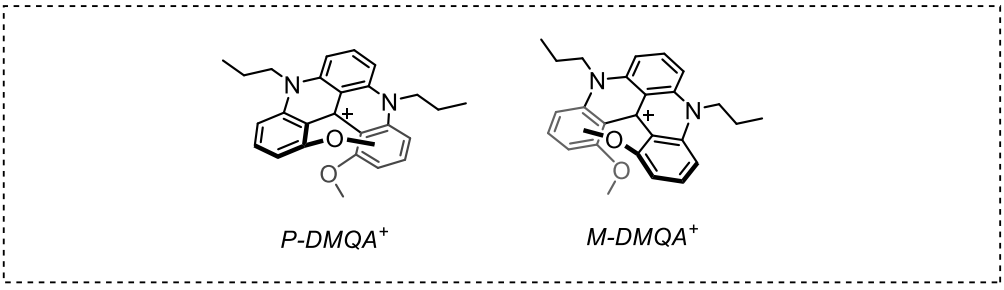

Figure 1.30 3-dimensional representation of the P, M enantiomers of the helicene DMQA⁺.

Several classes of helicenes are known from the literature (*Figure 1.31*)[73] but aza-derivatives in particular have important applications[73] especially as organic dyes, sensors and liquid crystals. The key aspect is the extensive conjugated π-system that determines the absorption and the emission in the visible region. Of particularly interest, enantiopure helix compounds (*P* or *M* enantiomers) possess

chirooptical properties, i.e. electronic circular dichroism (ECD) and circularly polarized luminescence (CPL), that can be exploited in chirooptical sensors.

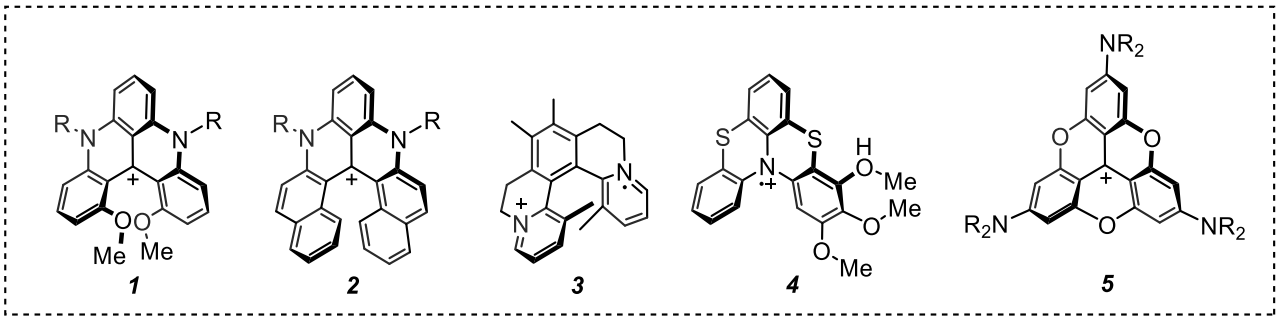

Figure 1.31 Different classes of helicenes known in the literature.

Of particular relevance for this introduction is the azahelicene structure **1**, known as dimethoxyquinacridinium ions (DMQA).

Chronologically, the Laursen group made a major contribution to the development of this class of dyes and their photophysical characterization and functionalization. Harrit and Lacour in 1998 reported for the first time the synthesis of the exceptionally stable helical 2,6,10-tris(dialkylamino)trioxatriangulenium carbenium ions **5**.[76] They evaluated the chemical stability of the carbenium ions using the parameter pK_{R+},[77] a value that quantifies the affinity of these carbenium ions for hydroxide ions in water. The higher and more positive the pK_{R+} value, the greater the chemical stability of the carbenium ion. The pK_{R+} parameter is defined as:

$$pK_{R+} = H_x + log\frac{[R^+]}{[ROH]} \tag{18}$$

where H_x is an acidity function characteristic of the carbenium/carbinol equilibrium and the solvent. In water, for example H_x corresponds to the pH scale.
The stability of the carbenium ions can be correlated with the delocalization of the positive charge along the aromatic nucleus. Moreover, the introduction of three dimethylamino substituents with strong electron-donating ability can increase the stability by simple resonance delocalization.
In the following years, Krebs and Lacour reported the synthesis of di- and triazangulenium ions **1** by the multiple aromatic substitution of the 4-methoxy groups on the aromatic core of the triaryl carbenium ion by a suitable amine forming multiple nitrogen bridges (*Figure 1.32*).[78] By controlling the reaction conditions it is possible to stop the reaction to the bis-substitution.

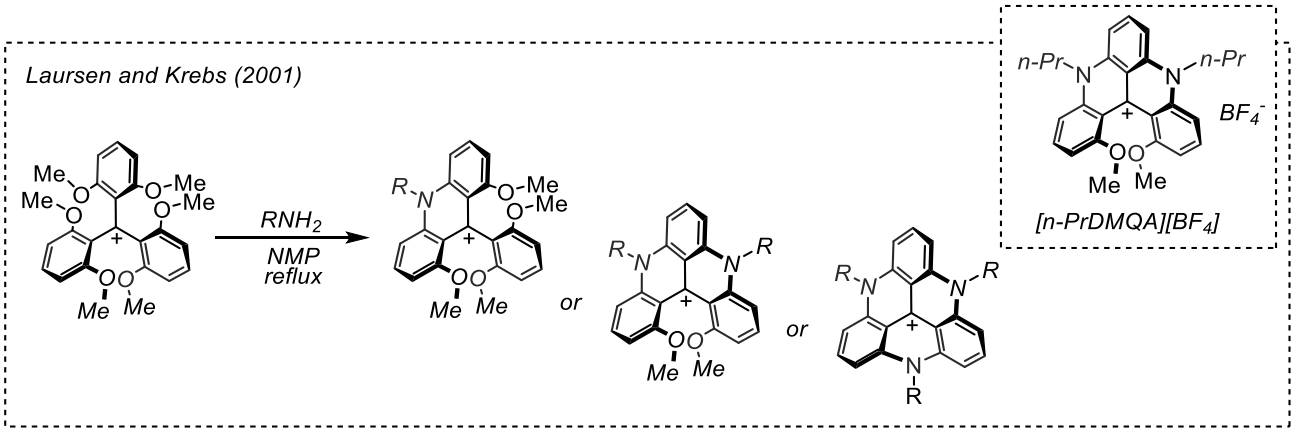

Figure 1.32 Synthesis of di- and triazangulenium ions as reported by Laursen and Krebs.

In particular, using *n*-propylamine as the RNH_2 source, they prepared the so-called [*n*-PrDMQA$^+$][BF_4^-]. The molecular backbone of [*n*-PrDMQA$^+$][BF_4^-] contains four *ortho*-condensed aromatic rings. The helicene structure is due to the steric repulsions between the two remaining methoxy substituents, inducing a twisted helical conformation and, therefore, the formation of two enantiomers *P* and *M*. This compound has attracted much interest for its high chemical (pK_{R+} = 19) and configurational stability ($\Delta G^{\ddagger}_{racemization}$ = 42 kcal mol^{-1}). In addition, its photophysical properties, reported in *Figure 1.33* make it a good candidate as a photocatalyst.[79]

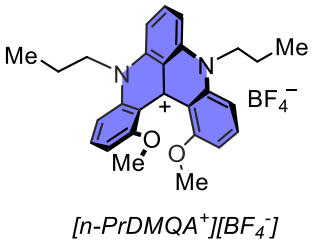

[*n*-PrDMQA$^+$][BF_4^-]

***E*$_{ox}$** = -0.52 V
***E*$_{red}$** = +1.14 V
***E*$_{ox}$** = +1.44 V
***E*$_{red}$** = -0.82 V
τ = 12.3 ns
λ$_{abs}$ = 614 nm
λ$_{em}$ = 648 nm
Φ$_{em}$ = 0.26

Figure 1.33 Photophysical and redox properties of [n-PrDMQA$^+$][BF_4^-].

After a pioneering application by Lacour in the photooxidation of benzylamines to benzylimines,[80] the Gianetti group was the first to fully exploit the photoredox properties of [*n*-PrDMQA$^+$][BF_4^-] in red-light-mediated photoredox transformations (*Figure 1.34*)[81] through both oxidative (*Figure 1.34 A*) and reductive quenching (*Figure 1.34 B*) pathways, taking advantage of the multiple accessible redox states of the photocatalyst.[82]

In the former case, no external redox-active reagents are required, since the aryldiazonium salt acts as the quencher ($E_{red}(PhN_2^+/Ph^{\bullet})$ = −0.10 V *vs* SCE) for the excited photocatalyst ($^*E_{ox}(DMQA^{\bullet++}/^*DMQA^+)$ = −0.61 V *vs* SCE in MeCN) through oxidative quenching, while the palladium(III) intermediate acts as the reductant, restoring the photocatalytic cycle. On the contrary, in the latter case, a stoichiometric amount of an external reductant has to be used for the reductive quenching of the excited photocatalyst *[DMQA$^+$]. DIPEA can be used since its oxidation potential (E_{ox}(DIPEA$^{\bullet+}$/DIPEA) = +0.65 V *vs* SCE) makes the reduction of the excited photocatalyst *[DMQA$^+$] ($^*E_{red}$(*DMQA$^+$/DMQA$^{\bullet}$) = +1.15 V *vs* SCE) thermodynamically feasible. Finally, oxygen ($E_{red}(O_2/O_2^{\bullet-})$ = −0.57 V *vs* SCE) ensures the turnover of the photocatalytic cycle by the oxidation of the reduced photocatalyst [DMQA$^{\bullet}$] (E_{red}(DMQA$^+$/DMQA$^{\bullet}$) = −0.78 V *vs* SCE) with the formation of the superoxide radical anion $O_2^{\bullet-}$, that is implicated in the aerobic oxidative hydroxylation of the arylboronic acid.

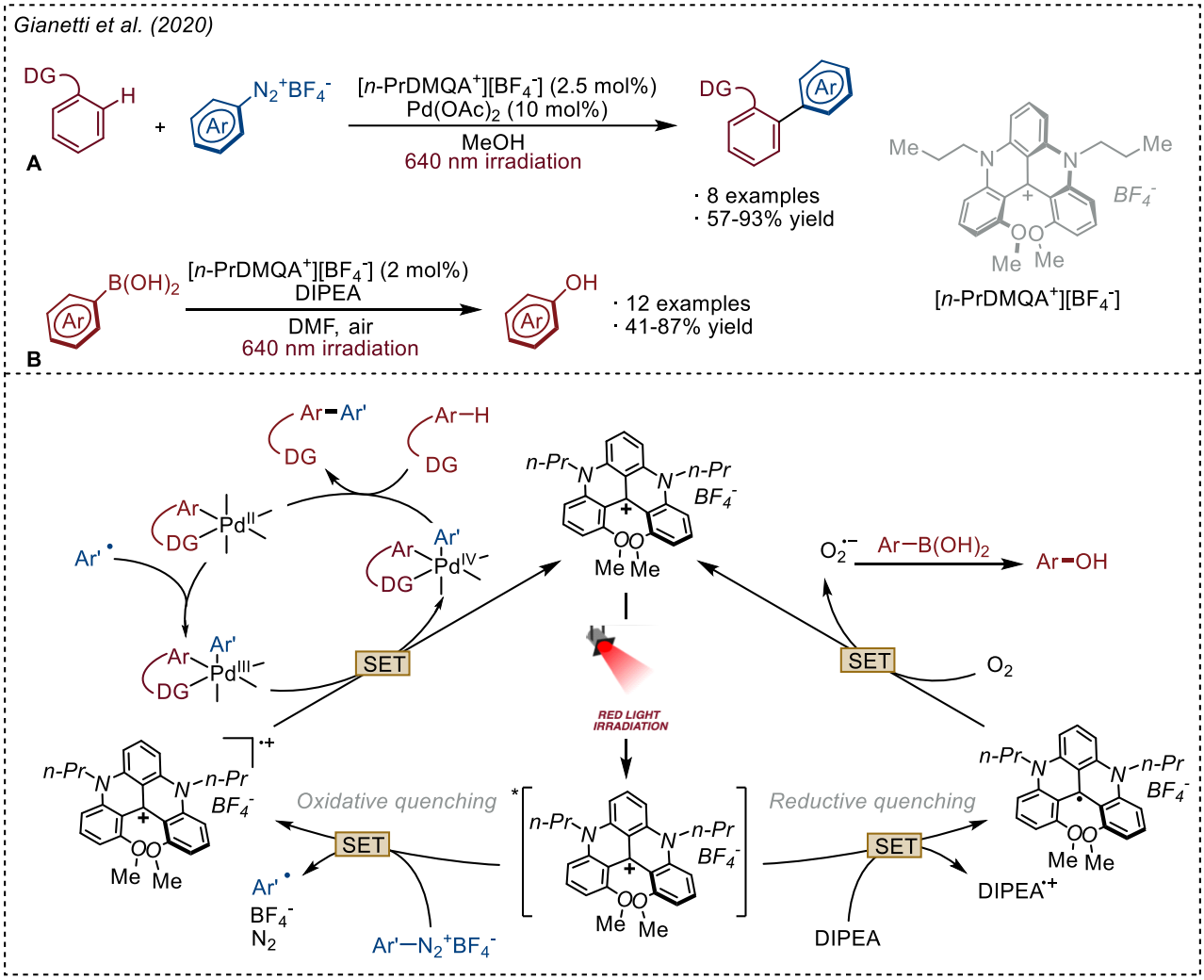

Figure 1.34 Selected applications of [n-PrDMQA$^+$][BF$_4^-$] reported by the Gianetti group.

More recently, our group has exploited the photophysical properties of the same photocatalyst in the dual photoredox- and titanium-[83] or vanadium-[84] mediated pinacol coupling of aromatic aldehydes. The results are described in more detail in Chapter 4.

Finally, this class of helicene photocatalysts is amenable to an extensive functionalization to fine tune their electrochemical, photophysical and chiroptical properties (*Figure 1.35*). This can be made either by cyclization steps generating new and valuable classes of photocatalysts absorbing in the green region,[85] or by the introduction of different auxochrome groups on the aromatic ring nucleus, as reported by the Lacour group.[86] In fact, they reported a simple and straightforward functionalization of racemic and enantioenriched [*n*-PrDMQA$^+$][BF$_4^-$] using peripheral substituents to modulate the electronic absorption and the circular dichroism from the orange to near-infrared spectral range (575-750 nm), increasing the fluorescence quantum efficiency up to 0.55 (631 nm) and also recording circularly polarized luminescence in the red region ($|g_{lum}|$ = ~10^{-3}). These functionalizations are not only important from a research point of view, but also demonstrate the versatility of the helicene structure as a chromophore motif.

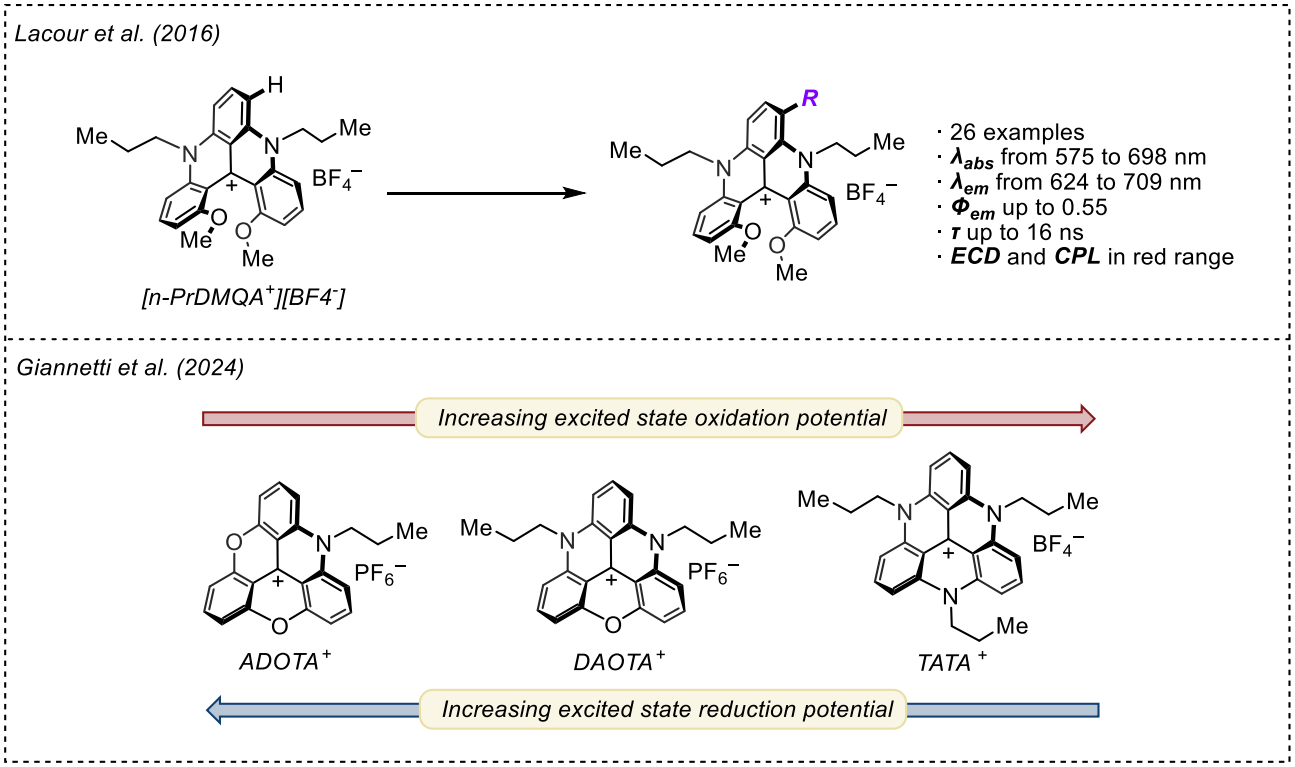

Figure 1.35 Functionalization of [n-PrDMQA$^+$][BF$_4^-$] reported by the Lacour group (above) and by the Gianetti group (below).

1.5.2 Cyanoarene–based photocatalysts

Cyanoarenes are a class of fully organic photocatalysts that have shown very interesting reactivity in photoredox catalysis over the last thirty years. The first examples of this large family of molecules were reported by the Pandey group using the unsubstituted 1,4-dicyanobenzene (p-DCB), 1,4-dicyanonapthalene (DCN), and 9,10-anthracenedicarbonitrile (DCA) (*Figure 1.36*).[87]

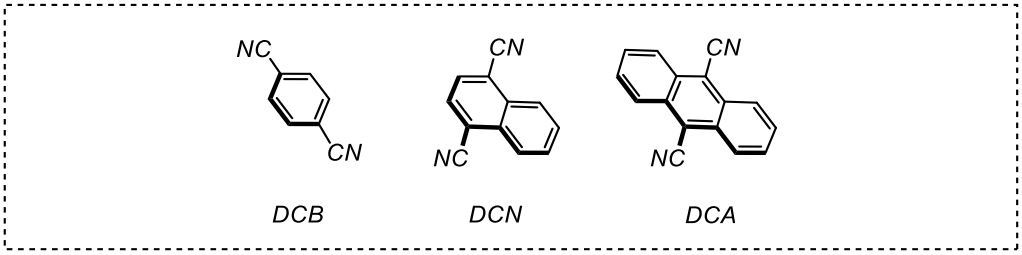

Figure 1.36 First examples of cyanoarene-based photocatalysts reported by the Pandey group.

These unsubstituted cyanoarenes absorb light in the UV region and possess a high energy singlet excited state that allows the oxidation of substrates with potentials above +2.0 V *vs* SCE. Consequently, the corresponding radical anions formed during the SET event are moderate reductants, that can be reduced to ensure the turnover of the catalytic cycle. From a practical point of view, cyanoarenes with an increased π-extension (i.e. DCN and DCA) are most useful, as they absorb light in the near UV and have longer singlet lifetimes than simple cyanobenzenes. However, the use of UV light is associated with several problems such as health hazards and possible parasitic reactions due to the absorption of photons by unwanted reactants.

With this in mind, the Adachi group in 2012 reported the 1,2,3,5-tetrakis(carbazol-9-yl)-4,6-dicyanobenzene (4CzIPN) as an organic light-emitting dye for the development of optical materials (e.g. OLEDs).[88] The turning point of this work lies on the development by design of a series of highly efficient electroluminescent organic molecules based on simple aromatic compounds. One of the key aspects of the carbazolyl dicyanobenzene structure is the thermally activated delayed fluorescence (TADF) phenomenon. As shown in *Figure 1.37*,[89] the TADF phenomenon is based on highly coupled S_1 and T_1 excited state levels, allowing the intersystem crossing (ISC) from S_1 to T_1 ($S_1 \rightarrow T_1$), and a small energy gap ΔE_{ST} (generally less than 0.2 eV).[88] Because the small energy gap, it is possible to populate the higher energy S_1 excited state from the lower energy T_1 state ($T_1 \rightarrow S_1$) by *reverse inter system crossing* (rISC) through a thermal input. Experimentally, what is observed after the visible light excitation is a first *prompt* fluorescence ($S_1 \rightarrow S_0$) in the range of nanoseconds, and a second *delayed* fluorescence occurring after the reverse intersystem crossing, allowing the molecule to emit delayed fluorescence in the range of microseconds. The mechanism of the TADF allows for enhanced quantum yields compared to other common organic dyes, comparable to those observed for iridium-, platinum-, gold- and other transition metal-based complexes.[89] Finally, TADF emitters exhibit photoredox activity from the singlet excited state and, due to the small energy ΔE_{ST}, the loss of energy associated with the active excited state is minimized. For example, for 4CzIPN (ΔE_{ST} = 0.08 eV)[90] the ground state redox potentials (*vs* SCE) are $E_{ox}(4CzIPN^{\bullet+}/4CzIPN)$ = +1.49 V, $E_{red}(4CzIPN/4CzIPN^{\bullet-})$ = −1.24 V, and considering E_{00} = 2.67 eV, according to the Rehm-Weller theory[1] $^*E_{ox}(4CzIPN^{\bullet+}/^*4CzIPN)$ = −1.18 V and $^*E_{red}(^*4CzIPN/4CzIPN^{\bullet-})$ = +1.43 V. The balance between the oxidation and reduction potentials, both in the ground- and in the excited state, makes 4CzIPN one of the most used photocatalysts.[91]

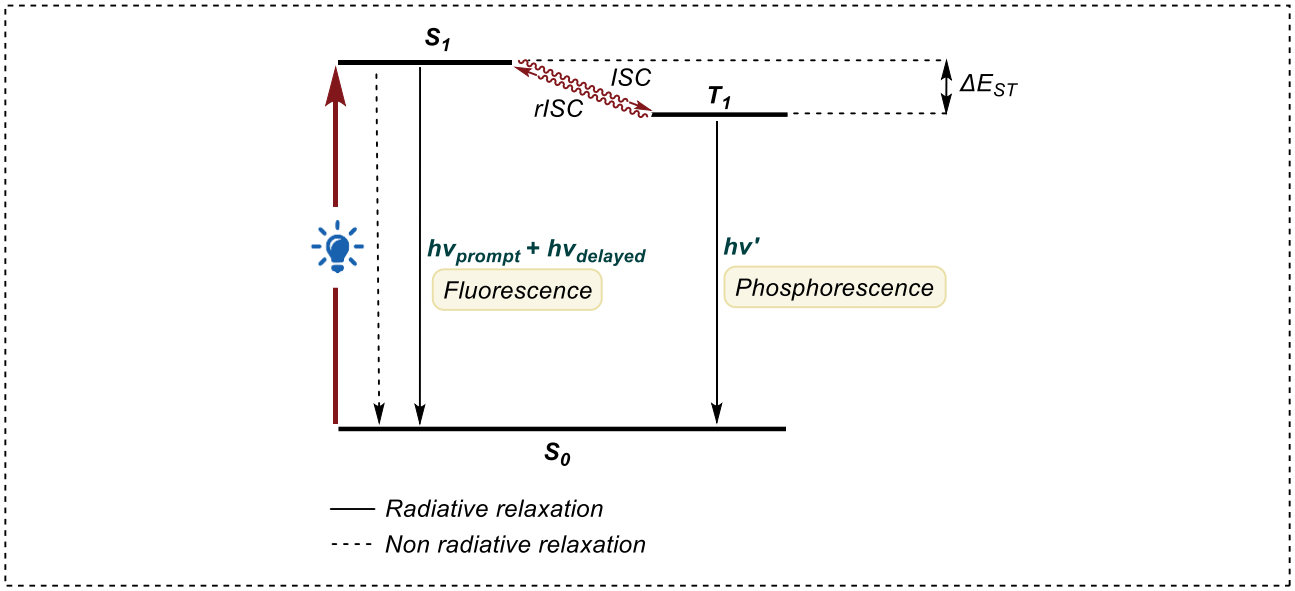

Figure 1.37 Graphical explanation of the TADF phenomenon.

In the following years, the group of Zhang[92] and Zeitler[90] reported the design of a large library of cyanoarene-based TADF-emitters with a fine-tuning of the photophysical and photoredox properties. More specifically, cyanoarene-based TADF emitters are conventionally described as donor–acceptor type (D–A type) molecules, with the *N*-aromatic rings as the donor moiety, and the central cyanobenzene ring as the acceptor moiety. The key aspect in inducing TADF-properties is the introduction of a twisted angle between the donor and the acceptor moieties, which avoids a significant overlap between the highest occupied molecular orbital (HOMO) and the lowest unoccupied molecular orbital (LUMO), generating a non-overlapping frontier molecular orbital (FMO) and a charge-transfer excited state.[93]

This class of photocatalysts can be manipulated starting from inexpensive building blocks (cyanobenzenes and aromatic amines) by modifying the structure and the presence of substituents to tune the electrochemical and photophysical properties of the products, both in the ground state and in the excited state, without affecting the chemical stability.

Based on a DFT approach to predict the spatial localization of FMO orbitals, the LUMO is predicted to be centered on the electron-withdrawing cyanoarene moiety, while the HOMO is predicted to be centered on the electron-donating portions of the molecule (the aromatic pendants). The spatial separation of the FMO allows to consider nearly independently the reduction and oxidation energies by changing the donor or the acceptor part of the molecule. Since the ground state reduction potential $E_{red}(PC/PC^{\bullet-})$ is therefore mainly determined by the HOMO of the donor and the ground state oxidation potential $E_{ox}(PC^{\bullet+}/PC)$ is determined by the LUMO of the acceptor, a structural modification of the photocatalyst core could lead to a decrease in the LUMO energy, thus increasing the E_{ox}. At the same time, the introduction of different electron donating substituents could lead to an increase in the HOMO with a consequent increase of the ground state reduction potential E_{red}.

Thus, the authors distinguished between a *donor–based* and a *core–based* effect.

To summarize the *donor-based* effects, increasing or decreasing the donor strength (or the number) resulted in an alteration of the electrondonating ability of the molecule leading, respectively to an increase or a decrease in the reduction potential (*Figure 1.38*).

To summarize the *core-based* effects, increasing or decreasing of the acceptor strength (or the number), resulted in a change in the electrondonating ability of the molecule leading, respectively to an increase or a decrease in the oxidation potential (*Figure 1.38*). In addition, the presence of halogen atoms with their strong σ-acceptor and π–donor nature is particularly relevant, and they will be discussed.

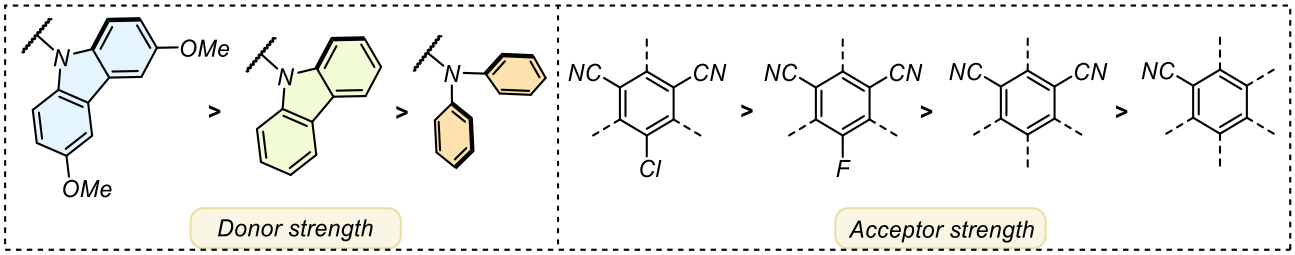

Figure 1.38 Different donor (left) and acceptor (right) building blocks and their different strength for the design and the synthesis of TADF-emitters, as reported by the Zeitler group.

The resulting redox potentials are determined by a combination of both donor- and core-based effects. *Figure 1.39* shows all the examples reported by the Zeitler group and their photoredox potentials, both in the ground- and in the excited states.

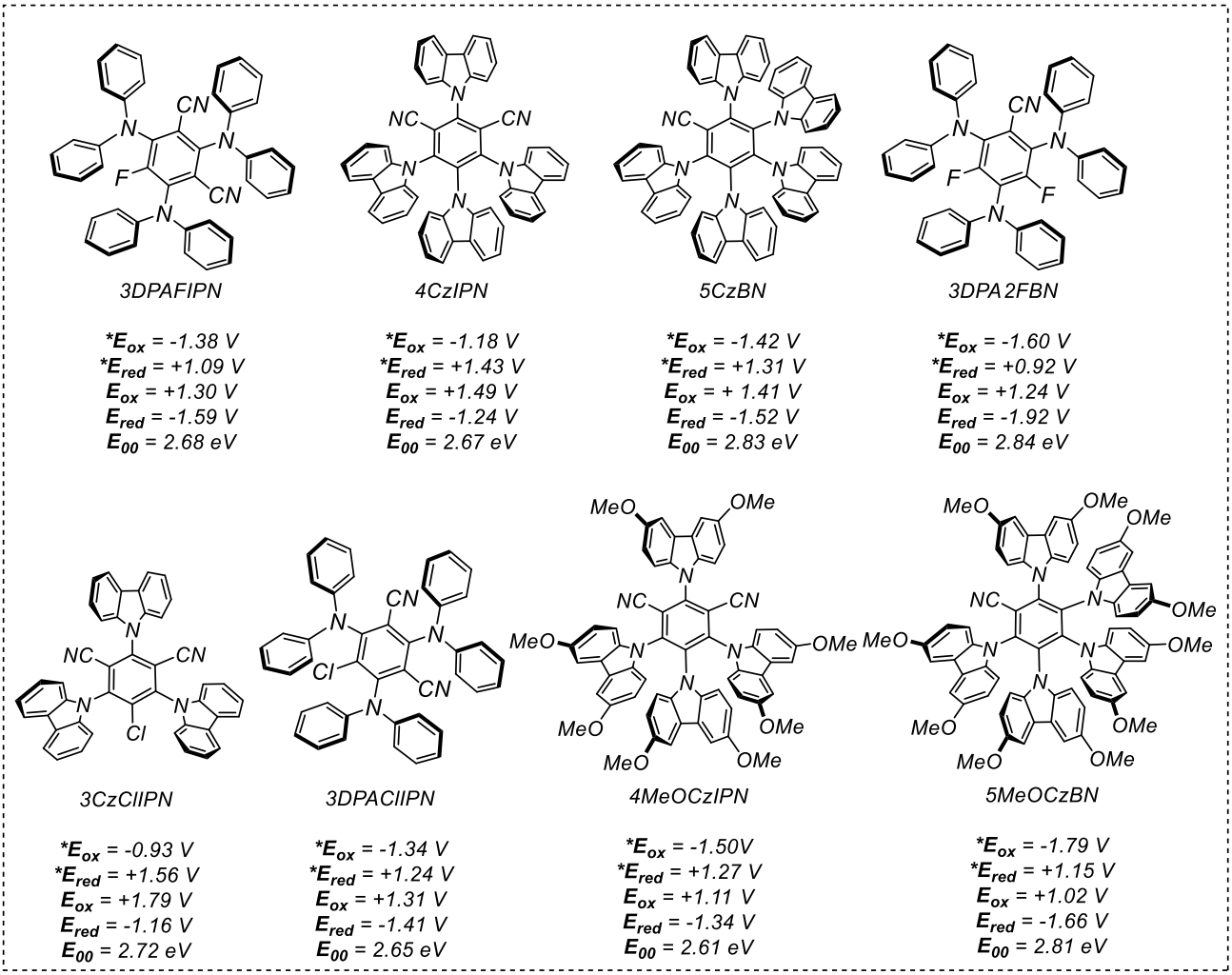

Figure 1.39 New cyanoarene-based TADF-emitters reported by the Zeitler group and their redox potentials.

Let's consider a practical example of a structure-property relationship starting from 3CzClIPN. According to *Figure 1.38*, the ClIPN nucleus has the highest acceptor strength, which together with the carbazolyl moiety (Cz), which has the lowest donor strength, explains the highest ground state oxidation potential (E_{ox}(3CzClIPN$^{\bullet+}$/3CzClIPN) = +1.79 V *vs* SCE).

On the contrary, by replacing the three carbazolyl groups with the stronger electron-donating diphenylamine, the resulting 3DPAClIPN shows an enhanced ground state reduction potential (E_{red}(3DPAClIPN/3CzClIPN$^{\bullet-}$) = –1.41 V *vs* SCE), while the oxidation potential is reduced (E_{ox}(3DPAClIPN$^{\bullet+}$/3DPAClIPN) = +1.31 V *vs* SCE). The substitution of the chlorine atom by a fluorine atom has a particular effect. While the oxidation potential of the resulting 3DPAFIPN is unaffected by the halogen exchange, the reduction potential is dramatically affected and shifted to more negative values (E_{red}(3DPAFIPN/3DPAFIPN$^{\bullet-}$) = –1.59 V *vs* SCE). This could be explained by the strong inductive σ-effect with no counteracting π-effect of the fluoride atom, which is instead present in the chlorine atom. Finally, the substitution of another cyano-group with a fluorine, leading to 3DPA2FIBN, give rise to the same behavior: while the oxidation potential is not affected, the reduction potential is strongly enhanced (E_{red}(3DPA2FBN/3DPA2FBN$^{\bullet-}$) = –1.92 V *vs* SCE) making it the strongest reducing agent in its radical anion form.

Finally, organic dyes with TADF-emitter properties offer suitable electrochemical and photophysical properties that have been widely exploited in the recent decades. The possibility of virtually unlimited,

deliberate and possibly predictable functionalizations[94] makes this class of fully organic dyes very attractive. All these features makes them good alternatives to metal-based photocatalysts.

1.6 Dual photoredox catalysis

The use of light, and in particular visible light as an energy source to promote the formation of organic radicals under mild and reproducible conditions avoiding the use of hazardous radical initiators, such as Bu_3SnH, or harsh conditions, such as high temperature or high energy UV irradiation, allows organic chemists to promote a wide library of manipulations with a high degree of selectivity and tolerance toward different functional groups.[95] However, the inherent disadvantage of generating radicals with an open shell configuration is their high reactivity, which could lead to poor control in the presence of several functional groups or to uncontrolled photodecomposition processes. Moreover, several organic reactions require a metal to transfer the reactivity of a radical to another functional groups,[96,97] e.g. in Cu-mediated transfer of radical carbenes,[98] Fe(II)-mediated Fenton reactions,[99] or Pd-mediated cross coupling reactions.[100] Finally, enantioselective reactions generally rely on the action of a complementary chiral catalyst.[101]

At this stage, the concept of *synergistic catalysis* becomes central. Synergistic catalysis is a specific type of multi-catalytic platform, i.e. a system in which different reaction partners are activated toward the formation of a new bond. In particular, synergistic catalysis is a catalytic strategy which involves the simultaneously activation of the nucleophile and electrophile partners of a reaction by two separate catalysts (*Figure 1.40*). The activated species can rapidly couple enabling reactions that could be impossible of less efficient under other catalytic conditions, e.g. under mono-catalytic systems, in which a unique catalyst activates a single substrate toward the reaction with a second unactivated substrate.[102]

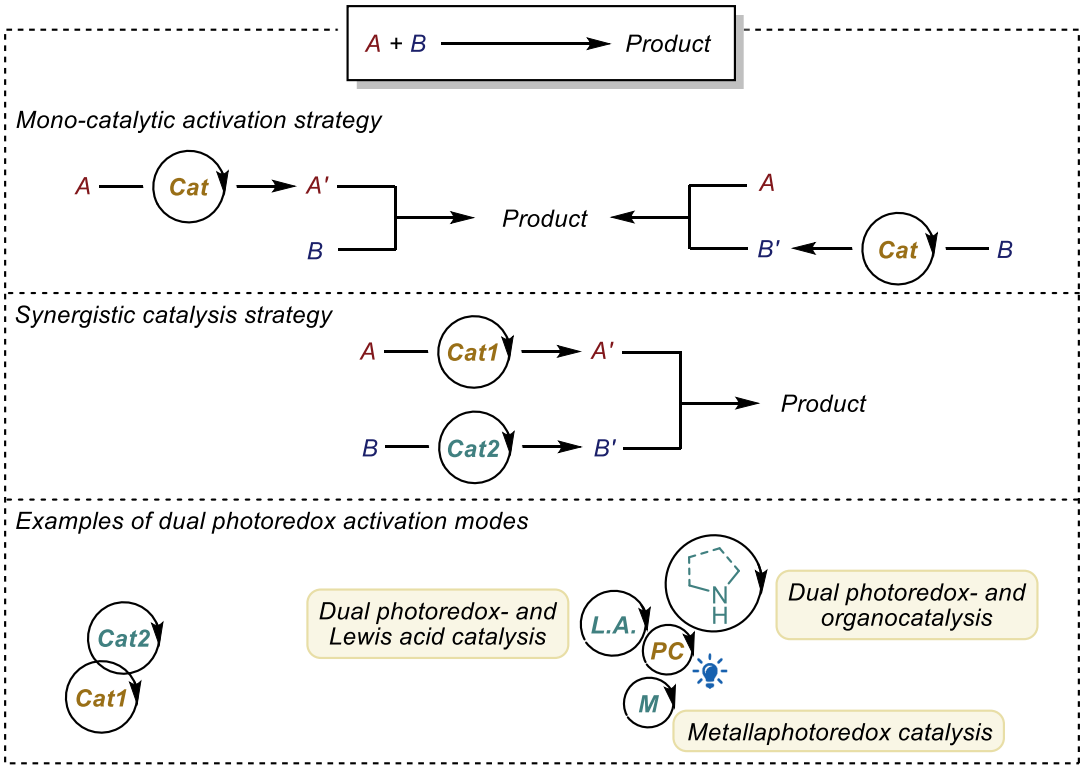

Figure 1.40 Schematic representation of the synergistic catalysis approach.

With this in mind, in the past decades photocatalytic cycles have been combined with a second catalytic cycle, that operates synergistically with the light-driven cycle and intercepts reactive radicals and manipulate and control their reactivity. Indeed, photoredox catalysis is particularly amenable to be merged with complementary activation modes because 1. the mild operational conditions (e.g. room temperature or visible light irradiation) are well tolerated by most of the other catalytic systems, 2. a wide range of reaction conditions, solvents, additives, and substrates do not react and do not take part in parasitic side-reactions, 3. in commonly employed organometallic photocatalysts, e.g. Ru- or Ir-based, the metal coordination sphere is saturated. Thus, usually it prevents the photocatalyst to engage deleterious *inner-sphere* interactions with the complementary catalyst, substrates or other reactants in the reaction media. Finally, 4. the thermodynamics of the single electron transfer event can be predicted by the redox potentials, enabling chemists to carefully choose the photocatalyst and the substrates, avoiding non-compatible matches.[101]

In this chapter three dual photoredox activation modes will be discussed: first the combination of photoredox- and organocatalysis, second the combination of photocatalysis with Brønsted- and Lewis acids and, finally, the combination of photoredox and transition metal catalysis.

1.6.1 Dual photoredox and organocatalytic processes

Chronologically, dual photoredox and organocatalytic processes are the first modern examples of dual photoredox catalysis. In particular, the pioneering work of MacMillan on the dual photoredox and secondary amine organocatalysis laid the foundations for the subsequent development of the field.

In this regard, in 2008 Nicewicz and MacMillan reported the first enantioselective α-alkylation of aldehydes merging photoredox catalysis and organocatalysis (*Figure 1.41*). The transformation was considered challenging as the enamine catalysis was not productive by its own, but became straightforward by combining it with a photocatalytic cycle.[27] This protocol was developed according to the concept of *singly occupied molecular orbital* (SOMO) organocatalysis[103] introduced by the same group in 2007 as a one-electron mode of activation which involves the formation of a transient radical species from an enamine and thus activates it toward the addition of a range of different electrophiles in an enantioselective manner.

The proposed mechanism depicted in *Figure 1.41* is initiated by a SET event between the excited $^*[Ru(bpy)_3]^{2+}$ and a sacrificial amount of the enamine. The reduced $[Ru(bpy)_3]^{+}$ can reduce ($E_{red}(Ru^{II}/Ru^{I})$ = –1.33 V *vs* SCE) the bromo derivative (i.e. the phenacylbromide used in the scope, E_{red}(phenacylbromide/phenacyl$^{\bullet}$) = –0.49 V *vs* SCE) leading to a bromide anion and a C-centered electrophilic radical, that can be trapped by the SOMOphile enamine. This is the key step, where the enantioselectivity of the coupling is controlled by the chiral imidazolidinone leading to an enantioenriched and electronrich α-amino radical, a single electron species that exhibits a low barrier oxidation (–0.92 to –1.12 V *vs* SCE in MeCN) which can act as the quencher for the excited photocatalyst ($^*E_{red}(Ru^{II}*/Ru^{I})$ = +0.77 V *vs* SCE) restoring the photoredox catalytic cycle and leading to the formation of an iminium ion, which can be hydrolyzed by the water present in the reaction medium giving the α-alkylated enantioenriched aldehyde and restoring the organocatalytic cycle.

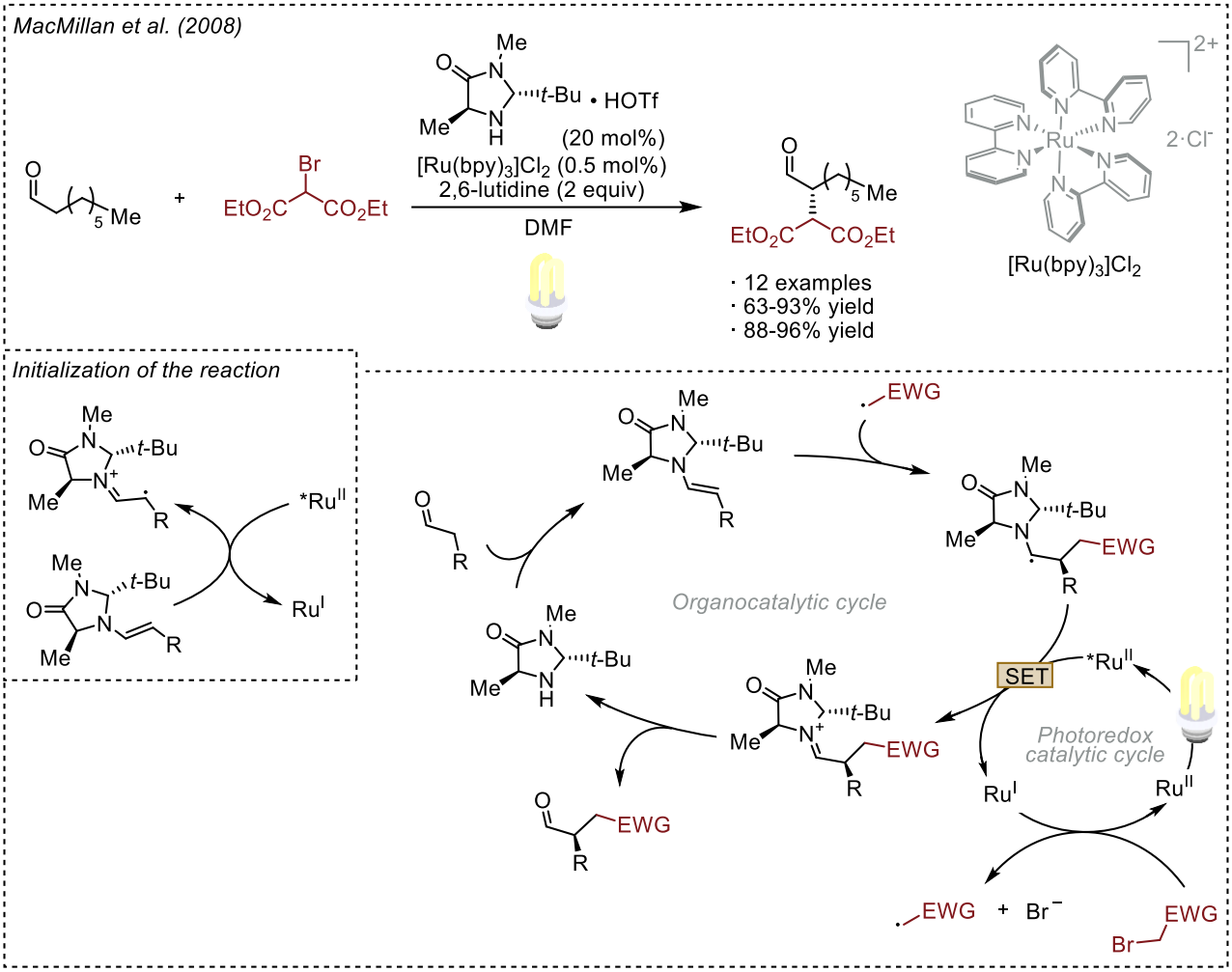

Figure 1.41 First dual photoredox and organocatalytic enantioselective α-alkylation of aldehydes reported by Nicewicz and MacMillan.

The mechanism was reinvestigated by the Yoon group several years later.[104] They calculated a quantum yield of Φ = 18, indicating a radical chain mechanism. From the combination of the quantum yield calculation and luminescence quenching measurements it was ruled out that the photoredox initiation is quite inefficient and the mechanism is dominated by a radical chain, as described in *Figure 1.42*.

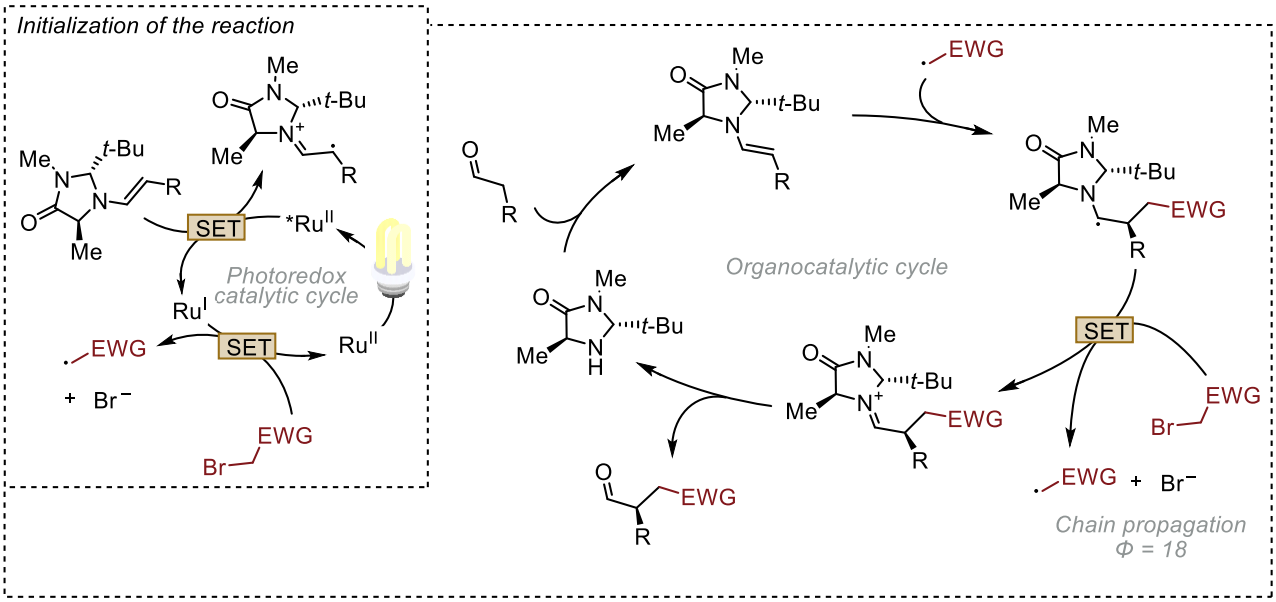

Figure 1.42 The revised mechanism reported by Yoon on the α-alkylation of aldehydes reported by Nicewicz and MacMillan.

This example was a milestone for the future developments in the field. In the following years, using the same dual activation approach, the same group and others reported the enantioselective α-trifluoromethylation,[105] oxyamination[106] and benzylation[107] of aldehydes.

More recently, the combination of photoredox- and secondary amine catalysis has been reported to activate the β-position on saturated carbonyl compounds instead of the α-position. The key point of these transformations is the oxidation of the enamine to a radical cation, which lowers the pK_a of the proton on the β-carbon. In the presence of a weak base, such as DABCO, a strong nucleophilic β-enaminyl radical is formed, which has a radical character at the β-carbon position (*Figure 1.43*). With this strategy, the coupling between saturated aldehydes and arenes,[108] aromatic ketones,[109] Michael acceptors, such as acrylates[110] and, more recently, also the use of organic TADF-emitters instead of iridium-based photocatalysts have been reported.[111]

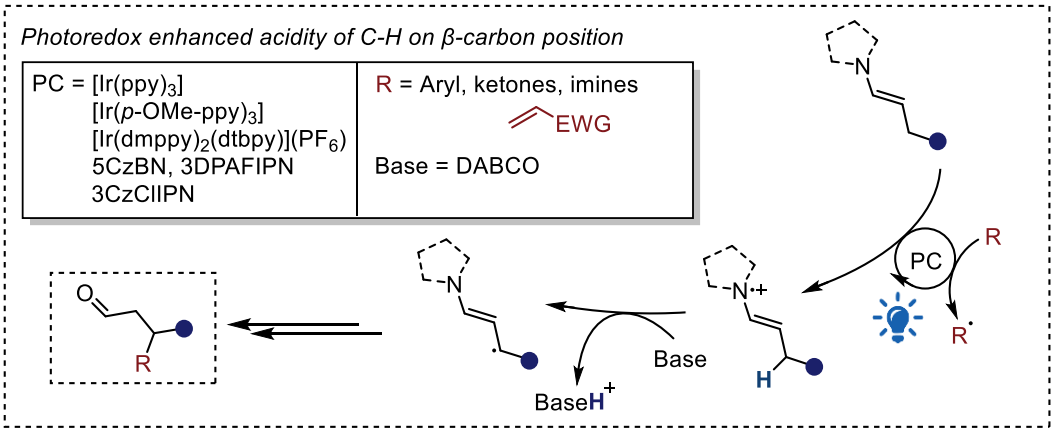

Figure 1.43 The formation of β-enaminyl radicals though the oxidation of the enamine radical cation.

The dual organo- and photocatalytic activation mode has recently been explored from a different perspective by the Melchiorre group. Indeed, the group reported the first enantioselective conjugate addition of allyl groups to α,β-unsaturated aldehyde (*Figure 1.44*).[112] The innovative strategy is based on the formation of a redox-active chiral iminium ions derived from a modified Jørgensen

organocatalyst, which can be directly excited under blue light irradiation. The excited iminium ion can be reductively quenched by an allylsilyl derivative to form a β-enaminyl radical. The oxidized allylsilyl derivative fragments into the allyl radical. Enantiocontrolled radical-radical coupling leads to the conjugated allylated enamine which upon hydrolysis by the water present in the reaction medium releases the desired product and the catalytic cycle is restored. The protocol was found to be tolerant to different functional groups and showed complete chemoselectivity towards the 1,4-coupling, high regiocontrol towards α-addition of the allyl moiety over the Y-addition and excellent enantioselectivity.

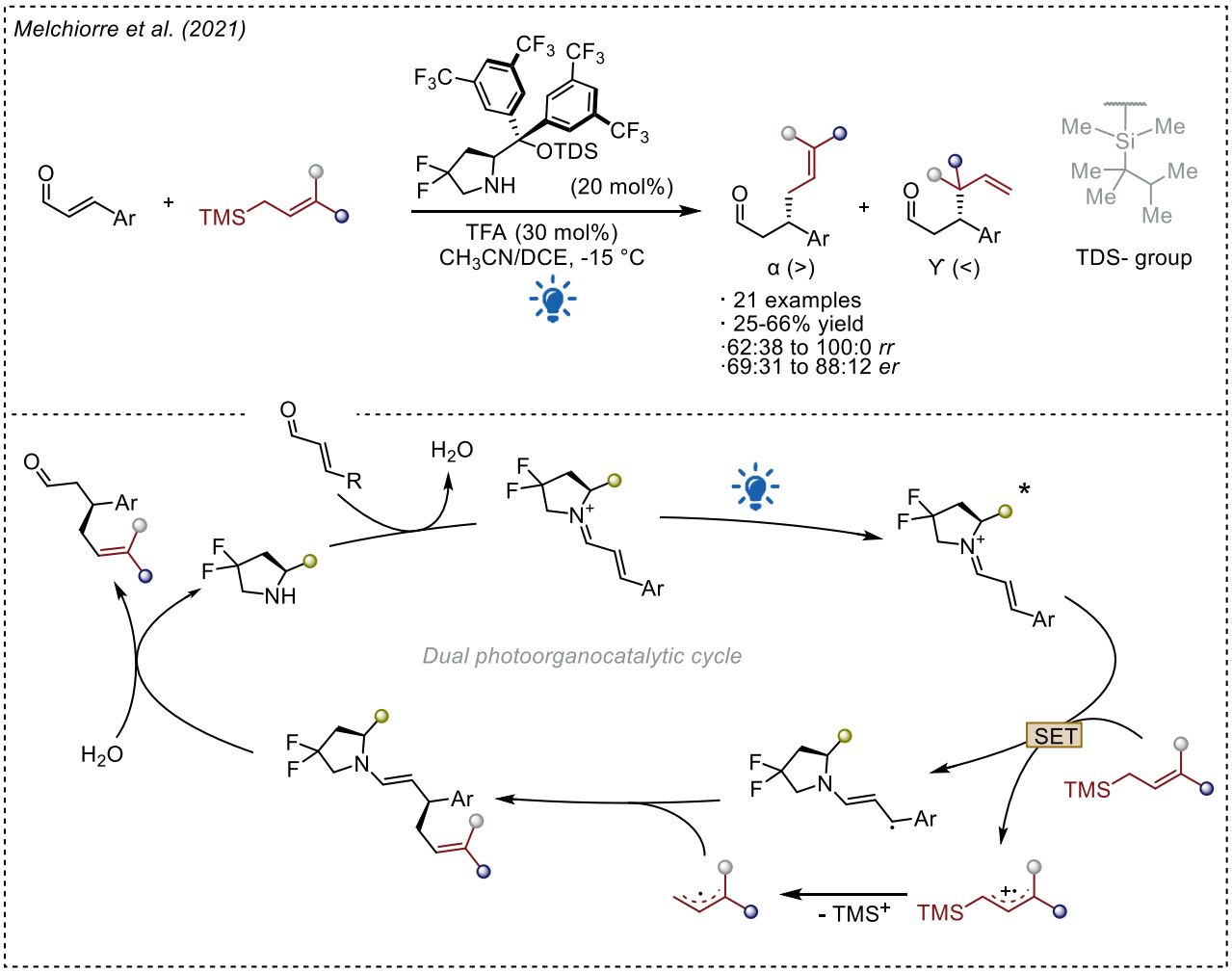

Figure 1.44 First dual photoredox and organocatalytic enantioselective addition of allyl groups to α,β-unsaturated aldehydes reported by the Melchiorre group.

1.6.2 Dual photoredox and Brønsted acids processes

Photoredox processes can take advantage of the presence of a catalytic amount of a Brønsted acid in the reaction media. This dual activation mode has been reported in several different transformations. Yoon described the dual photoredox- and formic acid-catalyzed reductive cyclization of bis(enones) to give cyclopentane products.[24] The key aspect is the acid activation of the carbonyl group towards a SET reduction with the reduced photocatalyst. The acid is essential to modulate the high reduction potential of the ketones (e.g. for acetophenone E_{red} = −2.10 V *vs* SCE) which could not be reduced by the reduced ruthenium photocatalyst ($E_{red}(Ru^{II}/Ru^{I})$ = −1.33 V *vs* SCE) from a thermodynamics perspective. A closely related mechanism for modulating the redox properties in the presence of Brønsted acids is called *proton-coupled electron transfer* (PCET) which involves the independent transfer of a proton and an

electron in a single elementary step. The concerted nature of the events lowers the energetic barrier compared to sequential steps involving proton and electron transfer. This strategy has been exploited by the Knowles group in the ketyl-olefin coupling reaction (*Figure 1.45*).[113] The authors used catalytic $[Ru(bpy)_3]^{2+}$ and diphenylphosphoric acid as the electron-donor/proton-donor pair allowing the reduction and protonation of the carbonyl moiety leading to a ketyl radical (PCET step). The latter undergoes an intramolecular radical cyclization to give an α-carbonyl radical. The abstraction of a hydrogen atom (HAT step) from 2-phenyl-dihydrobenzothiazole (BT) leads to the *cis*-cyclopentane alcohol as the major diastereoisomer and to the radical BT. The latter can act as the reductant for the excited photocatalyst leading to the reduced Ru(I) photocatalyst and 2-phenyl-benzothiazole, with the release of a proton that restores the catalytic acid previously consumed in the PCET step. The final intramolecular transesterification leads to desired bicyclic product.

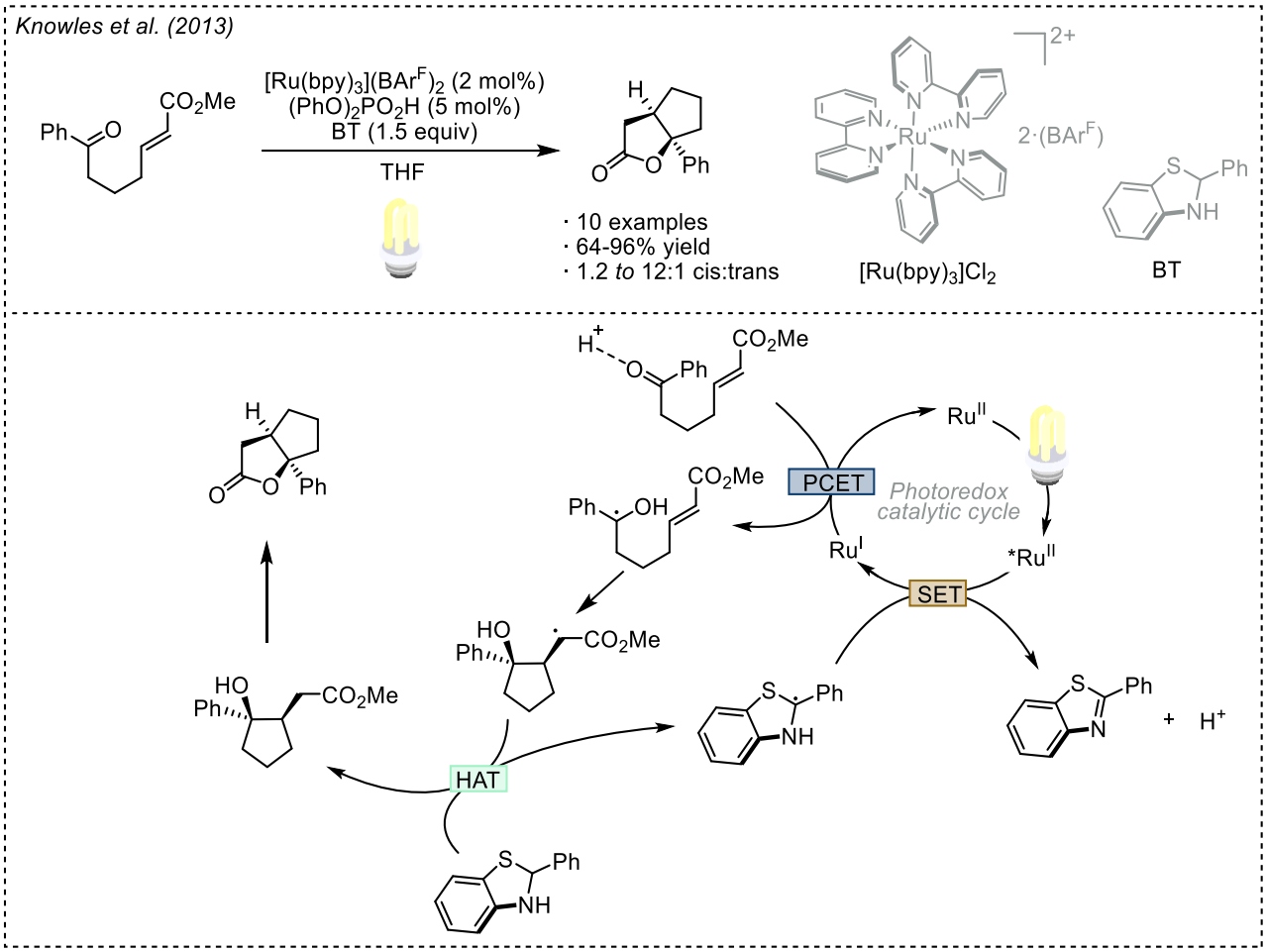

Figure 1.45 Dual photoredox and Brønsted acid ketyl-olefin coupling reaction reported by the Knowles group.

In the same year, the group reported an enantioselective variant using a chiral phosphoric acid to promote an asymmetric intramolecular aza-pinacol cyclization between an aromatic ketone and a hydrazone (*Figure 1.46*).[114] Compared to the previous protocol, $[Ru(bpy)_3]^{2+}$ is replaced by $[Ir(ppy)_2(dtbpy)](PF_6)$ as the photocatalyst, and the Hantzsch ester is used as the terminal reductant and proton source. The key aspect of the protocol is the formation of a stable non-covalent interaction between the phosphate and the radical substrate during the C-C bond formation step which provides the asymmetric induction.

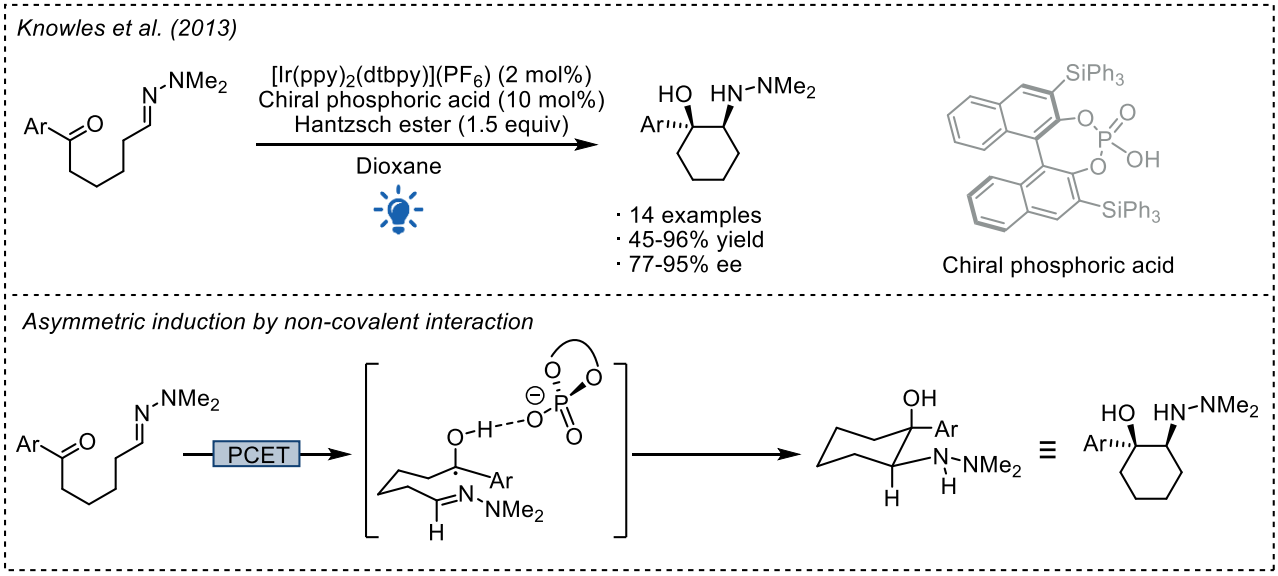

Figure 1.46 Dual photoredox- and Brønsted acid- enantioselective ketyl-hydrazone coupling reaction reported by the Knowles group.

1.6.3 Dual photoredox and transition metal processes

Transition metal catalysis is considered a fundamental tool for the activation and manipulation of chemical bonds. Usually the oxidation state of the metal center is an important element of design in a metal-mediated transformation, and the adjustment of this property is necessary to ensure the desired chemo-, regio- or stereoselectivity of the process.[115] The use of suitable ligands to stabilize a specific oxidation state of the metal or the addition of stoichiometric oxidants or reductants makes it possible to control, although not always easily, the oxidation state of the metal.[116]

The combination of metal catalysis with a photoredox cycle, known as metallaphotoredox catalysis, makes it possible to directly modify under mild conditions the oxidation state of the metal, even with appropriate ligands,[117] altering or adjusting its reactivity for the specific transformation and allowing oxidative addition/elimination cycles using even non-reactive substrate precursors activated by the photoredox cycle in order to pursue novel or unprecedented reactivities.[116] The unlimited potential of this dual strategy has been exploited with many metals, e.g. palladium,[118,119] copper,[120] titanium,[121] nickel,[122–125] gold,[126] chromium,[71,127] cobalt,[128] bismuth[129] and many others and has been extensively reviewed in recent years.[58,59,59,130] The vastness of the field precludes a detailed description in few pages. In the next section some chronological and relevant examples of metallaphotoredox catalysis will be described. The first metal will be palladium, which was the first to be reported under these dual conditions, followed by a few processes that use Earth abundant metals, such as nickel, chromium and titanium.

1.6.3.1 Dual photoredox and palladium processes

Palladium has a rich and well-studied chemistry as a reactive and versatile metal in catalysis with widespread applications in academia and industry.[131]

In 2011 the Sanford group reported a dual photoredox- and $Pd(OAc)_2$-directed C-H arylation at room temperature (*Figure 1.47*).[118] The protocol is based on the C-C bond formation under a Pd(II)/Pd(IV)

catalytic cycle that is combined with a photocatalytic cycle. The photoredox conditions allow the formation of an aryl radical at room temperature compared to the high temperatures (100°C) previously required in the past for the same Pd-catalyzed transformation using diaryliodonium salts[132] or dibenzoyl peroxides.[133] After the oxidative quenching of the photocatalyst ($*E_{ox}(Ru^{III}/*Ru^{II})$ = −0.86 *vs* SCE) by the aryldiazonium salt ($E_{red}(ArN_2^+/Ar^\bullet)$ ~ −0.2 V *vs* SCE[134]), an aryl radical is formed with nitrogen extrusion. The radical can be trapped by a cyclometalated Pd(II) complex leading to a Pd(III) intermediate. In order to induce the reductive elimination, the Pd(III) intermediate must be oxidized to a Pd(IV) intermediate. The oxidized photocatalyst is powerful enough to oxidize the Pd(III) intermediate to a Pd(IV) intermediate after its SET back-reduction restoring the Ru-catalytic cycle. Reductive elimination leads to the desired arylated product restoring the Pd-catalytic cycle.

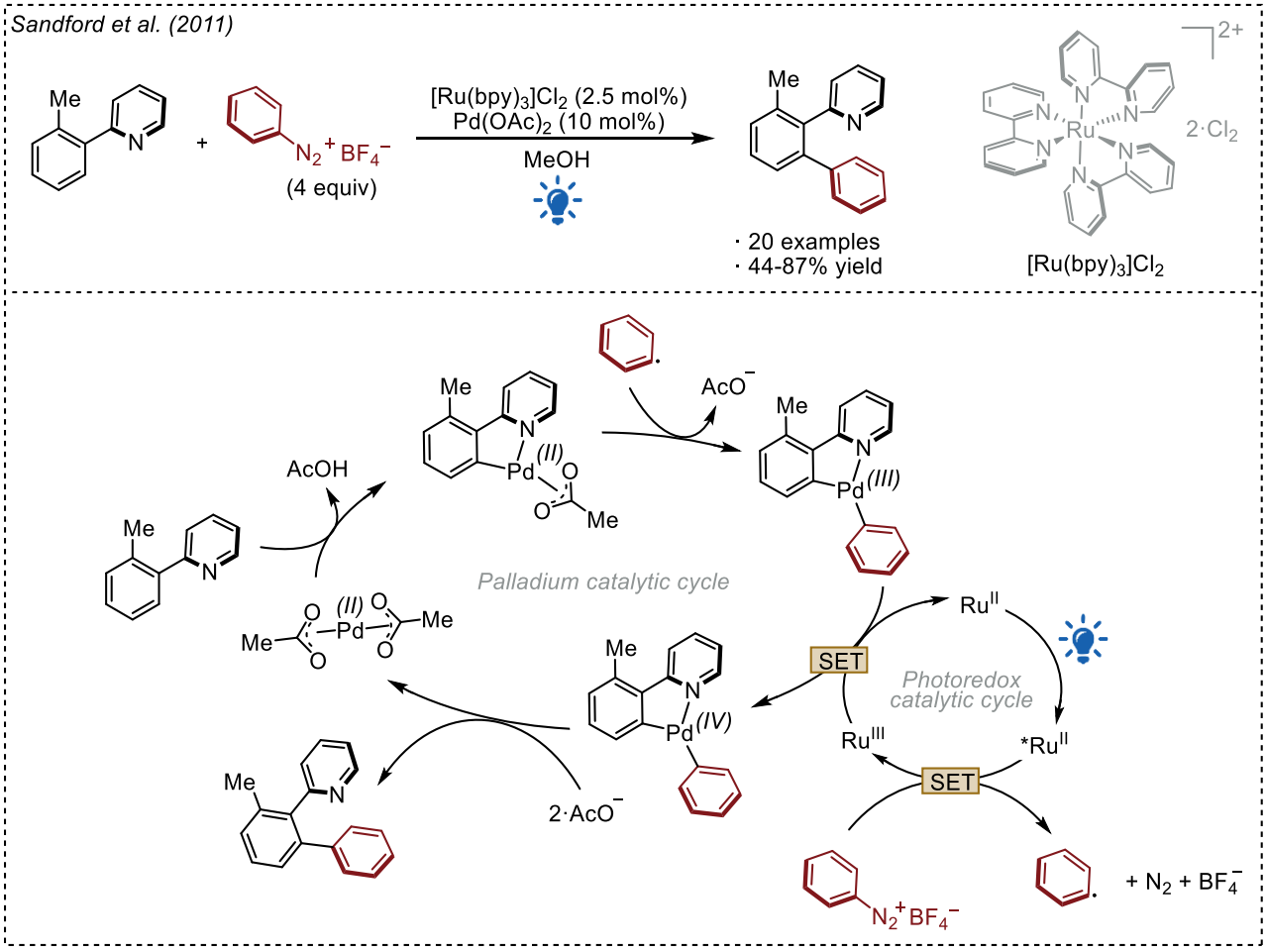

Figure 1.47 Dual photoredox- and palladium-directed C-H arylation reported by the Sandford group.

A few years later the Rueping group reported a straightforward dual photoredox- and palladium-catalyzed C-H olefination of aromatic enamines for the synthesis of indoles (*Figure 1.48*).[135] The protocol uses air as a mild redox mediator in combination with an iridium photocatalytic cycle to perform a Pd(0)/Pd(II) catalytic cycle. The proposed mechanism starts with the C-H activation of the olefin, followed by the activation of the arene. After the reductive elimination, the desired indole is produced and the resulting Pd(0) can now be reoxidized by either the reductive quenching of the excited photocatalyst or by the peroxy species $O_2^{\bullet-}$ formed during the back-oxidation of the reduced photocatalyst by molecular oxygen O_2.[136] The resulting reduced species O_2^{2-} was detected in the reaction media by colorimetric assay. Finally, using potassium superoxide KO_2 as an external oxidant in

the absence of a photoredox catalyst, the product was obtained in a discrete yield (53%) indicating that peroxy species may be involved in the process.

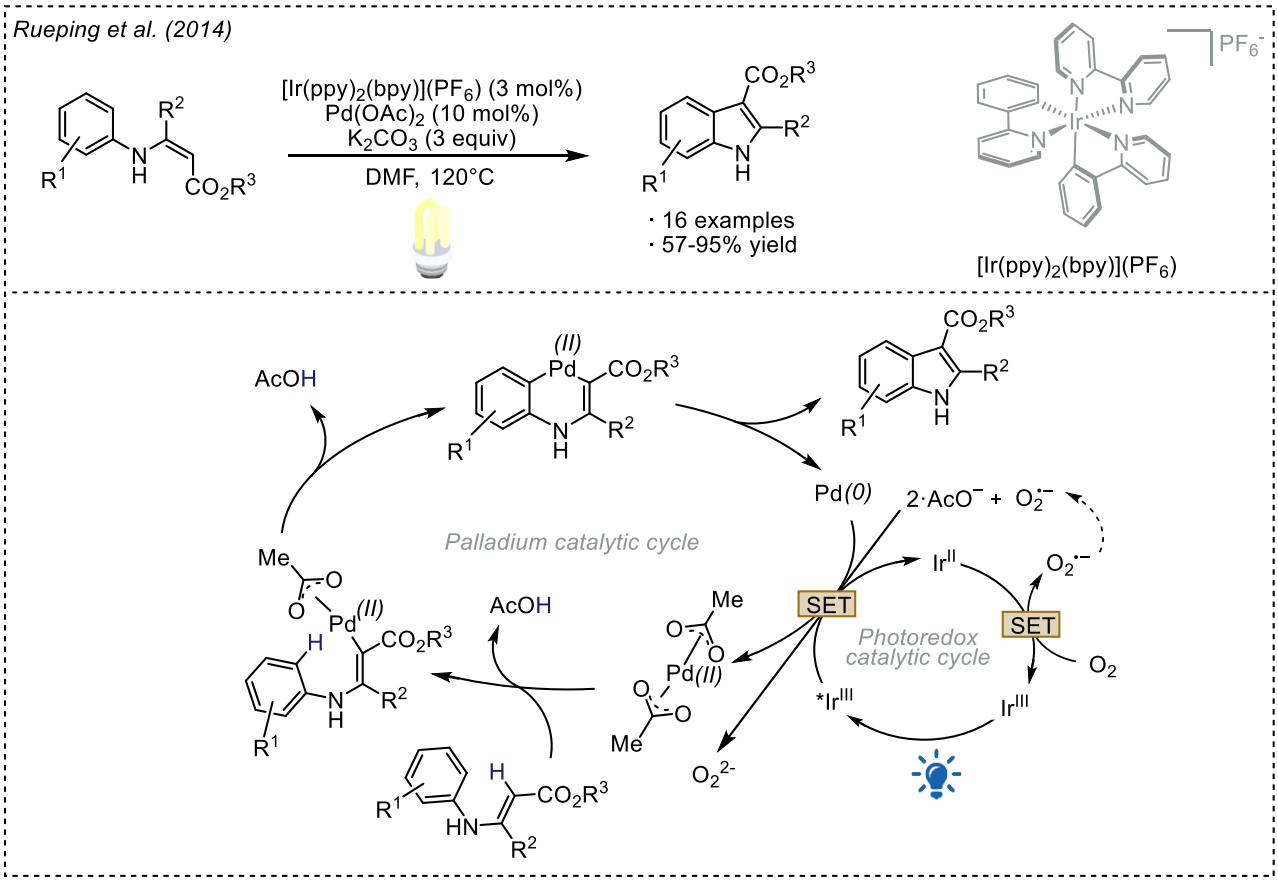

Figure 1.48 Synthesis of indoles under dual photoredox/palladium conditions reported by the Rueping group.

In the following years other dual palladium and photoredox protocols were reported.[100] These include name reactions, such as Sonogashira,[137] Suzuki-Miyaura[138] and Heck[139] couplings.

1.6.3.2 Dual photoredox and nickel processes

Palladium and nickel share some chemical properties in the elementary steps of a catalytic cycle, although they have their own distinct behaviors and properties. Like palladium, nickel has a range of contiguous and accessible oxidation states, ranging from -1 to +4, and exhibits both oxidative addition and reductive elimination processes. Nickel is more electropositive, favouring the oxidative addition even in the presence of substrates that are poorly reactive with palladium, such as aryl fluorides.[140] On the other hand, reductive elimination events are less favoured.[141] Compared to palladium, the reduced ability of nickel alkyl species to undergo β-hydride elimination prevents parasitic side-reactions.[59] For such properties, both nickel and palladium are suitable in cross-coupling protocols.[142]

It is commonly assumed that palladium-mediated cross-couplings follow a Pd(0)/Pd(II) catalytic cycle, operating via a non-radical mechanism,[125] although, as shown in the previous paragraph, it is possible to extend the repertoire of palladium chemistry by exploiting radical cycles. On the contrary, the Ni(I) and Ni(III) oxidation states are particularly well suited to be combined with radical cycles. Moreover, the formation of unstable Ni(III) intermediates are prone to undergo reductive elimination.[143]

The combination of photocatalysis and nickel catalysis is considered to be one of the most fruitful and widely explored in metallaphotoredox catalysis[125] which precludes a detailed discussion in this introduction. In the following paragraph only a few relevant and useful examples for this general introduction to dual photoredox/nickel cross couplings will be described.

Doyle and MacMillan in 2014 reported a dual photoredox- and nickel-catalyzed C(sp^3)-C(sp^2) decarboxylative arylation (*Figure 1.49*).[122] The combination of a photoredox- and a nickel catalytic cycle allows the use of carboxylic acids as unconventional coupling partners in cross coupling reactions: after their oxidation in a SET event by the excited photocatalyst and subsequent decarboxylation, the radical thus formed can be intercepted by a low-oxidation-state nickel intermediate, generated *in situ* from a Ni precursor in a reductive SET event, which can be combined with an aryl halide in a cross-coupling reaction to yield an (aryl)(alkyl)-Ni(III) intermediate. Reductive elimination leads the desired product and the formation a Ni(I) species, closing the Ni catalytic cycle. The protocol uses $NiCl_2$·glyme as Ni(II) source, [Ir{*d*F(CF_3)ppy}$_2$(dtbpy)](PF_6) as the photocatalyst and Cs_2CO_3 as the base with a CFL irradiation.

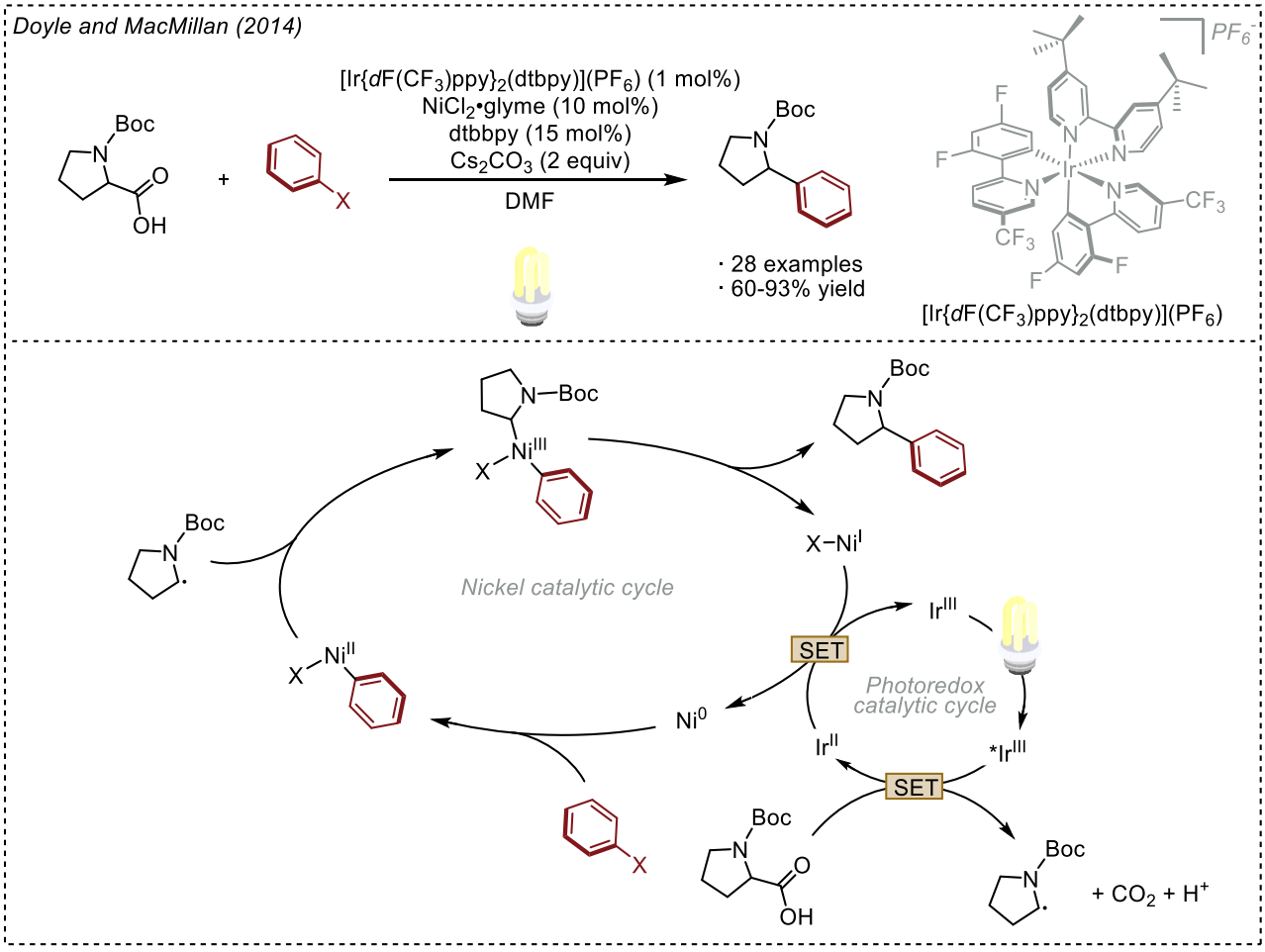

Figure 1.49 Dual photoredox- and nickel-catalyzed decarboxylative arylation reported by Doyle and MacMillan.

At the same time, the Molander group reported a dual photoredox- and nickel-catalyzed C(sp^3)-C(sp^2) coupling using aryl bromides and benzylic trifluoroborates (*Figure 1.50*).[123] In this case, trifluoroborates are introduced as a source of benzylic radicals and Ni(0) is used instead of Ni(II), dtbpy as the ligand and 2,6-lutidine as the base. The proposed mechanism[144] is similar to that using carboxylate precursors and involves the reductive quenching of the Ir-based photocatalyst ($*E_{red}(*Ir^{III}/Ir^{II})$ = +1.21 V *vs* SCE) by the trifluoroborate derivative ($E_{ox}(benzyl^{\bullet}/benzylBF_3^-)$ = +1.2 V *vs* SCE) and its subsequent fragmentation into a C-centered radical and BF_3. The reduced form of the photocatalyst can reduce a Ni(I)

intermediate, formed *in situ* in the nickel catalytic cycle, to an active Ni(0) species restoring the photocatalytic cycle. Addition of the C-centered radical to the Ni(0) species leads to an alkyl-Ni(I) intermediate that can undergo oxidative addition towards the aryl halide forming an (aryl)(alkyl)-Ni(III) intermediate. Reductive elimination leads to the desired product leading to a Ni(I) complex that can be reduced by the excited photocatalyst restoring the nickel catalytic cycle.

It is important to highlight that Ru-based photocatalysts, i.e. $[Ru(bpy)_3]^{2+}$, cannot be used in this transformation: considering the same mechanism, $[Ru(bpy)_3]^{2+}$ cannot be reduced ($*E_{red}(*Ru^{II}/Ru^{I})$ = +0.84 V *vs* SCE) by the trifluoroborate derivative ($E_{ox}(benzyl^{\bullet}/benzylBF_3^{-})$ = +1.2 V *vs* SCE) since it has a lower potential.

In the same work, the authors briefly demonstrated the feasibility of coupling secondary aliphatic trifluoroborates with aryl bromides in a potential enantioselective variant using a chiral bisoxazoline ligand (BiOX) with a promising 50% *ee*.

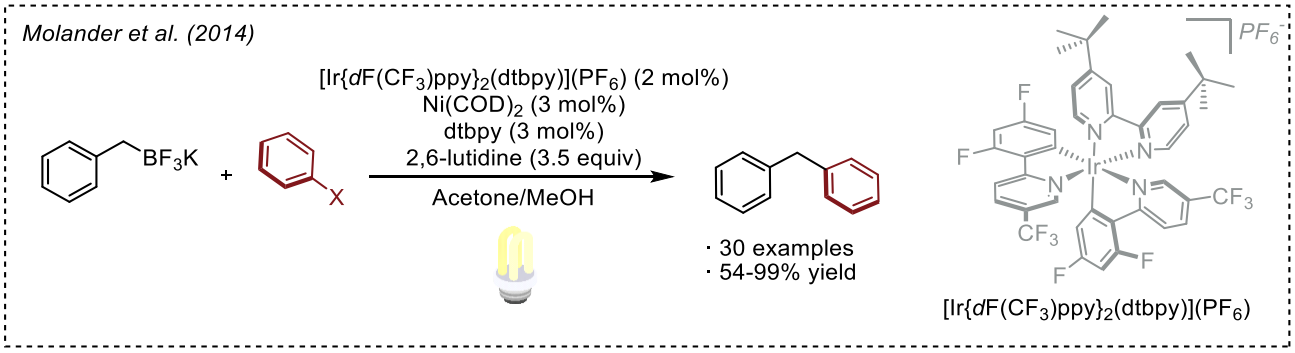

Figure 1.50 Dual photoredox- and nickel-catalyzed cross coupling of aryl bromides with benzylic trifluoroborates reported by the Molander group.

Years later, the Reisman group reported a detailed enantioselective protocol using a BiOX ligand in the enantioselective cross-coupling between α-*N*-heterocyclic trifluoroborates and aryl bromides under dual photoredox- and nickel catalysis (*Figure 1.51*).[145] The protocol uses $NiCl_2$·glyme as Ni(II) source, $[Ir\{dF(CF_3)ppy\}_2(bpy)](PF_6)$ as the photocatalyst (from 0.125 to 1 mol%) and K_2HPO_4 as the base under blue light irradiation.

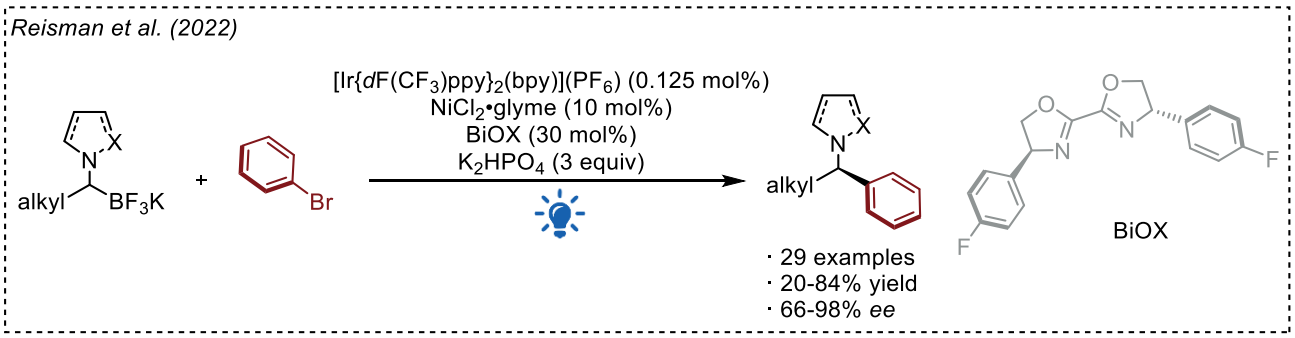

Figure 1.51 Dual photoredox- and nickel-catalyzed enantioselective cross-coupling between α-N-heterocyclic trifluoroborates and aryl bromides reported by the Reisman group.

Trifluoroborate salts were found to be suitable for a library of different functionalizations. Various radical precursors have been explored by the Molander group in the coupling of benzylic,[146] secondary alkyl,[147] α-alkoxy,[148] and α-amino[149] radicals using dual photoredox/nickel platforms.

Although trifluoroborate salts are indeed a valuable source of C-centered radicals, they suffer from some drawbacks that may limit their applicability. In particular, 1. primary alkyl trifluoroborate salts

cannot be oxidized by common Ir-based photocatalysts due to their high oxidation potentials (E_{ox} > +1.50 V *vs* SCE),[150] 2. alkyl trifluoroborates are poorly soluble in several solvents and 3. the stoichiometric amount of BF_3 released upon their oxidation is corrosive and can interfere with the reaction, requiring the addition of a stoichiometric amount of base. To overcome these drawbacks, the group of Molander[151] and Goddard, Ollivier and Fensterbank[152] reported the use of primary and secondary ammonium alkyl bis(catecholato) silicates (*Figure 1.52*). Of particular relevance is that the use of a dual photoredox and nickel catalysis also allows the coupling between aryl bromides and primary aliphatic ammonium bis(catecholato) silicates, as the measured oxidation potentials were in the range between +0.34 and +0.89 V *vs* SCE,[152] allowing the oxidation with commonly excited Ir- and Ru-based photocatalysts.

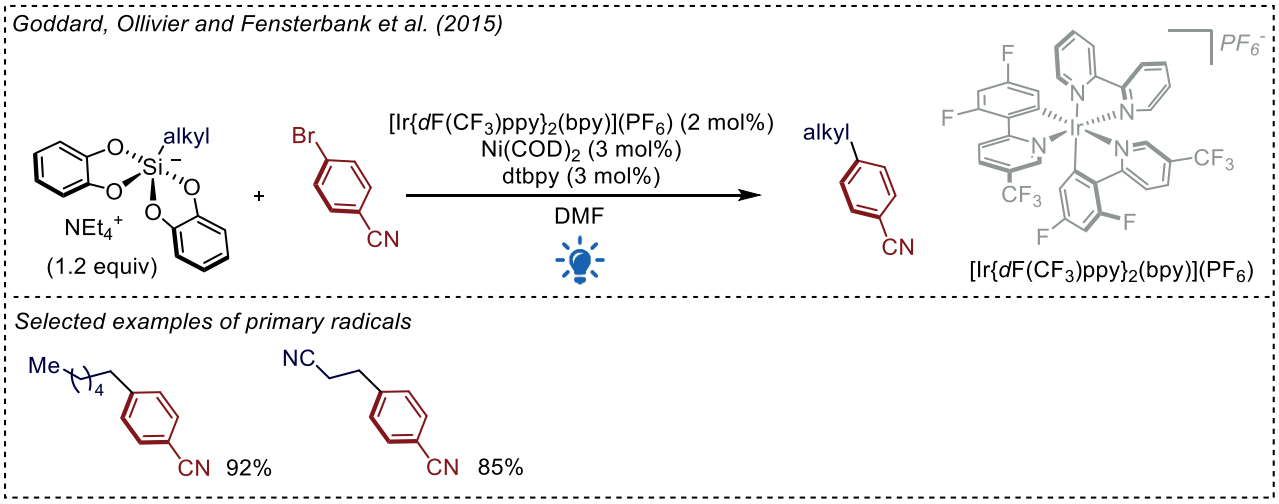

Figure 1.52 Dual photoredox- and nickel-catalyzed cross coupling between aryl bromides and ammonium alkyl bis(catecholato) silicates reported by Goddard, Ollivier and Fensterbank.

An alternative source of C(sp^2) radicals are 1,4-dihydropyridines (DHP). The Molander group reported in 2016 a dual photoredox and nickel cross coupling between (hetero)aryl bromides and substituted DHPs in the presence of a catalytic amount of 4CzIPN as an organic photosensitizer, Ni(dtbpy)Cl_2·$4H_2O$ as the Ni(II) precursor under blue light irradiation (*Figure 1.53*).[153] In this protocol the organic carbazole-based photocatalyst 4CzIPN gave better results compared to Ru- or Ir-based photocatalysts since its redox potential ($*E_{red}$(*4CzIPN/4CzIPN$^{\bullet-}$) = +1.32 *vs* SCE) allows the oxidation of the substituted DHP (E_{ox}(alkyl$^{\bullet}$/alkyl-DHP) ~ +1 V *vs* SCE) and the reduction of the nickel complex triggering its catalytic activity in the cross coupling reaction.

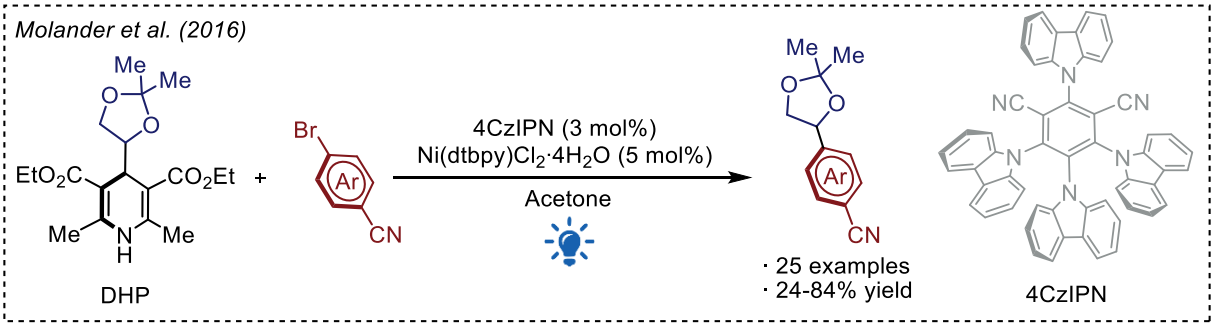

Figure 1.53 Dual photoredox- and nickel-catalyzed cross-coupling between (hetero)aryl bromides and substituted DHPs reported by the Molander group.

An attractive strategy made possible under metal- and photoredox conditions is the possibility of directly using aliphatic C-H bonds as a source of C-centered radicals in the presence of a suitable HAT agent without any further derivatization. The MacMillan group reported in 2016 the arylation of α-amino and α-oxy(sp^3) C–H bonds in both cyclic and acyclic systems combining a triple photoredox-, nickel- and HAT- catalytic cycle (*Figure 1.54*).[154] The protocol uses $NiBr_2 \cdot 3H_2O$ as the Ni-precursor, 4,7-*d*OMe-phen as the ligand, 3-acetoxyquinuclidine as the HAT agent, [Ir{*d*F(CF_3)ppy}$_2$(dtbpy)](PF_6) as the photocatalyst under blue light irradiation.

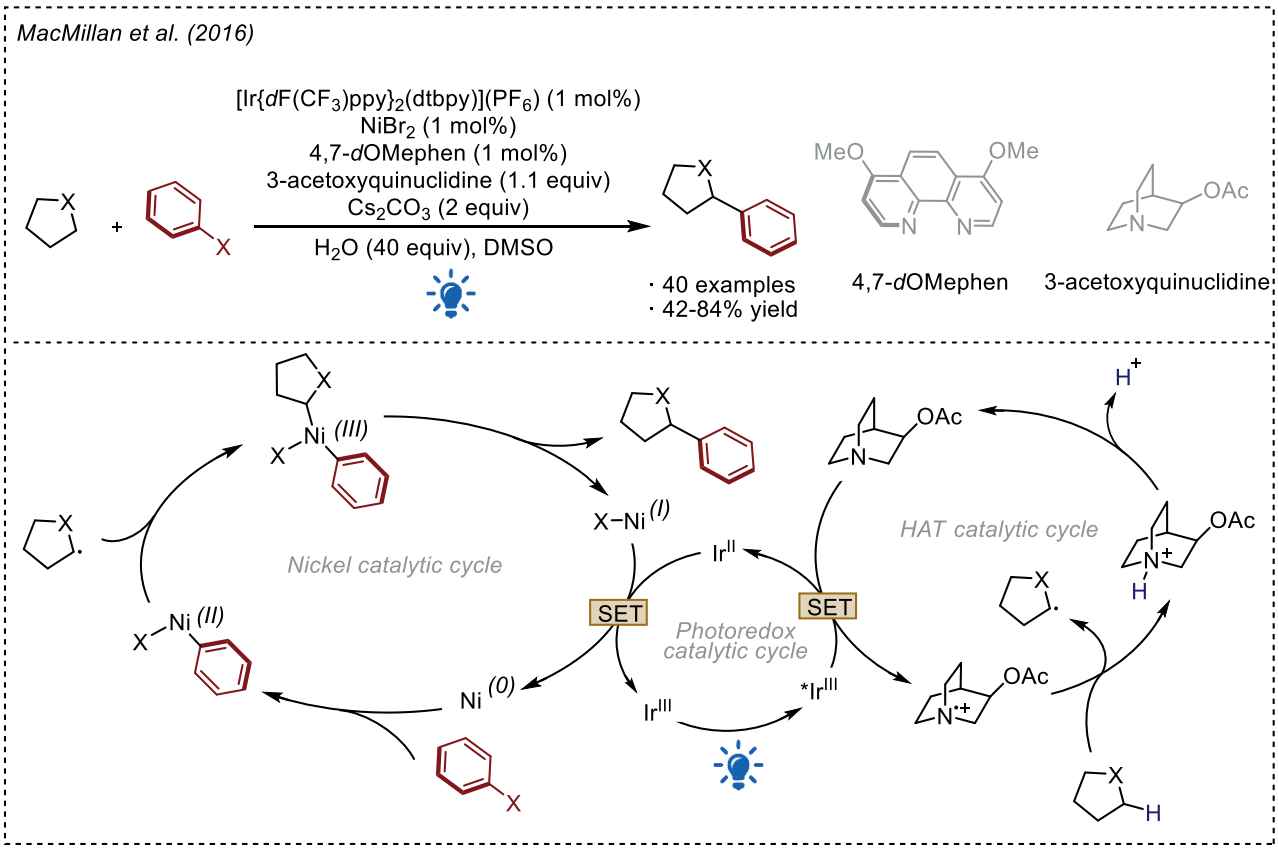

Figure 1.54 Triple photoredox-, nickel- and HAT-catalyzed arylation of α-amino and α-oxy(sp^3) C–H bonds reported by the MacMillan group.

The mechanism involves three catalytic cycles working cooperatively. The mechanism starts with the reductive quenching of the excited photocatalyst ($^*E_{red}(^*Ir^{III}/Ir^{II})$ = +1.21 V *vs* SCE in MeCN) by 3-acetoxyquinuclidine (E_{ox}(acetoxyquinuclidine$^{\bullet+}$/acetoxyquinuclidine) = +1.22 V *vs* SCE in MeCN) leading to an Ir(II) species that can act as a reductant ($E_{red}(Ir^{III}/Ir^{II})$ = −1.37 V *vs* SCE in MeCN) towards the Ni(II)-phenantroline complex ($E_{red}(Ni^{II}/Ni^0)$ = −1.2 V *vs* SCE in DMF) restoring the photocatalytic cycle and leading to a Ni complex in low oxidation state. The latter undergoes oxidative addition with the aryl bromide leading to a Ni(II)-aryl intermediate.

The quinuclidine radical cation is sufficiently electron-deficient to undergo a kinetically selective HAT process at the most electron-rich C-H site on the amine, i.e. the α-amino position. This event leads to an α-amino radical and a quinuclidinium cation, in equilibrium with the neutral form, restoring the HAT catalytic cycle. The HAT event is thermodynamically favoured considering the difference in the bond dissociation enthalpies (BDEs) of the hydridic α-amino C-H bonds (α-amino C-H = 89-94 kcal mol^{-1}) and the resultant N-H bond of quinuclidinium cation (BDE = 100 kcal mol^{-1}).

The α-amino radical is captured by the Ni(II)-aryl intermediate leading to a (aryl)(alkyl)-Ni(III) intermediate which upon reductive elimination provides the desired $C(sp^3)$-$C(sp^2)$ coupled product restoring the Ni-catalytic cycle.

Finally, the dual nickel/photoredox platform allows for a wide range of manipulations that cannot be fully described in just few pages. The applications and innovations of this dual activation mode have been extended in a very recent work by MacMillan in the activation of non-trivial functional groups, such as alcohols in deoxygenative cross-coupling protocols enabling C-centered radicals,[155–158] as well as the nickel-mediated C-O and C-N cross couplings using organic cyanoarene-based photocatalysts by the Pignataro group.[159] These works demonstrate the possibilities offered by metallaphotoredox catalysis to unveil new and elusive reactivities under mild conditions and with a high, and probably not fully explored, application potential.[160]

1.6.3.3 Dual photoredox and chromium processes

Chromium is an earth abundant transition metal which is widely used in metallurgy, materials science and in catalysis.[161] Chromium(III) has a rich chemistry and it has been extensively studied in recent decades. The Nozaki-Hiyama-Kishi (NHK) reaction is probably the best known protocol using organochromium reagents and has recently been reviewed.[162] In Nozaki-Hiyama-type reactions (NH), different organohalides can be used in the presence of stoichiometric amounts of chromium(II) to form different organochromium reagents *in situ*, i.e. allyl- or propargyl-chromium derivatives. On the contrary, in the preparation of alkenylchromium reagents starting from alkenyl halides, i.e. the Nozaki-Hiyama-Kishi (NHK) reaction, a catalytic amount of nickel(II) is required: first an alkenyl-Ni(II) intermediate is formed, then transmetalation as alkenyl-Cr(III) occurs.[163,164] The high stability of Cr-O bonds is a limitation of the reaction and is the reason why the first applications were stoichiometric in chromium. However, the use of chromium under stoichiometric conditions is associated with a large production of metal waste and is a concern for the scalability of the methodology. The Fürstner group in 1996 solved the problem and developed the first catalytic NHK reaction using Me_3SiCl as scavenger allowing the use of a catalytic amount of chromium(II) (*Figure 1.55 A*)[165]: as shown in the mechanism, given the oxophilicity of silicon, it was possible to force the Cr(III)-alkoxide to react, releasing the Cr(III) and restoring the metal catalytic cycle. More in detail into the mechanism by considering the vinylation reaction, since Cr^{2+} is a one-electron donor, two molecules of Cr(II) are required to form the vinyl-Cr(III) species: the first one reduces the vinyl bromide regenerating a Cr(III) species, while the second one can trap the vinyl radical forming the nucleophilic organometallic chromium(III) reagent. Addition to the carbonyl leads to the product as chromium alkoxide. Finally, the Cr-O bond is broken by Me_3SiCl, leading to the TMS-protected alcohol and the formation of a Cr(III) intermediate which can be reduced by a stoichiometric amount of Mn(0) reductant.

The authors reported an extensive use of aryl, heteroaryl, allyl and alkynyl halides, and alkenyl triflates and halides as the starting materials with both aromatic and aliphatic aldehydes. Different Cr(II)- and Cr(III)-sources were tested: $CrCl_2$ (doped with catalytic $NiCl_2$), $CrCl_3$, Cp_2Cr and $CpCrCl_2$·THF. The last two complexes gave the best efficiency in such C-C bond formations, as less than 1 mol % of chromium was required for quantitative conversions.

This catalytic protocol has been used years later by the Cozzi-Umani-Ronchi group in the first catalytic enantioselective NH reaction (*Figure 1.55 B*).[166]

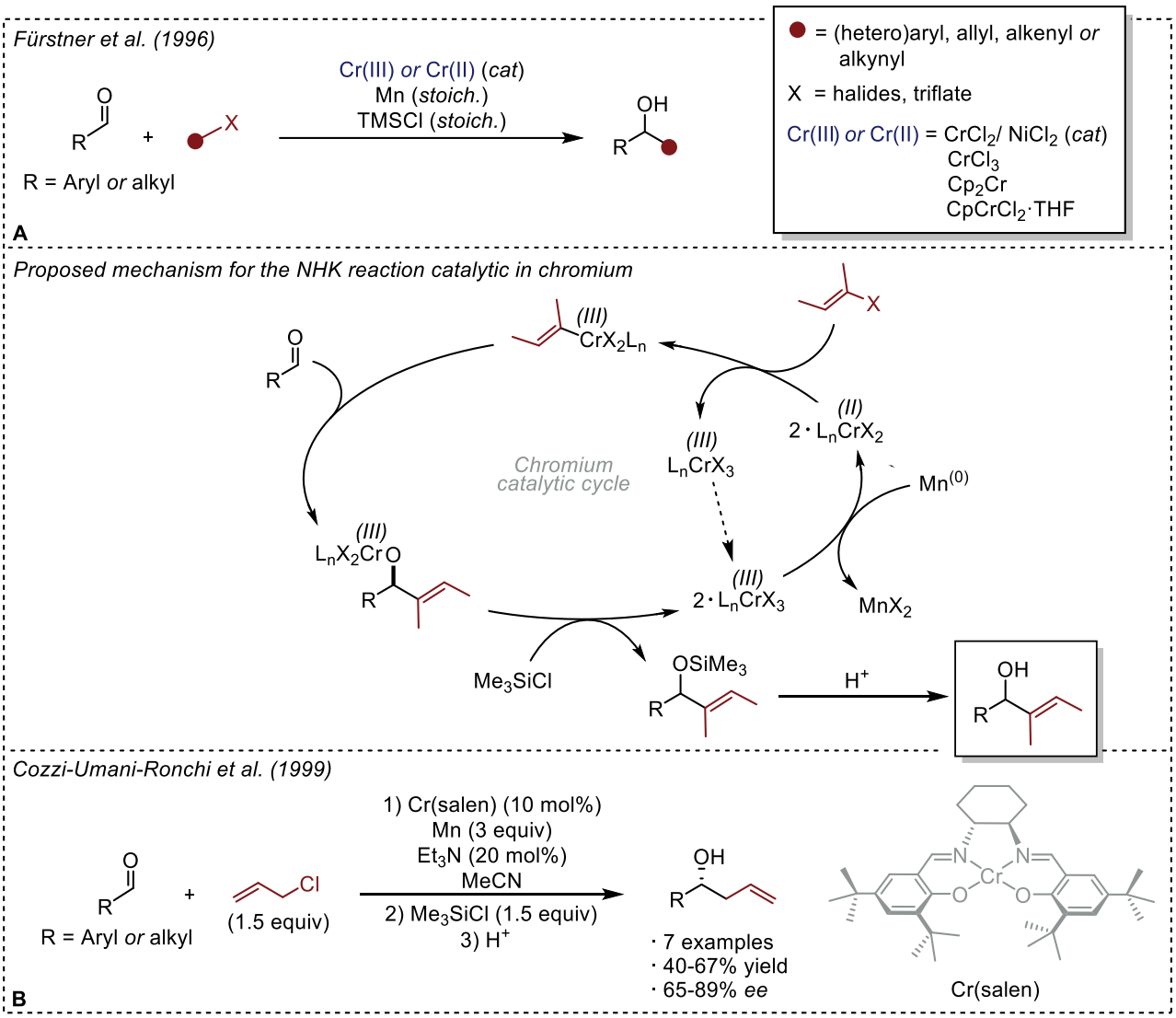

*Figure 1.55 First NHK (**A**) and first enantioselective NH (**B**) reaction catalytic in chromium.*

The protocol was applied to both aromatic and aliphatic aldehydes with generally good yields: the greatest erosion of the yield was due to the formation of a non-negligible amount (up to 40%) of the non-diastereoselective pinacol coupling product, observed more in the case of aldehydes substituted with electron-withdrawing groups.

In recent years, the combination of photoredox catalysis and chromium catalysis has been successfully applied to several transformations involving carbonyls as electrophiles. This dual platform has long been associated with the concept of *Reductive Radical-Polar Crossover* (RRPCO).[167] This approach involves the transfer of two electrons in two different SET steps: in the first SET event a radical is formed, under both oxidative or reductive conditions starting from a pronucleophile species, in the second SET event, chromium is reduced to a low oxidation state. The radical trapping by the low-valent Cr(II) leads to a transient nucleophilic organometallic Cr(III) species that exhibits a polar reactivity towards the carbonyl. Photoredox catalysis is well suited to the RRPCO strategy as it involves two single electron transfer steps that can generate both the radical partner and the chromium in a low oxidation state (*Figure 1.56*).

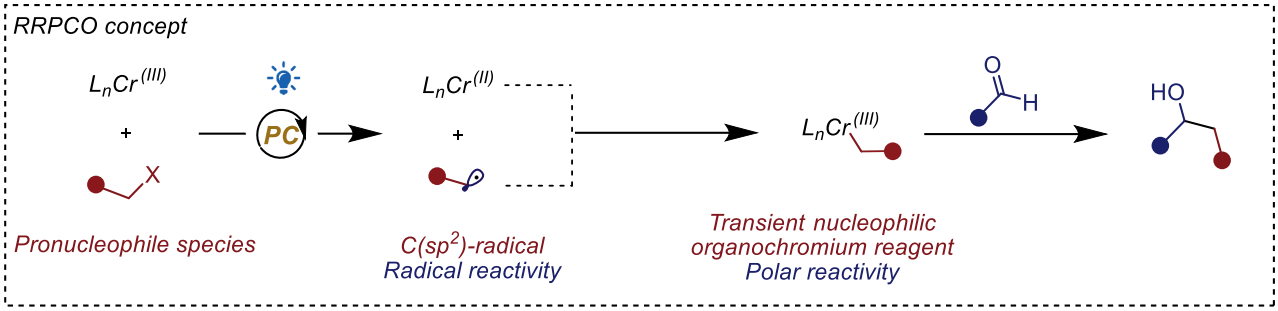

Figure 1.56 Schematic representation of the RRPCO concept.

The first dual photoredox and chromium protocols exploiting the RRPCO concept in the allylation of aldehydes were reported by the Glorius[168] and Kanai groups.[169]

The Glorius group reported in 2018 a highly diastereoselective protocol for the allylation of aldehydes using β-alkyl styrenes and allyl-diarylamines with both aromatic and aliphatic aldehydes using a catalytic amount of $CrCl_2$, [Ir{*d*F(CF$_3$)ppy}$_2$(dtbpy)](PF$_6$) as the photocatalyst, catalytic Li_2CO_3 as the base under blue light irradiation (*Figure 1.57*).[168]

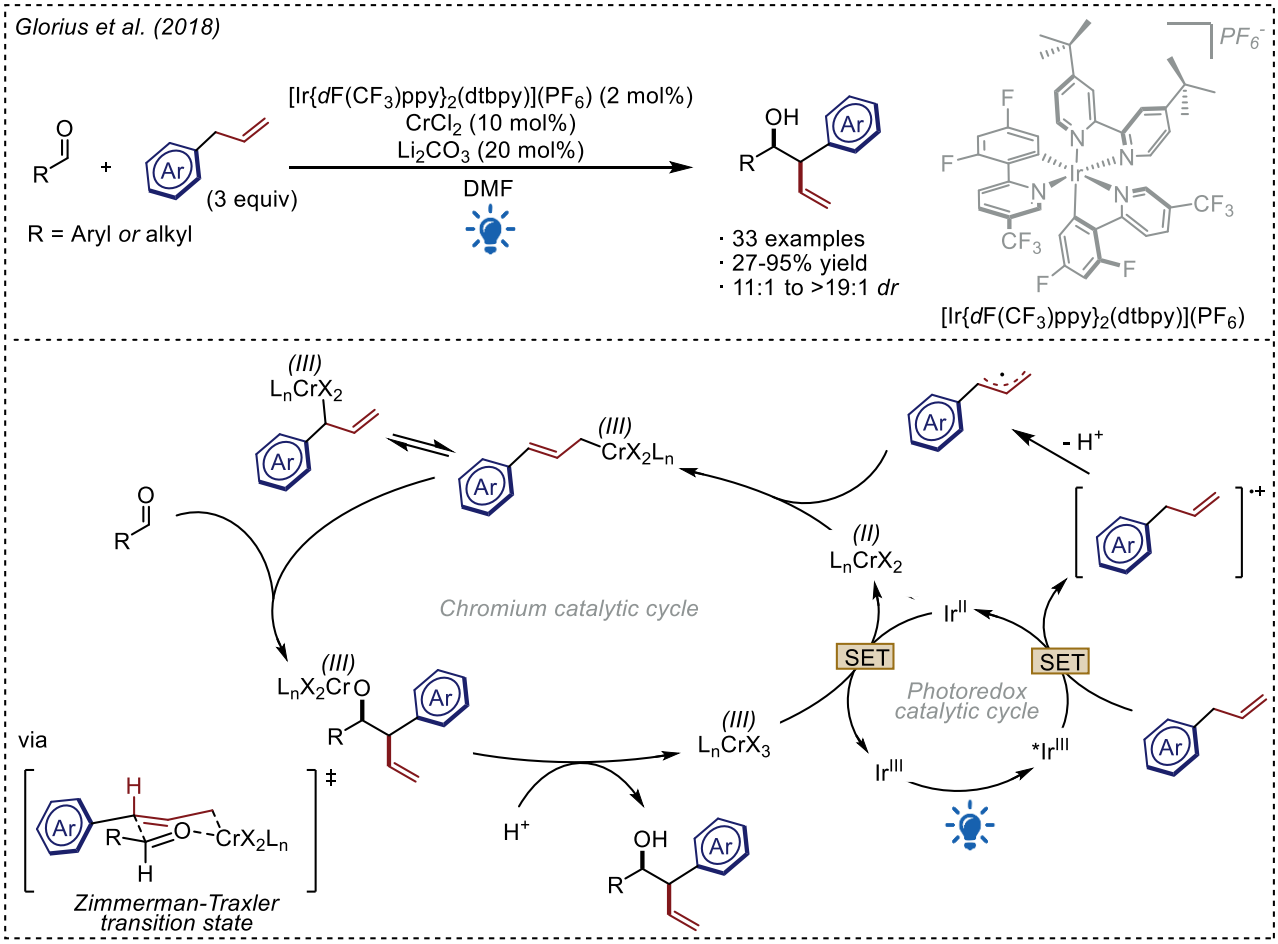

Figure 1.57 First dual photoredox- and chromium-catalyzed allylation of aldehydes reported by the Glorius group exploiting the RRPCO concept.

The mechanism involves the reductive quenching of the excited *Ir(III) photocatalyst ($^*E_{red}(Ir^{III}*/Ir^{II})$ = +1.21 V *vs* SCE in MeCN) by the allyl source leading to an allylic radical cation intermediate, which can be deprotonated by the catalytic base to give a radical allyl source which can then be trapped by the Cr(II) with the formation of a transient nucleophilic allyl-chromium(III) intermediate. The latter can

undergo a 1,2 nucleophilic addition to the carbonyl leading to the homoallylic chromium(III) alkoxide. The subsequent hydrolysis of the chromium alkoxide produces the desired homoallylic alcohol and a Cr(III) species which is supposed to be reduced ($E_{red}(Cr^{III}/Cr^{II})$ = −0.51 V *vs* SCE in DMF) by the Ir(II) ($E_{red}(Ir^{III}/Ir^{II})$ = −1.37 V *vs* SCE) thus restoring both the catalytic cycles. The high diastereoselectivity in favour of the *syn*-diastereoisomer is attributed to a cyclic Zimmerman-Traxler transition state. The reaction was completely inhibited in the presence of TEMPO as a radical-trapping agent confirming the formation of a free radical in the process. Moreover, using a cyclopropane carbaldehyde as a radical clock substrate, the product was obtained in high yield confirming that no ketyl radicals are involved in the reaction.

The Kanai group in 2019 reported a diastereo- and enantioselective protocol using unactivated alkenes as allyl source, $CrCl_2$ as Cr(II) source and the Fukuzumi photocatalyst (*Figure 1.58*).[169] The strong oxidation power of the excited photocatalyst ($^*E_{red}$(Mes-Acr-Me^{+*}/Mes-Acr-Me$^{\bullet}$) = +2.06 V *vs* SCE) allowed the use of unactivated alkenes, while the low reduction power of the reduced photocatalyst (E_{red}(Mes-Acr-Me^{+}/Mes-Acr-Me$^{\bullet}$) = −0.57 V *vs* SCE) was nevertheless sufficient to reduce the Cr(III) to an active Cr(II) species ($E_{red}(Cr^{III}/Cr^{II})$ = −0.51 V *vs* SCE in DMF). Again, the presence of radical intermediates were demonstrated using TEMPO as a radical-trapping agent. The diastereoselectivity was explained again by a Zimmerman-Traxler transition state, while the enantioselectivity of the protocol was ensured by an aminoindanol-derived bis(oxazoline).

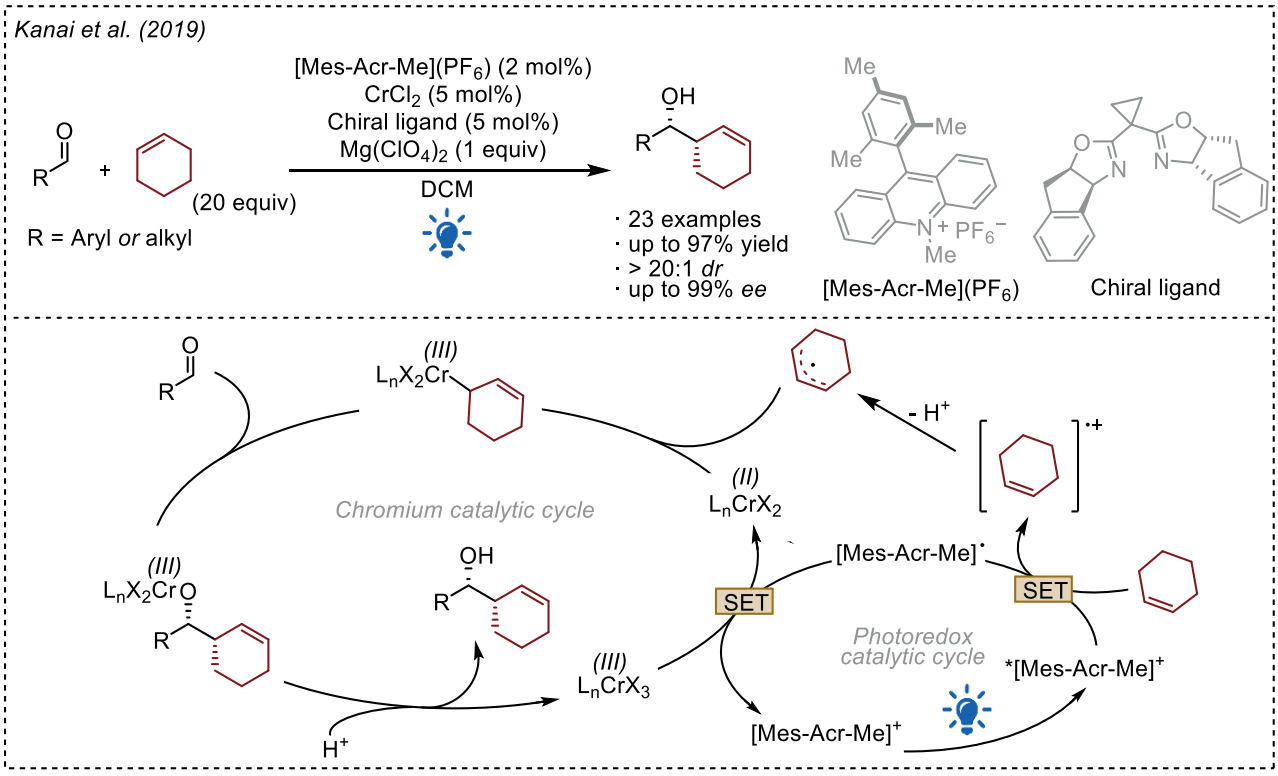

Figure 1.58 Dual photoredox- and chromium-catalyzed allylation of aldehydes reported by the Kanai group exploiting the RRPCO concept.

Both protocols were limited to relatively electron-rich alkenes, respectively α-aryl- or α-amino alkenes for Glorius' protocol and cyclic or tri- and tetrasubstituted alkenes for Kanai's protocol. Using a similar photoredox approach but introducing a HAT catalyst, the Kanai group was able to extend the applicability of the protocol to various inert alkenes that could not be directly oxidized (E_{ox} > +2.5 V *vs* SCE).[170] Under these conditions, 1-butene, 2-butene and 3-methyl-1-butene could be successfully used as allylic precursors in a diastereo- and enantioselective fashion (*Figure 1.59*).

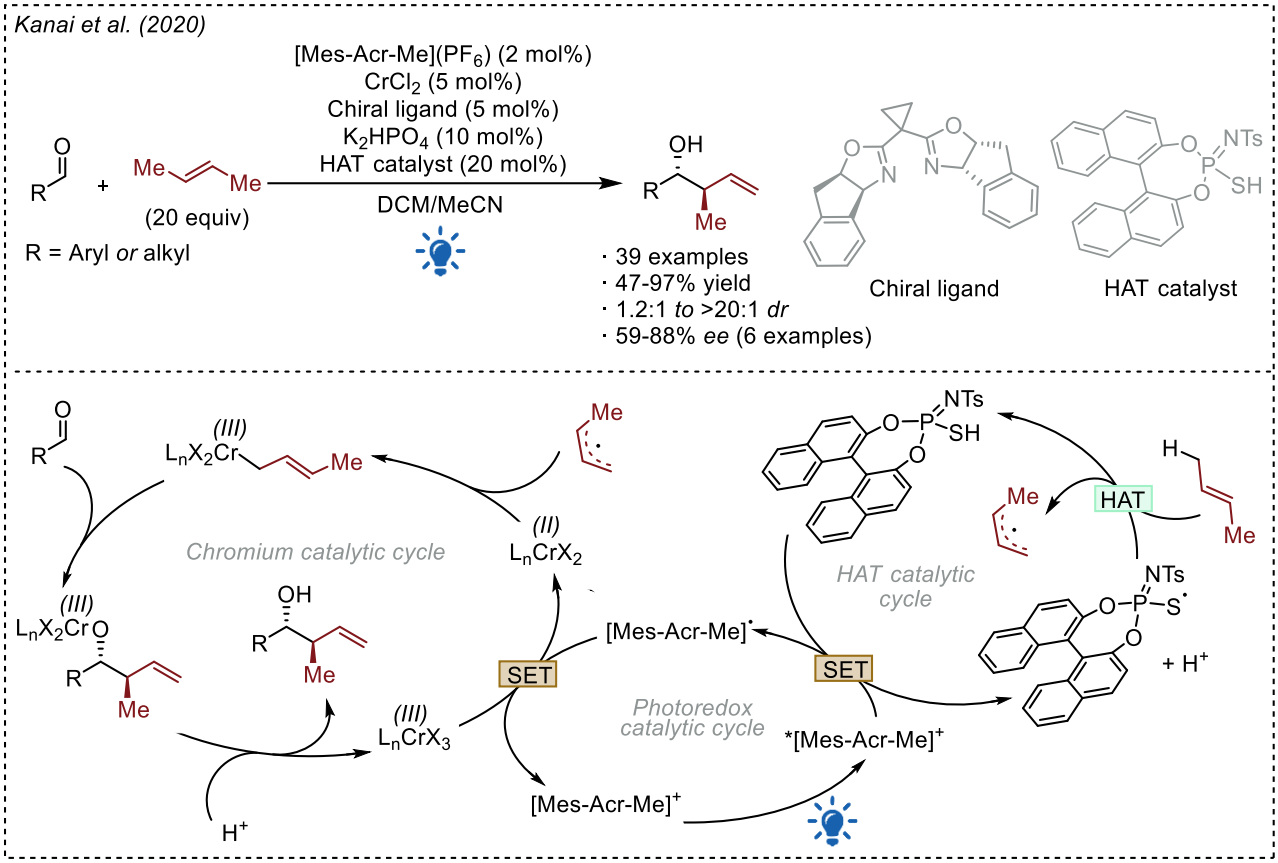

Figure 1.59 Triple photoredox-, chromium- and HAT-catalyzed allylation of aldehydes reported by the Kanai group using unactivated allyl sources.

In the dual photoredox/chromium arena, the Glorius group reported in the same year a diastereoselective allylation protocol using two radical sources: 1,3-dienes as the starting material and structural simple allylic source and substituted 1,4-dihydropyridines (*Figure 1.60*).[171] The dihydropyridine is responsible for the reductive quenching of the organic photocatalyst 4CzIPN. The dihydropyridine radical cation, upon rearomatization releases the relative pyridine and liberates an alkyl radical, which is trapped by 1,3-butadiene forming *in situ* the allyl radical which is then coupled with a Cr(II) leading to the nucleophilic allyl-Cr(III) intermediate. This strategy allows the formation of quaternary homoallylic alcohols with high structural diversity. The enantioselectivity was briefly tested with the same chiral ligand used by Kanai[170] with excellent enantioselectivity but reduced diastereoselectivity.

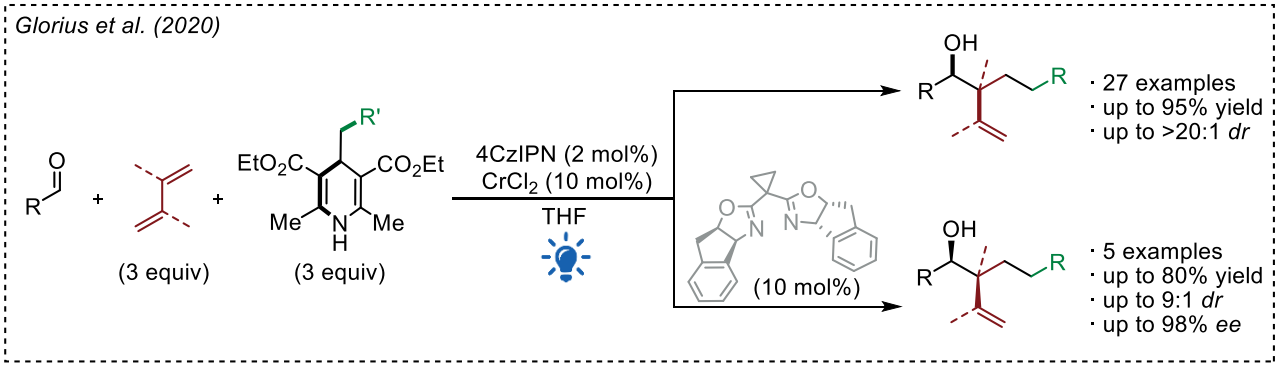

Figure 1.60 Dual photoredox- and chromium-catalyzed allylation of aldehydes reported by the Glorius group using two different radical sources to assemble in situ the allyl source and preliminary enantioselective variant of the protocol.

The four examples described so far demonstrate the versatility and robustness of the dual photoredox/chromium platform and show the enormous structural diversity that can be achieved. However, the simpler allyl moiety cannot be introduced under any of these protocols. To overcome this limitation, the Cozzi group has recently reported a dual photoredox and chromium Nozaki-Hiyama reaction using allyl bromide as the allyl source, $CrCl_3 \cdot 3THF$ as Cr(III)-source, 5CzBN as the organic photocatalyst, and Hantzsch ester as the stoichiometric reducing agent under blue light irradiation (*Figure 1.61*).[172] An important aspect of this work compared to the works described above is the use of an air-stable chromium(III) complex compared to the air-sensitive chromium(II), which requires handling under inert atmosphere.

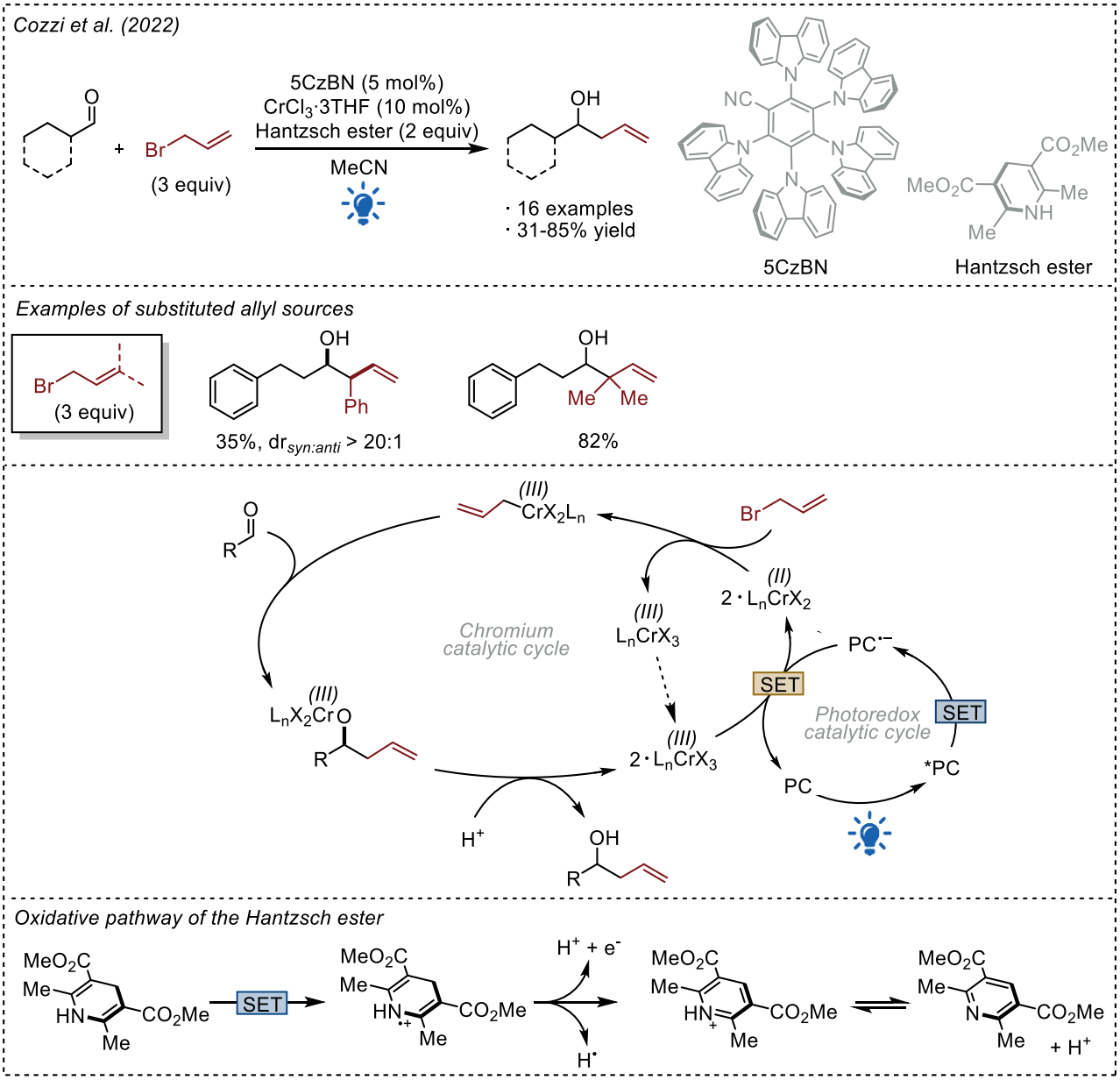

Figure 1.61 Dual photoredox- and chromium-catalyzed allylation of aldehydes reported by the Cozzi group using allylbromide as the allyl source.

The mechanism involves the reductive quenching of the excited *5CzBN ($*E_{red}$(*5CzBN/5CzBN$^{\bullet-}$) = +1.31 V *vs* SCE) by the Hantzsch ester (E_{ox}(HE$^{\bullet+}$/HE) = +1.0 V *vs* SCE). The reduced photocatalyst can reduce (E_{red}(5CzBN/5CzBN$^{\bullet-}$) = –1.52 V *vs* SCE) the Cr(III) salt to an active Cr(II) (E_{red}(Cr^{III}/Cr^{II}) = −0.51 V

vs SCE in DMF) triggering its catalytic activity. Due to the high reduction potential of the excited photocatalyst ($*E_{ox}$(5CzBN$^{\bullet+}$/*5CzBN) = –1.42 V *vs* SCE) the reduction of Cr(III) could be thermodynamically favoured. However, a quenching efficiency η_q = 0.6% for the Cr(III) salt has been calculated (see Equation 17). The reduction of $CrCl_3$·3THF is characterized by a large inner sphere reorganization energy and a slow electron transfer kinetics, as recently reported by Baran, Reisman and Blackmond.[173] This may explain why a direct oxidative quenching of the photocatalyst by the Cr(III) salt does not occur and a strong reducing agent is required, making it usually necessary to use a Cr(II) salt.

Additionally, two molecules of Cr(II) are required to form the allyl-Cr(III) species: the first one reduces the allyl bromide forming an allyl radical and regenerating a Cr(III) species, while the second one can trap the allyl radical forming the nucleophilic organometallic chromium(III) reagent. Addition to the carbonyl leads to the homoallyl product as chromium alkoxide. Finally, the Cr-O bond is broken by protons derived from the oxidation of the Hantzsch ester radical cation, releasing the product and restoring the metal catalytic cycle.

The main drawback of the reaction is that aromatic aldehydes cannot be used since the activation of the carbonyl by the Brønsted acids generated in the reaction media, i.e. the Hantzsch ester radical cation, in the presence of the strong reductant 5CzBN, both in the ground state and in its excited state, lead only to the non-diastereoselective pinacol coupling. The protocol was briefly investigated with substituted allyl bromides, with good yields and excellent regio- and diastereocontrol in favour of the *syn*-diastereoisomer, as expected from a Zimmerman-Traxler transition state.

Finally, chromium is a versatile metal that can provide several useful bond manipulations. A great deal of research has been carried out in the recent decades and the combination of its activity under photoredox conditions allows the introduction of molecular complexity under mild and catalytic conditions. Research into new transformations is still active,[174,175] as in the case of the diastereo- and enantioselective protocol reported by the Wang group for the synthesis of densely functionalized chiral allenols (*Figure 1.62*).[174]

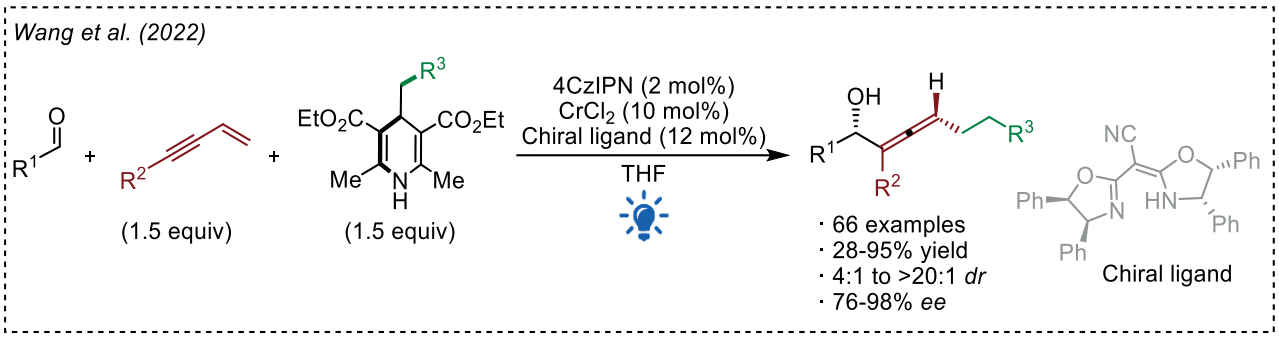

Figure 1.62 Dual photoredox- and chromium-catalyzed enantioselective synthesis of allenols reported by the Wang group.

1.6.3.4 Dual photoredox and titanium processes

Titanium is one of the most abundant transition metals on Earth, and has attracted particular attention because it is considered to be non-toxic and biocompatible, relatively inexpensive and environmentally friendly.[176] In the literature it is widely reported in many C-C, C-O and C-N bond-forming protocols as well as in several name reactions involving redox processes, e.g. Pauson-Khand,[177] Kulinkovich,[178] Reformatsky,[179] or McMurry reductive couplings,[180–182] or in radical reactions,[183] e.g. in the opening and transformation of epoxide rings[184] and in pinacol coupling reactions.[185] For these reasons, there has

been great interest in the use of titanium in the manipulation of small molecules, in the synthesis of fine chemicals[186] and natural products.[181,187–189]

The wide range of organic titanium-mediated transformations is due to the easy accessibility of Ti(III) oxidation state and, albeit under harsher conditions, of Ti(II) oxidation state,[190–193] triggering their different and unique reactivities. Since the broad development and application of this chemistry and the reactivity of Ti(II) complexes is beyond the purpose of this introduction, only the reactivity of Ti(III) will be discussed.

The reactivity of Ti(III) as a single electron transfer agent is dominated by titanocene chloride Cp_2TiCl, which is readily available from the bench-stable and inexpensive Cp_2TiCl_2.[194] First reported by the Wilkinson group in 1955[195] and studied in more detail by the Green group in 1972,[196] the synthesis involves the reduction of Cp_2TiCl_2 in THF in the presence of zinc metal, or other metals such as Al(0) or Mn(0),[197] followed by recrystallization from diethyl ether. In the solid state, the Ti(III) complex exists as the dimeric species $[Cp_2TiCl]_2$, whereas in the presence of a coordinating solvent such as THF, the dimer exists in equilibrium with the monomeric $Cp_2Ti(THF)Cl$ species, which may be considered as a loosely solvated "transition-metal-centered radical'' (*Figure 1.63*).[198] The Cp_2TiCl has an empty coordination site, that allows heteroatoms with free valence electrons to perform electron transfer via an inner-sphere mechanism.

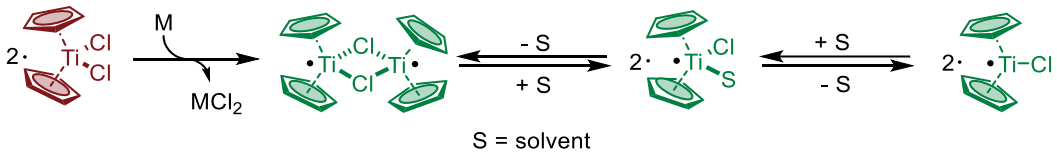

Figure 1.63 Equilibrium of Ti(III) species after the reduction of Cp_2TiCl_2 by a metal reductant M.

The complex is a greenish solid that can be stored for long periods in a nitrogen-filled glovebox. The first stoichiometric applications were reported in 1988 and 1994 by Nugent and Rajanbabu in the Ti(III)-mediated reduction of epoxides.[184,199] Different epoxide manipulations were reported, such as deoxygenation (**A**) and reductive ring opening (**B**) (*Figure 1.64*). Moreover, the authors reported many examples of a tandem ring opening procedure followed by epoxyolefin cyclization. The mechanism was investigated experimentally by isotopically labelled solvents and quenchers, and the evidence suggests that after the Cp_2TiCl-mediated one-electron reduction of the epoxide ring and the subsequent ring opening, the radical thus formed can be trapped by a second Cp_2TiCl if its concentration is kept high (case **A**, in which a solution of the epoxide is added dropwise into a solution of Cp_2TiCl) leading to a polar elimination process and the formation of the olefin, whereas if the concentration is kept as low as possible (case **B**, in which a solution of Cp_2TiCl is added dropwise into a solution of the epoxide), the intermediate can be trapped by other species, e.g. by a $H^{\bullet}$ derived from 1,4-cyclohexadiene (CHD) or from the solvent.

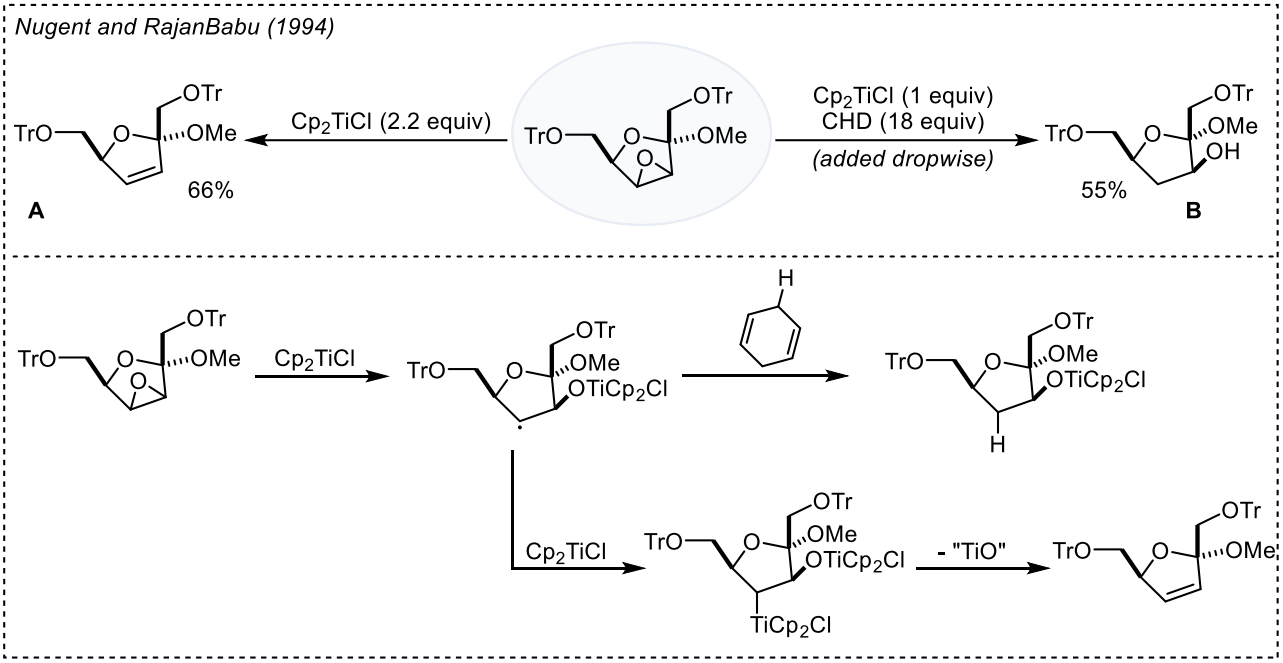

Figure 1.64 Titanium-mediated epoxide ring opening protocols reported by Nugent and RajanBabu.

At this stage, although Nugent and RajanBabu demonstrated the usefulness of Cp_2TiCl as a SET reagent, the main drawback was that it had to be used in a stoichiometric amount. Preliminary catalytic applications of Ti(III) complexes were described by the reduction of Cp_2TiCl_2 with organolithium reagents[200,201] or Grignard reagents[202,203] generating Cp_2TiR (R = alkyl) species, which possess a high electron density at the metal and are capable of reducing carbonyls groups. A major contribution was made by the Gansäuer group, which introduced stoichiometric metal reductants such as elemental zinc or manganese as cheap reductants (*Figure 1.65*).[204]

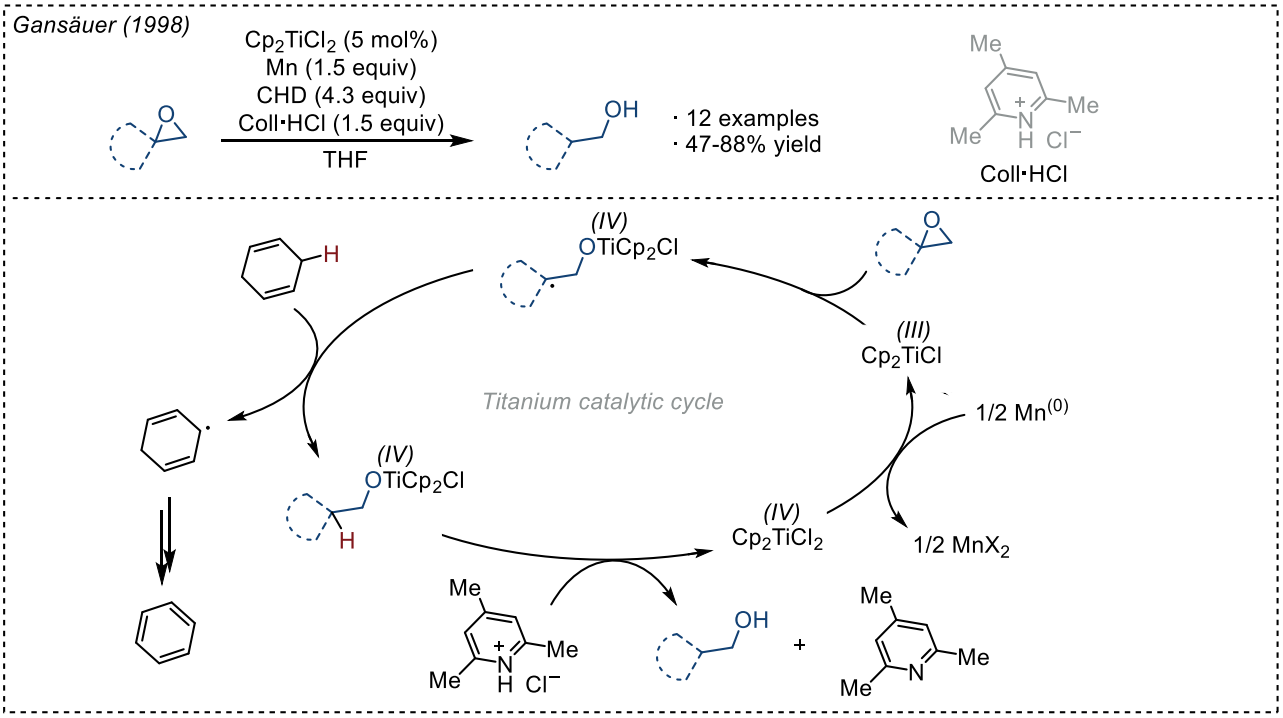

Figure 1.65 First titanium-catalyzed epoxide ring opening protocol reported by the Gansäuer group.

In particular, Mn dust can generate *in situ* Cp_2TiCl from the bench stable Cp_2TiCl_2 triggering its reactivity for the SET reduction and the opening of the epoxide ring with the concomitant formation of a strong Ti-O bond and a C-centered radical. The regiochemistry of the process is dictated by the formation of the more substituted C-radical. The latter can abstract a $H^{\bullet}$ from the CHD leading to the product protected as titanium alkoxide. Finally, Ti-O bond is broken by protons derived from the collidinium hydrochloride restoring the titanium catalytic cycle and releasing the desired product.

Although titanium is used in a catalytic amount, the need for a stoichiometric metal reductant to sustain the titanium catalytic cycle is associated with a large production of metal waste. As already pointed out in the previous sections, photoredox catalysis can replace the reductive behavior of metals with a milder photoredox catalytic cycle. From this perspective, the first important example of a dual photoredox/titanium platform in the epoxide ring opening was reported by the Gansäuer group in 2019 (*Figure 1.66 A*).[205] In the same work, the reactivity of titanium in low oxidation state was exploited in a tandem epoxide ring-opening-cyclization process to form indoline derivatives (*Figure 1.66 B*).

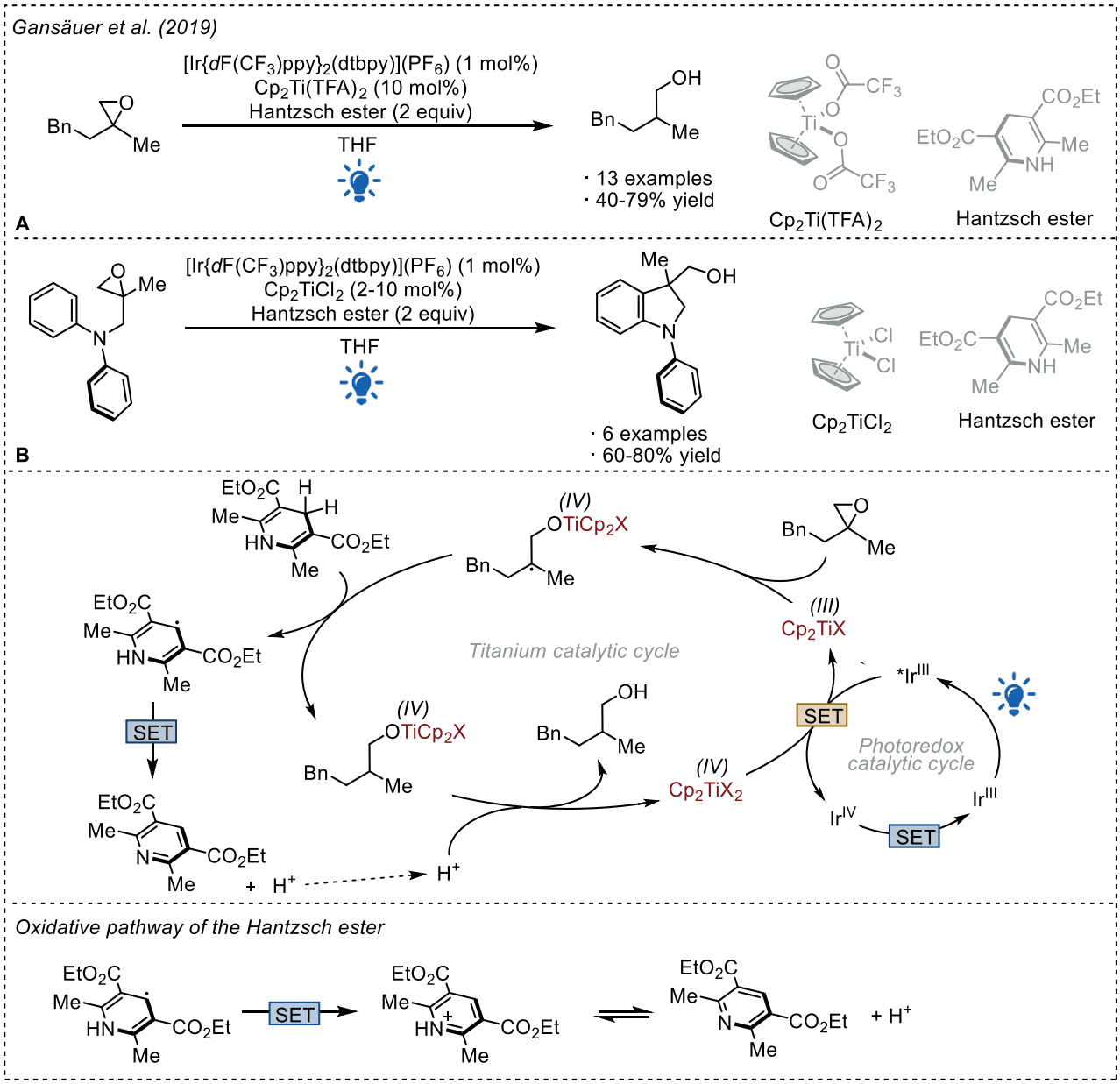

*Figure 1.66 Dual photoredox- and titanium-catalyzed **A**) epoxide ring opening and **B**) tandem epoxide ring-opening-cyclization process to form indoline derivatives reported by the Gansäuer group.*

The mechanism involves the oxidative quenching of the Ir-based photocatalyst ($*E_{ox}(Ir^{IV}/*Ir^{III})$ = –0.89 V *vs* SCE) by the titanocene complex $Cp_2Ti(CF_3CO_2)_2$ ($E_{red}(Ti^{IV}/Ti^{III})$ = –0.89 V *vs* SCE) forming a Ti(III) species and triggering its reactivity towards the epoxide. The epoxide ring opening event leads to a titanium alkoxide radical intermediate which can abstract a proton from the Hantzsch ester via a PCET mechanism generating a 1,4-dihydropyridine radical intermediate. The oxidized Ir(IV) photocatalyst can be reduced ($E_{ox}(Ir^{IV}/Ir^{III})$ = +1.69 V *vs* SCE) by the stoichiometric Hantzsch ester ($E_{ox}(HE^{\bullet+}/HE)$ = +1.0 V *vs* SCE) or by the 1,4-dihydropyridine radical intermediate restoring the photocatalytic cycle and leading to the rearomatized pyridinium salt. The latter acts as a scavenger for the Ti-O bond forming the free alcohol and liberating the Ti(IV).

The Doyle group in 2020 extended the application of the dual photoredox/titanium platform by coupling it with a Ni-mediated cross-coupling with aryl iodides (*Figure 1.67*).[206] The protocol was investigated with benzylic, aliphatic and cyclic aliphatic epoxides.

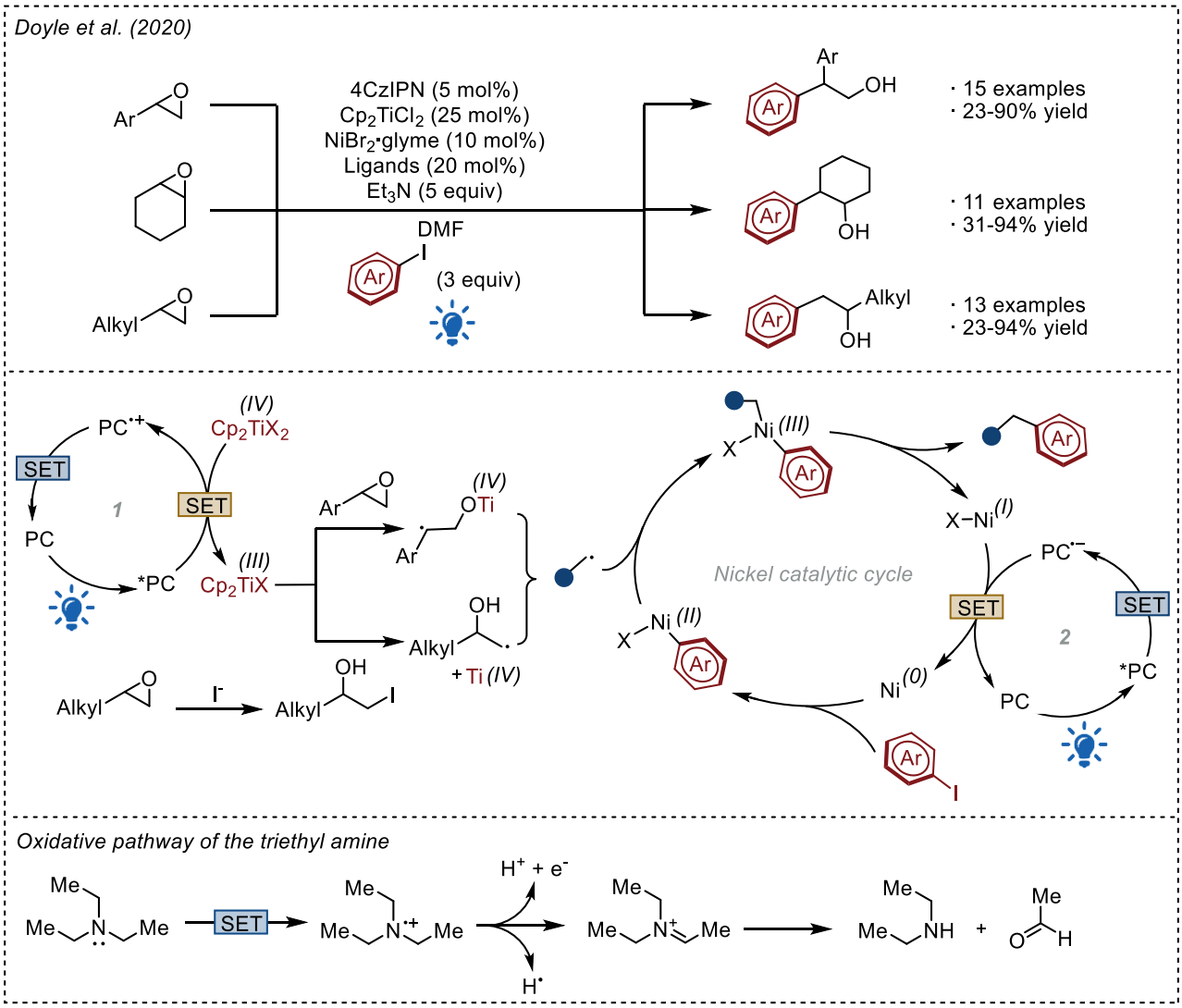

Figure 1.67 Triple photoredox-, titanium- and nickel-catalyzed epoxide ring opening arylation reported by the Doyle group.

The mechanism is complex and has been studied in detail. From the Stern-Volmer quenching experiments, it can proceed either by 1. an oxidative quenching of the organic photocatalyst 4CzIPN ($*E_{ox}(4CzIPN^{\bullet+}/*4CzIPN)$ = –1.18 V *vs* SCE) by the Cp_2TiCl_2 ($E_{red}(Ti^{IV}/Ti^{III})$ = –0.57 V *vs* SCE) or by 2. a reductive quenching of the photocatalyst ($*E_{red}(*4CzIPN/4CzIPN^{\bullet-})$ = +1.43 V *vs* SCE) by the

stoichiometric amine ($E_{ox}(Et_3N^{\bullet+}/Et_3N)$ = +0.93 V *vs* SCE). The two catalytic cycles work cooperatively forming respectively the active Ti(III) and Ni(0) species.

From the catalytic cycle 1. after the oxidative quenching of the photocatalyst, the turnover of the photocatalytic cycle is ensured by the reduction of $4CzIPN^{\bullet+}$ ($E_{ox}(4CzIPN^{\bullet+}/4CzIPN)$ = +1.49 V *vs* SCE) by the amine ($E_{ox}(Et_3N^{\bullet+}/Et_3N)$ = +0.93 V *vs* SCE). The Cp_2TiCl formed *in situ* can carry out the ring-opening reaction leading to a titanium-alkoxide radical intermediate.

From the catalytic cycle 2. after the reductive quenching of the photocatalyst, $4CzIPN^{\bullet-}$ can reduce ($E_{red}(4CzIPN/4CzIPN^{\bullet-})$ = –1.24 V *vs* SCE) the Ni(I) intermediate ($E_{red}(Ni^{I}/Ni^{0})$ = –1.17 V *vs* SCE) recovering both the nickel and the photocatalytic cycle. The Ni(0) species undergoes oxidative addition with the aryl iodide and can then react with the titanium alkoxide radical intermediate formed in the cycle 1. Reductive elimination and proton scavenging leads to the desired product liberating both the Ni(I) and Ti(IV) species and restoring the metal catalytic cycles.

In the case of terminal alkyl substituted epoxides, the formation of a transient iodohydrin should occur. In this case, Ti(III) acts as a halogen-atom-abstractor (HAA) restoring the titanium catalytic cycle and leading the formation of a nucleophilic C-centered radical which reacts into the nickel catalytic cycle.

As we have seen, photoredox catalysis is complex and requires, especially when applied to metal cycles, considerable and varied skills. These skills were applied during my PhD in the investigation of various processes.

1.7 Bibliography

[1] L. Buzzetti, G. E. M. Crisenza, P. Melchiorre, *Angew. Chem. Int. Ed.* **2019**, *58*, 3730–3747.
[2] V. Balzani, P. Ceroni, A. Juris, *Photochemistry and Photophysics: Concepts, Research, Applications, First Edition*, Wiley-VCH Verlag GmbH & Co, Weinheim, **2014**.
[3] B. Reiß, Q. Hu, E. Riedle, H.-A. Wagenknecht, *ChemPhotoChem* **2021**, *5*, 1009–1019.
[4] M. Kasha, *Discuss. Faraday Soc.* **1950**, *9*, 14–19.
[5] N. A. Romero, D. A. Nicewicz, *Chem. Rev.* **2016**, *116*, 10075–10166.
[6] F. Strieth-Kalthoff, M. J. James, M. Teders, L. Pitzer, F. Glorius, *Chem. Soc. Rev.* **2018**, *47*, 7190–7202.
[7] A. Kaur, P. Kaur, S. Ahuja, *Anal. Methods* **2020**, *12*, 5532–5550.
[8] S. Bai, P. Zhang, D. N. Beratan, *J. Phys. Chem. C* **2020**, *124*, 18956–18960.
[9] L. Capaldo, D. Ravelli, M. Fagnoni, *Chem. Rev.* **2022**, *122*, 1875–1924.
[10] D. C. Duncan, M. A. Fox, *J. Phys. Chem. A* **1998**, *102*, 4559–4567.
[11] V. D. Waele, O. Poizat, M. Fagnoni, A. Bagno, D. Ravelli, *ACS Catal.* **2016**, *6*, 7174–7182.
[12] P. J. Sarver, V. Bacauanu, D. M. Schultz, D. A. DiRocco, Y. Lam, E. C. Sherer, D. W. C. MacMillan, *Nat. Chem.* **2020**, *12*, 459–467.
[13] Z. Yuan, R. Britton, *Chem. Sci.* **2023**, *14*, 12883–12897.
[14] D. M. Hedstrand, W. H. Kruizinga, R. M. Kellogg, *Tetrahedron Lett.* **1978**, *19*, 1255–1258.
[15] T. J. Van Bergen, D. M. Hedstrand, W. H. Kruizinga, R. M. Kellogg, *J. Org. Chem.* **1979**, *44*, 4953–4962.
[16] C. Pac, M. Ihama, M. Yasuda, Y. Miyauchi, H. Sakurai, *J. Am. Chem. Soc.* **1981**, *103*, 6495–6497.
[17] C. Pac, Y. Miyauchi, O. Ishitani, M. Ihama, M. Yasuda, H. Sakurai, *J. Org. Chem.* **1984**, *49*, 26–34.
[18] O. Ishitani, M. Ihama, Y. Miyauchi, C. Pac, *J. Chem. Soc. Perkin 1* **1985**, 1527–1531.
[19] O. Ishitani, C. Pac, H. Sakurai, *J. Org. Chem.* **1983**, *48*, 2941–2942.
[20] O. Ishitani, S. Yanagida, S. Takamuku, C. Pac, *J. Org. Chem.* **1987**, *52*, 2790–2796.
[21] K. Hironaka, S. Fukuzumi, T. Tanaka, *J. Chem. Soc. Perkin Trans. 2* **1984**, 1705–1709.
[22] S. Fukuzumi, S. Koumitsu, K. Hironaka, T. Tanaka, *J. Am. Chem. Soc.* **1987**, *109*, 305–316.
[23] M. A. Ischay, M. E. Anzovino, J. Du, T. P. Yoon, *J. Am. Chem. Soc.* **2008**, *130*, 12886–12887.
[24] J. Du, L. R. Espelt, I. A. Guzei, T. P. Yoon, *Chem Sci* **2011**, *2*, 2115–2119.
[25] J. M. R. Narayanam, J. W. Tucker, C. R. J. Stephenson, *J. Am. Chem. Soc.* **2009**, *131*, 8756–8757.
[26] J. D. Nguyen, E. M. D'Amato, J. M. R. Narayanam, C. R. J. Stephenson, *Nat. Chem.* **2012**, *4*, 854–859.
[27] D. A. Nicewicz, D. W. C. MacMillan, *Science* **2008**, *322*, 77–80.
[28] E. Vitaku, D. T. Smith, J. T. Njardarson, *J. Med. Chem.* **2014**, *57*, 10257–10274.
[29] A. M. de P. Nicholas, D. R. Arnold, *Can. J. Chem.* **1982**, *60*, 2165–2179.
[30] A. McNally, C. K. Prier, D. W. C. MacMillan, *Science* **2011**, *334*, 1114–1117.
[31] A. G. Condie, J. C. González-Gómez, C. R. J. Stephenson, *J. Am. Chem. Soc.* **2010**, *132*, 1464–1465.
[32] W.-J. Chung, C. D. Vanderwal, *Angew. Chem. Int. Ed.* **2016**, *55*, 4396–4434.
[33] D. Cantillo, C. Oliver Kappe, *React. Chem. Eng.* **2017**, *2*, 7–19.
[34] P. Annamalai, K.-C. Liu, S. S. Badsara, C.-F. Lee, *Chem. Rec.* **2021**, *21*, 3674 – 3688.
[35] S. Marsden, Boronic Acids. Preparation, Applications in Organic Synthesis and Medicine (Ed.: D. Hall), Wiley-VCH Verlag GmbH & Co, Weinheim, **2005**.
[36] D. S. Matteson, in *Reactivity and Structure: Concepts in Organic Chemistry (REACTIVITY, volume 32),* Springer-Verlag, Berlin Heidelberg, **1995**.
[37] D. Leonori, V. K. Aggarwal, *Acc. Chem. Res.* **2014**, *47*, 3174–3183.
[38] A. Sáenz-Galindo, L. I. López-López, F. N. de la Cruz-Duran, A. O. Castañeda-Facio, L. A. Rámirez-Mendoza, K. C. Córdova-Cisneros, D. de Loera-Carrera, A. Sáenz-Galindo, L. I. López-López, F. N. de la Cruz-Duran, A. O. Castañeda-Facio, L. A. Rámirez-Mendoza, K. C. Córdova-Cisneros, D. de Loera-Carrera, in *Carboxylic Acid - Key Role Life Sci.*, IntechOpen, **2018**.

[39] S. B. Beil, T. Q. Chen, N. E. Intermaggio, D. W. C. MacMillan, *Acc. Chem. Res.* **2022**, *55*, 3481–3494.
[40] S. L. Goldschmid, N. E. Soon Tay, C. L. Joe, B. C. Lainhart, T. C. Sherwood, E. M. Simmons, M. Sezen-Edmonds, T. Rovis, *J. Am. Chem. Soc.* **2022**, *144*, 22409–22415.
[41] S. Murarka, *Adv. Synth. Catal.* **2018**, *360*, 1735–1753.
[42] A. Fawcett, J. Pradeilles, Y. Wang, T. Mutsuga, E. L. Myers, V. K. Aggarwal, *Science* **2017**, *357*, 283–286.
[43] J. Wu, C. Shu, Z. Li, A. Noble, V. K. Aggarwal, *Angew. Chem. Int. Ed.* **2023**, *62*, e202309684.
[44] N. W. Dow, P. S. Pedersen, T. Q. Chen, D. C. Blakemore, A.-M. Dechert-Schmitt, T. Knauber, D. W. C. MacMillan, *J. Am. Chem. Soc.* **2022**, *144*, 6163−6172.
[45] P. S. Pedersen, D. C. Blakemore, G. M. Chinigo, T. Knauber, D. W. C. MacMillan, *J. Am. Chem. Soc.* **2023**, *145*, 21189–21196.
[46] Q. Y. Li, S. N. Gockel, G. A. Lutovsky, K. S. DeGlopper, N. J. Baldwin, M. W. Bundesmann, J. W. Tucker, S. W. Bagley, T. P. Yoon, *Nat. Chem.* **2022**, *14*, 94–99.
[47] S. P. Pitre, L. E. Overman, *Chem. Rev.* **2022**, *122*, 1717–1751.
[48] Y. Sun, R. Li, W. Zhang, A. Li, *Angew. Chem. Int. Ed.* **2013**, *52*, 9201 –9204.
[49] D. J. Tao, Y. Slutskyy, M. Muuronen, A. Le, P. Kohler, L. E. Overman, *J. Am. Chem. Soc.* **2018**, *140*, 3091–3102; *J. Am. Chem. Soc.* **2019**, *141*, 706.
[50] Y. Slutskyy, C. R. Jamison, P. Zhao, J. Lee, Y. H. Rhee, L. E. Overman, *J. Am. Chem. Soc.* **2017**, *139*, 7192–7195.
[51] J. Li, J. Ren, S. Li, G. Li, M. M.-J. Li, R. Li, Y. S. Kang, X. Zou, Y. Luo, B. Liu, Y. Zhao, *Green Energy Environ.* **2024**, *9*, 859–876.
[52] Z. Kuspanov, B. Bakbolat, A. Baimenov, A. Issadykov, M. Yeleuov, C. Daulbayev, *Sci. Total Environ.* **2023**, *885*, 163914.
[53] S. Cañellas, M. Nuño, E. Speckmeier, *Nat. Commun.* **2024**, *15*, 307.
[54] J. Dhainaut, A. Dlubala, R. Guevel, A. Medard, G. Oddon, N. Raymond, J. Turconi, **2011**.
[55] J. Turconi, F. Griolet, R. Guevel, G. Oddon, R. Villa, A. Geatti, M. Hvala, K. Rossen, R. Göller, A. Burgard, *Org. Process Res. Dev.* **2014**, *18*, 417–422.
[56] C. Förster, K. Heinze, *Chem. Soc. Rev.* **2020**, *49*, 1057–1070.
[57] L. Flamigni, A. Barbieri, C. Sabatini, B. Ventura, F. Barigelletti, in *Photochem. Photophysics Coord. Compd. II* (Eds.: V. Balzani, S. Campagna), Springer, Berlin, Heidelberg, **2007**, 143–203.
[58] C. K. Prier, D. A. Rankic, D. W. C. MacMillan, *Chem. Rev.* **2013**, *113*, 5322–5363.
[59] J. Twilton, C. (Chip) Le, P. Zhang, M. H. Shaw, R. W. Evans, D. W. C. MacMillan, *Nat. Rev. Chem.* **2017**, *1*, 1–19.
[60] K. Teegardin, J. I. Day, J. Chan, J. Weaver, *Org. Process Res. Dev.* **2016**, *20*, 1156–1163.
[61] V. Balzani, A. Juris, M. Venturi, S. Campagna, S. Serroni, *Chem. Rev.* **1996**, *96*, 759–834.
[62] D. M. Arias-Rotondo, J. K. McCusker, *Chem. Soc. Rev.* **2016**, *45*, 5803-5820.
[63] A. F. Henwood, E. Zysman-Colman, *Chem. Commun.* **2017**, *53*, 807–826.
[64] M. S. Lowry, S. Bernhard, *Chem. Eur. J.* **2006**, *12*, 7970–7977.
[65] S. DiLuzio, T. U. Connell, V. Mdluli, J. F. Kowalewski, S. Bernhard, *J. Am. Chem. Soc.* **2022**, *144*, 1431–1444.
[66] M. S. Lowry, J. I. Goldsmith, J. D. Slinker, R. Rohl, R. A. Pascal, G. G. Malliaras, S. Bernhard, *Chem. Mater.* **2005**, *17*, 5712–5719; *Chem. Mater.* **2023**, *35*, 1466.
[67] D. Volz, M. Wallesch, C. Fléchon, M. Danz, A. Verma, J. M. Navarro, D. M. Zink, S. Bräse, T. Baumann, *Green Chem.* **2015**, *17*, 1988–2011.
[68] C. Bizzarri, E. Spuling, D. M. Knoll, D. Volz, S. Bräse, *Coord. Chem. Rev.* **2018**, *373*, 49–82.
[69] A. Gualandi, M. Marchini, L. Mengozzi, M. Natali, M. Lucarini, P. Ceroni, P. G. Cozzi, *ACS Catal.* **2015**, *5*, 5927–5931.
[70] J. Beaudelot, S. Oger, S. Peruško, T.-A. Phan, T. Teunens, C. Moucheron, G. Evano, *Chem. Rev.* **2022**, *122*, 16365–16609.
[71] L. A. Büldt, O. S. Wenger, *Chem. Sci.* **2017**, *8*, 7359–7367.

[72] C. Onneken, T. Morack, J. Soika, O. Sokolova, N. Niemeyer, C. Mück-Lichtenfeld, C. G. Daniliuc, J. Neugebauer, R. Gilmour, *Nature* **2023**, *621*, 753–759.
[73] D. C. Harrowven, I. L. Guy, L. Nanson, *Angew. Chem. Int. Ed.* **2006**, *45*, 2242–2245.
[74] B. Laleu, P. Mobian, C. Herse, B. W. Laursen, G. Hopfgartner, G. Bernardinelli, J. Lacour, *Angew. Chem.* **2005**, *117*, 1913–1917.
[75] B. Laleu, M. S. Machado, J. Lacour, *Chem. Commun.* **2006**, 2786–2788.
[76] B. W. Laursen, F. C. Krebs, M. F. Nielsen, K. Bechgaard, J. B. Christensen, N. Harrit, *J. Am. Chem. Soc.* **1998**, *120*, 12255–12263.
[77] G. A. Olah, *Angew. Chem. Int. Ed. Engl.* **1973**, *12*, 173–212.
[78] B. W. Laursen, F. C. Krebs, *Chem. Eur. J.* **2001**, *7*, 1773–1783.
[79] T. J. Sørensen, M. F. Nielsen, B. W. Laursen, *ChemPlusChem* **2014**, *79*, 1030–1035.
[80] C. Nicolas, C. Herse, J. Lacour, *Tetrahedron Lett.* **2005**, *46*, 4605–4608.
[81] L. Mei, J. M. Veleta, T. L. Gianetti, *J. Am. Chem. Soc.* **2020**, *142*, 12056–12061.
[82] A. C. Shaikh, J. Moutet, J. M. Veleta, M. Mubarak Hossain, J. Bloch, A. V. Astashkin, T. L. Gianetti, *Chem. Sci.* **2020**, *11*, 11060–11067.
[83] F. Calogero, G. Magagnano, S. Potenti, F. Pasca, A. Fermi, A. Gualandi, P. Ceroni, G. Bergamini, P. G. Cozzi, *Chem. Sci.* **2022**, *13*, 5973–5981.
[84] E. Pinosa, Y. Gelato, F. Calogero, M. M. Moscogiuri, A. Gualandi, A. Fermi, P. Ceroni, P. G. Cozzi, *Adv. Synth. Catal.* **2024**, *366*, 798-805.
[85] M. H. Nowack, J. Moutet, B. W. Laursen, T. L. Gianetti, *Synlett* **2023**, *35*, 307–312.
[86] I. H. Delgado, S. Pascal, A. Wallabregue, R. Duwald, C. Besnard, L. Guénée, C. Nançoz, E. Vauthey, R. C. Tovar, J. L. Lunkley, G. Muller, J. Lacour, *Chem. Sci.* **2016**, *7*, 4685–4693.
[87] G. Pandey, M. Karthikeyan, A. Murugan, *J. Org. Chem.* **1998**, *63*, 2867–2872.
[88] H. Uoyama, K. Goushi, K. Shizu, H. Nomura, C. Adachi, *Nature* **2012**, *492*, 234–238.
[89] J. Eng, T. J. Penfold, *Chem. Rec.* **2020**, *20*, 831–856.
[90] E. Speckmeier, T. G. Fischer, K. Zeitler, *J. Am. Chem. Soc.* **2018**, *140*, 15353–15365.
[91] T.-Y. Shang, L.-H. Lu, Z. Cao, Y. Liu, W.-M. He, B. Yu, *Chem. Commun.* **2019**, *55*, 5408–5419.
[92] J. Luo, J. Zhang, *ACS Catal.* **2016**, *6*, 873–877.
[93] C.-Y. Chan, Y.-T. Lee, M. Mamada, K. Goushi, Y. Tsuchiya, H. Nakanotani, C. Adachi, *Chem. Sci.* **2022**,*13*, 7821-7828.
[94] A. Tlili, S. Lakhdar, *Angew. Chem. Int. Ed.* **2021**, *60*, 19526–19549.
[95] M. M. Mastandrea, M. A. Pericàs, *Eur. J. Inorg. Chem.* **2021**, 3421–3431.
[96] Z. Huang, Y. Yang, J. Mu, G. Li, J. Han, P. Ren, J. Zhang, N. Luo, K.-L. Han, F. Wang, *Chin. J. Catal.* **2023**, *45*, 120–131.
[97] A. Kaga, S. Chiba, *ACS Catal.* **2017**, *7*, 4697–4706.
[98] R. F. J. Epping, D. Vesseur, M. Zhou, B. de Bruin, *ACS Catal.* **2023**, *13*, 5428–5448.
[99] R. C. III, B. Lujan, A. Martinez, R. Manasi, J. D. DeBow, K. G. M. Kou, *J. Org. Chem.* **2023**, *88*, 15060–15066.
[100] M. Shee, N. D. P. Singh, *Catal. Sci. Technol.* **2021**, *11*, 742–767.
[101] C. K. Prier, D. W. C. MacMillan, in *Visible Light Photocatal. Org. Chem.*, John Wiley & Sons, Ltd, **2018**, pp. 299–333.
[102] A. E. Allen, D. W. C. MacMillan, *Chem. Sci.* **2012**, *3*, 633–658.
[103] T. D. Beeson, A. Mastracchio, J.-B. Hong, K. Ashton, D. W. C. MacMillan, *Science* **2007**, *316*, 582-585.
[104] M. A. Cismesia, T. P. Yoon, *Chem. Sci.* **2015**, *6*, 5426–5434.
[105] D. A. Nagib, M. E. Scott, D. W. C. MacMillan, *J. Am. Chem. Soc.* **2009**, *131*, 10875–10877.
[106] T. Koike, M. Akita, *Chem. Lett.* **2009**, *38*, 166–167.
[107] H.-W. Shih, M. N. V. Wal, R. L. Grange, D. W. C. MacMillan, *J. Am. Chem. Soc.* **2010**, *132*, 13600–13603.
[108] M. T. Pirnot, D. A. Rankic, D. B. C. Martin, D. W. C. MacMillan, *Science* **2013**, *339*, 1593-1596.
[109] F. R. Petronijević, M. Nappi, D. W. C. MacMillan, *J. Am. Chem. Soc.* **2013**, *135*, 18323–18326.
[110] J. A. Terrett, M. D. Clift, D. W. C. MacMillan, *J. Am. Chem. Soc.* **2014**, *136*, 6858–6861.

[111] L. Dolcini, T. Gandini, R. Castiglioni, A. Bossi, M. Penconi, A. Dal Corso, C. Gennari, L. Pignataro, *J. Org. Chem.* **2023**, *88*, 14283–14291.
[112] M. Berger, D. Carboni, P. Melchiorre, *Angew. Chem. Int. Ed.* **2021**, *60*, 26373–26377.
[113] K. T. Tarantino, P. Liu, R. R. Knowles, *J. Am. Chem. Soc.* **2013**, *135*, 10022–10025.
[114] L. J. Rono, H. G. Yayla, D. Y. Wang, M. F. Armstrong, R. R. Knowles, *J. Am. Chem. Soc.* **2013**, *135*, 17735–17738.
[115] T.-Y. Zou, Q.-W. Zhang, *ChemCatChem* **2024**, *16*, e202301423.
[116] A. Y. Chan, I. B. Perry, N. B. Bissonnette, B. F. Buksh, G. A. Edwards, L. I. Frye, O. L. Garry, M. N. Lavagnino, B. X. Li, Y. Liang, E. Mao, A. Millet, J. V. Oakley, N. L. Reed, H. A. Sakai, C. P. Seath, D. W. C. MacMillan, *Chem. Rev.* **2022**, *122*, 1485–1542.
[117] R. J. Lundgren, M. Stradiotto, in *Ligand Des. Met. Chem.*, John Wiley & Sons, Ltd, **2016**, pp. 1–14.
[118] D. Kalyani, K. B. McMurtrey, S. R. Neufeldt, M. S. Sanford, *J. Am. Chem. Soc.* **2011**, *133*, 18566–18569.
[119] P. Chuentragool, D. Kurandina, V. Gevorgyan, *Angew. Chem. Int. Ed.* **2019**, *58*, 11586–11598.
[120] A. Hossain, A. Bhattacharyya, O. Reiser, *Science* **2019**, *364*, eaav9713.
[121] J.-L. Tu, B. Huang, *Org. Biomol. Chem.* **2024**, *22*, 6650–6664.
[122] Z. Zuo, D. T. Ahneman, L. Chu, J. A. Terrett, A. G. Doyle, D. W. C. MacMillan, *Science* **2014**, *345*, 437–440.
[123] J. C. Tellis, D. N. Primer, G. A. Molander, *Science* **2014**, *345*, 433–436.
[124] R. Wang, P. Fan, C. Wang, *ACS Catal.* **2023**, *13*, 141–146.
[125] A. Gualandi, F. Calogero, D. Corbisiero, E. Pinosa, P. G. Cozzi, *Asian J. Org. Chem.* **2024**, *13*, e202300574.
[126] M. N. Hopkinson, A. Tlahuext-Aca, F. Glorius, *Acc. Chem. Res.* **2016**, *49*, 2261–2272.
[127] F. Calogero, S. Potenti, G. Magagnano, G. Mosca, A. Gualandi, M. Marchini, P. Ceroni, P. G. Cozzi, *Eur. J. Org. Chem.* **2022**, e202200350.
[128] M. Kojima, S. Matsunaga, *Trends Chem.* **2020**, *2*, 410–426.
[129] S. Potenti, A. Gualandi, A. Puggioli, A. Fermi, G. Bergamini, P. G. Cozzi, *Eur. J. Org. Chem.* **2021**, *2021*, 1624–1627.
[130] K. L. Skubi, T. R. Blum, T. P. Yoon, *Chem. Rev.* **2016**, *116*, 10035–10074.
[131] A. Biffis, P. Centomo, A. Del Zotto, M. Zecca, *Chem. Rev.* **2018**, *118*, 2249–2295.
[132] D. Kalyani, N. R. Deprez, L. V. Desai, M. S. Sanford, *J. Am. Chem. Soc.* **2005**, *127*, 7330–7331.
[133] W.-Y. Yu, W. N. Sit, Z. Zhou, A. S.-C. Chan, *Org. Lett.* **2009**, *11*, 3174–3177.
[134] N. K. Kvasovs, V. Gevorgyan, *Chem. Soc. Rev.* **2021**, *50*, 2244-2259.
[135] J. Zoller, D. C. Fabry, M. A. Ronge, M. Rueping, *Angew. Chem. Int. Ed.* **2014**, *53*, 13264–13268.
[136] D. C. Fabry, M. Rueping, *Acc. Chem. Res.* **2016**, *49*, 1969–1979.
[137] K. C. Dissanayake, P. O. Ebukuyo, Y. J. Dhahir, K. Wheeler, H. He, *Chem. Commun.* **2019**, *55*, 4973–4976.
[138] K. Mori, M. Kawashima, H. Yamashita, *Chem. Commun.* **2014**, *50*, 14501–14503.
[139] H. Zhang, X. Huang, *Adv. Synth. Catal.* **2016**, *358*, 3736–3742.
[140] M. Tobisu, T. Xu, T. Shimasaki, N. Chatani, *J. Am. Chem. Soc.* **2011**, *133*, 19505–19511.
[141] S. Z. Tasker, E. A. Standley, T. F. Jamison, *Nature* **2014**, *509*, 299–309.
[142] G. A. Dawson, E. H. Spielvogel, T. Diao, *Acc. Chem. Res.* **2023**, *56*, 3640–3653.
[143] C. Zhu, H. Yue, L. Chu, M. Rueping, *Chem. Sci.* **2020**, *11*, 4051–4064.
[144] O. Gutierrez, J. C. Tellis, D. N. Primer, G. A. Molander, M. C. Kozlowski, *J. Am. Chem. Soc.* **2015**, *137*, 4896–4899.
[145] L.-M. Chen, S. E. Reisman, *Acc. Chem. Res.* **2024**, *57*, 751–762.
[146] D. Ryu, D. N. Primer, J. C. Tellis, G. A. Molander, *Chem. Eur. J.* **2016**, *22*, 120–123.
[147] D. N. Primer, I. Karakaya, J. C. Tellis, G. A. Molander, *J. Am. Chem. Soc.* **2015**, *137*, 2195–2198.
[148] J. Amani, E. Sodagar, G. A. Molander, *Org. Lett.* **2016**, *18*, 732–735.
[149] M. El Khatib, R. A. M. Serafim, G. A. Molander, *Angew. Chem. Int. Ed.* **2016**, *55*, 254–258.
[150] Y. Yasu, T. Koike, M. Akita, *Adv. Synth. Catal.* **2012**, *354*, 3414–3420.
[151] M. Jouffroy, D. N. Primer, G. A. Molander, *J. Am. Chem. Soc.* **2016**, *138*, 475–478.

[152] V. Corcé, L.-M. Chamoreau, E. Derat, J.-P. Goddard, C. Ollivier, L. Fensterbank, *Angew. Chem. Int. Ed.* **2015**, *54*, 11414–11418.
[153] Á. Gutiérrez-Bonet, J. C. Tellis, J. K. Matsui, B. A. Vara, G. A. Molander, *ACS Catal.* **2016**, *6*, 8004–8008.
[154] M. H. Shaw, V. W. Shurtleff, J. A. Terrett, J. D. Cuthbertson, D. W. C. MacMillan, *Science* **2016**, *352*, 1304–1308.
[155] Z. Dong, D. W. C. MacMillan, *Nature* **2021**, *598*, 451–456.
[156] Q. Cai, I. M. McWhinnie, N. W. Dow, A. Y. Chan, D. W. C. MacMillan, *J. Am. Chem. Soc.* **2024**, *146*, 12300–12309.
[157] J. Z. Wang, W. L. Lyon, D. W. C. MacMillan, *Nature* **2024**, *628*, 104–109.
[158] H. A. Sakai, D. W. C. MacMillan, *J. Am. Chem. Soc.* **2022**, *144*, 6185–6192.
[159] T. Gandini, L. Dolcini, L. Di Leo, M. Fornara, A. Bossi, M. Penconi, A. Dal Corso, C. Gennari, L. Pignataro, *ChemCatChem* **2022**, *14*, e202200990.
[160] L. Guillemard, N. Kaplaneris, L. Ackermann, M. J. Johansson, *Nat. Rev. Chem.* **2021**, *5*, 522–545.
[161] H.-J. Lunk, *ChemTexts* **2015**, *1*, 6.
[162] P. G. Cozzi, A. Gualandi, F. Calogero, E. Pinosa, D. Corbisiero, in *Ref. Module Chem. Mol. Sci. Chem. Eng.*, Elsevier, **2024**.
[163] K. Takai, M. Tagashira, T. Kuroda, K. Oshima, K. Utimoto, H. Nozaki, *J. Am. Chem. Soc.* **1986**, *108*, 6048–6050.
[164] H. Jin, J. Uenishi, W. J. Christ, Y. Kishi, *J. Am. Chem. Soc.* **1986**, *108*, 5644–5646.
[165] A. Fürstner, N. Shi, *J. Am. Chem. Soc.* **1996**, *118*, 12349–12357.
[166] M. Bandini, P. G. Cozzi, P. Melchiorre, A. Umani-Ronchi, *Angew. Chem. Int. Ed.* **1999**, *38*, 3357–3359.
[167] L. Pitzer, J. L. Schwarz, F. Glorius, *Chem. Sci.* **2019**, *10*, 8285–8291.
[168] J. L. Schwarz, F. Schäfers, A. Tlahuext-Aca, L. Lückemeier, F. Glorius, *J. Am. Chem. Soc.* **2018**, *140*, 12705–12709.
[169] H. Mitsunuma, S. Tanabe, H. Fuse, K. Ohkubo, M. Kanai, *Chem. Sci.* **2019**, *10*, 3459–3465.
[170] S. Tanabe, H. Mitsunuma, M. Kanai, *J. Am. Chem. Soc.* **2020**, *142*, 12374–12381.
[171] J. L. Schwarz, H.-M. Huang, T. O. Paulisch, F. Glorius, *ACS Catal.* **2020**, *10*, 1621–1627.
[172] F. Calogero, S. Potenti, G. Magagnano, G. Mosca, A. Gualandi, M. Marchini, P. Ceroni, P. G. Cozzi, *Eur. J. Org. Chem.* **2022**, *2022*, e202200350.
[173] Y. Gao, D. E. Hill, W. Hao, B. J. McNicholas, J. C. Vantourout, R. G. Hadt, S. E. Reisman, D. G. Blackmond, P. S. Baran, *J. Am. Chem. Soc.* **2021**, *143*, 9478–9488.
[174] F.-H. Zhang, X. Guo, X. Zeng, Z. Wang, *Nat. Commun.* **2022**, *13*, 5036.
[175] J. Liu, L.-Q. Lu, Y. Luo, W. Zhao, P.-C. Sun, W. Jin, X. Qi, Y. Cheng, W.-J. Xiao, *ACS Catal.* **2022**, *12*, 1879–1885.
[176] M. C. Rodríguez, I. R. García, R. N. R. Maecker, L. P. Morales, J. E. Oltra, A. R. Martínez, *Org. Process Res. Dev.* **2017**, *21*, 911–923.
[177] J. Blanco-Urgoiti, L. Añorbe, L. Pérez-Serrano, G. Domínguez, J. Pérez-Castells, *Chem. Soc. Rev.* **2004**, *33*, 32–42.
[178] S. Okamoto, *Chem. Rec.* **2016**, *16*, 857–872.
[179] L. Sgreccia, M. Bandini, S. Morganti, A. Quintavalla, A. Umani-Ronchi, P. G. Cozzi, *J. Organomet. Chem.* **2007**, *692*, 3191–3197.
[180] A. Bongso, R. Roswanda, Y. Maolana Syah, *RSC Adv.* **2022**, *12*, 15885–15909.
[181] J. E. McMurry, *Chem. Rev.* **1989**, *89*, 1513–1524.
[182] A. de Meijere, S. I. Kozhushkov, A. I. Savchenko, in *Titan. Zircon. Org. Synth.*, John Wiley & Sons, Ltd, **2002**, pp. 390–434.
[183] T. McCallum, X. Wu, S. Lin, *J. Org. Chem.* **2019**, *84*, 14369–14380.
[184] T. V. RajanBabu, W. A. Nugent, *J. Am. Chem. Soc.* **1994**, *116*, 986–997.
[185] A. Chatterjee, N. N. Joshi, *Tetrahedron* **2006**, *62*, 12137–12158.
[186] M. Manßen, L. L. Schafer, *Chem. Soc. Rev.* **2020**, *49*, 6947–6994.

[187] N. M. Padial, E. Roldan-Molina, A. Rosales, M. Álvarez-Corral, I. Rodríguez-García, M. Muñoz-Dorado, J. E. Oltra, in *Stud. Nat. Prod. Chem.* (Ed.: Atta-ur-Rahman), Elsevier, **2018**, pp. 31–71.
[188] J. Justicia, A. G. Campaña, B. Bazdi, R. Robles, J. M. Cuerva, J. E. Oltra, *Adv. Synth. Catal.* **2008**, *350*, 571–576.
[189] S. P. Morcillo, D. Miguel, A. G. Campaña, L. Á. de Cienfuegos, J. Justicia, J. M. Cuerva, *Org. Chem. Front.* **2014**, *1*, 15–33.
[190] F. Sato, H. Urabe, in *Titan. Zircon. Org. Synth.*, John Wiley & Sons, Ltd, **2002**, pp. 319–354.
[191] U. Rosenthal, V. V. Burlakov, in *Titan. Zircon. Org. Synth.*, John Wiley & Sons, Ltd, **2002**, pp. 355–389.
[192] L. B. Kool, M. D. Rausch, H. G. Alt, M. Herberhold, B. Honold, U. Thewalt, *J. Organomet. Chem.* **1987**, *320*, 37-45.
[193] E. M. Zolnhofer, G. B. Wijeratne, T. A. Jackson, S. Fortier, F. W. Heinemann, K. Meyer, J. Krzystek, A. Ozarowski, D. J. Mindiola, J. Telser, *Inorg. Chem.* **2020**, *59*, 6187–6201.
[194] R. J. Enemærke, J. Larsen, T. Skrydstrup, K. Daasbjerg, *J. Am. Chem. Soc.* **2004**, *126*, 7853–7864.
[195] J. M. Birmingham, A. K. Fischer, G. Wilkinson, *Naturwissenschaften* **1955**, *42*, 96–96.
[196] M. L. H. Green, C. R. Lucas, *J Chem Soc Dalton Trans* **1972**, 1000–1003.
[197] A. Rosales, I. Rodríguez-García, J. Muñoz-Bascón, E. Roldan-Molina, N. M. Padial, L. P. Morales, M. García-Ocaña, J. E. Oltra, *Eur. J. Org. Chem.* **2015**, 4567–4591.
[198] R. J. Enemærke, G. H. Hjøllund, K. Daasbjerg, T. Skrydstrup, *Comptes Rendus Académie Sci. - Ser. IIC - Chem.* **2001**, *4*, 435–438.
[199] W. A. Nugent, T. V. RajanBabu, *J. Am. Chem. Soc.* **1988**, *110*, 8561–8562.
[200] E. Klei, J. H. Telgen, J. H. Teuben, *J. Organomet. Chem.* **1981**, *209*, 297–307.
[201] E. Klei, J. H. Teuben, *J. Organomet. Chem.* **1980**, *188*, 97–107.
[202] Y. Zhang, T. Liu, *Synth. Commun.* **1988**, *18*, 2173–2178.
[203] F. Sato, T. Jinbo, M. Sato, *Tetrahedron Lett.* **1980**, *21*, 2171–2174.
[204] A. Gansäuer, H. Bluhm, M. Pierobon, *J. Am. Chem. Soc.* **1998**, *120*, 12849–12859.
[205] Z. Zhang, R. B. Richrath, A. Gansäuer, *ACS Catal.* **2019**, *9*, 3208–3212.
[206] M. Parasram, B. J. Shields, O. Ahmad, T. Knauber, A. G. Doyle, *ACS Catal.* **2020**, *10*, 5821–5827.

Chapter 2. Aim of the Project

The main purpose of my doctoral studies was the development of new organic methodologies using the combination of photoredox- and metal catalysis. As mentioned in the Chapter 1, the number of metallaphotoredox protocols has grown exponentially over the last few decades and an enormous number of different protocols have been reported so far. It was therefore necessary to focus the research activity on specific transformations. The main aspects on which we based our research were:

1. The use of organic photocatalysts, avoiding the more commonly used metal-based ones due to their cost, potential toxicity and low availability.
2. The use of earth-abundant transition metals, avoiding the use of precious metals such as palladium or rhodium. Finally, metals with lower toxicity, air stability and ease of manipulation are preferred.
3. The use of catalytic amounts of both photocatalysts and transition metals, making a trade-off between the catalyst loading and the reaction time required to achieve the best conversions.
4. The use of stoichiometric organic reductants to ensure the turnover of the photocatalytic cycles, avoiding the use of stoichiometric metal reductants which, despite their relatively low cost and abundance, are associated with a large metal waste production. The reductant of choice was the Hantzsch ester due its trivial and scalable synthesis using cheap reagents, its high reactivity and its suitable oxidation potential.
5. The use of standard Schlenk techniques, avoiding reactions that strictly require a glove box.

With these key aspects in mind, four novel protocols are described in the following chapters. Each chapter introduces innovative and unprecedented aspects in the metallaphotoredox field.

Chapter 3 focuses on the combination of photoredox- and cobalt catalysis for the allylation of carbonyl groups. The innovative aspect is the introduction of a novel TADF-emitter photocatalyst derived from the degradation of the commercially available 3DPAFIPN, which can sustain the dual catalytic protocol, where the latter and other common TADF-emitters failed.

Chapter 4 focuses on the combination of photoredox- and vanadium catalysis for the diastereoselective pinacol coupling of aromatic aldehydes. The use of vanadium under photoredox conditions for the functionalization of small molecules is an underexplored field: only few papers can be found in the literature. The key aspects of this work are the high reactivity and the high functional group tolerance of the vanadium complex used. Despite its extreme sensitivity to air, which would require the use of a glovebox, the use of commercial and inexpensive stock solution of the vanadium complex made it easy to handle and the results were highly reproducible.

Chapter 5 focuses on the combination of photoredox- and nickel catalysis for the diastereoselective allylation of carbonyl groups. The key aspect of this work is the use of Morita-Baylis-Hillman acetates as unprecedented pronucleophiles. The protocol was found to be highly regio- and diastereoselective, and tolerant to different functional groups. The products are useful intermediates for the synthesis of bioactive molecules, making the protocol highly desirable.

Chapter 6 focuses on the combination of photoredox and titanium catalysis for the allylation of carbonyl groups. The key aspect of this work is the use of 4-bromo crotonates as an unprecedented allyl source under photoredox/vinylogous conditions for the fast, highly regioselective and moderately diastereoselective synthesis of α-vinyl-β-hydroxy esters. The presence of multiple functional groups was exploited with some post-functionalization.

Chapter 3. Light-induced access to a novel TADF photocatalyst for a dual photoredox- and cobalt-catalyzed allylation of aldehydes

3.1 Background introduction

Cobalt is the first and the lightest element in the group 9 of transition metals and one of the most abundant on the Earth.[207] Because its relatively high abundancy, low price and low toxicity it is widely used in industrial processes, such as Fischer-Tropsch process[208] or in the energy and environmental sectors to such an extent that it is included in the list of critical raw materials of the European Union.[209]

As a catalyst, cobalt has been reported in various processes such as hydrogenation and dehydrogenation reactions,[210,211] name reactions, e.g. the Pauson-Khand reaction,[177] or the Reformatsky reaction,[212] and C-H activations to install new and valuable bonds (*Figure 3.1*), e.g. C-C, C-N, C-O bonds,[213–215] as well as to introduce molecular complexity, such as alkynyl or alkenyl groups, on a variety of substrates,[210,213,216] and, for the purposes of this chapter, allyl groups.

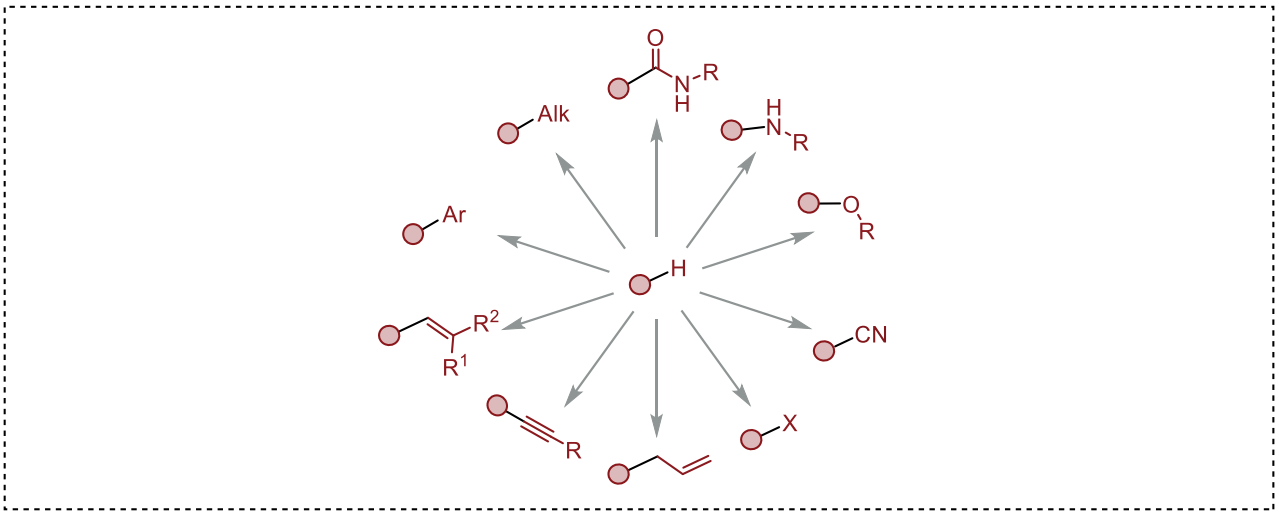

Figure 3.1 Different new bonds that can be forged in cobalt-mediated reactions.

The key point in the allylation reactions is the formation of a Co(I) intermediate starting from stable and commercially available Co(II) salts in the presence of an allyl derivative and a reductant, usually a metal e.g. Zn(0) or Mn(0), which triggers the ability of low-valent cobalt to coordinate the allyl species leading to an (π-allyl)-cobalt. This one-step strategy is known as the *Barbier-type* reaction.[217] (π-allyl)-cobalt complexes, like other (π-allyl)-metals, e.g. palladium,[218,219] are known to exhibit an amphiphilic character[220] depending on the oxidation state of the cobalt center, the ligand and the electronic environment (*Figure 3.2*).

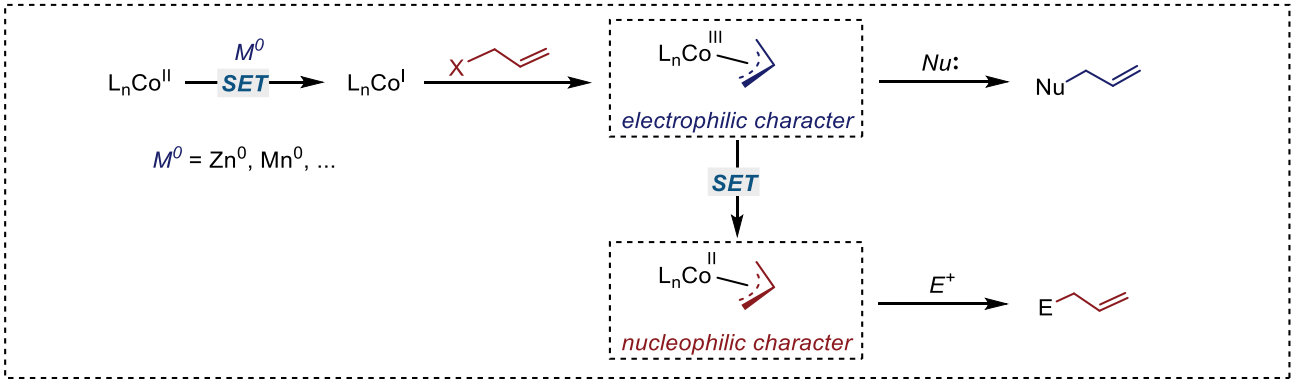

Figure 3.2 Different reactivity of (π -allyl)-cobalt intermediates.

(π-allyl)-cobalt(III) species display an electrophilic character and their reactivity has been recently reviewed.[221] The allylic functionalization can be achieved under both polar and radical conditions and using both hard and soft nucleophiles. *Figure 3.3* shows an example of the use of organozinc reagents as hard nucleophiles reported by the Knochel group[222] and the use of amines as softer nucleophiles reported by the Li group[223] allowing complete regiocontrol in favor of the linear and branched products respectively.

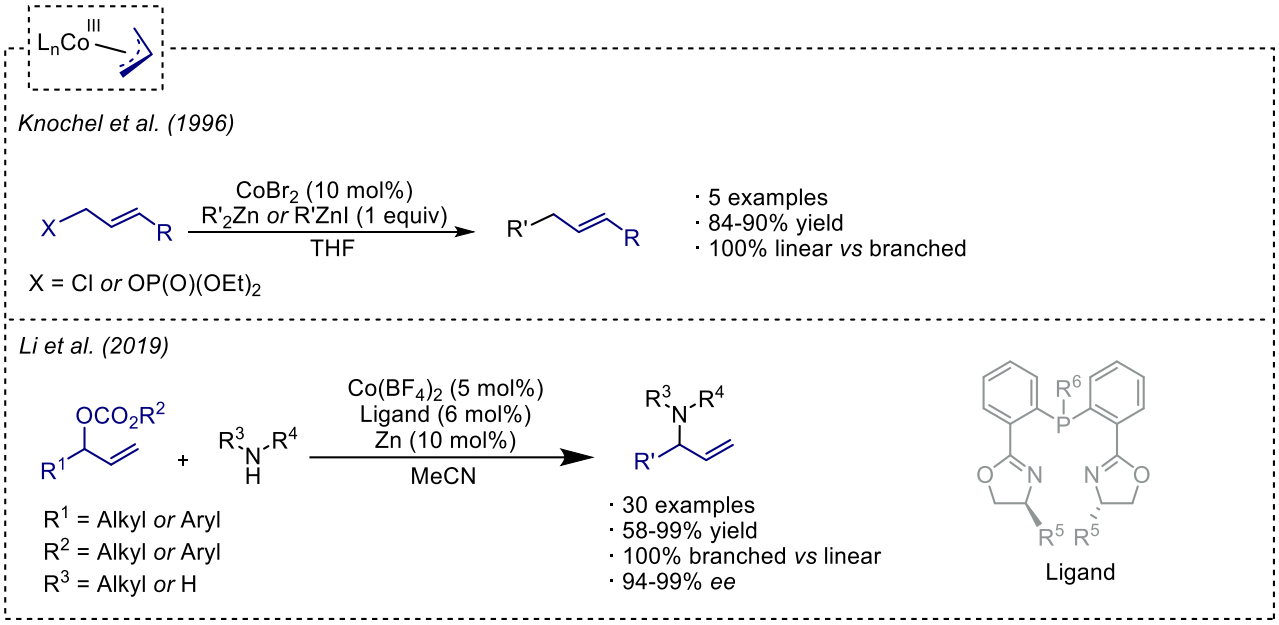

Figure 3.3 Reactivity of (π-allyl)-cobalt(III) intermediates as electrophiles.

However, in the presence of a suitable reducing agent it is possible to reduce the (π-allyl)-cobalt (III) to a (π-allyl)-cobalt(II) intermediate which has a nucleophilic character, and couple it to different reaction partners. Several protocols have been reported in this way in the literature.[224] Among all of them, the Perichon group reported in 2003 a cobalt-catalyzed allylation of aryl bromides, and the Gosmini group in 2011 a cobalt-catalyzed allylation of alkyl halides (*Figure 3.4*).

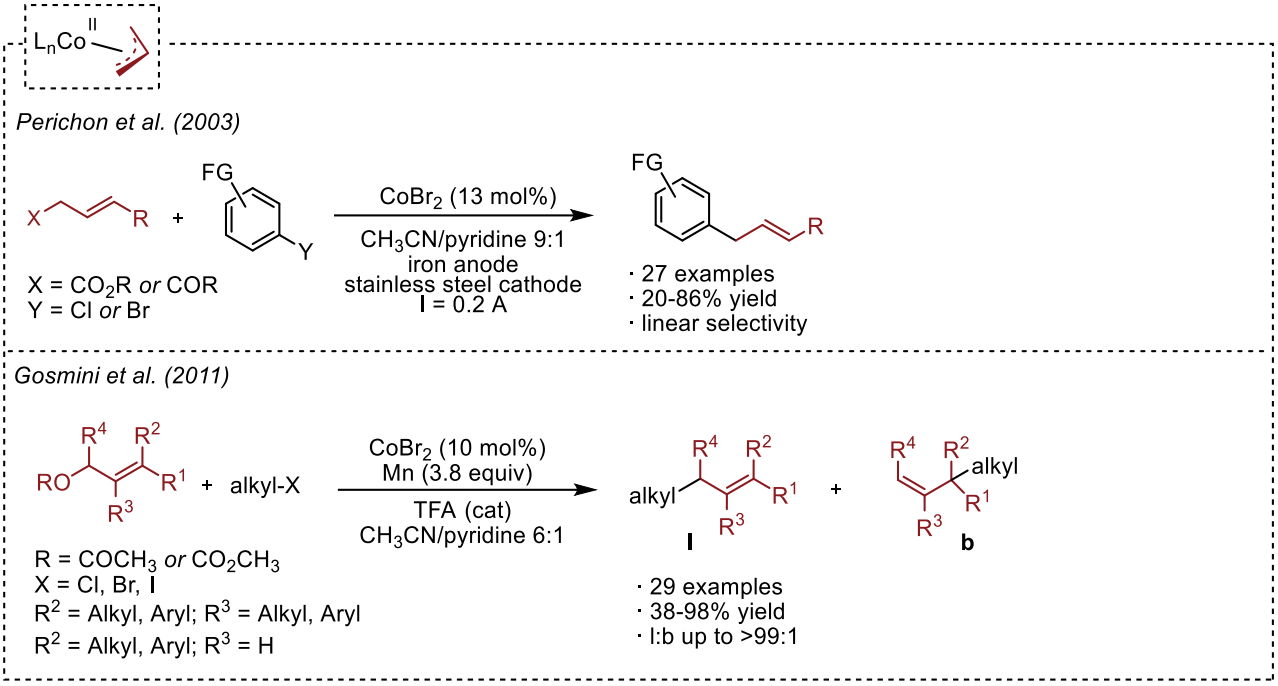

Figure 3.4 Reactivity of (π-allyl)-cobalt(II) intermediates as nucleophiles.

These two examples have in common use of $CoBr_2$ as a cheap and available source of Co(II) and the pyridine as the ligand to stabilize the Co(I) generated *in situ*[225] under two different reducing systems: 1. by electroreduction in the first example and 2. by overstoichiometric Mn(0) in the presence of trifluoroacetic acid (TFA) as the activator in the second example. The mechanism postulated by Gosmini (*Figure 3.5*) involves the reduction of the Co(II) precatalyst by the stoichiometric manganese in the presence of pyridine to form an active low-valent pyridine-Co(I) species which undergoes the oxidative addition to the allyl acetate forming the (π-allyl)-cobalt(III) intermediate that is subjected to a second reduction event. The nucleophilic (π-allyl)-cobalt(II) complex reacts with the alkyl halide to give an allyl-alkyl-Co(III) complex. This step was demonstrated by the formation of an alkyl radical using bromomethylcyclopropane as a radical clock and observing the ring-opening derivative as the main product. Furthermore, the addition of TEMPO as a radical inhibitor before the addition of the alkyl halide resulted in the complete inhibition of the reaction. Finally, reductive elimination provides the cross-coupling product and the turnover of the catalytic cycle.

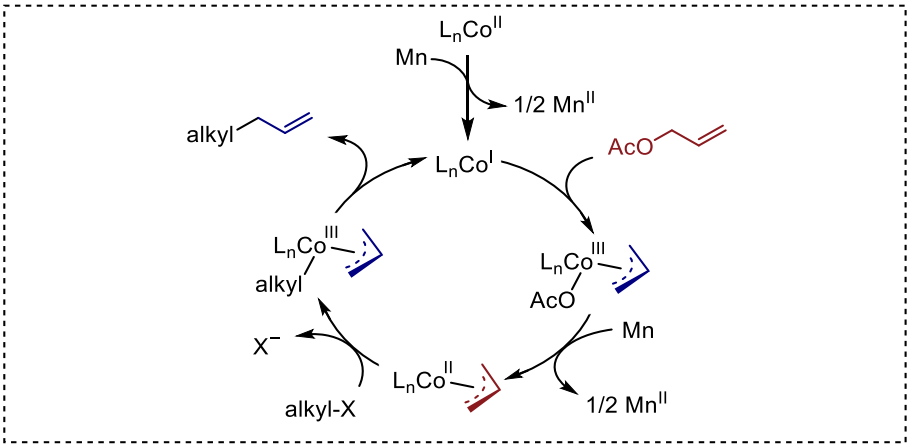

Figure 3.5 General mechanism for the cobalt-mediated cross coupling between allyl acetate and alkyl halides.

The same concept was reported in 2003 by the Perichon group in the allylation of carbonyls (*Figure 3.6*).

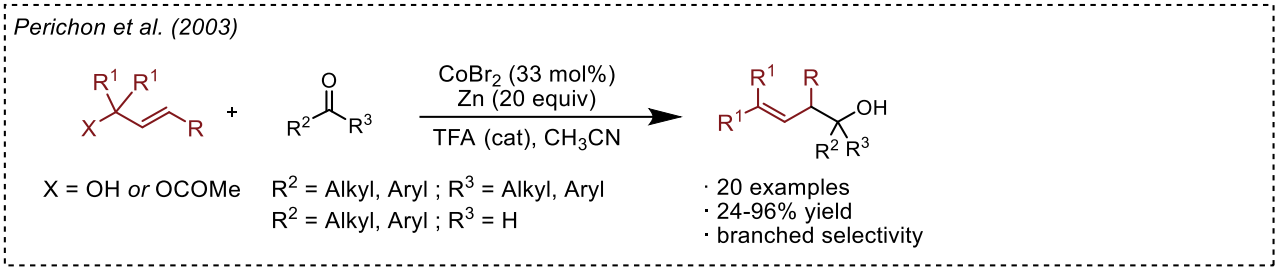

Figure 3.6 Cobalt-mediated allylation of carbonyls reported by the Perichon group.

The protocol is very tolerant to aromatic and aliphatic aldehydes and ketones with high yields also in the case of cyclic aliphatic ketones. When substituted allyl acetates are used, the protocol only leads the branched homoallylic alcohols. As before, using a catalytic amount of $CoBr_2$ in the presence of an overstoichiometric amount of zinc and a catalytic amount of TFA, a transient (π-allyl)-cobalt(II) complex is generated, and it is trapped by the electrophilic carbonyl, leading to the product as a cobalt alkoxide. Release of the product by proton scavenging restores the metal catalytic cycle (*Figure 3.7*).

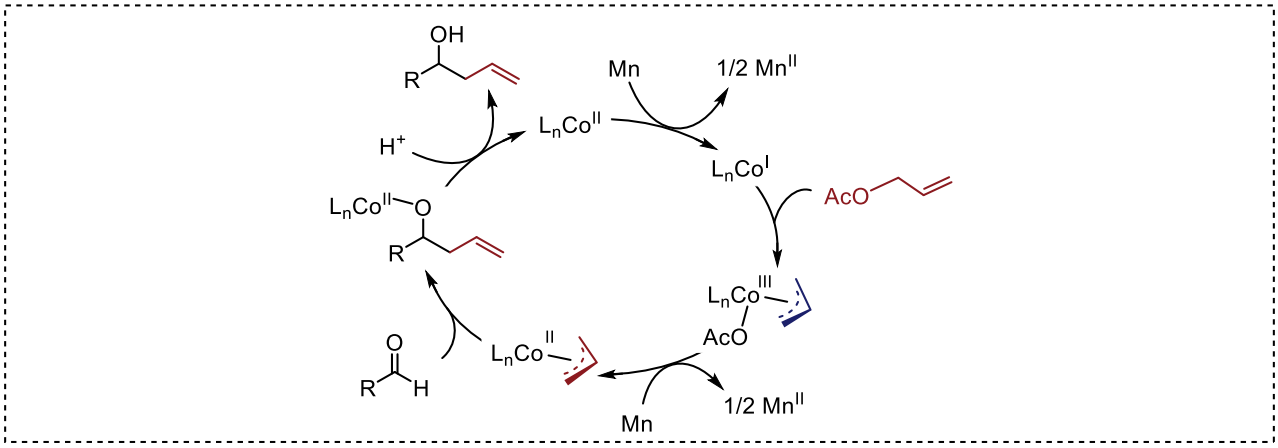

Figure 3.7 General mechanism for the cobalt-mediated allylation of carbonyls reported by the Perichon group.

Although these protocols provide a valuable route to useful products using a catalytic amount of an abundant transition metal, the use of a stoichiometric metal reductant is associated with a large amount of metal waste. In this perspective, our group[226] and the Shi group[227] reported in 2021 a dual photoredox- and cobalt-catalyzed allylation of aromatic and aliphatic aldehydes (*Figure 3.8*).

Two different sources of Co(II) were chosen: $CoBr_2$ in Cozzi's work and $CoSO_4 \cdot H_2O$ in Shi's work, with the same loading, and dtbpy as the ligand. Also, both the protocols use the same Ir-based photocatalyst $[Ir(ppy)_2(dtbpy)](PF_6)$ and stoichiometric DIPEA as the reductant, but with a different loading (respectively 2 mol% and 4 equivalents in Cozzi's work and 1 mol% and 3 equivalents in Shi's work). Finally, both the protocols use DMF as the main solvent, in Cozzi work the addition of a 10% of water was found to be beneficial.

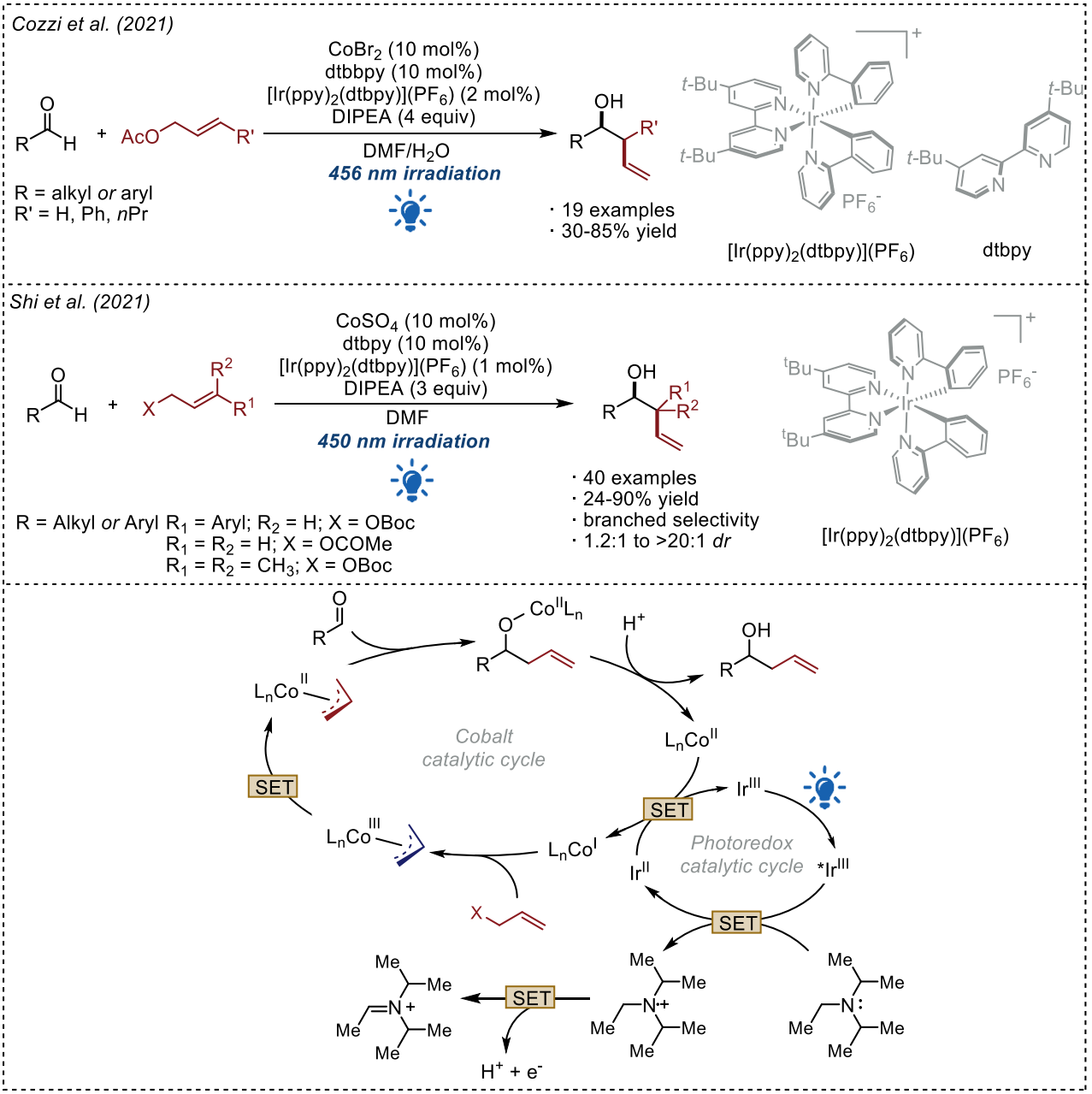

Figure 3.8 Dual photoredox- and cobalt-mediated allylation of carbonyls reported by the Cozzi and Shi group.

If we compare the two protocols, yields are slightly higher in Shi's work. Using substituted allyl moieties, they found it convenient to use the more reactive *tert*-butyl carbonates instead of the acetate with excellent control of the regioselectivity. The diastereoselectivity was highly dependent on the substrate, spanning from 1.2:1 to >20:1 with the cyclic cyclohexane carboxaldehyde. The major diastereoisomer, identified as the *syn* isomer is compatible with a Zimmerman-Traxler transition state. The use of substituted allyl acetates resulted in lower control over the regio- and diastereoselectivity.

An interesting observation for the purposes of this chapter is that in Shi's work, the organic photocatalyst 4CzIPN only gave traces of the products.

The mechanism was investigated using Stern–Volmer luminescence quenching experiments. As expected, the reaction proceeds in the same way in both the protocols. The photocatalyst reaches its excited state upon excitation and it is reductively quenched ($*E_{red}(*Ir^{III}/Ir^{II})$ = +0.66 V *vs* SCE in MeCN) by the DIPEA ($E_{ox}(DIPEA^{\bullet+}/DIPEA)$ = +0.65 V *vs* SCE) via SET generating an Ir(II) species and $DIPEA^{\bullet+}$. The

reduction of the ligand-coordinated Ln-Co(II) complex ($E_{red}(Co^{II}/Co^{I})$ = −1.30 V *vs* SCE)[228] by the reduced photocatalyst ($E_{red}(Ir^{III}/Ir^{II})$ = −1.51 V *vs* SCE in MeCN) leads to a ligand-stabilized Ln-Co(I) intermediate restoring the photocatalytic cycle. The Ln-Co(I) undergoes oxidative addition with the allylic acetate to generate the electrophilic (π-allyl)-cobalt(III) species which is readily reduced by another Ir(II) species to the key transient nucleophilic (π-allyl)-cobalt(II). Addition to the carbonyl forms a new C-C bond and the cobalt alkoxy product. Hydrolysis of the Co-O bond by protons derived from the degradation of the $DIPEA^{\bullet+}$ releases the homoallylic alcohol and restores the catalytic cycle.

3.2 Presented work

Cobalt catalysis has emerged as an attractive platform in a wide range of catalytic processes and, in particular, photoredox catalysis has been shown to be effective in generating active cobalt species from suitable and cheap precursors in the allylation of aldehydes. A possible evolution of this dual photoredox- and cobalt-mediated transformation could be the replacement of the expensive Ir-based photocatalysts with cheaper, readily available and fully organic photoreductants. This idea must deal with the fact that both 3DPAFIPN (as will be shown in the Paragraph 3.3) and 4CzIPN are not effective in this transformation. Although more recently the Kleij and Shi groups have recently disclosed two new protocols using 4CzIPN as the photocatalyst (*Figure 3.9*), respectively in a cobalt-mediated allylation of aldehydes using vinyl ethylene carbonates as 1,3-diene surrogates[229] and allyl aryls as allyl source,[230] to date, there is no example in the literature using allyl acetate, an inexpensive raw material, as the allyl source with organic photocatalysts.

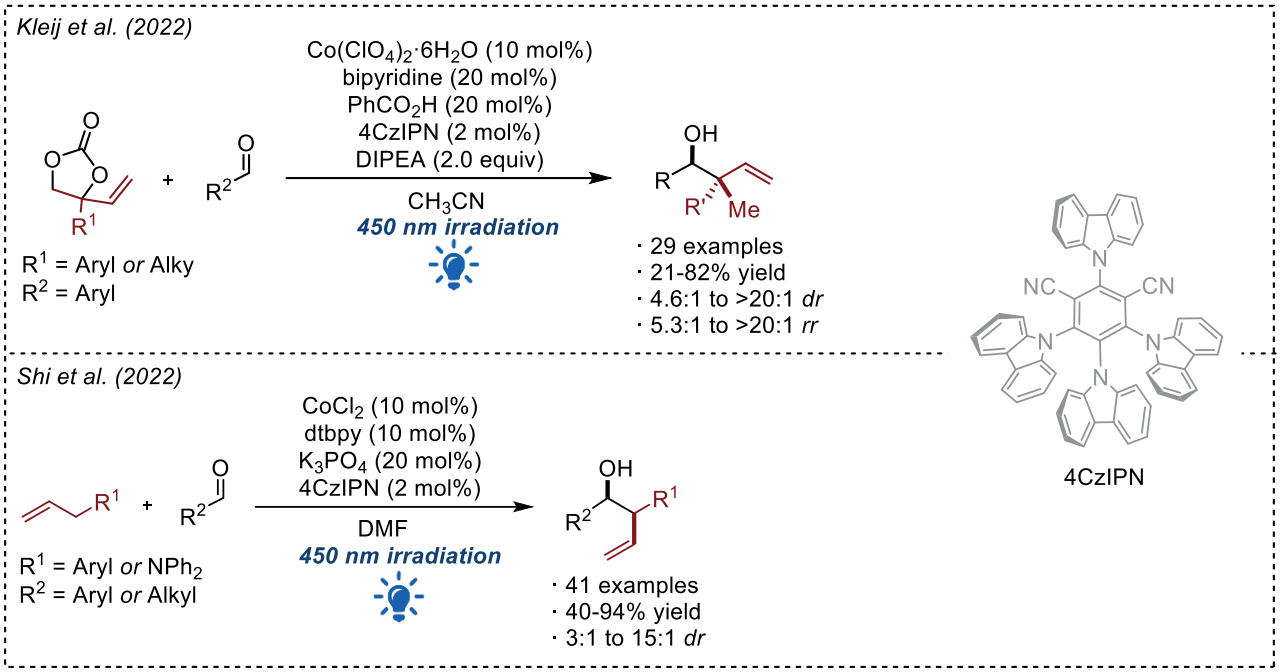

Figure 3.9 Dual photoredox- and cobalt-mediated allylation of carbonyls reported by the Kleij and Shi groups using 4CzIPN as the photocatalyst.

As will be shown, aromatic aldehydes in the presence of a Co(II) source, 3DPAFIPN or 4CzIPN as photocatalysts under blue light irradiation gave mixtures of non-diastereoselective pinacol coupling, benzylic alcohol and homoallylic product.

This limitation was overcome during my PhD when we investigated the stability of 3DPAFIPN under blue light irradiation. As already mentioned in Section 1.5.2, dicyanobenzene-based photocatalysts have

been reported to be stable under irradiation in the reaction media as it was possible, in some cases, to recover them after the reaction.[92,231,232] However, in the presence of certain reactants or intermediates generated in a light-driven reaction, the stability can be severely affected. The König group reported in 2019 the photocatalytic benzylation of aldehydes using 4CzIPN as the photocatalyst.[233] More specifically, benzylic carboxylates were used as a source of benzylic radicals. The key point was the photooxidation of the benzylic carboxylate by the excited photocatalyst with the CO_2 extrusion forming a benzyl radical, which can be reduced in another SET event by the reduced photocatalyst forming the effective electrophile. During the reaction the mono-substitution of a cyanide group of 4CzIPN by a benzylic group was observed. The mechanism for the formation of the new product, named 4CzBnBN, is shown in *Figure 3.10* and involves the formation of a Meisenheimer complex between the reduced photocatalyst $4CzIPN^{\bullet-}$ and the benzyl radical followed by the elimination of cyanide group.

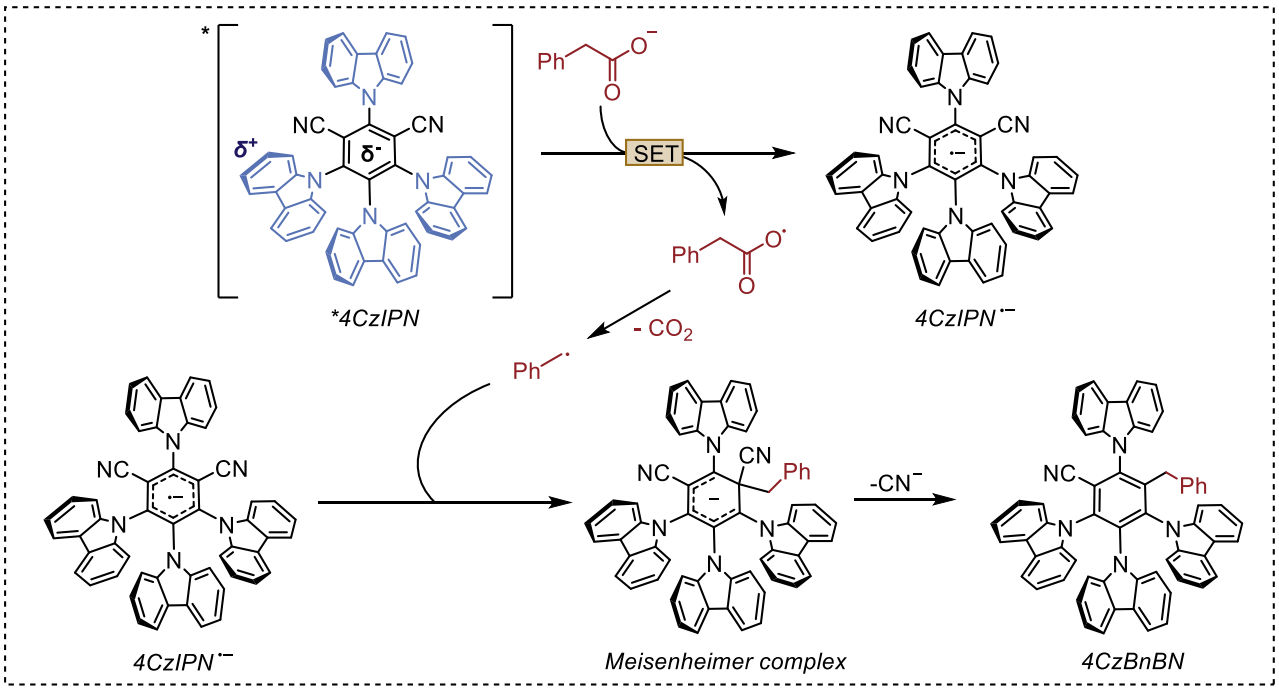

Figure 3.10 Mechanism for the mono-substitution of a cyanide group of 4CzIPN by a benzylic group reported by the König group.

The resulting photoproduct exhibits a blue-shifted absorption and emission, and a more negative reduction potential. The authors demonstrated that the photo-substituted TADF chromophore is responsible for the observed photocatalytic reaction. Besides the cyanide group, photo-induced nucleophilic substitution reactions are known to occur on other substituted benzenes[234] (e.g. on fluorobenzenes[235]).

In the following paragraph a detailed investigation of the unreported 2,4-bis(diphenylamino)-9-phenyl-9*H*-carbazole-1,3-dicarbonitrile 2DPAPhCzDCN derived from the photodegradation of 3DPAFIPN, its TADF and photoredox properties compared to the parent photocatalyst, and its application in the dual photoredox- and cobalt-mediated allylation of aldehydes is presented (*Figure 3.11*). Following the discovery of 2DPAPhCzDCN, we were able to scale-up and optimize its synthesis and fully characterize its structure and the photophysical properties. As the reduced form $2DPAPhCzDCN^{\bullet-}$ is a stronger reductant compared to the reduced form of the parent $3DPAFIPN^{\bullet-}$ it was possible to replace the Ir-based photocatalyst used in the previous protocol[226] with comparable yields and results.

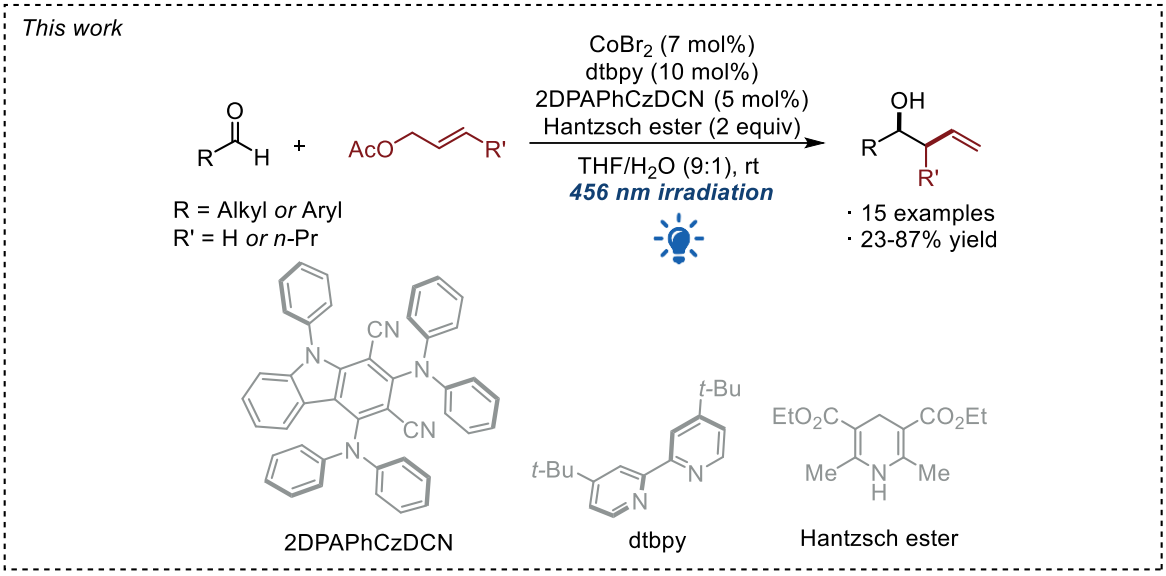

Figure 3.11 Presented work.

3.3 Optimization

To optimize the reaction, it was first necessary to obtain a sufficient amount of the photoproduct 2DPAPhCzDCN in high purity, as well as the parent 3DPAFIPN. Normally, the synthesis of 3DPAFIPN is carried out under nucleophilic displacement starting from a tetrasubstituted fluoro-derivative (See *Figure 3.12*). However, in the reaction conditions, traces of monocyano derivative are detected by HPLC/MS. In order to obtain 3DPAFIPN in high purity, without traces of other fluorinated cyanoarenes, which could be detrimental for the photosubstitution step, we carried out a careful chromatographic purification, and we isolated a pure sample of 3DPAFIPN.

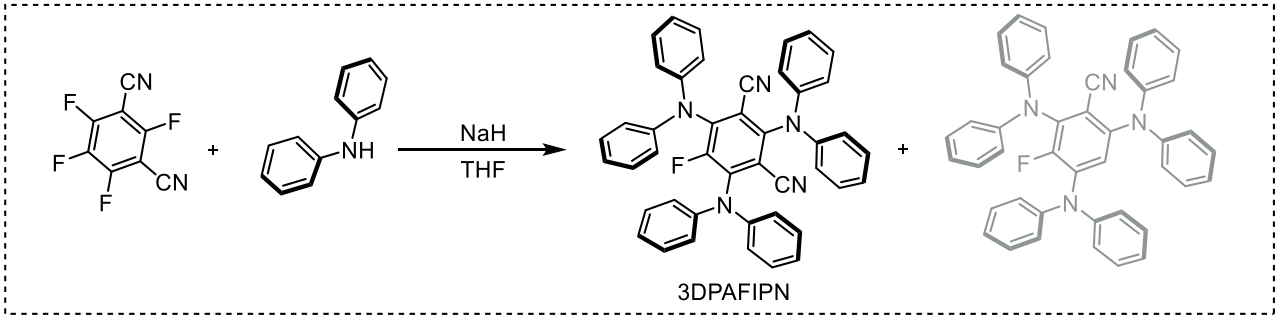

Figure 3.12 Synthesis of 3DPAFIPN. The monocyano side-product is represented in grey.

Preliminary cyclization tests (*Figure 3.13*) were carried out on a 0.1 mmol scale in THF under argon atmosphere at a low concentration (0.009 M). After 24h of irradiation with a blue Kessil lamp (456 nm) we obtained a complete conversion of the starting material in a 78% of isolated yield. Other solvents were investigated, such as toluene, DMF, or MeCN and they gave similar results. Interestingly, the presence of oxygen in the mixture did not inhibit the photocyclization.

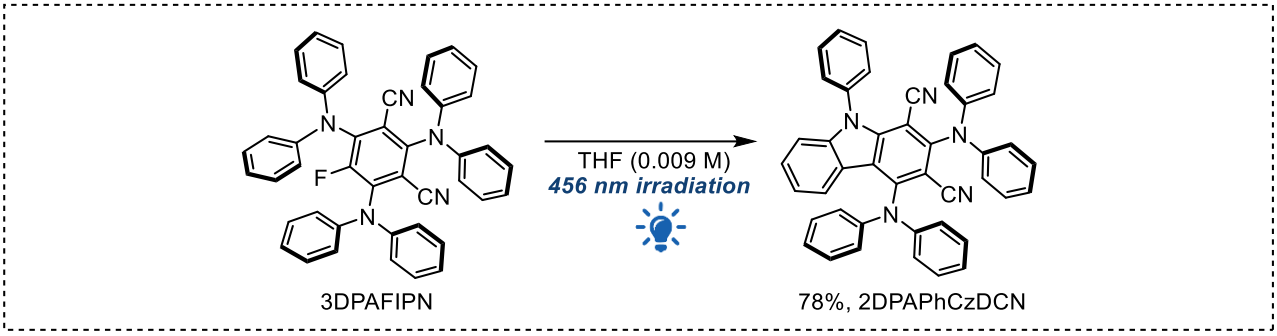

Figure 3.13 Synthesis of 2DPAPhCzDCN by photocyclization of 3DPAFIPN.

To scale up the reaction it was necessary to extend the reaction time to 48h to ensure the complete conversion of 3DPAFIPN. The presence of the starting material had to be avoided due to its similar polarity to that of the product, making the purification more difficult. The photocyclization was carried out up to 0.6 mmol with comparable isolated yield (70%).

With the pure 2DPAPhCzDCN in hand, we started the study of the dual photoredox- and cobalt-allylation reaction on a 0.1 mmol scale using 4-chlorobenzaldehyde **1a** as the model substrate and 3 equivalents of allyl acetate **2a**, 7 mol% of $CoBr_2$ as Co(II) precatalyst, 10 mol% of dtbpy as the ligand and 2 equivalents of Hantzsch ester as the terminal organic reductant. Taking into account our previous metallaphotoredox methodologies using TADF chromophores,[232,236,237] we choose tetrahydrofuran as the selected solvent (*Table 3.1*).

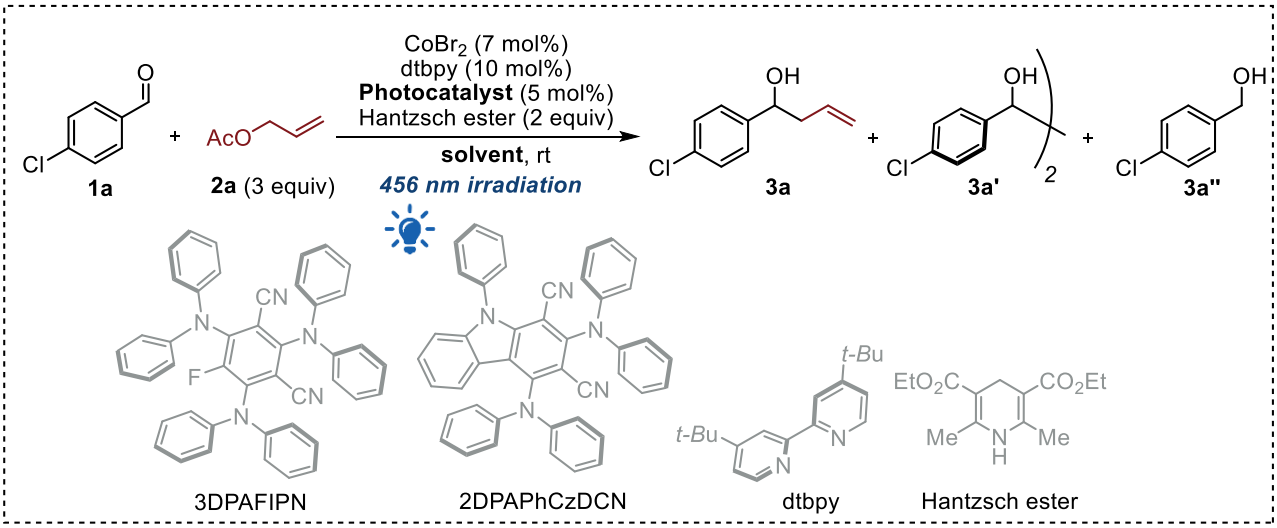

Entry	Solvent	Photocatalyst	Conversion (%)[a]	**3a:3a'[b]:3a''[c]**
1	THF	2DPAPhCzDCN	99	10:60:30
2	THF	3DPAFIPN	96	12:69:19
3	**THF/H_2O 9:1**	**2DPAPhCzDCN**	**96**	**94 (87)[d]:4:2**
4	THF/H_2O 9:1	3DPAFIPN	99	2:97:1
5	THF/H_2O 9:1	4CzIPN	99	0:100:0

Table 3.1 [a][c] Determined by ^{1}H NMR analysis on the reaction crude.[b] 1:1 ratio of meso:d/l pinacol coupling was observed by ^{1}H NMR analysis on the reaction crude.[c] Isolated yields after chromatographic purification are given in parentheses.

Under these preliminary conditions (entry 1) the aldehyde was almost completely converted to the pinacol derivative **3a'** and the benzylic alcohol **3a''** (**3a'**:**3a''** = 2:1) and only 10% of the homoallylic product **3a** was observed. Similar results were obtained using 3DPAFIPN instead of 2DPAPhCzDCN (entry 2). The addition of 10% of water as additive using 2DPAPhCzDCN (entry 3) led to 96% of

conversion with **3a** as the main product, highlighting its impact on the reaction outcome.[226] In comparison, the use of 3DPAFIPN instead of 2DPAPhCzDCN under the same conditions (entry 4), resulted in the formation of **3a'** as the main product, suggesting that the less powerful reducing TADF-emitter cannot sustain the cobalt catalytic cycle while being able to induce the reductive ketyl dimerization. Finally, considering the recent literature on the dual photoredox- and cobalt-catalysis promoted by 4CzIPN as the photocatalyst,[229],[230] we tested 4CzIPN under our conditions (entry 5) giving only the pinacolization product, confirming the superiority of 2DPAPhCzDCN in this transformation.

At this point we evaluated which cobalt precatalyst was the best for the reaction (*Table 3.2*).

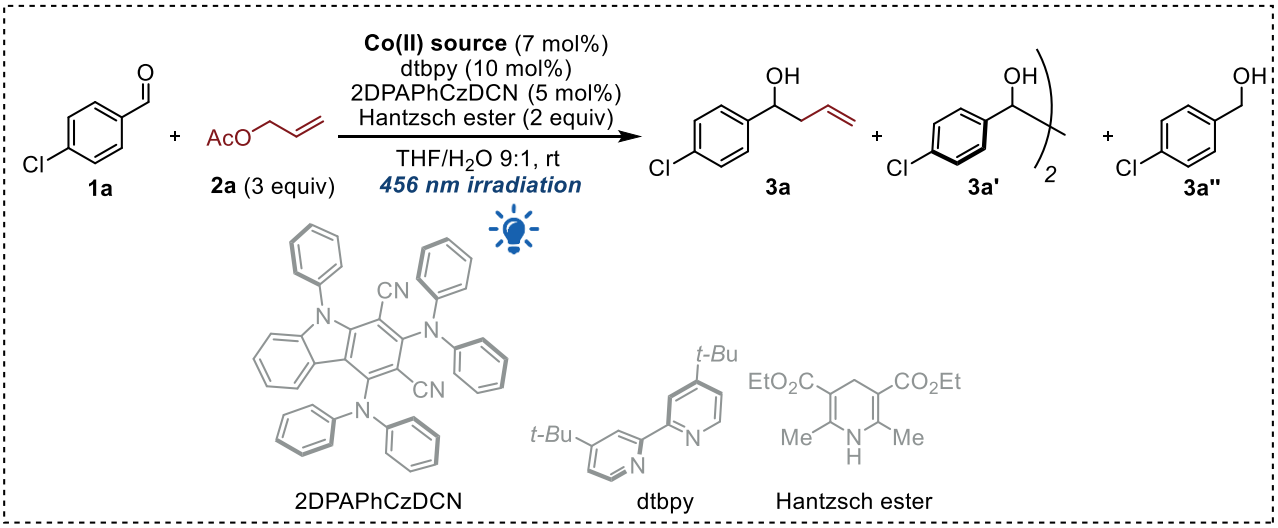

Entry	Co-source	Conversion (%)[a]	**3a**:**3a'**[b]:**3a''**[c]
0	**$CoBr_2$**	**96**	**94 (87):4:2**
1	$CoCl_2$	99	1:99:0
2	$CoCO_3$	78	62:30:8
3	$Co(acac)_2$	17	100:0:0
4	$Co(OAc)_2$	89	100:0:0
5[d]	$Co(OAc)_2$	92	48:41:11

Table 3.2 [a][c] Determined by ^{1}H NMR analysis on the reaction crude.[b] 1:1 ratio of meso:d/l pinacol coupling was observed by ^{1}H NMR analysis on the reaction crude.[c] Isolated yields after chromatographic purification are given in parentheses.[d] 4CzIPN was used instead of 2DPAPhCzDCN.

$CoCl_2$ (entry 1) gave only the pinacol coupling product compared to $CoBr_2$. While $CoCO_3$ (entry 2) gave good conversion but a mixture of **3a** and **3a'**, $Co(acac)_2$ (entry 3) gave only the desired product but with a low conversion. $Co(OAc)_2$ (entry 4) gave only the homoallylic product but with a lower conversion than $CoBr_2$. The use of 4CzIPN with the same Co(II) source (entry 5) gave a mixture of **3a** and **3a'** providing further evidence that the conditions reported by Kleij[229] and Shi[230] cannot be extended in this dual photoredox- and cobalt- catalyzed methodology and confirming the superiority of 2DPAPhCzDCN.

Once the optimized conditions were available, the necessary control experiments were carried out to provide further confirmations about the reaction mechanism. The essential roles of the photoirradiation (entry 1), the photocatalyst (entry 2), the Hantzsch ester (entry 3), the cobalt (entry 4) and the ligand (entry 5) are shown in *Table 3.3*. The ligand is required as it could affect the reduction potential of the cobalt complex and the stability of the reduced Co(I) intermediate.

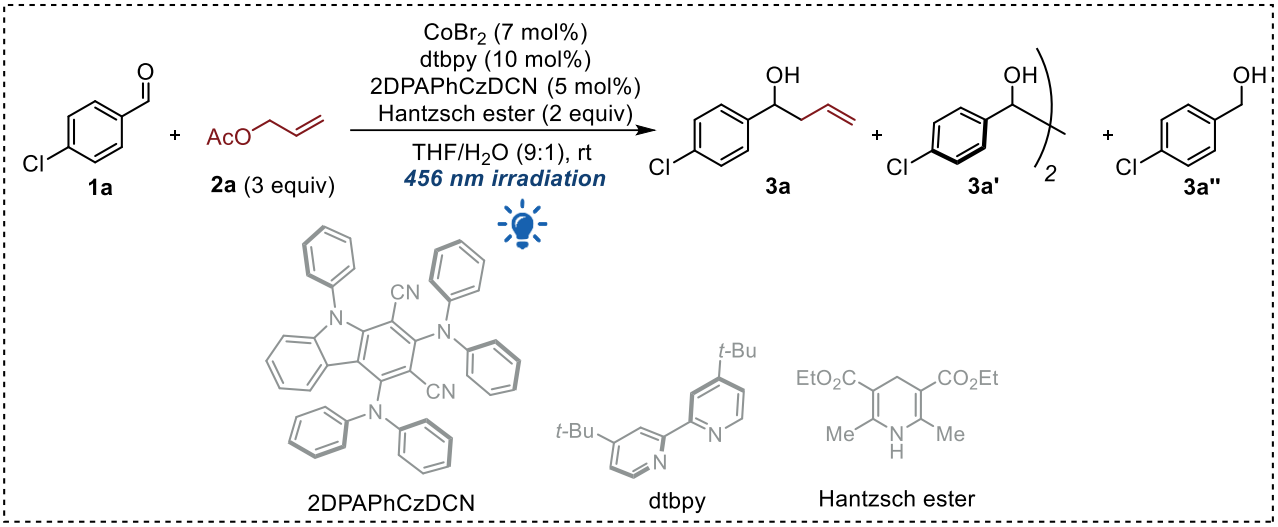

Entry	Deviation from standard conditions	Conversion (%)[a]	**3a**:**3a'**[b]:**3a''**[c]
0	**None**	**96**	**94 (87):4:2**
1	No light irradiation	NR	
2	No photocatalyst	NR	
3	No Hantzsch ester	NR	
4	No CoBr2	NR	
5	No ligand	99	10:90:0

Table 3.3 [a][c] Determined by ^{1}H NMR analysis on the reaction crude. Isolated yields after chromatographic purification are given in parentheses.[b] 1:1 ratio of meso:d/l pinacol coupling was observed by ^{1}H NMR analysis on the reaction crude. NR = No reaction.

After a systematic evaluation of all the reaction parameters, we were able to reveal the optimized conditions, shown in *Figure 3.11* which gave the product **3a** in 87% yield.

3.4 Scope evaluation

The optimized conditions were applied to a library of substituted aromatic and aliphatic aldehydes reported in *Figure 3.14* on a scale up to 0.2 mmol. To ensure complete conversion of the starting material, the reaction time was extended up to 72h in the case of the aliphatic substrates **3k**, **3l**, **3m** and **3o**. In general, complete conversion of aromatic aldehydes was always observed. Yields were generally moderate as the concomitant formation of pinacols (10-20%) and benzylic alcohols (10-15%) could not be completely avoided. As observed in the previous cobalt- mediated allylation,[226] the reactivity was strongly influenced by the aromatic moiety of the aldehydes: electronrich substrates showed a reduced reactivity, and in some cases, we tried to improve the yields by extending the reaction time to 40h (**3g**).

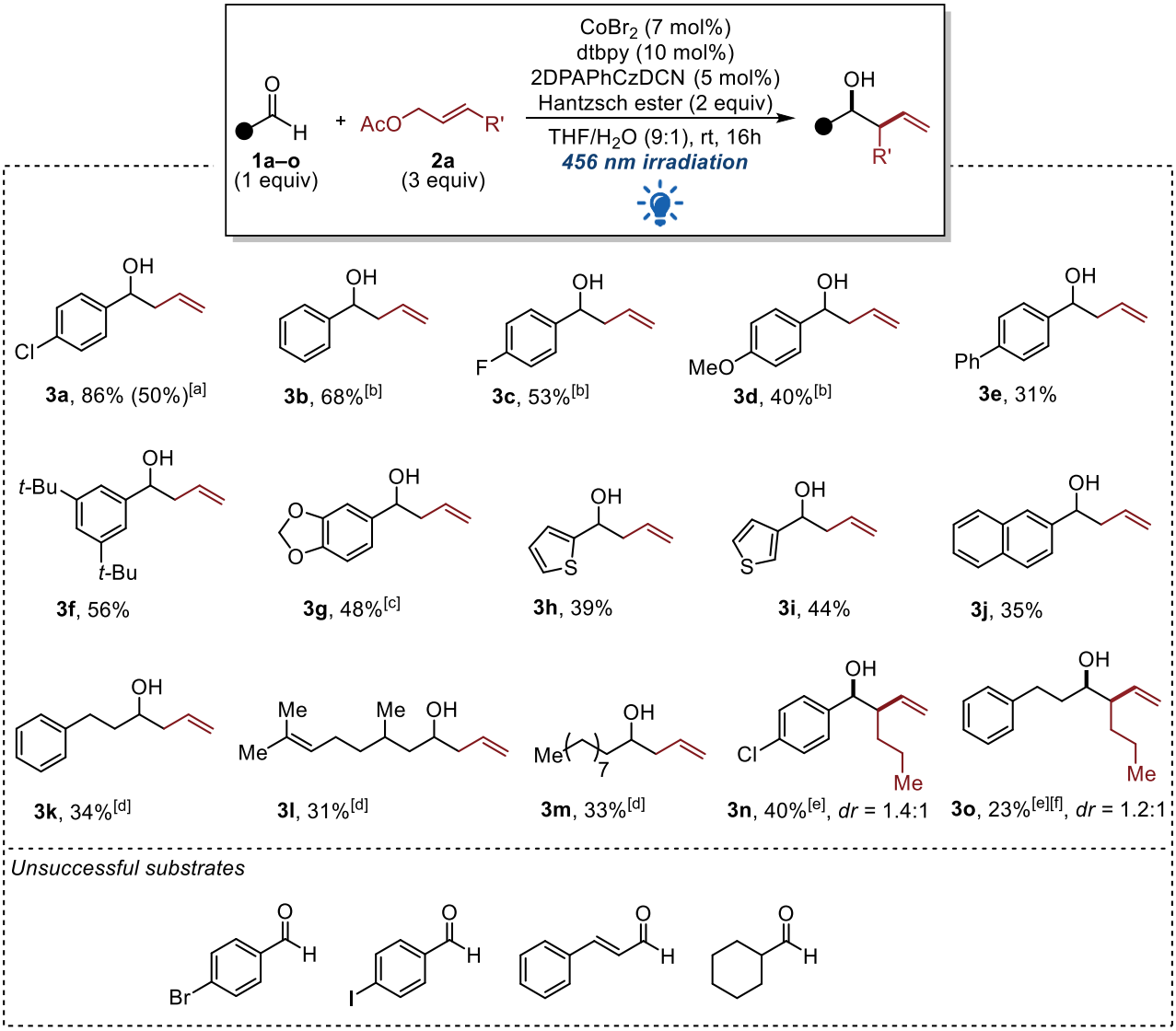

Figure 3.14 [a] *1 mmol scale of* ***1a*** *with* $Co(OAc)_2$ *instead of* $CoBr_2$. [b] *Reaction performed on a 0.1 mmol scale.* [c] *Reaction time extended to 40h.* [d] *Reaction time extended to 72h.* [e] $Co(OAc)_2$ *was used instead of* $CoBr_2$. [f] *Reaction time extended to 48h.*

As reported in Section 3.3, $Co(OAc)_2$ was found to be less active than $CoBr_2$, but it gave a lower amount of side-products. It was, therefore, decided to scale-up to 1 mmol scale the model substrate in the presence of this cobalt salt. The reaction was irradiated for 72h to ensure complete conversion of the starting material. Unfortunately, operating at 1 mmol scale made the reaction heterogeneous, and this probably affected the reaction outcome: ^1H NMR analysis showed 80% conversion of the starting aldehyde. In contrast to the 0.1 mmol experiment we also observed the presence of pinacol coupling (18%) and benzylic alcohol (8%) in the reaction mixture, which affected the isolated yield. Unfortunately, some substrates were found incompatible with the protocol: the stronger reduction potential of 2DPAPhCzDCN prevented the use of substrates containing bromine or iodine groups, as we observed partial dehalogenation in the isolated products.

Furthermore, the hindered cyclohexane carboxaldehyde was found to be unreactive. In fact, generally, aliphatic aldehydes suffered from a reduced reactivity. This trend was observed in our previous protocol and in the protocol reported by Shi.[230] In fact, we extended the reaction time to 72h and we obtained lower yields with linear aliphatic aldehydes, while branched aldehydes were found not to be reactive at all.

Two aldehydes, one aromatic (**1n**) and one aliphatic (**1o**), were chosen as model substrates, and the reaction was performed with the prochiral hex-2-en-1-yl acetate. In both the experiments $Co(OAc)_2$ was used to minimize the tendency to form side-products with less reactive substrates. The products, **3n** and **3o**, respectively were obtained with a pronounced branched selectivity but with a low diastereomeric control. In both cases a lower reactivity was observed, especially with the aliphatic aldehyde (**3o**), in line with the previous considerations, but with a predominant γ -regioselectivity. This is an evidence for a Zimmerman-Traxler transition state. In the case of 4-chlorobenzaldehyde, the desired product **3n** was obtained in 40% yield with a diastereomeric ratio of 1.4:1 (*syn*:*anti*).

3.5 Photophysical studies and reaction mechanism

The discovery of a new carbazole-1,3-dicarbonitrile chromophore capable of inducing a metallaphotoredox transformation prompted us to study in depth its unknown photophysical and electrochemical properties in order to rationalize the effect of the cyclization on its electronic properties and to fully unveil the mechanism of the reaction. These studies were carried out in collaboration with the research group led by Prof. P. Ceroni and the results are presented in *Table 3.4*.

Based on the literature, three mechanisms can be envisaged for the photo-induced photocyclization of fluorinated molecules, involving 1. electron transfer, 2. photo-nucleophilic substitution or 3. homolysis of the C-F bond . The charge-transfer nature of the lowest excited state of 3DPAFIPN, with an increased electronic density on the fluorinated aryl moiety, would favour a mechanism involving an electron transfer. However, a photo nucleophilic substitution is also plausible, and it is difficult to distinguish between these two mechanisms. The pathway involving the homolytic cleavage of the C-F bond in 3DPAFIPN can be excluded on the basis of the insufficient energy of the absorbed photons (E(λ = 480 nm) = 60 kcal/mol) compared to that of the C-F bond (127 kcal/mol).[238] We suggest that the most plausible mechanism for the photoinduced cyclization of 3DPAFIPN involves the photo-nucleophilic substitution and it is shown in *Figure 3.15*.

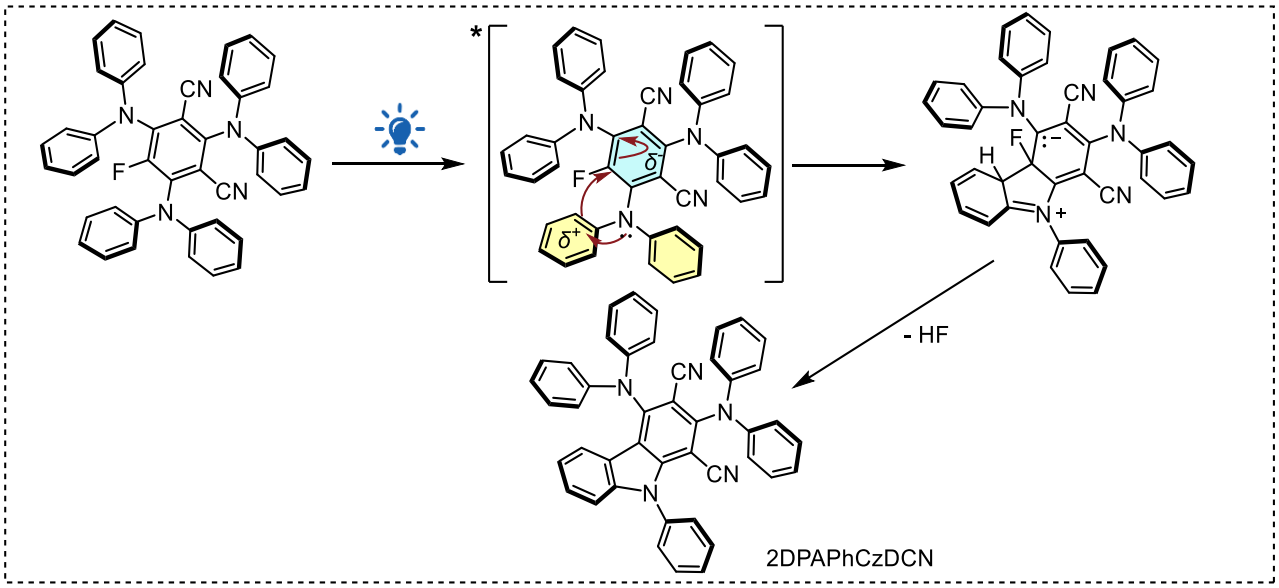

Figure 3.15 Most plausible mechanisms for the photoinduced cyclization of 3DPAFIPN to give 2DPAPhCzDCN.

The photophysical properties of 2DPAPhCzDCN were studied in THF. Compared to 3DPAFIPN, the absorption spectrum of 2DPAPhCzDCN appears to be blue-shifted in terms of absorption onsets (ε_{364nm} = 15700 $M^{-1}cm^{-1}$ in THF, λ^{abs}_{max} = 364 nm for 3DPAFIPN, ε_{377nm} = 10500 $M^{-1}cm^{-1}$ in THF, λ^{abs}_{max} = 377 nm for 2DPAPhCzDCN) (*Figure 3.16*).

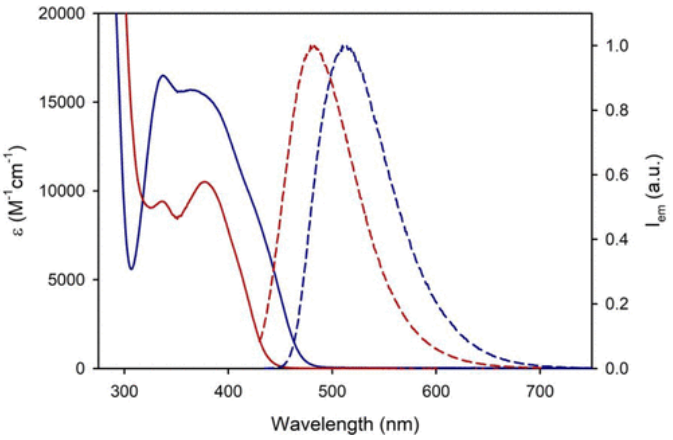

Figure 3.16 Absorption (solid line) and emission (dotted line) of 3DPAFIPN (blue) and 2DPAPhCzDCN (red).

The same trend is observed in the fluorescence emission spectra (λ_{max}= 510 nm and 479 nm of 3DPAFIPN and 2DPAPhCzDCN in THF at rt, respectively). The small Stokes shift in 2DPAPhCzDCN, reduced compared to value of the TADF parent (102 nm *vs* 146 nm) suggests that the excited state S_1 in 2DPAPhCzDCN has a charge transfer character, consistent with the property of TADF emitters.[88]

For both compounds, two lifetimes are observed in degassed THF:H_2O 9:1 solutions at room temperature. The short one, in the range of nanoseconds, has been attributed to the prompt fluorescence (τ_{PROMPT}), while the longer one, in the range of microseconds, has been attributed to the delayed fluorescence (TADF) (τ_{TADF}). In fact, the shape of the emission spectra for both 3DPAFIPN and 2DPAPhCzDCN is not affected by the presence of molecular oxygen, suggesting that the transition responsible for the longer lifetime is the same radiative deactivation $S_1 \rightarrow S_0$. On the contrary, the emission quantum yield is reduced in air-equilibrated solutions due to the efficient quenching of the chromophores' triplet excited state T_1 by dioxygen, which consequently prevents the thermally activated Reverse Inter-System Crossing (rISC) $T_1 \rightarrow S_1$.

The quantum yield of prompt fluorescence (Φ_{FLUO}) is increased from 5.7% to 21% for 3DPAFIPN and 2DPAPhCzDCN, respectively. This result is consistent with the more rigid structure of 2DPAPhCzDCN which prevents the non-radiative decay.[89] The rigidity of the new chromophore also causes an increase in τ_{PROMPT}, τ_{TADF}, and τ_{PHOS}.

Finally, the phosphorescence emission was recorded in a glassy matrix of DCM/MeOH 1:1 at 77 K (*Figure 3.17*) in order to reduce the quenching effect of vibrations. It shows the presence of phosphorescence for both chromophores (λ_{max} = 518 and 513 nm, for 3DPAFIPN and 2DPAPhCzDCN, respectively).

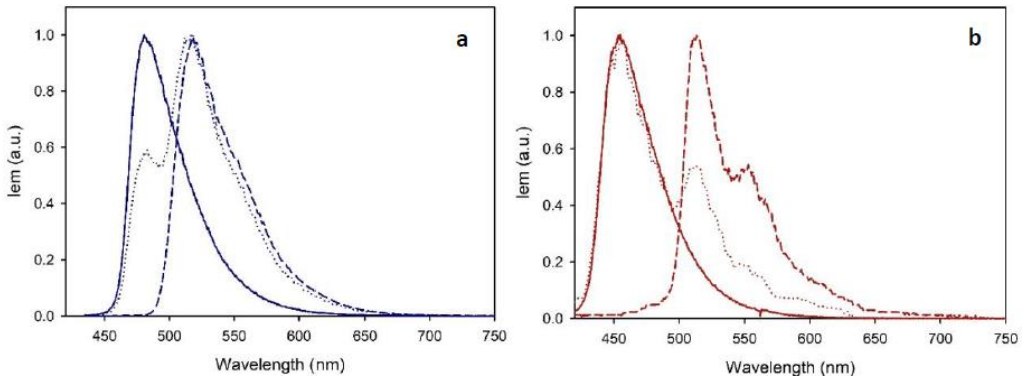

*Figure 3.17 Emission of 3DPAFIPN (**a**) and 2DPAPhCzDCN (**b**) recorded in a glassy matrix of DCM/MeOH 1:1 at 77 K. Fluorescence emission is represented with solid lines, while phosphorescence emission is represented with dotted lines.*

Under these experimental conditions, the phosphorescence bands are slightly red-shifted with respect to their fluorescence, indicating that the S_1 and T_1 excited states are close in energy. In particular, the $S_1 \rightarrow T_1$ energy gap (Δ_{EST}) is larger for 2DPAPhCzDCN than for 3DPAFIPN (320 meV and 190 meV, respectively). It is expected that the same trend is maintained at room temperature, explaining the lower TADF quantum yield Φ_{TADF} and the longer τ_{TADF} for 2DPAPhCzDCN than for 3DPAFIPN. In fact, higher Δ_{EST}, associated with an increased activation energy for the $T_1 \rightarrow S_1$ intersystem crossing, should lead to lower k_{RISC}. Lower k_{RISC}, according to the inverse proportionality between kinetic constants and lifetimes, should be accompanied by higher τ_{TADF}. However, this assumption cannot always be generalized because relatively small differences in Δ_{EST} can result in great differences in k_{RISC}, as reported for other classes of TADF-active chromophores.[239,240] *Table 3.4* lists all the photophysical and electrochemical properties of 3DPAFIPN and 2DPAPhCzDCN.

	Absorption		Emission								Electrochemistry	
	λ_{ABS}^{MAX} (nm)	ε (M-1 cm-1)	λ_{FLUO}^{MAX} (nm)	λ_{PHOS}^{MAX} (nm)[a]	τ_{FLUO} (ns)	τ_{TADF} (μs)[b]	τ_{PHOS} (ms)[a]	Φ_{FLUO}	Φ_{TADF}	Φ_{Δ}	E(A•+/A) (V)[c]	E(A/A•-) (V)[c]
1	364	15700	510	518	3.3	130	180	5.7%	35%	88%	+1.31[d]	-1.53
2	377	10500	479	513	9.1	680	374	21%	6.2%	55%	+1.31	-1.74

*Table 3.4 Photophysical and electrochemical properties of 3DPAFIPN (**1**) and 2DPAPhCzDCN (**2**).[a] At 77 K in a glassy matrix (DCM:MeOH 1:1 v/v).[b] Degassed solution.[c] In MeCN. Potentials vs SCE.[d] Anodic peak potential at 1 V/s, chemically irreversible electron transfer process.*

Cyclic voltammetry was then used to investigate the electrochemical properties of 2DPAPhCzDCN (*Figure 3.18*).

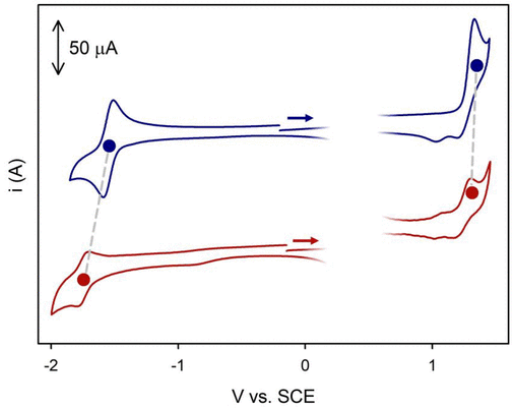

Figure 3.18 Cyclic voltammetry of 3DPAFIPN (blue) and 2DPAPhCzDCN (red).

In the case of 3DPAFIPN, the reduction process (–1.53 V *vs* SCE) is chemically and electrochemically reversible at a scan rate of 1 V/s, while the oxidation process (+1.31 V *vs* SCE) shows only partial chemical reversibility. The photoproduct 2DPAPhCzDCN shows less chemically reversible electron transfer processes. While its oxidation potential is unchanged compared to that of 3DPAFIPN (+1.28 V *vs* SCE), its reduction potential is cathodically shifted to –1.74 V *vs* SCE, making it a stronger reductant compared to the parent compound.

Let's consider the localized nature of frontier molecular orbitals in TADF molecules. In 3DPAFIPN the HOMO is delocalized over the three diphenylamino groups, whereas the LUMO is centered on the dicyanobenzene moiety.[2,88] The electrochemical data indicate that the LUMO orbital is destabilized in 2DPAPhCzDCN compared to 3DPAFIPN, as expected upon removal of the fluorine atom from the dicyanobenzene fragment. On the other hand, the HOMO orbital is not appreciably affected, as two electron-donating diphenylamine groups are also present in the molecule. Finally, the larger energy gap derived from electrochemical measurements of 2DPAPhCzDCN is consistent with its blue-shifted absorption and emission spectra.

After a careful photophysical and electrochemical characterization, the analysis of the luminescence quenching in the presence of all the reaction components was carried out.

Figure 3.19 a shows the absorption spectra of each species at the same concentrations as in the reaction. Considering only the emission region of the Kessil lamp (400-500 nm with λ_{max}= 456 nm) (*Figure 3.19 b*) the photocatalyst is not the only species capable of absorbing light, since both the Hantzsch ester and the bipyridine-Co(II) complex have a significant absorption in this region. Based on the absorption spectra of these species and the profile of the irradiation source, it is estimated that 65% of the light is absorbed by 2DPAPhCzDCN, 10% by the Hantzsch ester and 25% by the bipyridine-Co(II) complex, while 4-chlorobenzaldehyde and allyl acetate do not absorb light in this wavelengths range. We chose to irradiate at 456 nm to reduce the absorption of both species and maximize the light absorbed by the photocatalyst. At lower wavelength, the Hantzsch ester absorbs more light than the photocatalyst.

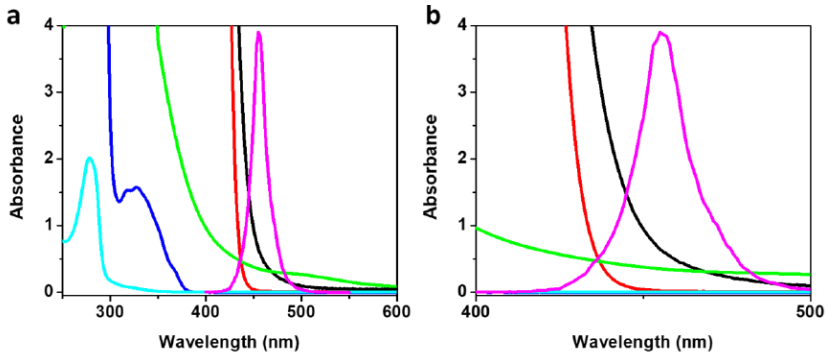

*Figure 3.19 (**a**) Absorption spectra of 2DPAPhCzDCN (2.5×10^{-3} M, black line), Hantzsch ester (0.5 M, red line), $CoBr_2$/dtbpy (each of them at concentration of 5×10^{-3} M, green line), 4-chlorobenzaldehyde (0.05 M, blue line), allyl acetate (0.15 M, cyan line) in THF/H_2O (9:1 v/v) and Kessil lamp profile (λ_{em} = 456 nm, purple line). The concentrations are the same used in the reaction conditions. (**b**) Absorption spectra of the reaction components in the region of the emission of the Kessil Lamp (420 nm – 500 nm).*

No relevant change in the TADF emission lifetime was observed upon addition of 4-chlorobenzaldehyde at reaction conditions (0.05 M) (*Figure 3.20*).

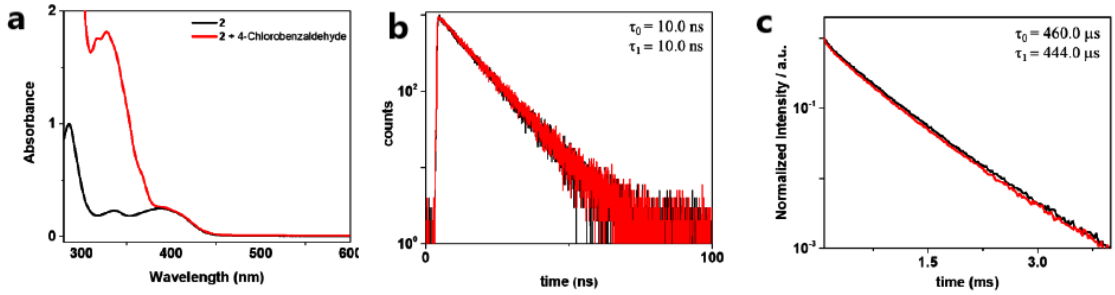

*Figure 3.20 Absorption spectra (**a**), time resolved decay of prompt (**b**) and delayed (**c**) fluorescence of 2DPAPhCzDCN (ca. 10^{-5} M, in THF/H_2O 9:1, v/v) upon addition of 4-chlorobenzaldehyde 5×10^{-2} M. λ_{exc} = 405 nm (**b**); λ_{exc} = 420 nm (**c**).*

On the other hand, quenching processes were observed for allyl acetate upon its addition at the same concentration as the reaction conditions (0.1 M) (k_q= 2.5 x 10^4 $M^{-1}s^{-1}$) (*Figure 3.21 a, b, c*) and for the corresponding complex formed after the addition of dtbpy to $CoBr_2$ at different concentrations (25 µM and 125 µM) (k_q = 1.0 x 10^8 $M^{-1}s^{-1}$) (*Figure 3.21 d, e, f*). It is important to note that the bipyridine-Co(II) complex absorbs light at the excitation wavelength, so it is necessary to perform the quenching experiments at more diluted concentrations.

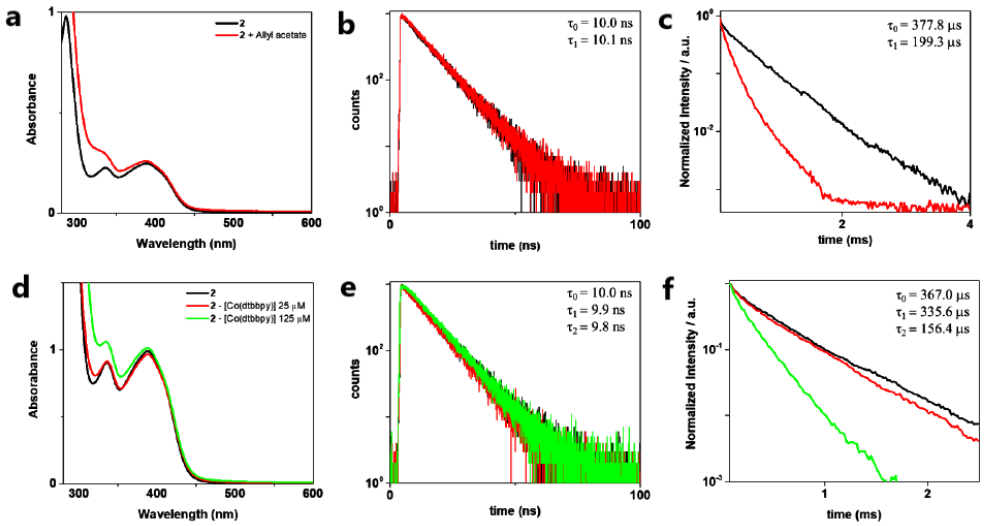

*Figure 3.21 Absorption spectra (**a**, **d**), time resolved decay of prompt (**b**, **e**) and delayed (**c**, **f**) fluorescence of 2DPAPhCzDCN (ca. 10^{-5} M, in THF/H_2O 9:1, v/v) upon addition of allyl acetate 1.5 × 10^{-1} M (**a**, **b**, **c**) and a solution of $CoBr_2$ and dtbpy (**d**, **e**, **f**). λ_{exc} = 405 nm (**b**, **e**); λ_{exc} = 420 nm (**c**, **f**).*

Unfortunately, it was not possible to study the quenching of the excited *2DPAPhCzDCN by the Hantzsch ester because its absorption spectrum largely overlaps with that of the photocatalyst and, under the experimental conditions used for the luminescence measurements, most of the light is absorbed by it. Although a strong quenching was observed for the delayed emission, a reliable value of the Stern-Volmer quenching constant was not obtained. Therefore, the quenching efficiency η of each species under the reaction conditions was not determined.

With all this experimental evidence, we can propose a mechanistic cycle for the presented protocol (*Figure 3.22*).

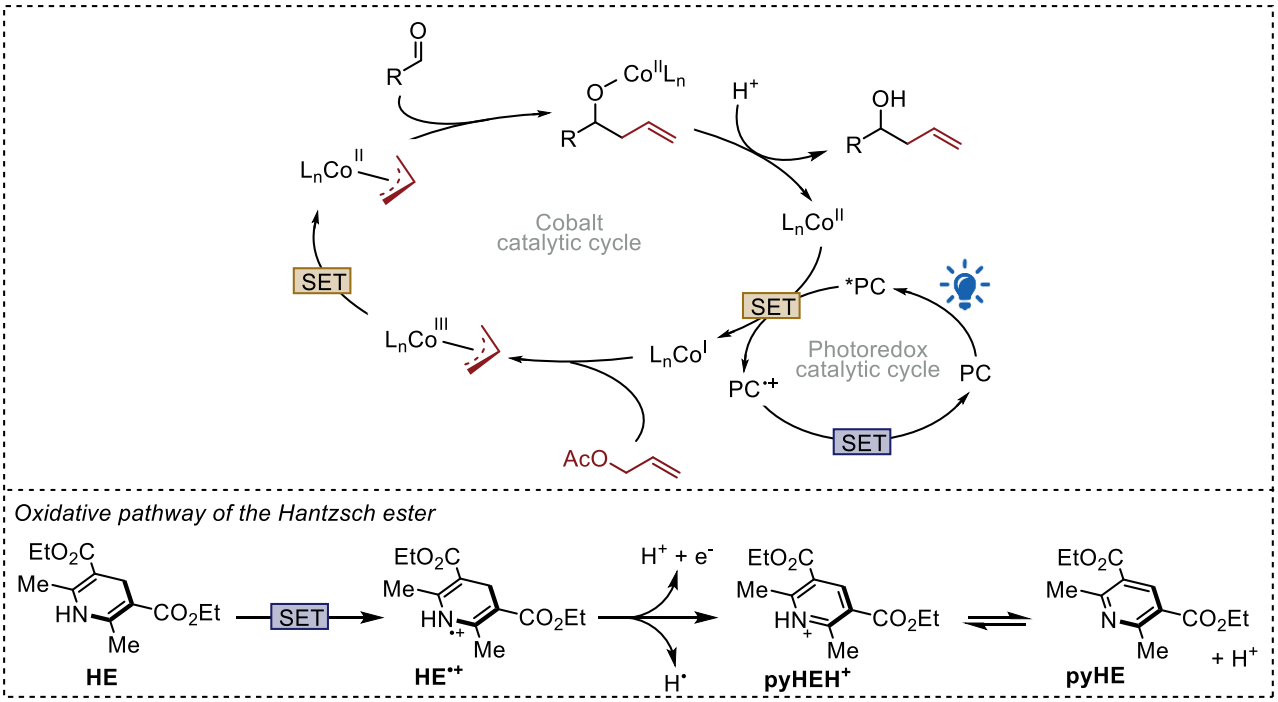

Figure 3.22 Proposed mechanism for the dual photoredox- and cobalt-catalyzed allylation of aldehydes.

The process is initiated by the absorption of visible radiation by the photocatalyst. The long-lived excited photocatalyst *2DPAPhCzDCN is oxidatively quenched ($*E_{ox}$(2DPAPhCzDCN$^{\bullet+}$/*2DPAPhCzDCN) = −1.31 V *vs* SCE) in the presence of the bipyridine-Co(II) complex (E_{red}(Co^{II}/Co^{I}) = −1.05 V *vs* SCE), which is reduced to form the corresponding bipyridine-Co(I) complex. The oxidation of the Hantzsch ester (E_{ox}(HE$^{\bullet+}$/HE) = +1.0 V *vs* SCE) by the oxidized 2DPAPhCzDCN$^{\bullet+}$ (E_{ox}(2DPAPhCzDCN$^{\bullet+}$/2DPAPhCzDCN) = +1.31 V *vs* SCE in MeCN) leads to the Hantzsch ester radical cation (HE$^{\bullet+}$) and provides the turnover of the photocatalytic cycle. Co(I) undergoes oxidative addition with the allylic acetate to form an electrophilic (π-allyl)-cobalt(III) which is readily reduced by the photocatalyst, or by the strong reductant HE$^{\bullet+}$, in another SET event to produce a transient nucleophilic (π-allyl)-cobalt(II). Addition of this intermediate to the aldehyde creates a new C–C bond and the cobalt alkoxide product is formed. Hydrolysis of the Co-O bond by protons arising from the oxidative pathway of the Hantzsch ester releases the homoallylic alcohol and restores the cobalt catalytic cycle.

3.6 Conclusions

In conclusion, we have described for the first time the photoconversion of the common 3DPAFIPN photocatalyst into a new chemical species, named 2DPAPhCzDCN. A complete structural characterization revealed the photo-induced cleavage of the C-F bond, already known in the literature,[235] and the cyclization leading to a carbazole-1,3-dicarbonitrile derivative. Photophysical and electrochemical characterization showed similar TADF properties as the parent compound but a stronger reducing potentials, making it a suitable photocatalyst for the dual photoredox- and cobalt-catalyzed allylation of aldehydes, where the parent compound 3DPAFIPN was found to be not suitable. Although two cobalt-photoredox allylation strategies using 4CzIPN, one of the best known TADF photosensitizers, have recently been reported in the literature,[227,230] the dual photoredox- and cobalt-catalyzed allylation of aldehydes with the simple allyl acetate remains challenging, as it has only been reported using an Ir(III)-based photocatalyst. This work provides the first example of a dual photoredox/cobalt platform using a fully organic photocatalyst and provides insight into a new chemical structure with suitable TADF properties. The photodegradation of TADF-active halo-isophthalonitriles must be considered as a key factor for their use as photocatalysts[241] and for the design of suitable photoredox-promoted chemical transformations.

The ability of this new organic photocatalyst to trigger the reactivity of cobalt in low oxidation state could be further used in a future research in the development of dual photoredox- and cobalt-catalyzed protocols, e.g. in the asymmetric dual photoredox- and cobalt-catalyzed allylation of aldehydes and in the Reformatsky reaction. To date, although two light-driven Reformatsky protocols are reported in the literature,[242,243] a metallaphotoredox reaction using a fully organic photocatalyst under visible light irradiation has not been achieved yet and could be a significant implementation for more benign conditions.

Full account and description of the content of the chapter have been published in: E. Pinosa, E. Bassan, S. Cetin, M. Villa, S. Potenti, F. Calogero, A. Gualandi, A. Fermi, P. Ceroni, P. G. Cozzi, *J. Org. Chem.* **2023**, 88, 6390–6400.

3.7 Experimental section

General Methods

^{1}H NMR and ^{13}C NMR spectra were recorded on a Varian Mercury 400 spectrometer. Chemical shifts are reported in parts per million from TMS with the solvent resonance as the internal standard ($CHCl_3$, δ = 7.26; $CDCl_3$, δ = 77.0). Data are reported as follows: chemical shift, multiplicity (s, singlet; d, duplet; t, triplet; q, quartet; dd, double duplet; m, multiplet), coupling constants (hertz). Structural assignments were made with additional information from gCOSY, gHSQC, and gHMBC experiments. Chromatographic purification was performed with 240–400 mesh silica gel. HPLC-MS analyses were performed on an Agilent Technologies HP1100 instrument coupled with an Agilent Technologies MSD1100 single-quadrupole mass spectrometer using a Phenomenex Gemini C18 3 µm (100 mm × 3 mm) column; mass spectrometric detection was performed in full-scan mode from m/z 50 to 2500, with a scan time of 0.1 s in positive ion mode, an ESI spray voltage of 4500 V, nitrogen gas at 35 psi, a drying gas flow rate of 11.5 mL min^{-1}, and a fragmentor voltage of 30 V. HRMS was performed on a Waters Xevo G2-XS QTof instrument, ESI+, with a cone voltage of 40 V, a capillary voltage of 3 kV, and a source temperature of 120°C. All reactions were set up under an argon atmosphere in oven-dried glassware using standard Schlenk techniques. The reaction mixture was irradiated with a Kessil PR160L@456 nm instrument (see *Figure 3.23* for the emission profile). Diethyl 2,6-dimethyl-1,4-dihydropyridine-3,5-dicarboxylate (Hantzsch ester) was prepared following a literature procedure.[244]

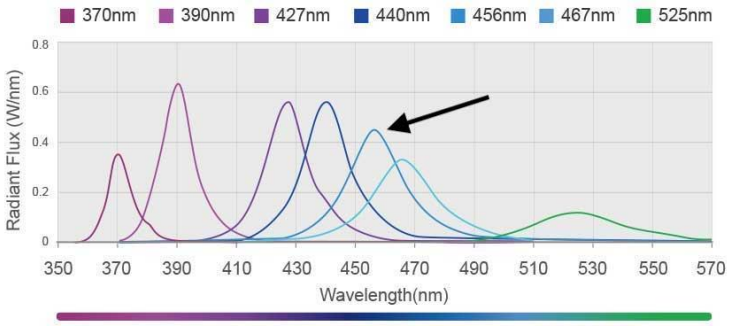

Figure 3.23 Emission profile of the Kessil® PR160L@456 nm used to irradiate the solutions (from Kessil® website: https://www.kessil.com/science/PR160L.php).

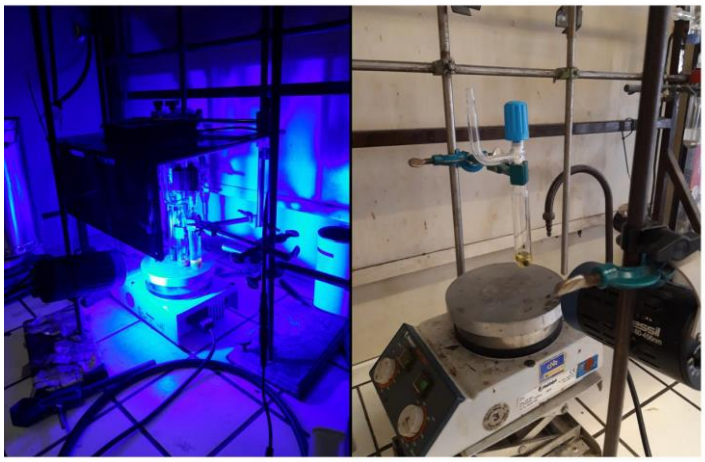

Figure 3.24 Reaction set-up with Kessil® PR160L@456 nm lamp. Reaction flasks were positioned approximatively at 18 cm from the light source.

Photophysical analyses

General Methods

All of the photophysical analyses were carried out in air-equilibrated tetrahydrofuran at 298 K, unless otherwise specified. UV–vis absorption spectra were recorded with a PerkinElmer λ40 spectrophotometer using quartz cells with an optical path length of 1.0 cm. Degassed solutions were obtained by means of repeated pump–freeze–thaw cycles (~4 × 10^{-6} mbar) in sealed quartz cuvettes. Luminescence spectra were recorded with a PerkinElmer LS-50, a Varian Cary Eclipse, or an Edinburgh FLS920 spectrofluorimeter equipped with a Hamamatsu R928 phototube. The estimated experimental errors are 2 nm on the band maximum and 5% on the molar absorption coefficient and luminescence lifetime. Luminescence measurements at 77 K were performed in a DCM/MeOH 1:1 (v/v) mixture using quartz tubes. Fluorescence lifetimes were measured with an Edinburgh FLS920 spectrofluorometer by a time-correlated single-photon counting (TCSPC) technique. Thermally-activated delayed fluorescence (TADF) lifetimes were measured with a PerkinElmer LS55 spectrofluorometer. Emission quantum yields were measured using perylene in MeOH (Φ_{FLUO} = 92%) as the standard.[245] TADF quantum yields were calculated by knowing Φ_{FLUO} and the intensity ratio between prompt and delayed fluorescence. Singlet oxygen quantum yields were measured with an Edinburgh FLS920 spectrofluorometer equipped with a Ge detector using tetraphenyl porphyrin (TPP) in THF (ΦΔ = 62%) as the standard.[246] Cyclic voltammetry was performed at room temperature by using an EcoChemie Autolab 30 potentiostat in a three-electrode setup [glassy carbon working electrode (d = 3 mm), silver wire quasi-reference electrode, and Pt wire counter electrode] in anhydrous MeCN (supporting electrolyte, 0.05 M $TEAPF_6$) and using Fc^+/Fc as the internal standard (Fc^+/Fc = +0.38 V *vs* SCE). The working electrode was polished with 0.03 μm alumina paste, rinsed with water and acetone, and finally blow-dried

Synthesis of 2,4,6-Tris(diphenylamino)-5-fluoroisophthalonitrile (3DPAFIPN)

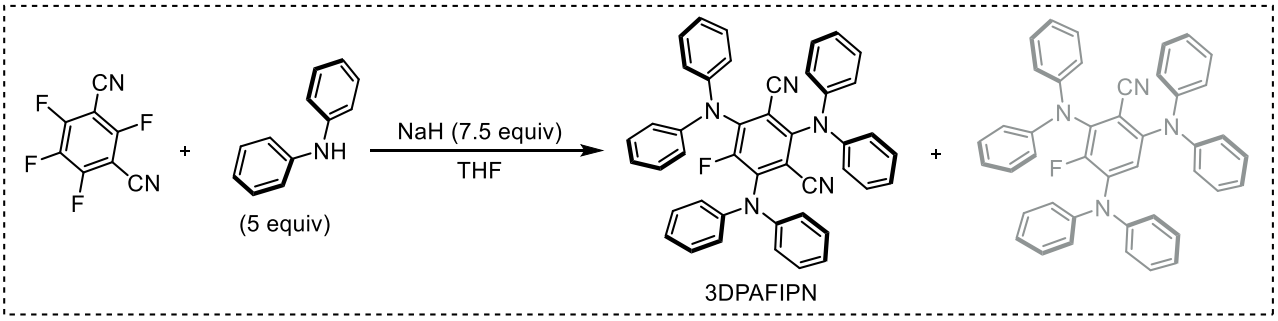

Diphenylamine (1.69 g, 10 mmol, 5.0 equiv.) and dry THF (20 mL) were added to a 50 mL round-bottom-flask, equipped with a magnetic stirring bar rod. The solution was cooled down to 0 °C and NaH (60% in mineral oil, 600 mg, 15 mmol, 7.5 equiv.) was slowly added while stirring vigorously. After 2 hours, tetrafluoroisophthalonitrile (400 mg, 2 mmol, 1 equiv.) was added, and the mixture was stirred at room temperature. The solution slowly turned from colorless to dark brown. When the TLC showed a complete consumption of the starting material (usually 2 days are required), water (1 mL) was added dropwise under vigorous stirring to neutralize the excess of NaH, and the mixture was evaporated to give a yellow solid. The residue was purified by flash chromatography (SiO_2, cyHexane/EtOAc 2:1) to obtain 3DPAFIPN as bright yellow solid (1.04 g, 1.6 mmol, 80% yield). By HPLC/MS analysis, the formation of the monocyano side-product in 5-7 mol%, that was not detected by ^{1}H NMR, was observed after purification. To obtain pure 3DPAFIPN, the product was further purified by flash chromatography (SiO_2, 98:2 cyHexane/Et_2O) to obtain pure 3DPAFIPN as a bright yellow solid. ^{1}H NMR (400 MHz, $CDCl_3$) δ = 7.25 (m, 12H), 7.11-7.01 (m, 6H), 7.01-6.86 (m, 12H); ^{13}C NMR (100 MHz, $CDCl_3$) δ = 152.4 (d, J = 259.5

Hz, 1C), 151.8 (d, *J* = 4.0 Hz, 1C), 145.5 (2C), 145.3 (4C), 143.0 (d, *J* = 11.0 Hz, 2C), 129.43 (8C), 129.36 (4C), 124.6 (4C), 124.0 (2C), 122.73 (8C), 122.70 (4C), 112.6 (d, *J* = 3.4 Hz, 2C) 108.9 (d, *J* = 3.2 Hz, 2C).

Synthesis of 2,4-bis(diphenylamino)-9-phenyl-9H-carbazole-1,3-dicarbonitrile (2DPAPhCzDCN)

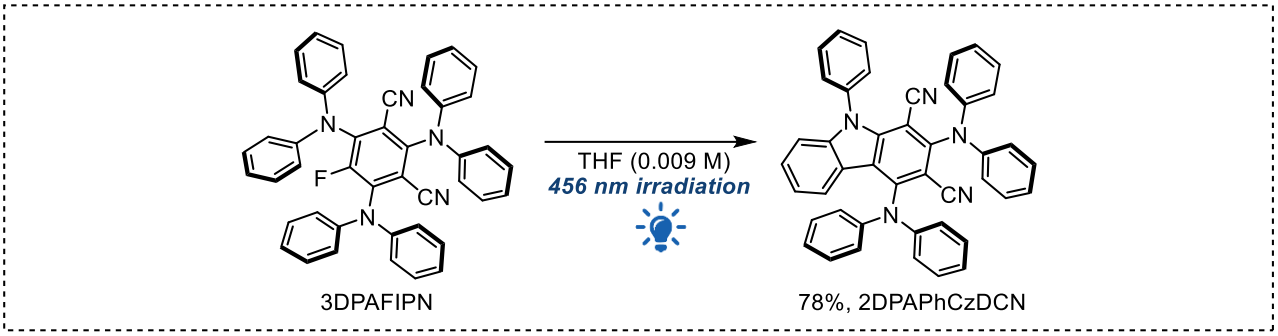

3DPAFIPN 78%, 2DPAPhCzDCN

A dry 20 mL Schlenk tube, equipped with a Rotaflo stopcock and a magnetic stirring bar under an argon atmosphere, was first charged with 3DPAFIPN (0.09 mmol, 60 mg). Then, inhibitor-free dry THF (10 mL) was added, and the reaction mixture was irradiated with a blue Kessil lamp (456 nm) ~15 cm from the light source, under vigorous stirring for 48h. After that, the solvent was removed under reduced pressure. The crude solid was purified by flash column chromatography (SiO_2, DCM) to afford 2DPAPhCzDCN as a bright yellow solid in 78% yield (44 mg, 0.07 mmol).

^{1}H NMR (400 MHz, $CDCl_3$) δ= 7.69 (d, J = 8.0 Hz, 1H), 7.57 (m, 3H), 7.49 (m, 2H), 7.36 (t, J = 7.5 Hz, 1H), 7.30-7.15 (m, 16H overlapped with the residual peak of the solvent), 7.12-7.04 (m, 3H), 7.04-6.96 (m, 8H);^{13}C NMR (100 MHz, $CDCl_3$) δ = 153.2, 148.2, 146.0 (2C), 145.1 (2C), 144.5, 143.2, 134.9, 130.4, 129.8, 129.4 (4C), 129.43, 129.37, 129.2, 129.2 (4C), 129.1, 127.7, 124.6, 123.5 (2C), 123.5 (2C), 122.9, 122.74 (4C), 122.4, 121.8 (4C), 121.7, 121.0, 120.9, 119.6, 114.2, 112.2, 110.5, 108.0;

HRMS (ESI/Q-TOF) m/z $[M + H]^+$ calcd for $C_{44}H_{30}N_5$ 628.2496, found 628.2495

HRMS (ESI/Q-TOF) m/z $[M + K]^+$ calcd for $C_{44}H_{29}KN_5$ 666.2055, found 666.2054.

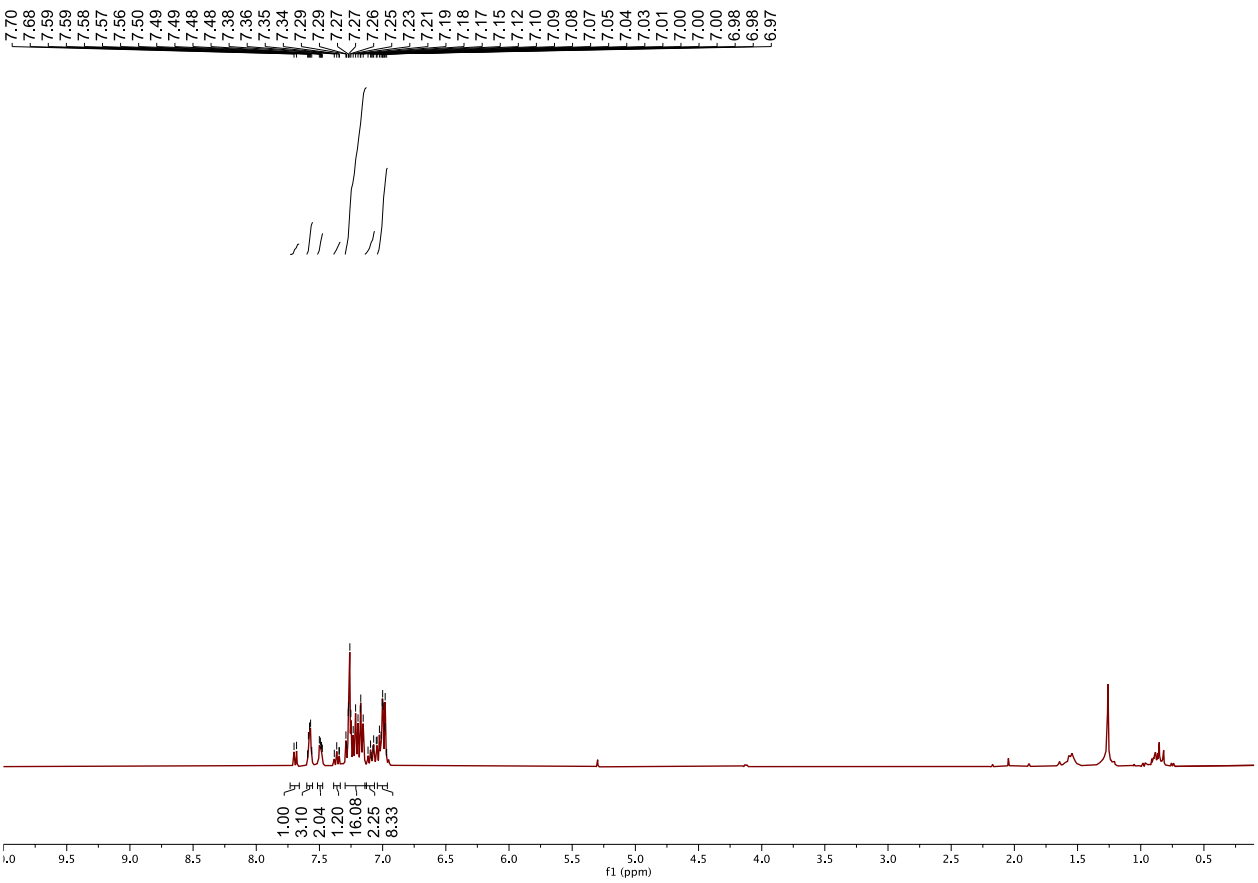

Figure 3.25 ^{1}H NMR (400 MHz, $CDCl_3$) of 2DPAPhCzDCN.

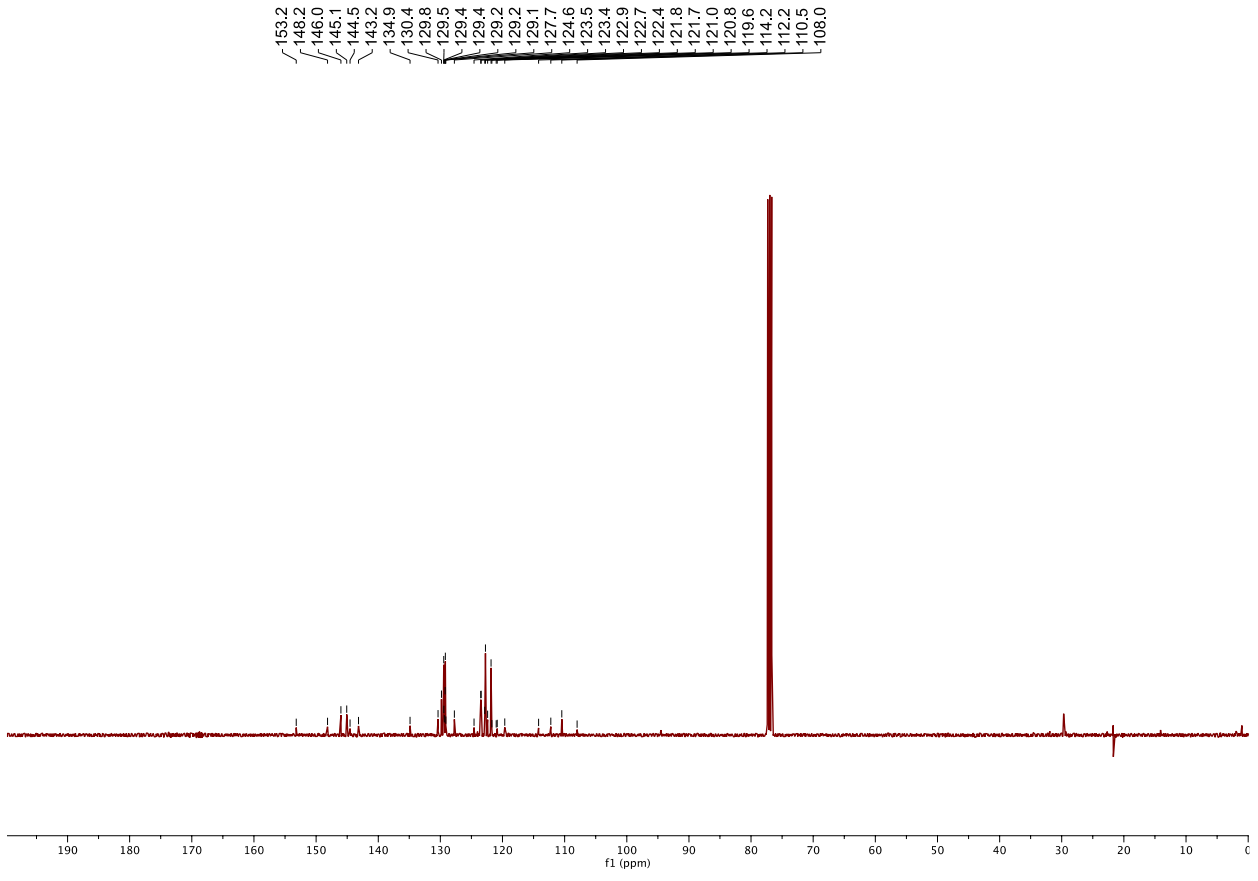

Figure 3.26 ^{13}C NMR (100 MHz, $CDCl_3$) of 2DPAPhCzDCN.

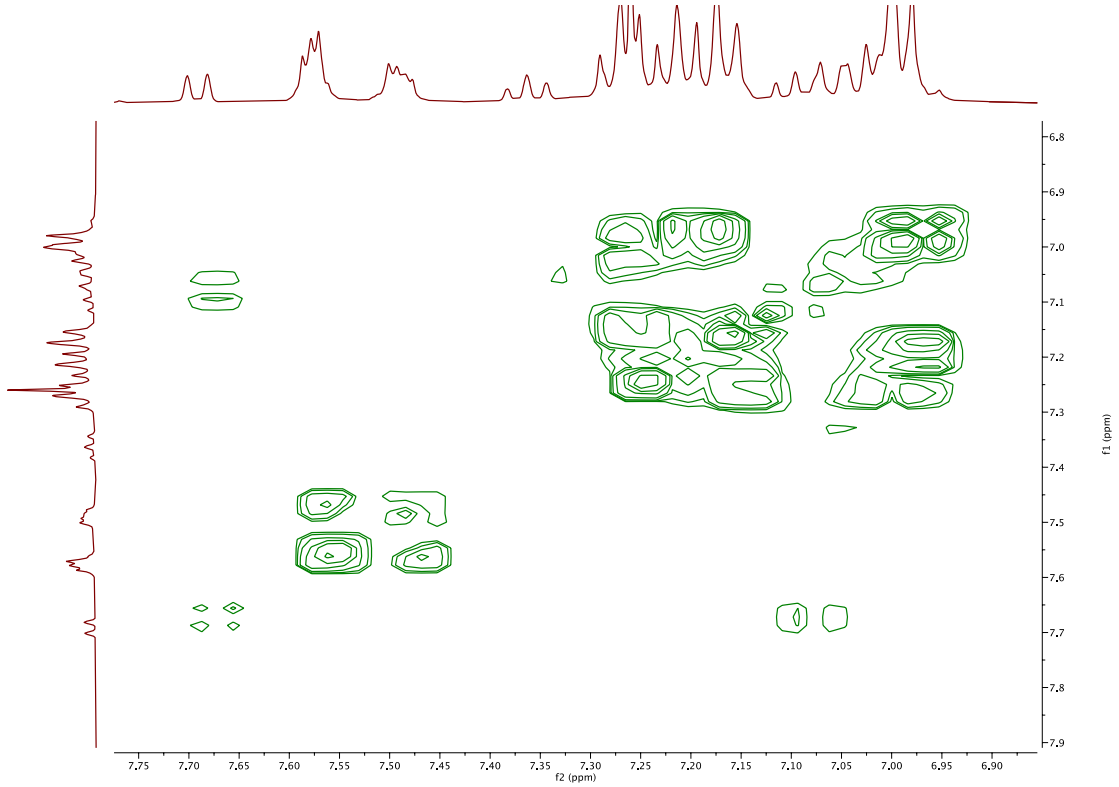

Figure 3.27 *COSY spectrum (400 MHz, $CDCl_3$) of 2DPAPhCzDCN.*

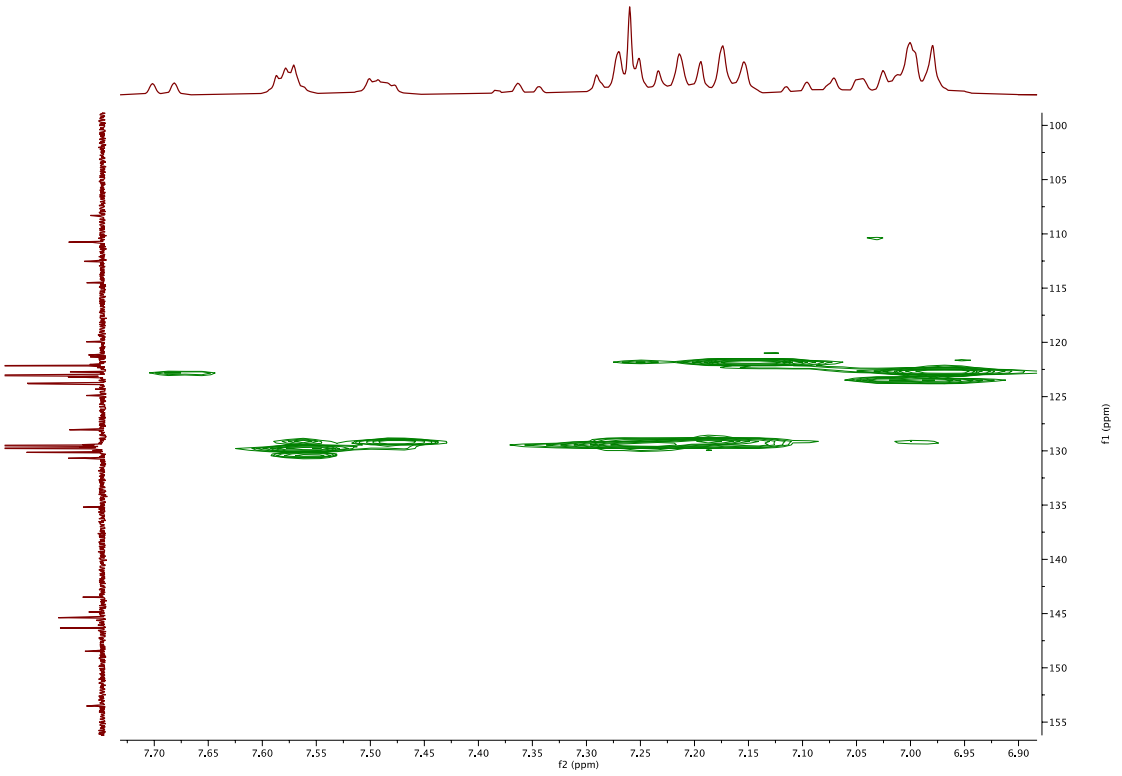

Figure 3.28 *HSQC spectrum (400 MHz, $CDCl_3$) of 2DPAPhCzDCN.*

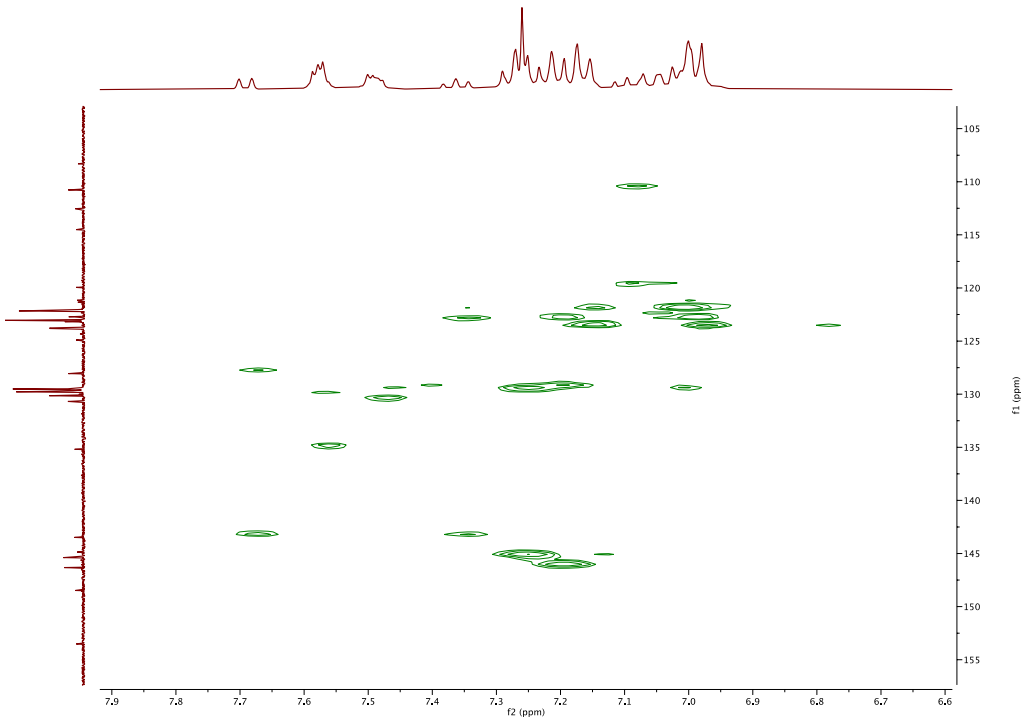

Figure 3.29 HMBC spectrum (400 MHz, $CDCl_3$) of 2DPAPhCzDCN.

Peaks assignments for 2

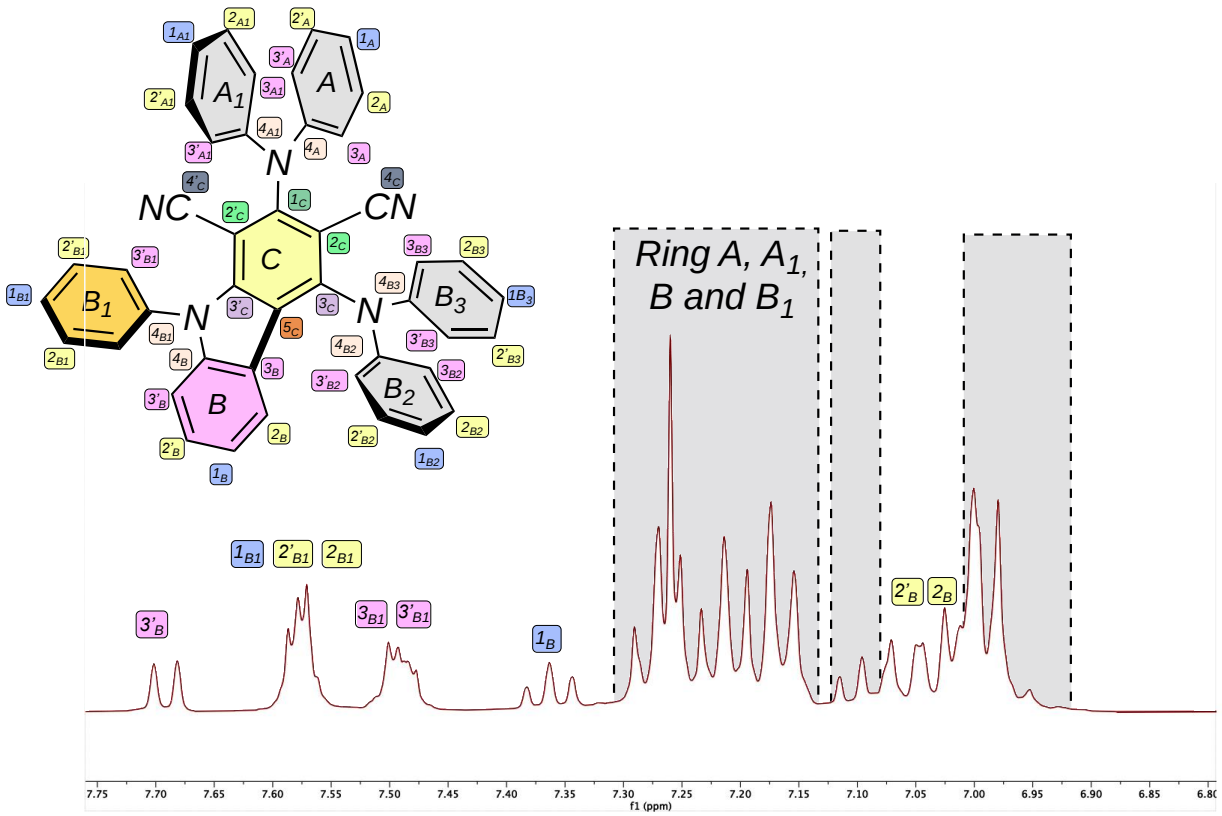

Figure 3.30 Graphical peak assignment for ^1H NMR: spectrum of 2DPAPhCzDCN.

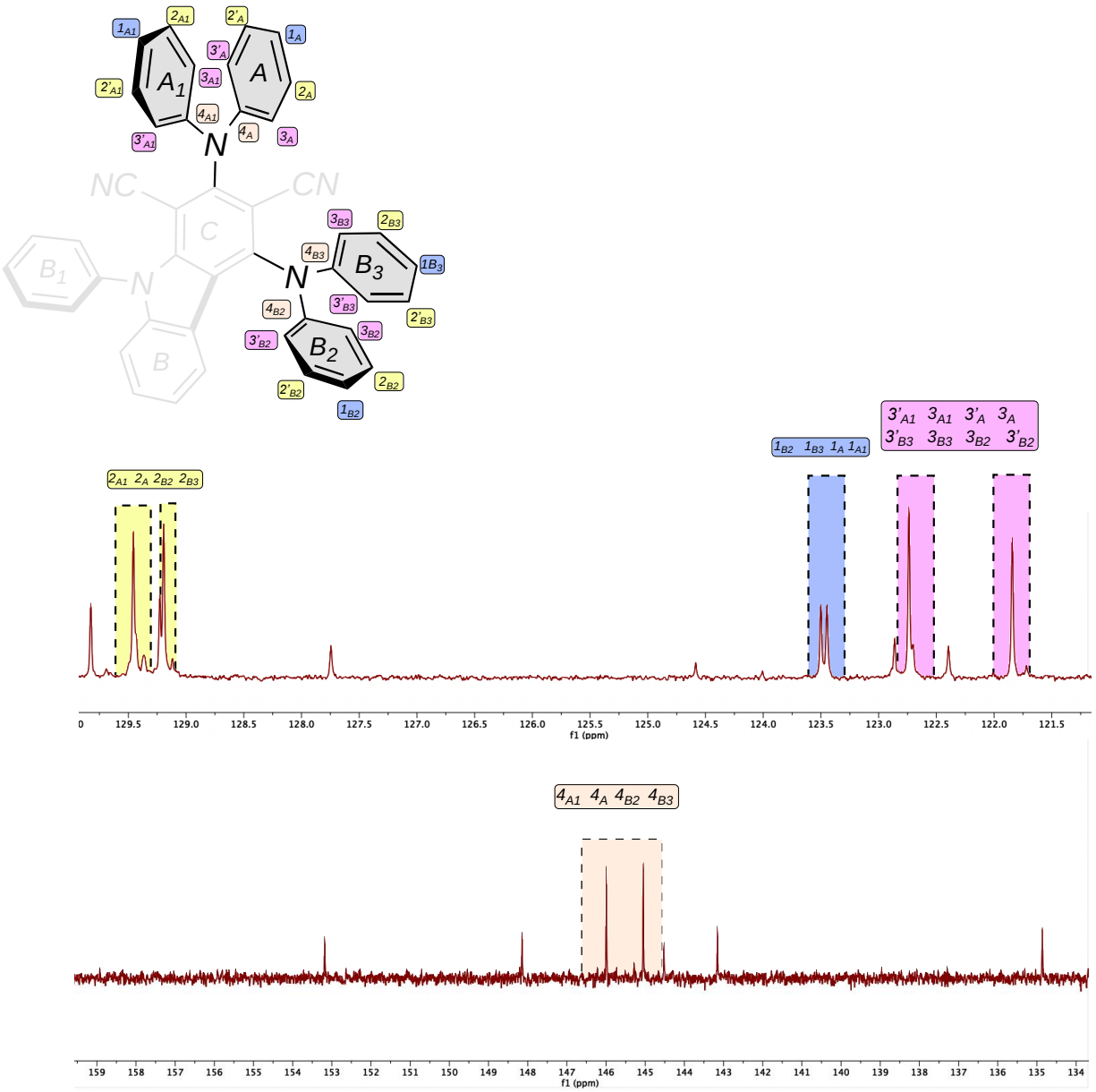

Figure 3.31 Graphical peak assignment for ^{13}C NMR: spectrum of 2DPAPhCzDCN (diphenyl amine region zoom)

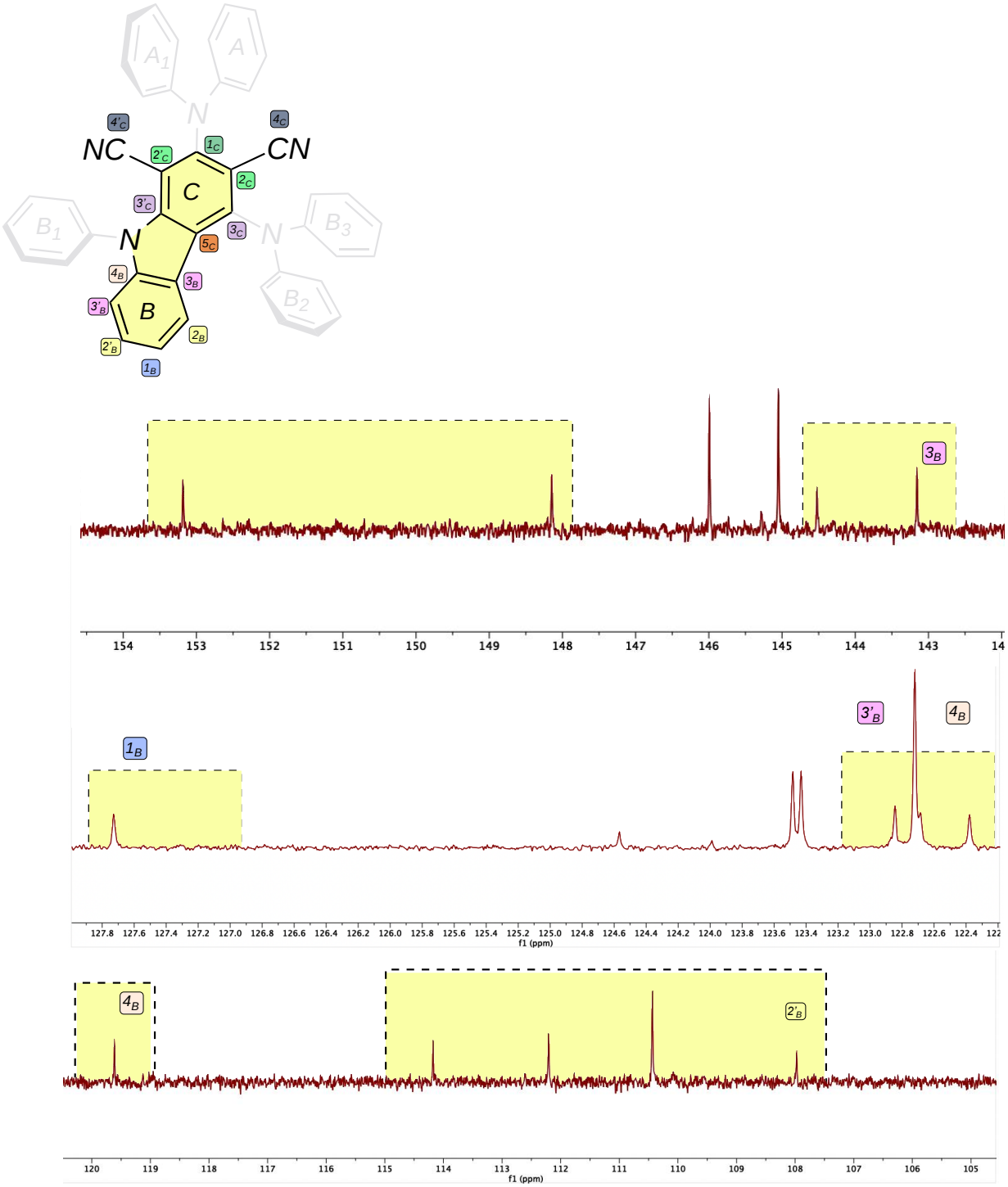

Figure 3.32 Graphical peak assignment for ^{13}C NMR: spectrum of 2DPAPhCzDCN (core region zoom)

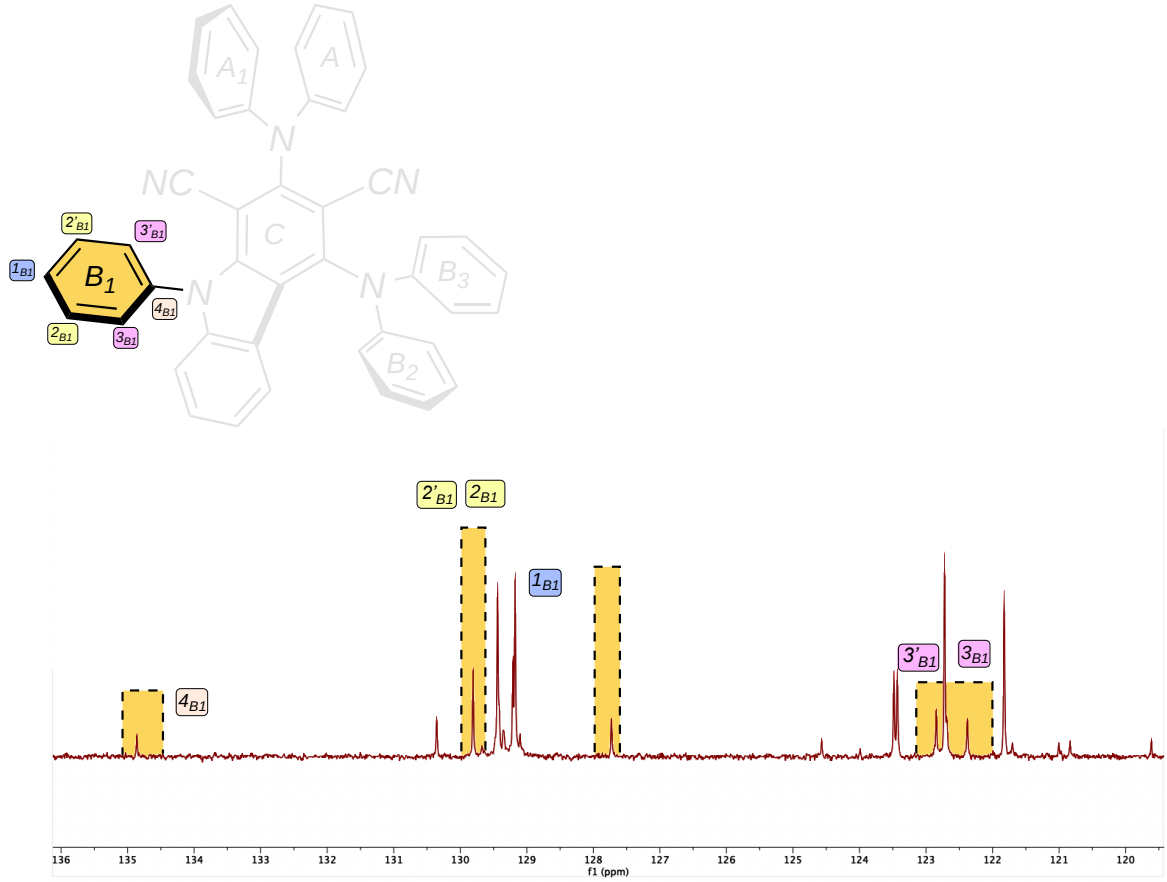

Figure 3.33 Graphical peak assignment for ^{13}C NMR: spectrum of 2DPAPhCzDCN (N-phenyl region zoom)

General procedure for the dual photoredox- and cobalt-catalyzed allylation of aldehydes

All of the reactions were performed on a 0.2 mmol scale of aldehyde, or in duplicate on a 0.1 mmol scale. A dry 10 mL Schlenk tube, equipped with a Rotaflo stopcock, a magnetic stirring bar, and an argon supply tube, was first charged with $CoBr_2 \cdot 6H_2O$ (4.6 mg, 14 µmol, 7 mol%) that was flame-dried under vacuum to remove the presence of water. Then 4,4-di-tert-butyl-2,2-dipyridyl (dtbpy, 5.4 mg, 20 µmol, 10 mol%) and freshly distilled inhibitor-free THF (1 mL) were added. The reaction was kept under vigorous stirring for a few minutes, and then substrate (0.2 mmol, 1 equiv.), the organic photocatalyst 2DPAPhCzDCN (6.3 mg, 0.01 mmol, 5 mol%), and diethyl 1,4-dihydro-2,6-dimethyl-3,5-pyridinedicarboxylate (Hantzsch ester) (101 mg, 0.4 mmol, 2 equiv.) were added. THF (2.6 mL) and distilled water (0.4 mL) were then added; the reaction mixture was further subjected to a freeze-pump-thaw procedure (three cycles), and the vessel was refilled with argon. Then, allyl acetate **2a** (65 µL, 0.6 mmol, 3 equiv.) was added. The reaction mixture was irradiated with a blue Kessil lamp (456 nm) ~15 cm from the light source, under vigorous stirring from 16 to 72h. After that, the reaction was quenched with water (approximately 4 mL) and the mixture extracted with EtOAc (3 x 10 mL). The combined organic layers were dried over anhydrous Na_2SO_4, and the solvent was removed under reduced pressure. The crude was purified by flash column chromatography (100% DCM) to afford the products in the stated yields.

General procedure for the 1 mmol scale reaction

A dry 30 mL Schlenk tube, equipped with a Rotaflo stopcock, a magnetic stirring bar, and an argon supply tube, was first charged with $Co(OAc)_2 \cdot 4H_2O$ (18 mg, 0.07 mmol, 7 mol%) that was flame-dried under vacuum to remove the presence of water. Then 4,4-di-tert-butyl-2,2-dipyridyl (dtbbpy, 27 mg, 0.1

mmol, 10 mol%) and freshly distilled inhibitor-free THF (5 mL) were added. The reaction was kept under vigorous stirring for a few minutes, and then substrate **1a** (140 mg, 1 mmol, 1 equiv.), the organic photocatalyst 2DPAPhCzDCN (31 mg, 0.05 mmol, 5 mol%), and diethyl 1,4-dihydro-2,6-dimethyl-3,5-pyridinedicarboxylate (Hantzsch ester) (506 mg, 2 mmol, 2 equiv.) were added. THF (13 mL) and distilled water (2 mL) were then added; the reaction mixture was further subjected to a freeze-pump-thaw procedure (three cycles), and the vessel was refilled with argon. Then, allyl acetate **2a** (0.33 mL, 3 mmol, 3 equiv.) was added. The reaction mixture was irradiated with a blue Kessil lamp (456 nm) ~15 cm from the light source, under vigorous stirring for 16h. After that, the reaction was quenched with water (approximately 20 mL) and the mixture extracted with EtOAc (3 x 20 mL). The combined organic layers were dried over anhydrous Na_2SO_4, and the solvent was removed under reduced pressure. The title compound was isolated by flash column chromatography (7:3 DCM/hexane) as a pale yellow oil in 50% yield (90 mg, 0.49 mmol). Spectroscopic data were according to the literature.[247]

Characterization of the products

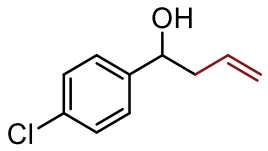

1-(4-Chlorophenyl) But-3-en-1-ol (3a). Pale yellow oil, 87% (16 mg, 0.088 mmol).

The general procedure (16 h) was applied using **1a** (14 mg, 0.1 mmol) and **2a** (32 µL, 0.3 mmol, 3 equiv.). The title compound was isolated by flash column chromatography (100% DCM). Spectroscopic data were according to the literature.[247]

^{1}H NMR (400 MHz, $CDCl_3$) δ = 7.31–7.26 (m, 4H), 5.81–5.71 (m, 1H), 5.17–5.11 (m, 2H), 4.71 (dd, J = 7.8, 5.1 Hz, 1H), 2.52–2.39 (m, 2H); ^{13}C NMR (100 MHz, $CDCl_3$) δ = 142.2, 133.9, 133.1, 128.5 (2C), 127.2 (2C), 118.9, 72.5, 43.9.

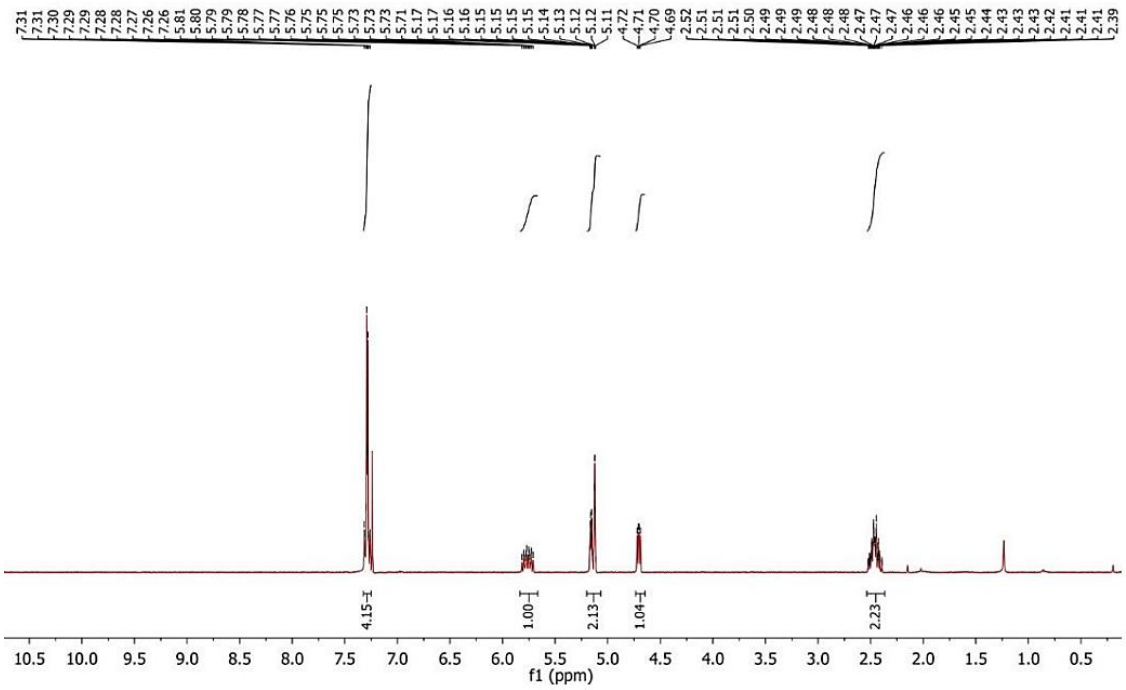

*Figure 3.34 ^{1}H NMR of **3a**.*

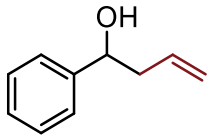

1-Phenylbut-3-en-1-ol (3b). Pale yellow oil, 68% (10 mg, 0.068 mmol).

The general procedure (16 h) was applied using previously distilled **1b** (10 µL, 0.1 mmol) and **2a** (32 µL, 0.3 mmol, 3 equiv.). The title compound was isolated by flash column chromatography (100% DCM). Spectroscopic data were according to the literature.[247]

^{1}H NMR (400 MHz, $CDCl_3$) δ = 7.35–7.24 (m, 5H), 5.81–5.76 (m, 1H), 5.18–5.11 (m, 2H), 4.72 (dd, J = 7.6, 5.4 Hz, 1H), 2.52–2.49 (m, 2H), 2.10 (br s, 1H); ^{13}C NMR (100 MHz, $CDCl_3$) δ = 143.9, 134.5, 128.4 (2C), 127.5, 125.8 (2C), 118.3, 73.3, 43.8.

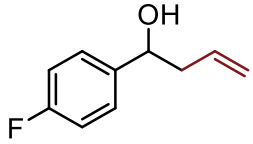

1-(4-Fluorophenyl) But-3-en-1-ol (3c). Pale yellow oil, 53% (9 mg, 0.054 mmol).

The general procedure (16 h) was applied using previously distilled **1c** (11 µL, 0.1 mmol) and **2a** (32 µL, 0.3 mmol, 3 equiv.). The title compound was isolated by flash column chromatography (100% DCM). Spectroscopic data were according to the literature:[129]

^{1}H NMR (400 MHz, $CDCl_3$) δ = 7.33–7.29 (m, 2H), 7.05–6.99 (m, 2H), 5.82–5.72 (m, 1H), 5.17–5.12 (m, 2H), 4.71 (dd, J = 7.9, 4.8 Hz, 1H), 2.52–2.43 (m, 2H), 1.88 (br s, 1H); ^{13}C NMR (100 MHz, $CDCl_3$) δ = 163.3, 160.9 139.5, 134.1, 127.4 (2C), 118.7, 115.3, 115.1, 72.6, 43.9; ^{19}F NMR (377 MHz, $CDCl_3$) δ = −115.23 (m, 1F).

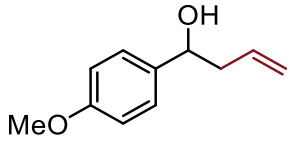

1-(4-Methoxyphenyl) But-3-en-1-ol (3d). Pale yellow oil, 40% (7.2 mg, 0.040 mmol).

The general procedure (16 h) was applied using previously distilled **1d** (12 µL, 0.1 mmol) and **2a** (32 µL, 0.3 mmol, 3 equiv.). The title compound was isolated by flash column chromatography (100% DCM). Spectroscopic data were according to the literature.[247]

^{1}H NMR (400 MHz, $CDCl_3$) δ = 7.29–7.24 (m, 2H), 6.89–6.85 (m, 2H), 5.79 (ddt, J = 17.2, 10.2, 7.1 Hz, 1H), 5.17–5.09 (m, 2H), 4.67 (t, J = 6.5 Hz, 1H), 3.79 (s, 3H), 2.51–2.47 (m, 2H); ^{13}C NMR (100 MHz, $CDCl_3$) δ = 159.0, 136.0, 134.6, 127.0 (2C), 118.2, 113.8 (2C), 72.9, 55.3, 43.7.

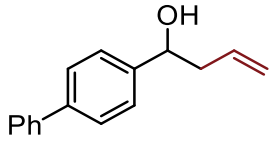

1-([1,1-Biphenyl]-4-yl) But-3-en-1-ol (3e). Pale yellow oil, 31% (14 mg, 0.063 mmol).

The general procedure (16 h) was applied using **1e** (36 mg, 0.2 mmol) and **2a** (65 µL, 0.6 mmol, 3 equiv.). The title compound was isolated by flash column chromatography (100% DCM). Spectroscopic data were according to the literature.[247]

^{1}H NMR (400 MHz, $CDCl_3$) δ = 7.59–7.57 (m, 4H), 7.43–7.41 (m, 4H), 7.35–7.31 (m, 1H), 5.89–5.79 (m, 1H), 5.22–5.14 (m, 2H), 4.78 (t, J = 5.4 Hz, 1H), 2.58–2.52 (m, 2H), 2.07 (br s, 1H); ^{13}C NMR (100 MHz, $CDCl_3$) δ = 142.9, 140.8, 140.5, 134.4, 128.7 (2C), 127.2, 127.1 (2C), 127.0 (2C), 126.2 (2C), 118.5, 73.0, 43.8.

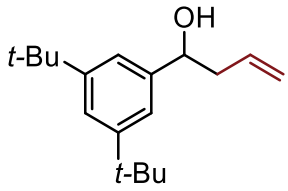

1-(3,5-Di-tert-butylphenyl) But-3-en-1-ol (3f). Pale yellow oil, 56% (29 mg, 0.11 mmol).

The general procedure (16 h) was applied using **1f** (44 µL, 0.2 mmol) and **2a** (65 µL, 0.6 mmol, 3 equiv.). The title compound was isolated by flash column chromatography (100% DCM). Spectroscopic data were according to the literature.[248]

^{1}H NMR (400 MHz, $CDCl_3$) δ = 7.35 (s, 1H), 7.20 (s, 2H), 5.91–5.81 (m, 1H), 5.21–5.13 (m, 2H), 4.71 (t, J = 5.4 Hz, 1H), 1.94 (br s, 1H), 1.33 (s, 18H); ^{13}C NMR (100 MHz, $CDCl_3$) δ = 150.8, 143.1, 135.0, 121.6, 120.0, 118.0, 74.1, 43.9, 34.9, 31.5.

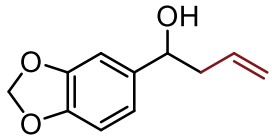

1-(Benzo[d][1,3]dioxol-5-yl) But-3-en-1-ol (3g). Pale yellow oil, 49% (19 mg, 0.096 mmol).

The general procedure (16 h) was applied using **1g** (30 mg, 0.2 mmol) and **2a** (65 µL, 0.6 mmol, 3 equiv.). The title compound was isolated by flash column chromatography (100% DCM). Spectroscopic data were according to the literature.[247]

^{1}H NMR (400 MHz, $CDCl_3$) δ = 6.86 (d, J = 1.5 Hz, 1H), 6.80–6.74 (m, 2H), 5.93 (s, 2H), 5.82–5.72 (m, 1H), 5.16–5.10 (m, 2H), 4.62 (t, J = 6.5 Hz, 1H), 2.47–2.43 (m, 2H), 2.01 (br s, 1H); ^{13}C NMR (100 MHz, $CDCl_3$) δ = 147.7, 146.9, 137.9, 134.4, 119.2, 118.4, 108.0, 106.4, 101.0, 73.2, 43.8.

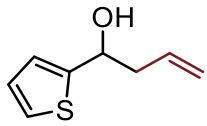

1-(Thiophen-2-yl) But-3-en-1-ol (3h). Pale yellow oil, 39% (12 mg, 0.078 mmol).

The general procedure (16 h) was applied using previously distilled **1h** (19 µL, 0.2 mmol) and **2a** (65 µL, 0.6 mmol, 3 equiv.). The title compound was isolated by flash column chromatography (100% DCM). Spectroscopic data were according to the literature.[129]

^{1}H NMR (400 MHz, $CDCl_3$) δ = 7.25–7.21 (m, 1H), 7.00–6.92 (m, 2H), 5.82 (ddt, J = 17.2, 10.2, 7.1 Hz, 1H), 5.23–5.11 (m, 2H), 4.98 (t, J = 6.4 Hz, 1H), 2.69–2.53 (m, 2H), 2.19 (s, 1H); ^{13}C NMR (100 MHz, $CDCl_3$) δ = 147.76, 133.79, 126.60, 124.54, 123.66, 118.80, 69.34, 43.76.

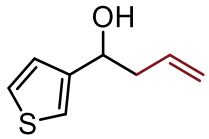

1-(Thiophen-3-yl) But-3-en-1-ol (3i). Pale yellow oil, 45% (14 mg, 0.09 mmol).

The general procedure (16 h) was applied using previously distilled **1i** (19 µL, 0.2 mmol) and **2a** (65 µL, 0.6 mmol, 3 equiv.). The title compound was isolated by flash column chromatography (100% DCM). Spectroscopic data were according to the literature.[129]

^{1}H NMR (400 MHz, $CDCl_3$) δ = 7.29 (dd, *J* = 5.0, 3.0 Hz, 1H), 7.19 (d, *J* = 2.9 Hz, 1H), 7.07 (dd, *J* = 5.0, 1.2 Hz, 1H), 5.84–5.74 (m, 1H), 5.18–5.11 (m, 2H), 4.83 (dt, *J* = 8.0, 4.2 Hz, 1H), 2.58–2.45 (m, 2H), 2.09 (br s, 1H); ^{13}C NMR (100 MHz, $CDCl_3$) δ = 145.3, 134.2, 126.0, 125.6, 120.7, 118.5, 69.5, 43.0.

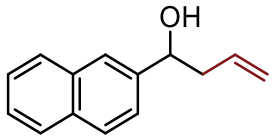

1-(Naphthalen-2-yl) But-3-en-1-ol (3j). Pale yellow oil, 35% (14 mg, 0.070 mmol).

The general procedure (16 h) was applied using **1j** (31 mg, 0.2 mmol) and **2a** (65 µL, 0.6 mmol, 3 equiv.). The title compound was isolated by flash column chromatography (100% DCM). Spectroscopic data were according to the literature.[247]

^{1}H NMR (400 MHz, $CDCl_3$) δ = 7.84–7.79 (m, 4H), 7.49–7.45 (m, 3H), 5.88–5.77 (m, 1H), 5.21–5.12 (m, 2H), 4.89 (dd, *J* = 7.2, 5.9 Hz, 1H), 2.66–2.53 (m, 2H), 2.12 (br s, 1H); ^{13}C NMR (100 MHz, $CDCl_3$) δ = 141.2, 134.3, 133.2, 132.9, 128.2, 127.9, 127.6, 126.1, 125.8, 124.5, 124.0, 118.5, 73.5, 43.7.

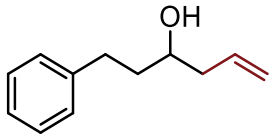

1-Phenylhex-5-en-3-ol (3k). Pale yellow oil, 34% (12 mg, 0.068 mmol).

The general procedure (72 h) was applied using previously distilled **1k** (26 µL, 0.2 mmol) and **2a** (65 µL, 0.6 mmol, 3 equiv.). The title compound was isolated by flash column chromatography (100% DCM). Spectroscopic data were according to the literature.[247]

^{1}H NMR (400 MHz, $CDCl_3$) δ = 7.29–7.17 (m, 5H), 5.81–5.79 (m, 1H), 5.16–5.11 (m, 2H), 3.66 (ddd, *J* = 12.2, 7.6, 4.7 Hz, 1H), 2.80–2.75 (m, 1H), 2.72–2.64 (m, 1H), 2.31–2.28 (m, 1H), 2.24–2.15 (m, 1H), 1.81–1.75 (m, 2H), 1.61 (br s, 1H); ^{13}C NMR (100 MHz, $CDCl_3$) δ = 142.0, 134.6, 128.4 (2C), 128.4 (2C), 125.8, 118.3, 69.9, 42.0, 38.4, 32.0.

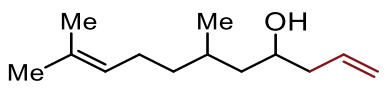

6,10-Dimethylundeca-1,9-dien-4-ol (3l). Pale yellow oil, 31% (12 mg, 0.061 mmol).

The general procedure (72 h) was applied using previously distilled **1l** (36 µL, 0.2 mmol) and **2a** (65 µL, 0.6 mmol, 3 equiv.). The title compound was isolated by flash column chromatography (100% DCM) as a mixture of *syn* and *anti* diastereoisomers. Spectroscopic data were according to the literature.[247]

^{1}H NMR (400 MHz, $CDCl_3$) mixture of diastereoisomers δ = 5.86–5.76 (m, 1H), 5.14–5.08 (m, 3H), 3.76–3.70 (m, 1H), 2.28–2.22 (m, 1H), 2.16–2.04 (m, 1H), 2.04–1.87 (m, 2H), 1.66 (s, 3H), 1.69–1.55 (m, 3H), 1.58 (s, 3H), 1.51–1.05 (m, 2H), 0.90 (dd, *J* =6.4, 6.4 Hz, 3H); ^{13}C NMR (100 MHz, $CDCl_3$) mixture of diastereoisomers δ = 135.1, 135.0, 131.4, 124.9, 118.3, 118.2, 68.9, 68.5, 44.5, 44.4, 42.9, 42.3, 38.0, 36.9, 29.5, 29.1, 25.9, 25.6, 25.6, 20.4, 19.3, 17.8.

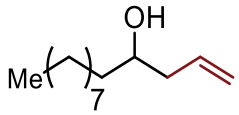

Tridec-1-en-4-ol (3m). Pale yellow oil, 33% (13 mg, 0.066 mmol).

The general procedure (72 h) was applied using previously distilled **1m** (38 µL, 0.2 mmol) and **2a** (65 µL, 0.6 mmol, 3 equiv.). The title compound was isolated by flash column chromatography (100% DCM). Spectroscopic data were according to the literature.[129]

^{1}H NMR (400 MHz, $CDCl_3$) δ = 5.83 (dddd, *J* = 20.4, 9.6, 7.9, 6.5 Hz, 1H), 5.17–5.10 (m, 2H), 3.64 (dtd, *J* = 7.7, 5.9, 4.1 Hz, 1H), 2.34–2.26 (m, 1H), 2.13 (dt, *J* = 13.7, 7.9 Hz, 1H), 1.60 (s, 2H), 1.44 (d, *J*= 2.7 Hz, 1H), 1.26 (t, *J* = 3.2 Hz, 12H), 0.90–0.85 (m, 4H); ^{13}C NMR (100 MHz, $CDCl_3$) δ = 134.9, 118.0, 70.7, 41.9, 36.8, 31.9, 29.6, 29.6, 29.5, 29.3, 25.6, 22.6, 14.1.

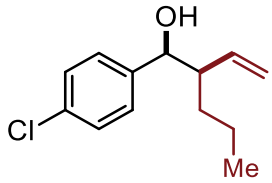

1-(4-Chlorophenyl)-2-vinylpentan-1-ol (3n). Isolated as mixture of diastereoisomers $dr_{syn:anti}$= 1.4:1, colorless oil, 40% (9 mg, 0.040 mmol).

The general procedure (16 h) was applied using **1a** (14 mg, 0.1 mmol) and **2b** (43 mg, 0.3 mmol, 3 equiv.). The title compound was isolated by two consecutive flash column chromatography (7:3 DCM/hexane, then 8:1 Hexane/EtOAc). Spectroscopic data were according to the literature.[249]

^{1}H NMR (400 MHz, $CDCl_3$) δ = 7.31–7.25 (m, 6H), 7.20–7.17 (m, 2H), 5.61 (ddd, *J* = 17.2, 10.3, 9.2 Hz, 1H, *anti*), 5.45 (ddd, *J* = 17.1, 10.3, 9.1 Hz, 1H, *syn*), 5.27–5.13 (m, 2H, *anti*), 5.09–4.96 (m, 2H, *syn*), 4.59 (m, 1H, *syn*), 4.35 (d, *J* = 8.2 Hz, 1H, *anti*), 2.37 (m, 1H), 2.27–2.19 (m, 1H), 2.18 (d, *J* = 2.3 Hz, 1H), 2.00 (d, *J* = 4.6 Hz, 1H), 1.51–1.36 (m, 2H), 1.35–1.27 (m, 2H), 1.14 (m, 6H), 0.84 (t, *J* = 7.1 Hz, 3H), 0.77 (t, *J*= 7.0 Hz, 3H); ^{13}C NMR (100 MHz, $CDCl_3$) δ = 141.0 (*anti*), 140.9 (*syn*), 138.9 (*anti*), 138.1 (*syn*), 133.2 (*anti*), 133.0 (*syn*), 128.3 (*syn*+*anti*), 128.1 (*anti*), 128.0 (*syn*), 119.1 (*anti*), 117.7 (*syn*), 76.2 (*syn*), 75.9 (*anti*), 52.6 (*anti*), 51.2 (*syn*), 32.5 (*anti*), 31.7 (*syn*), 20.3 (*syn*+*anti*), 14.0 (*syn*), 13.8 (*anti*).

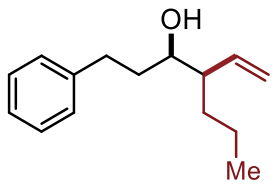

1-phenyl-4-vinylheptan-3-ol (3o). Isolated as mixture of diastereoisomers, $dr_{syn:anti}$= 1.2:1, colorless oil, 23% (5 mg, 0.023 mmol).

The general procedure (48 h) was applied using previously distilled **1k** (13 µL, 0.1 mmol) and **2b** (43 mg, 0.3 mmol, 3 equiv.). The title compound was isolated by two consecutive flash column chromatography (7:3 DCM/hexane, then 8:1 Hexane/EtOAc). Spectroscopic data were according to the literature.[250]

^{1}H NMR (400 MHz, $CDCl_3$, *syn*+*anti*) δ = 7.28 (d, *J* = 7.7 Hz, 2H), 7.22–7.12 (m, 3H), 5.63–5.51 (m,1H), 5.19–5.03 (m, 2H), 3.54–3.41 (m, 1H), 2.87–2.77 (m, 1H), 2.70–2.58 (m, 1H), 2.14–2.01 (m, 1H), 1.89–1.77 (m, 1H), 1.76–1.57 (m, 1H), 1.43–1.28 (m, 4H), 0.85 (t, *J* = 8.0 Hz, 3H); ^{13}C NMR (100 MHz, $CDCl_3$) δ = 142.3 (*syn*+*anti*), 138.9 (*anti*),138.8 (*syn*), 128.4 (2H, *syn*), 128.3 (2H, *anti*), 125.7 (*syn*+*anti*), 118.0 (*syn*), 117.4 (*anti*), 73.7 (*anti*), 72.9 (*syn*), 50.6 (*anti*), 50.3 (*syn*), 36.5 (*syn*), 35.7 (*anti*), 32.9 (*syn*), 32.4 (*anti*), 32.3 (*anti*), 32.1 (*syn*), 20.4 (*syn*+*anti*), 14.0 (*syn*+*anti*).

3.8 Bibliography

[207] B. Su, Z.-C. Cao, Z.-J. Shi, *Acc. Chem. Res.* **2015**, *48*, 886–896.
[208] F. Hebrard, P. Kalck, *Chem. Rev.* **2009**, *109*, 4272–4282.
[209] S. Gupta, R. Fernandes, R. Patel, M. Spreitzer, N. Patel, *Appl. Catal. Gen.* **2023**, *661*, 119254.
[210] M. M. Tohidi, B. Paymard, S. R. Vasquez-García, D. Fernández-Quiroz, *Tetrahedron* **2023**, *136*, 133352.
[211] H. Wang, X. Jie, T. Su, Q. Wu, J. Kuang, Z. Sun, Y. Zhao, Q. Chong, Y. Guo, Z. Zhang, F. Meng, *J. Am. Chem. Soc.* **2024**, *146*, 23476–23486.
[212] M. Lombardo, A. Gualandi, F. Pasi, C. Trombini, *Adv. Synth. Catal.* **2007**, *349*, 465–468.
[213] M. Moselage, J. Li, L. Ackermann, *ACS Catal.* **2016**, *6*, 498–525.
[214] V. Dwivedi, D. Kalsi, B. Sundararaju, *ChemCatChem* **2019**, *11*, 5160–5187.
[215] Y. Xu, Y. Lin, S. L. Homölle, J. C. A. Oliveira, L. Ackermann, *J. Am. Chem. Soc.* **2024**, *146*, 24105–24113.
[216] R. Mei, U. Dhawa, R. C. Samanta, W. Ma, J. Wencel-Delord, L. Ackermann, *ChemSusChem* **2020**, *13*, 3306–3356.
[217] M. Smith, *Organic Synthesis*, Academic Press, **2011**.
[218] B. M. Trost, M. L. Crawley, *Chem. Rev.* **2003**, *103*, 2921–2944.
[219] G. Zanoni, A. Pontiroli, A. Marchetti, G. Vidari, *Eur. J. Org. Chem.* **2007**, *2007*, 3599–3611.
[220] K. Spielmann, G. Niel, R. M. De Figueiredo, J.-M. Campagne, *Chem. Soc. Rev.* **2018**, *47*, 1159–1173.
[221] E. Joseph, J. A. Tunge, *Chem. Eur. J.* **2024**, *30*, e202401707.
[222] C. K. Reddy, P. Knochel, *Angew. Chem. Int. Ed.* **1996**, *35*, 1700–1701.
[223] S. Ghorai, S. S. Chirke, W.-B. Xu, J.-F. Chen, C. Li, *J. Am. Chem. Soc.* **2019**, *141*, 11430–11434.
[224] A. Moncomble, C. Gosmini, *Isr. J. Chem.* **2010**, *50*, 568 – 576.
[225] O. Buriez, C. Cannes, J.-Y. Nédélec, J. Périchon, *J. Electroanal. Chem.* **2000**, *495*, 57–61.
[226] A. Gualandi, G. Rodeghiero, R. Perciaccante, T. P. Jansen, C. Moreno-Cabrerizo, C. Foucher, M. Marchini, P. Ceroni, P. G. Cozzi, *Adv. Synth. Catal.* **2021**, *363*, 1105–1111.
[227] C. Shi, F. Li, Y. Chen, S. Lin, E. Hao, Z. Guo, U. T. Wosqa, D. Zhang, L. Shi, *ACS Catal.* **2021**, *11*, 2992–2998.
[228] P. Gomes, O. Buriez, E. Labbé, C. Gosmini, J. Périchon, *J. Electroanal. Chem.* **2004**, *562*, 255–260.
[229] S. Xue, À. Cristòfol, B. Limburg, Q. Zeng, A. W. Kleij, *ACS Catal.* **2022**, 12, *6*, 3651–3659.
[230] D. Zhang, H. Li, Z. Guo, Y. Chen, H. Yan, Z. Ye, F. Zhang, B. Lu, E. Hao, L. Shi, *Green Chem.* **2022**, *24*, 9027–9032.
[231] J. Luo, J. Zhang, *ACS Catal.* **2020**, *10*, 14302–14303.
[232] A. Gualandi, F. Calogero, M. Mazzarini, S. Guazzi, A. Fermi, G. Bergamini, P. G. Cozzi, *ACS Catal.* **2020**, *10*, 3857–3863.
[233] K. Donabauer, M. Maity, A. L. Berger, G. S. Huff, S. Crespi, B. König, *Chem. Sci.* **2019**, *10*, 5162–5166.
[234] J. Cornelisse, E. Havinga, *Chem. Rev.* **1975**, *75*, 353–388.
[235] J. A. Barltrop, N. J. Bunce, A. Thomson, *J. Chem. Soc. C Org.* **1967**, 1142–1145.
[236] F. Calogero, A. Gualandi, M. Di Matteo, S. Potenti, A. Fermi, G. Bergamini, P. G. Cozzi, *J. Org. Chem.* **2021**, 86, *9*, 7002–7009.
[237] F. Calogero, S. Potenti, E. Bassan, A. Fermi, A. Gualandi, J. Monaldi, B. Dereli, B. Maity, L. Cavallo, P. Ceroni, P. G. Cozzi, *Angew. Chem. Int. Ed.* **2022**, *61*, e202114981.
[238] S. J. Blanksby, G. B. Ellison, *Acc. Chem. Res.* **2003**, 36, *4*, 255–263.
[239] F. B. Dias, T. J. Penfold, A. P. Monkman, *Methods Appl. Fluoresc.* **2017**, *5*, 012001.
[240] J. S. Ward, R. S. Nobuyasu, A. S. Batsanov, P. Data, A. P. Monkman, F. B. Dias, M. R. Bryce, *Chem. Commun.* **2016**, *52*, 2612–2615.
[241] S. Grotjahn, B. König, *Org. Lett.* **2021**, *23*, 3146–3150.
[242] Q.-L. Chen, L. Mao, Y.-F. Pan, H. Cai, X.-M. Zhang, F.-M. Zhang, A.-J. Ma, J.-B. Peng, Y.-Q. Tu, *Chem. Commun.* **2023**, *59*, 14427–14430.

[243] Y.-F. Lv, G. Liu, Z. Shi, Z. Wang, *Angew. Chem. Int. Ed.* **2024**, *63*, e202406109.
[244] E. Tatunashvili, B. Chan, P. E. Nashar, C. S. P. McErlean, *Org. Biomol. Chem.* **2020**, *18*, 1812–1819.
[245] M. Montalti, A. Credi, L. Prodi, M. Gandolfi, *Handbook of Photochemistry*. Taylor and Francis, Boca Raton, **2006**.
[246] F. Wilkinson, W. P. Helman, A. B. Ross, *J. Phys. Chem. Ref. Data* **1993**, *22*, 113–262.
[247] A. Gualandi, G. Rodeghiero, A. Faraone, F. Patuzzo, M. Marchini, F. Calogero, R. Perciaccante, T. P. Jansen, P. Ceroni, P. G. Cozzi, *Chem. Commun.* **2019**, *55*, 6838–6841.
[248] J. Chen, D. Liu, D. Fan, Y. Liu, W. Zhang, *Tetrahedron* **2013**, *69*, 8161–8168.
[249] Y.-Z. Huang, L.-J. Zhang, C. Chen, G.-Z. Guo, *J. Organomet. Chem.* **1991**, *412*, 47–52.
[250] Y. Xiong, G. Zhang, *J. Am. Chem. Soc.* **2018**, 140, *8*, 2735–2738.

Chapter 4. Accessing vanadium in low oxidation state: a diastereoselective pinacol coupling

4.1 Background introduction

The venerable pinacol coupling reaction is one of the oldest, most studied and most developed protocol in organic chemistry. The key point and the beauty of this protocol lies in the installation of a new C-C bond and two new adjacent stereocenters by the reductive coupling of two carbonyl groups in the presence of an electron donor in a free radical process.[251]

The reaction was first reported almost 130 years ago by the Fittig group who induced the pinacolization of acetone in the presence of Mg(0) as a single electron reductant.[252] During the last 50 years the reaction has undergone a continuous development and improvement, in particular new reagents have been introduced to control the radical dimerization. Among them, several transition metal-catalyzed pinacol coupling strategies have been reported and applied in the synthesis of complex molecules and drugs (*Figure 4.1*), e.g. stoichiometric Nb(III)[253] and Sn(IV)[254] have been used in the synthesis of amino alcohols, or Sm(II) in the preparation of cyclic diols[255] and simpler homopinacols.[256] Ytterbium[257] and magnesium[258] were reported in stoichiometric protocols but with discrete results.

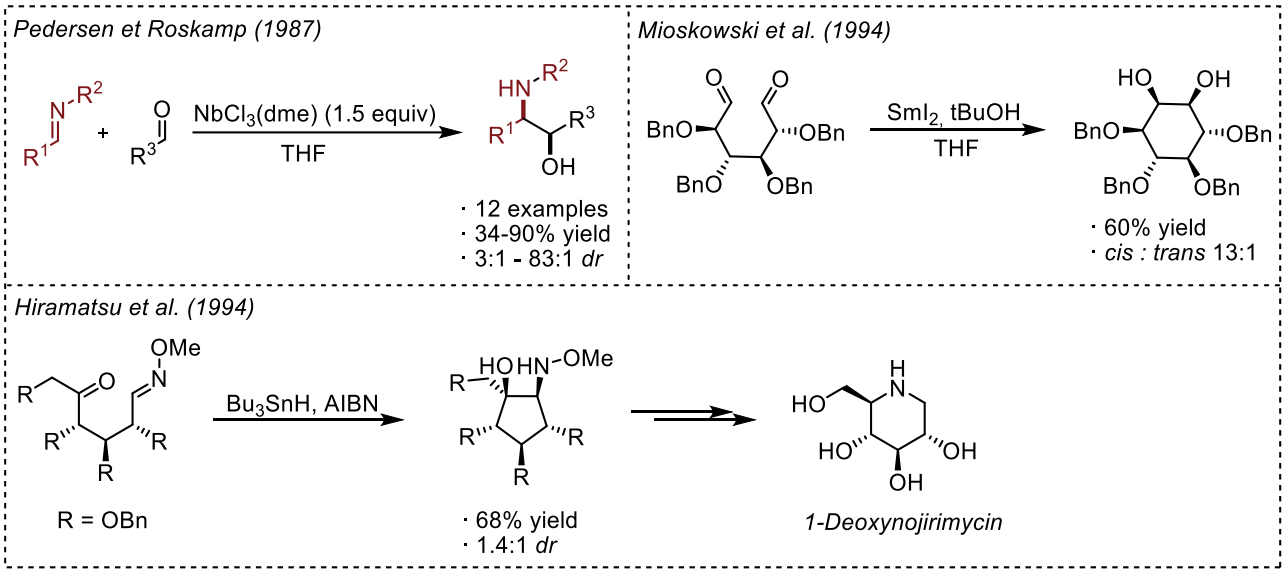

Figure 4.1 Examples of pinacol coupling protocols mediated by stoichiometric transition metals in the synthesis of complex organic scaffolds.

To induce the reductive coupling using a catalytic amount of transition metals, the Liu group reported a protocol using 10 mol% of titanocene dichloride in the presence of a stoichiometric amount of Grignard reagent as the final reductant.[202] The protocol was found to be suitable also for aromatic ketones. The mechanism involves the reduction of Cp_2TiCl_2 to $[TiCp_2H]$, then the unpaired electron of the metal center is transferred to the ketone ligand by back-donation to the π* orbital of the carbonyl giving a radical character to the ketone. The coupling of two radicals gives the desired 1,2-diol. The Inanaga group reported the homocoupling of aromatic and α,β-unsaturated aldehydes using an overstoichiometric amount of $[Cp_2TiCl]$ obtained after *in situ* reduction of Cp_2TiCl_2 with *s*-BuMgCl, to give the diol with high *syn*-selectivity (*Figure 4.2*).[259] The coexistence of a trimetal system Ti(III)-Mg(II)-Ti(III) and Ti(IV)-Mg(II)-Ti(IV) which is used for the reduction of the titanocene complex and persists during the reaction is thought to be the key factor in the *syn*-diastereoselective outcome of the reaction.

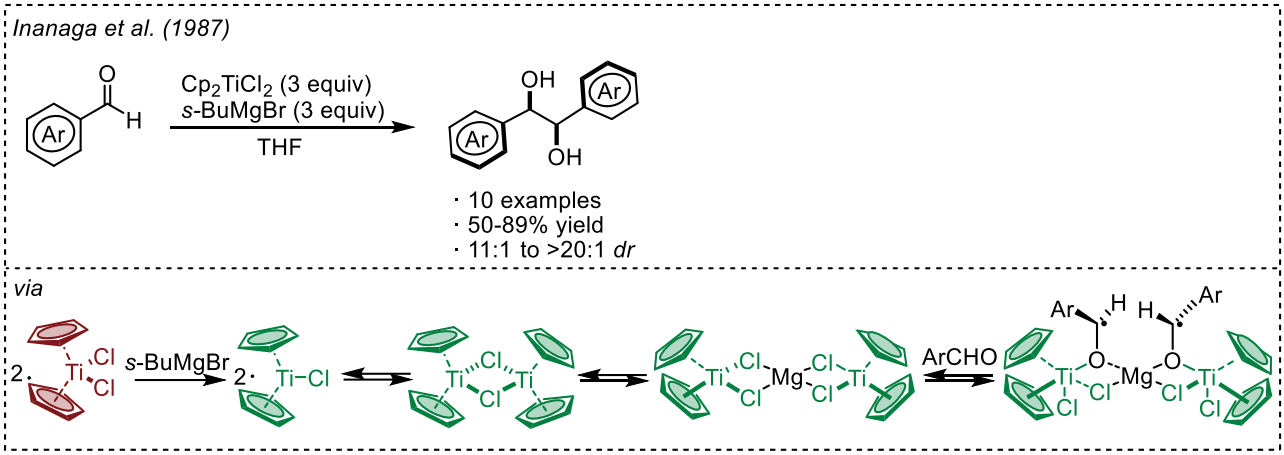

Figure 4.2 Diastereoselective pinacol coupling using stoichiometric Cp_2TiCl_2 reported by the Inanaga group.

A major impact on the development of catalytic protocols was made by the Fürstner group in 1995, who introduced zinc powder as a cheap, abundant and easy-to-use terminal reducing agent.[260] The mechanism in *Figure 4.3* first involves the reduction of the catalytic transition metal (MX_n) by a suitable reductant e.g. Zn(0) or Mg(0) triggering its ability to induce a single electron transfer to the carbonyl. The metal-assisted dimerization leads to the diol, that is coordinated to the metal centers. A stoichiometric amount of trimethylchlorosilane (Me_3SiCl) or other stoichiometric scavengers are added to liberate the product from the metal and to restore the metal catalytic cycle. Finally, Si-O bonds can be cleaved after the work-up, usually by acidic treatment, releasing the 1,2-diol.

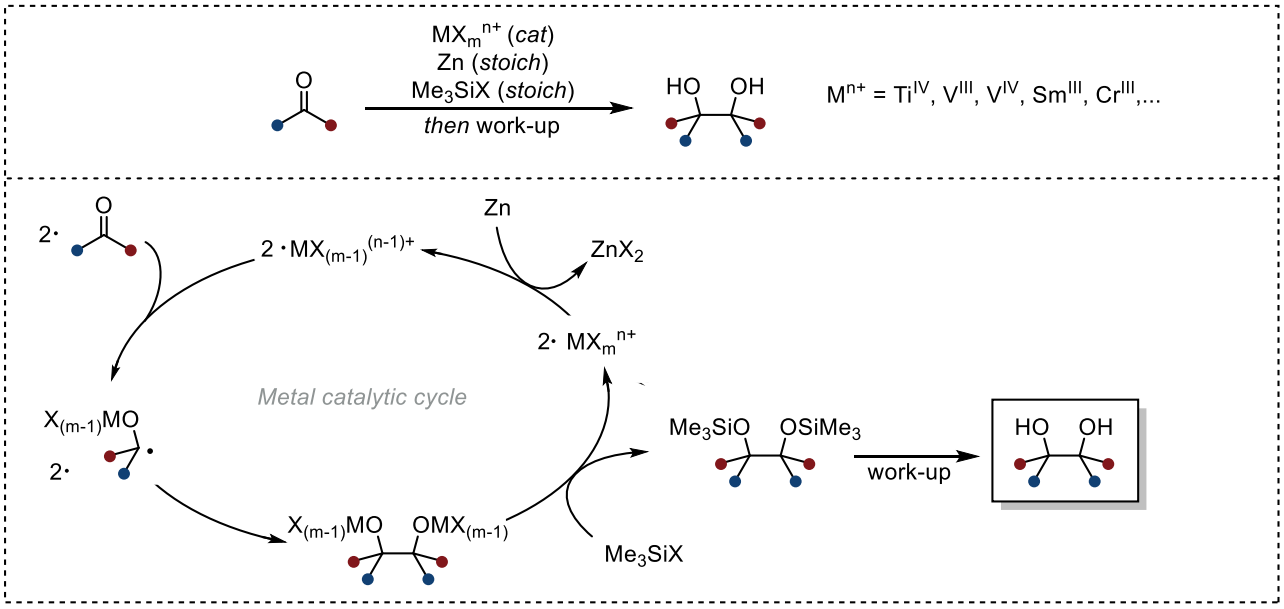

Figure 4.3 General protocol for the pinacol coupling mediated by a catalytic transition metal, and relative mechanism.

This strategy was first applied in the titanium-catalyzed McMurry reductive coupling of ketones and amides[261,262] in order to access lower Ti-oxidation states in a mild way and then extended to other metals such as samarium,[263] chromium,[264] titanium[265] (*Figure 4.4*) and in particular for the chapter, to vanadium.

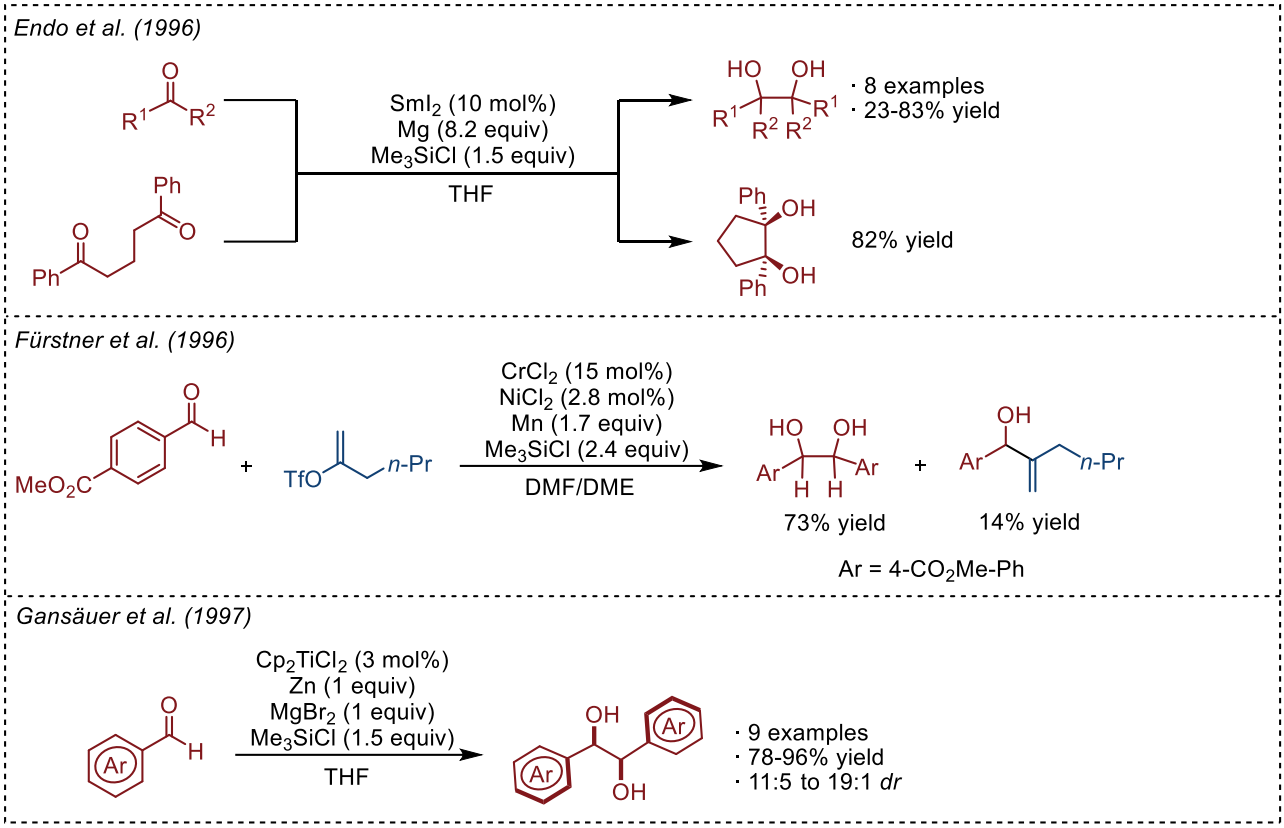

Figure 4.4 Examples of pinacol coupling protocols mediated by catalytic amounts of transition metals.

The use of vanadium(III) in pinacol coupling protocols was firstly described by the Pedersen group in 1989 in two seminal works. In the first work the group reported the cross-pinacol coupling between simple aliphatic aldehydes, which are almost inert in the presence of reduced metal complex due to their high reduction potential (E_{red} < −2 V *vs* SCE)[266], and other aliphatic aldehydes capable of forming a chelate, expecially six- or seven-membered ring, with the metal center, thus accelerating the reaction rate and yielding the unsymmetrical diol in good yields and with good diastereoselectivity (*Figure 4.5*).[267]

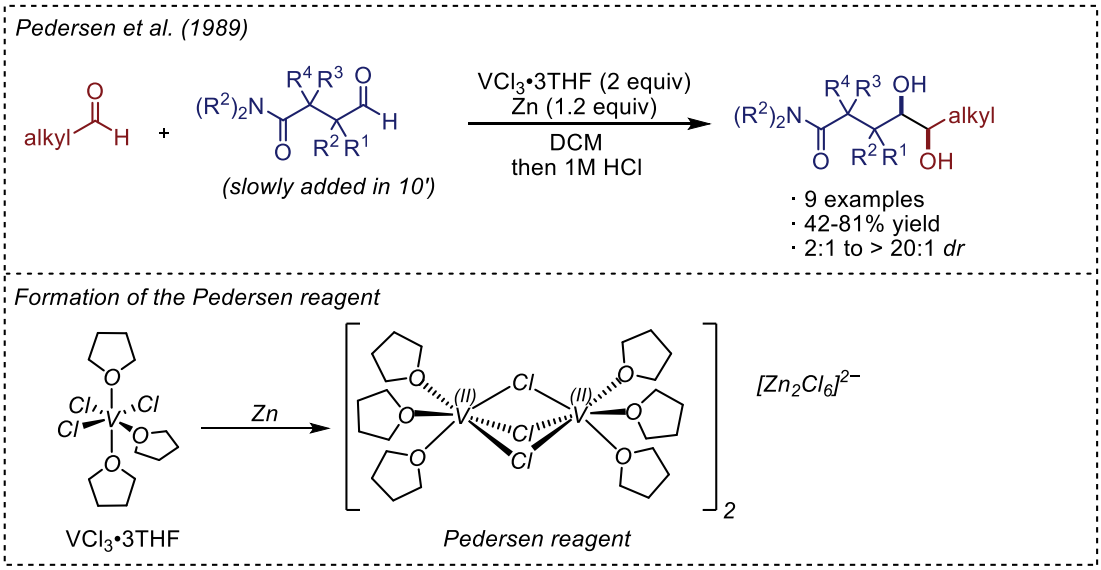

Figure 4.5 Vanadium-mediated cross-pinacol coupling of aliphatic aldehydes reported by the Pedersen group.

The key step is the reduction of the stoichiometric V(III) by zinc powder producing a cationic V(II) dimer known as the *Pedersen reagent*.[268,269] A plausible mechanism involves first the formation of a chelate complex with one of the aliphatic partners, the reductive formation of a ketyl radical by one of the V(II) centers followed by its rapid reduction by the other V(II) center generating an organometallic intermediate and finally the controlled insertion of a second carbonyl leading to the coordinated diol which is liberated by the acidic work-up.

In the second mentioned paper the group reported the cross-pinacol coupling between aromatic and aliphatic aldehydes exploiting the ability of V(II) to induce the single electron transfer only on the aromatic carbonyls (*Figure 4.6*).[270] If the reaction is carried out by slowly adding the aromatic substrate in the presence of the entire amount of the inert aliphatic aldehyde, the cross-pinacol coupled product can be obtained as the main product. Conversely, the rapid addition of the aromatic aldehyde results in approximately 1:1 mixtures of cross- and homo-coupled products. Cross-pinacol coupling reactions work best when the aromatic substrate has an *ortho*- or *para*-electron withdrawing group or when it is able to form a chelate with the metal, as was also observed in the first paper.

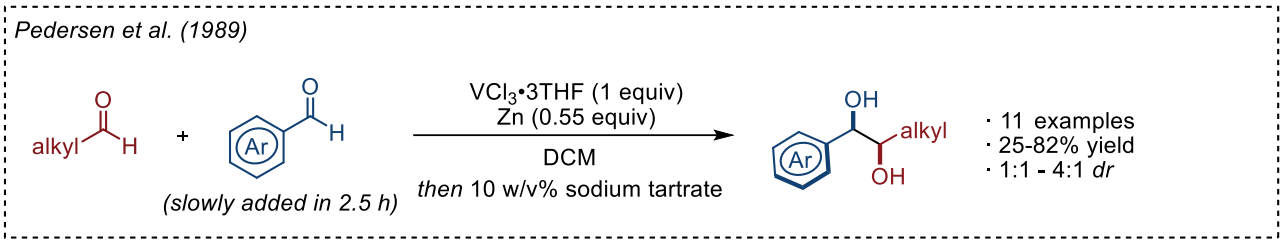

Figure 4.6 Vanadium-mediated cross-pinacol coupling between aliphatic and aromatic aldehydes reported by the Pedersen group.

The ability of vanadium to induce the unsymmetrical reductive pinacol coupling by intramolecular complexation of a coordinating substrate has also been exploited by the Cinquini-Cozzi group in the enantioselective cross-pinacol coupling between aliphatic and aromatic aldehydes bearing a chiral amide in the *ortho*-position (*Figure 4.7*). The diastereoselectivity and enantioselectivity, determined after the treatment of the diol with PTSA to form chiral lactones, are generally high.[271] The authors explained the stereoselectivity of the reaction by considering vanadium coordinated in a seven-member chelate to the oxygen of the aldehyde, to the amide and to the anion radical derived from the aliphatic aldehyde, which attacks the *si*-face of the aldehyde to minimize the steric repulsion with the methoxymethyl group of the chiral auxiliary forced into the indicated conformation by the ligands on the vanadium center. The more favorable arrangement of the alkyl group with respect to the aromatic ring in **A** explains the preferential formation of the *syn*-isomer. This is in agreement with the experimental results, since an increase in the steric hindrance on the alkyl residue leads to an increase of the stereoselectivity.

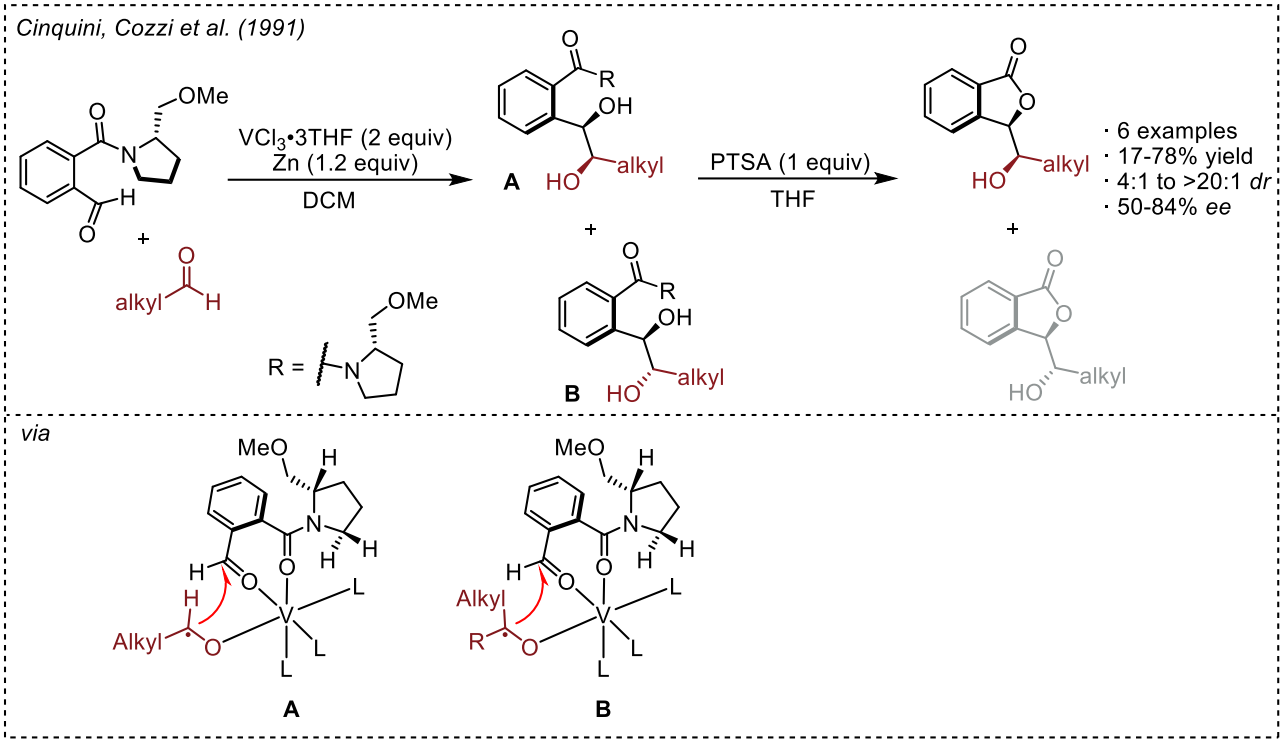

Figure 4.7 Vanadium-mediated cross-pinacol coupling between aliphatic and aromatic coordinating aldehydes reported by the Cinquini-Cozzi group.

To promote the homopinacol coupling of non-coordinating aliphatic aldehydes, VCl_3•3THF is not suitable since it cannot induce the reductive ketyl formation due to the higher reduction potentials required. The Hirao group reported in 2005 a protocol for the homopinacol coupling of aliphatic aldehydes using a catalytic amount of vanadocene dichloride Cp_2VCl_2 in the presence of an overstoichiometric amount of zinc and Me_3SiCl as scavenger agent (*Figure 4.8*).[272]

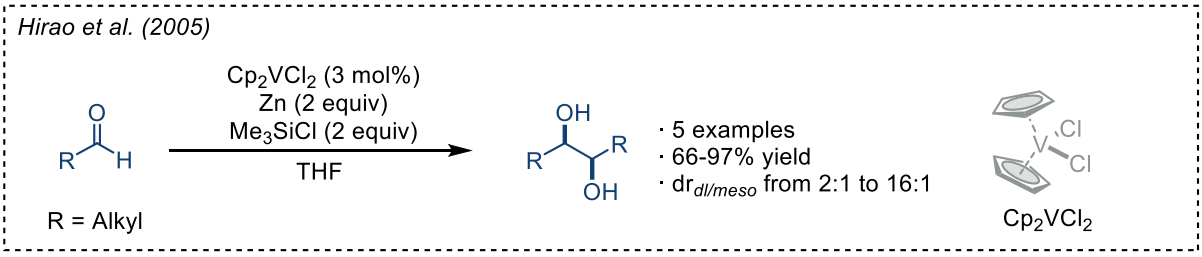

Figure 4.8 Vanadium-catalyzed homopinacol coupling or aliphatic aldehydes reported by the Hirao group.

These four examples are the cornerstone of vanadium-mediated pinacol coupling protocols. The main drawback is the stoichiometric amount of vanadium and zinc usually required, which is associated with a large production of metal waste. As already mentioned, the use of a stoichiometric amount of metal complex is necessary due to the poisoning of the metal by the strong coordination with the diol product. In fact, it is necessary to liberate it by an acid treatment or a treatment with sodium tartrate solution.[270]

An improvement in this respect was made by the Zhu group in the asymmetric pinacol coupling of aromatic aldehydes using a catalytic amount of a chiral Salan-VO complex, a stoichiometric amount of zinc metal and an overstoichiometric amount of chlorotrimethylsilane as the scavenger. The homo-coupled diols are generally obtained in good yields and with discrete diastereo- and enantioselectivity (*Figure 4.9*).

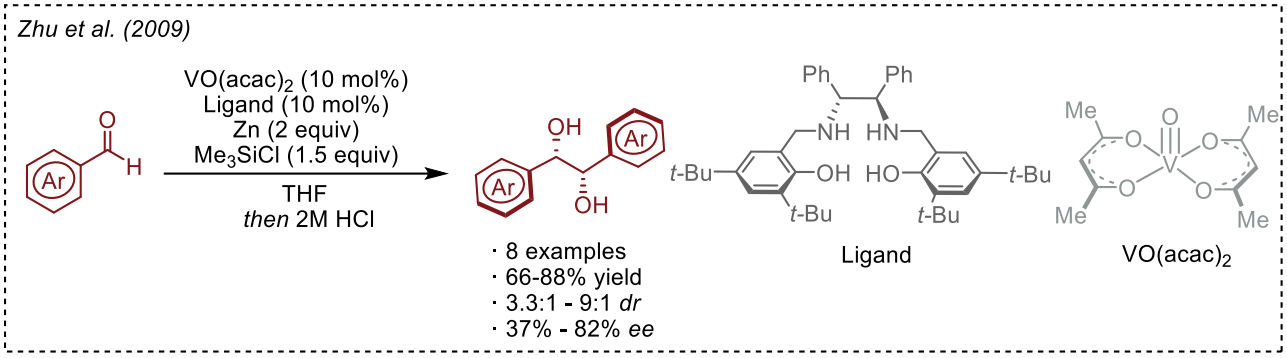

Figure 4.9 Vanadium-catalyzed enantio- and diastereoselective pinacol coupling of aromatic aldehydes reported by the Zhu group.

The need for a stoichiometric amount of zinc or other metals to ensure the turnover of the vanadium catalytic cycle remains the main drawback of these reactions. Photoredox catalysis offers the possibility of replacing the reductive behavior of the metal with a milder photocatalytic cycle. In this respect, the Rueping group reported the first photoredox pinacol coupling of aromatic aldehydes, ketones and imines using 1 mol% of Iridium-based photocatalyst and 2 equivalents of Bu_3N (*Figure 4.10*).[273] The reaction gave good results in terms of yield and functional group compatibility both on the aldehydes and ketones.

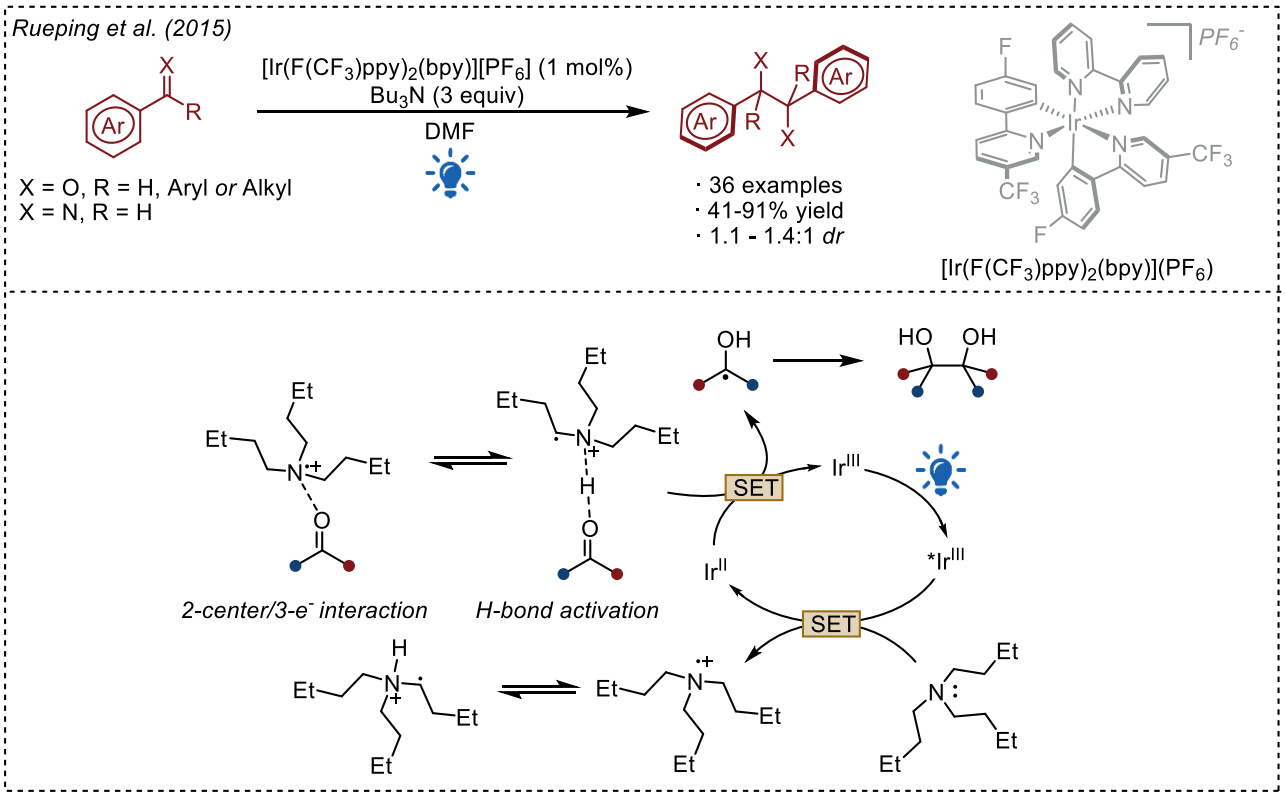

Figure 4.10 First photoredox pinacol coupling of aromatic carbonyls reported by the Rueping group.

The amine, as explained by the authors, has a dual role in making the reaction work: as a reducing agent, it is the effective quencher of the excited photocatalyst. The reduced form of the photocatalyst in its ground state can reduce the carbonyl group to a ketyl radical, which induces the reductive coupling. However, there is a discrepancy between the reduction potential of the ketone (E_{red} = −2.08 V *vs* SCE) and the photocatalyst ($E_{red}(Ir^{III}/Ir^{II})$ = −1.29 V *vs* SCE) making the SET significantly endergonic. The results indicate that the driving force of the reaction is the C=O activation by the so-formed amino radical

cation, which can act as a Lewis acid in a 2-center/3-electron interaction or as a Brønsted acid changing the reduction potential of the carbonyl and making the elementary step exergonic.

Based on this pioneering work, our group introduced coumarins as efficient photocatalysts as an alternative to toxic, rare and expensive iridium-based complexes in the same reaction on aromatic aldehydes, ketones and imines (*Figure 4.11*).[274]

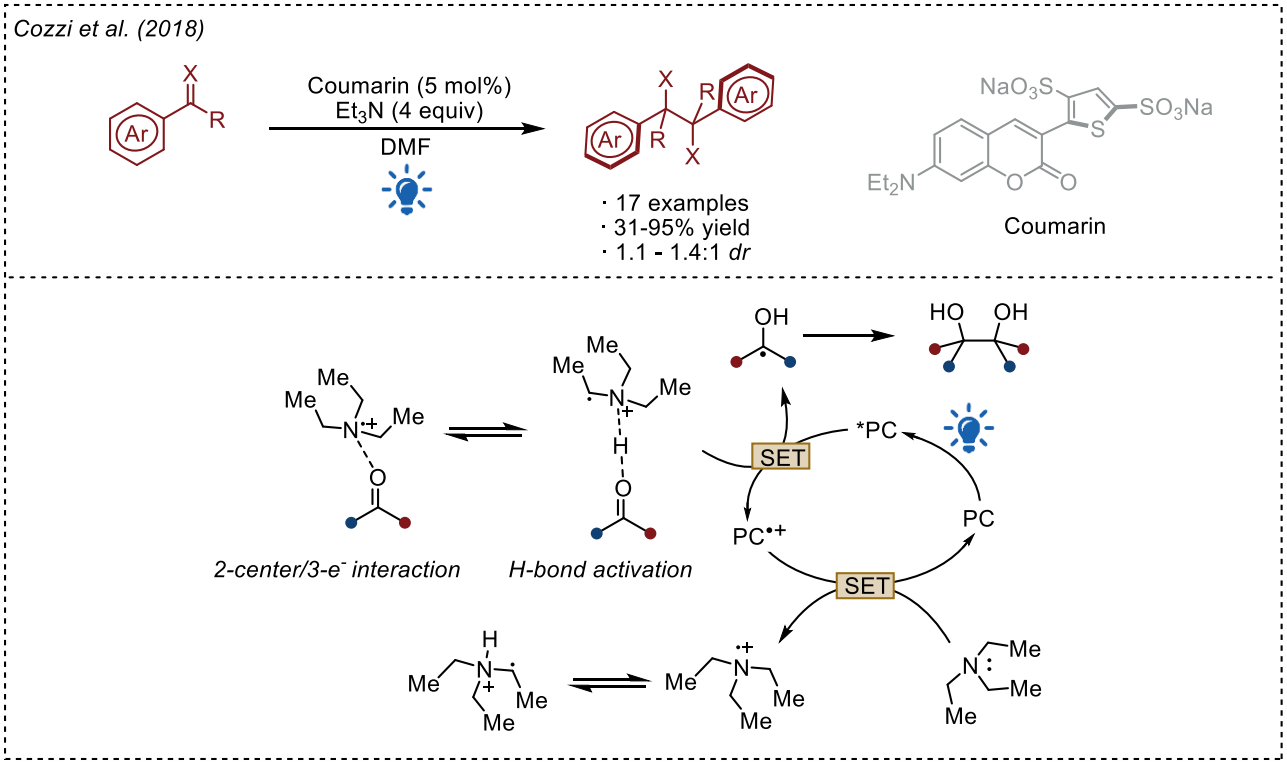

Figure 4.11 Photoredox pinacol coupling of aromatic carbonyls promoted by a coumarin reported by the Cozzi group.

The reaction mechanism is different, and it is dictated by the stronger reduction potential of the excited coumarin ($^*E_{ox}(PC^{\bullet+}/^*PC)$ = -1.89 V *vs* SCE) which is able to directly reduce the carbonyl. The oxidized form of the coumarin is back-reduced ($E_{ox}(PC^{\bullet+}/PC)$ = +0.83 V *vs* SCE) by the amine ($E_{ox}(Et_3N^{\bullet+}/Et_3N)$ = +0.77 V *vs* SCE) restoring the catalytic cycle.

In these two seminal works, the generation of free ketyl radicals leads to an uncontrolled pinacol coupling without any diastereocontrol. To overcome this limitation, it is necessary to introduce a metal to trap the free radicals and direct the C-C bond formation. A few years later, our group published the first example of a dual photoredox- and titanium-mediated pinacol coupling of aromatic aldehydes[83] combining the photophysical properties of [*n*-PrDMQA$^+$][BF_4^-] as the photocatalyst, already described in Section 1.5.1, with the known reactivity of titanocene dichloride and the Hantzsch ester as the stoichiometric organic reductant under red light irradiation (*Figure 4.12*). This protocol is the first highly diastereoselective pinacol coupling that completely replaces the use of both metal-based photocatalysts and stoichiometric metal terminal reductants and uses the less energetic, less harmful and more penetrating red light. In addition, using a chiral Salen-$TiCl_2$ complex it was possible to obtain diols with a high control of both diastereo- and enantioselectivity.

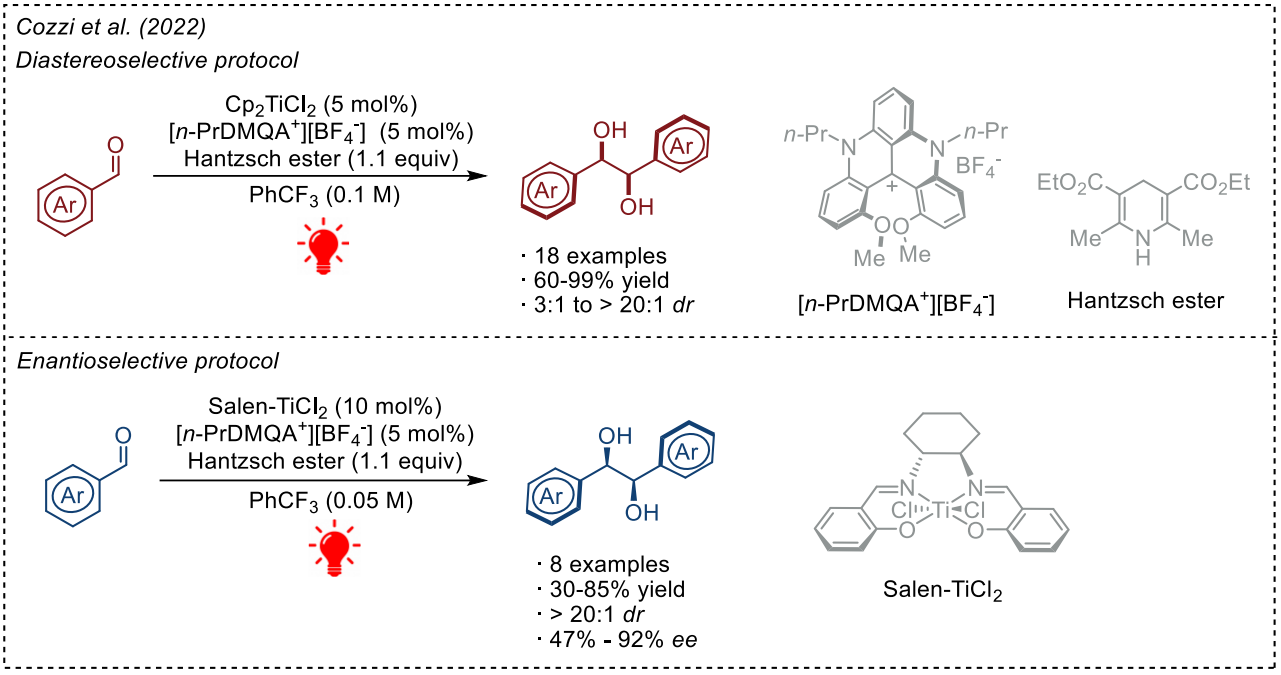

Figure 4.12 Dual photoredox- and titanium-catalyzed pinacol coupling of aromatic aldehydes reported by the Cozzi group.

The reaction was found to be tolerant to many functional groups in the *para*- and *meta*-positions, while the substitution in the *ortho*-position was detrimental to the diastereoselective outcome. Moreover, the reaction requires long reaction times, extended up to 72h to ensure complete conversion of the starting materials. The possibility of an enantioselective variant, however, made this protocol attractive and opened up further investigation in the area.

4.2 Presented work

The reductive coupling of two carbonyl functionalities to give 1,2-diols has been extensively studied in recent years. Several transition metals in low oxidation state have been exploited to induce the pinacol coupling reaction and, among them, vanadium has found many applications in the literature both in the homocoupling of aromatic aldehydes and in the cross-pinacol coupling of two different aldehydes to obtain useful moieties. However, the use of stoichiometric amounts of vanadium complex and reducing agents, particularly zinc powder to reduce V(III) to V(II), is associated with a large amount of metal waste. This limitation has been overcome by our group by combining titanium in catalytic amounts with a photoredox system that does not require stoichiometric metal reductants but instead a stoichiometric amount of an organic, cheap and easy-to-prepare Hantzsch ester can be used as the final reductant.

With these premises during my PhD we wanted to combine photoredox- and vanadium-catalysis to promote the single electron reduction of the metal and then to promote the single electron reduction of carbonyl compounds.

In the following paragraphs a highly diastereoselective pinacol coupling of aromatic aldehydes promoted by a catalytic amount of VCl_3·3THF as V(III) source, [*n*-PrDMQA$^+$][BF_4^-] as the photocatalyst under red light irradiation is reported (*Figure 4.13*). After a long optimization process, 6,6'-dimethylbipyridine was found to be the best ligand to induce the complete diastereoselection in favor of the *d/l* 1,2-diol. The protocol was found to be more reactive than the previous one reported by our

group using titanocene dichloride and also suitable for *ortho*-substituted substrates, which was the main limitation of the previous work.

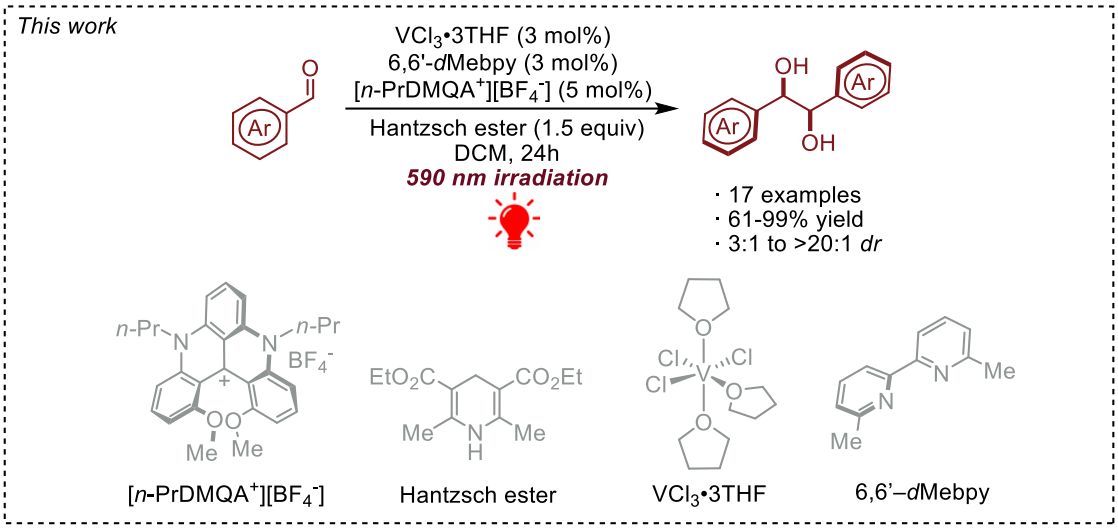

Figure 4.13 Presented work.

4.3 Optimization

In order to optimize the reaction and taking into account the knowledge acquired in this field by our group in recent years, we started to study this new reaction using 4-chlorobenzaldehyde as the model substrate. Taking into account the state-of-the-art of vanadium chemistry, we initially chose dichloromethane as the solvent. Since the previous dual photoredox and titanium protocol reported by our group demonstrated the efficient formation of titanium in a low oxidation state promoted by [*n*-PrDMQA$^+$][BF_4^-] under red light irradiation, we postulated that an effective diastereoselective pinacol coupling could be also achieved under this dual platform.

Due to the known sensitivity of V(III) complexes to oxygen and water, and in order to obtain reproducible results, we found it convenient to use a commercially available solution of VCl_3·3THF in DCM.

In preliminary experiments (*Table 4.1*) using 10 mol% of VCl_3·3THF as vanadium precatalyst, 5 mol% of [*n*-PrDMQA$^+$][BF_4^-] as the photocatalyst and 1.5 equivalents of Hantzsch ester as organic sacrificial reductant in dichloromethane (0.1 M) under red light irradiation (590 nm) (entry 1) we observed no conversion of the starting material. Reducing the vanadium catalyst loading to a 3 mol% under the same conditions (entry 2) we observed complete conversion of the aldehyde with a poor diastereoselection (*d/l:meso* 2.8:1). This result is attributed to the absorption of the vanadium complex in the visible region of the spectrum leading to a complete inhibition of the reaction (see the section 4.6 dedicated to the Photophysical studies for more details). Performing the reaction in THF as an alternative solvent (entry 3) did not improve the diastereoselection, while the reactivity was dramatically reduced.

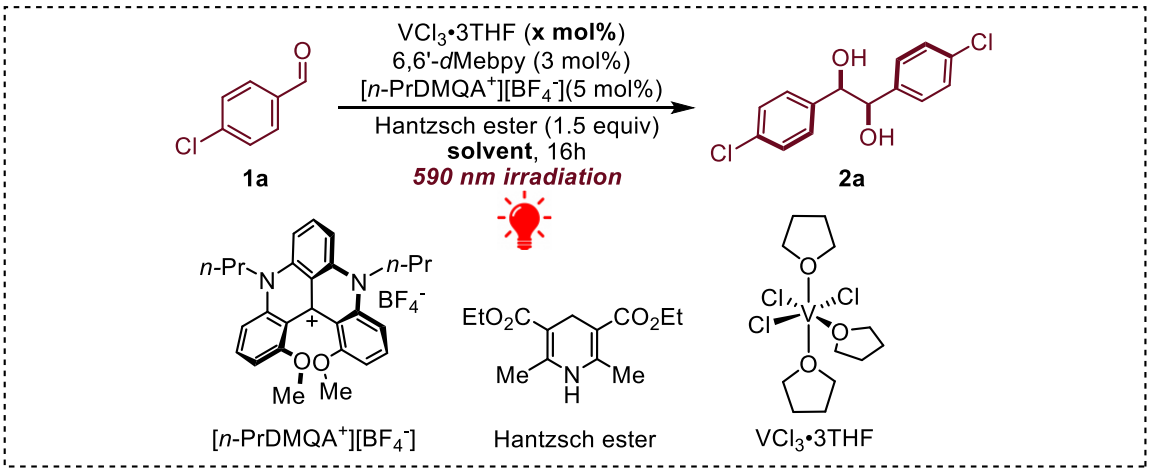

Entry	x mol%	Solvent	Conversion (%)[a]	*dr* **2a** (*dl:meso*)[b]
1	10	DCM	NR	
2	**3**	**DCM**	**99**	**2.8:1**
3	3	THF	28	2:1

Table 4.1 [a] *Determined by ^{1}H NMR analysis on the reaction crude.* [b] *Determined by ^{1}H NMR analysis on the reaction crude by integration of the benzylic C-H signals. NR = No reaction*

At this point, an extensive screening of ligands was undertaken to improve the diastereoselectivity of the protocol. Several classes of ligands that are known to coordinate vanadium were investigated (*Table 4.2*).

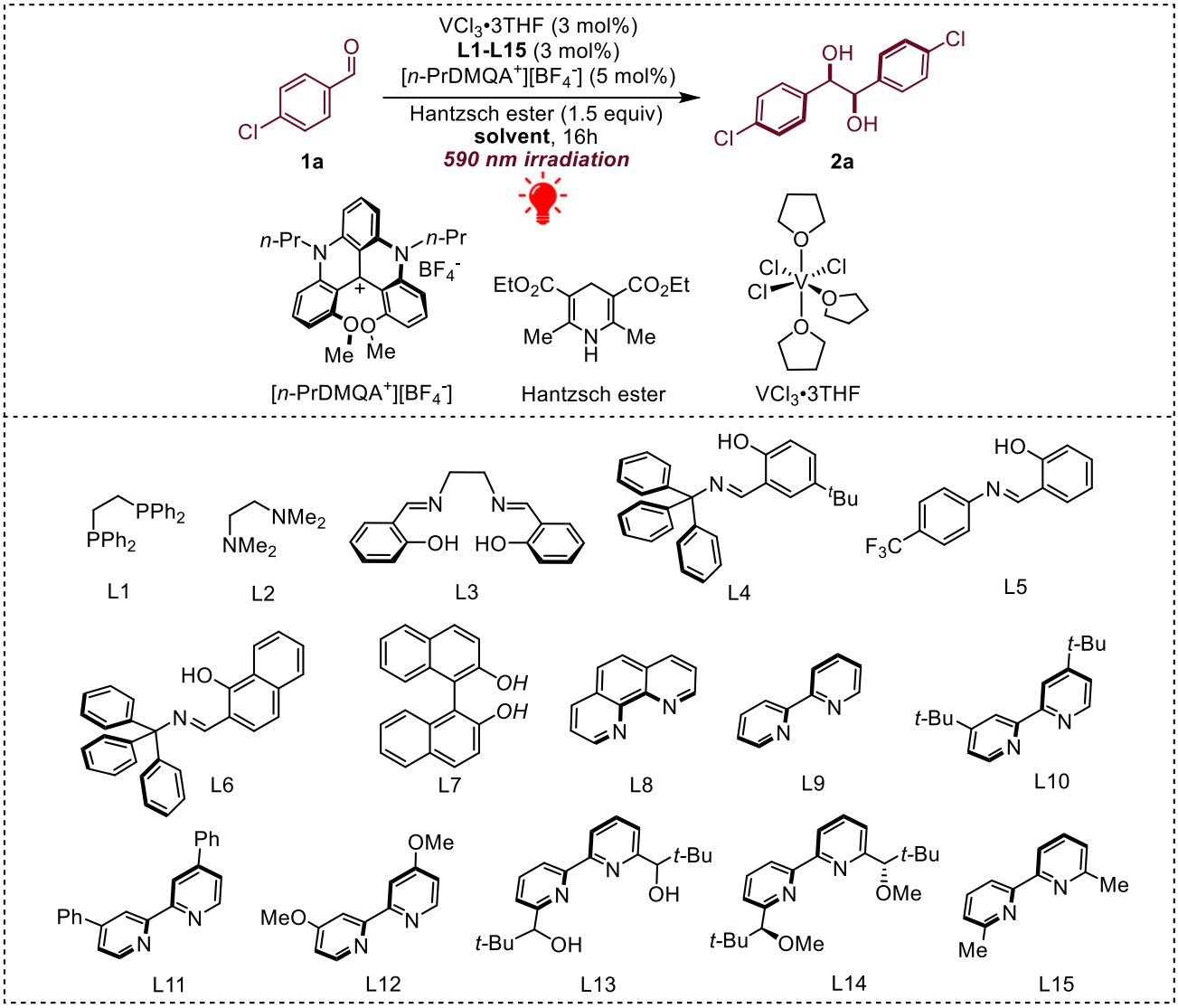

Entry	Ligand	Conversion (%)[a]	*dr* **2a** (*dl:meso*)[b]
0	-	99	2.8:1
1	L1	NR	
2	L2	NR	
3	L3	NR	
4	L4	99	2.3:1
5	L5	99	2.4:1
6	L6	99	2.3:1
7	L7	99	2.5:1
8	L8	74	6:1
9	L9	90	6.3:1
10	L10	92	6:1
11	L11	NR	
12	L12	NR	
13	L13	99	3:1
14	L14	99	> 20:1
15	**L15**	**99**	**> 20:1**

Table 4.2 [a] Determined by ^{1}H NMR analysis on the reaction crude. [b] Determined by ^{1}H NMR analysis on the reaction crude by integration of the benzylic C-H signals. NR = No reaction.

While bis-phosphine (entry 1), TMEDA (entry 2)[275] and the achiral Salen ligand (*N,N'*-ethylenebis(salicylaldiminato)dianion)[276] (entry 3) stopped the reactivity of vanadium, bidentate Schiff

bases (entries 4-6) did not improve the diastereoselection. Encouraging results were obtained when o-phenanthroline (entry 8) or bipyridine (entry 9)[277,278] were used for the reaction. The optimization was therefore focused on substituted bipyridines. The presence of an electrondonating group on the 4,4'-positions with a positive inductive effect +I (entry 10) did not improve the *dr* ratio, whereas the presence of a substituent at the same position with a positive mesomeric effect +M (entries 11 and 12) shut the reactivity down. Investigating the substitution at the 6,6'-positions, the presence of the sterically hindered *t*-butyl alcohol (entry 13) gave complete conversion of the aldehyde but with no improvement in the *dr* ratio. A detrimental effect of the free alcohol in the diastereocontrol was confirmed using the O-methylated chiral ligand (entry 14) and complete conversion and diastereocontrol was observed. As the steric hindrance at this position was found to be beneficial, we also tested 6,6'-dimethylbipyridine (entry 15) and the same excellent results were observed. Since L15 is commercially available, whereas L14 has to be prepared in a multi-step synthesis [279] we chose L15 as the ligand of choice.

Finally, to have a complete investigation of the possible reaction condition, other photocatalysts were evaluated (*Table 4.3*).

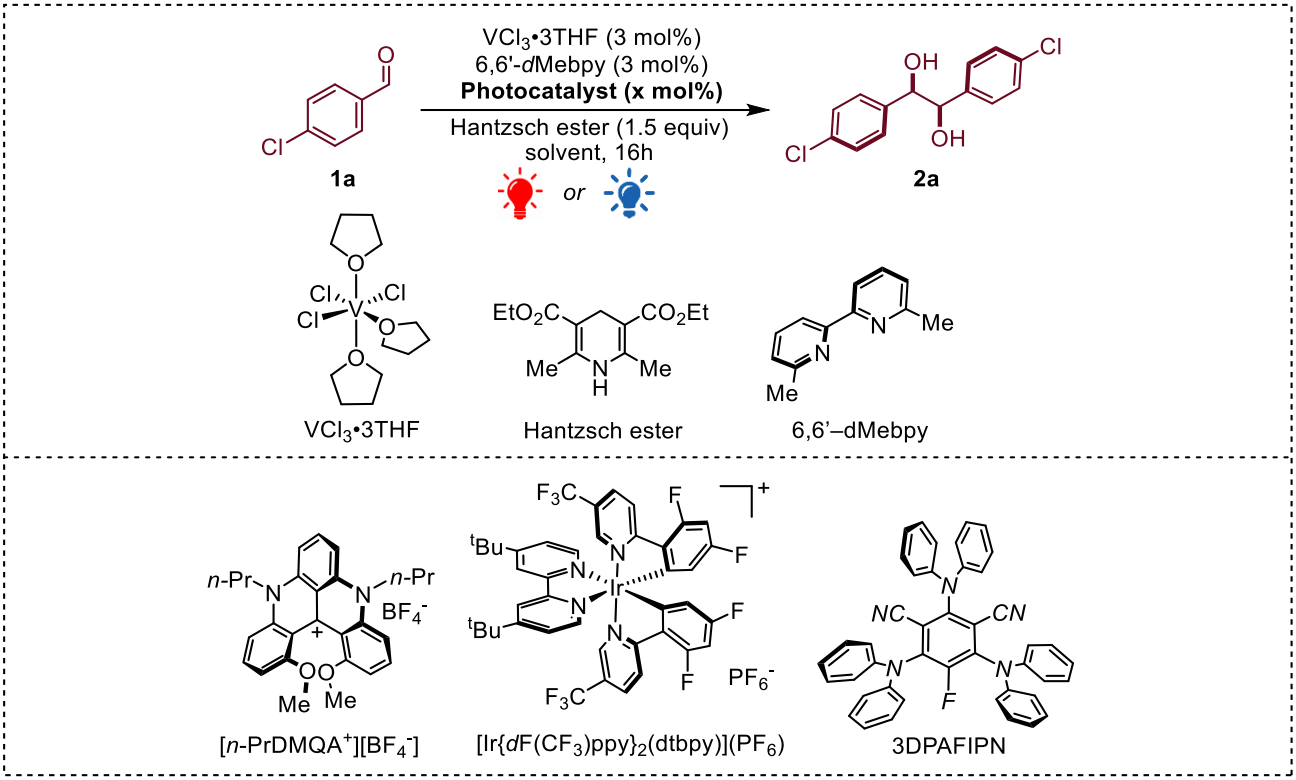

Entry	Photocatalyst, x mol% (nm irradiation)	Conversion (%)[a]	*dr* **2a** (*dl:meso*)[b]
0	**DMQA, 5 mol% (595 nm)**	**99**	**>20:1**
1	[Ir{*d*F(CF$_3$)ppy}$_2$(dtbpy)](PF$_6$), 1 mol% (427 nm)	99	13:1
2	3DPAFIPN, 5 mol% (456 nm)	99	15:1

Table 4.3 [a] Determined by ^{1}H NMR analysis on the reaction crude. [b] Determined by ^{1}H NMR analysis on the reaction crude by integration of the benzylic C-H signals.

Both [Ir{*d*F(CF$_3$)ppy}$_2$(dtbpy)](PF$_6$) (entry 1) and 3DPAFIPN (entry 2) have the maximum absorption in the blue region of the visible spectra. The reaction proceeded to completion as expected, affording the product with a good *dr* ratio, contrary to the case of titanium. Although the *dr* ratio was lower than that obtained with [*n*-PrDMQA$^+$][BF$_4^-$], these results remain quite interesting, since two possible non-diastereoselective pathways may be involved under blue light irradiation.[273] As described in the section 4.1 and as already observed by our group in a previous work,[236] the presence of a pyridinium salt,

derived from the oxidation of the sacrificial reductant, influences the redox potential of the carbonyl compound allowing its reduction by the excited state of the photocatalyst or by the excited state of the Hantzsch ester itself, which is able to absorb light around 400 nm, and can behave as a strong reductant in its excited state ($*E_{ox}(HE^{\bullet+}/*HE)$ = –2.28 V *vs* SCE).[280–282]

With the optimized conditions in hand, all the necessary control experiments were carried out to provide further confirmations about the reaction mechanism (*Table 4.4*). As expected, photoexcitation (entry 1) of the photocatalyst is mandatory for the reaction. Even though vanadium itself could absorb light radiation at 590 nm (see the section 4.6 dedicated to the Photophysical studies for more details), the photocatalyst is the only species capable of undergoing a productive catalytic cycle (entry 2). Hantzsch ester is essential to maintain the catalytic cycle as the reducing agent (entry 3), and since it does not absorb in the red region, it cannot promote the reaction. Finally, vanadium is required to maintain the catalytic cycle, as the photocatalyst does not have suitable redox potentials to induce the pinacolization (entry 4).

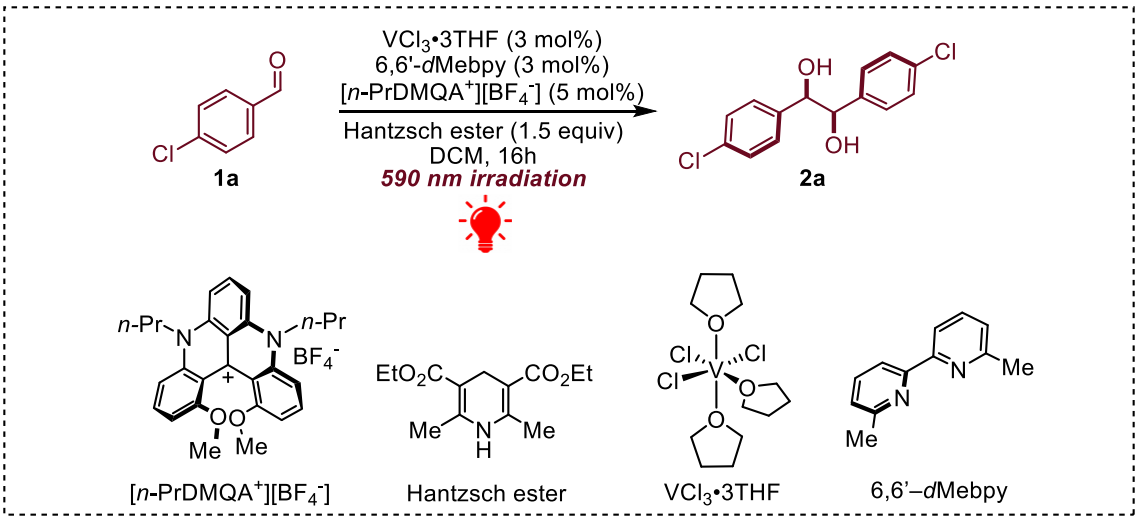

Entry	Deviation from standard conditions	Conversion (%)[b]	*dr* **2a** (*dl:meso*)[b]
0	**none**	**99**	**>20:1**
1	No light irradiation	NR	
2	No photocatalyst	NR	
3	No Hantzsch ester	NR	
4	No VCl_3•3THF	NR	

Table 4.4 [a] Determined by ^{1}H NMR analysis on the reaction crude. [b] Determined by ^{1}H NMR analysis on the reaction crude by integration of the benzylic C-H signals. NR = No reaction.

After a systematic evaluation of all the reaction parameters, we were able to reveal the optimized conditions, shown in *Figure 4.13* which gave the product **2a** in quantitative isolated yield and with complete diastereocontrol in favor of the *d/l* isomers.

4.4 Scope evaluation

The optimized conditions were applied to a library of substituted aromatic aldehydes shown in *Figure 4.14* on a 0.2 mmol scale. To ensure complete conversion of the starting material the reaction time was extended to 24h.

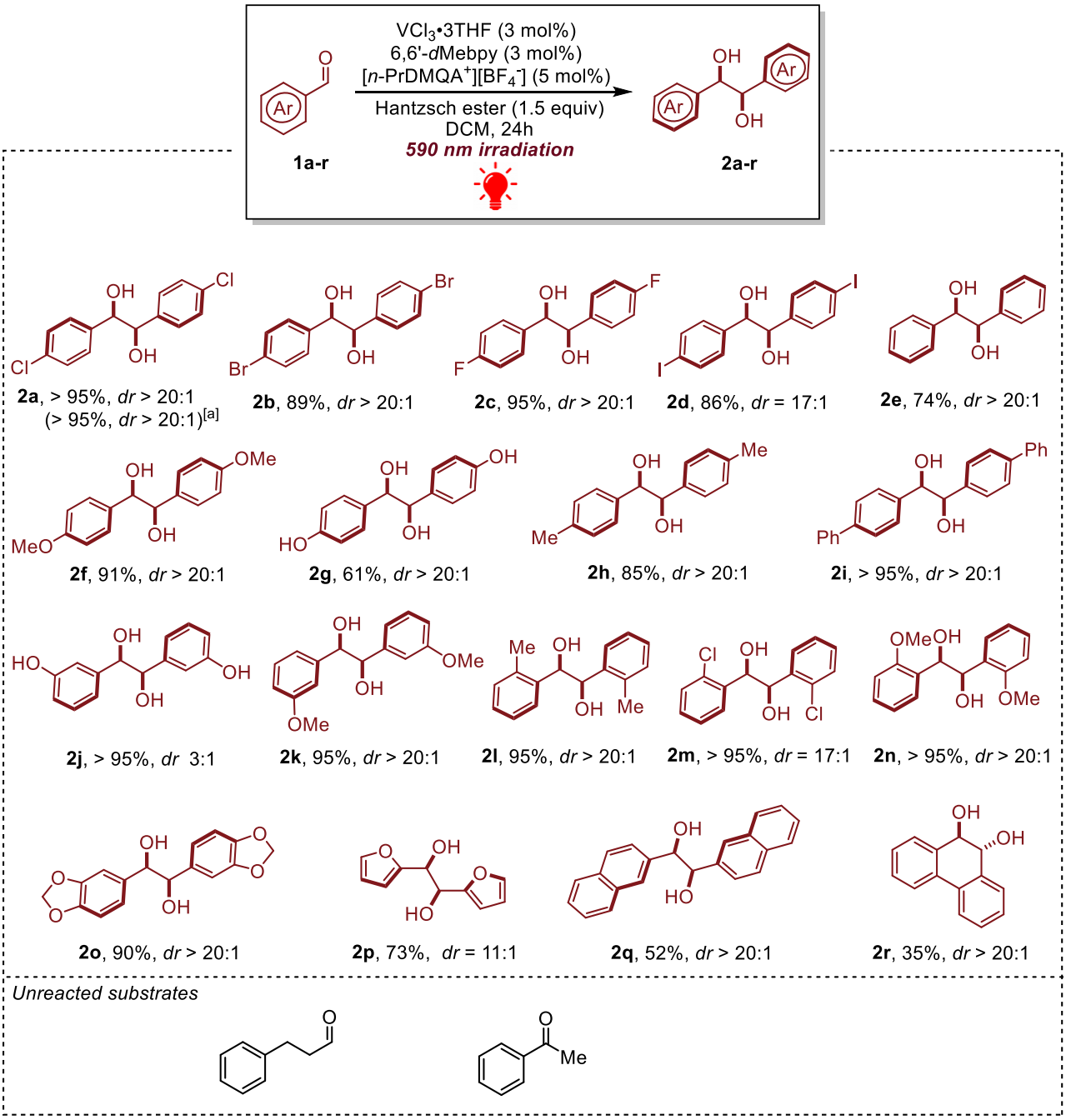

Figure 4.14 Substrate scope. [a] *Reaction performed on 1 mmol of* ***1a****.*

Yields are generally from high to quantitative regardless of the aromatic ring substitution, and the *dr* ratio is almost always >20:1 in favor of the *d/l* isomers. Very interestingly, comparing this protocol with the titanium one, the steric effect on the *ortho*-position or the presence of an acidic hydroxy group (**1g**) in the *para*-position did not affect the diastereoselective outcome, whereas in the titanium protocol a dramatic decrease was observed. The same protocol on 3-hydroxybenzaldehyde (**1j**) gave the desired product **2j** in quantitative yield but with a significant detrimental effect on the diastereocontrol, while

the same substrate O-methylated (**1k**) gave the product **2k** in a quantitative yield and *dr* >20:1. A plausible explanation could be the strong coordination of the hydroxyl group to the metal center, which could hinder the diastereocontrol.

The superiority of vanadium- over the titanium-mediated photoredox pinacol coupling was also observed in the case of heterocyclic compounds such as furfural (**1p**), which was not suitable for the titanium protocol, probably due to the strong coordination and deactivation of the oxophilic titanium center.[83] Although vanadium is still oxophilic, the product **2p** was obtained in a good yield and diastereoselectivity (*dr* = 11:1).

Finally, it is worth noting that this protocol requires 24h to achieve full conversion of the starting materials using a 3 mol% of vanadium catalyst, whereas 72h are required to achieve the same results using a 5 mol% of titanium catalyst. Scaling up the reaction to 1 mmol did not require any additional time, and full conversion and *dr* >20:1 was achieved within 24h of reaction.

Although the protocol was found to be suitable for different functional groups and heteroaromatic rings, as expected, it was not possible to extend it to either ketones or to aliphatic aldehydes. Both classes of carbonyl compounds have very different reduction potentials than the aromatic aldehydes and they are much less prone to engage a single electron reduction.[283] As reported in Paragraph 4.1, the homopinacol coupling of aliphatic aldehydes cannot be performed with VCl_3·3THF but it requires Cp_2VCl_2.[272]

To extend the methodology, we attempted to replicate known vanadium-mediated cross-pinacol coupling protocols between a coordinating aromatic and an aliphatic aldehyde (*Figure 4.15 A*)[270] and between an aliphatic aldehyde and paraformaldehyde[284] (*Figure 4.15 B*). No reaction was observed other than the degradation of the photocatalyst. Finally, the coupling between an aromatic aldehyde and an imine (*Figure 4.15 C*) gave, as usual, the homopinacol coupling of the aldehyde as the only product with *dr* >20:1.

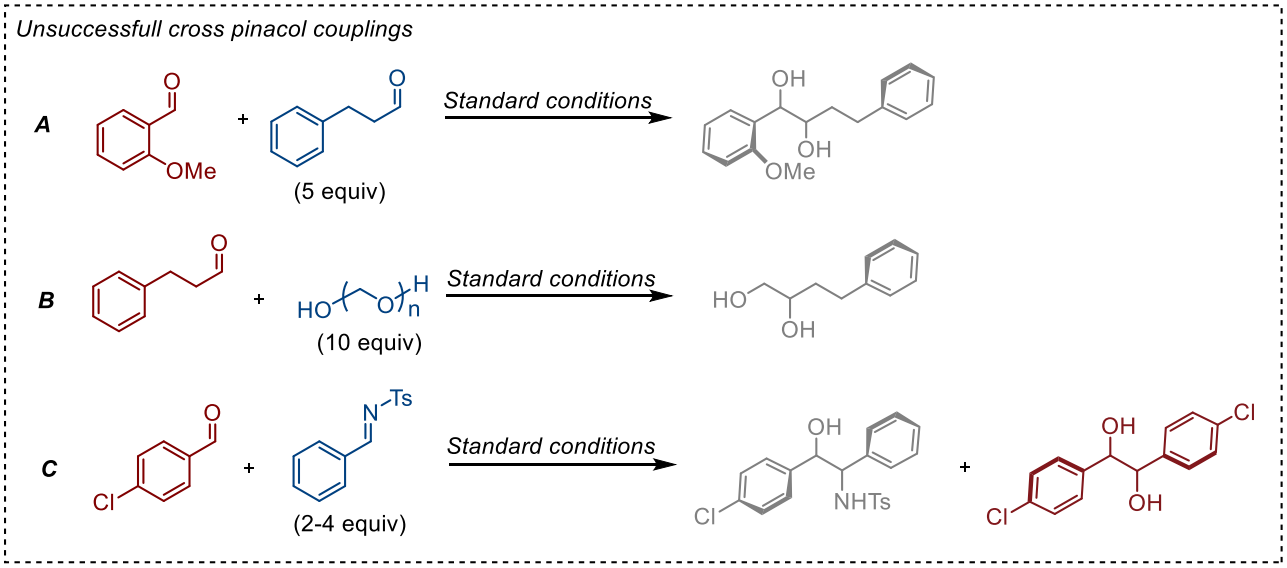

Figure 4.15 Unsuccessful cross-pinacol couplings tested.

4.5 Enantioselective attempts

After disclosing and exploring the diastereoselective protocol on a library of substrates, motivated by the good reactivity and the high diastereoselectivity, we focused on the enantioselective variant of the protocol. Since the bipyridine class gave the best results in the diastereocontrol, we focused mainly on bi-and tridentate *N*-ligands such as bisoxazoline, pyOX, pyBOX and bipyridines with different steric hindrance in 6,6'- and 2,2'-positions (*Table 4.5*). While almost all the tests performed gave complete conversion, only bipyridine L14 gave an acceptable *dr* ratio, but no promising enantioselective results have been obtained so far.

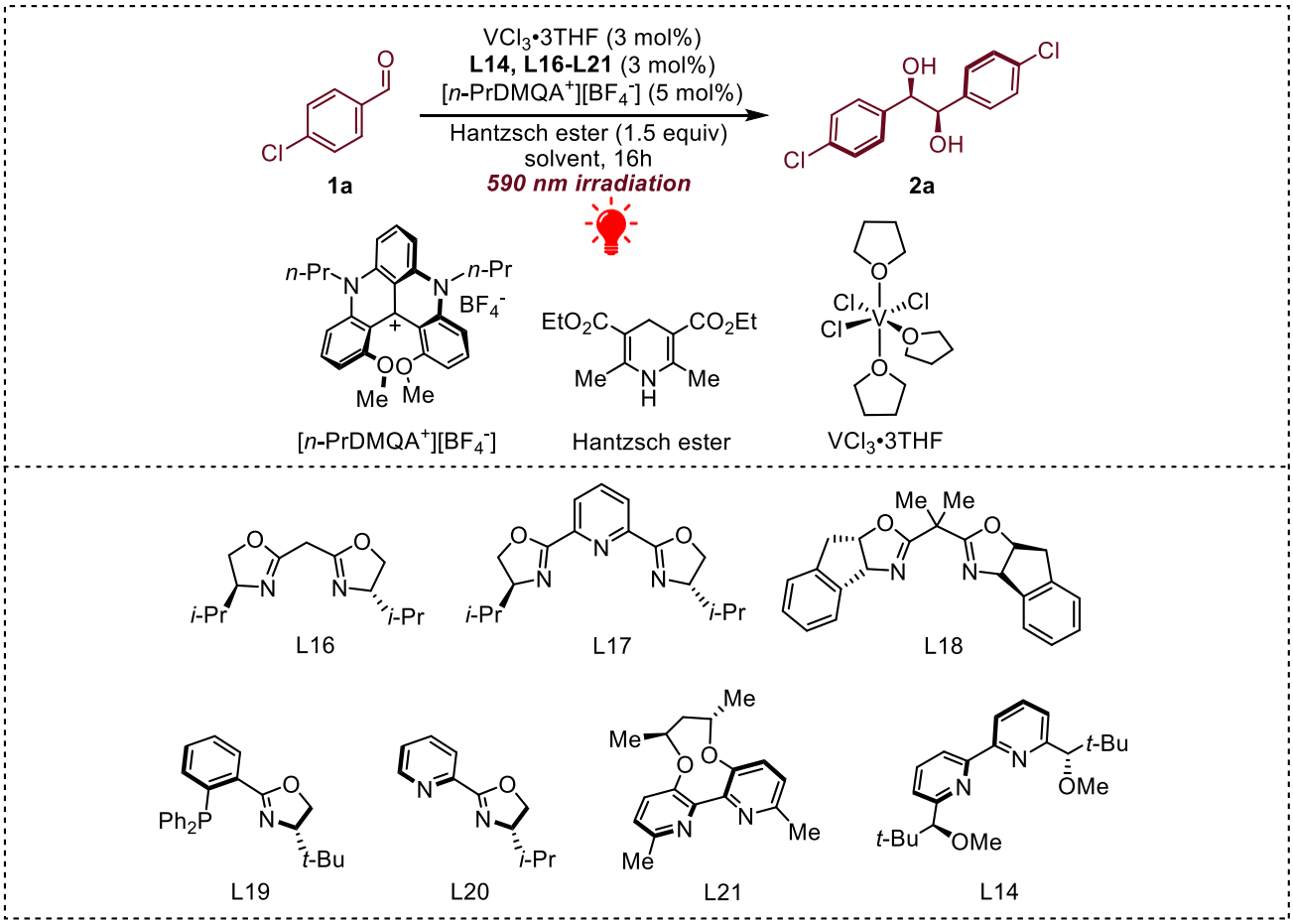

Entry	Ligand	Conversion (%)[a]	*dr* **2a** (*dl:meso*)[b]	*ee* % **2a**[c]
1	L16	99	4:1	-
2	L17	99	2.5:1	-
3	L18	67	3:1	-
4	L19	99	4.4:1	-
5	L20	60	12:1	-
6	L21	99	6:1	-
7	L14	92	>20:1	10

Table 4.5 [a] Determined by ^{1}H NMR analysis on the reaction crude. [b] Determined by ^{1}H NMR analysis on the reaction crude by integration of the benzylic C-H signals.[c] Ees determined by chiral HPLC (ID, n-hexane/i-PrOH = 90:10, 0.75 mL/min, 40°C, 214 nm. t_R(R,R-enantiomer) = 9.878 min, t_R-(meso-diastereoisomer) = 13.839 min, t_R(S,S-enantiomer) = 15.205 min).

4.6 Photophysical studies and reaction mechanism

In order to fully elucidate the reaction mechanism, a careful photophysical analysis was carried out. Thanks to the collaboration with the research group supervised by Prof. P. Ceroni, the analysis of the photophysical behavior of [*n*-PrDMQA$^+$][BF_4^-] in the presence of the different components of the reaction mixture, shed light on the key aspects of the photoredox catalytic cycle. As for the synthetic protocol, DCM was chosen as the solvent of choice for the photophysical characterization of [*n*-PrDMQA$^+$][BF_4^-]. In agreement with published results, it exhibits a low-energy lying absorption band with a maximum at 614 nm (ε_{614nm} = 10300 $M^{-1}cm^{-1}$ in DCM, λ_{onset} ~ 680 nm; *Figure 4.16*) allowing its excitation with red light (λ_{max} = 590 nm). The emission band is peaked at 648 nm – with a lifetime of 12.3 ns and a quantum yield of 0.26 in air-equilibrated DCM solution, corresponding to a spectroscopic energy E_{00} of 1.96 eV. As shown in the figure, the presence of molecular oxygen has a negligible effect on the emission lifetime (τ_{degas} = 12.6 ns *vs* $\tau_{air\ eq.}$ = 12.3 ns), as expected for fluorescent dyes.

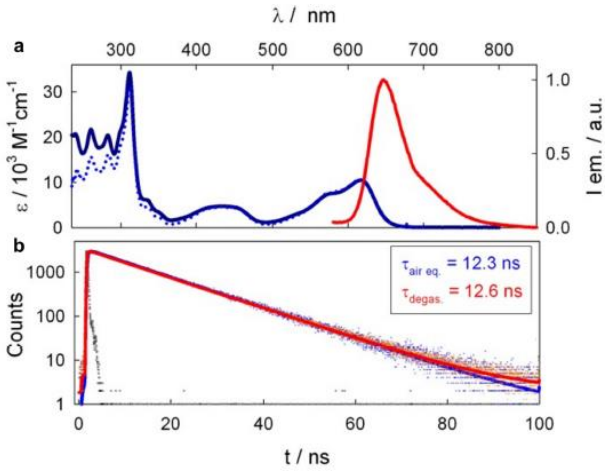

*Figure 4.16 Absorption (**a**, blue line) and emission (**a**, red line) spectrum of [n-PrDMQA$^+$][BF_4^-] in air-equilibrated DCM. Excitation spectrum (**a**, blue dotted line) is shown. (**b**) Comparison between fluorescence decays in air-equilibrated (**b**, blue dots) and N_2-saturated (**b**, red dots) DCM. The instrument response function (IRF) is also shown (grey dots).*

The photocatalyst is used as a racemic mixture, therefore no studies on electronic circular dichroism nor circular polarized luminescence have been carried out.

After having analyzed the main aspects regarding the photocatalyst, the analysis of the luminescence quenching in the presence of all the reaction components has been conducted. As expected, the modest reduction potentials of the photocatalyst in its excited state $^*E_{ox}$(DMQA$^{\bullet+}$/*DMQA$^+$) = −0.52 V *vs* SCE) and in its ground state (E_{red}(DMQA$^+$/DMQA$^\bullet$) = −0.82 V *vs* SCE in DCM) do not allow direct reduction of the model substrate **1a** (E_{red} = −1.82 V *vs* SCE) preventing its non-diastereoselective metal-free dimerization, since no relevant quenching mechanism has been observed upon addition of increasing amounts of **1a** (up to about 16.5 mM) (*Figure 4.17*).

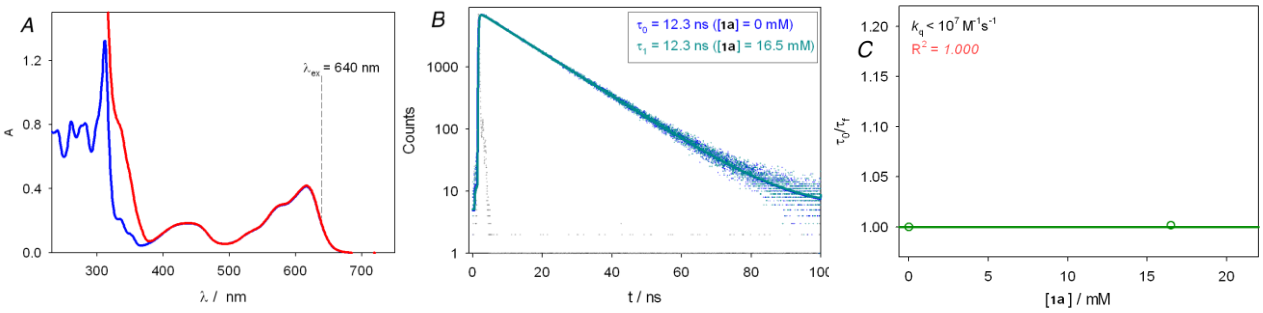

Figure 4.17 **A**) Absorption spectra of solutions of [n-PrDMQA$^+$][BF_4^-] in air-equilibrated DCM at rt (ca. 37 μM, blue line) obtained upon addition of increasing amounts of 4-chlorobenzaldehyde (**1a**, up to ca. 16.5 mM, red line). **B**) Fluorescence decays of [n-PrDMQA$^+$][BF_4^-] obtained from the same solutions at λ_{em}= 680 nm (λ_{ex} = 640 nm). The instrument response function (IRF) is also shown (grey dots). **C**) Stern-Volmer diagram relative to the fluorescence lifetimes.

At the same time no relevant quenching was observed upon the addition of free ligand 6,6-*d*Mebpy (up to *ca*. 9.2 mM, $k_{q2} = 7.2 \cdot 10^7$ $M^{-1}s^{-1}$) (*Figure 4.18*).

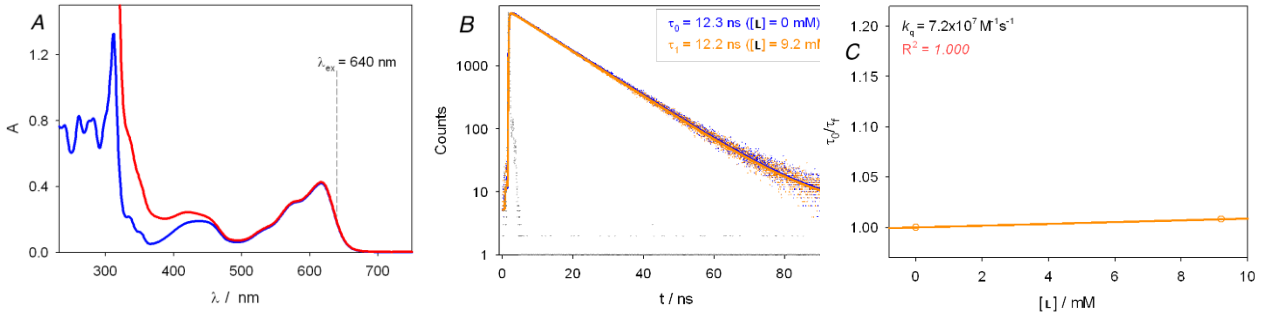

Figure 4.18 ***A****) Absorption spectra of solutions of [n-PrDMQA$^+$][BF_4^-] in air-equilibrated DCM at r.t. (ca. 37μM, blue line) obtained upon addition of increasing amounts of 6,6-dMebpy (**L**, up to ca. 9.2 mM, red line).* ***B****) Fluorescence decays of [n-PrDMQA$^+$][BF_4^-] obtained from the same solutions at λ_{em}= 680 nm (λ_{ex} = 640 nm). The instrument response function (IRF) is also shown (grey dots).* ***C****) Stern-Volmer diagram relative to the fluorescence lifetimes.*

On the other hand, quenching processes were observed for VCl_3·3THF (k_q= 8.0x10^9 $M^{-1}s^{-1}$) (*Figure 4.19*), for the corresponding complex formed after the equimolar addition of the ligand 6,6-*d*Mebpy to VCl_3·3THF (k_{q3} = 8.5x10^9 $M^{-1}s^{-1}$) in a degassed solution (*Figure 4.20*), and for the Hantzsch ester (k_{q4}=1.1x10^9 $M^{-1}S^{-1}$) in air-equilibrated solution (*Figure 4.21*).

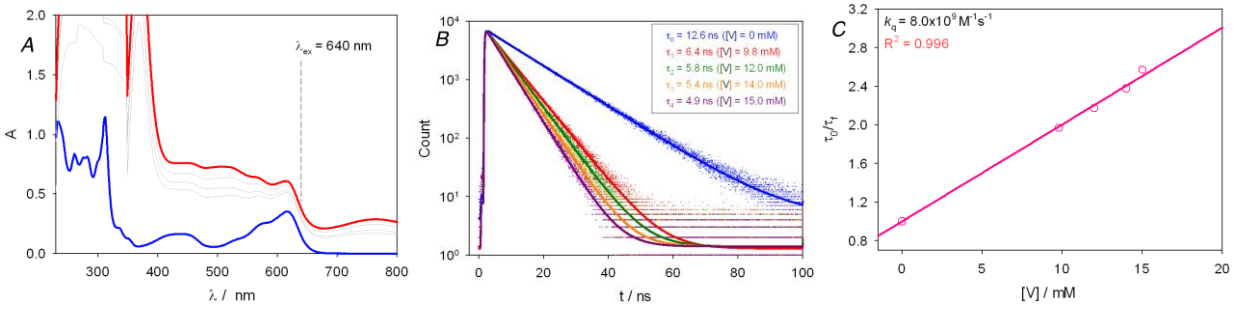

Figure 4.19 ***A****) Absorption spectra of solutions of [n-PrDMQA$^+$][BF_4^-] in air-equilibrated DCM at r.t. (ca. 37μM, blue line) obtained upon addition of increasing amounts of VCl_3·3THF (**V**, up to ca. 15 mM, red line).* ***B****) Fluorescence decays of [n-PrDMQA$^+$][BF_4^-] obtained from the same solutions at λ_{em}= 680 nm (λ_{ex} = 640 nm). The instrument response function (IRF) is also shown (grey dots).* ***C****) Stern-Volmer diagram relative to the fluorescence lifetimes.*

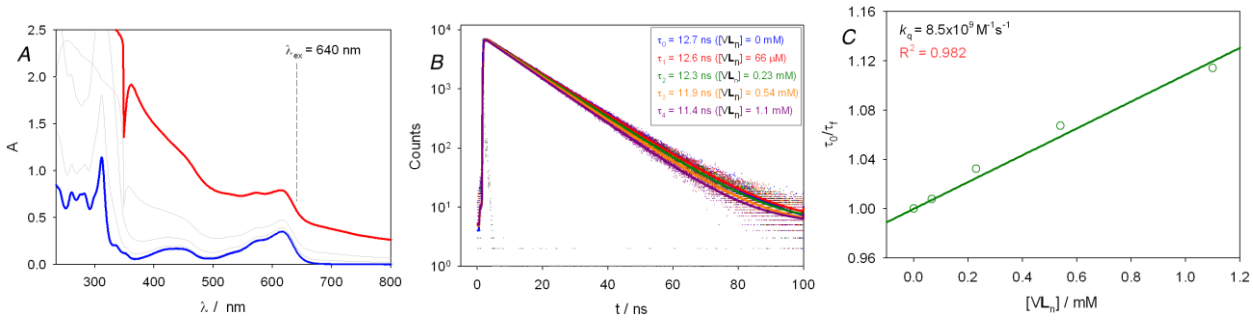

Figure 4.20 ***A****) Absorption spectra of solutions of [n-PrDMQA$^+$][BF$_4^-$] in air-equilibrated DCM at r.t. (ca. 37μM, blue line) obtained upon addition of increasing amounts of the complex obtained between equimolar amounts of VCl$_3$·3THF and 6,6-dMebpy (****VL$_n$****, up to ca. 15 mM, red line).* ***B****) Fluorescence decays of [n-PrDMQA$^+$][BF$_4^-$] obtained from the same solutions at λ$_{em}$= 680 nm (λ$_{ex}$ = 640 nm). The instrument response function (IRF) is also shown (grey dots).* ***C****) Stern-Volmer diagram relative to the fluorescence lifetimes.*

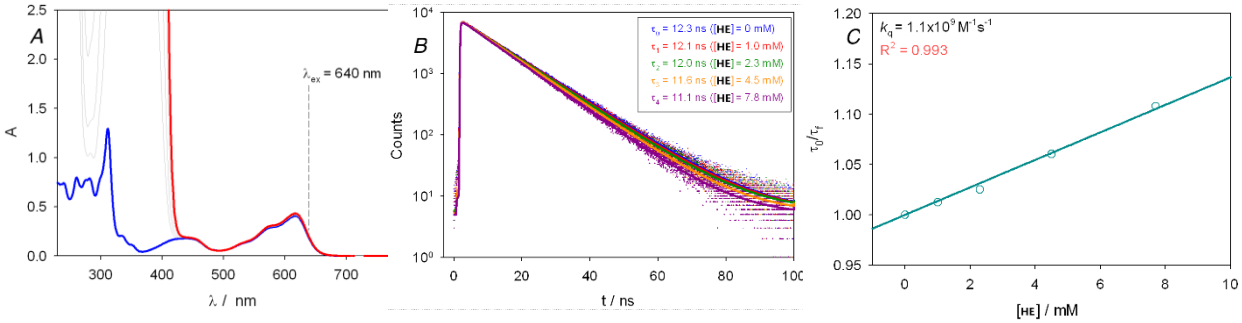

Figure 4.21 ***A****) Absorption spectra of solutions of [n-PrDMQA$^+$][BF$_4^-$] in air-equilibrated DCM at r.t. (ca. 37μM, blue line) obtained upon addition of increasing amounts of Hantzsch ester (****HE****, up to ca. 7.8 mM, red line).* ***B****) Fluorescence decays of [n-PrDMQA$^+$][BF$_4^-$] obtained from the same solutions at λ$_{em}$= 680 nm (λ$_{ex}$ = 640 nm). The instrument response function (IRF) is also shown (grey dots).* ***C****) Stern-Volmer diagram relative to the fluorescence lifetimes.*

Important note for the preparation of the complex between VCl$_3$·3THF and 6,6-*d*Mebpy: a solution containing VCl$_3$·3THF and 6,6-*d*Mebpy was prepared in a nitrogen-filled glovebox, reproducing the concentration obtained during the photocatalytic reaction. To ensure the formation of the desired complex, the solution was stirred 30 minutes before use.

Although the Hantzsch ester has a lower quenching constant compared to that determined for the vanadium complex (k_q = 1.1x10^9 M^{-1}s^{-1} *vs* 8.5x10^9 M^{-1}s^{-1}, respectively), it is the most efficient quencher with an efficiency η = 61%, due to the higher concentration. The experimental evidence agrees with the results obtained in the dual photoredox and titanium-mediated pinacol coupling.

In conclusion, from the evidence obtained from the photophysical study we have been able to propose a mechanistic cycle for the presented protocol (*Figure 4.22*). The mechanism starts with the reductive quenching of the excited photocatalyst ($^*E_{red}$(*DMQA$^+$/DMQA$^\bullet$) = +1.14 V *vs* SCE) by the Hantzsch ester (E_{ox}(HE$^{\bullet+}$/HE) = +1.0 V *vs* SCE) leading to the formation of [DMQA$^\bullet$]. The latter can reduce (E_{red}(DMQA$^+$/DMQA$^\bullet$) = −0.82 V *vs* SCE) in a second step, the V(III) complex (E_{red}(V^{III}/V^{II}) = −0.255 V *vs* SCE[285]) triggering its redox activity towards the carbonyl group of the substrate. The influence of the ligand in the reduction potential of the resulting V(III) complex was not elucidated due to its sensitivity. The vanadium complex in low oxidation state thus generated can undergo a single electron transfer in the presence of the substrate, leading to the formation of the corresponding ketyl radical. The metal-assisted dimerization of this radical is the key step that determines the formation of the new C-C bond. In the ketyl approach, in order to rationalize the exclusive formation of the *d*/*l* products, a transition state

is proposed in which the two aryl groups are in a *gauche* relationship, while the vanadium complexes are in *anti*-position.[286] In our case the presence of a decorated bipyridyl ligand is crucial in defining the transition state, forcing the *gauche* relationship of the two aryl moieties. Finally, the V-O bond is broken by the scavenging effect of the protons resulting from the oxidative pathway of the Hantzsch ester, restoring the metal catalytic cycle and releasing the desired product.

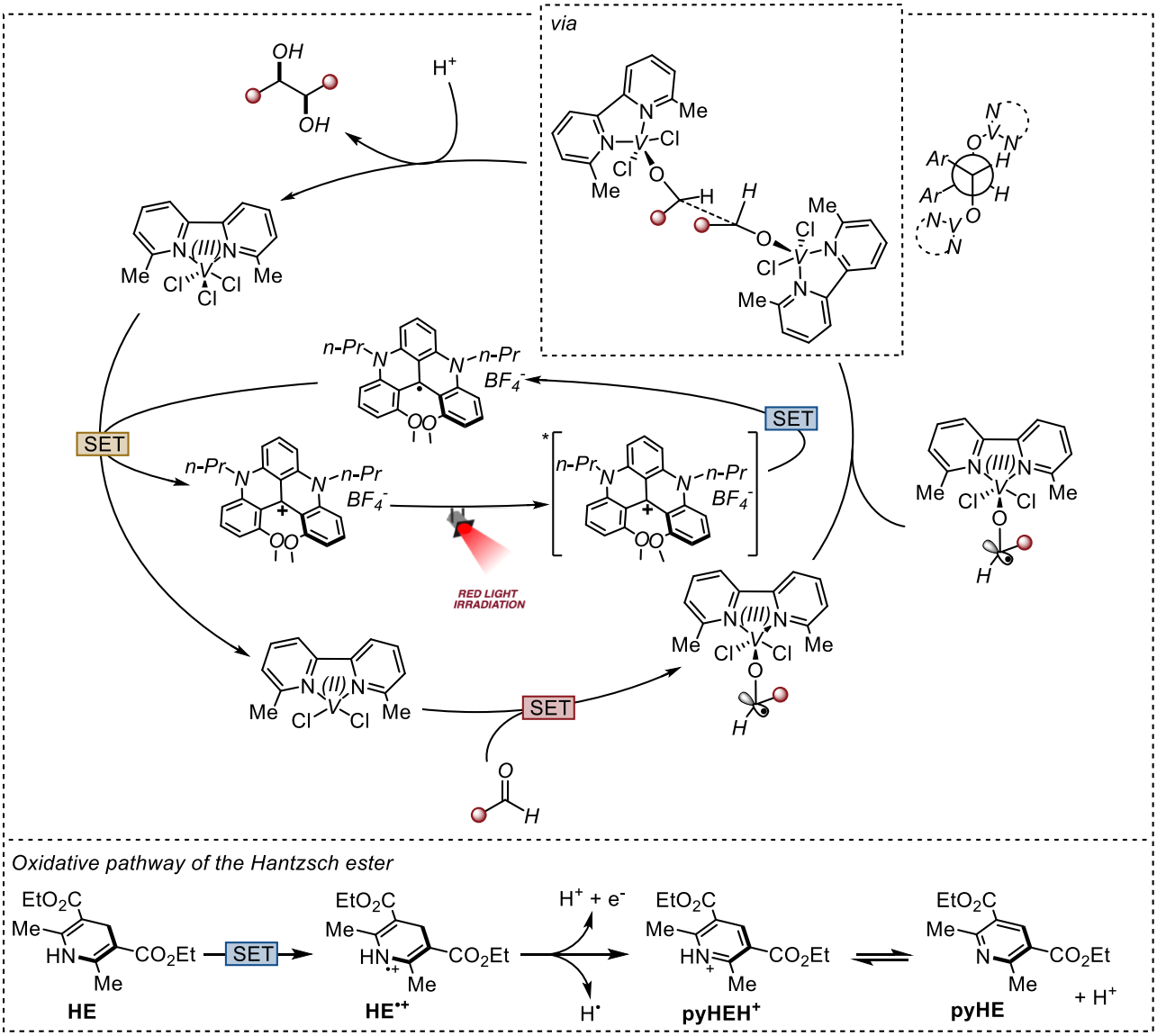

Figure 4.22 Proposed mechanism for the dual photoredox- and vanadium-catalyzed pinacol coupling of aromatic aldehydes.

4.7 Conclusions

In conclusion, we have described a novel dual photoredox- and vanadium-catalyzed diastereoselective pinacol coupling under orange/red light irradiation. The combination of the earth-abundant and low-toxic vanadium complex with low catalyst loading and the use of the less energetic and safer visible light to generate ketyl radicals and control their dimerization in a highly diastereoselective manner makes this procedure quite attractive, as it could potentially be used in different types of couplings.

Compared to our previous titanium-mediated protocol, this protocol offers a superior reactivity (24h *vs* 72h reaction time) with a lower catalyst loading (3 mol% *vs* 5 mol%) and a better substrate compatibility. If these features are the strengths of this work, the extreme oxygen and moisture sensitivity of VCl_3·3THF and the need for a ligand are the major drawbacks of the protocol compared to the air-stable and cheaper Cp_2TiCl_2. The use of a commercial and inexpensive solution of VCl_3·3THF mitigated this problem and made the protocol more attractive. The enantioselective version of this protocol is still ongoing in our research group. To date, only a chiral pyOX and a substituted 6,6'-bipyridine have been found to provide the pinacolization product with a decent diastereoselectivity. Although no promising enantioselective results have been found so far, in the future a detailed screening of different substituents on these classes of ligands will be performed.

The application of vanadium complexes under photoredox conditions is an underrated research topic and a major advance in the field could be the development of a dual photoredox- and vanadium-catalyzed pinacol coupling of aliphatic aldehydes. Further studies on this challenging reaction are in progress in our research group.

Full account and description of the content of the chapter have been published in: E. Pinosa, Y. Gelato, F. Calogero, M. M. Moscogiuri, A. Gualandi, A. Fermi, P. Ceroni, P. G. Cozzi, *Adv. Synth. Catal.* **2024**, *366*, 798–805.

4.8 Experimental section

General Methods

^{1}H NMR spectra were recorded on Varian Mercury 400 spectrometer or Bruker 600 spectrometer. Chemical shifts are reported in ppm from TMS with the solvent resonance as the internal standard ($CDCl_3$, δ = 7.26 ppm, DMSO-*d6*, δ = 2.50 ppm, CD_3CN, δ = 1.94 ppm, CD_3OD, δ = 3.31 ppm). Data are reported as follows: chemical shift, multiplicity (s = singlet, d = doublet, m= multiplet), coupling constants (Hz), number of protons. ^{13}C NMR spectra were recorded on Varian Mercury 400 spectrometer or Bruker 600 spectrometer. Chemical shifts are reported in ppm from TMS with the solvent as the internal standard ($CDCl_3$, δ = 77.2 ppm, DMSO-*d6*, δ = 39.5 ppm, CD_3CN, δ = 118.3, CD_3OD, δ = 49.0 ppm). ^{19}F NMR spectra were recorded on Varian Mercury 400 spectrometer or Bruker 600. Chemical shifts are reported in ppm from $CFCl_3$. HRMS was performed on a Waters Xevo G2-XS QTof, ESI+, cone voltage 40 V, Capillary 3KV, with a source temperature of 120°C. Chromatographic purifications were done with 240-400 mesh silica gel. All reactions were set up under an argon atmosphere in oven-dried glassware using standard Schlenk techniques. All the reagents were purchased from commercial sources (Sigma-Aldrich, Alfa Aesar, Fluorochem, Strem Chemicals, TCI) and used without further purification unless specified. Liquid aldehydes were purified by distillation prior to use. Ligands L1, L2, L7-L12, L15, L17 and L19 were purchased from commercial sources. All reactions requiring inert atmosphere were set up under an argon atmosphere in heat gun-dried glassware using standard Schlenk techniques. Anhydrous solvents were supplied by Aldrich in Sureseal® bottles and, unless specified, were used without further treatment. Trichlorotris(tetrahydrofuran)vanadium 0.5 M solution in dichloromethane was purchased from Thermo Scientific. To perform all the catalysis some millilitres were cannulated from the bottle in a heat gun-dried Schlenk tube and stored under argon atmosphere. Kessil® PR160L@595 nm were used as light source for the photocatalytic reactions (see *Figure 4.23* for the emission profile). Synthesis of Hantzsch ethyl ester was achieved following the reported literature procedure.[244] Ligands L3-L6,[287,288] L13,[289] L16,[290] L18,[291] L20,[292] were synthetized following standard literature procedures. Ligands L14 and L21 were kindly supplied by the Bandini group.

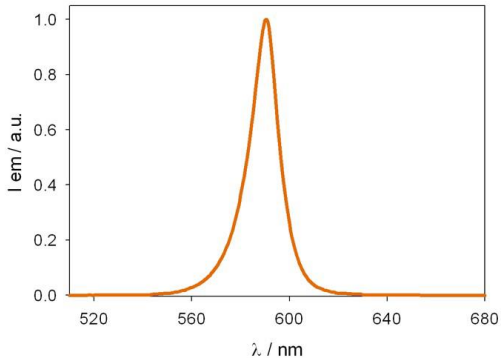

Figure 4.23 Emission spectrum collected from the Kessil® lamp (PR160L@595 nm) used in the experimental setup (λ_{max} = 590 nm; FWHM = 13 nm).

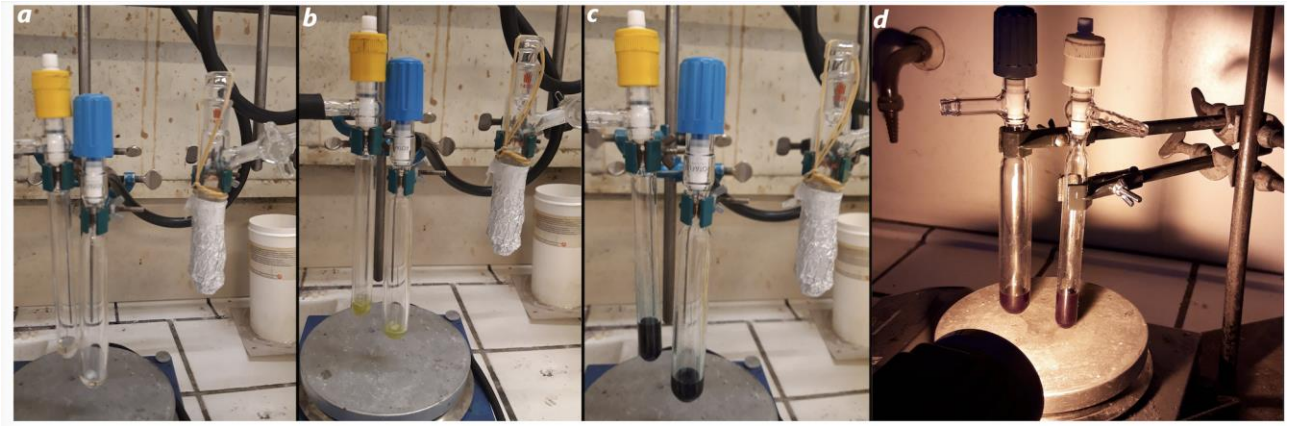

Figure 4.24 ***a****) Solution of the ligand in DCM.* ***b****) Formation of the complex between VCl_3·3THF and 6,6-dMebpy (left), solution of VCl_3·3THF in a Schlenk under Ar atmosphere (right).* ***c****) Reaction mixture after the addition of all the reagents.* ***d****) Reaction mixture under irradiation with Kessil® PR160L@595 nm lamp. The reaction flasks were positioned approximatively at 10 cm from the light source and Kessil® PR160. The reaction temperature was close to room temperature (25-28°C) during the irradiation.*

Photophysical analyses

General Methods

All the photophysical analyses were carried out in dichloromethane at 298 K, unless otherwise specified. UV–vis absorption spectra were recorded with a PerkinElmer λ40 spectrophotometer using quartz cells with path length of 1.0 cm. Luminescence spectra were performed with a PerkinElmer LS-50, an Edinburgh FS5 spectrofluorometer equipped with a Hamamatsu Photomultiplier R928P phototube or on an Edinburgh FLS920 equipped with a Ge detector for NIR emissions. Lifetimes were measured by the same Edinburgh FLS920 spectrofluorometer by time-correlated single-photon counting (TCSPC) technique. Quantum yields are determined with the method of Demas and Crosby[293] Cresyl Violet in air-equilibrated methanol as a standard (Φ = 0.54). Experiments in absence of oxygen were carried out in sealed custom-made quartz cuvettes and the samples were prepared inside a nitrogen filled glovebox. The estimated experimental errors are 2 nm on the band maximum, 5% on the molar absorption coefficient and luminescence lifetime.

Synthesis of *N,N'*-di-*n*-propyl-1,13-dimethoxyquinacridinium tetrafluoroborate[*n*-PrDMQA$^+$][BF_4^-]

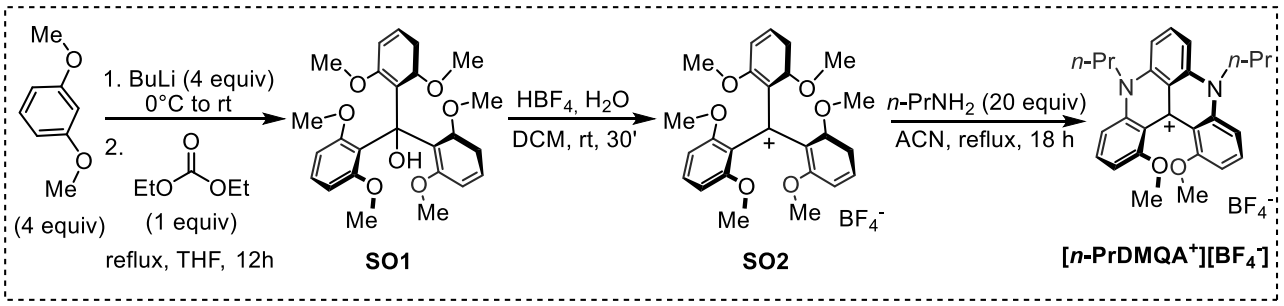

Carbinol **S01** was synthetized modifying the procedure reported by Martin and Smith.[294] In a flame dried 250 mL three-necked round bottom flask equipped with a magnetic stirring bar, under nitrogen atmosphere, 1,3-dimethoxybenzene (2.1 mL, 16 mmol, 4 equiv.) was dissolved in dry THF (8 mL). The solution was cooled to 0°C with an ice bath, and *n*-BuLi (2.5 M in hexane, 6.4 mL, 16 mmol, 4 equiv.) was added dropwise. The solution was allowed to stir 4h at room temperature, then diethyl carbonate (0.49 mL, 4 mmol, 1 equiv.) was added to the reaction mixture. The solution was heated to reflux for 8h. The reaction was quenched at 0 °C upon slow addition of *ca.* 20 mL of water. Volatiles were removed under

reduced pressure and the resulting mixture was extracted with DCM (3x10 mL). The combined organic phase was dried with Na_2SO_4 and concentrated under reduced pressure to yield a colorless oil which was employed in the next step without further purifications.

Synthesis of ***S02***

Compound **S02** was synthetized adapting the procedure reported by Laursen.[78] In a one-necked round bottom flask equipped with a magnetic stir bar, the crude carbinol **S01** was dissolved in absolute EtOH (30 mL), and HBF_4 (48% wt. in H_2O, 1.57 mL, 12 mmol, 3 equiv.) was added dropwise. The mixture become immediately black. After 0.5h a 1:1 solution of diethyl ether and hexane (60 mL) was added, and the formation of a violet precipitate was observed. **S02** was allowed to precipitate overnight in the reaction mixture. The crude was filtered and washed with hexane (*ca.* 20 mL). Compound **S02** was isolated as a dark violet solid (1.11 g, 2.2 mmol, 54% yield over two steps). Spectroscopic data matched those previously reported in the literature.

Synthesis of **[*n*-PrDMQA$^+$][BF_4^-]**

Adapting the procedure reported by Giannetti and co-workers.[81] In a flame dried 250 mL Schlenk tube equipped with a magnetic stirring bar, under argon atmosphere **S02** (1.1 g, 2.15 mmol, 1 equiv.) was dissolved in dry MeCN (25 mL). The mixture was degassed for few minutes, then propylamine (4.42 mL, 53.7 mmol, 25 equiv.) was added to the solution, and the reaction mixture was heated to 80 °C and stirred until HPLC/MS analysis showed a complete conversion of the starting material. Volatiles were removed under reduced pressure and the crude was washed with diethyl ether, then it was dissolved in the minimum volume of DCM (*ca.* 10 mL), reprecipitated with EtOAc (*ca.* 100 mL) and filtrated to afford **[*n*-PrDMQA$^+$][BF_4^-]** as a dark green solid (700 mg, 1.4 mmol, 65%). Spectroscopic data matched those previously reported in the literature.

General procedure for the dual photoredox- and vanadium-diastereoselective photoredox pinacol coupling

All the reactions were performed on 0.2 mmol of aldehyde. In a flame dried 10 mL Schlenk tube, equipped with a Rotaflo stopcock, magnetic stirring bar, and an argon supply tube, under vigorous argon flux, 6,6'-dimethyl-2,2'-dipyridyl (6,6-*d*Mebpy, 1.1 mg, 0.006 mmol, 3 mol%) was dissolved in anhydrous dichloromethane (0.6 mL), then trichlorotris(tetrahydrofuran)vanadium (0.5 M in DCM, 12 µL, 0.006 mmol, 3 mol%) was added. Reaction mixture turned instantly into green color. The mixture was let stirring at room temperature for one hour, then the aldehyde **1a-q** (0.2 mmol), the photocatalyst (5.0 mg, 0.01 mmol, 5 mol%) and the diethyl 1,4-dihydro-2,6-dimethyl-3,5-pyridinedicarboxylate (Hantzsch ester) (76 mg, 0.3 mmol, 1.5 equiv.) were added in the Schlenk tube. Anhydrous dichloromethane (1.4 mL) was then added, and the reaction mixture was further subjected to a freeze-pump-thaw procedure (three cycles), and the vessel was then refilled with argon. The reaction was irradiated under vigorous stirring for 24h at room temperature. The crude reaction was filtered over a pad of silica, the solvent was evaporated under reduced pressure and the reaction crude was analyzed by ^{1}H NMR to evaluate the diastereomeric ratio of the products. The crude was subject to flash column chromatography (SiO_2, Hexane/AcOEt) to afford products **2a–q** in the stated yields.

General procedure for the 1 mmol scale reaction

In a flame dried 30 mL Schlenk tube, equipped with a Rotaflo stopcock, magnetic stirring bar, and an argon supply tube, under vigorous argon flux, 6,6'-dimethyl-2,2'-dipyridyl (6,6-*d*Mebpy, 5.5 mg, 0.03 mmol, 3 mol%) was dissolved in anhydrous dichloromethane (3 mL), then trichlorotris(tetrahydrofuran)vanadium (0.5 M in DCM, 60 µL, 0.03 mmol, 3 mol%) was added. Reaction mixture turned instantly into green colour. The mixture was let stirring at room temperature for one hour,

then the aldehyde **1a** (140 mg, 1 mmol, 1 equiv.), the photocatalyst (25 mg, 0.05 mmol, 5 mol%) and the diethyl 1,4-dihydro-2,6-dimethyl-3,5-pyridinedicarboxylate (Hantzsch ester) (380 mg, 1.5 mmol, 1.5 equiv.) were added in the Schlenk tube. Anhydrous dichloromethane (7 mL) was then added, and the reaction mixture was further subjected to a freeze-pump-thaw procedure (three cycles), and the vessel was then refilled with argon. The reaction was irradiated under vigorous stirring for 24h at room temperature. A small portion of the crude reaction was filtered over a pad of silica, the solvent was evaporated under reduced pressure and the reaction crude was analyzed by 1H NMR to evaluate the diastereomeric ratio of the product. The crude was subject to flash column chromatography (SiO_2, 5:1 Hexane/AcOEt, then 4:1, then 1:1) to afford products **2a** in quantitative yield (0.49 mmol, 139 mg).

Characterization of the products

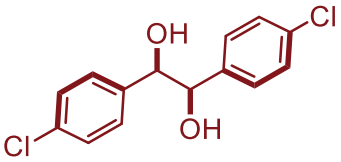

1,2-bis(4-chlorophenyl)ethane-1,2-diol (2a). White solid; Yield >95% (0.099 mmol, 28 mg); $dr_{d/l\text{-}meso}$ > 20:1 calculated considering the ^{1}H NMR spectrum of the reaction crude and comparing the integral of the benzylic CH. The general procedure was applied using **1a** (0.2 mmol, 28 mg). The title compound was isolated by flash column chromatography (SiO_2, 5:1 Hexane/AcOEt). Spectroscopic data matched those previously reported in the literature.[83]

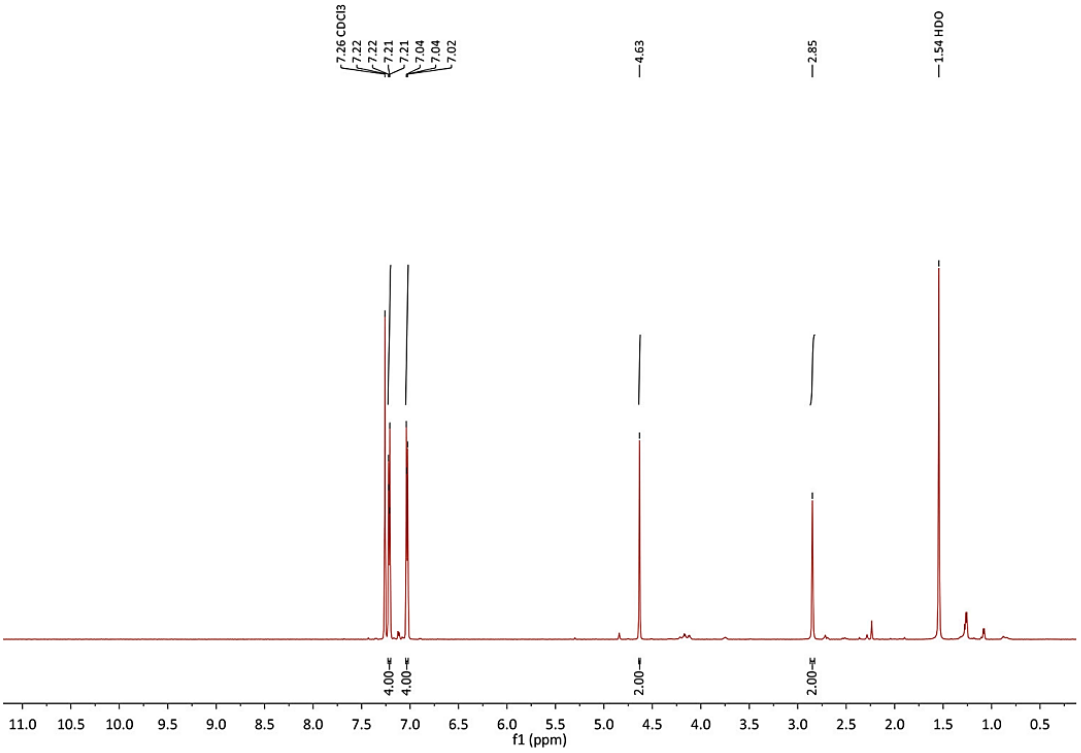

*Figure 4.25 ^{1}H NMR of **2a**.*

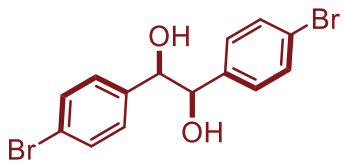

1,2-bis(4-bromophenyl)ethane-1,2-diol (2b). White solid; Yield 89% (0.089 mmol, 33 mg); $dr_{d/l\text{-}meso}$ > 20:1 calculated considering the ^{1}H NMR spectrum of the reaction crude and comparing the integral of the benzylic CH. The general procedure was applied using **1b** (0.2 mmol, 37 mg). The title compound was isolated by flash column chromatography (SiO_2, 5:1 Hexane/AcOEt). Spectroscopic data matched those previously reported in the literature.[83]

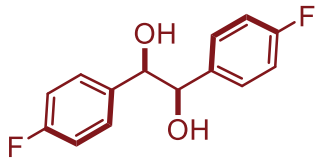

1,2-bis(4-fluorophenyl)ethane-1,2-diol (2c). White solid; Yield 95% (0.095 mmol, 24 mg); $dr_{d/l\text{-}meso}$ > 20:1 calculated considering the ^{1}H NMR spectrum of the reaction crude and comparing the integral of the benzylic CH. The general procedure was applied using **1c** (0.2 mmol, 22 µL). The title compound was isolated by flash column chromatography (SiO_2, 5:1 Hexane/AcOEt). Spectroscopic data matched those previously reported in the literature.[83]

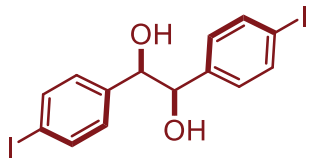

1,2-bis(4-iodophenyl)ethane-1,2-diol (2d). White solid; Yield 86% (0.086 mmol, 40 mg); $dr_{d/l\text{-}meso}$ = 17:1 calculated considering the ^{1}H NMR spectrum of the reaction crude and comparing the integral of the benzylic CH. The general procedure was applied using **1d** (0.2 mmol, 47 mg). The title compound was isolated by flash column chromatography (SiO_2, 4:1 Hexane/AcOEt).

d/l-**2d**. 1H NMR (600 MHz, DMSO_*d6*) δ = 7.60 – 7.55 (m, 4H), 6.87 – 6.83 (m, 4H), 4.60 (s, 2H). ^{13}C NMR (151 MHz, DMSO_*d6*) δ = 139.2 (2C), 137.3 (4C), 128.9 (4C), 93.8 (2C), 78.6 (2C).

HRMS (ESI/Q-TOF) m/z: $[M + Na]^+$ calcd for $C_{14}H_{12}I_2NaO_2$ 488.8819; found 488.8812.

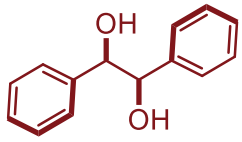

1,2-diphenylethane-1,2-diol (2e). White solid; Yield 74% (0.074 mmol, 16 mg); $dr_{d/l\text{-}meso}$ > 20:1 calculated considering the ^{1}H NMR spectrum of the reaction crude and comparing the integral of the benzylic CH. The general procedure was applied using **1e** (0.2 mmol, 21 µL). The title compound was isolated by flash column chromatography (SiO_2, 5:1 Hexane/AcOEt). Spectroscopic data matched those previously reported in the literature.[83]

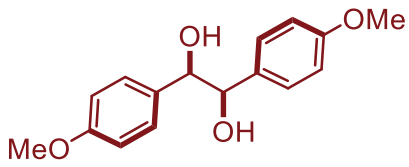

1,2-bis(4-methoxyphenyl)ethane-1,2-diol (2f). White solid; Yield 91% (0.091 mmol, 25 mg); $dr_{d/l\text{-}meso}$ > 20:1 calculated considering the ^{1}H NMR spectrum of the reaction crude and comparing the integral of the benzylic CH. The general procedure was applied using **1f** (0.2 mmol, 24 µL). The title compound was isolated by flash column chromatography (SiO_2, 5:1 Hexane/AcOEt). Spectroscopic data matched those previously reported in the literature.[83]

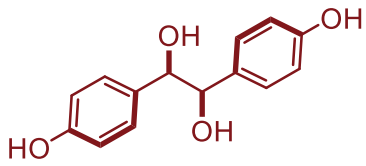

1,2-bis(4-hydroxyphenyl)ethane-1,2-diol (2g). White solid; Yield 61% (0.061 mmol, 15 mg); $dr_{d/l\text{-}meso}$ > 20:1 calculated considering the ^{1}H NMR spectrum of the reaction crude and comparing the integral of the benzylic CH. The general procedure was applied using **1g** (0.2 mmol, 24.8 mg). The title compound was isolated by flash column chromatography (SiO_2, 3:1 Hexane/AcOEt, then 100% AcOEt). Spectroscopic data matched those previously reported in the literature.[83]

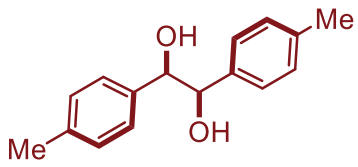

1,2-di-p-tolylethane-1,2-diol (2h). White solid; Yield 85% (0.085 mmol, 21 mg); $dr_{d/l\text{-}meso}$ > 20:1 calculated considering the ^{1}H NMR spectrum of the reaction crude and comparing the integral of the benzylic CH. The general procedure was applied using **1h** (0.2 mmol, 24 µL). The title compound was isolated by flash column chromatography (SiO_2, 5:1 Hexane/AcOEt). Spectroscopic data matched those previously reported in the literature.[83]

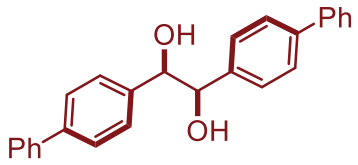

1,2-di([1,1'-biphenyl]-4-yl)ethane-1,2-diol (2i). White solid; Yield >95% (0.096 mmol, 35 mg); $dr_{d/l\text{-}meso}$ > 20:1 calculated considering the ^{1}H NMR spectrum of the reaction crude and comparing the integral of the benzylic CH. The general procedure was applied using **1i** (0.2 mmol, 37 mg). The title compound was isolated by flash column chromatography (SiO_2, 10:1 Hexane/AcOEt, then 5:1). Spectroscopic data matched those previously reported in the literature.[83]

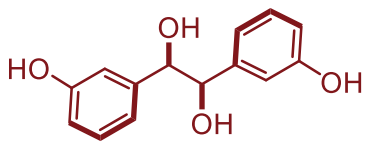

1,2-bis(3-hydroxyphenyl)ethane-1,2-diol (2j). Colorless oil; Yield > 95% (0.098 mmol, 24 mg); $dr_{d/l\text{-}meso}$ = 3:1 calculated considering the ^{1}H NMR spectrum of the reaction crude and comparing the integral of

the benzylic CH. The general procedure was applied using **1j** (0.2 mmol, 24.8 mg). The title compound was isolated by flash column chromatography (SiO_2, 3:1 Hexane/AcOEt, then 1:1).

d/l-**2j**. ^{1}H NMR (600 MHz, CD_3OD) δ = 6.99 (t, J = 7.8 Hz, 2H), 6.77 – 6.73 (m, 1H d/l + 1H meso), 6.64 (dd, J = 2.4, 1.5 Hz, 2H), 6.61 – 6.57 (m, 3H dl + 3H meso), 4.55 (s, 2H), 3.35 (s, 2H). ^{13}C NMR (151 MHz, CD_3OD) δ =157.9 (2C), 144.1 (2C), 129.7 (2C), 119.7 (2C), 115.3 (2C), 115.2 (2), 80.1 (2C).

meso-**2j**. ^{1}H NMR (600 MHz, CD_3OD) δ = 7.08 (t, J = 7.8 Hz, 2H), 6.77 – 6.73 (m, 1H meso + 1H d/l), 6.66 (ddd, J = 8.1, 2.6, 1.1 Hz, 2H), 6.61 – 6.57 (m, 3H meso + 3H dl), 4.68 (s, 2H). ^{13}C NMR (151 MHz, CD_3OD) δ = 157.9 (2C), 144.4 (2C), 129.7 (2C), 119.9 (2C), 115.4 (2C), 115.2 (2C), 78.9 (2C).

HRMS (ESI/Q-TOF) m/z: $[M + Na]^+$ calcd for $C_{14}H_{14}NaO_4$ 269.0784; found 269.0780.

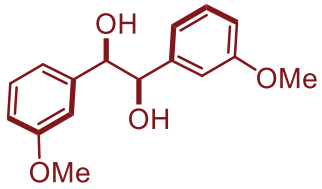

1,2-bis(3-methoxyphenyl)ethane-1,2-diol (2k). White solid; Yield 95% (0.095 mmol, 26 mg); $dr_{d/l\text{-}meso}$ > 20:1 calculated considering the ^{1}H NMR spectrum of the reaction crude and comparing the integral of the benzylic CH. The general procedure was applied using **1k** (0.2 mmol, 25 µL). The title compound was isolated by flash column chromatography (SiO_2, 4:1 Hexane/AcOEt). Spectroscopic data matched those previously reported in the literature.[83]

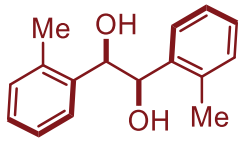

1,2-di-o-tolylethane-1,2-diol (2l). White solid; Yield 95% (0.095 mmol, 23 mg); $dr_{d/l\text{-}meso}$ > 20:1 calculated considering the ^{1}H NMR spectrum of the reaction crude and comparing the integral of the benzylic CH. The general procedure was applied using **1l** (0.2 mmol, 23 µL). The title compound was isolated by flash column chromatography (SiO_2, 10:1 Hexane/AcOEt). Spectroscopic data matched those previously reported in the literature.[295]

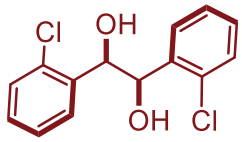

1,2-bis(2-chlorophenyl)ethane-1,2-diol (2m). White solid; Yield >95% (0.099 mmol, 28 mg); $dr_{d/l\text{-}meso}$ = 17:1 calculated considering the ^{1}H NMR spectrum of the reaction crude and comparing the integral of the benzylic CH. The general procedure was applied using **1m** (0.2 mmol, 23 µL). The title compound was isolated by flash column chromatography (SiO_2, 7:1 Hexane/AcOEt, then 5:1). Spectroscopic data matched those previously reported in the literature.[83]

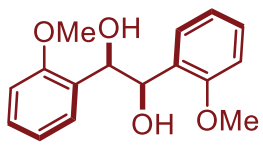

1,2-bis(2-methoxyphenyl)ethane-1,2-diol (2n). White solid; Yield >95% (0.099 mmol, 27 mg $dr_{d/l\text{-}meso}$ > 20:1 calculated considering the ^{1}H NMR spectrum of the reaction crude and comparing the integral of

the benzylic CH. The general procedure was applied using **1n** (0.2 mmol, 27 mg). The title compound was isolated by flash column chromatography (SiO_2, 4:1 Hexane/AcOEt). Spectroscopic data matched those previously reported in the literature.[295]

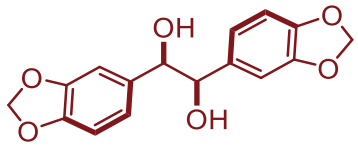

1,2-bis(benzo[d][1,3]dioxol-5-yl)ethane-1,2-diol (2o). White solid; Yield 90% (0.090 mmol, 27 mg); $dr_{d/l\text{-}meso}$ > 20:1 calculated considering the ^{1}H NMR spectrum of the reaction crude and comparing the integral of the benzylic CH. The general procedure was applied using **1o** (0.2 mmol, 30 mg). The title compound was isolated by flash column chromatography (SiO_2, 5:1 Hexane/AcOEt). Spectroscopic data matched those previously reported in the literature.[83]

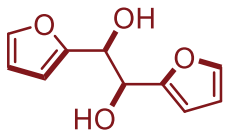

1,2-di(furan-2-yl)ethane-1,2-diol (2p). White solid; Yield 73% (0.073 mmol, 14 mg); $dr_{d/l\text{-}meso}$ = 11:1 calculated considering the ^{1}H NMR spectrum of the reaction crude and comparing the integral of the aromatic CH at 7.44 ppm for the meso- diastereoisomer and at 7.38 ppm for the d/l- diastereoisomer. The general procedure was applied using **1p** (0.2 mmol, 17 µL). The title compound was isolated by flash column chromatography (SiO_2, 5:1 Hexane/AcOEt). Spectroscopic data matched those previously reported in the literature.[296]

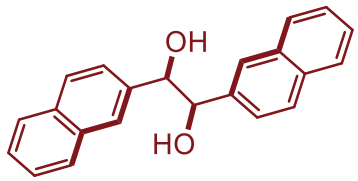

1,2-di(naphthalen-2-yl)ethane-1,2-diol (2q). White solid; Yield 52% (0.052 mmol, 31 mg); $dr_{d/l\text{-}meso}$ > 20:1 calculated considering the ^{1}H NMR spectrum of the reaction crude and comparing the integral of the benzylic CH. The general procedure was applied using **1q** (0.2 mmol, 24.8 mg). The title compound was isolated by flash column chromatography (SiO_2, 6:1 Hexane/AcOEt). Spectroscopic data matched those previously reported in the literature.[83]

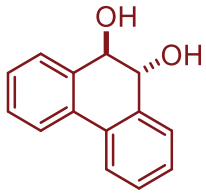

9,10-dihydrophenanthrene-9,10-diol (2r). White solid; Yield = 35% (0.07 mmol, 15 mg); $dr_{d/l\text{-}meso}$ > 20:1 calculated considering the ^{1}H NMR spectrum of the reaction crude and comparing the integral of the benzylic CH. The general procedure was applied using **1r** (0.2 mmol, 21 mg). The title compound was isolated by flash column chromatography (SiO_2, 10:1 Hexane/AcOEt, then 5:1). Spectroscopic data matched those previously reported in the literature.[297]

4.9 Bibliography

[251] J. Streuff, *Synthesis* **2013**, *45,* 281–307.
[252] R. Fittig, *Liebigs Ann.* **1859**, 110, 17–23.
[253] E. J. Roskamp, S. F. Pedersen, *J. Am. Chem. Soc.* **1987**, *109*, 6551–6553.
[254] T. Kiguchi, K. Tajiri, I. Ninomiya, T. Naito, H. Hiramatsu, *Tetrahedron Lett.* **1995**, *36*, 253–256.
[255] J. P. Guidot, T. Le Gall, C. Mioskowski, *Tetrahedron Lett.* **1994**, *35*, 6671–6672.
[256] J. L. Namy, J. Souppe, H. B. Kagan, *Tetrahedron Lett.* **1983**, 24, *8*, 765–766.
[257] Z. Hou, K. Takamine, Y. Fujiwara, H. Taniguchi, *Chem. Lett.* **1987**, 2061–2064.
[258] W.-C. Zhang, C.-J. Li, *J. Chem. Soc. Perkin 1* **1998**, 3131–3132.
[259] Y. Handa, J. Inanaga, *Tetrahedron Lett.* **1987**, 28, *46*, 5717–5718.
[260] A. Fürstner, A. Hupperts, *J. Am. Chem. Soc.* **1995**, *117*, 4468–4475.
[261] A. Fürstner, *Pure Appl. Chem.* **1998**, *70*, 1071–1076.
[262] A. Fürstner, *Chem. Eur. J.* **1998**, *4*, 567–570.
[263] R. Nomura, T. Matsuno, T. Endo, *J. Am. Chem. Soc.* **1996**, *118*, 11666–11667.
[264] A. Fürstner, N. Shi, *J. Am. Chem. Soc.* **1996**, *118*, 2533–2534.
[265] A. Gansäuer, *Chem. Commun.* **1997**, 457–458.
[266] H. G. Roth, N. A. Romero, D. A. Nicewicz, *Synlett* **2015**, *27*, 714–723.
[267] J. H. Freudenberger, A. W. Konradi, S. F. Pedersen, *J. Am. Chem. Soc.* **1989**, *111*, 8014–8016.
[268] F. A. Cotton, S. A. Duraj, M. W. Extine, G. E. Lewis, W. J. Roth, C. D. Schmulbach, W. Schwotzer, *J. Chem. Soc. Chem. Commun.* **1983**, 1377.
[269] F. A. Cotton, S. A. Duraj, W. J. Roth, *Inorg. Chem.* **1985**, *24*, 913–917.
[270] P. M. Takahara, J. H. Freudenberger, A. W. Konradi, S. F. Pedersen, *Tetrahedron Lett.* **1989**, 30, *51*, 7177–7180.
[271] R. Annunziata, M. Cinquini, F. Cozzi, P. Giaroni, M. Benaglia, *Tetrahedron* **1991**, 41, *30*, 5137–5158.
[272] T. Hirao, A. Ogawa, M. Asahara, Y. Muguruma, H. Sakurai, *Org. Synth.* **2005**, *81*, 26–32.
[273] M. Nakajima, E. Fava, S. Loescher, Z. Jiang, M. Rueping, *Angew. Chem. Int. Ed.* **2015**, *54*, 8828–8832.
[274] A. Gualandi, G. Rodeghiero, E. D. Rocca, F. Bertoni, M. Marchini, R. Perciaccante, T. P. Jansen, P. Ceroni, P. G. Cozzi, *Chem. Commun.* **2018**, *54*, 10044–10047.
[275] J. J. H. Edema, W. Stauthamer, F. Van Bolhuis, S. Gambarotta, W. J. J. Smeets, A. L. Spek, *Inorg. Chem.* **1990**, *29*, 1302–1306.
[276] S. Gambarotta, M. Mazzanti, C. Floriani, A. Chiesi-Villa, C. Guastini, *Inorg. Chem.* **1986**, *25*, 2308–2314.
[277] C. Kaes, A. Katz, M. W. Hosseini, *Chem. Rev.* **2000**, *100*, 3553–3590.
[278] I. S. Tidmarsh, L. J. Batchelor, E. Scales, R. H. Laye, L. Sorace, A. Caneschi, J. Schnack, E. J. L. McInnes, *Dalton Trans.* **2009**, 9402–9409.
[279] C. Bolm, M. Zehnder, D. Bur, *Angew. Chem.* **1990**, *102*, 206–208.
[280] S. Lin, Y. Chen, H. Yan, Y. Liu, Y. Sun, E. Hao, C. Shi, D. Zhang, N. Zhu, L. Shi, *Org. Lett.* **2021**, *23*, 8077–8081.
[281] J. Jung, J. Kim, G. Park, Y. You, E. J. Cho, *Adv. Synth. Catal.* **2016**, *358*, 74–80.
[282] H. Li, C. Pan, X. Li, Z. He, X. Sun, J. Xu, K. Wang, B. Fan, *J. Org. Chem.* **2024**, *89*, 11537–11541.
[283] Á. Péter, S. Agasti, O. Knowles, E. Pye, D. J. Procter, *Chem. Soc. Rev.* **2021**, *50*, 5349–5365.
[284] J. Park, S. F. Pedersen, *Tetrahedron* **1992**, *48*, 2069–2080.
[285] X. Li, H. Zhang, Z. Mai, H. Zhang, I. Vankelecom, *Energy Environ. Sci.* **2011**, *4*, 1147–1160.
[286] R. J. Enemaerke, J. Larsen, G. H. Hjøllund, T. Skrydstrup, K. Daasbjerg, *Organometallics* **2005**, *24*, 1252–1262.
[287] T. Kawasaki, T. Kamata, H. Ushijima, M. Kanakubo, S. Murata, F. Mizukami, Y. Fujii, Y. Usui, *J. Chem. Soc. Perkin Trans. 2* **1999**, 193–198.
[288] A. L. Johnson, M. G. Davidson, M. D. Lunn, M. F. Mahon, *Eur. J. Inorg. Chem.* **2006**, *2006*, 3088–3098.

[289] S. Lauzon, L. Schouwey, T. Ollevier, *Org. Lett.* **2022**, *24*, 1116–1120.
[290] C. C. Tyrol, N. S. Yone, C. F. Gallin, J. A. Byers, *Chem. Commun.* **2020**, *56*, 14661–14664.
[291] J. L. Hofstra, T. J. DeLano, S. E. Reisman, *Org. Synth. Annu. Publ. Satisf. Methods Prep. Org. Chem.* **2020**, *97*, 172–188.
[292] C. Bolm, K. Weickhardt, M. Zehnder, T. Ranff, *Chem. Ber.* **1991**, *124*, 1173–1180.
[293] G. A. Crosby, J. N. Demas, *J. Am. Chem. Soc.* **1971**, *93*, 2841–2847.
[294] J. C. Martin, R. G. Smith, *J. Am. Chem. Soc.* **1964**, *86*, 2252–2256.
[295] F. Lan, C.-S. Liu, C. Zhou, X. Huang, J.-Y. Wu, X. Zhang, *J. Mater. Chem. A* **2022**, *10*, 16578–16584.
[296] M. Jiang, J. Tan, Y. Chen, W. Zhang, P. Chen, Y. Tang, Q. Gao, *Chem. Commun.* **2023**, *59*, 3103–3106.
[297] X. Wang, J. Zhong, M. Luo, X. Zeng, *Org. Lett.* **2024**, *26*, 4093–4097.

Chapter 5. A dual photoredox- and nickel-catalyzed diastereoselective allylation of aldehydes with Morita-Baylis-Hillman adducts

5.1 Background introduction

Nickel is an abundant and inexpensive transition metal and, despite some problems related to health hazards, its industrial, technological and academic applications are growing rapidly.[298–301] Apart from its abundance and lower cost, nickel derivatives display some useful properties in catalysis, such as the formation of highly reactive organometallic intermediates, the ready availability of many contiguous oxidation states (from -1 to +4), easy homolytic bond cleavage, and the ability to react with unsaturated systems and activate multiple bonds by coordination. These properties are similar to those of the more expensive palladium, e.g. in cross-coupling reactions involving oxidative addition-reductive elimination steps, and can be used in a variety of different transformations such as cross-couplings and C-H activation, even with unreactive substrates,[299] under different modes of activation, e.g. photocatalysis, electrocatalysis or metal reduction. Among this wide range of useful transformations, the application of nickel catalysis in allylation methods is particularly relevant to this introduction. Transition metal-catalyzed allylations are considered one of the most important tools for the formation of new C-C bonds and many metals can be used in this transformation.[302]

The Durandetti-Perichon group in 1987 reported a pioneering protocol for the formation of nucleophilic (π-allyl)-Ni species under electrochemical/Barbier conditions using methallyl chloride as pronucleophile species.[303] In addition, in the same work methyl chloroacetate was used in the Reformatsky reaction. The reaction was applied to aliphatic and aromatic ketones and aldehydes with yields from good to high. The following year the same group studied more in detail the same electrochemical protocol using both methallyl chloride and methallyl acetate.[304] In more recent years the group reported a few examples of the synthesis of homoallylic alcohols using a catalytic amount of Ni(II) precatalyst in the presence of allyl acetate and a stoichiometric amount of manganese as reducing agent (*Figure 5.1*).[305] In a preliminary test crotyl acetate was used and the branched product was obtained as the major regioisomer in a 19:1 branched/linear ratio. A good conversion of the starting materials was observed when the reaction was carried out at 80°C.

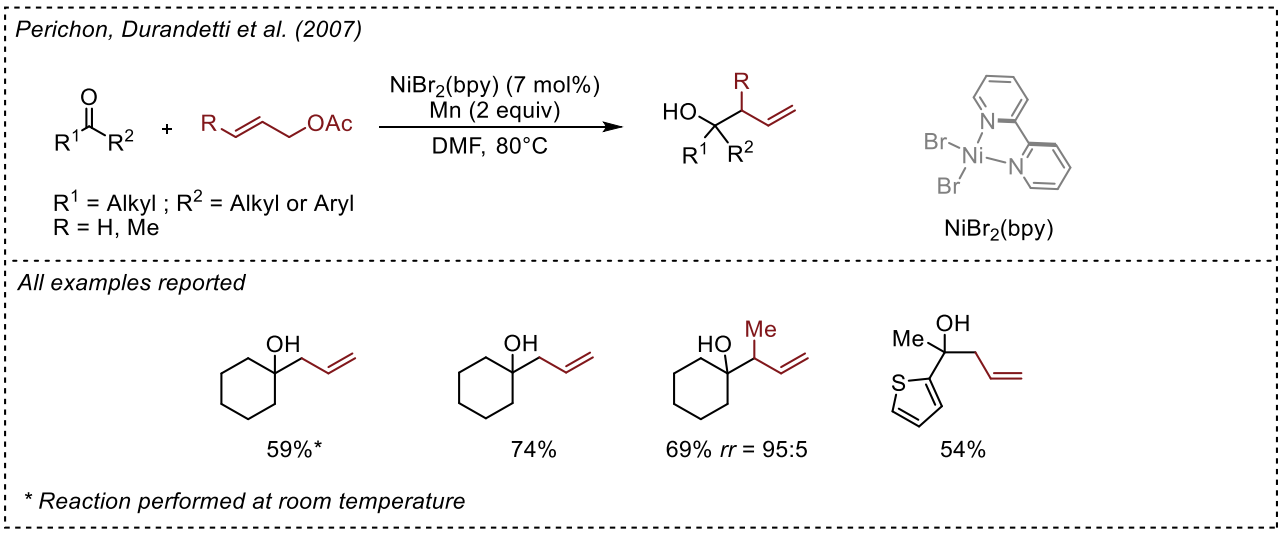

Figure 5.1 Nickel-catalyzed allylation of carbonyls reported by the Durandetti-Perichon group.

In 2014 the Gong group published the first asymmetric Ni-catalyzed reductive coupling of allylic carbonates with aldehydes in the presence of a pyBOX ligand and zinc as the stoichiometric terminal reductant.[306] The reaction conditions were found to be particularly effective for the 2-aryl-allylic carbonates, producing the desired alcohols with generally moderate enantiomeric ratios for both aromatic and aliphatic aldehydes. Preliminary studies ruled out that the enantioselectivity of the protocol was due to the addition of the weaker (π-allyl)-Ni nucleophile to the carbonyl rather than to the more reactive allyl-Zn that may be generated in the reaction. Finally, using substituted allyl acetates, the Y-isomer was obtained as the major regioisomer, suggesting a Zimmerman-Traxler transition state (*Figure 5.2*).

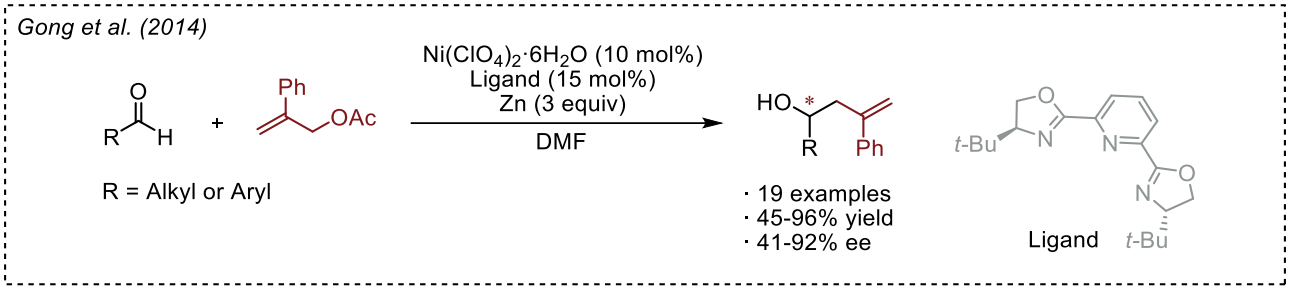

Figure 5.2 Nickel-catalyzed enantioselective allylation of carbonyls reported by the Gong group.

To date, the formation of a (π-allyl)-Ni nucleophiles has been achieved using activated allyl sources, such as allyl halides or acetates. The Martin group reported in 2017 the Ni-catalyzed carboxylation of unactivated allyl alcohols using CO_2 as the electrophile partner and additives to facilitate the C-O cleavage, generating a carbonate *in situ*.[307] The protocol is characterized by an exquisite regiodivergence which can be modulated by the type of ligand chosen (*Figure 5.3*).

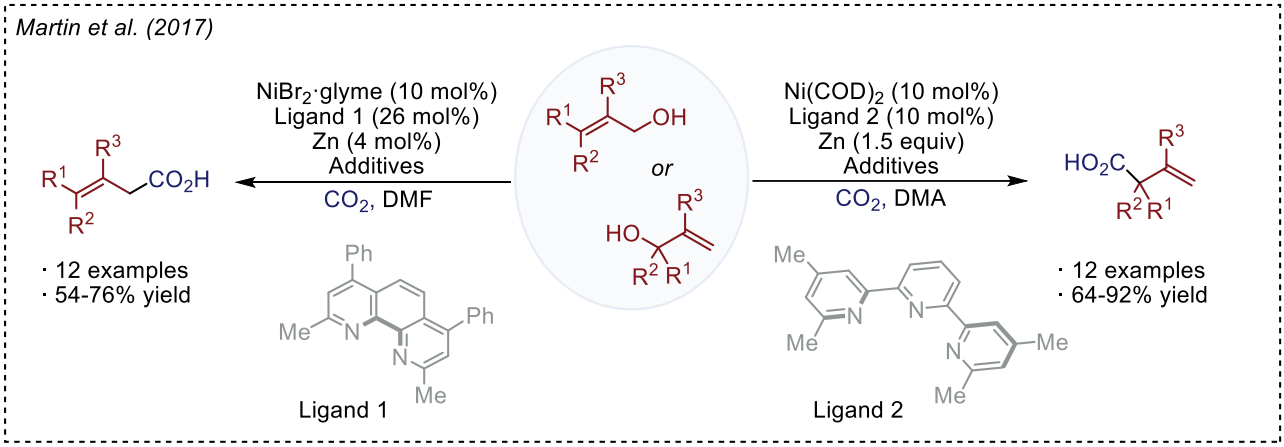

Figure 5.3 Nickel-catalyzed regiodivergent carboxylation of unactivated allyl alcohols reported by the Martin group.

Even though the protocols described so far use catalytic amounts of relatively cheap and air-stable Ni(II) complexes under mild conditions, avoiding the use of high sensitive Ni(0), e.g. $Ni(COD)_2$, the use of stoichiometric metals, e.g. Zn(0) or Mn(0), required to get access to the catalytically active Ni in a low oxidation state, is associated with a large amount of metal waste. Photoredox catalysis offers the possibility of replacing the reductive behaviour of the metal with a milder photocatalytic cycle.

For example, the Cozzi group in 2019 reported the first dual photoredox- and nickel-catalyzed allylation of aldehydes using the inexpensive $NiBr_2$·glyme as a ready-available, commercial and air-stable Ni(II) source, $[Ru(bpy)_3]Cl_2$ as the photocatalyst, o-phenanthroline as the ligand and DIPEA as the final organic reductant (*Figure 5.4*).[247] Under blue light irradiation the protocol was found to be suitable for

aromatic and aliphatic aldehydes, but ketones were found to be poorly reactive, as were 1-substituted allyl derivatives.

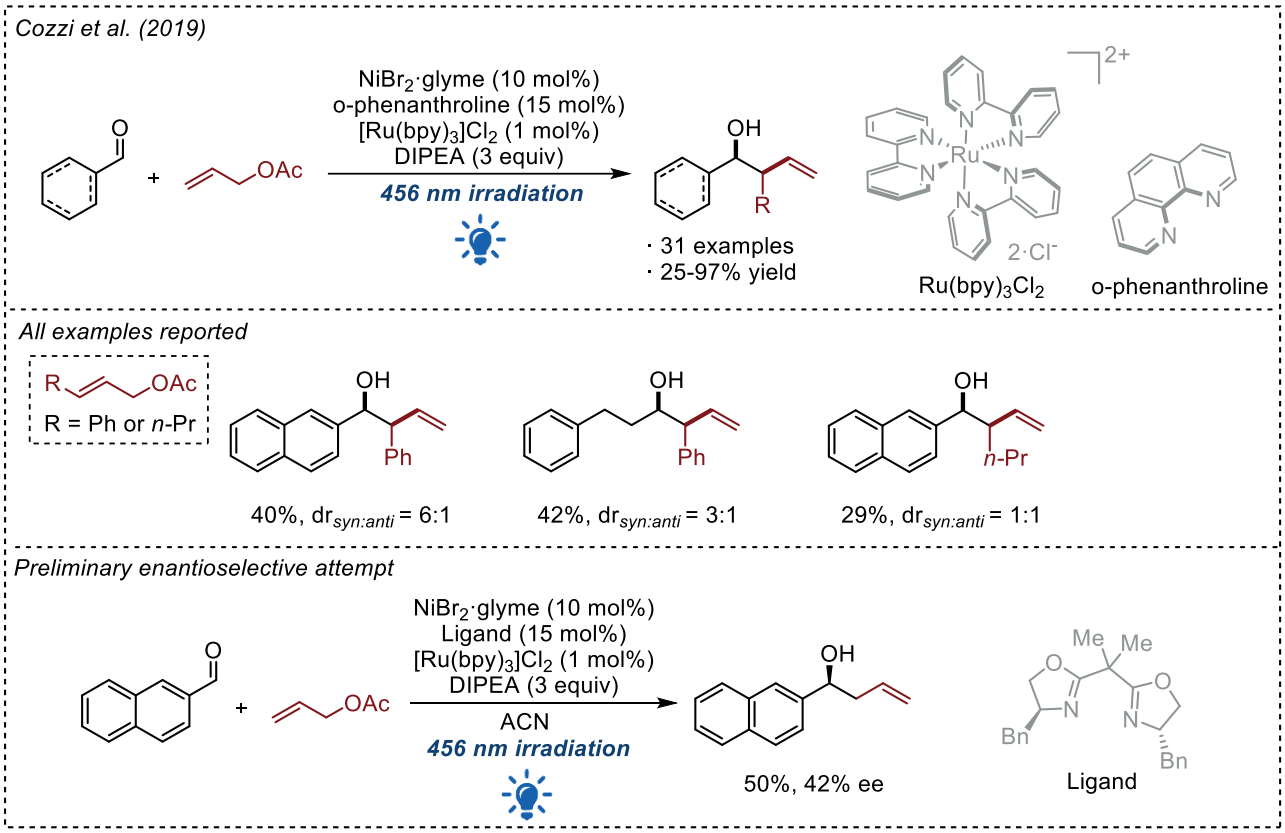

Figure 5.4 First dual photoredox- and nickel-catalyzed allylation of aldehydes reported by the Cozzi group and preliminary enantioselective attempt.

The group reported a first attempt of an enantioselective version of the reaction but only a modest 42% *ee* was achieved using a BOX ligand. The search for the optimal enantioselective conditions took 3 years, as it was reported by our group in 2022 (*Figure 5.5*).[237]

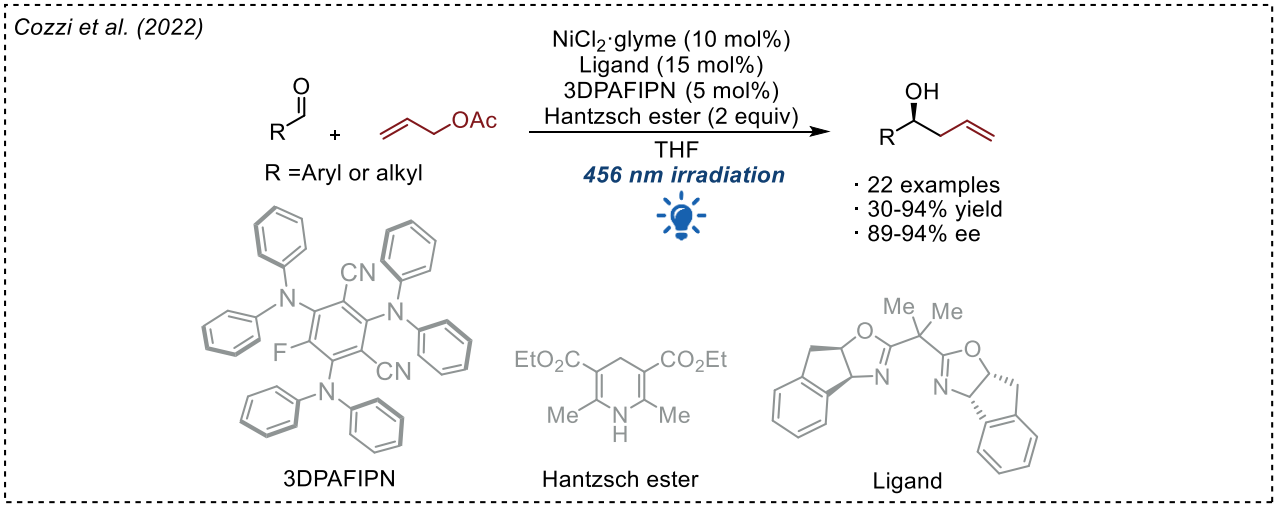

Figure 5.5 First dual photoredox- and nickel-enantioselective allylation of aldehydes reported by the Cozzi group.

The optimal conditions greatly differ from the previous protocol, since our group switched from a metal-based photocatalyst to the fully organic and stronger reductant 3DPAFIPN. DIPEA was replaced with

Hantzsch ester to avoid the use of a large excess of a coordinating amine which could hamper an effective and enantioselective catalytic cycle.

The mechanism was investigated by Stern-Volmer luminescence quenching studies and at a computational level, and the experimentally favoured cycle is shown in *Figure 5.6*. From photophysical analyses it was determined that 3DPAFIPN in the presence of an overstoichiometric amount of Hantzsch ester (HE) is expected to quantitatively form with the HE the photoactive complex [3DPAFIPN·HE]. The process is initiated by the absorption of visible radiation by the photocatalyst. The Hantzsch ester can act as an efficient reductant of the excited dye leading to the formation of $[3DPAFIPN{\cdot}HE]^{\bullet-}$ and the concomitant formation of $HE^{\bullet+}$. The former can reduce ($E_{red}([3DPAFIPN{\cdot}HE]/[3DPAFIPN{\cdot}HE]^{\bullet-})$ = –1.63 V *vs* SCE) in a second step the Ni(II) complex to the active Ni(0) species ($E_{red}(Ni^{II}/Ni^{I})$ = –0.58 V *vs* SCE; $E_{red}(Ni^{I}/Ni^{0})$ = –1.46 V *vs* SCE) in a sequence of SET events, triggering its redox activity towards the allyl acetate and simultaneously restoring the photoredox catalytic cycle. Ni(0) undergoes oxidative addition with the allyl acetate and generates the electrophilic (π-allyl)-nickel(II) species that is readily reduced in another SET event to the key transient nucleophilic (π-allyl)-nickel(I). Enantioselective addition of this intermediate to the aldehyde forges a new stereodefined C-C bond and the formation of the product as nickel alkoxide. Finally, the Ni-O bond is cleaved in a proton-coupled electron transfer (PCET) process in which the independent transfer of a proton and an electron liberates the homoallylic alcohol and restores the nickel catalytic cycle.

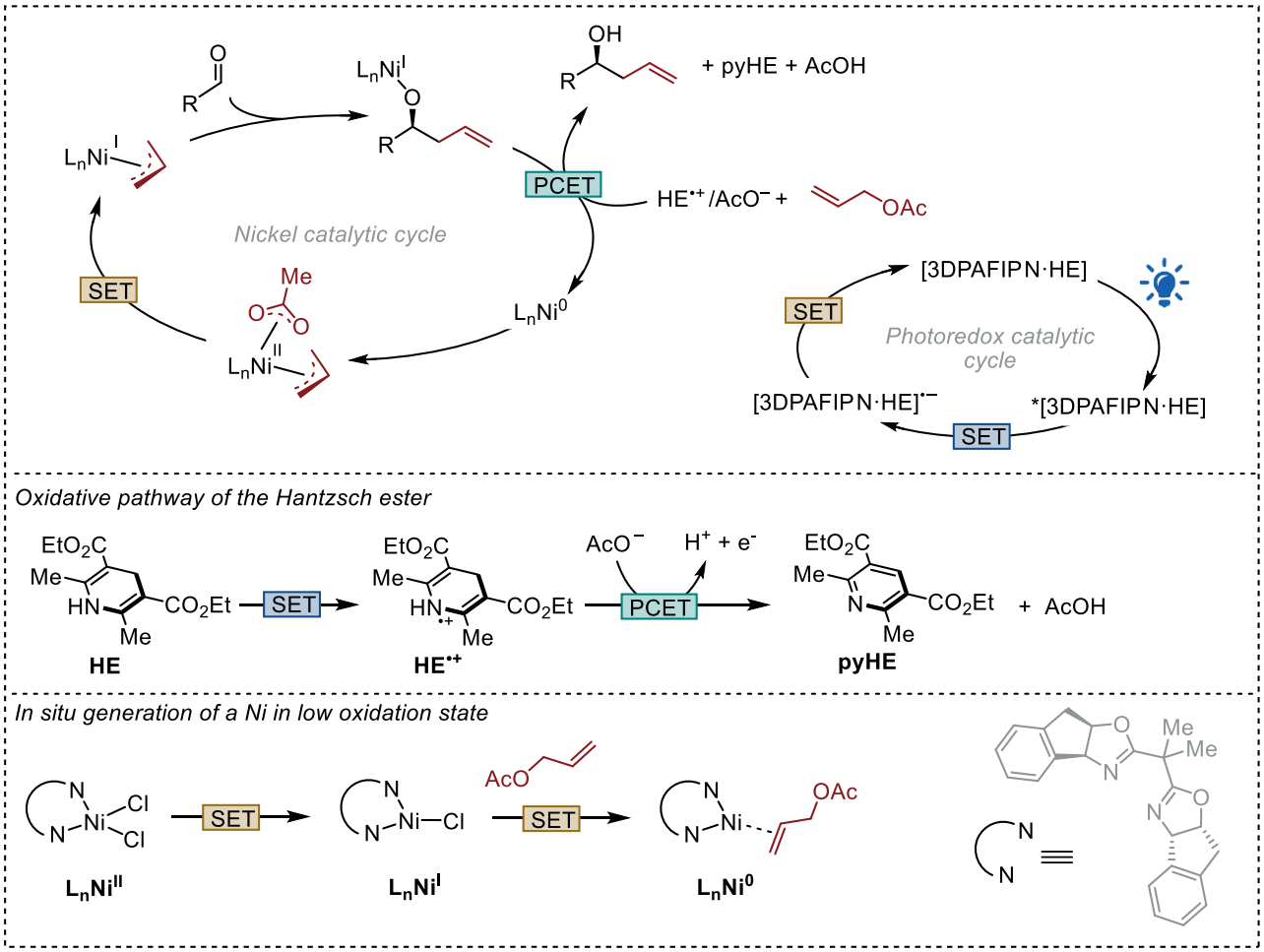

Figure 5.6 Proposed mechanism for the dual photoredox- and nickel-catalyzed enantioselective allylation reported by the Cozzi group.

Recently the Xi group reported a dual photoredox- and nickel-catalyzed diastereoselective allylation of aldehydes using unactivated allyl alcohol derivatives in the presence of CO_2 (*Figure 5.7*).[308] In contrast to the previous dual role of the CO_2,[307] in this work, CO_2 acts only as an activator for the C-O cleavage and the formation of the (π-allyl)-Ni(II) species. The protocol shows a high branched selectivity. The authors reported an in-depth theoretical study of the intermediates involved in the transformation.

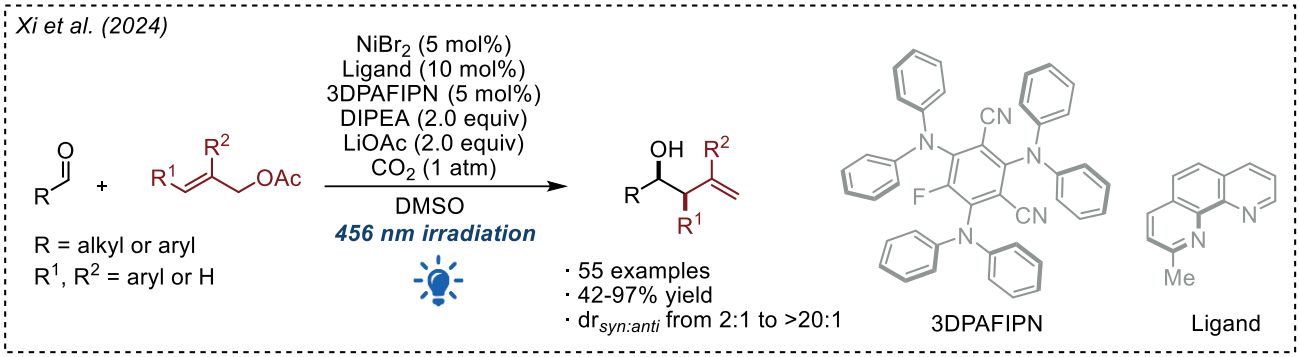

Figure 5.7 Dual photoredox- and nickel-catalyzed diastereoselective carboxylation of allyl acetates reported by the Xi group.

Finally, with regards to the use of unactivated allyl sources, it is also worth mentioning the work of the groups of Xia[309] and Breit,[310] who reported respectively the use of 1,3-dienes and allenes which can be converted into (π-allyl)-Ni(II) species in the presence of a Ni-H intermediate generated under photoredox conditions (*Figure 5.8*). These protocols allow the high functionalization of carbonyl compounds in regioselective and diastereoselective manners.

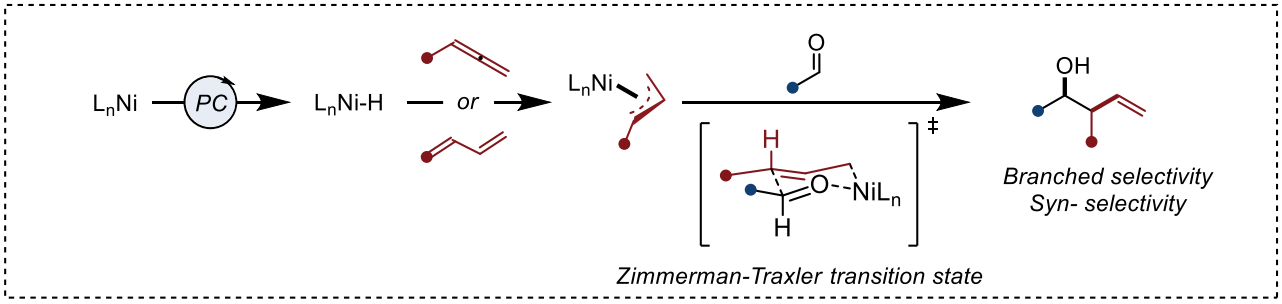

Figure 5.8 Schematic formation of nucleophilic (π-allyl)-nickel species through the reaction between Ni-H and unactivated allyl sources.

5.2 Presented work

The abundance of nickel on Earth and its versatility in a wide range of transformations make it an excellent transition metal for catalysis. The possibility of accessing Ni in low oxidation states using commercially available and stable Ni(II) sources under mild photoredox or electrochemical conditions and avoiding the use of stoichiometric metal reductants or highly sensitive Ni(0) complexes makes the use of nickel even more attractive. Despite the large and comprehensive number of protocols already reported in the literature,[311] the development or the implementation of dual photoredox- and nickel-mediated transformations remains intriguing. In particular, given the expertise in nickel-mediated allylations gained by our group in recent years, a reasonable implementation could be the use of more functionalized allyl sources for the synthesis of homoallylic alcohols with greater structural complexity. To this end, during my PhD studies I focused on Morita-Baylis-Hillmann (MBH) acetates as a novel allyl source to couple with photoredox and Ni in low oxidation state (*Figure 5.9*).

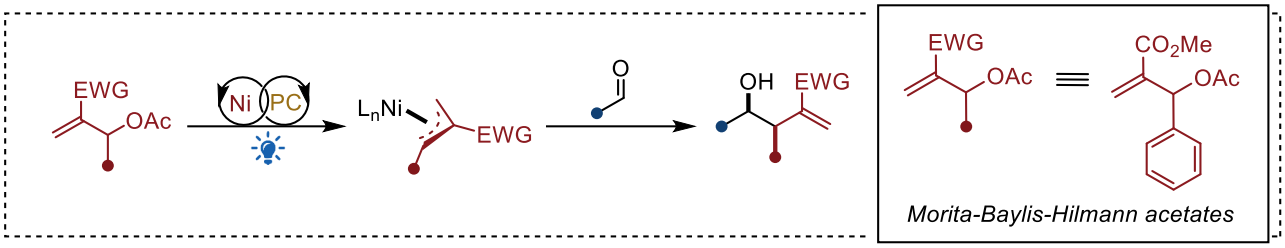

Figure 5.9 Expanding metallaphotoredox allylation protocols using a multi-decorated allylic source: the MBH strategy.

MBH acetates have a long history and a rich chemistry[312] mainly as electrophilic partners.[313] The presence of a good leaving group (OAc) and a conjugated double bond allows various electrophilic substitutions, both under S_N2 and S_N2' pathways and mainly under suitable polar and chemoselective conditions.[314] However, MBH acetates are also prone to react in the presence of nucleophilic radicals, e.g. generated under electrochemical or photoredox conditions, following both S_N2 and S_N2' pathways (*Figure 5.10*).

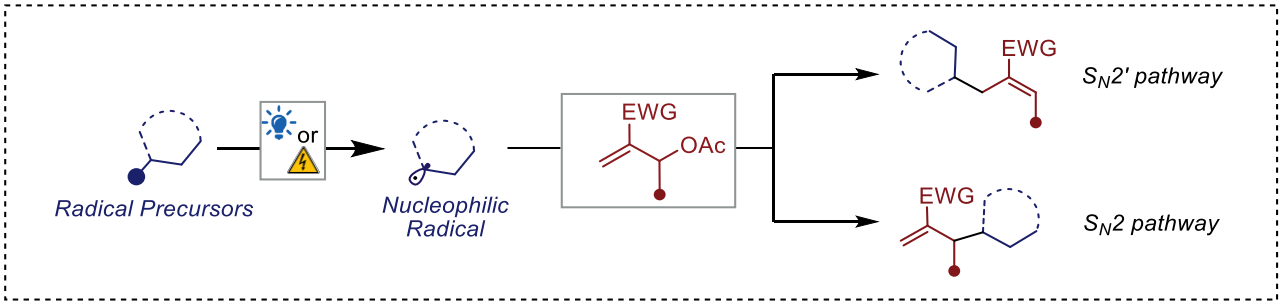

Figure 5.10 S_N2 and S_N2' mechanism pathway for the nucleophilic addition of a radical to MBH acetates.

Compared to polar conditions, radical conditions are an underexplored field, and in this perspective, the Bandini group reported the electrochemical functionalization of MBH acetates using redox-active esters (RAE) as pronucleophiles.[315] RAE esters under reductive electrochemical conditions underwent fragmentation generating C-centered nucleophilic radicals that could attack the MBH acetates following a S_N2' mechanism (*Figure 5.11*).

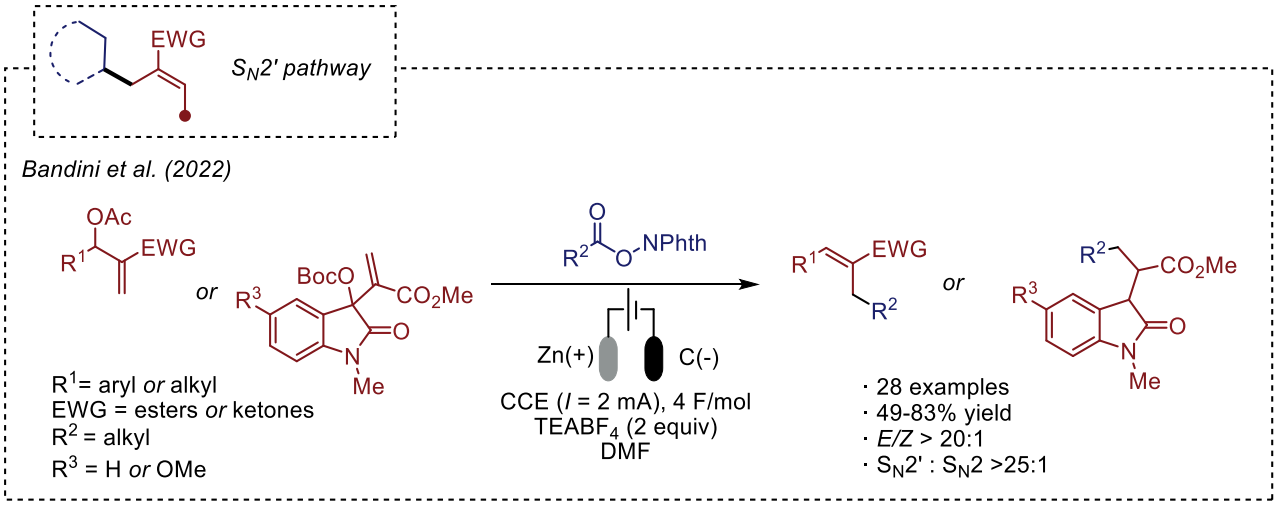

Figure 5.11 Electrochemical functionalization of MBH acetates with RAEs reported by the Bandini group.

Recently, the radical functionalization of MBH acetates under photoredox conditions has experienced a rapid development providing high regioselectivity following both the S_N2' mechanism, using diversified C- and S-centered nucleophilic radicals generated *in situ,*[316–318] and the S_N2 mechanism using metal catalysis to reverse the regioselectivity of the non-metal mediated radical addition. In this regard, dual photoredox- and palladium-catalysis has been reported in the literature.[319] Of particular relevance to this chapter is the work of the Wang group on the dual photoredox- and nickel-catalyzed cross-coupling between MBH acetates and aldehydes (*Figure 5.12*).[124] The mechanism involves the C-H activation of the carbonyl group by the photoexcited *TBADT^{4-}, as previously described in the Paragraph 1.1.4, generating an acyl radical, that can be coordinated to a nickel complex in low oxidation state. Nickel can coordinate also the MBH acetate forming, as usual, a (π-allyl)-Ni species. The so-formed (π-allyl)(acyl)-Ni(III) intermediate undergoes reductive elimination forming a new C-C bond and restoring the metal catalytic cycle.

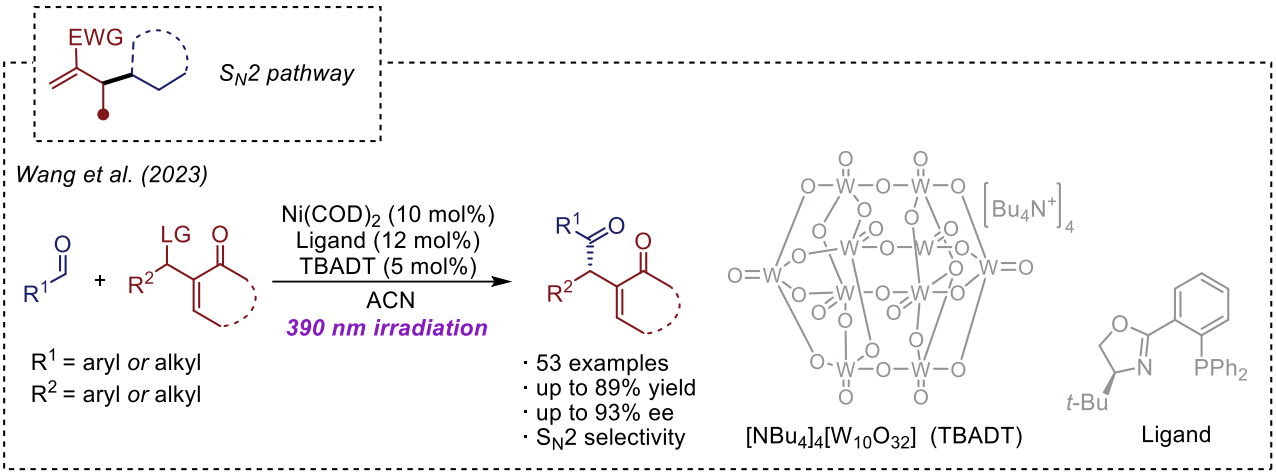

Figure 5.12 Dual photoredox- and nickel-catalyzed cross-coupling between MBH acetates and aldehydes reported by the Wang group.

Herein, a novel dual photoredox- and nickel-catalyzed allylation of aldehydes using MBH acetates is reported. The protocol uses 3DPAFIPN as the photocatalyst, $NiCl_2$·glyme as a commercially available Ni(II) source and Hantzsch ester as the stoichiometric organic reductant under blue light irradiation. Under these conditions, MBH acetates can be used as an unprecedented pronucleophile source to yield homoallylic alcohols with high regio- and diastereocontrol (*Figure 5.13*).

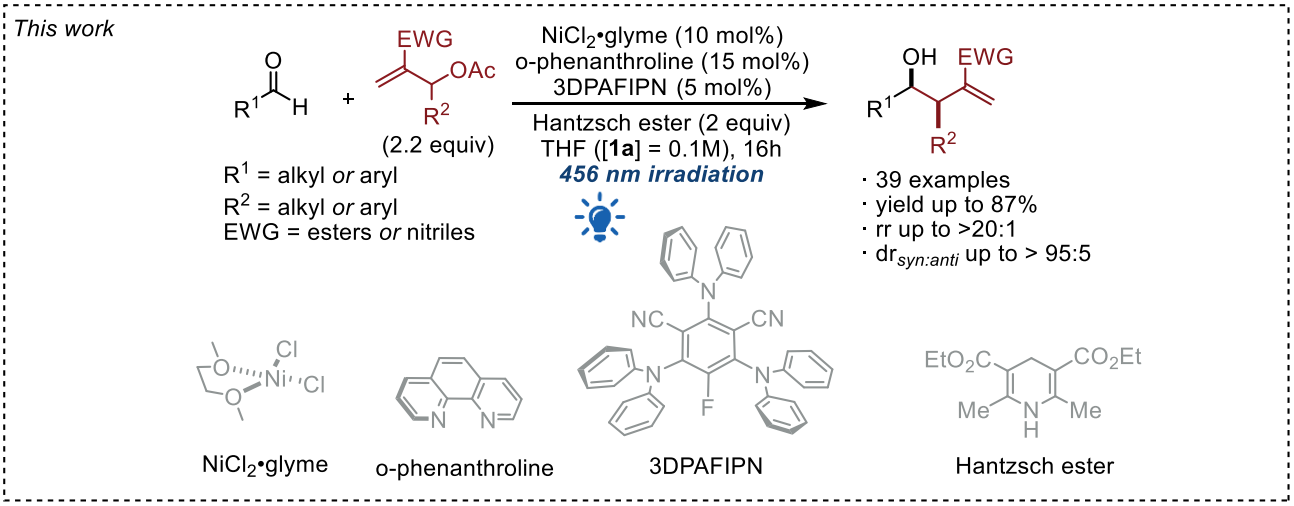

Figure 5.13 Presented work.

5.3 Optimization

To optimize the reaction and taking into account the knowledge gained during the study of our previous dual photoredox- and nickel-protocol,[237] we started the study of this protocol on 4-chlorobenzaldehyde **1a** as the model substrate on a 0.1 mmol scale, using 2.2 equivalents of MBH acetate **2a**, 10 mol% of $NiCl_2$·glyme as Ni(II) precatalyst, 2 equivalents of Hantzsch ester as the organic reductant in THF as the solvent under blue light irradiation. Three different classes of ligands were tested: substituted o-phenanthrolines (entries 1-3), substituted 2,2'-bipyridines (entries 4 and 5) and the phosphines dppe (entry 6), dppp (entry 7) and (±)–BINAP (entry 8) (*Table 5.1*).

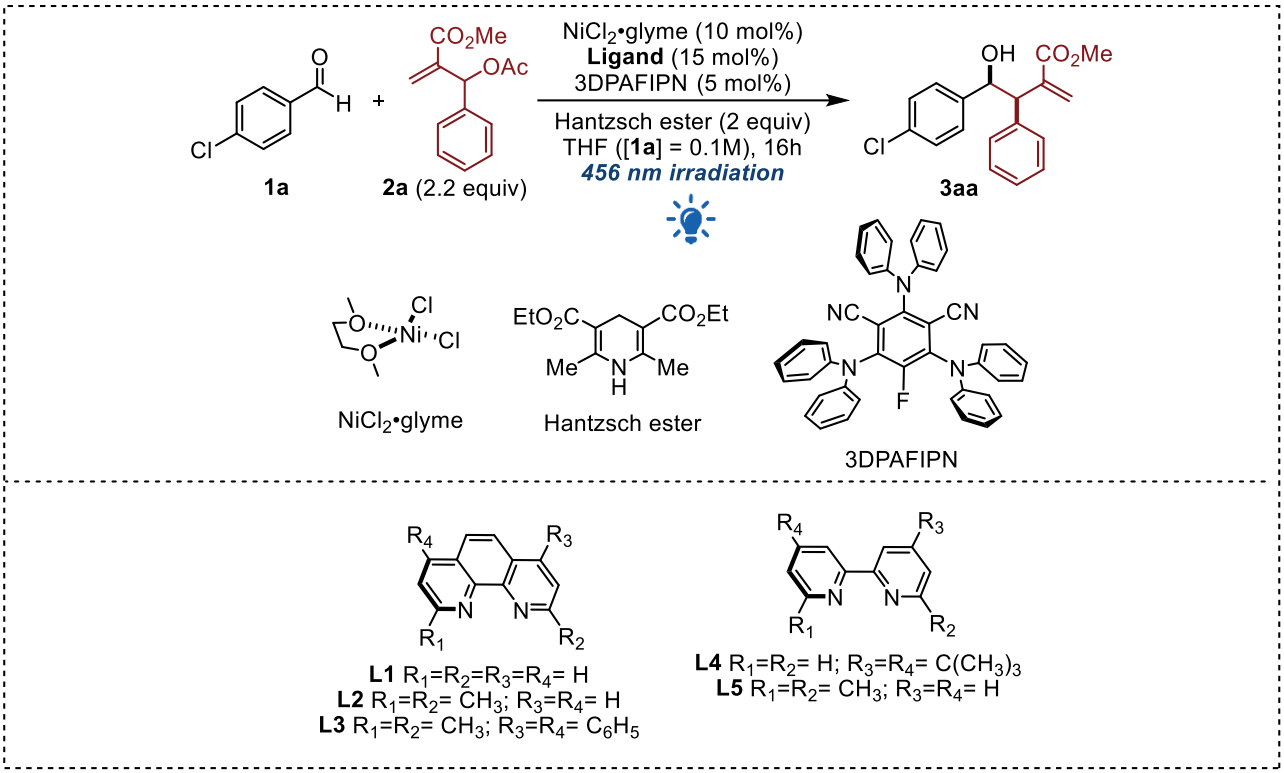

Entry	Ligand	Conversion (%)[a]	*dr* (*syn:anti*)[b]
1	**L1**	**99 (87)**	**>95:5**
2	L2	73	80:20
3	L3	50	94:6
4	L4	95	>95:5
5	L5	56	80:20
6	DPPE	traces[c]	–
7	DPPP	traces[c]	–
8	(±)–BINAP	28[c]	66:34
9	-	36	94:6

*Table 5.1 [a] Determined by ^{1}H NMR analysis on the reaction crude. Isolated yields are reported in brackets.[b] Determined by ^{1}H NMR analysis on the reaction crude by integration of the benzylic C-H signals.[c] Pinacolization of **1a** was detected as main side-product with a dl/meso 1:1.*

The standard procedure is to complex *in situ* $NiCl_2$·glyme with the appropriate ligand. In general, P-based ligands gave traces of the desired product along with the non-diastereoselective pinacol coupling as the major side-product. Unsubstituted o-phenanthroline (entry 1) and bipyridine (entry 4) gave very similar and excellent results, while any substitution at the *ortho*-positions of the *N,N*-ligands led to a decrease in the conversion and in the diastereoselectivity. The use of a ligand was found to be crucial (entry 9).

Since the initial conditions were already satisfactory, we briefly tested other solvents (*Table 5.2*). Compared to the THF, a decrease in the diastereoselectivity was observed when the more coordinating DMF was used (entry 1). The same result, although less pronounced, was observed with the less coordinating toluene (entry 2).

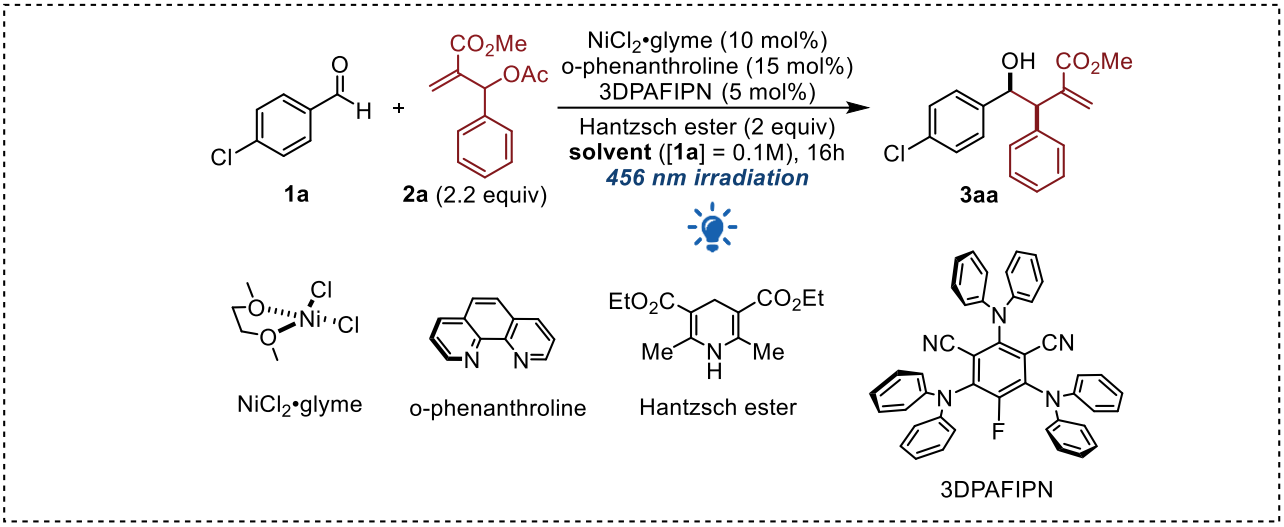

Entry	Solvent	Conversion (%)[a]	*dr* (*syn:anti*)[b]
0	**THF**	**99 (87)**	**>95:5**
1	DMF	97	90:10
2	Toluene	90	93:7

Table 5.2 [a] Determined by ^{1}H NMR analysis on the reaction crude. Isolated yields are reported in brackets.[b] Determined by ^{1}H NMR analysis on the reaction crude by integration of the benzylic C-H signals.

With these preliminary conditions, we tested different Ni(II) sources (*Table 5.3*).

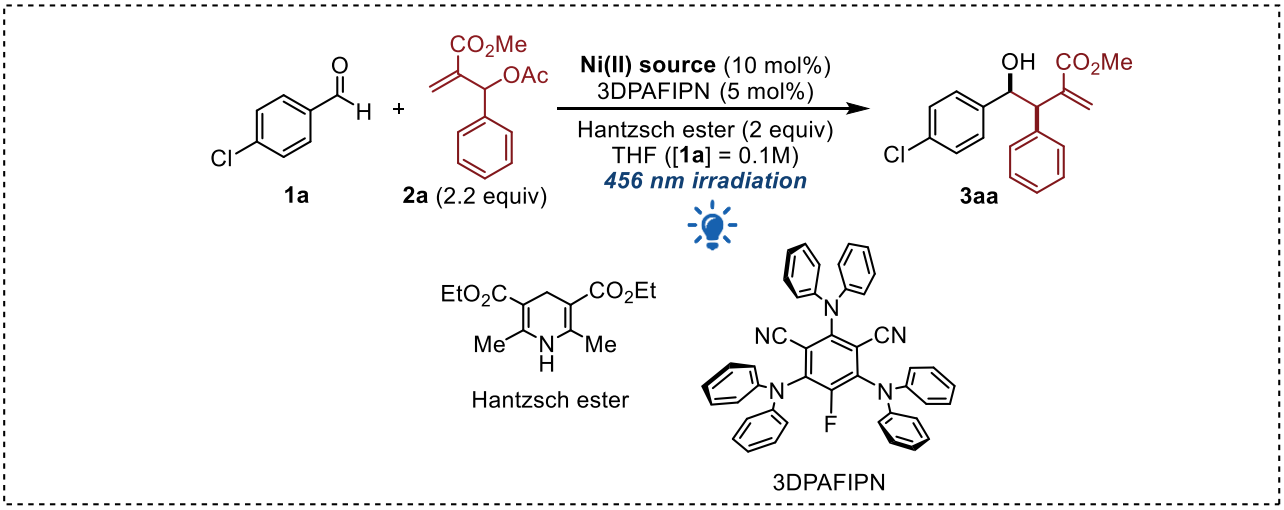

Entry	Ni(II) source	Conversion (%)[a]	*dr* (*syn:anti*)[b]
0[c]	**$NiCl_2$·glyme[d]**	**99 (87)**	**>95:5**
1[e]	$Ni(AcO)_2$[d]	>99	>95:5
2[c]	$NiCl_2(PBu_3)_2$	82	>95:5
3[e]	$Ni(acac)_2$[d]	95	86:14

Table 5.3 [a] Determined by ^{1}H NMR analysis on the reaction crude. Isolated yields are reported in brackets.[b] Determined by ^{1}H NMR analysis on the reaction crude by integration of the benzylic C-H signals.[c] 16h irradiation time.[d] 15 mol% o-phenanthroline added as ligand.[e] 5h irradiation time.

In the case of $Ni(acac)_2$ and $Ni(AcO)_2$ a 15 mol% of o-phenanthroline was added as in the case of $NiCl_2$·glyme. $Ni(OAc)_2$ (entry 1) was found to be as reactive as $NiCl_2$·glyme giving complete regio- and diastereocontrol within 5h of irradiation. It is worth mentioning that the protocol with $NiCl_2$·glyme was not tried under 5h of irradiation, since it was preferred to maintain an irradiation time of 16h in order to ensure the complete conversion of even less reactive substrates than the model **1a**. On the contrary, $NiCl_2(PBu_3)_2$ was found to be as suitable as $NiCl_2$·glyme to ensure complete regio- and diastereocontrol, but after 16h of irradiation the conversion was lower. Finally, $Ni(acac)_2$ (entry 3) gave complete conversion of **1a** within 5h of irradiation as $Ni(OAc)_2$ but with a significant decrease in the diastereoselectivity.

Because of the high reactivity in 16h of reaction, we also try to reduce the catalyst loading, as well as the ligand loading to maintain a 1.5:1 ligand:$NiCl_2$·glyme ratio (*Table 5.4*). Since the diastereoselectivity was found to be slightly lower (entry 1), we decided to keep the initial catalyst loading. The presence of the nickel catalyst, as expected, was found to be crucial to ensure the formation of a nucleophilic allyl species. Without the metal catalyst (entry 2), only the non-diastereoselective pinacol coupling was observed, as already highlighted in the previous chapters.

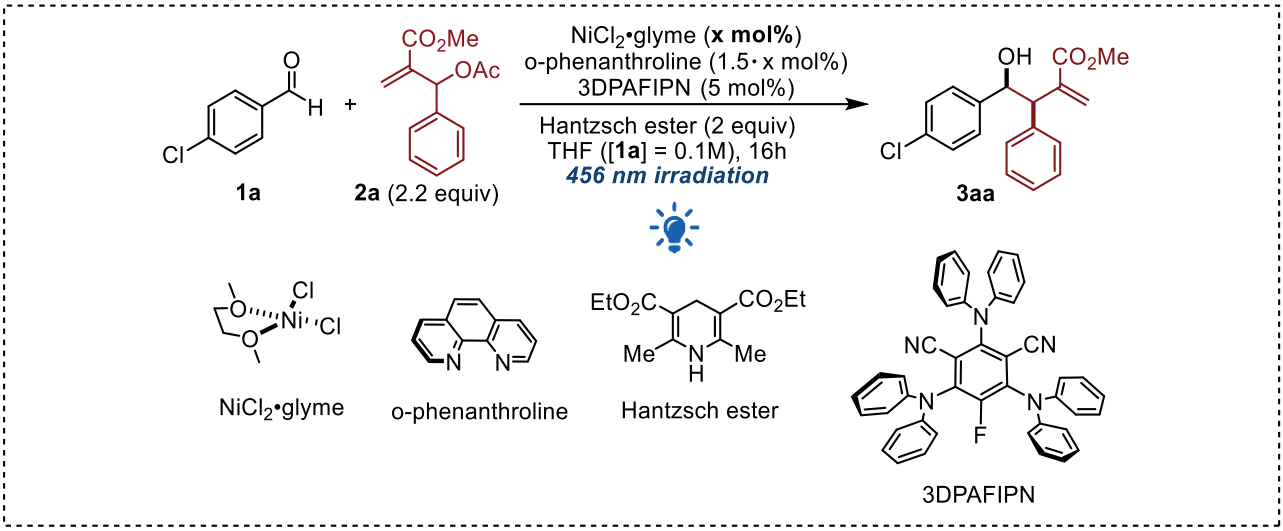

Entry	Catalyst loading (x mol)	Conversion (%)[a]	*dr* (*syn:anti*)[b]
0	**10%**	**99 (87)**	**>95:5**
1	5%	99	95:5
2	0	NR	

Table 5.4 [a] Determined by ^{1}H NMR analysis on the reaction crude. Isolated yields are reported in brackets.[b] Determined by ^{1}H NMR analysis on the reaction crude by integration of the benzylic C-H signals. NR = No reaction.

We also tested different amounts of Hantzsch ester (*Table 5.5*), with the goal of reducing the amount of stoichiometric reactants. Unfortunately, using 1.5 (entry 1) and 1.1 (entry 2) equivalents of Hantzsch ester the conversion decreased. As expected, Hantzsch ester is mandatory to maintain the photoredox catalytic cycle (entry 3).

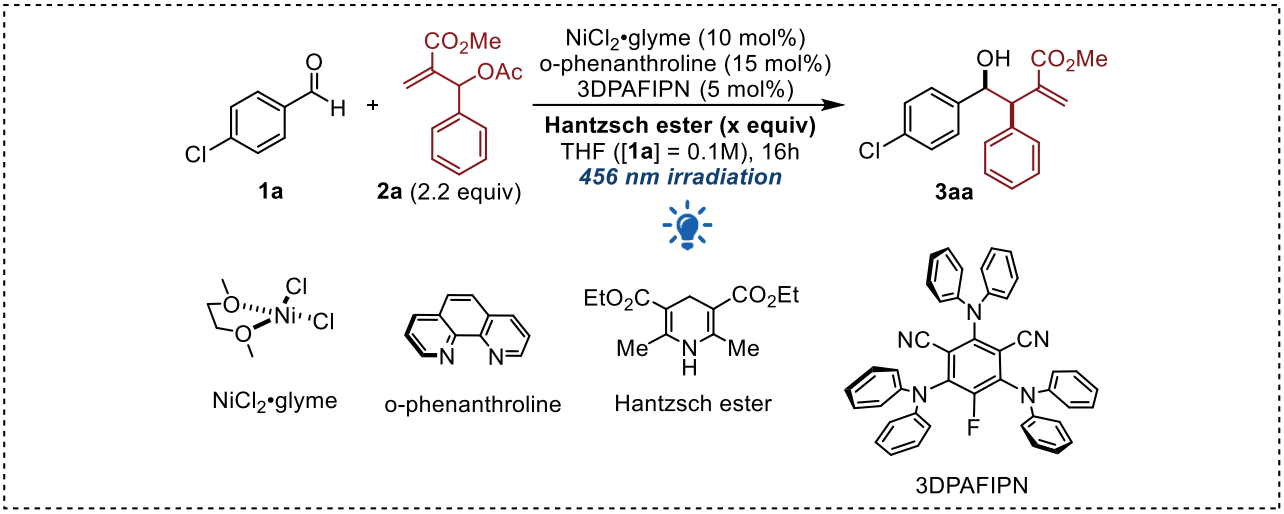

Entry	Hantzsch ester (x equiv.)	Conversion (%)[a]	*dr* (*syn:anti*)[b]
0	**2**	**99 (87)**	**>95:5**
1	1.5	86	>95:5
2	1.1	86	>95:5
3	0	NR	

Table 5.5 [a] Determined by ^{1}H NMR analysis on the reaction crude. Isolated yields are reported in brackets.[b] Determined by ^{1}H NMR analysis on the reaction crude by integration of the benzylic C-H signals. NR = No reaction.

Finally, other TADF-emitter photocatalysts were evaluated (*Table 5.6*). 4CzIPN was tested as an alternative TADF-emitter photocatalyst (entry 1), with very similar results. As a confirmation of the photo-promoted protocol, in the presence of the photocatalyst without any irradiation (entry 2), the reaction did not occur between the reactants, which were revealed unreacted by ^{1}H NMR. On the contrary, when the reaction mixture was irradiated in the absence of any photocatalyst (entry 3) no conversion was observed. These results are in contrast with the usual non-diastereoselective pinacolization of the aldehyde promoted by the excited Hantzsch ester, already described in the previous chapters.

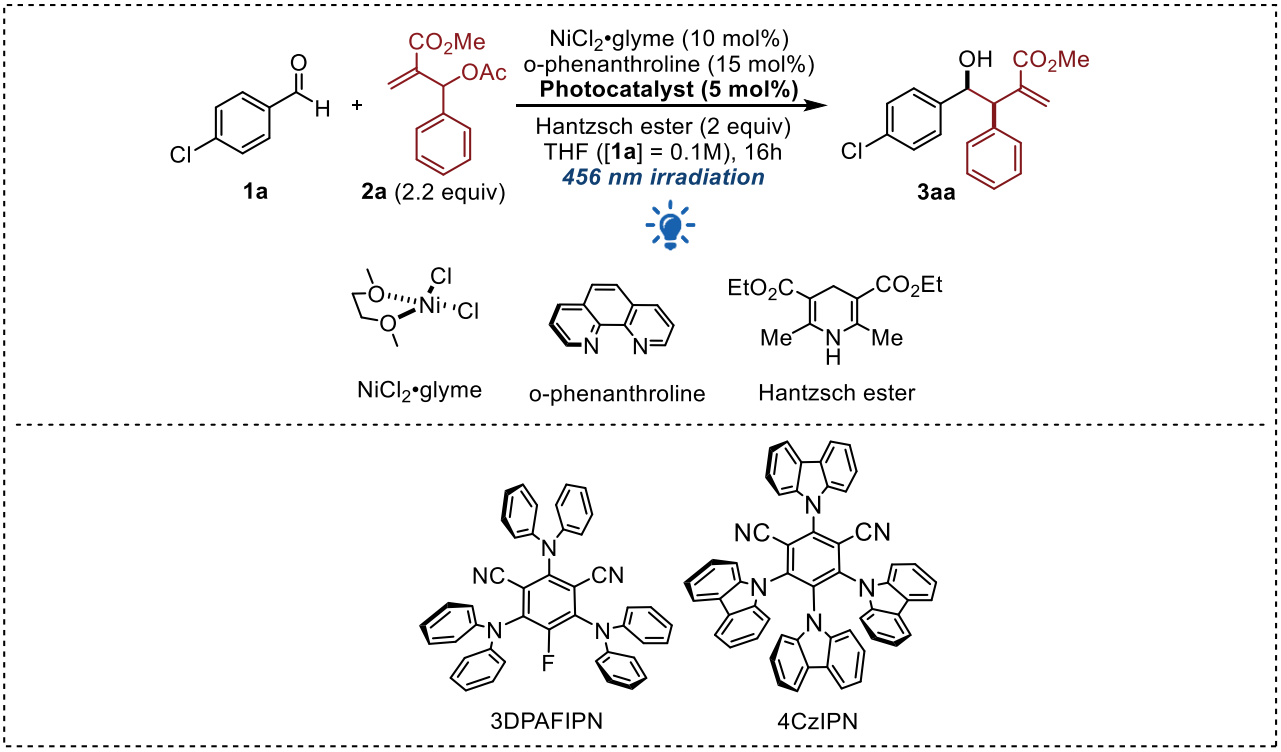

Entry	Photocatalyst	Conversion (%)[a]	*dr* (*syn*:*anti*)[b]
0	**3DPAFIPN**	**99 (87)**	**>95:5**
1	4CzIPN	86	>95:5
2[c]	3DPAFIPN	-	-
3	-	NR	

Table 5.6 [a] Determined by ^{1}H NMR analysis on the reaction crude. Isolated yields are reported in brackets.[b] Determined by ^{1}H NMR analysis on the reaction crude by integration of the benzylic C-H signals.[c] Reaction performed in the dark. NR = No reaction

At this point, other MBH derivatives were evaluated (*Table 5.7*). The unprotected MBH alcohol **2b** could be used (entry 1) but with a significant loss of reactivity and diastereoselectivity. Using MBH trifluoroacetate ester **2c** (entry 2) or a MBH carbonate **2d** (entry 3) the non-diastereoselective pinacol coupling was observed as the main side-product.

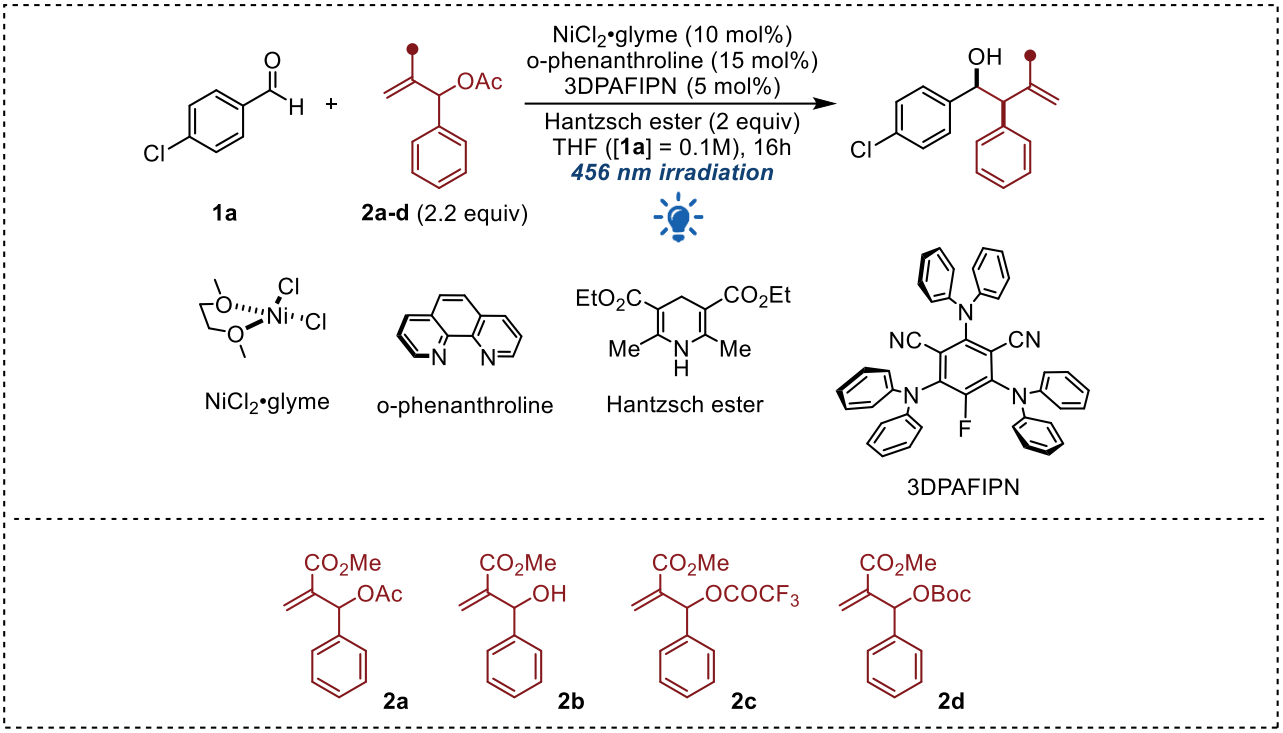

Entry	MBH derivative	Conversion (%)[a]	*dr* (*syn:anti*)[b]
0	**2a**	**99 (87)**	**>95:5**
1	2b	45[c]	66:34
2	2c	18%[c]	83:17
3	2d	95%[c]	–

*Table 5.7 [a] Determined by ^{1}H NMR analysis on the reaction crude. Isolated yields are reported in brackets.[b] Determined by ^{1}H NMR analysis on the reaction crude by integration of the benzylic C-H signals.[c] Pinacolization of **1a** was detected as main side-product with a dl/meso 1:1.*

After a systematic evaluation of all the reaction parameters, we were able to reveal the optimized conditions shown in *Figure 5.13*, obtaining the product **3aa** in 87% of isolated yield and with a *dr* >95:5 in favor of the *syn*-isomer and complete regiocontrol in favor of the branched homoallylic alcohol.

5.4 Scope evaluation

The optimized conditions were applied to an extended library of substituted aromatic and aliphatic aldehydes. Different substituted aromatic and aliphatic MBH acetates and MBH adducts bearing different electron-withdrawing groups were tested. All the reactions were carried out on a 0.2 mmol scale. *Figure 5.14* shows the range of aromatic aldehydes tested in the reaction.

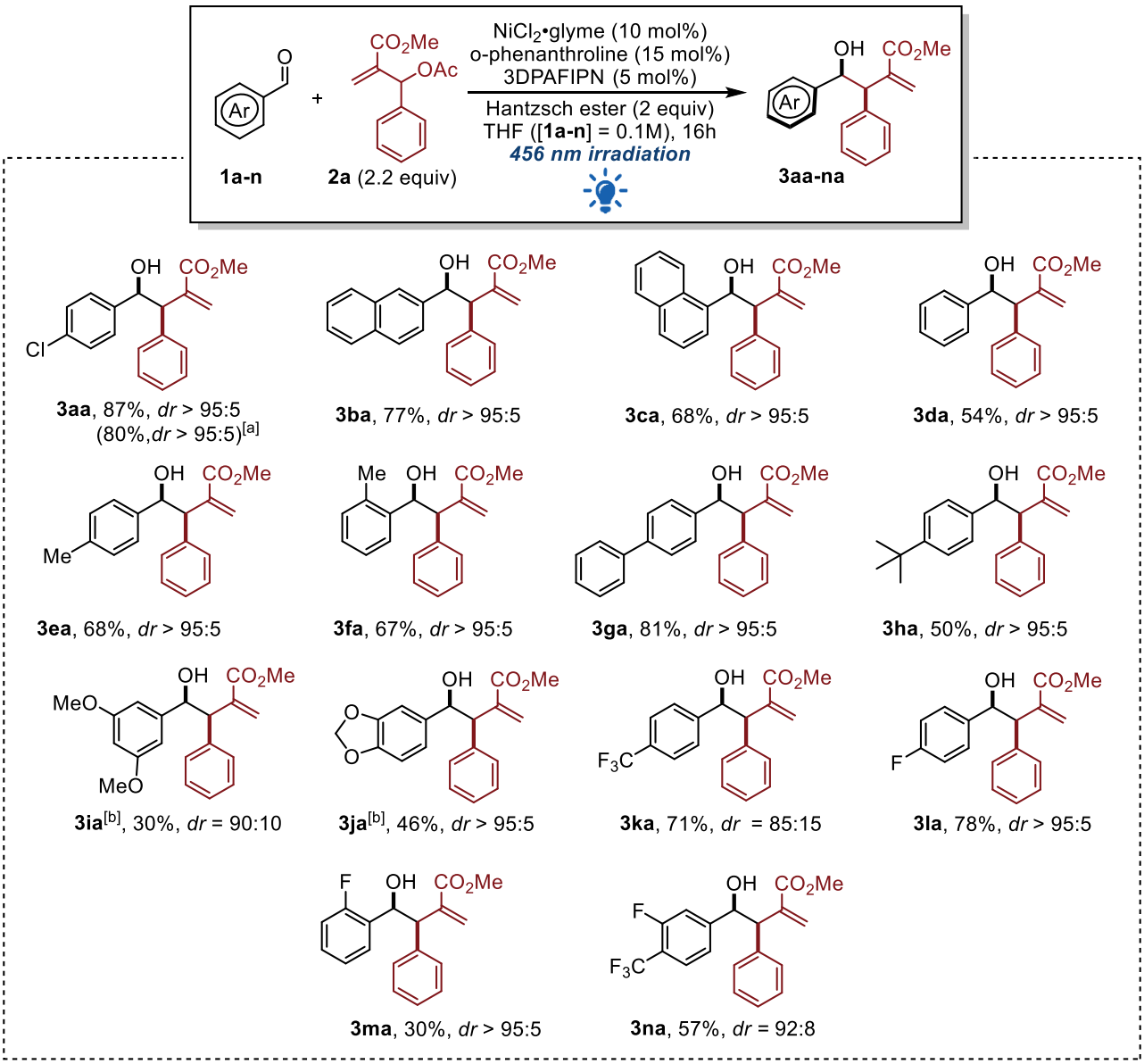

*Figure 5.14 Scope of aromatic aldehydes. [a] Reaction performed on 2 mmol of **1a**. Reaction conditions: $NiCl_2$·glyme 5 mol%, o-phenanthroline 7.5 mol%, 3DPAFIPN 3 mol%, HE 2 equiv, THF [**1a**]= 0.1M, irradiation time 60h.[b] Reaction time extended to 48h.*

In general, isolated yields differ from the ^{1}H NMR conversion of the starting aldehyde due to the unavoidable pinacol coupling promoted by the Hantzsch ester radical cation, already discussed in Paragraph 4.1. Moreover, the purification of the products was sometimes complicated by the presence of side-products derived from the decomposition of the MBH adducts (reduction, deacetylation, etc).

Aromatic aldehydes substituted with electron withdrawing groups showed a better reactivity (e.g. **3aa**, **3ka** or **3la**), compared to electron rich ones (**3ea**, **3ha** or **3ia**). The diastereoselection was quite high, greater than 95:5 in most of the cases. An outlier case was the highly electronrich 3,5-dimethoxybenzaldehyde **3ia**: although the reaction time was extended to ensure a better conversion, we obtained only a 30% of isolated yield and a reduced diastereoselectivity. The presence of steric hindrance in proximity of the carbonyl group, as in the case of 1-naphtaldehyde **3ca**, 2-methylbenzaldehyde **3fa** or 2-fluorobenzaldehyde **3ma** did not affect the diastereoselectivity, while in the latter case only the yield was lower.

Scaling up the reaction to 2 mmol, we decided to reduce the amount of both the Ni(II) complex to 5 mol%, keeping constant the $NiCl_2$·glyme/o-phenanthroline ratio (1:1.5) and the photocatalyst (3 mol%). To ensure complete conversion of the starting aldehyde, the reaction time was extended to 60h, obtaining a comparable yield with respect to the 0.2 mmol scale (80% *vs* 87%) and with complete diastereocontrol.

Figure 5.15 shows the range of aliphatic aldehydes which were tested. Because of the known reduced reactivity of aliphatic aldehydes,[237,320–322] we extended the reaction time to 48h to ensure better conversions of the starting materials. In addition, the amount of MBH acetate was reduced to 2 equivalents to avoid the presence of unreacted MBH acetate at the end of the reaction. In this way, it was possible to isolate the desired products without any contamination by the starting MBH adduct. In general, the yields and diastereoselectivity are quite similar to those obtained for the aromatic aldehydes.

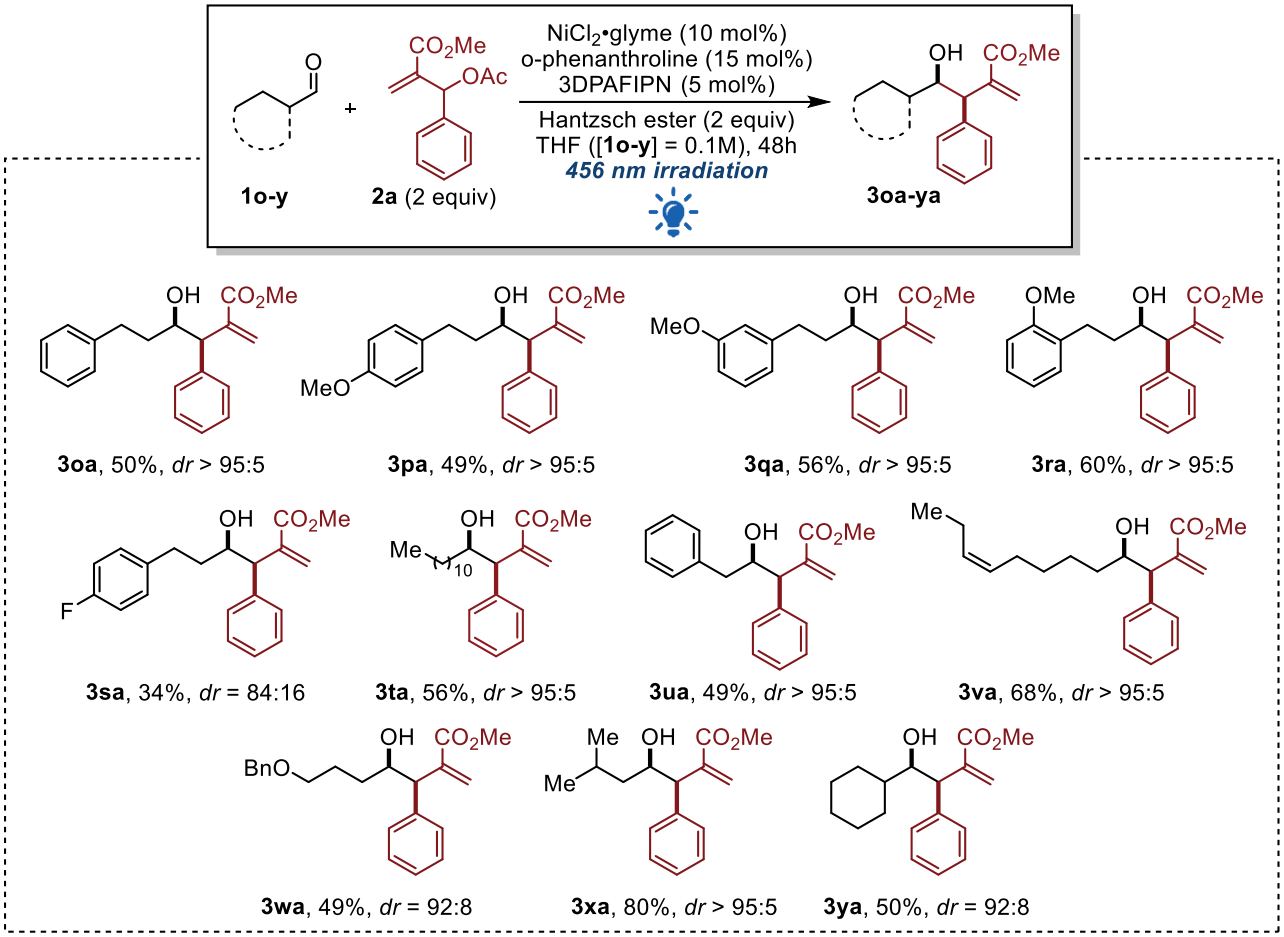

Figure 5.15 Scope of aliphatic aldehydes.

The protocol was also extended to other MBH acetates with different electron withdrawing groups (*Figure 5.16*). Three different esters (**2e**, **2g** and **2h**), the ketone **2i** and the nitrile **2f** were evaluated.

Moving from the methyl ester derivative **2a** to the more sterically demanding *t*-butyl ester (**3ae**+**3ae'**), a significant decrease in the regioselectivity was observed (*rr* = 80:20), while the diastereoselectivity remained completely in favor of the *syn*-diastereoisomer. In the case of the nitrile (product **3af**+**3af'**) the regioisomeric drop can be explained by electronic factors because of the different electronic distribution of the ester compared to the nitrile. The protocol was found not to be suitable using a MBH ketone (product **3ai**) or a MBH acetate bearing a propargyl ester (product **3ah**).

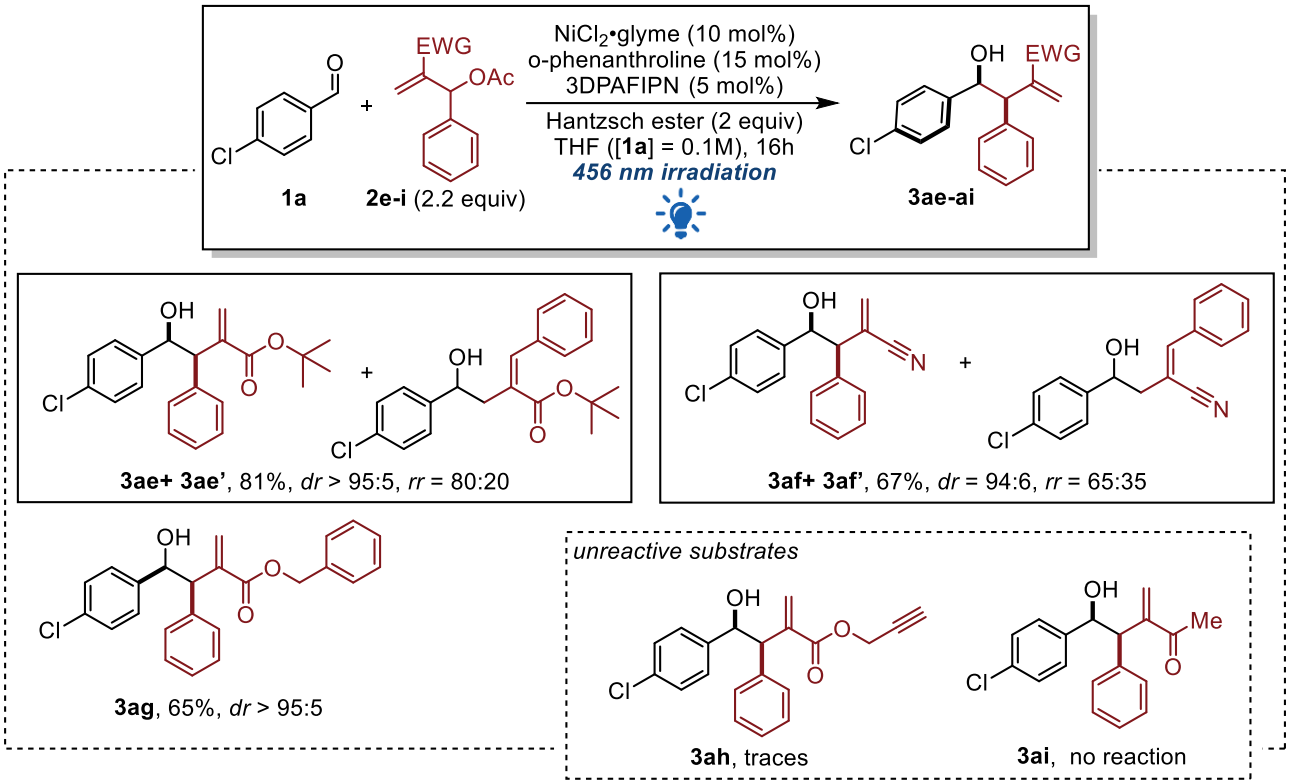

Figure 5.16 Scope of different MBH acetates.

Taking advantage of the relative ease of synthesis of the MBH adducts, we subjected various substituted methyl ester MBH adducts to the protocol (*Figure 5.17*).

A direct comparison of reactivity can be made considering the same moiety included in the aldehyde or in the MBH acetate, and it shows a dramatic difference. The examples reported in *Figure 5.17* show that differently substituted aromatic moieties introduced into the MBH acetate (**3aj-aq**) are well tolerated. It was also possible to incorporate sensitive heteroaromatic structures such as furan (**3ap**) or thiophene (**3aq**) into the MBH adducts, resulting in a densely functionalized products. In all cases the diastereoselection was again quite high, favoring the usual diastereoisomer. The introduction of an aliphatic group into the MBH adduct (**3ar** and **3as**) although the diastereoselection was good to high, considerably reduced the reactivity of the MBH adduct.

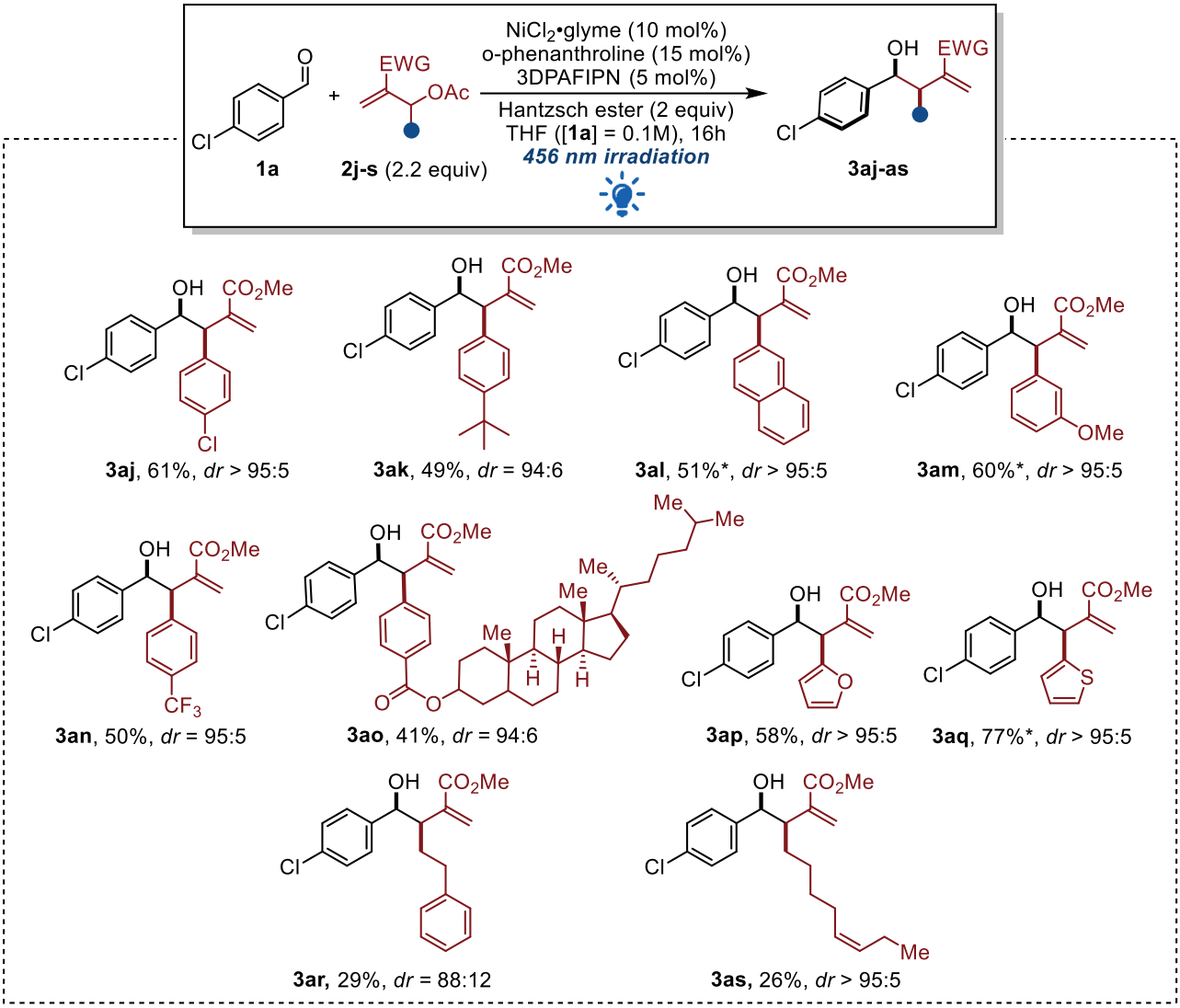

*Figure 5.17 Scope of different methyl ester MBH derivatives. *48h irradiation.*

Finally, we have briefly investigated the reactivity and the synthetic utility of the standard product **3aa** by performing some further functionalization, as shown in *Figure 5.18*. First, the OH group of *syn*-**3aa** was protected as OTBS (**4a**) without altering the diastereomeric ratio. Then the conjugated double bond was exploited in two Michael additions. Taking advantage of the reactivity of the double bonds in the presence of secondary amines[323] it was possible to induce a cyclative aza-Michael reaction leading to a γ-butyrolactones derivative (**4b**). This class of cyclic compounds has been proven to be a NF-kB inhibitor for the treatment of pancreatic cancer.[324] The possibility of getting easy access to this class of compounds in a straightforward manner demonstrates the usefulness of this new allylation protocol. Finally, the double bond was again exploited as an electrophilic site in a sulfa-Michael addition using 2-naphthalenethiol as the Michael donor (**4c**). In both Michael additions, three contiguous stereocenters were formed with quite good diastereoselectivity and yields.

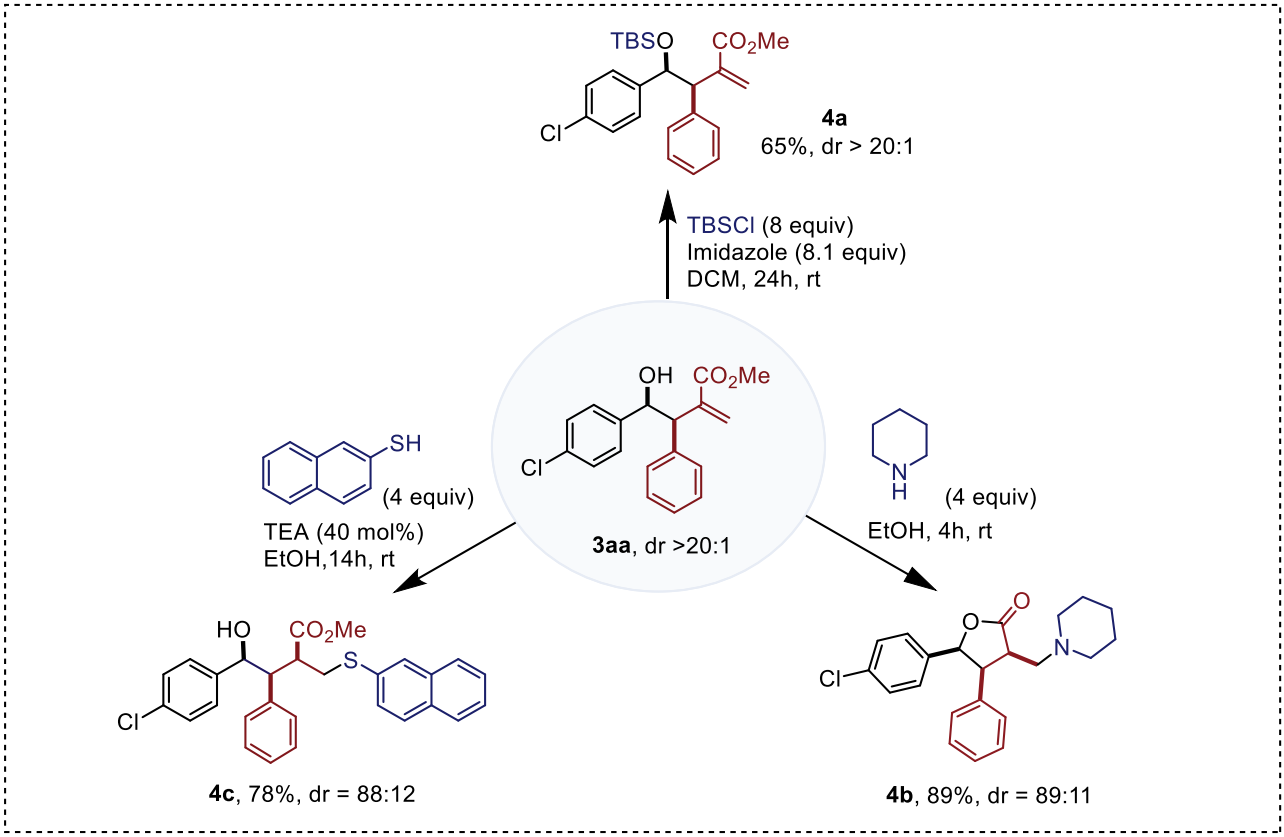

*Figure 5.18 Post functionalization of the model substrate **3aa**.*

5.5 Photophysical, theoretical and experimental studies and reaction mechanism

In order to fully elucidate the reaction mechanism, a careful photophysical analysis was carried out in collaboration with the research group led by Prof. P. Ceroni. In order to present a plausible catalytic cycle, as well as the possible intermediates involved in the process, DFT calculations were carried out by the research group led by Prof. L. Cavallo. Finally, some experimental tests have also been carried out to confirm the mechanistic proposal.

Photophysical studies

The analysis of the photophysical behavior of 3DPAFIPN in the presence of the different components of the reaction mixture shed light on the key aspects of the photoredox catalytic cycle. As shown in a previous publication, by a combined photophysical and computational study,[237] catalytic 3DPAFIPN in the presence of an overstoichiometric amount of Hantzsch ester (HE) at concentrations near to its solubility limit in THF (0.1 M), is expected to quantitatively form with the HE the photoactive complex [3DPAFIPN·HE] (*Figure 5.19*).

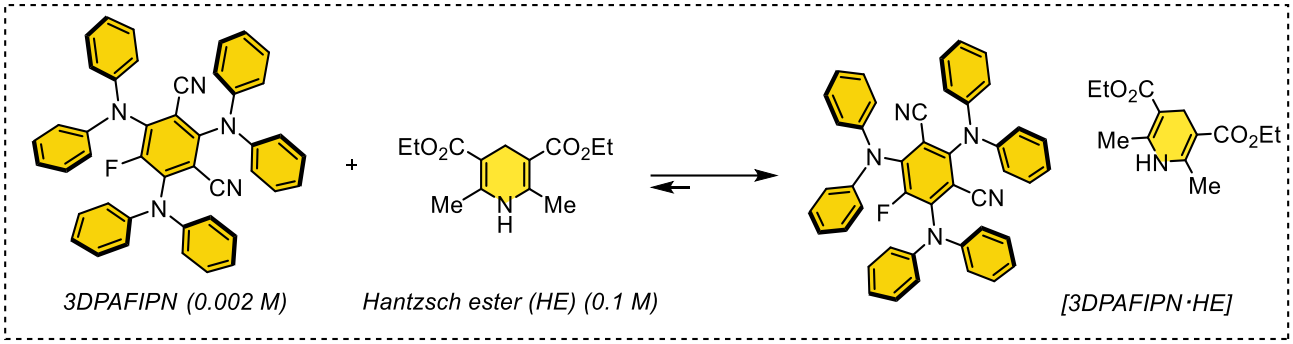

Figure 5.19 Formation of the photoactive complex [3DPAFIPN·HE] in the reaction conditions.

The complex thus formed still possesses suitable redox potentials for the efficient photoinduced electron transfer to the reactants involved in the transformation. As previously reported, in a deaerated, stabilizer-free THF solution, it exhibits an absorption band in the visible range (ε = 14900 $M^{-1}cm^{-1}$ at λ = 370 nm) with an absorption onset at 470 nm, and an emission band centered at 520 nm, attributed to prompt fluorescence (τ = 3.6 ns) and delayed fluorescence (τ = 110 µs).

In particular, a quenching constant (k_q) of 2.1×10^8 M^{-1} s^{-1} was measured in the presence of an excess of Hantzsch ester (HE), which can effectively quench the excited photocatalyst *[3DPAFIPN·HE] at concentrations above 130 µM. In addition, aldehyde **1a** does not significantly affect the luminescence lifetime (k_q < 1.0×10^6 M^{-1} s^{-1}).[237] To fully understand the catalytic picture of the photocatalyst, luminescence quenching analyses were performed using the Stern-Volmer kinetics, taking into account the other reaction partners of the presented protocol. In agreement with our previous reports, it is noteworthy that the pronucleophilic species **2a** and the model ligand o-phenantroline (**L1**) alone do not interact with the excited state of the photocatalyst and do not alter its luminescence lifetime, even when working at concentrations comparable to or exceeding those used in the reaction conditions. Finally, the ability of quenching the luminescence of *[3DPAFIPN·HE] was evaluated in the presence of increasing concentrations of the complex formed *in situ* between $Ni(OAC)_2$ and phenanthroline. It is important to emphasize that, in contrast to the standard conditions, the precatalyst $Ni(OAC)_2$ was used in the analysis, since it ensures the same results and increases the solubility of the resulting complex. In this context, a significant quenching constant (k_q = 7.0×10^7 $M^{-1}s^{-1}$, *Figure 5.20*) was measured; however, this value remains incomparable to the static quenching observed for HE.

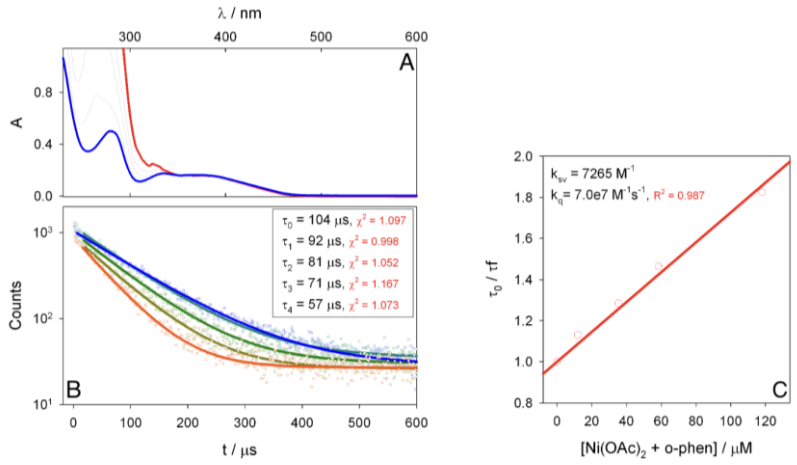

Figure 5.20 ***A****) Absorption spectra of solutions of 3DPAFIPN in degassed THF at r.t. (ca. 11 µM, blue line) obtained upon addition of increasing amounts of the complex between o-phenanthroline and* $Ni(OAc)_2$ *(1.5:1.0 eqv in THF; up to ca. 0.12 mM).* ***B****) Delayed fluorescence decays of 3DPAFIPN obtained from the same solutions at* λ_{em} *= 530 nm (*λ_{ex} *= 475 nm) and corresponding monoexponential fitting functions.* ***C****) Stern-Volmer diagram relative to the determined decay lifetimes.*

DFT calculations

The reaction starts with the coordination of **L1** to the nickel precatalyst **$^{T}NiCl_2 \cdot glyme$**, resulting in the octahedral Ni(II) species **^{T}INT-A**, from which the liberation of glyme yields **^{T}INT-B** (*Figure 5.21*). **^{T}INT-B** is then reduced to **INT-C** by **[3DPAFIPN · HE]$^{\bullet-}$** (SET1) after the reductive quenching within the photoredox catalytic cycle. This step is exergonic by 26.6 kcal/mol with a free energy barrier of 6.2 kcal/mol, estimated using the Marcus-Hush theory.[325–327] This is in agreement with our previous finding which showed that the associated species **[3DPAFIPN · HE]** plays the role of photocatalyst in the reaction.[237] In addition, a 20-fold higher concentration of **HE** compared to **$^{T}NiCl_2 \cdot glyme$** under the experimental conditions suggests for a preference for the reductive quenching of the photoexcited **^{T}3DPAFIPN · HE** over oxidative quenching.[237,328] The oxidative addition of allyl acetate (**2a**) to the Ni(I) intermediate **INT-C**, leading to a significantly less stable Ni(III) intermediate, requires an unattainable energy barrier of 35.0 kcal/mol, and can therefore be ruled out. Rather, single electron transfer (SET2) from **[3DPAFIPN · HE]$^{\bullet-}$** to **INT-C** with concomitant coordination of **2a** leads to an appreciably stable Ni(0) species **INT-D** which acts as the active catalyst in the nickel catalytic cycle. Furthermore, the generation of **INT-D** from **INT-C** *via* the disproportionation route is thermodynamically unfavorable by 9.2 kcal/mol, and can therefore be discarded.

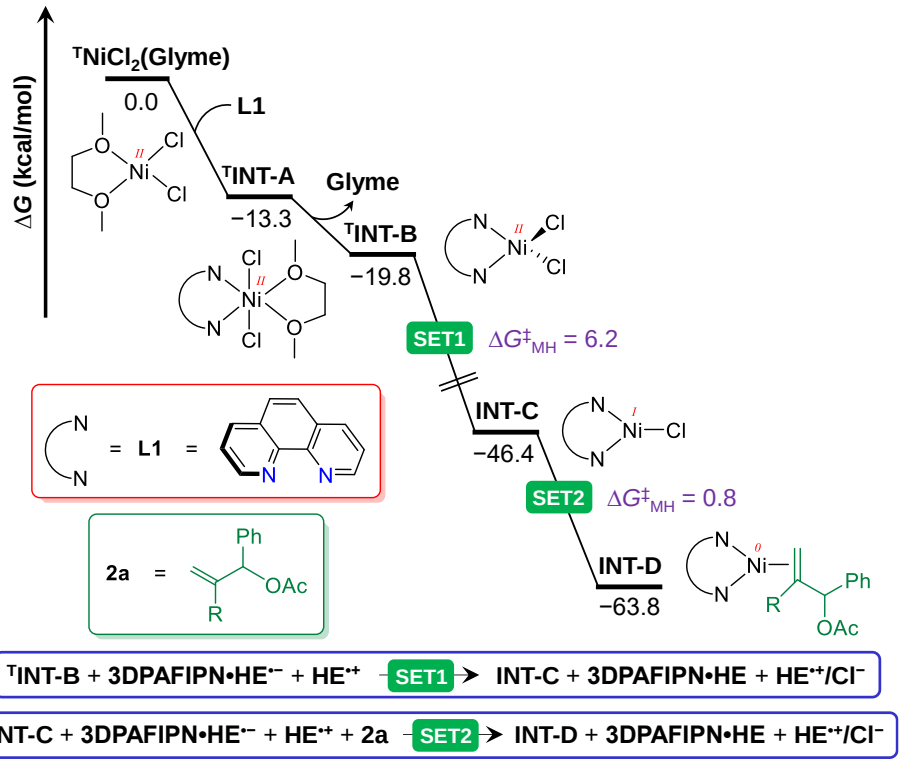

*Figure 5.21 Free energy profile for the formation of Ni(0) species **INT-D** at the M06(SMD,THF)/def2-TZVPP//PBE-D3(SMD,THF)/def2-TZVP(Ni)/def2-SVP level of theory.*

The nickel catalytic cycle begins with the oxidative addition of coordinated allyl acetate in **INT-D** via the transition state **TS-A** (*Figure 5.22*). This step must overcome the rate-limiting energy barrier of 22.6 kcal/mol. The simple 1e^{-} reduction of the resulting intermediate **^{T}INT-E** by **[3DPAFIPN · HE]$^{\bullet-}$** (SET3) and an estimated energy barrier of 5.5 kcal/mol, yields the Ni(I) species **INT-F**. The subsequent insertion of 4-chlorobenzaldehyde (**1a**) into the Ni-allyl bond in **INT-F** from its more hindered site leads to a slightly more stable intermediate **INT-G** via transition state **TS-B**. The insertion step has to overcome an energy barrier of 12.5 kcal/mol. In addition, a similar carbonyl insertion from the less hindered site of **INT-F** via

the **TS-B1** transition state requires a significantly higher energy barrier of 22.5 kcal/mol, which explains the diastereoselective outcome of the reaction. The reaction further continues with the coordination of **HE$^{\bullet+}$/AcO^{-}** to **INT-G**, resulting in the intermediate **^{T}INT-H**, which undergoes intramolecular hydrogen atom transfer (HAT) involving the transition state **^{T}TS-C** to yield a remarkably stable intermediate **INT-I** with the release of Hantzsch pyridine (**HP**) and acetic acid.[237] Finally, another molecule of **2a** replaces the desired product (**3aa**) already formed in **INT-I** to regenerate **INT-D** for the next catalytic cycle.

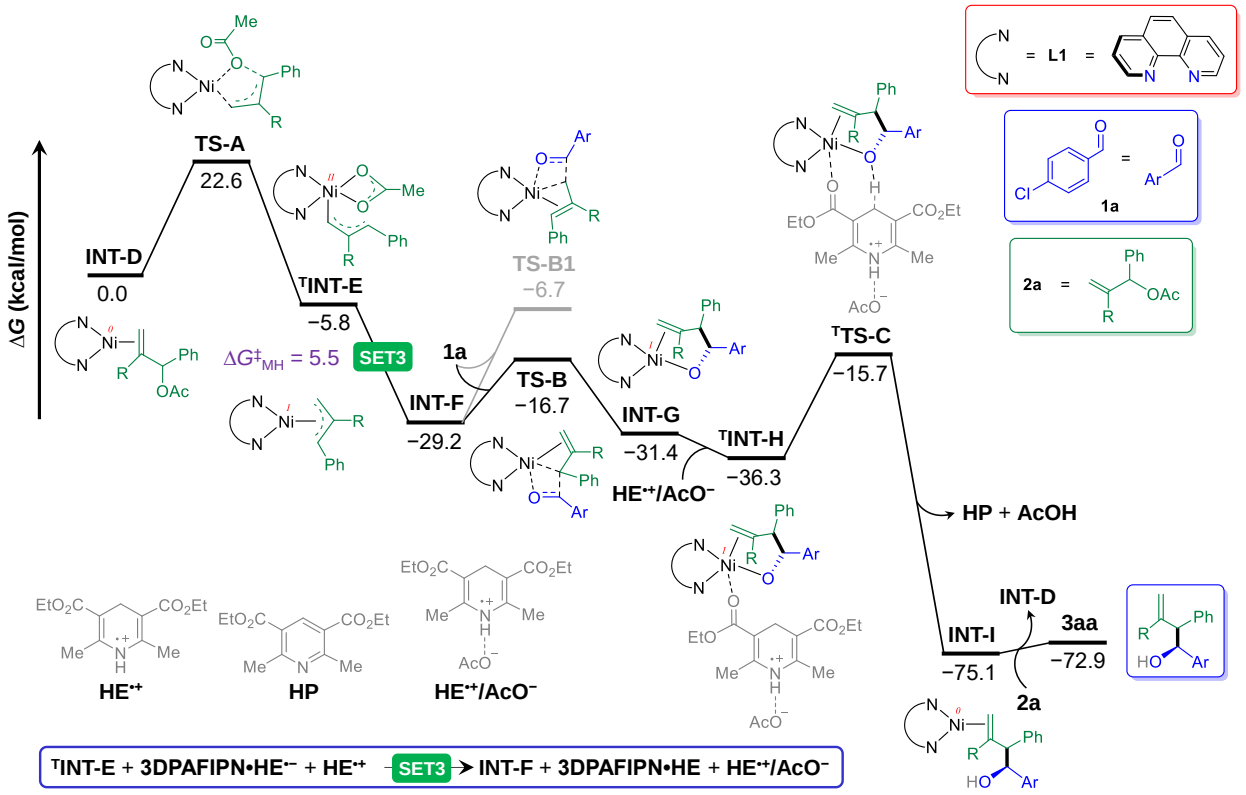

Figure 5.22 Free energy profile for the nickel catalytic cycle of allylation of aldehydes.

To shed light on the origin of the activation barriers associated with the diastereoselectivity-determining steps, a distortion-interaction analysis[329,330] was performed on the transition states **TS-B** and **TS-B1**, considering **INT-F** and **1a** as the interacting fragments (*Figure 5.23*). The remarkably lower activation barrier for **TS-B** than for **TS-B1** is attributed to the significantly higher interaction energy (in absolute values) between the two distorted fragments in **TS-B**, which offset the higher distortion energy of the Ni fragment of **TS-B**, reflected in the stretching of the Ni-allyl bond (3.503/2.403 Å in **TS-B**/**TS-B1**) involved in the aldehyde insertion. In addition, the distortion energy of the aldehyde fragment is slightly lower in **TS-B** compared to **TS-B1**.

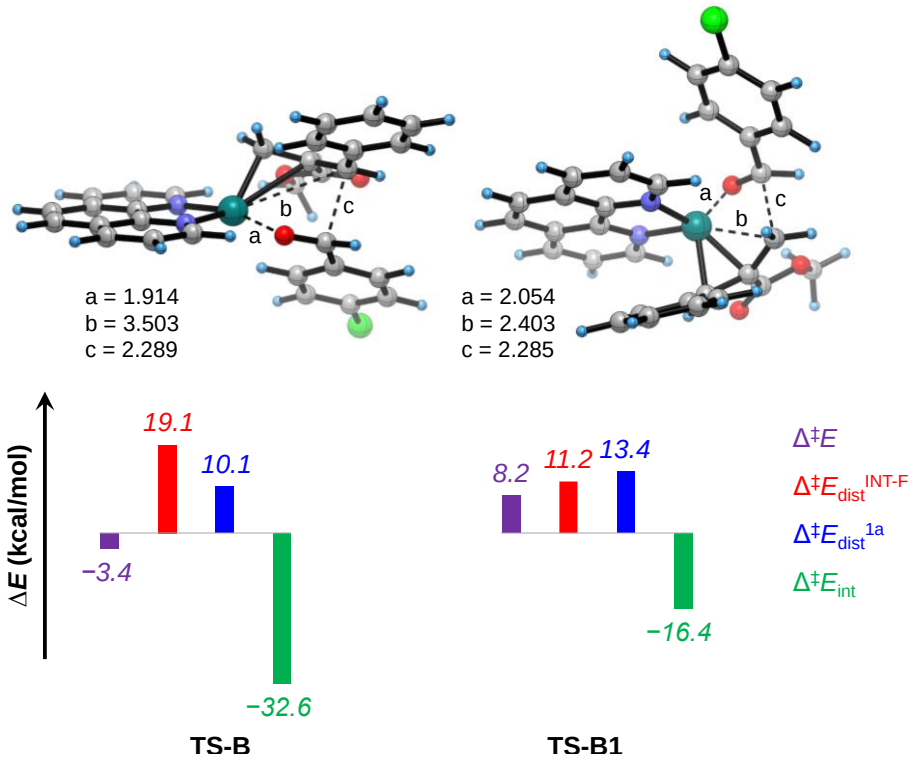

*Figure 5.23 Distortion–interaction analysis of **TS-B** and **TS-B1**. Optimized geometries of the transition states with selected bond distances in angstroms (Å).*

Experimental tests

To better understand the intermediates involved in the process, some experimental tests were performed (*Figure 5.24*).

First, the presence of intermediate radical species was tested by running the standard conditions in the presence of a stoichiometric amount of TEMPO as the radical trap. The isolation of the desired product in a very similar yield and with the usual high regio- and diastereoselectivity indicates there are no free-radicals present in the reaction media, e.g. generated from the reduction of the MBH acetate in a photoredox or metal-mediated event.

As mentioned above, the isolation of the products was complicated by the presence of side-products derived from MBH acetates. The nature and the structure of these side-products have been investigated by submitting the MBH adduct under the reaction conditions, in the absence of the aldehyde. We were able to confirm and verify by GC-MS the presence of the reduced product **bp1**, generated in the presence of Ni-H and in absence of an electrophile, the isomerized reduced product **bp2**, generated in an energy-transfer process by the photoexcited photocatalyst, and the fully hydrogenated reduced product **bp3**.

Finally, starting from the “normal” MBH adduct, or from the isomer, simply obtained by reported procedures,[331] we have isolated the same homoallylic product, indicating the formation of a (π-allyl)-Ni intermediate, which is well evident in the DFT calculation.

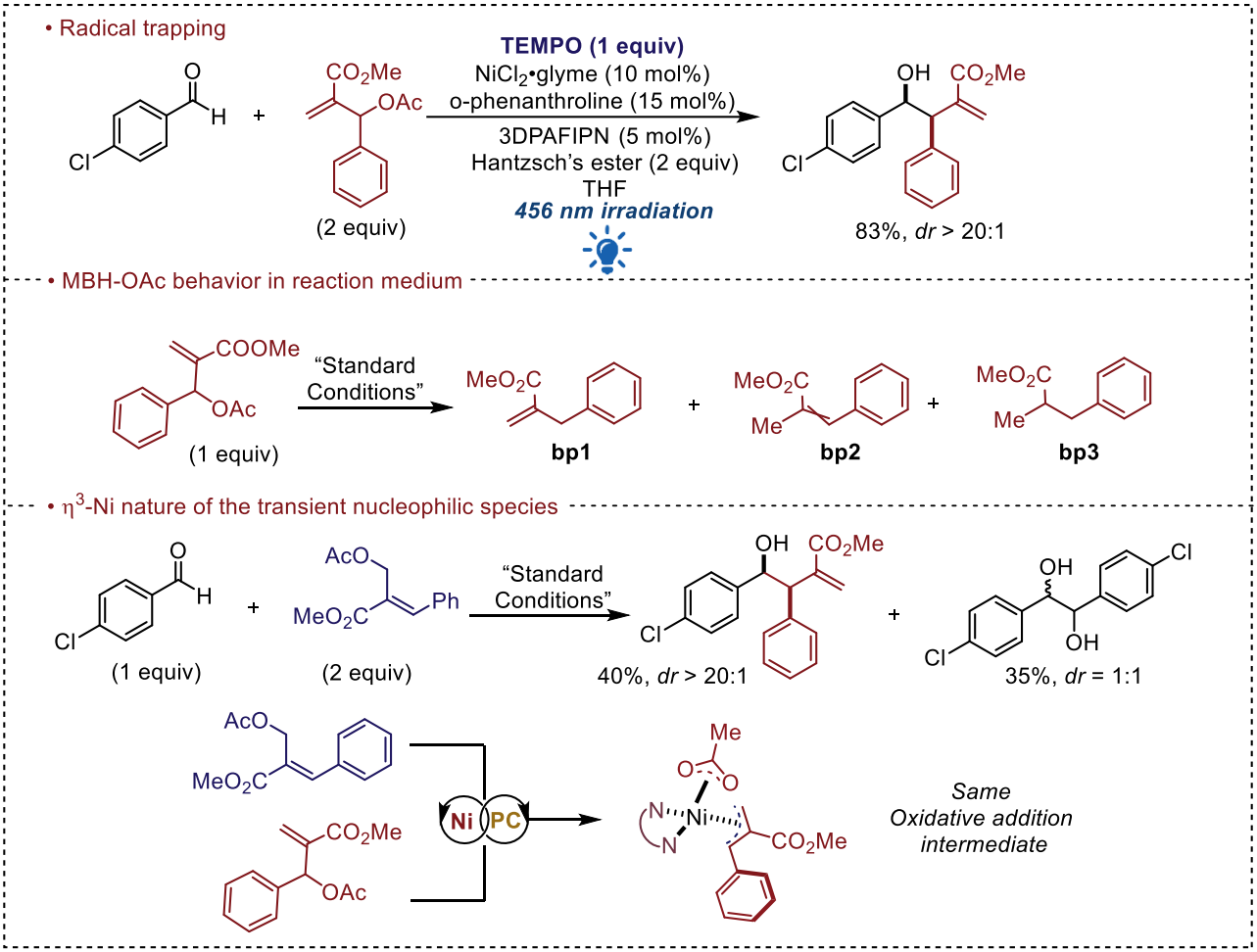

Figure 5.24 Experimental tests performed.

Taking into account the photophysical studies, the computational investigation and the experimental evidence derived from the experimental tests we were able to propose a mechanistic cycle for the presented protocol (*Figure 5.25*).

The process is initiated by the absorption of visible radiation by the photocatalyst. The Hantzsch ester can act as an efficient reductant ($E_{ox}(HE^{\bullet+}/HE)$ = +1.0 V *vs* SCE) for the excited photoactive complex *[3DPAFIPN·HE] ($^*E_{red}(^*[3DPAFIPN·HE]/[3DPAFIPN·HE]^{\bullet-})$ = +0.58 V *vs* SCE) even if the SET event is endergonic, leading to the formation of $[3DPAFIPN·HE]^{\bullet-}$ and the concomitant formation of $HE^{\bullet+}$. The former can reduce ($E_{red}([3DPAFIPN·HE]/[3DPAFIPN·HE]^{\bullet-})$ = –1.63 V *vs* SCE) in a second step the Ni(II) complex to the active Ni(0) species in a sequence of SET events, triggering its redox activity towards the MBH acetate and simultaneously restoring the photoredox catalytic cycle. Ni(0) undergoes oxidative addition with the MBH acetate and generates the electrophilic (π-allyl)-nickel(II) species that is readily reduced by another SET event to the key transient nucleophilic (π-allyl)-nickel(I). Addition of this intermediate to the aldehyde forges a new C-C bond and the formation of the product as nickel alkoxide. In order to rationalize the exclusive formation of the *syn*-products, a Zimmerman-Traxler transition state is suggested. Finally, the Ni-O bond is cleaved in a proton-coupled electron transfer (PCET) process in which the independent transfer of a proton and an electron liberates the product and restores the nickel catalytic cycle.

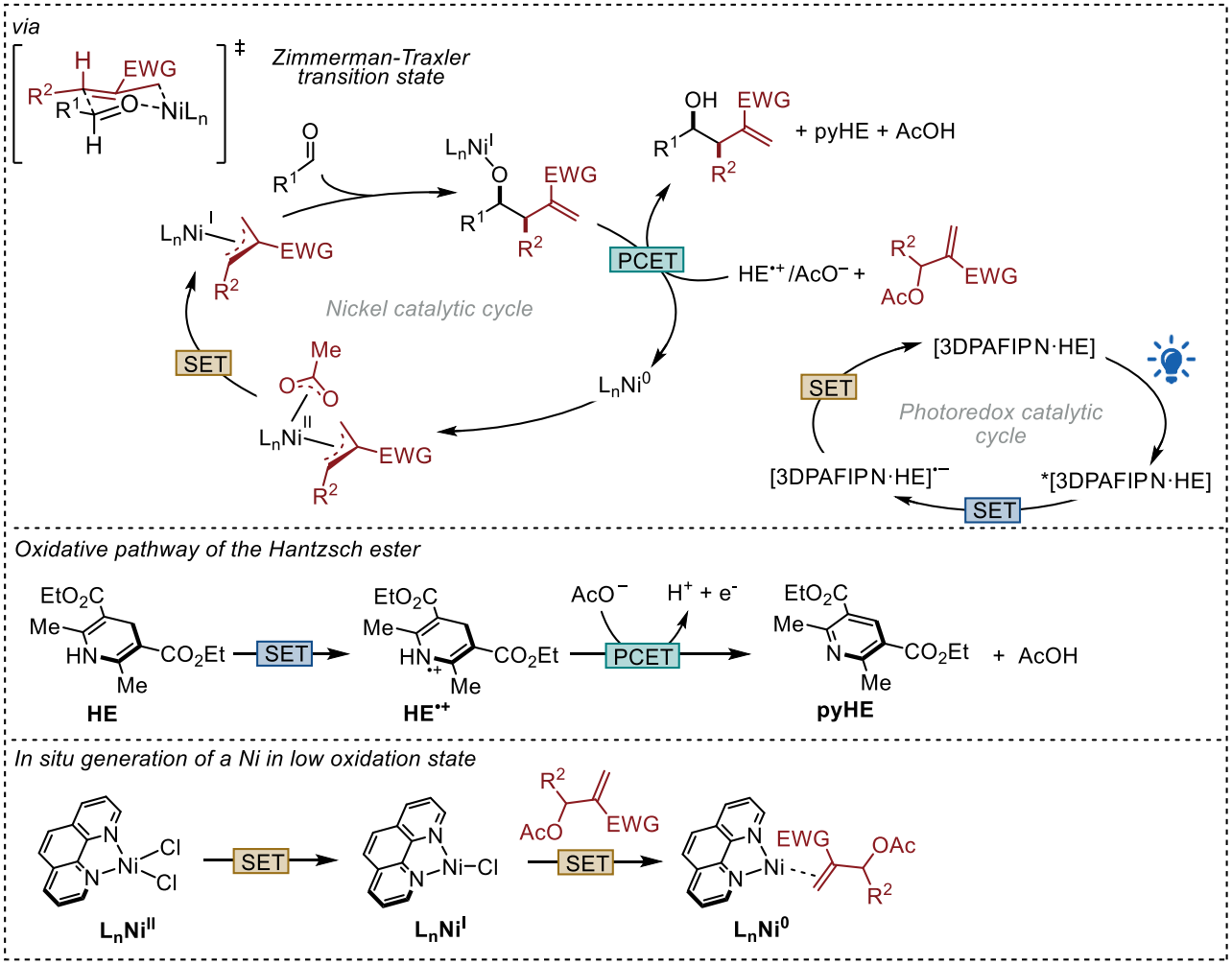

Figure 5.25 Proposed mechanism.

5.6 Conclusions

In conclusion, we have described a novel dual photoredox- and nickel-mediated allylation of aldehydes using MBH acetates as an unprecedented pronucleophile allylic source. The main advantages of this protocol compared to other allylation routes already reported in the literature are the low Ni- and photocatalyst loading, the rapid, reproducible, robust, regioselective and diastereoselective conditions of the methodology and the broad compatibility of substrates. The higher molecular complexity of the homoallylic alcohol can be directly exploited in the straightforward synthesis of bioactive products, demonstrating the utility of the protocol. A complete photophysical analysis, DFT calculations together with some experimental tests provided a deep understanding of the reaction mechanism. Further studies, directed towards an enantioselective version of this protocol are in progress in our research group.

Full account and description of the content of the chapter have not been published yet. The manuscript is in preparation.

5.7 Experimental section

General Methods

^{1}H NMR spectra were recorded on Varian Mercury 400 spectrometer. Chemical shifts are reported in ppm from TMS with the solvent resonance as the internal standard ($CHCl_3$, δ = 7.27 ppm). Data are reported as follows: chemical shift, multiplicity (s = singlet, d = duplet, t = triplet, q = quartet, dd = double duplet, m = multiplet), coupling constants (Hz). ^{13}C NMR spectra were recorded on Varian Mercury 400 spectrometer. Chemical shifts are reported in ppm from TMS with the solvent as the internal standard ($CDCl_3$, δ = 77.0 ppm). GC-MS spectra were taken by EI ionization at 70 eV on a Hewlett-Packard 5971 with GC injection. Chromatographic purifications were done with 240-400 mesh silica gel. HRMS spectra were obtained with a G2XS QTof mass spectrometer using either ESI or APCI ionization techniques. All the reagents were purchased from commercial sources (Sigma-Aldrich, Alfa Aesar, Fluorochem, Strem Chemicals, TCI) and used without further purification unless specified.
All reactions requiring inert atmosphere were set up under an argon atmosphere in heat gun-dried glassware using standard Schlenk techniques. Anhydrous solvents were supplied by Aldrich in Sureseal® bottles and, unless specified, were used without further treatments. Anhydrous tetrahydrofuran (THF) was obtained by standard Sodium/benzophenone ketyl distillation starting from reagent grade THF, supplied by TCI® or Sigma Aldrich®.
Freshly distilled THF was stored under argon atmosphere in a dry Schlenk tube, equipped with a Rotaflo® stopcock with activated 3Å molecular sieves (ca. 5 g of MS for 100 mL of solvent). 3Å molecular sieves were supplied by Sigma-Aldrich®. Activation of the MS was performed through five 6-minute cycles in microwave (750W). Once the cycles are completed the MS are rapidly inserted in a dry Schlenk tube, equipped with a Rotaflo® stopcock and then flame-dried for 5 minutes under vacuum before starting the distillation. Photocatalytic reactions were irradiated with Kessil® PR160L@456 nm (see *Figure 5.26* for the emission profile). Ligands employed for the dual nickel/photoredox catalytic reaction (L1–5, DPPE, DPPP, BINAP), as well as the nickel complexes $NiCl_2$·glyme, $NiCl_2(PBu_3)_2$, $Ni(acac)_2$ and $Ni(OAc)_2$ were purchased from commercial sources (Sigma-Aldrich, Fluorochem) and were used without further treatment.
2,4,6-tri(diphenylamino)-5-fluoroisophthalonitrile (3DPAFIPN) and 2,4,5,6-tetrakis(carbazol-9-yl)-isophthalonitrile (4CzIPN), were prepared according to published literature procedures.[90] Synthesis of Hantzsch ethyl ester was achieved following the known literature procedure.[244]
Substrates **2a-s** were prepared according to the two-step standard Morita-Baylis-Hillman acetate (MBH–acetate) synthetic protocol.[332] Spectroscopic data for MBH-alcohols **2b**, **S1-17** and for MBH-acetates **2a-s** match or are consistent with those already been reported in the literature.
Substrates **1k**, **1q**, **1r**, **1s**, **1t** and **1w** were synthetized according to the known literature protocols and the related spectroscopic data match with those already reported.

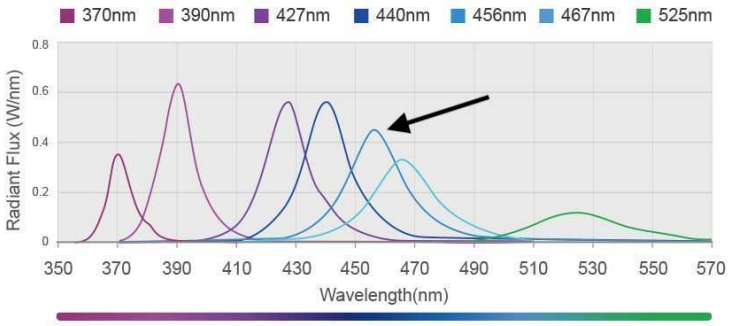

Figure 5.26 Emission profile of the Kessil® PR160L@456 nm used to irradiate the solutions (from Kessil® website: https://www.kessil.com/science/PR160L.php).

Figure 5.27 Reaction set-up with Kessil® PR160L@456 nm lamp.

Reaction flasks were positioned approximatively at 18 cm from the light source. The reaction temperature was close to room temperature (22-28°C) during the irradiation.

Photophysical analyses

General Methods

All the photophysical analyses were carried out in deoxygenated, stabilizer-free tetrahydrofuran (THF) at 298 K, unless otherwise specified. Experiments in absence of oxygen were carried out in a nitrogen-filled glovebox in a custom-made quartz cuvette. UV–vis absorption spectra were recorded with a PerkinElmer λ40 spectrophotometer using quartz cells with 1.0 cm optical path. Luminescence spectra were performed with an Edinburgh FS5 spectrofluorometer equipped with a Hamamatsu Photomultiplier R928P phototube. Lifetimes shorter than 10 μs were measured by an Edinburgh FLS920 spectrofluorometer by time-correlated single-photon counting (TCSPC) technique. Lifetimes longer than 10 μs were measured by the above-mentioned Edinburgh FS5 spectrofluorometer or by a Varian Cary Eclipse fluorescence spectrophotometer. The estimated experimental errors are 2 nm on the band maximum, 5% on the molar absorption coefficient and luminescence lifetimes.

General procedure for dual photoredox- and nickel-catalyzed reaction between aldehydes and MBH-acetates.

All the reactions were performed on 0.2 mmol scale. A heat-gun dried 10 mL Schlenk tube, equipped with a Rotaflo® stopcock, magnetic stirring bar and an argon supply tube, was firstly charged under vigorous argon flux with $NiCl_2$·glyme (4.4 mg, 0.02 mmol, 10 mol%), the substrate if solid **1** (0.2 mmol) the organic photocatalyst 3DPAFIPN (6.5 mg, 0.01 mmol, 5 mol%), diethyl 1,4-dihydro-2,6-dimethyl-3,5-pyridinedicarboxylate Hantzsch ester (101 mg, 0.4 mmol, 2 equiv.) and o-phenanthroline (10.8 mg, 0.03 mmol, 15 mol%). Then, inhibitor-free and freshly distilled dry THF (2 mL in order to obtain a 0.1 M substrate solution) was added. Finally, MBH acetate **2** (103 mg, 0.44 mmol, 2.2 equiv.) were added to the solution that was further subjected to a freeze-pump-thaw procedure (three cycles, 5 minutes per cycle) and then refilled with argon. Then substrate **1** if liquid was added. The degassed reaction mixture was irradiated under vigorous stirring for 16h. After that, the reaction mixture was quenched with HCl 1M (approx. 10 mL) and extracted with EtOAc (10x3 mL). The combined organic layers were dried over anhydrous Na_2SO_4 and the solvent was removed under reduced pressure. The reaction crude was analyzed by ^1H NMR for the evaluation of the diastereomeric ratio. The NMR sample was carefully recovered, the solvent was removed under reduced pressure and purified by flash column chromatography (SiO_2) to afford products **3** in the stated yields.

General procedure for the 2 mmol scale reaction.

A heat-gun dried 50 mL Schlenk tube, equipped with a magnetic stirring bar and an argon supply tube, was firstly charged under vigorous argon flux with $NiCl_2 \cdot$glyme (5 mol%, 0.1 mmol, 22 mg), the substrate **1a** (280 mg, 2 mmol, 1 equiv.) the organic photocatalyst 3DPAFIPN (39 mg, 0.06 mmol, 3 mol%), diethyl 1,4-dihydro-2,6-dimethyl-3,5-pyridinedicarboxylate Hantzsch ester (1.01 g, 4 mmol, 2 equiv.) and o-phenanthroline (27 mg, 0.15 mmol, 7.5 mol%). Then, Inhibitor-free and freshly distilled dry THF (20 mL in order to obtain [**1a**] = 0.1 M) was added. Finally, MBH acetate **2a** (1.030 g, 4.4 mmol, 2.2 equiv.) was added to the solution that was further subjected to a freeze-pump-thaw procedure (three cycles, 5 minutes per cycle) and then refilled with argon. The degassed reaction mixture was irradiated under vigorous stirring for 60h. After that, the reaction mixture was quenched with HCl 1M (approx. 20 mL) and extracted with EtOAc (15x3 mL). The combined organic layers were dried over anhydrous Na_2SO_4 and the solvent was removed under reduced pressure. The reaction crude was analyzed by ^{1}H NMR for the evaluation of the diastereomeric ratio. The NMR sample was carefully recovered, the solvent was removed under reduced pressure and purified by flash chromatography (SiO_2 DCM/Hexane from 6:4 to 8:2) to afford product **3aa** in 80% yield (506 mg, 1.6 mmol).

Characterization of the products

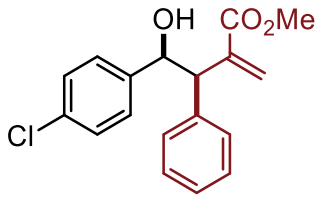

Methyl 4-(4-chlorophenyl)-4-hydroxy-2-methylene-3-phenylbutanoate (3aa). Yield 87% (0.174 mmol, 55 mg). Pale yellow oil. $dr_{syn:anti}$ > 95:5 determined from ^{1}H NMR of the reaction crude by integration of the 2 C-H in the benzylic position. **3aa** was obtained following the general procedure as stated above employing 0.2 mmol (28 mg, 1 equiv.) of **1a** and 0.44 mmol (103 mg, 2.2 equiv.) of **2a**. The title compound was isolated by flash column chromatography (SiO_2, 50-30% Hexane in DCM). Spectroscopical data are in accordance with the reported literature.[333]

^{1}H NMR (401 MHz, $CDCl_3$) δ = 7.37 – 7.21 (m, 10H, overlapped with the residual peak of NMR solvent), 6.25 (s, 1H), 5.80 (s, 1H), 5.27 (d, J = 7.8 Hz, 1H), 4.24 (d, J = 7.7 Hz, 1H), 3.60 (s, 3H).^{13}C NMR (101 MHz, $CDCl_3$) δ = 166.6, 140.5, 140.2, 137.8, 133.1, 128.8 (2C), 128.3 (2C), 128.0 (2C), 128.0 (2C), 127.1, 126.8, 74.7, 54.2, 51.6.

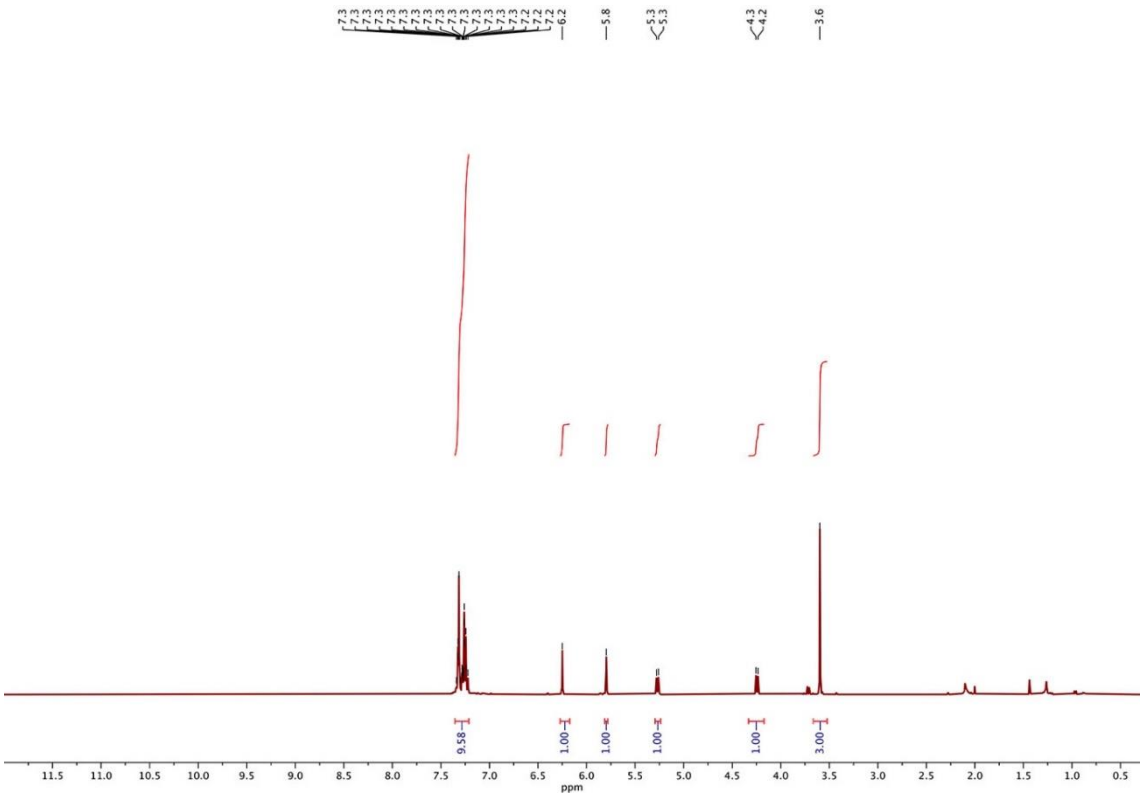

*Figure 5.28 [1]H NMR of **3aa**.*

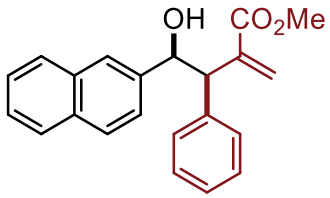

Methyl 4-hydroxy-2-methylene-4-(naphthalen-2-yl)-3-phenylbutanoate (3ba). Yield 77% (0.154 mmol, 51 mg). Pale yellow oil. $dr_{syn:anti}$ > 95:5 determined from ^{1}H NMR of the reaction crude by integration of the 2 C-H in the benzylic position. **3ba** was obtained following the general procedure as stated above employing 0.2 mmol (31.2 mg, 1 equiv.) of **1b** and 0.44 mmol (103 mg, 2.2 equiv.) of **2a.** The title compound was isolated by flash column chromatography (SiO_2, 50-30% Hexane in DCM). Spectroscopical data are in accordance with the reported literature.[334]

^{1}H NMR (401 MHz, $CDCl_3$) δ = 7.80 (m, 3H), 7.72 – 7.69 (m, 1H), 7.49 – 7.44 (m, 3H), 7.38 – 7.23 (m, 6H overlapped with the residual peak of NMR solvent), 6.22 (d, *J* = 0.9 Hz, 1H), 5.85 (s, 1H), 5.44 (d, *J* = 7.8 Hz, 1H), 4.43 (d, *J* = 7.9 Hz, 1H), 3.51 (s, 3H). ^{13}C NMR (101 MHz, $CDCl_3$) δ = 166.6, 140.7, 139.1, 138.2, 132.7, 132.7, 128.9 (2C), 128.2 (2C), 127.7, 127.7, 127.3, 126.9, 126.59, 125.9, 125.7, 125.6, 124.4, 75.5, 53.9, 51.5.

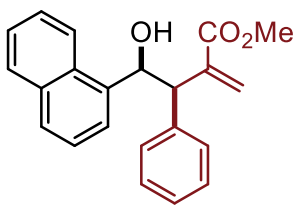

Methyl 4-hydroxy-2-methylene-4-(naphthalen-1-yl)-3-phenylbutanoate (3ca). Yield 68% (0.136 mmol, 45 mg). Pale yellow oil. $dr_{syn:anti}$ > 95:5 determined from ^{1}H NMR of the reaction crude by

integration of the 2 C-H in the benzylic position. **3ca** was obtained following the general procedure as stated above employing 0.2 mmol (31.2 mg, 27.1 µl 1 equiv.) of **1c** and 0.44 mmol (103 mg, 2.2 equiv.) of **2a**. The title compound was isolated by flash column chromatography (SiO_2, 50-30% Hexane in DCM). Spectroscopical data are in accordance with the reported literature.[334]

^{1}H NMR (401 MHz, $CDCl_3$) δ = 8.24 (m, 1H), 7.92 – 7.86 (m, 1H), 7.76 (m, 1H), 7.54 (m, 2H), 7.37 – 7.16 (m, 8H overlapped with the residual peak of NMR solvent), 6.35 (s, 1H), 6.07 (d, *J* = 5.7 Hz, 1H), 6.00 (s, 1H), 4.61 (d, *J* = 5.7 Hz, 1H), 3.59 (s, 3H). ^{13}C NMR (101 MHz, $CDCl_3$) δ = 167.5, 141.5, 137.9, 137.9, 134.6, 130.9, 129.9 (2C), 129.3, 128.5(2C), 128.5, 127.5, 127.2, 126.6, 125.8, 125.3, 124.7, 123.4, 72.0, 52.9, 52.2.

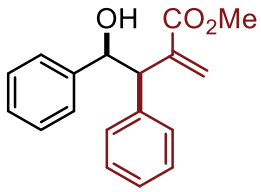

Methyl 4-hydroxy-2-methylene-3,4-diphenylbutanoate (3da). Yield 54% (0.108 mmol, 30.5 mg). Pale yellow oil. $dr_{syn:anti}$ > 95:5 determined from ^{1}H NMR of the reaction crude by integration of the 2 C-H in the benzylic position. **3da** was obtained following the general procedure as stated above employing 0.2 mmol (21.2 mg, 20.3 µl, 1 equiv.) of **1d** and 0.44 mmol (103 mg, 2.2 equiv.) of **2a**.The title compound was isolated by flash column chromatography (SiO_2, 50-30% Hexane in DCM). Spectroscopical data are in accordance with the reported literature.[334]

^{1}H NMR (401 MHz, $CDCl_3$) δ = 7.34 – 7.21 (m, 10H overlapped with the residual peak of NMR solvent), 6.23 (s, 1H), 5.80 (s, 1H), 5.26 (d, *J* = 7.9 Hz, 1H), 4.31 (d, *J* = 7.6 Hz, 1H), 3.56 (s, 3H).^{13}C NMR (101 MHz, $CDCl_3$) δ = 166.9, 142.0, 141.1, 138.6, 129.2 (2C), 128.5(2C), 128.2(2C), 127.8, 127.2, 127.0(2C), 126.8, 75.8, 54.3, 51.8.

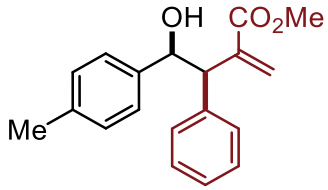

Methyl 4-hydroxy-2-methylene-3-phenyl-4-(p-tolyl)butanoate (3ea). Yield 68% (0.136 mmol, 40.2 mg). Pale yellow oil. $dr_{syn:anti}$ > 95:5 determined from ^{1}H NMR of the reaction crude by integration of the 2 C-H in the benzylic position. **3ea** was obtained following the general procedure as stated above employing 0.2 mmol (24.3 mg, 23.8 µl, 1 equiv.) of **1e** and 0.44 mmol (103 mg, 2.2 equiv.) of **2a**. The title compound was isolated by flash column chromatography (SiO_2, 50-30% Hexane in DCM). Spectroscopical data are in accordance with the reported literature.[335]

^{1}H NMR (401 MHz, $CDCl_3$) δ = 7.29 – 7.17 (m, 5H overlapped with the residual peak of NMR solvent), 7.14 – 7.10 (m, 2H), 7.03 (d, *J* = 7.8 Hz, 2H), 6.15 (s, 1H), 5.72 (s, 1H), 5.16 (d, *J* = 8.3 Hz, 1H), 4.24 (d, *J* = 8.2 Hz, 1H), 3.50 (s, 3H), 2.25 (s, 3H). ^{13}C NMR (101 MHz, $CDCl_3$) δ = 166.9, 141.1, 139.0, 138.8, 137.4, 136.0, 129.2 (2C), 128.9(2C), 128.5(2C), 127.2, 126.9(2C), 126.7, 75.6, 54.2, 51.8, 21.1.

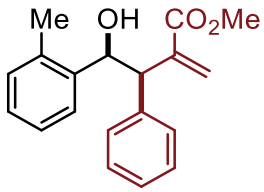

Methyl 4-hydroxy-2-methylene-3-phenyl-4-(o-tolyl)butanoate (3fa). Yield 68% (0.134 mmol, 39.7 mg). Pale yellow oil. $dr_{syn:anti}$ > 95:5 determined from ^{1}H NMR of the reaction crude by integration of the 2 C-H in the benzylic position. **3fa** was obtained following the general procedure as stated above employing 0.2 mmol (24.3 mg, 23.8 µl, 1 equiv.) of **1f** and 0.44 mmol (103 mg, 2.2 equiv.) of **2a**. The title compound was isolated by flash column chromatography (SiO_2, 50-30% Hexane in DCM).

^{1}H NMR (401 MHz, $CDCl_3$) δ = 7.25 (m, 5H overlapped with the residual peak of NMR solvent), 7.15 – 7.06 (m, 4H), 6.26 (s, 1H), 5.85 (s, 1H), 5.45 (d, J = 6.0 Hz, 1H), 4.38 (d, J = 7.0 Hz, 1H), 3.56 (s, 3H), 2.41 (s, 3H). ^{13}C NMR (101 MHz, $CDCl_3$) δ = 167.4, 141.6, 140.2, 138.5, 135.4, 130.8, 129.8, 128.7, 127.8, 127.5 (2C), 126.9(2C), 126.8, 126.2, 72.2, 52.6, 52.2, 19.7.

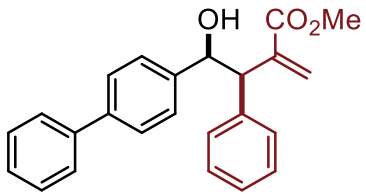

Methyl 4-([1,1'-biphenyl]-4-yl)-4-hydroxy-2-methylene-3-phenylbutanoate (3ga). Yield 81% (0.162 mmol, 58.0 mg). White solid. $dr_{syn:anti}$ > 95:5 determined from ^{1}H NMR of the reaction crude by integration of the 2 C-H in the benzylic position. **3ga** was obtained following the general procedure as stated above employing 0.2 mmol (36. 4mg, 1 equiv.) of **1g** and 0.44 mmol (103 mg, 2.2 equiv.) of **2a**. The title compound was isolated by flash column chromatography (SiO_2, 50-30% Hexane in DCM).

^{1}H NMR (401 MHz, $CDCl_3$) δ 7.61 – 7.53 (m, 4H), 7.44 (dd, *J* = 8.3, 6.9 Hz, 2H), 7.41 – 7.27 (m, 9H), 6.28 (s, 1H), 5.85 (s, 1H), 5.33 (d, *J* = 8.0 Hz, 1H), 4.38 (d, *J* = 8.0 Hz, 1H), 3.59 (s, 3H). ^{13}C NMR (101 MHz, $CDCl_3$) δ = 166.9, 141.0, 141.0, 140.7, 140.6, 138.6, 129.2 (2C), 128.7(2C), 128.6(2C), 127.6, 127.4 (2C), 127.3 (2C), 127.0, 126.9, 126.9, 75.5, 54.2, 51.8.

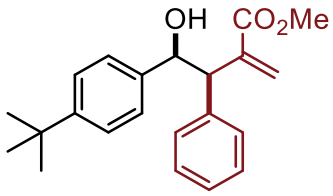

Methyl 4-(4-(*tert*-butyl)phenyl)-4-hydroxy-2-methylene-3-phenylbutanoate (3ha). Yield 50% (0.10 mmol, 33.8 mg). Pale yellow oil. $dr_{syn:anti}$ > 95:5 determined from ^{1}H NMR of the reaction crude by integration of the 2 C-H in the benzylic position. **3ha** was obtained following the general procedure as stated above employing 0.2 mmol (32. 4mg, 33.4 µl,1 equiv.) of **1h** and 0.44 mmol (103 mg, 2.2 equiv.) of **2a.** The title compound was isolated by flash column chromatography (SiO_2, 50-30% Hexane in DCM).

^{1}H NMR (401 MHz, $CDCl_3$) δ = 7.45 – 7.18 (m, 9H overlapped with the residual peak of NMR solvent), 6.24 (s, 1H), 5.79 (s, 1H), 5.22 (d, *J* = 8.4 Hz, 1H), 4.35 (d, *J* = 8.4 Hz, 1H), 3.56 (s, 3H), 1.31 (s, 9H). ^{13}C NMR (101 MHz, $CDCl_3$) δ = 167.0, 150.7, 141.2, 139.0, 138.8, 129.2(2C), 128.5 (2C), 127.2, 126.8 (2C), 126.6, 125.2 (2C), 75.7, 53.9, 51.8, 34.4, 31.3 (3C).

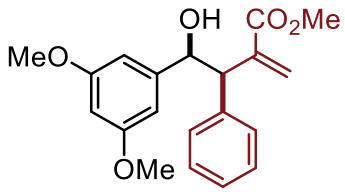

Methyl 4-(3,5-dimethoxyphenyl)-4-hydroxy-2-methylene-3-phenylbutanoate (3ia). Yield 30% (0.06 mmol, 20.5 mg). Pale yellow oil. $dr_{syn:anti}$ = 90:10 determined from ^{1}H NMR of the reaction crude by integration of the 2 C-H in the benzylic position. **3ia** was obtained modifying the general procedure extending the reaction time from 16 to 48h, employing 0.2 mmol (33. 2 mg,1 equiv.) of **1i** and 0.44 mmol (103 mg, 2.2 equiv.) of **2a**. The title compound was isolated by flash column chromatography (SiO_2, 100% DCM). Spectroscopical data are given only for the major diastereoisomer.

^{1}H NMR (401 MHz, $CDCl_3$) δ = 7.34 – 7.30 (m, 4H), 6.45 (m, 2H), 6.35 (m, 1H), 6.26 (d, *J* = 0.8 Hz, 1H), 5.86 (s, 1H), 5.22 (d, *J* = 7.6 Hz, 1H), 4.27 (d, *J* = 7.1 Hz, 1H), 3.75 (s, 6H), 3.61 (s, 3H). ^{13}C NMR (101 MHz, $CDCl_3$) δ = 166.7, 160.3, 144.2, 140.7, 138.17, 129.0 (2C), 128.2 (2C), 126.9, 126.5, 104.6, 99.6, 75.4, 55.0 (2C), 53.9, 51.6

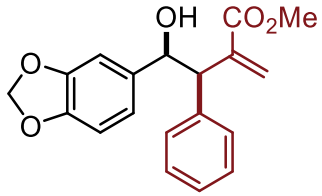

Methyl 4-(benzo[*d*][1,3]dioxol-5-yl)-4-hydroxy-2-methylene-3-phenylbutanoate (3ja). Yield 46% (0.092 mmol, 30.0 mg). Pale yellow oil. $dr_{syn:anti}$ > 95:5 determined from ^{1}H NMR of the reaction crude by integration of the 2 C-H in the benzylic position. **3ja** was obtained modifying the general procedure extending the reaction time from 16 to 48h, employing 0.2 mmol (30.0 mg,1 equiv.) of **1j** and 0.44 mmol (103 mg, 2.2 equiv.) of **2a.** The title compound was isolated by flash column chromatography (SiO_2, 100% DCM).

^{1}H NMR (401 MHz, $CDCl_3$) δ = 7.39 – 7.23 (m, 5H, overlapped with the residual peak of NMR solvent), 6.84 (m, 1H), 6.80 – 6.67 (m, 2H), 6.23 (d, J = 0.9 Hz, 1H), 5.8 (s, 2H), 5.77 (s, 1H), 5.21 (d, J = 8.3 Hz, 1H), 4.24 (dd, J = 8.3, 0.9 Hz, 1H), 3.61 (s, J = 0.9 Hz, 3H). ^{13}C NMR (101 MHz, $CDCl_3$) δ = 166.9, 147.6, 147.8, 141.0, 138.7, 136.0, 129.1(2C), 128.6(2C), 127.3, 126.8, 120.7, 107.9, 107.3, 100.9, 75.5, 54.6, 51.9.

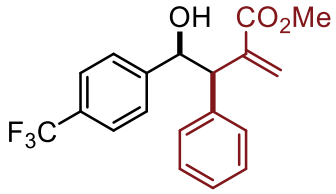

Methyl 4-hydroxy-2-methylene-3-phenyl-4-(4-(trifluoromethyl)phenyl)butanoate (3ka). Yield 71% (0.142 mmol, 49.7 mg). Pale yellow oil. $dr_{syn:anti}$ = 85:15 determined from ^{19}F NMR of the reaction crude. **3ka** was obtained following the general procedure as stated above employing 0.2 mmol (34.8 mg, 27 µl, 1 equiv.) of **1k** and 0.44 mmol (103 mg, 2.2 equiv.) of **2a**. The title compound was isolated by flash column chromatography (SiO_2, 50-30% Hexane in DCM). Spectroscopical data are given only for the major diastereoisomer.

^{1}H NMR (401 MHz, $CDCl_3$) δ = 7.50 (m, 2H), 7.37 (m, 2H), 7.33 – 7.16 (m, 5H overlapped with the residual peak of NMR solvent), 6.21 (s, 1H), 5.76 (s, 1H), 5.30 (d, *J* = 7.6 Hz, 1H), 4.22 (d, *J* = 7.6 Hz, 1H), 3.53 (s, 3H). ^{13}C NMR (101 MHz, $CDCl_3$) δ = 167.2, 146.3, 141.0, 138.2, 130.2 (q, *J* = 32.4 Hz, 1C), 129.5 (2C),

129.4, 129.0 (2C),128.7, 127.8, 127.6 (2C), 125.4 (q, *J* = 3.8 Hz), 75.4, 54.9, 52.3. ^{19}F NMR (377 MHz, CDCl3) δ = -61.29 (s, 3F).

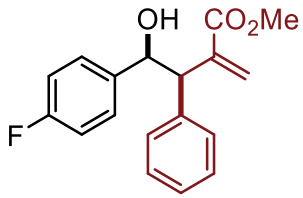

Methyl 4-(4-fluorophenyl)-4-hydroxy-2-methylene-3-phenylbutanoate (3la). Yield 78% (0.156 mmol, 46.8 mg). Pale yellow oil. $dr_{syn:anti}$ >95:5 determined from ^{19}F NMR of the reaction crude. **3la** was obtained following the general procedure as stated above employing 0.2 mmol (24.8 mg, 21.4 µl, 1 equiv.) of **1l** and 0.44 mmol (103 mg, 2.2 equiv.) of **2a**. The title compound was isolated by flash column chromatography (SiO_2, 50-30% Hexane in DCM).

^{1}H NMR (401 MHz, $CDCl_3$) δ = 7.36 – 7.21 (m, 7H overlapped with the residual peak of NMR solvent), 6.97 (m, 2H), 6.22 (s, 1H), 5.77 (s, 1H), 5.26 (d, *J* = 8.0 Hz, 1H), 4.24 (d, *J* = 8.0 Hz, 1H), 3.57 (s, 3H). ^{13}C NMR (101 MHz, $CDCl_3$) δ = 166.9, 162.3 (d, *J* = 246.0 Hz, 1C), 140.9, 138.4, 137.7 (d, *J* = 3.2 Hz, 1C), 129.1 (2C), 128.6 (d, *J* = 8.1 Hz, 2C), 128.6 (2C), 127.4, 127.0, 115.1 (d, *J* = 21.4 Hz, 2C), 75.1, 54.6, 51.9. ^{19}F NMR (377 MHz, $CDCl_3$) δ = -114.6 (m 1F).

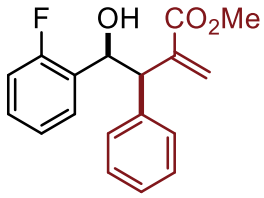

Methyl 4-(2-fluorophenyl)-4-hydroxy-2-methylene-3-phenylbutanoate (3ma). Yield 30% (0.06 mmol, 18.0 mg). Pale yellow oil. $dr_{syn:anti}$ >95:5 determined from ^{19}F NMR of the reaction crude. **3ma** was obtained following the general procedure as stated above employing 0.2 mmol (24.8 mg, 21.1 µl, 1 equiv.) of **1m** and 0.44 mmol (103 mg, 2.2 equiv.) of **2a.** The title compound was isolated by flash column chromatography (SiO_2, 50-30% Hexane in DCM).

^{1}H NMR (401 MHz, $CDCl_3$) δ = 7.36 – 7.21 (m, 7H overlapped with the residual peak of NMR solvent), 7.11 – 6.96 (m, 2H), 6.28 (s, 1H), 5.93 (s, 1H), 5.58 (d, *J* = 7.9 Hz, 1H), 4.40 (d, *J* = 7.9 Hz, 1H), 3.59 (s, 3H). ^{13}C NMR (101 MHz, $CDCl_3$) δ = 166.6, 159.6 (d, *J* = 245.7 Hz, 1C), 140.3, 138.0, 129.0 (d, *J* = 8.5 Hz, 1C), 128.7 (2C), 128.3 (2C), 128.0 (d, *J* = 4.1 Hz, 1C), 127.0, 126.3 (d, *J* = 1.6 Hz, 1C), 123.9, 123.8, 114.9 (d, *J* = 22.3 Hz, 1C), 69.0 (d, *J* = 2.2 Hz, 1C), 52.7, 51.6. ^{19}F NMR (377 MHz, $CDCl_3$) δ = -118.5 (m 1F).

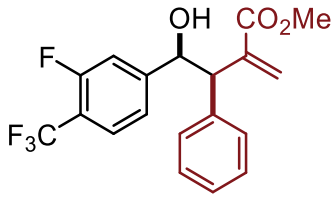

Methyl 4-(3-fluoro-4-(trifluoromethyl)phenyl)-4-hydroxy-2-methylene-3-phenylbutanoate (3na). Yield 57% (0.114 mmol, 41.9 mg). Pale yellow oil. $dr_{syn:anti}$ = 92:8 determined from ^{19}F NMR of the reaction crude. **3na** was obtained following the general procedure as stated above employing 0.2 mmol (38.4 mg, 1 equiv.) of **1n** and 0.44 mmol (103 mg, 2.2 equiv.) of **2a**. The title compound was isolated by flash column chromatography (SiO_2, 50-30% Hexane in DCM).

^{1}H NMR (401 MHz, $CDCl_3$) Spectroscopical data are given only for the major diastereoisomer. δ = 7.54 – 7.43 (m, 2H), 7.35 – 7.22 (m, 5H overlapped with the residual peak of NMR solvent), 7.13 – 7.07 (m, 1H),

6.25 (s, 1H), 5.78 (s, 1H), 5.34 (d, *J* = 8.4 Hz, 1H), 4.19 (dd, *J* = 7.7, 0.9 Hz, 1H), 3.60 (s, 3H). ^{13}C NMR (101 MHz, $CDCl_3$) all peaks are given without assignment. δ = 166.9, 160.3, 160.3, 157.8, 157.8, 140.6, 138.3, 138.3, 137.7, 132.4, 132.3, 129.5, 129.2, 129.2, 129.1, 129.0, 129.0, 128.8, 128.8, 128.6, 128.6, 127.9, 127.6, 127.4, 126.0, 125.9, 125.9, 125.8, 125.8, 125.8, 125.8, 125.7, 125.7, 123.9, 123.5, 123.4, 122.7, 121.8, 121.2, 118.2, 118.1, 117.9, 117.7, 116.7, 116.6, 116.5, 116.4, 81.0, 74.6, 60.4, 55.0, 52.0, 51.5. ^{19}F NMR (377 MHz, $CDCl_3$) Spectroscopical data are given only for the major diastereoisomer. δ = -61.42 (d, *J* = 12.7 Hz, 3F), -115.60 – -116.71 (m, 1F).

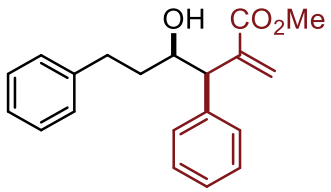

Methyl 4-hydroxy-2-methylene-3,6-diphenylhexanoate (3oa). Yield 50% (0.10 mmol, 31.0 mg). Pale yellow oil. $dr_{syn:anti}$ > 95:5 determined from ^{1}H NMR of the reaction crude by integration of the C-H in the benzylic position. **3oa** was obtained modifying the general procedure extending the reaction time from 16 to 48h, employing 0.2 mmol (26.8 mg, 26.3 µl, 1 equiv.) of **1o** and 0.4 mmol (93.6 mg, 2.0 equiv.) of **2a**. The title compound was isolated by flash column chromatography (SiO_2, 50-30% Hexane in DCM).

^{1}H NMR (401 MHz, $CDCl_3$) δ = 7.36 – 7.22 (m, 7H, overlapped with the residual signal of the NMR solvent), 7.23 – 7.13 (m, 3H), 6.32 (d, J = 0.8 Hz, 1H), 5.74 (d, J = 1.0 Hz, 1H), 4.13 (ddd, J = 9.4, 6.9, 3.0 Hz, 1H), 3.92 (dd, J = 6.9, 1.0 Hz, 1H), 3.66 (s, 3H), 2.86 (ddd, J = 14.4, 9.7, 5.2 Hz, 1H), 2.70 (ddd, J = 13.8, 9.4, 7.0 Hz, 1H), 1.90 (dddd, J = 13.9, 9.9, 7.1, 3.0 Hz, 1H), 1.70 (ddt, J = 13.7, 9.1, 4.6 Hz, 1H). ^{13}C NMR (101 MHz, $CDCl_3$) δ = 167.2, 141.9, 141.4, 138.8, 129.2 (2C), 128.6 (2C), 128.5 (2C), 128.3 (2C), 127.2, 126.1, 125.8, 72.1, 52.7, 52.0, 37.0, 32.2.

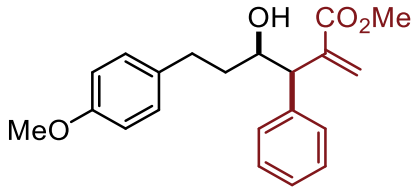

Methyl 4-hydroxy-6-(4-methoxyphenyl)-2-methylene-3-phenylhexanoate (3pa). Yield 49% (0.10 mmol, 33.3 mg). Pale yellow oil. $dr_{syn:anti}$ >95:5 determined from ^{1}H NMR of the reaction crude by integration of the C-H in the benzylic position. **3pa** was obtained modifying the general procedure extending the reaction time from 16 to 48h, employing 0.2 mmol (32.8, 1 equiv.) of **1p** and 0.4 mmol (93.6 mg, 2.0 equiv.) of **2a**. The title compound was isolated by flash column chromatography (SiO_2, 40-30% Hexane in DCM).

^{1}H NMR (401 MHz, $CDCl_3$) δ = 7.29 (d, *J* = 4.3 Hz, 4H, overlapped with the residual signal of the NMR solvent), 7.25 – 7.19 (m, 1H), 7.10 – 7.05 (m, 2H), 6.83 – 6.77 (m, 2H), 6.31 (d, *J* = 0.8 Hz, 1H), 5.74 (d, *J* = 1.0 Hz, 1H), 4.10 (d, *J* = 8.6 Hz, 1H), 3.91 (dd, *J* = 6.9, 1.0 Hz, 1H), 3.76 (s, 3H), 3.65 (s, 3H), 2.78 (ddd, *J* = 14.4, 9.5, 5.2 Hz, 1H), 2.64 (ddd, *J* = 13.9, 9.2, 7.1 Hz, 1H), 1.85 (dddd, *J* = 13.9, 9.8, 7.1, 3.0 Hz, 1H), 1.66 (ddt, *J* = 13.6, 9.0, 4.6 Hz, 1H), 1.46 (d, *J* = 4.7 Hz, 1H). ^{13}C NMR (101 MHz, $CDCl_3$) δ = 167.2, 157.7, 141.4, 138.8, 133.9, 129.4 (2C), 129.2 (2C), 128.6 (2C), 127.2, 126.1, 113.8 (2C), 72.0, 55.2, 52.6, 52.0, 37.3, 31.2.

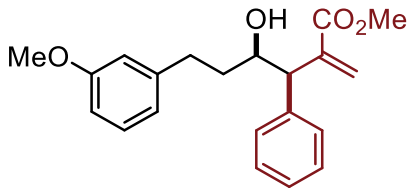

Methyl 4-hydroxy-6-(3-methoxyphenyl)-2-methylene-3-phenylhexanoate (3qa). Yield 56% (0.112 mmol, 38.1 mg). Pale yellow oil. $dr_{syn:anti}$ > 95:5 determined from ^{1}H NMR of the reaction crude by integration of the C-H in the benzylic position. **3qa** was obtained modifying the general procedure extending the reaction time from 16 to 48h, employing 0.2 mmol (32.8, 1 equiv.) of **1q** and 0.4 mmol (93.6 mg, 2.0 equiv.) of **2a.** The title compound was isolated by flash column chromatography (SiO_2, 60-30% Hexane in DCM).

^{1}H NMR (401 MHz, $CDCl_3$) δ = 7.29 (m, 4H), 7.25 – 7.22 (m, 1H), 7.20 – 7.14 (m, 1H), 6.78 – 6.69 (m, 3H), 6.32 (s, 1H), 5.75 (s, 1H), 4.13 (ddd, *J* = 9.3, 6.8, 2.9 Hz, 1H), 3.93 – 3.89 (m, 1H), 3.77 (s, 3H), 3.65 (s, 3H), 2.83 (ddd, *J* = 14.4, 9.7, 5.2 Hz, 1H), 2.67 (ddd, *J* = 13.7, 9.4, 7.0 Hz, 1H), 1.89 (dddd, *J* = 13.9, 9.9, 7.0, 3.0 Hz, 1H), 1.69 (ddt, *J* = 13.6, 9.0, 4.6 Hz, 1H). ^{13}C NMR (101 MHz, $CDCl_3$) δ = 167.2, 159.6, 143.6, 141.4, 138.8, 129.3, 129.2 (2C), 128.6 (2C), 127.2, 126.1, 120.9, 114.2, 111.1, 72.1, 55.1, 52.7, 52.0, 36.9, 32.3.

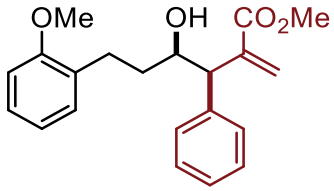

Methyl 4-hydroxy-6-(2-methoxyphenyl)-2-methylene-3-phenylhexanoate (3ra). Yield 60% (0.12 mmol, 40.8 mg). Pale yellow oil. $dr_{syn:anti}$ > 95:5 determined from ^{1}H NMR of the reaction crude by integration of the C-H in the benzylic position. **3ra** was obtained modifying the general procedure extending the reaction time from 16 to 48h, employing 0.2 mmol (32.8, 1 equiv.) of **1r** and 0.4 mmol (93.6 mg, 2.0 equiv.) of **2a.** The title compound was isolated by flash column chromatography (SiO_2, 60-30% Hexane in DCM).

^{1}H NMR (401 MHz, $CDCl_3$) δ = 7.30 – 7.09 (m, 7H, overlapped with the residual signal of the NMR solvent), 6.89 – 6.80 (m, 2H), 6.31 (s, 1H), 5.79 (s, 1H), 4.13 – 4.05 (m, 1H), 3.93 – 3.90 (m, 1H), 3.78 (s, 3H), 3.63 (s, 3H), 2.83 – 2.70 (m, 2H), 1.92 – 1.82 (m, 1H), 1.76 (s, 1H), 1.64 (qd, *J* = 8.6, 4.4 Hz, 1H). ^{13}C NMR (101 MHz, $CDCl_3$) δ = 167.2, 157.3, 141.7, 138.9, 130.1, 130.1, 129.3 (2C), 128.4 (2C), 127.1, 127.0, 126.0, 120.6, 110.3, 72.1, 55.3, 52.2, 51.9, 35.7, 26.6.

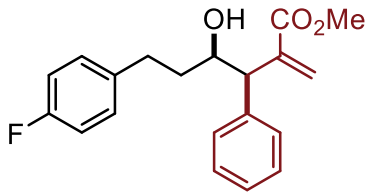

Methyl 6-(4-fluorophenyl)-4-hydroxy-2-methylene-3-phenylhexanoate (3sa). Yield 34% (0.07 mmol, 22.3 mg). Pale yellow oil. $dr_{syn:anti}$ = 84:16 determined from ^{19}F NMR of the reaction crude. **3sa** was obtained modifying the general procedure extending the reaction time from 16 to 48h, employing 0.2 mmol (30.4 mg, 1 equiv.) of **1s** and 0.4 mmol (93.6 mg, 2.0 equiv.) of **2a.** The title compound was isolated by flash column chromatography (SiO_2, 60-30% Hexane in DCM). Spectroscopical data are given only for the major diastereoisomer.

^{1}H NMR (401 MHz, $CDCl_3$) δ = 7.34 – 7.27 (m, 5H, overlapped with the residual signal of the NMR solvent), 7.14 – 7.09 (m, 2H), 6.97 – 6.91 (m, 2H), 6.32 (d, *J* = 0.8 Hz, 1H), 5.73 (s, 1H), 4.10 (ddd, *J* = 9.1, 7.0, 3.0 Hz, 1H), 3.91 (dd, *J* = 6.9, 1.0 Hz, 1H), 3.66 (s, 3H), 2.82 (ddd, *J* = 14.4, 9.5, 5.1 Hz, 1H), 2.72 – 2.63 (m, 1H), 1.86 (dddd, *J* = 13.9, 9.9, 7.2, 3.0 Hz, 1H), 1.72 – 1.60 (m, 1H). ^{13}C NMR (101 MHz, $CDCl_3$) δ = 167.1, 161.2 (d, *J* = 243 Hz), 141.3, 138.7, 137.5 (d, *J* = 3.3 Hz), 129.8, 129.7, 129.1 (2C), 129.0, 128.8, 128.7 (2C), 127.2, 126.1, 115.1, 114.9, 71.9, 52.7, 52.0, 37.1, 31.3. ^{19}F NMR (377 MHz, $CDCl_3$) δ = -116.6 (m, 1F).

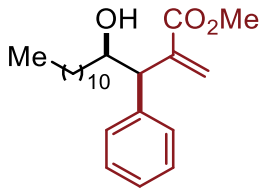

Methyl 4-hydroxy-2-methylene-3-phenylpentadecanoate (3ta). Yield 56% (0.112 mmol, 40.3 mg). Pale yellow oil. $dr_{syn:anti}$ > 95:5 determined from ^{1}H NMR of the reaction crude by integration of the C-H in the benzylic position. **3ta** was obtained modifying the general procedure extending the reaction time from 16 to 48h, employing 0.2 mmol (36.8, 44.3 µl, 1 equiv.) of **1t** and 0.4 mmol (93.6 mg, 2.0 equiv.) of **2a**. The title compound was isolated by flash column chromatography (SiO_2, 60-30% Hexane in DCM).

^{1}H NMR (401 MHz, $CDCl_3$) δ = 7.33 – 7.19 (m, 6H, overlapped with the residual signal of the NMR solvent), 6.35 (s, 1H), 5.87 (s, 1H), 4.12 (ddt, J = 8.3, 6.4, 3.3 Hz, 1H), 3.90 (d, J = 6.4 Hz, 1H), 3.67 (s, 3H), 1.53 – 1.23 (m, 20H), 0.86 (t, J = 6.8 Hz, 3H). ^{13}C NMR (101 MHz, $CDCl_3$) δ = 167.3, 141.7, 138.8, 129.3 (2C), 128.5 (2C), 127.1, 126.1, 72.8, 52.5, 52.0, 35.4, 31.9, 29.6, 29.6, 29.6, 29.5, 29.3, 25.9, 22.7, 21.5, 14.1.

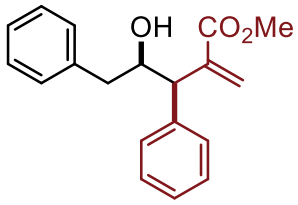

Methyl 4-hydroxy-2-methylene-3,5-diphenylpentanoate (3ua). Yield 49% (0.098 mmol, 29.0 mg). Pale yellow oil. $dr_{syn:anti}$ > 95:5 determined from ^{1}H NMR of the reaction crude by integration of the C-H in the benzylic position. **3ua** was obtained modifying the general procedure extending the reaction time from 16 to 48h, employing 0.2 mmol (24.0 mg , 22,3 µl, 1 equiv.) of **1u** and 0.4 mmol (93.6 mg, 2.0 equiv.) of **2a**. The title compound was isolated by flash column chromatography (SiO_2, 60-30% Hexane in DCM). Spectroscopical data are in accordance with the reported literature.[336]

^{1}H NMR (401 MHz, $CDCl_3$) δ = 7.37 – 7.28 (m, 5H), 7.27 – 7.17 (m, 5H, overlapped with the residual signal of the NMR solvent), 6.38 (s, 1H), 5.91 (s, 1H), 4.41 (td, *J* = 6.4, 3.4 Hz, 1H), 3.98 (d, *J* = 1.0 Hz, 1H), 3.68 (s, 3H), 2.90 (dd, *J* = 13.9, 3.5 Hz, 1H), 2.63 (dd, *J* = 13.9, 9.0 Hz, 1H), 1.58 (s, 1H). ^{13}C NMR (101 MHz, $CDCl_3$) δ = 167.2, 141.6, 138.7, 138.6, 129.4 (2C), 129.3 (2C), 128.5 (2C), 128.5 (2C), 127.1, 126.5, 126.4, 73.7, 52.3, 52.0, 41.9.

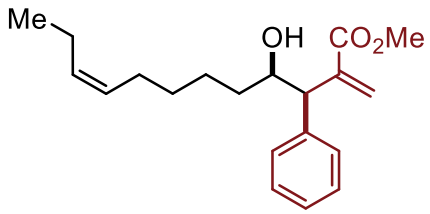

Methyl 4-hydroxy-2-methylene-3-phenyldodec-9-enoate (3va). Yield 68% (0.136 mmol, 42.9 mg). Pale yellow oil. $dr_{syn:anti}$ > 95:5 determined from ^{1}H NMR of the reaction crude by integration of the C-H in the benzylic position. **3va** was obtained modifying the general procedure extending the reaction time from 16 to 48h, employing 0.2 mmol (28.4 mg, 33.8 µl, 1 equiv.) of **1v** and 0.4 mmol (93.6 mg, 2.0 equiv.) of **2a.** The title compound was isolated by flash column chromatography (SiO_2, 60-30% Hexane in DCM).

^{1}H NMR (401 MHz, $CDCl_3$) δ = 7.32 – 7.28 (m, 4H, overlapped with the residual signal of the NMR solvent), 7.22 (ddt, *J* = 8.6, 3.6, 2.4 Hz, 1H), 6.34 (s, 1H), 5.86 (s, 1H), 5.40 – 5.22 (m, 2H), 4.15 – 4.08 (m, 1H), 3.89 (dd, *J* = 6.5, 1.0 Hz, 1H), 3.66 (s, 3H), 2.00 (qdd, *J* = 8.7, 4.6, 2.0 Hz, 4H), 1.61 – 1.25 (m, 7H), 0.92 (t, *J* = 7.6 Hz, 3H). ^{13}C NMR (101 MHz, $CDCl_3$) δ = 167.2, 141.7, 138.8, 131.7, 129.3 (2C), 128.9, 128.5 (2C), 127.1, 126.1, 72.7, 52.5, 52.0, 35.3, 29.6, 27.0, 25.6, 20.5, 14.4.

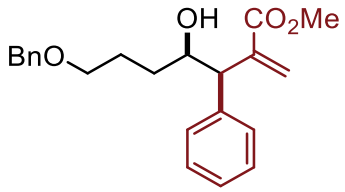

Methyl 7-(benzyloxy)-4-hydroxy-2-methylene-3-phenylheptanoate (3wa). Yield 49% (0.098 mmol, 34.7 mg). Pale yellow oil. $dr_{syn:anti}$ = 92:8 determined from ^{1}H NMR of the reaction crude by integration of the C-H in the benzylic position. **3wa** was obtained modifying the general procedure extending the reaction time from 16 to 48h, employing 0.2 mmol (35.6, 1 equiv.) of **1w** and 0.4 mmol (93.6 mg, 2.0 equiv.) of **2a.** The title compound was isolated by flash column chromatography (SiO_2, 60-30% Hexane in DCM). Spectroscopical data are given only for the major diastereoisomer.

^{1}H NMR (401 MHz, $CDCl_3$) δ = 7.33 – 7.21 (m, 10H, overlapped with the residual signal of the NMR solvent), 6.34 (s, 1H), 5.86 (s, 1H), 4.48 (s, 2H), 4.20 – 4.13 (m, 1H), 3.90 (d, *J* = 6.5 Hz, 1H), 3.67 (s, 3H), 3.47 (t, *J* = 5.9 Hz, 2H), 2.02 (d, *J* = 5.4 Hz, 1H), 1.74 (ddd, *J* = 12.4, 6.3, 4.4 Hz, 2H), 1.58 (m, 2H). ^{13}C NMR (101 MHz, $CDCl_3$) δ = 167.3, 141.7, 139.0, 138.3(2C), 129.3 (2C), 129.1(2C), 128.7(2C), 128.5, 128.3, 128.3, 127.6, 127.5, 127.5, 127.0, 126.1, 72.9, 72.5, 70.2, 52.6, 52.0, 32.5, 26.2.

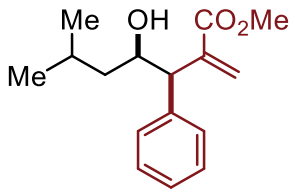

Methyl 4-hydroxy-6-methyl-2-methylene-3-phenylheptanoate (3xa). Yield 80% (0.160 mmol, 41.9 mg). Pale yellow oil. $dr_{syn:anti}$ > 95:5 determined from ^{1}H NMR of the reaction crude by integration of the C-H in the benzylic position. **3xa** was obtained modifying the general procedure extending the reaction time from 16 to 48h, employing 0.2 mmol (17.2, 21.4 µl, 1 equiv.) of **1x** and 0.4 mmol (93.6 mg, 2.0 equiv.) of **2a**. The title compound was isolated by flash column chromatography (SiO_2, 60-30% Hexane in DCM).

^{1}H NMR (401 MHz, $CDCl_3$) δ = 7.34 – 7.29 (m, 4H , overlapped with the residual signal of the NMR solvent), 6.36 (s, 1H), 5.87 (s, 1H), 4.24 – 4.16 (m, 1H), 3.86 (dd, *J* = 6.5, 1.1 Hz, 1H), 3.67 (s, 3H), 1.83 (tt,

J = 13.4, 6.7 Hz, 1H), 1.32 (dd, *J* = 7.9, 5.2 Hz, 2H), 0.91 (d, *J* = 3.6 Hz, 3H), 0.90 (d, *J* = 3.9 Hz, 3H). ^{13}C NMR (101 MHz, $CDCl_3$) δ = 167.2, 141.7, 138.9, 136.1, 129.3 (2C), 128.5 (2C), 127.1, 126.0, 70.8, 52.9, 52.0, 44.6, 24.7, 23.6.

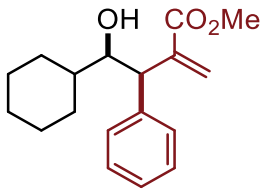

Methyl 4-cyclohexyl-4-hydroxy-2-methylene-3-phenylbutanoate (3ya). Yield 50% (0.100 mmol, 28.8 mg). Pale yellow oil. $dr_{syn:anti}$ = 92:8 determined from ^{1}H NMR of the reaction crude by integration of the C-H in the benzylic position. **3ya** was obtained modifying the general procedure extending the reaction time from 16 to 48h, employing 0.2 mmol (22.4, 24.2 µl, 1 equiv.) of **1y** and 0.4 mmol (93.6 mg, 2.0 equiv.) of **2a**. The title compound was isolated by flash column chromatography (SiO_2, 60-30% Hexane in DCM). Spectroscopical data are given only for the major diastereoisomer.

^{1}H NMR (401 MHz, $CDCl_3$) δ = 7.37 – 7.26 (m, 5H, overlapped with the residual signal of the NMR solvent), 7.23 (d, J = 9.1 Hz, 1H), 6.37 – 6.34 (m, 1H), 5.81 (s, 1H), 4.13 (d, J = 6.5 Hz, 1H), 3.88 (t, J = 6.0 Hz, 1H), 3.69 (s, 3H), 1.74 (s, 3H), 1.65 – 1.59 (m, 1H), 1.39 – 1.09 (m, 8H). ^{13}C NMR (101 MHz, $CDCl_3$) δ = 167.3, 141.7, 139.2, 129.4 (2C), 128.5 (2C), 127.0, 126.5, 76.8, 52.0, 49.0, 40.3, 30.3, 27.0, 26.4, 26.3, 26.0.

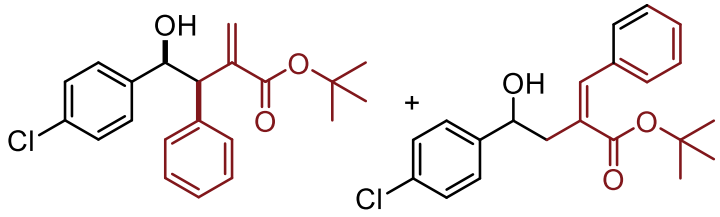

***Tert*-butyl-4-(4-chlorophenyl)-4-hydroxy-2-methylene-3-phenylbutanoate (3ae)** and ***tert*-butyl-2-benzylidene-4-(4-chlorophenyl)-4-hydroxybutanoate (3ae')**. Yield 81% (0.162 mmol, 57.9 mg) reported as sum of two regioisomers. Pale yellow oil. **3ae:3ae'** = 80:20. Regioisomeric ratio was determined ^{1}H NMR of the reaction crude by integration of the two different C-H in the benzylic position. **3ae, 3ae'** were obtained following the general procedure as stated above employing 0.2 mmol (28 mg, 1 equiv.) of **1a** and 0.44 mmol (121 mg, 2.2 equiv.) of **2e**. For **3ae**: $dr_{syn:anti}$ >95:5 determined from ^{1}H NMR of the reaction crude by integration of the C-H in the benzylic position. *E:Z* = 1.2:1 determined from ^{1}H NMR of the reaction crude by integration of the C-H in the benzylic position. The title compound was isolated by flash column chromatography (SiO_2, 60-30% Hexane in DCM). Spectroscopical data are given only for the major regioisomer.

^{1}H NMR (401 MHz, $CDCl_3$) δ = 7.43 – 7.17 (m, 9H overlapped with the residual peak of the NMR solvent), 6.17 (d, *J* = 1.0 Hz, 1H), 5.69 (t, *J* = 1.0 Hz, 1H), 5.26 (d, *J* = 7.4 Hz, 1H), 4.19 (d, *J* = 7.4 Hz, 1H), 1.31 (s, 9H). ^{13}C NMR (101 MHz, $CDCl_3$) δ = 165.7, 142.5, 141.5, 140.7, 138.5, 133.3, 129.2(2C), 129.0, 128.5(2C), 128.4, 128.4, 128.3(2C), 128.3 (2C), 127.2, 126.9, 126.0, 81.0, 75.0, 54.5, 27.8.

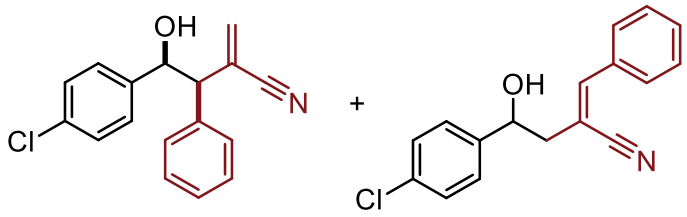

4-(4-chlorophenyl)-4-hydroxy-2-methylene-3-phenylbutanenitrile(3af) and **2-benzylidene-4-(4-chlorophenyl)-4-hydroxybutanenitrile (3af')**. Yield 67% (0.134 mmol, 37.9 mg) reported as sum of two regioisomers. Pale yellow oil. **3af:3af'** 65:35. Regioisomeric ratio was determined ^{1}H NMR of the reaction crude by integration of the two different C-H in the benzylic position. For **3af**: $dr_{syn:anti}$ = 94:6 determined from ^{1}H NMR of the reaction crude by integration of the C-H in the benzylic position. For **3af'**: *E*:*Z*= 1.2:1 determined from ^{1}H NMR of the reaction crude by integration of the C-H in the benzylic position. **3af, 3af'** were obtained following the general procedure as stated above employing 0.2 mmol (28 mg, 1 equiv.) of **1a** and 0.44 mmol (88.4 mg, 2.2 equiv.) of **2f**. The title compound was isolated by flash column chromatography (SiO_2, 60-30% Hexane in DCM). Spectroscopical data are given only for the major regioisomer.

^{1}H NMR (401 MHz, $CDCl_3$) δ = 7.43 – 7.05 (m, 9H overlapped with the residual peak of the NMR solvent and the other regioisomer), 6.00 (s, 1H), 5.96 – 5.92 (m, 1H), 5.15 (d, *J* = 9.4 Hz, 1H), 3.67 (d, *J* = 9.4 Hz, 1H). ^{13}C NMR (101 MHz, $CDCl_3$) δ = 147.0, 141.4, 139.9, 137.5, 128.8 (2C), 128.4 (2C), 128.0 (4C), 124.11, 118.35, 74.97, 58.0, 55.8.

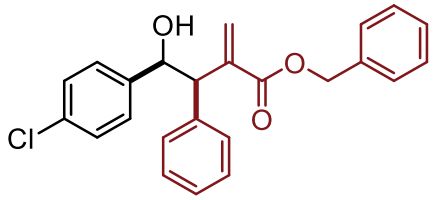

Benzyl-4-(4-chlorophenyl)-4-hydroxy-2-methylene-3-phenylbutanoate (3ag). Yield 65% (0.130 mmol, 51.0 mg). Pale yellow oil. $dr_{syn:anti}$ > 95:5 determined from ^{1}H NMR of the reaction crude by integration of the C-H in the benzylic position. **3ag** was obtained following the general procedure as stated above employing 0.2 mmol (28 mg, 1 equiv.) of **1a** and 0.44 mmol (124.8 mg, 2.2 equiv.) of **2g**. The title compound was isolated by flash column chromatography (SiO_2, 60-30% Hexane in DCM).

^{1}H NMR (401 MHz, $CDCl_3$) δ = 7.32 – 7.22 (m, 10H, overlapped with the residual signal of the NMR solvent), 6.31 (s, 1H), 5.83 (s, 1H), 5.29 (d, *J* = 7.7 Hz, 1H), 5.08 – 4.98 (m, 2H), 4.26 (d, *J* = 7.7 Hz, 1H). ^{13}C NMR (101 MHz, $CDCl_3$) δ = 166.2, 140.8, 140.1, 138.1, 135.6, 133.4, 129.2 (2C), 128.6 (2C), 128.6 (2C), 128.5 (2C), 128.4 (2C), 128.37, 128.3 (2C), 128.17, 128.14, 128.02, 127.97, 127.44, 127.39, 74.95, 66.65, 54.64.

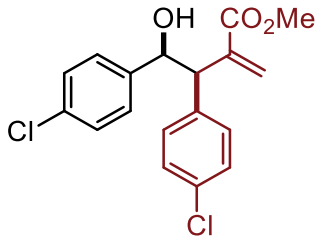

Methyl 3,4-bis(4-chlorophenyl)-4-hydroxy-2-methylenebutanoate (3aj). Yield 61% (0.122 mmol, 42.7.0 mg). Pale yellow oil. $dr_{syn:anti}$ > 95:5 determined from ^{1}H-NMR of the reaction crude by integration of the C-H in the benzylic position. **3aj** was obtained following the general procedure as stated above

employing 0.2 mmol (28 mg, 1 equiv.) of **1a** and 0.44 mmol (117.9 mg, 2.2 equiv.) of **2j**. The title compound was isolated by flash column chromatography (SiO_2, 60-30% Hexane in DCM).

^{1}H NMR (401 MHz, $CDCl_3$) δ = 7.32 – 7.12 (m, 8H overlapped with the residual peak of the NMR solvent), 6.25 (s, 1H), 5.80 (s, 1H), 5.26 (d, *J* = 7.1 Hz, 1H), 4.17 (d, *J* = 7.1 Hz, 1H), 3.61 (s, 3H). ^{13}C NMR (101 MHz, $CDCl_3$) δ = 166.8, 140.6, 140.5, 136.6 (2C), 133.5(2C), 133.1(2C), 130.7(2C), 128.6, 128.4, 128.1, 127.4, 74.7, 53.9, 52.0.

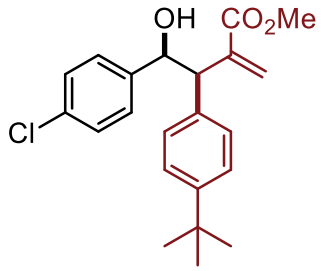

Methyl 3-(4-(*tert*-butyl)phenyl)-4-(4-chlorophenyl)-4-hydroxy-2-methylenebutanoate (3ak). Yield 49% (0.098 mmol, 36.5.0 mg). Pale yellow oil. $dr_{syn:anti}$ = 94:6 determined from ^{1}H NMR of the reaction crude by integration of the two C-H in the benzylic position. **3ak** was obtained following the general procedure as stated above employing 0.2 mmol (28 mg, 1 equiv.) of **1a** and 0.44 mmol (127.9 mg, 2.2 equiv.) of **2k.** The title compound was isolated by flash column chromatography (SiO_2, 60-30% Hexane in DCM). Spectroscopical data are given only for the major diastereoisomer.

^{1}H NMR (401 MHz, $CDCl_3$) δ = 7.34 (m, 2H), 7.25 (m, 6H overlapped with the residual peak of NMR solvent), 6.29 (s, 1H), 5.74 (s, 1H), 5.23 (d, *J* = 8.4 Hz, 1H), 4.22 (d, *J* = 8.4 Hz, 1H), 3.58 (s, 3H), 1.30 (s, 9H). ^{13}C NMR (101 MHz, $CDCl_3$) δ = 166.9, 150.3, 140.9, 140.5, 135.1, 133.4, 128.6 (2C), 128.5 (2C), 128.4 (2C), 126.9, 125.7 (2C), 75.3, 54.3, 51.9, 34.5, 31.3 (3C).

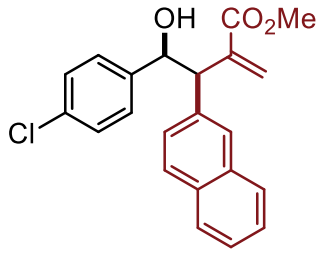

Methyl-4-(4-chlorophenyl)-4-hydroxy-2-methylene-3-(naphthalen-2-yl)butanoate (3al). Yield 51% (0.102 mmol, 37.3 mg). Pale yellow oil. $dr_{syn:anti}$ > 95:5 determined from ^{1}H NMR of the reaction crude by integration of the two C-H in the benzylic position. **3al** was obtained modifying the general procedure extending the reaction time from 16h to 48h, employing 0.2 mmol (28 mg, 1 equiv.) of **1a** and 0.4 mmol (113.6 mg, 2.0 equiv.) of **2l**. The title compound was isolated by flash column chromatography (SiO_2, 60-30% Hexane in DCM).

^{1}H NMR (401 MHz, $CDCl_3$) δ = 7.80 (d, *J* = 7.0 Hz, 4H), 7.48 – 7.36 (m, 3H), 7.26 (s, 4H overlapped with the residual peak of NMR solvent), 6.29 (s, 1H), 5.86 (s, 1H), 5.36 (d, *J* = 7.6 Hz, 1H), 4.42 (d, *J* = 7.7 Hz, 1H), 3.58 (s, 3H). ^{13}C NMR (101 MHz, $CDCl_3$) δ = 166.9, 140.8, 140.5, 135.7, 133.5, 133.4, 132.7, 128.4 (2C), 128.3(2C), 128.3, 128.0, 127.9, 127.6, 127.2, 126.2, 126.0, 75.0, 54.5, 52.0.

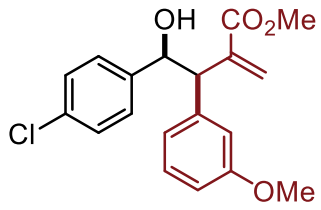

Methyl 4-(4-chlorophenyl)-4-hydroxy-3-(3-methoxyphenyl)-2-methylenebutanoate (3am). Yield 60% (0.120 mmol, 41.5 mg). Pale yellow oil. $dr_{syn:anti}$ > 95:5 determined from ^{1}H NMR of the reaction crude by integration of the two C-H in the benzylic position. **3am** was obtained modifying the general procedure extending the reaction time from 16h to 48h, employing 0.2 mmol (28 mg, 1 equiv.) of **1a** and 0.4 mmol (105.0 mg, 2.0 equiv.) of **2m**. The title compound was isolated by flash column chromatography (SiO_2, in DCM).

^{1}H NMR (401 MHz, $CDCl_3$) δ = 7.28 – 7.22 (m, 5H overlapped with the residual peak of NMR solvent), 6.93 – 6.81 (m, 3H), 6.25 (s, 1H), 5.80 (s, 1H), 5.25 (d, *J* = 7.8 Hz, 1H), 4.23 (d, *J* = 7.9 Hz, 1H), 3.78 (s, 3H), 3.60 (s, 3H). ^{13}C NMR (101 MHz, $CDCl_3$) δ = 167.2, 160.0, 141.0, 140.8, 140.1, 133.7, 129.9 (2C), 128.7(2C), 128.6, 127.4, 121.6, 115.3, 112.97, 75.3, 55.4, 54.8, 52.3.

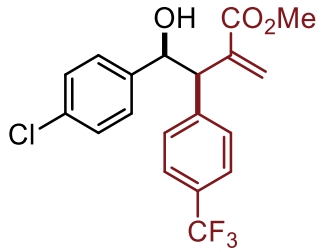

Methyl 4-(4-chlorophenyl)-4-hydroxy-2-methylene-3-(4-(trifluoromethyl)phenyl)butanoate (3an). Yield 50% (0.100 mmol, 38,4.0 mg). Pale yellow oil. $dr_{syn:anti}$ = 95:5 determined from ^{19}F NMR of the reaction crude. **3an** was obtained following the general procedure as stated above employing 0.2 mmol (28 mg, 1 equiv.) of **1a** and 0.4 mmol (120.9 mg, 2.0 equiv.) of **2n**. The title compound was isolated by flash column chromatography (SiO_2, 50%– 30% Hexane in DCM). Spectroscopical data are given only for the major diastereoisomer.

^{1}H NMR (401 MHz, $CDCl_3$) δ = 7.56 (d, *J* = 8.1 Hz, 2H), 7.43 (d, *J* = 8.1 Hz, 2H), 7.32 – 7.10 (m, 5H overlapped with the residual peak of the NMR solvent), 6.30 (s, 1H), 5.84 (s, 1H), 5.35 (dd, *J* = 7.2, 3.3 Hz, 1H), 4.28 (d, *J* = 7.1 Hz, 1H), 3.63 (s, 3H). ^{13}C NMR (101 MHz, $CDCl_3$) δ = 166.66, 142.51, 140.44, 140.32, 133.68, 129.67, 128.51 (2C), 128.06 (2C), 127.92, 127.78, 125.26 (q, *J* = 3.8 Hz), 74.66, 54.36, 52.07. ^{19}F NMR (377 MHz, $CDCl_3$) δ = -62.54 (m, 3F).

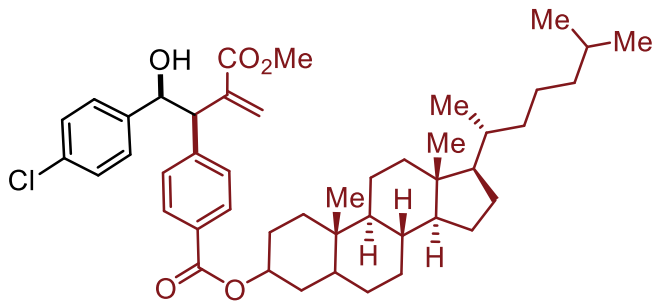

(8*R*,9*S*,10*S*,13*R*,14*S*,17*R*)-10,13-dimethyl-17-((*R*)-6-methylheptan-2-yl)hexadecahydro-1*H*-cyclopenta[*a*]phenanthren-3-yl 4-(1-(4-chlorophenyl)-1-hydroxy-3-(methoxycarbonyl)but-3-en-2-yl)benzoate (3ao). Yield 41% (0.082 mmol, 59.9 mg). White solid. $dr_{syn:anti}$ = 96:4 determined from ^{1}H

NMR of the reaction crude by integration of two C-H in the benzylic positions. **3ao** was obtained following the general procedure as stated above employing 0.2 mmol (28 mg, 1 equiv.) of **1a** and 0.4 mmol (256.0 mg, 2.0 equiv.) of **2o**. The title compound was isolated by two consecutive flash column chromatography (SiO_2, 1st 50%– 30% Hexane in DCM, 2nd 0%– 30% Et_2O in Hexane). Spectroscopical data are given only for the major diastereoisomer.

^{1}H NMR (401 MHz, $CDCl_3$) δ = 7.96 (m, 2H), 7.36 (m, 2H), 7.27 (m, 3H), 7.21 (m 2H), 6.30 (s, 1H), 5.84 (s, 1H), 5.34 (d, *J* = 7.1 Hz, 1H), 4.96 – 4.91 (m, 1H), 4.29 (d, *J* = 7.1 Hz, 1H), 3.62 (s, 3H), 2.04 – 1.89 (m, 3H), 1.88 – 1.75 (m, 3H), 1.59 (m, 11H), 1.39 – 1.23 (m, 14H), 1.16 – 0.99 (m, 11H), 0.92 (m, 5H). ^{13}C NMR (101 MHz, $CDCl_3$) δ = 166.7, 165.9, 143.3, 140.5, 140.4, 133.6, 129.9, 129.6 (2C), 129.3 (2C), 128.4(2C), 128.1 (2C), 127.6, 74.7, 74.4, 56.4, 56.3, 54.5, 54.2, 52.0, 44.7, 42.6, 39.9, 39.5, 36.8, 36.2, 35.8, 35.5, 34.1, 32.0, 28.6, 28.2, 28.0, 27.6, 24.2, 23.8, 22.8, 22.5, 21.2, 18.7, 12.2, 12.1.

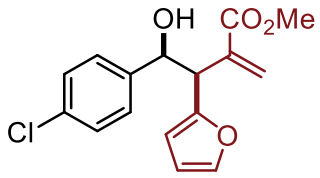

Methyl 4-(4-chlorophenyl)-3-(furan-2-yl)-4-hydroxy-2-methylenebutanoate (3ap). Yield 58% (0.116 mmol, 35.5 mg). Pale yellow oil. $dr_{syn:anti}$ > 95:5 determined from ^{1}H NMR of the reaction crude by integration of the C-H in the benzylic position. **3ap** was obtained following the general procedure as stated above employing 0.2 mmol (28 mg, 1 equiv.) of **1a** and 0.44 mmol (98.5 mg, 2.2 equiv.) of **2p**. The title compound was isolated by flash column chromatography (SiO_2, 60%– 30% Hexane in DCM).

^{1}H NMR (401 MHz, $CDCl_3$) δ = 7.37 (m, 1H), 7.29 – 7.16 (m, 4H overlapped with the residual peak of NMR solvent), 6.35 – 6.29 (m, 2H), 6.22 (d, *J* = 3.2 Hz, 1H), 5.78 (s, 1H), 5.15 (d, *J* = 6.7 Hz, 1H), 4.40 (d, *J* = 6.6 Hz, 1H), 3.66 (s, 3H). ^{13}C NMR (101 MHz, $CDCl_3$) δ = 167.0, 152.4, 142.4, 140.2, 138.5, 133.6, 128.8, 128.5 (2C), 128.3(2C), 110.7, 108.9, 75.2, 52.4, 48.7.

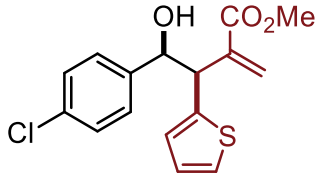

Methyl 4-(4-chlorophenyl)-4-hydroxy-2-methylene-3-(thiophen-2-yl)butanoate (3aq). Yield 77% (0.154 mmol, 49.6 mg). Pale yellow oil. $dr_{syn:anti}$ > 95:5 determined from ^{1}H NMR of the reaction crude by integration of the C-H in the benzylic position. **3aq** was obtained modifying the general procedure extending the reaction time from 16h to 48h, employing 0.2 mmol (28 mg, 1 equiv.) of **1a** and 0.4 mmol (96.5 mg, 2.0 equiv.) of **2q**. The title compound was isolated by flash column chromatography (SiO_2, 50%– 30% Hexane in DCM).

^{1}H NMR (401 MHz, $CDCl_3$) δ = 7.26 (m, 4H overlapped with the residual peak of NMR solvent), 7.22 (m, 1H), 6.99 – 6.95 (m, 2H), 6.29 (s, 1H), 5.83 (s, 1H), 5.20 (d, *J* = 6.7 Hz, 1H), 4.53 (d, *J* = 6.7 Hz, 1H), 3.69 (s, 3H). ^{13}C NMR (101 MHz, $CDCl_3$) δ = 166.8, 140.7, 140.4, 140.0, 133.4, 128.3 (2C), 128.1 (2C), 128.0, 127.0, 126.8, 125.2, 75.5, 52.1, 50.7.

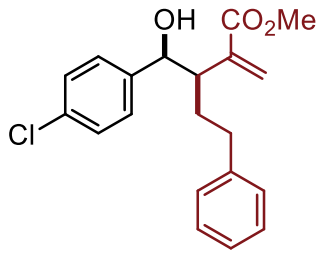

Methyl (4-chlorophenyl)(hydroxy)methyl)-2-methylene-5-phenylpentanoate (3ar). Yield 29% (0.058 mmol, 19.9 mg). Pale yellow oil. $dr_{syn:anti}$= 88:12 determined from ^{1}H NMR of the reaction crude by integration of the C-H in the benzylic position. **3ar** was obtained following the general procedure as stated above employing 0.2 mmol (28 mg, 1 equiv.) of **1a** and 0.4 mmol (104.8 mg, 2.0 equiv.) of **2r**. The title compound was isolated by flash column chromatography (SiO_2, 50%–30% Hexane in DCM). Spectroscopical data are given only for the major diastereoisomer.

^{1}H NMR (401 MHz, $CDCl_3$) δ = 7.31 – 7.09 (m, 7H overlapped with the residual peak of the NMR solvent), 7.11 – 6.80 (m, 2H), 6.29 (d, *J* = 1.0 Hz, 1H), 5.47 (s, 1H), 4.95 – 4.72 (m, 1H), 3.75 (s, 3H), 2.94 (dt, *J* = 10.9, 4.2 Hz, 1H), 2.55 (ddd, *J* = 14.6, 10.1, 4.9 Hz, 1H), 2.36 (ddd, *J* = 13.9, 9.9, 7.0 Hz, 1H), 1.94 (dtd, *J* = 13.7, 6.8, 3.6 Hz, 1H), 1.83 (ddt, *J* = 14.0, 9.7, 5.2 Hz, 1H). ^{13}C NMR (101 MHz, $CDCl_3$) δ = 168.4, 141.7, 140.9, 140.0, 132.9, 128.3 (2C), 128.3(2C), 128.1(2C), 127.8(2C), 127.7, 125.8, 75.6, 52.2, 49.1, 33.5, 29.0.

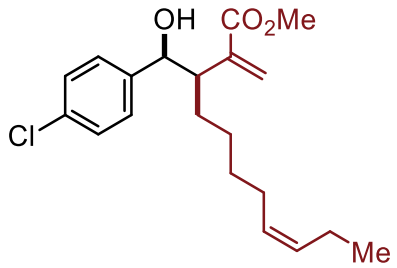

Methyl (*Z*)-3-((4-chlorophenyl)(hydroxy)methyl)-2-methyleneundec-8-enoate (3as). Yield 26% (0.052 mmol, 18.0 mg). Pale yellow oil. $dr_{syn:anti}$> 95:5 determined from ^{1}H NMR of the reaction crude by integration of the C-H in the benzylic position. **3as** was obtained following the general procedure as stated above employing 0.2 mmol (28 mg, 1 equiv.) of **1a** and 0.4 mmol (107.2 mg, 2.0 equiv.) of **2s**. The title compound was isolated by flash column chromatography (SiO_2, 50%– 30% Hexane in DCM).

^{1}H NMR (401 MHz, $CDCl_3$) δ = 7.80 (m, 1H), 7.72 – 7.68 (m, 2H), 7.64 (m, 1H), 7.57 – 7.40 (m, 3H), 7.32 – 7.04 (m, 12H overlapped with the residual peak of the nmr solvent), 5.31 (d, *J* = 8.0 Hz, 1H), 3.49 (d, *J* = 1.6 Hz, 3H), 3.41 (dd, *J* = 7.8, 5.8 Hz, 1H), 3.29 – 3.22 (m, 1H), 3.08 (m, 1H), 3.00 (dt, *J* = 8.3, 6.0 Hz, 1H). ^{13}C NMR (101 MHz, $CDCl_3$) δ = 172.9, 140.4, 136.6, 133.6, 133.4, 132.2, 131.9, 129.4 (2C), 128.6, 128.4 (2C), 128.3, 128.3 (2C), 128.2 (2C), 127.9, 127.7(2C), 127.7, 127.1, 126.6, 126.0, 73.7, 54.2, 51.6, 46.7, 34.1.

Post-functionalizations of the standard product 3aa

Synthesis of Methyl-4-((tert-butyldimethylsilyl)oxy)-4-(4-chlorophenyl)-2-methylene-3-phenylbutanoate (4a)

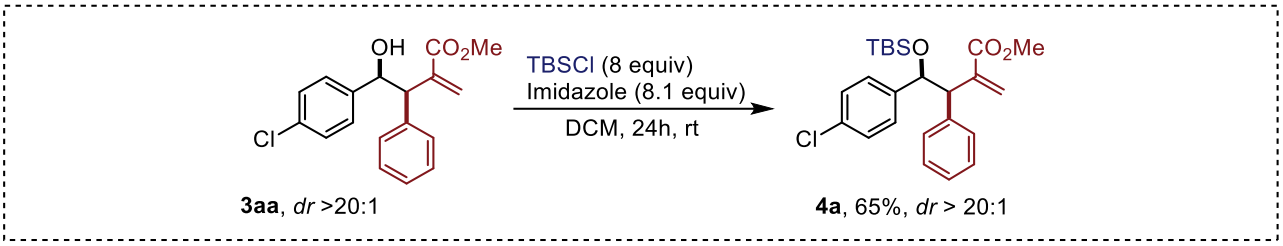

3aa, *dr* >20:1 **4a**, 65%, *dr* > 20:1

Product **4a** was synthetized according to a slightly modified procedure reported by the Nicponski group.[323] In a one-necked 5 mL round bottom flask equipped with a magnetic stirring bar, methyl 4-(4-chlorophenyl)-4-hydroxy-2-methylene-3-phenylbutanoate (**3aa**) (31.6 mg, 0.1 mmol, 1 equiv.) was dissolved in 2 mL of reagent-grade DCM. Imidazole (37 mg, 0.55 mmol, 5.5 equiv.) was then added to the reaction mixture. Finally, while stirring, TBSCl (81 mg, 0.44 mmol, 4.4 equiv.) were added to the solution. The reaction was allowed to stir at room temperature and after 2 hours was monitored by TLC analysis (eluent 10% EtOAc in Hexane). Showing a non-total conversion of the starting material, the reaction mixture was charged with 0.26 mmol (17.5 mg, 2.6 equiv.) of imidazole and 0.36 mmol (66 mg, 3.6 equiv.) of TBSCl and was allowed to stir overnight. After 24h TLC analysis showed a complete conversion of the starting material. The reaction was quenched with water (*ca.* 5ml) and extracted with DCM (3x *ca.* 5mL). The organic phase was dried over Na_2SO_4 and the solvent was removed under vacuum. Product **4a** was isolated as a white solid after flash chromatography (SiO_2, 5-15% EtOAc in Hexane) in 65% yield (28.0 mg, 0.065 mmol).

^{1}H NMR (401 MHz, $CDCl_3$) δ = 7.50 – 7.35 (m, 2H), 7.35 – 7.23 (m, 7H overlapped with the residual peak of the NMR solvent), 6.31 (s, 1H), 5.75 (t, *J* = 1.1 Hz, 1H), 5.30 (d, *J* = 7.0 Hz, 1H), 4.22 (d, *J* = 6.9 Hz, 1H), 3.74 (s, 3H), 0.79 (s, 9H), -0.14 (s, 3H), -0.27 (s, 3H). ^{13}C NMR (101 MHz, $CDCl_3$) δ = 167.3, 142.1, 140.7, 139.3, 132.7, 129.9 (2C), 128.4 (2C), 127.9 (4C), 127.5, 126.7, 76.0, 55.9, 51.9, 25.6, 17.9, -4.7, -5.5.

Synthesis of 5-(4-chlorophenyl)-4-phenyl-3-(piperidin-1-ylmethyl)dihydrofuran-2(3H)-one (4b)

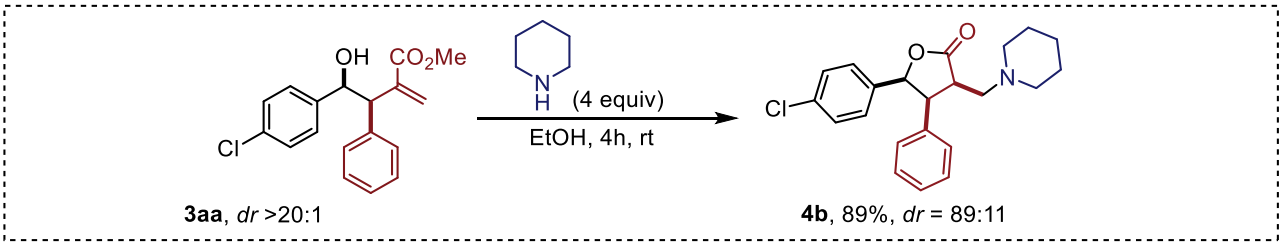

3aa, *dr* >20:1 **4b**, 89%, *dr* = 89:11

Product **4b** was synthetized according to a slightly modified procedure reported by the Nicponski group.[323] In a one-necked 5 mL round bottom flask equipped with a magnetic stirring bar, methyl -4-(4-chlorophenyl)-4-hydroxy-2-methylene-3-phenylbutanoate (**3aa**) (31.6 mg, 0.1 mmol, 1 equiv.) was dissolved in 1 mL of reagent-grade EtOH (to obtain [**3aa**] = 0.1 M). To the solution, piperidine (39.5 µl, 0.4 mmol, 4 equiv.) was added and the reaction was allowed to stir for 4h at room temperature. The reaction crude was monitored by TLC analysis and, upon confirming the complete conversion of the starting material, it was quenched with water (*ca.* 1ml). The reaction was extracted with Et_2O (3x *ca.* 5ml), dried over Na_2SO_4 and the solvent was removed under vacuum. The product **4b** was isolated without further purification as a white solid in 89% yield (32.8 mg, 0.089 mmol, *dr* = 89:11). Spectroscopical data are given only for the major diastereoisomer.

^{1}H NMR (401 MHz, $CDCl_3$) δ = 7.16 – 7.02 (m, 7H), 6.87 (dd, *J* = 6.7, 2.9 Hz, 2H), 5.78 (d, *J* = 5.2 Hz, 1H), 4.07 (dd, *J* = 7.5, 5.2 Hz, 1H), 3.43 (td, *J* = 8.2, 3.8 Hz, 1H), 2.72 (dd, *J* = 13.4, 3.8 Hz, 1H), 2.37 (br s, 2H), 2.19 (m, 1H), 2.08 (m, 2H), 1.50 (m, 4H), 1.38 (m, 2H), 1.26 (m,1H). ^{13}C NMR (101 MHz, $CDCl_3$) δ = 177.5, 134.4, 134.4, 133.1, 129.4 (2C), 129.1, 128.2, 128.2, 127.3 (2C), 126.8 (2C), 82.3, 54.6, 54.4 (2C), 51.9, 45.9, 26.0 (2C), 24.1.

Synthesis of Methyl 4-(4-chlorophenyl)-4-hydroxy-2-((naphthalen-2-ylthio)methyl)-3-phenylbutanoate (4c)

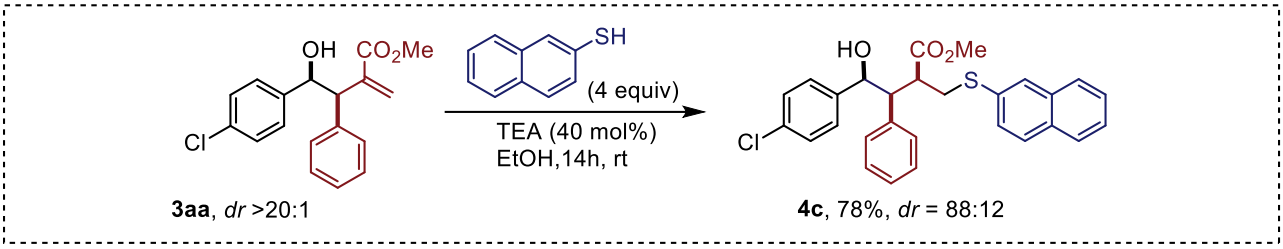

3aa, *dr* >20:1 **4c**, 78%, *dr* = 88:12

Product **4c** was synthetized applying standard conditions for sulfa-Micheal reaction.[337] In a one-necked 5 mL round bottom flask equipped with a magnetic stirring bar, methyl 4-(4-chlorophenyl)-4-hydroxy-2-methylene-3-phenylbutanoate (**3aa**) (31.6 mg, 0.1 mmol, 1 equiv.) was dissolved in 1 mL of reagent-grade EtOH (to obtain [**3aa**] = 0.1 M). To the solution, 2-thionaphtol (63.6 mg, 0.4 mmol, 4 equiv.) and triethylamine (6 µL, 0.02 mmol, 0.4 equiv.) were added, and the reaction was allowed to stir for 14h at room temperature. The reaction crude was monitored by TLC analysis and, upon confirming a complete conversion of the starting material, it was quenched with water (*ca.* 1ml). The reaction was extracted with Et_2O (3x *ca.* 5ml), dried over Na_2SO_4 and the solvent was removed under vacuum. The product **4c** was isolated without further purification as a white solid in 78% yield (37.2 mg, 0.078 mmol, *dr* = 88:12). Spectroscopical data are given only for the major diastereoisomer.

^{1}H NMR (401 MHz, $CDCl_3$) δ = 7.80 (m, 1H), 7.72 – 7.68 (m, 2H), 7.64 (m, 1H), 7.57 – 7.40 (m, 3H), 7.32 – 7.04 (m, 12H overlapped with the residual peak of the nmr solvent), 5.31 (d, *J* = 8.0 Hz, 1H), 3.49 (d, *J* = 1.6 Hz, 3H), 3.41 (dd, *J* = 7.8, 5.8 Hz, 1H), 3.29 – 3.22 (m, 1H), 3.08 (m, 1H), 3.00 (dt, *J* = 8.3, 6.0 Hz, 1H). ^{13}C NMR (101 MHz, $CDCl_3$) δ = 172.9, 140.4, 136.6, 133.6, 133.4, 132.2, 131.9, 129.4 (2C), 128.6, 128.4 (2C), 128.3, 128.3 (2C), 128.2 (2C), 127.9, 127.7(2C), 127.7, 127.1, 126.6, 126.0, 73.7, 54.2, 51.6, 46.7, 34.1.

Computational Methodology

Computations were carried out employing density functional theory (DFT) implemented in the Gaussian 16 suite of programs.[338] Geometry optimizations were carried out in tetrahydrofuran solvent (ε = 7.426) by a self-consistent reaction field (SCRF) approach using the SMD continuum solvation model[339] with the Perdew–Burke–Ernzerhof (PBE) exchange-correlation functional[340] including the Grimme's D3 empirical dispersion correction.[341] For geometry optimizations, we used Ahlrichs' split valence plus polarization basis set (def2-SVP)[342] for all the atoms except for nickel which was treated with Ahlrichs' triple-ζ valence plus polarization basis set (def2-TZVP).[342,343] No symmetry constraints were imposed during structural optimizations. The frequency analyses were executed on the optimized geometries at the same level to ascertain the nature of stationary points on the potential energy surface either as minima or the transition states characterized by first-order saddle points and also to obtain the thermochemical energy values. The minima were identified by having a full set of real frequencies, whereas the transition states possess only one imaginary frequency. The transition states were searched using the linear *synchronous* transit (LST) method,[344] and subsequent optimizations were performed by utilizing the default Berny algorithm, implemented in the Gaussian 16 code. Intrinsic reaction coordinate (IRC) calculations were enforced to ensure that the transition state connects the

corresponding real minima.[345] Furthermore, to improve the accuracy of the energies obtained from the PBE-D3(SMD,THF)/def2-TZVP(Ni)/def2-SVP level of theory, single-point calculations were performed on the optimized geometries with the M06 meta-hybrid functional[346] functional employing the def2-TZVPP basis set[342,343] for all the atoms. Similar to geometry optimizations, solvation energies in tetrahydrofuran solvent were evaluated using the SMD continuum solvation model. All the energy values (ΔG) presented herein were obtained at the M06(SMD,THF)/def2-TZVPP//PBE-D3(SMD,THF)/def2-TZVP(Ni)/def2-SVP level. To enrich our understanding toward the origin of activation barriers, distortion–interaction analysis was performed.[329,330] The distortion–interaction model allows for partitioning the activation barrier ($\Delta^{\ddagger}E$) of a transition state into destabilizing distortion energy ($\Delta^{\ddagger}E_{dist}$) and stabilizing interaction ($\Delta^{\ddagger}E_{int}$) energy terms. All the intermediates and transition states were reported in their most stable ground electronic states. Activation energy barriers ($\Delta G^{\ddagger}_{MH}$) of single electron transfer (SET) steps were estimated using the Marcus–Hush theory.[326,327,347] Tight wave function convergence criteria and "ultrafine" (99,950) grid were used in numerical integration during all theoretical calculations.

Estimation of energy barriers of single electron transfer steps using Marcus–Hush theory.

Applying the Marcus–Hush theory of electron transfer, the free energy barrier (ΔG‡MH) of a singlet electron transfer process can be estimated according to the following equation (19):

$$\Delta G^{\ddagger}_{\mathrm{MH}} = \frac{(\Delta G_r + \lambda)^2}{4\lambda} \tag{19}$$

where ΔG_r is the free energy change of the step, λ is the reorganization energy, which has two components, inner sphere and outer sphere. However, the first one is considered to be neglected, and hence, the total λ will the outer sphere reorganization energy, which can be calculated by the equation (20):

$$\lambda = \lambda_{\mathrm{outer}} = (332\ \mathrm{kcal/mol})\left(\frac{1}{2a_1} + \frac{1}{2a_2} - \frac{1}{\mathrm{R}}\right)\left(\frac{1}{\varepsilon_{\mathrm{opt}}} - \frac{1}{\varepsilon}\right) \tag{20}$$

where a_1 and a_2 are the radii of donor and acceptor, respectively. R is the sum of a_1 and a_2. ε_{opt} and ε are the optical dielectric constant (ε_{opt} = 1.974) and static dielectric constant (ε = 7.426) of tetrahydrofuran solvent, respectively.

SET	a_1 (Å)	a_2 (Å)	R (Å)	λ	ΔGr	$\Delta G^{\ddagger}_{MH}$
SET1	8.09	5.05	13.14	10.46	-26.6	6.2
SET2	8.09	4.63	12.72	11.26	-17.4	0.8
SET3	8.09	6.00	14.09	9.16	-23.4	5.5

Table 5.8 Calculated free energy barriers ($\Delta G^{\ddagger}_{MH}$) of single electron transfer (SET) steps and their relevant parameters.

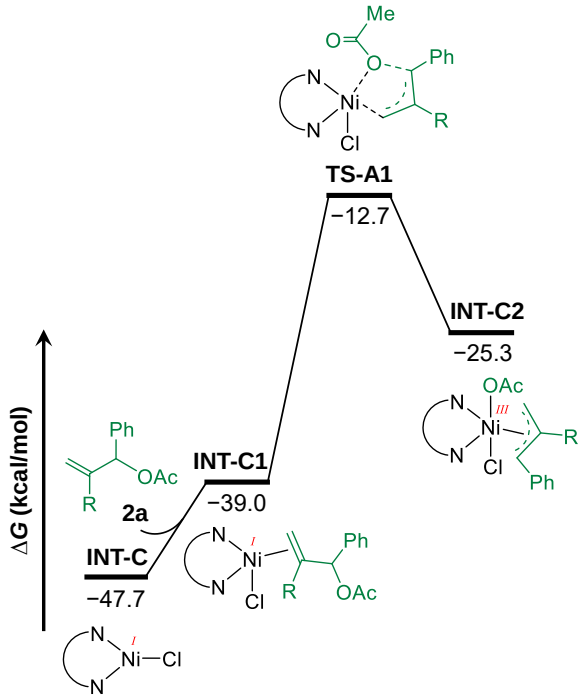

Figure 5.29 Free energy profile for the oxidative addition of ***2a*** to the Ni(I) species INT-C.

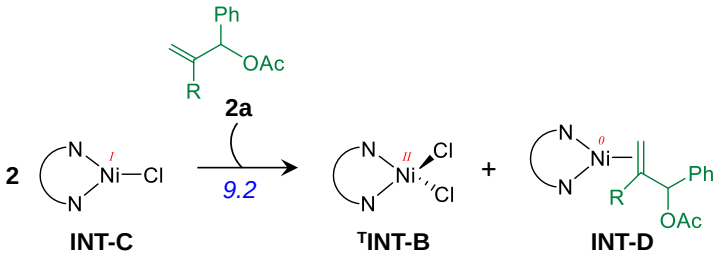

Figure 5.30 Energetics for the generation of Ni(0) species (INT-D) from INT-C via disproportionation reaction.

Species	E	Gcorr	G	No. of imaginary frequency
TNiCl$_2$(Glyme)	-2737.60740109	0.099836	-2737.5075650900	0
L1	-571.393997335	0.130996	-571.2630013350	0
TINT-A	-3309.04895633	0.257262	-3308.7916943300	0
Glyme	-308.785426641	0.103860	-308.6815666410	0
TINT-B	-3000.24659621	0.126031	-3000.1205652100	0
[3DPAFIPN · HE]$^{\bullet-}$	-2929.96755520	0.799848	-2929.1677072000	0
[3DPAFIPN · HE]	-2929.86542870	0.797991	-2929.0674377000	0
HE	-862.288834823	0.248015	-862.0408198230	0
HE•+	-862.092482878	0.247219	-861.8452638780	0
HE•+/Cl−	-1322.47366118	0.241962	-1322.2316991800	0
INT-C	-2540.00446800	0.127640	-2539.8768280000	0

2a	-804.512166387	0.190515	-804.3216513870	0
INT-D	-2884.28699880	0.346953	-2883.9400458000	0
INT-C1	-3344.53173710	0.347180	-3344.1845571000	0
TS-A1	-3344.48750199	0.344881	-3344.1426209900	1
INT-C2	-3344.50720939	0.344534	-3344.1626753900	0
TS-A	-2884.24885586	0.344845	-2883.9040108600	1
TINT-E	-2884.29307368	0.343784	-2883.9492896800	0
HE•+/AcO−	-1090.72138091	0.285554	-1090.4358269100	0
INT-F	-2655.79682175	0.300507	-2655.4963147500	0
1a	-805.059335325	0.064686	-804.9946493250	0
TS-B	-3460.86164164	0.390629	-3460.4710126400	1
TS-B1	-3460.84303277	0.387911	-3460.4551217700	1
INT-G	-3460.88472547	0.390259	-3460.4944664700	0
TINT-H	-4551.64323563	0.705063	-4550.9381726300	0
TTS-C	-4551.60735192	0.702025	-4550.9053269200	1
HP	-861.096087758	0.226952	-860.8691357580	0
AcOH	-229.066201523	0.032578	-229.0336235230	0
INT-I	-3461.50156900	0.404282	-3461.0972870000	0
3aa	-1381.72320434	0.247840	-1381.4753643400	0

Table 5.9 Absolute energies (in hartree) of all the intermediates and transition states at 298.15 K. E = electronic energy at the M06(SMD,THF)/def2-TZVPP//PBE-D3(SMD,THF)/def2-TZVP(Ni)/def2-SVP level, Gcorr = thermal correction to Gibbs free energy at the PBE-D3(SMD,THF)/def2-TZVP(Ni)/def2-SVP level, and G = Gibbs free energy at the M06(SMD,THF)/def2-TZVPP//PBE-D3(SMD,THF)/def2-TZVP(Ni)/def2-SVP level.

$^{T}NiCl_2$(Glyme)			
Charge = 0; Spin multiplicity = 3			
Ni	-0.036593000	-0.607783000	0.013895000
C	-0.587302000	2.210813000	0.126886000
H	-1.179640000	2.270176000	-0.814093000
H	-0.784253000	3.118796000	0.737215000
C	0.887363000	2.092166000	-0.170796000
H	1.484456000	2.044889000	0.767630000
H	1.226735000	2.961641000	-0.774550000
O	1.064551000	0.878613000	-0.924304000
C	2.429788000	0.600885000	-1.272698000
H	3.050868000	0.456725000	-0.364465000
H	2.829682000	1.434959000	-1.887404000
H	2.425647000	-0.330174000	-1.868956000

O	-0.965243000	1.036329000	0.868213000
C	-2.367918000	0.962018000	1.165412000
H	-2.524977000	0.037478000	1.750639000
H	-2.971265000	0.917961000	0.234936000
H	-2.662200000	1.843328000	1.773942000
Cl	1.506181000	-1.333808000	1.428946000
Cl	-1.644006000	-1.331081000	-1.319680000

L1

Charge = 0; Spin multiplicity = 1

N	1.385934000	-1.569634000	-0.001431000
N	-1.385929000	-1.569638000	0.001428000
C	2.716315000	-1.559885000	-0.001539000
C	0.731666000	-0.380342000	-0.000370000
C	-2.716310000	-1.559893000	0.001496000
C	-0.731665000	-0.380345000	0.000376000
C	3.499585000	-0.378378000	-0.000602000
H	3.217565000	-2.545630000	-0.002361000
C	1.424501000	0.878477000	-0.000044000
C	-3.499583000	-0.378389000	0.000545000
H	-3.217555000	-2.545640000	0.002340000
C	-1.424503000	0.878474000	0.000040000
H	4.598124000	-0.442256000	-0.000488000
C	2.844849000	0.846579000	0.000002000
C	0.686849000	2.113326000	0.000123000
C	-2.844850000	0.846571000	-0.000041000
H	-4.598122000	-0.442264000	0.000395000
C	-0.686853000	2.113324000	-0.000103000
H	3.406448000	1.794336000	0.000507000
H	1.249580000	3.060203000	0.000274000
H	-3.406454000	1.794324000	-0.000554000
H	-1.249586000	3.060200000	-0.000241000

^{T}INT-A

Charge = 0; Spin multiplicity = 3

C	-3.818838000	-0.554506000	-0.510723000
H	-3.732911000	-0.127264000	-1.536113000
H	-4.774043000	-1.124021000	-0.432203000
C	-3.819104000	0.553585000	0.509878000
H	-3.733323000	0.126417000	1.535309000
H	-4.774447000	1.122828000	0.431077000
O	-2.716460000	1.430061000	0.258290000
C	-2.652748000	2.465590000	1.236752000
H	-2.397954000	2.049602000	2.235584000

H	-3.621201000	3.013741000	1.283219000
H	-1.862260000	3.176584000	0.933790000
O	-2.715989000	-1.430675000	-0.258955000
C	-2.651774000	-2.465999000	-1.237617000
H	-1.860871000	-3.176668000	-0.934937000
H	-2.397273000	-2.049693000	-2.236393000
H	-3.619942000	-3.014652000	-1.284100000
Cl	-1.024274000	-0.219878000	2.346605000
Cl	-1.024405000	0.219846000	-2.347125000
Ni	-0.864854000	-0.000004000	-0.000272000
N	0.710930000	-1.341741000	0.094327000
N	0.710778000	1.342063000	-0.094585000
C	0.674038000	-2.661522000	0.286792000
C	1.919495000	-0.717320000	0.064444000
C	0.673784000	2.661880000	-0.286794000
C	1.919416000	0.717789000	-0.064536000
C	1.843458000	-3.444706000	0.409457000
H	-0.322265000	-3.121495000	0.359322000
C	3.156564000	-1.422167000	0.161593000
C	1.843139000	3.445211000	-0.409151000
H	-0.322539000	3.121806000	-0.359304000
C	3.156427000	1.422790000	-0.161344000
H	1.750785000	-4.529978000	0.559840000
C	3.088915000	-2.829380000	0.333206000
C	4.388996000	-0.682559000	0.082827000
C	3.088653000	2.830016000	-0.332789000
H	1.750367000	4.530495000	-0.559387000
C	4.388930000	0.683323000	-0.082358000
H	4.018390000	-3.413977000	0.412241000
H	5.336666000	-1.238195000	0.152742000
H	4.018074000	3.414729000	-0.411589000
H	5.336547000	1.239076000	-0.152070000

Glyme

Charge = 0; Spin multiplicity = 1

C	0.650105000	-0.394977000	0.000087000
C	-0.649933000	0.395412000	-0.000490000
H	0.679220000	-1.063597000	-0.897751000
H	0.678968000	-1.062852000	0.898486000
H	-0.679009000	1.064128000	0.897265000
H	-0.678748000	1.063082000	-0.899040000
O	1.722469000	0.521292000	-0.000136000
O	-1.722284000	-0.520847000	-0.000097000

C	-2.981224000	0.111484000	0.000268000
H	-3.759119000	-0.678633000	0.000463000
H	-3.133675000	0.755215000	0.902151000
H	-3.134200000	0.755257000	-0.901497000
C	2.981390000	-0.111063000	-0.000851000
H	3.759312000	0.679030000	-0.000710000
H	3.134398000	-0.755250000	0.900615000
H	3.133791000	-0.754392000	-0.903030000

^{T}INT-B

Charge = 0; Spin multiplicity = 3

Ni	1.637905000	-0.000234000	0.000017000
N	0.151301000	1.329690000	0.035534000
N	0.151030000	-1.329722000	-0.036258000
C	0.211068000	2.664538000	0.062647000
C	-1.066355000	0.717661000	0.016956000
C	0.210569000	-2.664584000	-0.063187000
C	-1.066506000	-0.717457000	-0.017949000
C	-0.955699000	3.461275000	0.075606000
H	1.216745000	3.112645000	0.072739000
C	-2.295379000	1.436037000	0.030096000
C	-0.956351000	-3.461101000	-0.076288000
H	1.216165000	-3.112877000	-0.073001000
C	-2.295664000	-1.435602000	-0.031271000
H	-0.855287000	4.555833000	0.097769000
C	-2.209049000	2.853097000	0.060000000
C	-3.526998000	0.688966000	0.013310000
C	-2.209589000	-2.852680000	-0.061029000
H	-0.856177000	-4.555682000	-0.098329000
C	-3.527138000	-0.688287000	-0.014759000
H	-3.130403000	3.455298000	0.069854000
H	-4.475670000	1.246873000	0.024150000
H	-3.131056000	-3.454709000	-0.071011000
H	-4.475923000	-1.245999000	-0.025763000
Cl	2.492041000	0.152128000	-2.045205000
Cl	2.486576000	-0.152468000	2.047757000

3DPAFIPN•HE$^{\bullet-}$

Charge = -1; Spin multiplicity = 2

N	-1.489280000	4.417322000	-2.782609000
C	-1.154423000	5.365919000	-2.155988000
C	-0.787306000	6.497693000	-1.405325000
C	-0.090890000	7.571597000	-2.027965000
C	-1.208232000	6.625868000	-0.009675000

C	0.059117000	8.806617000	-1.356207000
N	0.454169000	7.388729000	-3.327405000
C	-1.152307000	7.899386000	0.572323000
N	-1.606619000	5.492031000	0.746137000
C	-0.597908000	9.021977000	-0.067535000
C	0.887983000	9.820730000	-1.898319000
C	1.398702000	6.346523000	-3.525637000
C	0.057562000	8.268445000	-4.368356000
F	-1.635060000	8.050126000	1.826965000
C	-0.631165000	4.523667000	1.083963000
C	-2.936653000	5.454273000	1.239350000
N	-0.656388000	10.317605000	0.499682000
N	1.576138000	10.677940000	-2.331085000
C	2.300595000	6.012654000	-2.488671000
C	1.437280000	5.609758000	-4.731554000
C	0.968184000	8.682726000	-5.366691000
C	-1.262814000	8.774295000	-4.390806000
C	0.745353000	4.856987000	1.024520000
C	-0.987745000	3.200228000	1.445615000
C	-3.226807000	5.058268000	2.566302000
C	-3.999840000	5.866848000	0.402112000
C	-1.247982000	11.349805000	-0.275727000
C	-0.124179000	10.543561000	1.790636000
C	3.218529000	4.967059000	-2.657857000
H	2.277524000	6.582892000	-1.548374000
C	2.374079000	4.579550000	-4.897256000
H	0.721579000	5.841049000	-5.533728000
C	0.556726000	9.571972000	-6.369048000
H	2.005264000	8.318158000	-5.343152000
C	-1.656121000	9.680422000	-5.384766000
H	-1.978491000	8.452767000	-3.619749000
C	1.724706000	3.901761000	1.333271000
H	1.041118000	5.876736000	0.739129000
C	0.000346000	2.262035000	1.771214000
H	-2.044364000	2.899076000	1.464057000
C	-4.549583000	5.061207000	3.030101000
H	-2.407537000	4.763197000	3.237567000
C	-5.317582000	5.875212000	0.878811000
H	-3.779925000	6.175932000	-0.630813000
C	-0.740914000	12.671341000	-0.259660000
C	-2.318474000	11.041064000	-1.148202000
C	0.961160000	9.762934000	2.257211000
C	-0.685536000	11.511531000	2.659650000

C	3.269245000	4.248416000	-3.864578000
H	3.907043000	4.717008000	-1.835303000
H	2.388370000	4.014006000	-5.842237000
C	-0.753331000	10.081462000	-6.384628000
H	1.281037000	9.887919000	-7.136323000
H	-2.686151000	10.070476000	-5.379329000
C	1.364761000	2.600625000	1.720932000
H	2.787065000	4.188699000	1.276559000
H	-0.305387000	1.241046000	2.047917000
C	-5.604891000	5.467849000	2.194031000
H	-4.755264000	4.754624000	4.067938000
H	-6.131288000	6.194373000	0.208625000
C	-1.310178000	13.655131000	-1.077917000
H	0.115210000	12.918000000	0.384782000
C	-2.867718000	12.029787000	-1.976230000
H	-2.713100000	10.014305000	-1.170568000
C	1.471712000	9.953551000	3.547389000
H	1.401990000	9.003657000	1.593908000
C	-0.158990000	11.699712000	3.944596000
H	-1.547511000	12.107966000	2.327411000
H	3.992853000	3.429081000	-3.994332000
H	-1.066285000	10.789790000	-7.166852000
H	2.134399000	1.853870000	1.967018000
H	-6.641005000	5.470532000	2.565342000
C	-2.374594000	13.345016000	-1.944621000
H	-0.898702000	14.676673000	-1.053818000
H	-3.697384000	11.765671000	-2.651171000
C	0.921637000	10.925483000	4.402514000
H	2.318861000	9.335970000	3.885661000
H	-0.614842000	12.455404000	4.604093000
H	-2.807637000	14.119897000	-2.595425000
H	1.326245000	11.073334000	5.415364000
H	-1.473829000	2.555655000	-2.408880000
N	-1.382144000	1.666760000	-1.879513000
C	-0.083010000	1.225107000	-1.667168000
C	-2.449681000	1.332008000	-1.059780000
C	0.102731000	0.107135000	-0.878507000
C	0.967289000	2.104557000	-2.285040000
C	-2.312407000	0.232848000	-0.233199000
C	-3.614742000	2.278137000	-1.157003000
C	-1.121696000	-0.681710000	-0.453702000
C	1.389789000	-0.361340000	-0.350811000
H	1.409610000	2.771898000	-1.516143000

H	0.526500000	2.749935000	-3.067852000
H	1.796122000	1.516414000	-2.713343000
C	-3.199452000	-0.118579000	0.880705000
H	-3.606698000	2.795584000	-2.136116000
H	-3.558132000	3.062926000	-0.373613000
H	-4.577139000	1.756791000	-1.022057000
H	-1.367472000	-1.460252000	-1.219428000
H	-0.901920000	-1.242355000	0.473217000
O	1.514448000	-1.315815000	0.417356000
O	2.466537000	0.373097000	-0.760601000
O	-3.053209000	-1.113584000	1.591208000
O	-4.202860000	0.783798000	1.109190000
C	3.744076000	0.010506000	-0.210390000
C	-5.089303000	0.490429000	2.205435000
C	4.749560000	1.053813000	-0.654915000
H	4.023458000	-1.008210000	-0.559562000
H	3.666671000	-0.043708000	0.897192000
C	-6.196465000	1.523911000	2.197658000
H	-4.512029000	0.513844000	3.155888000
H	-5.483037000	-0.543192000	2.096397000
H	5.753002000	0.812337000	-0.249980000
H	4.824128000	1.094976000	-1.761097000
H	4.461102000	2.061479000	-0.291484000
H	-6.884958000	1.346558000	3.048573000
H	-5.786302000	2.549867000	2.291216000
H	-6.786638000	1.471895000	1.259814000

3DPAFIPN•HE

Charge = 0; Spin multiplicity = 1

N	-1.169923000	4.401003000	-2.103609000
C	-0.856512000	5.429158000	-1.628416000
C	-0.555516000	6.700409000	-1.070399000
C	-0.013786000	7.723743000	-1.896299000
C	-0.942677000	6.972457000	0.282710000
C	0.033513000	9.053273000	-1.395299000
N	0.468087000	7.420056000	-3.180986000
C	-0.967100000	8.316509000	0.704491000
N	-1.332633000	5.933172000	1.137104000
C	-0.533856000	9.380237000	-0.118360000
C	0.758630000	10.048120000	-2.113289000
C	1.411234000	6.362793000	-3.346225000
C	0.028610000	8.203868000	-4.290045000
F	-1.420271000	8.594575000	1.937494000

C	-0.475534000	4.797240000	1.268303000
C	-2.539747000	6.037123000	1.886374000
N	-0.602502000	10.707462000	0.316788000
N	1.398817000	10.851229000	-2.685540000
C	2.391341000	6.132258000	-2.355347000
C	1.374003000	5.535820000	-4.490016000
C	0.928683000	8.591933000	-5.305151000
C	-1.318477000	8.620543000	-4.356200000
C	0.925727000	4.970203000	1.251897000
C	-1.014628000	3.500580000	1.406083000
C	-2.608056000	5.565740000	3.215286000
C	-3.679264000	6.624613000	1.296010000
C	-1.089860000	11.701589000	-0.588390000
C	-0.190163000	11.063858000	1.633772000
C	3.313623000	5.087309000	-2.507516000
H	2.432189000	6.779785000	-1.466974000
C	2.317611000	4.510782000	-4.642996000
H	0.600846000	5.696814000	-5.255112000
C	0.479052000	9.383590000	-6.369969000
H	1.982894000	8.284968000	-5.246509000
C	-1.751545000	9.432220000	-5.414163000
H	-2.024303000	8.303973000	-3.573776000
C	1.771464000	3.855974000	1.355145000
H	1.349541000	5.981479000	1.160796000
C	-0.159677000	2.398485000	1.538808000
H	-2.104669000	3.359180000	1.398979000
C	-3.806446000	5.674086000	3.932906000
H	-1.718481000	5.121104000	3.684323000
C	-4.867604000	6.743566000	2.030089000
H	-3.631804000	6.980113000	0.255242000
C	-0.465877000	12.963497000	-0.674721000
C	-2.190571000	11.406601000	-1.420560000
C	0.928003000	10.430360000	2.216717000
C	-0.893039000	12.047478000	2.362441000
C	3.290060000	4.277337000	-3.654864000
H	4.067611000	4.915160000	-1.723634000
H	2.278268000	3.873263000	-5.539831000
C	-0.858165000	9.814369000	-6.428372000
H	1.190563000	9.685387000	-7.154137000
H	-2.802910000	9.757452000	-5.449970000
C	1.235480000	2.566318000	1.506487000
H	2.862565000	4.002908000	1.329132000
H	-0.591816000	1.391048000	1.634990000

C	-4.940853000	6.265046000	3.348886000
H	-3.848432000	5.303782000	4.968996000
H	-5.749672000	7.203758000	1.558362000
C	-0.943819000	13.915216000	-1.584880000
H	0.404275000	13.186967000	-0.040778000
C	-2.645406000	12.358412000	-2.344037000
H	-2.686489000	10.427560000	-1.341210000
C	1.329185000	10.771543000	3.515652000
H	1.486443000	9.674233000	1.644010000
C	-0.472134000	12.392488000	3.653474000
H	-1.771910000	12.534502000	1.915684000
H	4.020662000	3.463048000	-3.774890000
H	-1.201185000	10.446881000	-7.261146000
H	1.899471000	1.692234000	1.575585000
H	-5.877610000	6.351848000	3.920002000
C	-2.028705000	13.617511000	-2.428221000
H	-0.446536000	14.895273000	-1.650236000
H	-3.499310000	12.114402000	-2.994863000
C	0.636203000	11.756170000	4.239550000
H	2.202846000	10.269986000	3.960007000
H	-1.027959000	13.160415000	4.213606000
H	-2.390691000	14.364974000	-3.150358000
H	0.958430000	12.027733000	5.256258000
H	-1.257060000	2.410470000	-2.018304000
N	-1.119638000	1.450753000	-1.664391000
C	-2.173522000	0.881073000	-0.968109000
C	0.196096000	1.018176000	-1.580381000
C	-1.993486000	-0.366589000	-0.404675000
C	-3.401231000	1.750202000	-0.893706000
C	0.451061000	-0.204779000	-0.995186000
C	1.188011000	2.002628000	-2.131099000
C	-0.708880000	-1.130923000	-0.676889000
C	-2.974299000	-1.080298000	0.423688000
H	-4.289339000	1.226993000	-1.296583000
H	-3.250804000	2.692444000	-1.454683000
H	-3.644551000	2.000381000	0.156888000
C	1.783485000	-0.727566000	-0.664002000
H	0.716571000	2.624954000	-2.915355000
H	2.074169000	1.499423000	-2.549287000
H	1.544200000	2.690678000	-1.336211000
H	-0.458929000	-1.761146000	0.198279000
H	-0.862142000	-1.864757000	-1.508191000
O	-2.785905000	-2.206215000	0.883836000

O	-4.133616000	-0.394290000	0.655224000
O	1.991699000	-1.877321000	-0.279194000
O	2.791990000	0.190477000	-0.770782000
C	-5.119381000	-1.067782000	1.461815000
C	4.118745000	-0.267059000	-0.449903000
C	-6.303767000	-0.137663000	1.623767000
H	-4.669350000	-1.338745000	2.441480000
H	-5.407339000	-2.022153000	0.969314000
C	5.060984000	0.909213000	-0.607232000
H	4.393121000	-1.110112000	-1.121023000
H	4.127192000	-0.667934000	0.586900000
H	-7.085544000	-0.626136000	2.239712000
H	-6.006878000	0.804949000	2.127666000
H	-6.749571000	0.118961000	0.641025000
H	6.095926000	0.602887000	-0.354096000
H	5.059250000	1.289299000	-1.649552000
H	4.773054000	1.743601000	0.065097000

HE

Charge = 0; Spin multiplicity = 1

H	0.000001000	-1.608712000	0.861934000
C	0.000000000	-0.910193000	-0.006253000
C	-1.232920000	1.294692000	-0.002571000
C	1.232922000	1.294691000	-0.002570000
N	0.000001000	1.927194000	-0.003529000
C	1.274803000	-0.082608000	-0.003074000
C	-1.274803000	-0.082607000	-0.003070000
H	-0.000001000	-1.602521000	-0.879548000
H	0.000001000	2.949089000	-0.003158000
C	-2.403167000	2.242298000	-0.000668000
H	-3.050820000	2.080005000	-0.883290000
H	-2.058251000	3.295067000	-0.003162000
H	-3.045653000	2.082652000	0.886281000
C	2.403168000	2.242297000	-0.000667000
H	2.058254000	3.295066000	-0.003110000
H	3.050793000	2.080037000	-0.883319000
H	3.045684000	2.082615000	0.886252000
C	-2.499381000	-0.895622000	-0.001459000
O	-2.484283000	-2.126006000	-0.003106000
O	-3.666917000	-0.187903000	0.002167000
C	2.499381000	-0.895624000	-0.001469000
O	2.484282000	-2.126008000	-0.003079000
O	3.666918000	-0.187906000	0.002150000

C	4.879793000	-0.967385000	0.003592000
C	6.051702000	-0.008182000	0.007246000
H	4.890218000	-1.630234000	-0.888782000
H	4.886590000	-1.632518000	0.894303000
H	7.003385000	-0.576895000	0.008653000
H	6.040690000	0.642384000	-0.891120000
H	6.036751000	0.640280000	0.907075000
C	-4.879793000	-0.967382000	0.003588000
C	-6.051701000	-0.008178000	0.007228000
H	-4.886604000	-1.632517000	0.894297000
H	-4.890205000	-1.630228000	-0.888788000
H	-7.003385000	-0.576890000	0.008624000
H	-6.036761000	0.640283000	0.907058000
H	-6.040678000	0.642389000	-0.891138000

HE$^{\bullet+}$

Charge = +1; Spin multiplicity = 2

H	0.000017000	-1.578320000	0.827811000
C	-0.000001000	-0.842823000	-0.018193000
C	-1.239058000	1.323112000	-0.015273000
C	1.239024000	1.323131000	-0.015300000
N	-0.000021000	1.920383000	-0.016430000
C	1.268654000	-0.071314000	-0.015001000
C	-1.268667000	-0.071333000	-0.014967000
H	-0.000008000	-1.569980000	-0.871696000
H	-0.000029000	2.949921000	-0.018353000
C	-2.406056000	2.258910000	-0.015446000
H	-3.050492000	2.076481000	-0.896858000
H	-2.074158000	3.314595000	-0.024598000
H	-3.040635000	2.088733000	0.875668000
C	2.406008000	2.258947000	-0.015494000
H	2.074095000	3.314628000	-0.024542000
H	3.050374000	2.076594000	-0.896974000
H	3.040663000	2.088711000	0.875554000
C	-2.500569000	-0.918315000	-0.015166000
O	-2.441641000	-2.139881000	-0.029925000
O	-3.643731000	-0.213491000	0.004172000
C	2.500566000	-0.918280000	-0.015224000
O	2.441653000	-2.139847000	-0.029971000
O	3.643723000	-0.213443000	0.003985000
C	4.879179000	-0.982956000	0.008968000
C	6.034162000	-0.010247000	0.065719000
H	4.900335000	-1.613495000	-0.904875000

H	4.859574000	-1.669018000	0.881788000
H	6.988086000	-0.574357000	0.069900000
H	6.037751000	0.664136000	-0.814314000
H	5.995942000	0.607113000	0.985903000
C	-4.879180000	-0.983018000	0.009233000
C	-6.034167000	-0.010326000	0.066181000
H	-4.859473000	-1.669143000	0.882001000
H	-4.900428000	-1.613490000	-0.904654000
H	-6.988085000	-0.574447000	0.070440000
H	-5.995846000	0.606975000	0.986401000
H	-6.037870000	0.664113000	-0.813809000

$HE^{\bullet+}/Cl^{-}$

Charge = 0; Spin multiplicity = 2

H	-0.000039000	-2.122582000	0.854858000
C	-0.000032000	-1.399725000	-0.000031000
C	-1.228147000	0.778255000	-0.000072000
C	1.228148000	0.778218000	-0.000069000
N	0.000010000	1.392972000	-0.000062000
C	1.267010000	-0.616275000	-0.000067000
C	-1.267051000	-0.616236000	-0.000058000
H	-0.000048000	-2.122682000	-0.854829000
C	-2.403128000	1.710350000	-0.000093000
H	-3.042547000	1.528007000	-0.885398000
H	-2.057542000	2.762172000	-0.000245000
H	-3.042375000	1.528242000	0.885391000
C	2.403157000	1.710278000	-0.000086000
H	2.057602000	2.762110000	-0.000098000
H	3.042482000	1.528020000	-0.885479000
H	3.042487000	1.528046000	0.885310000
C	-2.495259000	-1.457635000	-0.000062000
O	-2.445050000	-2.682252000	-0.000166000
O	-3.647561000	-0.757886000	0.000065000
C	2.495192000	-1.457710000	-0.000096000
O	2.444947000	-2.682326000	-0.000026000
O	3.647516000	-0.757997000	-0.000003000
C	4.872439000	-1.535188000	0.000056000
C	6.036541000	-0.569830000	0.000024000
H	4.873033000	-2.195571000	-0.893166000
H	4.873006000	-2.195473000	0.893352000
H	6.988211000	-1.138012000	0.000076000
H	6.021910000	0.077808000	-0.899908000
H	6.021876000	0.077914000	0.899879000

C	-4.872509000	-1.535039000	0.000093000
C	-6.036579000	-0.569644000	0.000424000
H	-4.872989000	-2.195535000	0.893231000
H	-4.873230000	-2.195211000	-0.893287000
H	-6.988268000	-1.137795000	0.000460000
H	-6.021780000	0.077889000	0.900428000
H	-6.022041000	0.078204000	-0.899359000
H	0.000026000	2.493481000	-0.000073000
Cl	0.000093000	4.360313000	-0.001216000

INT-C

Charge = 0; Spin multiplicity = 2

Ni	-1.762178000	-0.071103000	-0.000201000
N	-0.334285000	1.267751000	0.000011000
N	-0.292316000	-1.344958000	0.000003000
C	-0.410937000	2.609435000	0.000039000
C	0.911861000	0.697527000	0.000024000
C	-0.319602000	-2.690176000	0.000026000
C	0.935543000	-0.732681000	0.000020000
C	0.736584000	3.431722000	0.000069000
H	-1.424544000	3.040176000	0.000029000
C	2.123673000	1.441904000	0.000049000
C	0.855908000	-3.471007000	0.000052000
H	-1.316152000	-3.158597000	0.000017000
C	2.172242000	-1.434547000	0.000041000
H	0.608489000	4.523970000	0.000089000
C	2.008486000	2.857782000	0.000069000
C	3.367459000	0.714071000	0.000056000
C	2.107422000	-2.853634000	0.000054000
H	0.765956000	-4.567062000	0.000068000
C	3.390494000	-0.664272000	0.000052000
H	2.914613000	3.482643000	0.000087000
H	4.307926000	1.286323000	0.000067000
H	3.034628000	-3.446573000	0.000068000
H	4.349622000	-1.204689000	0.000060000
Cl	-3.910360000	0.089983000	-0.000826000

2a

Charge = 0; Spin multiplicity = 1

C	-0.815123000	-0.898102000	0.435818000
C	0.460440000	-0.419964000	-0.239616000
C	-0.832285000	-1.631167000	1.568082000
H	0.393427000	-0.668991000	-1.317119000
H	-1.782657000	-1.947748000	2.021715000

H	0.105802000	-1.936915000	2.056559000
O	1.611104000	-1.091206000	0.325324000
C	2.029938000	-2.234960000	-0.294109000
C	3.186394000	-2.843854000	0.453412000
H	3.713686000	-3.565467000	-0.195660000
H	3.882011000	-2.064758000	0.819397000
H	2.795512000	-3.384821000	1.340988000
O	1.511652000	-2.687441000	-1.297705000
C	-2.063330000	-0.483006000	-0.278647000
O	-2.065335000	0.047397000	-1.381532000
O	-3.186952000	-0.761004000	0.416097000
C	-4.421540000	-0.414888000	-0.230521000
H	-5.225667000	-0.703962000	0.470134000
H	-4.469804000	0.673850000	-0.437207000
H	-4.536606000	-0.962560000	-1.188396000
C	0.674951000	1.076939000	-0.076099000
C	0.777342000	1.909319000	-1.205993000
C	0.785795000	1.642697000	1.210023000
C	0.989480000	3.289269000	-1.054306000
H	0.682459000	1.470365000	-2.211297000
C	1.006806000	3.019700000	1.362219000
H	0.696151000	0.997407000	2.098254000
C	1.106985000	3.846740000	0.229573000
H	1.064596000	3.932428000	-1.945050000
H	1.096565000	3.451997000	2.371128000
H	1.274752000	4.928611000	0.348982000

INT-D

Charge = 0; Spin multiplicity = 1

C	1.397034000	0.856309000	-0.474578000
C	2.143167000	-0.408769000	-0.079029000
C	1.086821000	1.884458000	0.493418000
H	1.971070000	-1.172571000	-0.865220000
H	1.008394000	2.931589000	0.150815000
H	1.479985000	1.764169000	1.519233000
O	1.596119000	-0.930458000	1.169081000
C	0.834897000	-2.054950000	1.108836000
C	0.179988000	-2.307702000	2.441947000
H	-0.270518000	-3.315680000	2.461413000
H	0.906327000	-2.188614000	3.269289000
H	-0.614109000	-1.545918000	2.591240000
O	0.695657000	-2.741902000	0.110969000
C	1.326701000	1.079644000	-1.932245000

O	1.485160000	0.208813000	-2.793306000
O	1.042967000	2.375538000	-2.268130000
C	0.837463000	2.618934000	-3.662010000
H	0.642182000	3.703202000	-3.760643000
H	1.729680000	2.340647000	-4.260387000
H	-0.032751000	2.046619000	-4.047974000
Ni	-0.495787000	0.868203000	0.039580000
N	-2.031941000	1.238018000	1.141433000
N	-1.627527000	-0.444653000	-0.834885000
C	-2.200783000	2.112585000	2.149706000
C	-3.063777000	0.369387000	0.872488000
C	-1.384032000	-1.260327000	-1.874382000
C	-2.844589000	-0.543994000	-0.210182000
C	-3.379548000	2.158923000	2.926008000
H	-1.363439000	2.799438000	2.343992000
C	-4.286120000	0.343486000	1.599279000
C	-2.327102000	-2.213240000	-2.320275000
H	-0.403550000	-1.143793000	-2.364487000
C	-3.849757000	-1.478240000	-0.581855000
H	-3.453236000	2.898348000	3.736823000
C	-4.427390000	1.278908000	2.660287000
C	-5.287487000	-0.618783000	1.215583000
C	-3.557986000	-2.335332000	-1.677940000
H	-2.069030000	-2.855828000	-3.174686000
C	-5.079211000	-1.490754000	0.168519000
H	-5.353571000	1.299176000	3.254604000
H	-6.232426000	-0.641990000	1.779994000
H	-4.301307000	-3.077544000	-2.006840000
H	-5.856812000	-2.217381000	-0.113258000
C	3.645473000	-0.243024000	0.114680000
C	4.394033000	-1.301980000	0.673065000
C	4.324325000	0.923309000	-0.288802000
C	5.783536000	-1.195115000	0.828846000
H	3.878168000	-2.221873000	0.990672000
C	5.717718000	1.029926000	-0.137921000
H	3.757069000	1.760857000	-0.721804000
C	6.452245000	-0.026431000	0.422900000
H	6.350173000	-2.031130000	1.268550000
H	6.230735000	1.950418000	-0.458417000
H	7.543503000	0.058761000	0.544190000

INT-C1

Charge = 0; Spin multiplicity = 2

C	1.318190000	1.127668000	-0.847436000
C	1.843210000	-0.168207000	-0.258559000
C	0.993899000	2.245721000	-0.020585000
H	1.614215000	-0.999440000	-0.953896000
H	0.908775000	3.241214000	-0.480767000
H	1.246948000	2.214599000	1.053210000
O	1.083950000	-0.405566000	0.980907000
C	0.581414000	-1.654391000	1.202847000
C	-0.174726000	-1.695273000	2.504920000
H	0.543337000	-1.928532000	3.319471000
H	-0.644604000	-0.722100000	2.738131000
H	-0.931465000	-2.499961000	2.470828000
O	0.752657000	-2.601008000	0.455059000
C	1.416474000	1.215580000	-2.328037000
O	1.393852000	0.242960000	-3.083126000
O	1.532021000	2.488238000	-2.766695000
C	1.306572000	2.690555000	-4.166143000
H	1.525723000	3.756142000	-4.364037000
H	1.963907000	2.044801000	-4.782866000
H	0.244732000	2.476600000	-4.407712000
Ni	-0.634149000	1.177995000	-0.388803000
N	-2.076934000	1.288558000	1.010220000
N	-1.608828000	-0.511085000	-0.916104000
C	-2.286945000	2.214311000	1.952845000
C	-2.902372000	0.201216000	0.962346000
C	-1.355858000	-1.362471000	-1.915582000
C	-2.652605000	-0.765582000	-0.077214000
C	-3.323067000	2.099507000	2.907166000
H	-1.607222000	3.080518000	1.948195000
C	-3.973020000	-0.002133000	1.880439000
C	-2.123970000	-2.532545000	-2.114839000
H	-0.507034000	-1.101643000	-2.570703000
C	-3.478232000	-1.920231000	-0.194612000
H	-3.448806000	2.889293000	3.661822000
C	-4.166693000	0.992146000	2.876150000
C	-4.784366000	-1.184721000	1.748399000
C	-3.180477000	-2.818459000	-1.254349000
H	-1.871460000	-3.205131000	-2.947173000
C	-4.547366000	-2.105157000	0.751958000
H	-4.980759000	0.878605000	3.608607000
H	-5.605943000	-1.336748000	2.465143000
H	-3.788781000	-3.726764000	-1.384927000
H	-5.177417000	-3.003265000	0.660787000

C	3.332512000	-0.201129000	0.060135000
C	3.936784000	-1.442158000	0.361878000
C	4.130301000	0.959745000	0.056809000
C	5.302143000	-1.515379000	0.672265000
H	3.322412000	-2.355841000	0.348161000
C	5.499847000	0.885347000	0.362867000
H	3.679108000	1.930710000	-0.196316000
C	6.089020000	-0.349894000	0.675112000
H	5.758438000	-2.490370000	0.905225000
H	6.110303000	1.801962000	0.353847000
H	7.162638000	-0.407255000	0.913559000
Cl	-1.627348000	2.546964000	-1.969144000

TS-A1

Charge = 0; Spin multiplicity = 2

C	1.672335000	1.110209000	-1.301801000
C	2.515139000	0.021086000	-0.939535000
C	1.159853000	2.052160000	-0.345770000
H	2.485299000	-0.844250000	-1.621606000
H	0.751786000	3.009030000	-0.702367000
H	1.580452000	2.043349000	0.672407000
O	0.935634000	-0.701554000	0.464442000
C	0.845462000	-1.865014000	1.068609000
C	-0.274682000	-2.016797000	2.093319000
H	-0.008540000	-2.816069000	2.810488000
H	-0.475989000	-1.071852000	2.632170000
H	-1.209298000	-2.322184000	1.580187000
O	1.626127000	-2.798093000	0.845894000
C	1.273304000	1.141579000	-2.750018000
O	1.129715000	0.151893000	-3.461324000
O	1.156580000	2.407896000	-3.196799000
C	0.576769000	2.559201000	-4.498896000
H	0.616348000	3.639379000	-4.730499000
H	1.138451000	1.983407000	-5.262008000
H	-0.478305000	2.216717000	-4.478727000
Ni	-0.315980000	0.704568000	-0.411661000
N	-1.610180000	0.962400000	1.146651000
N	-1.606592000	-0.784987000	-0.886581000
C	-1.573299000	1.844586000	2.147219000
C	-2.690924000	0.140938000	1.028884000
C	-1.552000000	-1.630183000	-1.916904000
C	-2.689433000	-0.797682000	-0.065103000
C	-2.615524000	1.950333000	3.097456000

H	-0.685423000	2.494026000	2.199893000
C	-3.789309000	0.171324000	1.935761000
C	-2.589642000	-2.555737000	-2.177301000
H	-0.660025000	-1.555691000	-2.561245000
C	-3.783046000	-1.692127000	-0.245091000
H	-2.534505000	2.692392000	3.904857000
C	-3.724442000	1.115426000	2.994905000
C	-4.882559000	-0.744308000	1.732759000
C	-3.704243000	-2.589860000	-1.343632000
H	-2.501408000	-3.236340000	-3.036334000
C	-4.880548000	-1.638368000	0.685634000
H	-4.549122000	1.176725000	3.721687000
H	-5.726730000	-0.714559000	2.438534000
H	-4.524769000	-3.301334000	-1.524157000
H	-5.722668000	-2.332703000	0.542629000
C	3.631308000	0.057624000	-0.003631000
C	4.241188000	-1.164896000	0.389312000
C	4.196675000	1.274085000	0.465270000
C	5.347799000	-1.168962000	1.244042000
H	3.781207000	-2.107352000	0.058557000
C	5.310549000	1.263202000	1.313713000
H	3.781523000	2.234275000	0.126947000
C	5.886882000	0.043946000	1.712596000
H	5.797183000	-2.126287000	1.551240000
H	5.742015000	2.216003000	1.657952000
H	6.762859000	0.039126000	2.379984000
Cl	-1.608507000	2.112229000	-1.723098000

INT-C2

Charge = 0; Spin multiplicity = 2

C	1.935765000	1.373207000	-1.585199000
C	3.096450000	0.643702000	-1.419656000
C	0.906249000	1.643250000	-0.589307000
H	3.621792000	0.396142000	-2.358822000
H	0.304482000	2.544744000	-0.787644000
H	1.196824000	1.516353000	0.464491000
O	0.845479000	-1.090485000	-0.131768000
C	1.146673000	-1.646376000	1.018374000
C	0.552014000	-1.014884000	2.273190000
H	1.036492000	-1.440914000	3.171288000
H	0.669428000	0.086347000	2.272748000
H	-0.536219000	-1.227110000	2.321807000
O	1.871871000	-2.642839000	1.080202000

C	1.696714000	1.848941000	-2.997623000
O	2.061029000	1.269532000	-4.010046000
O	1.079355000	3.052093000	-3.008823000
C	0.666194000	3.528776000	-4.293784000
H	0.241275000	4.535966000	-4.128745000
H	1.520190000	3.585243000	-4.999199000
H	-0.110300000	2.858061000	-4.716192000
Ni	-0.438292000	0.165845000	-0.768373000
N	-1.669116000	0.845295000	0.700313000
N	-1.809602000	-1.349748000	-0.820625000
C	-1.575808000	1.958660000	1.433056000
C	-2.756092000	0.037089000	0.868265000
C	-1.814239000	-2.438128000	-1.590188000
C	-2.826437000	-1.147800000	0.056226000
C	-2.556188000	2.321716000	2.383179000
H	-0.691183000	2.591735000	1.267611000
C	-3.793210000	0.318109000	1.805138000
C	-2.856060000	-3.392424000	-1.527939000
H	-0.965631000	-2.556452000	-2.281890000
C	-3.922866000	-2.048166000	0.190170000
H	-2.424664000	3.248968000	2.959050000
C	-3.665293000	1.503712000	2.575070000
C	-4.893831000	-0.604193000	1.918275000
C	-3.912061000	-3.199216000	-0.641376000
H	-2.817850000	-4.274242000	-2.183467000
C	-4.955758000	-1.741466000	1.144877000
H	-4.441639000	1.762551000	3.311190000
H	-5.689696000	-0.378246000	2.644173000
H	-4.736870000	-3.925499000	-0.576202000
H	-5.801190000	-2.439415000	1.243709000
C	3.732519000	0.135500000	-0.209187000
C	4.557020000	-1.014761000	-0.319864000
C	3.609513000	0.739922000	1.069849000
C	5.181453000	-1.570248000	0.802514000
H	4.680417000	-1.487272000	-1.307157000
C	4.244297000	0.189153000	2.189227000
H	3.037292000	1.671894000	1.180470000
C	5.023405000	-0.975268000	2.065031000
H	5.796681000	-2.476856000	0.692505000
H	4.138468000	0.679089000	3.169987000
H	5.515591000	-1.409595000	2.949126000
Cl	-1.458334000	1.156846000	-2.524151000

TS-A

Charge = 0; Spin multiplicity = 1

C	1.576921000	1.146844000	-0.938636000
C	2.409007000	0.023319000	-0.651470000
C	1.184214000	2.090436000	0.086351000
H	2.265245000	-0.857648000	-1.297133000
H	0.709114000	3.036551000	-0.218714000
H	1.783275000	2.140623000	1.010690000
O	1.283679000	-0.975347000	1.099604000
C	1.041217000	-2.223400000	0.843238000
C	0.084100000	-2.894473000	1.836471000
H	0.114581000	-3.995397000	1.730412000
H	0.320680000	-2.602245000	2.878710000
H	-0.950283000	-2.547310000	1.627522000
O	1.491928000	-2.875417000	-0.120501000
C	0.919891000	1.139153000	-2.285533000
O	0.975522000	0.218926000	-3.097637000
O	0.282371000	2.312914000	-2.549969000
C	-0.417529000	2.364657000	-3.798002000
H	-0.834989000	3.385567000	-3.874976000
H	0.261616000	2.166591000	-4.652419000
H	-1.240488000	1.619494000	-3.822506000
Ni	-0.060283000	0.584995000	0.066203000
N	-1.564633000	1.200751000	1.053626000
N	-1.294910000	-0.769831000	-0.667911000
C	-1.662219000	2.212166000	1.938766000
C	-2.686319000	0.434834000	0.830400000
C	-1.107221000	-1.748679000	-1.567300000
C	-2.538464000	-0.634069000	-0.108781000
C	-2.860717000	2.507222000	2.619523000
H	-0.751541000	2.805159000	2.106541000
C	-3.935235000	0.661867000	1.473646000
C	-2.143659000	-2.632118000	-1.943515000
H	-0.099402000	-1.826343000	-1.998799000
C	-3.639012000	-1.480768000	-0.419933000
H	-2.873894000	3.349120000	3.327011000
C	-4.004522000	1.740356000	2.394296000
C	-5.035824000	-0.210642000	1.150778000
C	-3.409431000	-2.509016000	-1.372338000
H	-1.931421000	-3.414666000	-2.686319000
C	-4.894605000	-1.237236000	0.242416000
H	-4.948561000	1.957716000	2.916579000

H	-6.002089000	-0.036616000	1.648757000
H	-4.227407000	-3.191671000	-1.649118000
H	-5.747223000	-1.891941000	0.004893000
C	3.656054000	0.037257000	0.113600000
C	4.288164000	-1.197683000	0.418699000
C	4.320930000	1.240032000	0.461843000
C	5.523547000	-1.226286000	1.070708000
H	3.761166000	-2.127141000	0.150267000
C	5.562147000	1.206283000	1.113721000
H	3.876452000	2.207907000	0.189503000
C	6.164681000	-0.023414000	1.426895000
H	5.996278000	-2.192560000	1.306723000
H	6.068029000	2.150009000	1.370850000
H	7.138372000	-0.046789000	1.940907000

^{T}INT-E

Charge = 0; Spin multiplicity = 3

C	1.270503000	0.786823000	-0.944539000
C	2.463825000	0.138597000	-1.271238000
C	0.812546000	1.271339000	0.334064000
H	2.528389000	-0.155331000	-2.331748000
H	0.045233000	2.058731000	0.280516000
H	1.571800000	1.467722000	1.107043000
O	0.840864000	-0.283762000	3.055362000
C	1.403155000	-1.371588000	2.691316000
C	2.366416000	-2.080076000	3.613125000
H	1.824938000	-2.888041000	4.149276000
H	3.180950000	-2.551993000	3.031387000
H	2.782305000	-1.383455000	4.364647000
O	1.130152000	-1.876529000	1.548092000
C	0.342549000	0.941657000	-2.124866000
O	0.524083000	0.478265000	-3.244389000
O	-0.758182000	1.684033000	-1.829969000
C	-1.683077000	1.880075000	-2.905162000
H	-2.545249000	2.422750000	-2.475948000
H	-1.225852000	2.482491000	-3.717671000
H	-2.015275000	0.912531000	-3.332397000
Ni	-0.215843000	-0.321403000	1.203593000
N	-1.883995000	0.719764000	1.553382000
N	-1.312720000	-1.086053000	-0.305669000
C	-2.121728000	1.642439000	2.496985000
C	-2.853777000	0.475303000	0.620675000
C	-0.976363000	-2.002836000	-1.223653000

C	-2.548587000	-0.509242000	-0.378378000
C	-3.334838000	2.360544000	2.560704000
H	-1.314261000	1.810525000	3.227031000
C	-4.107661000	1.151594000	0.602766000
C	-1.853544000	-2.384579000	-2.261717000
H	0.031212000	-2.437617000	-1.130634000
C	-3.498958000	-0.825723000	-1.390603000
H	-3.477426000	3.102658000	3.359652000
C	-4.333233000	2.119714000	1.615976000
C	-5.053184000	0.816733000	-0.432155000
C	-3.116290000	-1.798482000	-2.351327000
H	-1.524648000	-3.138537000	-2.991258000
C	-4.762257000	-0.133236000	-1.386486000
H	-5.286694000	2.668999000	1.645360000
H	-6.020913000	1.341401000	-0.444741000
H	-3.814529000	-2.075987000	-3.155794000
H	-5.494283000	-0.376609000	-2.171868000
C	3.645666000	-0.191482000	-0.498233000
C	4.743133000	-0.774221000	-1.202554000
C	3.818717000	0.006298000	0.903272000
C	5.933376000	-1.125897000	-0.558945000
H	4.638767000	-0.946265000	-2.286209000
C	5.013697000	-0.344795000	1.544285000
H	3.007090000	0.425527000	1.508137000
C	6.080753000	-0.911632000	0.824478000
H	6.756164000	-1.572584000	-1.139542000
H	5.109032000	-0.178928000	2.629285000
H	7.015850000	-1.187233000	1.336379000
$HE^{\bullet+}/AcO^{-}$			
Charge = 0; Spin multiplicity = 2			
H	-0.161652000	-2.676115000	-0.626492000
C	-0.149456000	-1.857584000	0.138056000
C	1.175906000	0.251075000	-0.005517000
C	-1.216698000	0.371448000	-0.237561000
N	0.015983000	0.949905000	-0.212307000
C	-1.362529000	-1.010344000	-0.024005000
C	1.156547000	-1.142122000	0.111235000
H	-0.221776000	-2.468189000	1.073348000
H	0.138326000	2.562849000	-0.486658000
C	2.395166000	1.124327000	0.100591000
H	3.249768000	0.608749000	0.565535000
H	2.129079000	2.027823000	0.686645000

H	2.712716000	1.464807000	-0.908417000
C	-2.359483000	1.318697000	-0.493327000
H	-1.973650000	2.325547000	-0.731879000
H	-3.017812000	1.388288000	0.395565000
H	-3.000380000	0.961901000	-1.321750000
C	2.333884000	-2.040649000	0.264890000
O	2.241591000	-3.173696000	0.724392000
O	3.492669000	-1.520158000	-0.194950000
C	-2.634820000	-1.773895000	0.043670000
O	-2.662664000	-2.994740000	0.166769000
O	-3.750470000	-1.013645000	-0.028849000
C	-5.012969000	-1.719557000	0.041550000
C	-6.124424000	-0.699351000	-0.070785000
H	-5.055073000	-2.281087000	0.999390000
H	-5.048925000	-2.470941000	-0.776043000
H	-7.105912000	-1.211477000	-0.015465000
H	-6.074890000	0.040763000	0.753535000
H	-6.073939000	-0.154211000	-1.035147000
C	4.665120000	-2.365920000	-0.082791000
C	5.844703000	-1.604478000	-0.645911000
H	4.474694000	-3.310863000	-0.635077000
H	4.810771000	-2.636907000	0.984607000
H	6.753946000	-2.236253000	-0.591993000
H	5.676064000	-1.333123000	-1.707713000
H	6.037172000	-0.675114000	-0.072435000
O	0.111550000	3.570075000	-0.756358000
C	0.499087000	4.339416000	0.264431000
O	0.921524000	3.903767000	1.332204000
C	0.362750000	5.814616000	-0.044625000
H	-0.702416000	6.065332000	-0.227906000
H	0.915132000	6.061681000	-0.973983000
H	0.747719000	6.420079000	0.795067000

INT-F

Charge = 0; Spin multiplicity = 2

C	1.463422000	1.709676000	-1.723860000
C	1.925862000	0.438992000	-1.218314000
C	1.097697000	2.743962000	-0.789607000
H	1.838019000	-0.396469000	-1.932587000
H	0.565679000	3.625732000	-1.180550000
H	1.698500000	2.927131000	0.114827000
C	0.985450000	1.714717000	-3.143105000
O	1.042396000	0.755215000	-3.906758000

O	0.466836000	2.914270000	-3.506675000
C	-0.078404000	2.978551000	-4.830590000
H	-0.445759000	4.012874000	-4.962300000
H	0.693286000	2.750054000	-5.594205000
H	-0.916718000	2.261369000	-4.952597000
Ni	0.049636000	1.072058000	-0.556006000
N	-1.170016000	1.364048000	0.892100000
N	-1.006704000	-0.528733000	-0.919411000
C	-1.252066000	2.378190000	1.785595000
C	-2.108885000	0.351608000	0.987294000
C	-0.889504000	-1.473111000	-1.873198000
C	-2.003487000	-0.685694000	0.022473000
C	-2.227826000	2.423151000	2.791878000
H	-0.497789000	3.173084000	1.688042000
C	-3.128307000	0.318036000	1.984540000
C	-1.733579000	-2.596519000	-1.936029000
H	-0.105138000	-1.304598000	-2.628853000
C	-2.902492000	-1.794937000	0.034644000
H	-2.229401000	3.271050000	3.492261000
C	-3.176566000	1.391068000	2.905600000
C	-4.027595000	-0.810590000	1.986118000
C	-2.743755000	-2.770750000	-0.976662000
H	-1.595953000	-3.321615000	-2.751216000
C	-3.916001000	-1.824142000	1.059254000
H	-3.945029000	1.408684000	3.693140000
H	-4.815142000	-0.847200000	2.754998000
H	-3.414079000	-3.643249000	-1.009373000
H	-4.613939000	-2.675672000	1.080047000
C	2.738921000	0.155713000	-0.035245000
C	2.765316000	-1.181116000	0.458521000
C	3.544701000	1.117296000	0.637165000
C	3.519325000	-1.527412000	1.583842000
H	2.161298000	-1.946175000	-0.055496000
C	4.301324000	0.764042000	1.762257000
H	3.602435000	2.144885000	0.250432000
C	4.289096000	-0.554711000	2.251612000
H	3.510706000	-2.567660000	1.946255000
H	4.920795000	1.528327000	2.258254000
H	4.883355000	-0.825927000	3.137845000

1a

Charge = 0; Spin multiplicity = 1

C	2.923887000	0.340161000	0.000068000

C	1.447259000	0.213649000	0.000032000
C	0.641104000	1.371152000	0.000021000
C	-0.754926000	1.267840000	-0.000040000
C	-1.338772000	-0.011849000	-0.000072000
C	-0.552896000	-1.182257000	0.000006000
C	0.838177000	-1.061245000	0.000040000
H	3.296258000	1.407758000	0.000070000
H	1.480645000	-1.955353000	0.000076000
H	1.116725000	2.365486000	0.000034000
H	-1.391693000	2.164081000	-0.000055000
H	-1.037359000	-2.169314000	0.000027000
Cl	-3.078804000	-0.155397000	-0.000065000
O	3.704808000	-0.601742000	0.000127000

TS-B

Charge = 0; Spin multiplicity = 2

C	0.390137000	-0.679333000	2.119554000
C	-1.013701000	-0.651163000	1.882123000
C	-1.812077000	0.482045000	1.556720000
C	-1.260930000	0.528415000	-0.664737000
O	0.018547000	0.652108000	-0.587562000
C	-1.909587000	-0.719736000	-1.107420000
C	-3.306601000	-0.762779000	-1.331010000
C	-3.946451000	-1.953400000	-1.683731000
C	-3.180383000	-3.126982000	-1.823423000
C	-1.788377000	-3.109878000	-1.644056000
C	-1.163420000	-1.906391000	-1.293983000
H	0.858645000	0.235946000	2.520779000
H	-0.064266000	-1.883476000	-1.163983000
H	-3.902535000	0.155266000	-1.201511000
H	-5.034581000	-1.985609000	-1.838955000
H	-1.202101000	-4.030791000	-1.776857000
Cl	-3.979654000	-4.640077000	-2.210730000
H	0.785100000	-1.602860000	2.571923000
C	-1.549750000	1.900534000	1.821293000
C	-0.263686000	2.508076000	1.860848000
C	-2.672275000	2.758907000	1.996346000
C	-0.119162000	3.886096000	2.084622000
H	0.633217000	1.907243000	1.670425000
C	-2.524781000	4.132125000	2.224793000
H	-3.682431000	2.319188000	1.956488000
C	-1.241948000	4.708537000	2.275515000
H	0.892110000	4.323665000	2.104182000

H	-3.419101000	4.760204000	2.365253000
H	-1.120771000	5.788032000	2.456318000
H	-2.883125000	0.239620000	1.472190000
C	-1.775051000	-1.942477000	1.834080000
O	-2.995021000	-2.044401000	1.792579000
O	-0.971532000	-3.047100000	1.876881000
C	-1.656266000	-4.304541000	1.846905000
H	-2.266623000	-4.406769000	0.926135000
H	-0.871772000	-5.084056000	1.867675000
H	-2.324354000	-4.419778000	2.725212000
Ni	1.237649000	-0.590131000	0.208169000
N	2.512623000	-2.037896000	0.481729000
N	2.857386000	0.389748000	-0.463577000
C	2.293893000	-3.279292000	0.955888000
C	3.801254000	-1.693571000	0.157135000
C	2.971005000	1.639601000	-0.936998000
C	3.987729000	-0.369888000	-0.353288000
C	3.331140000	-4.220352000	1.115712000
H	1.251283000	-3.514133000	1.221615000
C	4.912245000	-2.571751000	0.302868000
C	4.214683000	2.188535000	-1.315085000
H	2.031310000	2.209101000	-1.015153000
C	5.285486000	0.094444000	-0.712216000
H	3.085873000	-5.221721000	1.498715000
C	4.646057000	-3.875596000	0.796258000
C	6.218236000	-2.083601000	-0.064070000
C	5.377461000	1.422094000	-1.204903000
H	4.251576000	3.219912000	-1.695103000
C	6.398151000	-0.806493000	-0.549621000
H	5.469722000	-4.594733000	0.921758000
H	7.078441000	-2.761053000	0.050720000
H	6.356779000	1.832711000	-1.494836000
H	7.403645000	-0.452187000	-0.824625000
H	-1.852155000	1.458080000	-0.820104000

TS-B1

Charge = 0; Spin multiplicity = 2

C	-1.735278000	0.543017000	1.398929000
C	-0.586641000	1.149443000	2.044001000
C	0.630996000	0.448441000	2.320667000
C	-1.760423000	1.461589000	-0.692970000
O	-0.694223000	2.182269000	-0.764316000
C	-1.989256000	0.279360000	-1.577433000

C	-3.106997000	-0.567796000	-1.395613000
C	-3.328425000	-1.666695000	-2.235648000
C	-2.430293000	-1.915858000	-3.289338000
C	-1.329974000	-1.069857000	-3.515110000
C	-1.118547000	0.018525000	-2.660565000
H	-1.788093000	-0.552846000	1.332652000
H	-2.710575000	1.968864000	-0.391266000
H	-0.258061000	0.686639000	-2.816088000
H	-3.811102000	-0.369760000	-0.571530000
H	-4.190958000	-2.330946000	-2.079016000
H	-0.645508000	-1.268835000	-4.352812000
Cl	-2.685290000	-3.302080000	-4.334474000
H	-2.705861000	1.038552000	1.531053000
C	0.851565000	-0.979517000	2.600916000
C	-0.170861000	-1.915236000	2.905476000
C	2.188969000	-1.462369000	2.568171000
C	0.127718000	-3.269760000	3.118988000
H	-1.210645000	-1.572407000	3.002480000
C	2.483776000	-2.814874000	2.773247000
H	3.002654000	-0.751020000	2.353978000
C	1.451888000	-3.733651000	3.041980000
H	-0.687919000	-3.971029000	3.357393000
H	3.529560000	-3.157686000	2.724235000
H	1.680630000	-4.798504000	3.203283000
H	1.456228000	1.105773000	2.644191000
C	-0.545429000	2.628952000	2.254704000
O	0.428345000	3.274821000	2.636170000
O	-1.738303000	3.211213000	1.965654000
C	-1.752630000	4.641365000	1.988150000
H	-1.430752000	5.035725000	2.973753000
H	-1.082082000	5.052766000	1.205018000
H	-2.796073000	4.943450000	1.781497000
Ni	0.379328000	0.779314000	0.283078000
N	1.085761000	-0.901517000	-0.528709000
N	2.236762000	1.460521000	-0.134703000
C	0.478401000	-2.086407000	-0.696541000
C	2.414574000	-0.809494000	-0.838235000
C	2.773116000	2.664375000	0.099970000
C	3.035519000	0.470309000	-0.628932000
C	1.155986000	-3.226358000	-1.178122000
H	-0.591417000	-2.130394000	-0.438492000
C	3.183881000	-1.904853000	-1.327217000
C	4.133150000	2.945351000	-0.160381000

H	2.097303000	3.422259000	0.527603000
C	4.420339000	0.654300000	-0.911948000
H	0.600577000	-4.167936000	-1.296796000
C	2.511036000	-3.143620000	-1.496087000
C	4.580541000	-1.693215000	-1.611092000
C	4.960944000	1.944378000	-0.667798000
H	4.522603000	3.953151000	0.045142000
C	5.174333000	-0.466063000	-1.413009000
H	3.062085000	-4.019698000	-1.870882000
H	5.170238000	-2.542177000	-1.990214000
H	6.024657000	2.138797000	-0.874629000
H	6.243678000	-0.321743000	-1.631694000

INT-G

Charge = 0; Spin multiplicity = 2

C	0.394637000	-0.343365000	2.088573000
C	-0.914389000	-0.547956000	1.629348000
C	-1.697203000	0.527743000	0.911381000
C	-1.299956000	0.514157000	-0.639400000
O	0.062408000	0.597854000	-0.806462000
C	-1.946090000	-0.707977000	-1.303481000
C	-3.321236000	-0.710286000	-1.612657000
C	-3.947609000	-1.841317000	-2.152641000
C	-3.182152000	-2.996327000	-2.389780000
C	-1.807779000	-3.020133000	-2.108927000
C	-1.203911000	-1.871051000	-1.574157000
H	0.746742000	0.691619000	2.246375000
H	-0.118004000	-1.877367000	-1.363133000
H	-3.923103000	0.193007000	-1.418044000
H	-5.022149000	-1.835127000	-2.387109000
H	-1.217960000	-3.926471000	-2.310630000
Cl	-3.956269000	-4.425136000	-3.057561000
H	0.861439000	-1.108015000	2.729238000
C	-1.554421000	1.902239000	1.546485000
C	-0.597151000	2.850019000	1.123488000
C	-2.402942000	2.246461000	2.622649000
C	-0.494868000	4.101029000	1.756274000
H	0.067370000	2.583572000	0.287342000
C	-2.300322000	3.493700000	3.257663000
H	-3.156994000	1.518876000	2.965506000
C	-1.342820000	4.428646000	2.826622000
H	0.257857000	4.826550000	1.408037000
H	-2.975578000	3.739416000	4.092777000

H	-1.260464000	5.408552000	3.322745000
H	-2.763251000	0.234705000	0.975342000
C	-1.631851000	-1.830787000	1.808149000
O	-2.832130000	-2.000051000	1.613383000
O	-0.831966000	-2.846189000	2.261219000
C	-1.492651000	-4.099874000	2.470296000
H	-1.940649000	-4.478400000	1.528035000
H	-0.716872000	-4.802128000	2.828837000
H	-2.296863000	-4.009607000	3.229310000
Ni	1.178520000	-0.568013000	0.163043000
N	2.453839000	-2.009585000	0.603804000
N	2.885262000	0.357603000	-0.483048000
C	2.209094000	-3.207819000	1.167558000
C	3.752346000	-1.719497000	0.263407000
C	3.031202000	1.558317000	-1.055561000
C	3.983068000	-0.435391000	-0.330788000
C	3.222805000	-4.159280000	1.401647000
H	1.162320000	-3.397395000	1.448470000
C	4.839428000	-2.617445000	0.464192000
C	4.288810000	2.034931000	-1.487237000
H	2.105871000	2.143581000	-1.178182000
C	5.292641000	-0.044598000	-0.733628000
H	2.952659000	-5.121080000	1.861642000
C	4.543161000	-3.874804000	1.052304000
C	6.158013000	-2.199930000	0.057744000
C	5.424157000	1.239901000	-1.323591000
H	4.357596000	3.031541000	-1.947191000
C	6.376858000	-0.967626000	-0.518140000
H	5.349320000	-4.603811000	1.225450000
H	6.995487000	-2.896888000	0.215602000
H	6.415015000	1.592983000	-1.648549000
H	7.390575000	-0.667842000	-0.825775000
H	-1.798572000	1.418409000	-1.076515000

^{T}INT-H

Charge = 0; Spin multiplicity = 3

C	2.526250000	-0.745734000	2.532995000
C	2.456203000	-0.165133000	1.283942000
C	1.462776000	0.934096000	0.950588000
C	2.012832000	2.342057000	1.393644000
O	2.591913000	2.303325000	2.657950000
C	2.968346000	3.038248000	0.410777000
C	3.184780000	2.660844000	-0.927969000

C	4.121738000	3.334492000	-1.731869000
C	4.840616000	4.412144000	-1.195535000
C	4.616241000	4.839005000	0.124960000
C	3.686370000	4.148319000	0.911883000
H	3.523877000	4.450770000	1.956710000
H	2.657488000	1.800740000	-1.361676000
H	4.300069000	3.012351000	-2.768187000
H	5.177194000	5.692492000	0.533444000
Cl	6.043742000	5.229203000	-2.177005000
C	0.092273000	0.649260000	1.559224000
C	-0.313927000	1.186003000	2.799660000
C	-0.797129000	-0.205623000	0.872931000
C	-1.577832000	0.880322000	3.332621000
H	0.370879000	1.842088000	3.358904000
C	-2.057847000	-0.515459000	1.406454000
H	-0.492514000	-0.633010000	-0.096628000
C	-2.453579000	0.027677000	2.641185000
H	-1.869468000	1.305799000	4.304801000
H	-2.737522000	-1.181472000	0.851588000
H	-3.442784000	-0.211931000	3.062188000
H	1.338442000	0.931192000	-0.148812000
C	3.322724000	-0.667826000	0.173348000
O	3.098685000	-0.483145000	-1.017251000
O	4.379893000	-1.387246000	0.618061000
C	5.256188000	-1.909363000	-0.390796000
H	5.657314000	-1.094997000	-1.027823000
H	6.079642000	-2.410252000	0.149758000
H	4.728106000	-2.638938000	-1.038483000
Ni	3.835478000	1.010311000	3.184568000
N	4.705211000	-0.369651000	4.451643000
N	5.656345000	0.851214000	2.276676000
C	4.182777000	-0.953376000	5.535909000
C	5.996686000	-0.634098000	4.113178000
C	6.079882000	1.465099000	1.168363000
C	6.505085000	0.014401000	2.933912000
C	4.940994000	-1.832360000	6.345326000
H	3.126081000	-0.725283000	5.766596000
C	6.831937000	-1.514271000	4.859071000
C	7.382556000	1.276405000	0.653898000
H	5.360511000	2.129972000	0.670125000
C	7.838564000	-0.235265000	2.497288000
H	4.467702000	-2.283868000	7.229143000
C	6.261842000	-2.116410000	6.012270000

C	8.179245000	-1.741683000	4.404029000
C	8.265262000	0.428001000	1.315973000
H	7.675326000	1.810860000	-0.261359000
C	8.661435000	-1.131393000	3.267783000
H	6.867904000	-2.801452000	6.625058000
H	8.819124000	-2.422245000	4.986291000
H	9.287000000	0.266056000	0.939373000
H	9.691771000	-1.317162000	2.928252000
H	1.108551000	3.000949000	1.443175000
O	1.015602000	-0.375143000	6.047391000
C	0.327827000	0.613329000	6.343947000
C	0.849462000	1.978235000	6.359540000
O	-0.993977000	0.476823000	6.652169000
C	2.293385000	2.070561000	5.929590000
C	0.162282000	3.135826000	6.714091000
C	-1.528101000	-0.860554000	6.590283000
H	2.440549000	1.406947000	5.047529000
C	2.736079000	3.472338000	5.581379000
H	2.968199000	1.621578000	6.701569000
N	0.727156000	4.381074000	6.561748000
C	-1.246543000	3.169367000	7.257556000
C	-3.003647000	-0.788909000	6.923464000
H	-0.974160000	-1.509932000	7.302450000
H	-1.354156000	-1.275490000	5.574004000
C	1.931302000	4.560597000	5.953476000
C	3.994409000	3.535549000	4.881739000
H	0.132362000	5.517661000	7.240094000
H	-1.468675000	4.172031000	7.667460000
H	-1.406804000	2.403757000	8.038396000
H	-1.984099000	2.953474000	6.456408000
H	-3.445741000	-1.805110000	6.890998000
H	-3.167138000	-0.373641000	7.938852000
H	-3.549851000	-0.153115000	6.196869000
C	2.295934000	6.003785000	5.707453000
O	4.661446000	2.510041000	4.582668000
O	4.476227000	4.763988000	4.557877000
O	-0.353838000	6.362973000	7.774808000
H	2.496435000	6.182873000	4.633116000
H	3.222722000	6.283483000	6.245847000
H	1.474032000	6.663875000	6.037443000
C	5.762731000	4.808114000	3.905418000
C	0.379644000	6.748033000	8.811252000
C	6.038824000	6.248130000	3.526838000

H	5.750550000	4.141584000	3.017742000
H	6.535108000	4.409030000	4.598519000
O	1.475637000	6.275889000	9.110272000
C	-0.284103000	7.860072000	9.610492000
H	7.021096000	6.321038000	3.018038000
H	5.262456000	6.638049000	2.837078000
H	6.063609000	6.902265000	4.421941000
H	-1.261232000	7.513052000	10.005721000
H	-0.496548000	8.727992000	8.952914000
H	0.363820000	8.175906000	10.448428000
H	3.181198000	-1.611492000	2.698649000
H	1.751586000	-0.551403000	3.293194000

HP

Charge = 0; Spin multiplicity = 1

C	0.000001000	-0.731048000	0.000198000
C	-1.181521000	1.376209000	0.000254000
C	1.181516000	1.376213000	-0.000029000
N	-0.000003000	2.025027000	0.000083000
C	1.225610000	-0.049755000	0.000083000
C	-1.225610000	-0.049758000	0.000247000
C	-2.392792000	2.268155000	0.000477000
H	-3.033379000	2.082004000	-0.884463000
H	-2.056514000	3.321255000	0.000766000
H	-3.033461000	2.081504000	0.885245000
C	2.392785000	2.268162000	-0.000329000
H	2.056505000	3.321262000	-0.000601000
H	3.033363000	2.081526000	-0.885173000
H	3.033469000	2.081991000	0.884529000
C	-2.448840000	-0.919434000	0.000312000
O	-2.405555000	-2.142092000	0.000704000
O	-3.603566000	-0.222774000	-0.000192000
C	2.448842000	-0.919428000	-0.000020000
O	2.405560000	-2.142085000	-0.000580000
O	3.603567000	-0.222765000	0.000449000
C	4.826625000	-1.001361000	0.000169000
C	5.992167000	-0.037318000	-0.000022000
H	4.828340000	-1.661587000	-0.893070000
H	4.828697000	-1.661621000	0.893387000
H	6.943435000	-0.606473000	-0.000197000
H	5.978676000	0.610726000	-0.899783000
H	5.979003000	0.610704000	0.899760000
C	-4.826624000	-1.001372000	-0.000148000

C	-5.992166000	-0.037330000	-0.000336000
H	-4.828561000	-1.661508000	0.893157000
H	-4.828471000	-1.661721000	-0.893300000
H	-6.943434000	-0.606484000	-0.000365000
H	-5.978914000	0.610789000	0.899375000
H	-5.978763000	0.610618000	-0.900168000
H	0.000001000	-1.830807000	0.000208000

AcOH

Charge = 0; Spin multiplicity = 1

O	0.774592000	-1.049837000	0.000140000
C	0.091592000	0.122317000	-0.000051000
O	0.650648000	1.205400000	-0.000121000
C	-1.397390000	-0.104344000	0.000014000
H	-1.926442000	0.864384000	-0.001281000
H	-1.691484000	-0.696642000	-0.890279000
H	-1.691582000	-0.694137000	0.891956000
H	1.729285000	-0.808160000	0.000230000

INT-I

Charge = 0; Spin multiplicity = 1

C	2.808735000	-1.211692000	3.113299000
C	2.468592000	-0.791670000	1.772959000
C	1.423481000	0.276086000	1.425355000
C	1.330561000	1.515677000	2.355794000
O	0.906297000	1.117885000	3.653558000
C	2.621266000	2.328196000	2.377635000
C	2.983949000	3.107158000	1.259994000
C	4.164701000	3.862168000	1.252283000
C	4.983803000	3.856772000	2.395095000
C	4.633784000	3.116426000	3.533074000
C	3.464082000	2.338423000	3.508026000
H	3.177495000	1.755364000	4.394436000
H	2.334187000	3.120345000	0.369861000
H	4.450946000	4.454878000	0.371617000
H	5.284441000	3.123647000	4.419258000
Cl	6.465550000	4.797800000	2.396845000
C	0.044059000	-0.342728000	1.213882000
C	-0.563216000	-1.150905000	2.198855000
C	-0.659934000	-0.106538000	0.014863000
C	-1.838878000	-1.698813000	1.991602000
H	-0.023387000	-1.351656000	3.135172000
C	-1.935861000	-0.655031000	-0.197486000
H	-0.191981000	0.512174000	-0.768166000

C	-2.531518000	-1.453268000	0.792786000
H	-2.296700000	-2.326466000	2.772912000
H	-2.464605000	-0.462058000	-1.144587000
H	-3.530581000	-1.887490000	0.629708000
H	1.728582000	0.689600000	0.443407000
C	2.826303000	-1.623080000	0.600232000
O	2.676678000	-1.286296000	-0.579584000
O	3.366335000	-2.839672000	0.925917000
C	3.855861000	-3.607972000	-0.173784000
H	4.684933000	-3.083658000	-0.695856000
H	4.229502000	-4.557550000	0.253687000
H	3.056742000	-3.817380000	-0.914949000
Ni	4.273342000	-0.220781000	2.312793000
N	5.821008000	-0.022842000	3.462880000
N	5.392731000	0.597161000	0.944453000
C	5.997891000	-0.345015000	4.756824000
C	6.840954000	0.643149000	2.827698000
C	5.144876000	0.859969000	-0.349938000
C	6.609364000	0.975665000	1.452664000
C	7.173016000	-0.018499000	5.468071000
H	5.167908000	-0.879800000	5.242889000
C	8.060947000	1.010589000	3.460455000
C	6.074633000	1.527337000	-1.178034000
H	4.173915000	0.508686000	-0.736301000
C	7.603510000	1.658140000	0.698477000
H	7.253123000	-0.308319000	6.526030000
C	8.210439000	0.660035000	4.829498000
C	9.050078000	1.712376000	2.682650000
C	7.302255000	1.939216000	-0.661326000
H	5.810803000	1.717068000	-2.228840000
C	8.831352000	2.020779000	1.357876000
H	9.134237000	0.924123000	5.366550000
H	9.992258000	2.000522000	3.173911000
H	8.035961000	2.469501000	-1.287507000
H	9.597160000	2.558307000	0.777594000
H	0.551868000	2.165158000	1.886529000
H	3.110603000	-2.261664000	3.277176000
H	2.275432000	-0.741071000	3.954502000
H	0.688858000	1.931689000	4.148355000

3aa

Charge = 0; Spin multiplicity = 1

C	2.636702000	-1.169772000	3.065577000

C	2.296083000	-0.831879000	1.800940000
C	1.273514000	0.223522000	1.414464000
C	1.236270000	1.491474000	2.315554000
O	0.775552000	1.135464000	3.611022000
C	2.582107000	2.211581000	2.332870000
C	3.037404000	2.878767000	1.176906000
C	4.280375000	3.524845000	1.153504000
C	5.079758000	3.509136000	2.309675000
C	4.646010000	2.862795000	3.477026000
C	3.399603000	2.217206000	3.478150000
H	3.052723000	1.709655000	4.390112000
H	2.408219000	2.898340000	0.272169000
H	4.629447000	4.042931000	0.248480000
H	5.279598000	2.862966000	4.375861000
Cl	6.636484000	4.316061000	2.293754000
C	-0.125327000	-0.363082000	1.231382000
C	-0.720234000	-1.186269000	2.209131000
C	-0.868840000	-0.044021000	0.076278000
C	-2.026256000	-1.671720000	2.038442000
H	-0.151649000	-1.453469000	3.111870000
C	-2.174593000	-0.530576000	-0.099083000
H	-0.411347000	0.591812000	-0.699265000
C	-2.758709000	-1.346307000	0.883796000
H	-2.475096000	-2.313311000	2.813236000
H	-2.736012000	-0.274807000	-1.011567000
H	-3.781243000	-1.732393000	0.748584000
H	1.584869000	0.589932000	0.416388000
C	2.922817000	-1.522498000	0.623006000
O	2.758167000	-1.178065000	-0.540493000
O	3.697872000	-2.572715000	0.974765000
C	4.348971000	-3.257556000	-0.104425000
H	5.027800000	-2.576737000	-0.658355000
H	4.929846000	-4.076348000	0.357941000
H	3.607847000	-3.673648000	-0.817435000
H	0.501767000	2.172320000	1.821079000
H	3.385737000	-1.952712000	3.255181000
H	2.175537000	-0.663821000	3.925143000
H	0.601061000	1.964036000	4.098564000

Table 5.10 Cartesian coordinates (Å) of the reactants, intermediates and transition states.

5.8 Bibliography

[298] R. G. Kukushkin, P. M. Yeletsky, *Catalysts* **2023**, *13*, 968.
[299] V. P. Ananikov, *ACS Catal.* **2015**, *5*, 1964–1971.
[300] S. Z. Tasker, E. A. Standley, T. F. Jamison, *Nature* **2014**, *509*, 299-309.
[301] Y. Tamaru, *Modern Organonickel Chemistry*, John Wiley & Sons, Ltd, **2005**.
[302] M.-M. Zhang, Y.-N. Wang, L.-Q. Lu, W.-J. Xiao, *Trends Chem.* **2020**, *2*, 764–775.
[303] S. Sibille, E. d'Incan, L. Leport, M.-C. Massebiau, J. Perichon, *Tetrahedron Lett.* **1987**, *28*, 55–58.
[304] S. Durandetti, S. Sibille, J. Perichon, *J. Org. Chem.* **1989**, *54*, 2198–2204.
[305] M. Durandetti, C. Gosmini, J. Périchon, *Tetrahedron* **2007**, *63*, 1146–1153.
[306] Z. Tan, X. Wan, Z. Zang, Q. Qian, W. Deng, H. Gong, *Chem Commun* **2014**, *50*, 3827–3830.
[307] M. van Gemmeren, M. Börjesson, A. Tortajada, S.-Z. Sun, K. Okura, R. Martin, *Angew. Chem. Int. Ed Engl.* **2017**, *56*, 6558–6562.
[308] Z. Zhang, Z. Han, J. Li, H.-S. Hu, J. Li, C. Xi, *ACS Catal.* **2024**, *14*, 12392–12402.
[309] Y.-L. Li, W.-D. Li, Z.-Y. Gu, J. Chen, J.-B. Xia, *ACS Catal.* **2020**, *10*, 1528–1534.
[310] H. Xie, B. Breit, *ACS Catal.* **2022**, *12*, 3249–3255.
[311] A. Gualandi, F. Calogero, D. Corbisiero, E. Pinosa, P. G. Cozzi, *Asian J. Org. Chem.* **2024**, *13*, e202300574.
[312] D. Basavaiah, B. S. Reddy, S. S. Badsara, *Chem. Rev.* **2010**, *110*, 5447–5674.
[313] K. C. Bharadwaj, *RSC Adv.* **2015**, *5*, 75923–75946.
[314] D. Basavaiah, R. T. Naganaboina, *New J. Chem.* **2018**, *42*, 14036–14066.
[315] G. Bertuzzi, G. Ombrosi, M. Bandini, *Org. Lett.* **2022**, *24*, 4354–4359.
[316] S. Senapati, S. K. Parida, S. S. Karandikar, S. Murarka, *Org. Lett.* **2023**, *25*, 7900–7905.
[317] Z.-J. Song, Y. Bao, Y.-J. Sun, S. Yan, Y. Zhang, G. Li, J.-Y. Wang, *J. Org. Chem.* **2024**, *89*, 4877–4887.
[318] L. Marchini, J. A. C. Vélez, E. Andre, J. T. M. Correia, S. Moura, M. W. Paixão, *Adv. Synth. Catal.* **2024**, *366*, 2063–2071.
[319] X. Bai, L. Qian, H.-H. Zhang, S. Yu, *Org. Lett.* **2021**, *23*, 8322–8326.
[320] S. Potenti, A. Gualandi, A. Puggioli, A. Fermi, G. Bergamini, P. G. Cozzi, *Eur. J. Org. Chem.* **2021**, *2021*, 1624–1627.
[321] A. Gualandi, F. Calogero, M. Mazzarini, S. Guazzi, A. Fermi, G. Bergamini, P. G. Cozzi, *ACS Catal.* **2020**, *10*, 3857–3863.
[322] E. Pinosa, E. Bassan, S. Cetin, M. Villa, S. Potenti, F. Calogero, A. Gualandi, A. Fermi, P. Ceroni, P. G. Cozzi, *J. Org. Chem.* **2023**, 88, *10*, 6390–6400.
[323] P. V. Ramachandran, D. R. Nicponski, *Chem. Commun.* **2014**, *50*, 15216–15219.
[324] P. V. Ramachandran, D. Pratihar, H. N. G. Nair, M. Walters, S. Smith, M. T. Yip-Schneider, H. Wu, C. M. Schmidt, *Bioorg. Med. Chem. Lett.* **2010**, *20*, 6620–6623.
[325] B. Maity, S. Dutta, L. Cavallo, *Chem. Soc. Rev.* **2023**, *52*, 5373–5387.
[326] R. A. Marcus, *J. Chem. Phys.* **1956**, *24*, 966–978.
[327] N. S. Hush, *Trans. Faraday Soc.* **1961**, *57*, 557–580.
[328] B. Maity, C. Zhu, H. Yue, L. Huang, M. Harb, Y. Minenkov, M. Rueping, L. Cavallo, J. *Am. Chem. Soc.* **2020**, 142, *40*, 16942–16952.
[329] K. Kitaura, K. Morokuma, *Int. J. Quantum Chem.* **1976**, *10*, 325–340.
[330] F. M. Bickelhaupt, K. N. Houk, *Angew. Chem. Int. Ed Engl.* **2017**, *56*, 10070–10086.
[331] P. H. Mason, N. D. Emslie, *Tetrahedron* **1994**, *50*, 12001–12008.
[332] H. Huang, B. Sun, Y. Huang, J. Niu, *J. Am. Chem. Soc.* **2018**, *140*, 10402–10406.
[333] K.-H. Kim, H.-S. Lee, S.-H. Kim, K.-Y. Lee, J.-E. Lee, J.-N. Kim, *Bull. Korean Chem. Soc.* **2009**, *30*, 1012–1020.
[334] H. J. Hamann, N. S. Abutaleb, R. Pal, M. N. Seleem, P. V. Ramachandran, *Bioorganic Chem.* **2020**, *104*, 104183.
[335] B. R. Park, K. H. Kim, J. N. Kim, *Tetrahedron Lett.* **2010**, *51*, 6568–6571.
[336] P. V. Ramachandran, M. A. Helppi, A. L. Lehmkuhler, J. M. Marchi, C. M. Schmidt, M. T. Yip-Schneider, *Bioorg. Med. Chem. Lett.* **2015**, *25*, 4270–4273.

[337] M. Schaeffer, J. L. Stampf, C. Benezra, *J. Org. Chem.* **1989**, *54*, 6106–6113.
[338] M. J. Frisch *et al.*, *Gaussian 16*, *Revision B.01*, Gaussian, Inc., Wallingford CT, **2016**.
[339] A. V. Marenich, C. J. Cramer, D. G. Truhlar, *J. Phys. Chem. B* **2009**, *113*, 6378–6396.
[340] J. P. Perdew, K. Burke, M. Ernzerhof, *Phys. Rev. Lett.* **1996**, *77*, 3865–3868.
[341] S. Grimme, J. Antony, S. Ehrlich, H. Krieg, *J. Chem. Phys.* **2010**, *132*, 154104.
[342] F. Weigend, R. Ahlrichs, *Phys. Chem. Chem. Phys.* **2005**, *7*, 3297–3305.
[343] F. Weigend, *Phys. Chem. Chem. Phys.* **2006**, *8*, 1057–1065.
[344] T. A. Halgren, W. N. Lipscomb, *Chem. Phys. Lett.* **1977**, *49*, 225–232.
[345] H. P. Hratchian, H. B. Schlegel, *J. Chem. Phys.* **2004**, *120*, 9918–9924.
[346] Y. Zhao, D. G. Truhlar, *Theor. Chem. Acc.* **2008**, *120*, 215–241.
[347] R. A. Marcus, *J. Chem. Phys.* **1957**, *26*, 872–877.

Chapter 6. A dual photoredox- and titanium-catalyzed approach for the direct access to α-vinyl-β-hydroxy esters

6.1 Background introduction

Titanium is one of the most abundant transition metals on Earth, and has attracted particular attention because it is considered nontoxic and biocompatible, relatively inexpensive and environmentally friendly.[176] In the literature it is widely reported in many in C-C, C-O and C-N bond formation protocols[183,186] since the possibility to get easy access to Ti(III) species [348] and, although under harsher conditions, to Ti(II) species[190–193] triggering their different and unique reactivities. As already described in the section 1.6.3.4, the reactivity of Ti(III) as a single electron transfer agent is dominated by titanocene chloride Cp_2TiCl, readily available from the inexpensive and bench-stable titanocene dichloride Cp_2TiCl_2 by reduction with several metal reductants, e.g. Zn(0) or Mn(0)[199,203] or under photoredox conditions.[83,205,206]

In particular, among the wide range of titanium-mediated protocols reported in the literature, the high versatility of titanium in low oxidation state has been extensively reported in allylation reactions.[349] Typically, allyl-titanium species are generated *in situ* starting from a suitable allyl precursor and Cp_2TiCl, previously synthesized from Cp_2TiCl_2, or also generated *in situ* in the presence of metal reductants, as mentioned above. Although the synthesis of substituted $Cp_2Ti(\pi\text{-allyl})$ complexes has been reported,[350] their extreme air-sensitivity hinders their widespread application in allylation methodologies. This two-steps strategy (1. synthesis and 2. isolation of the $Cp_2Ti(\pi\text{-allyl})$ complex, then allylation of a substrate) is known as the *Grignard-type* reaction.

The concept of Ti-mediated allylations under Barbier conditions was first described by the Cuerva group in 2004.[351] The protocol combines a catalytic amount of Cp_2TiCl_2 as precatalyst, allyl bromide as an activated allyl precursor, Mn dust as reductant, 2,4,6-collidine and Me_3SiCl as scavengers (*Figure 6.1*).

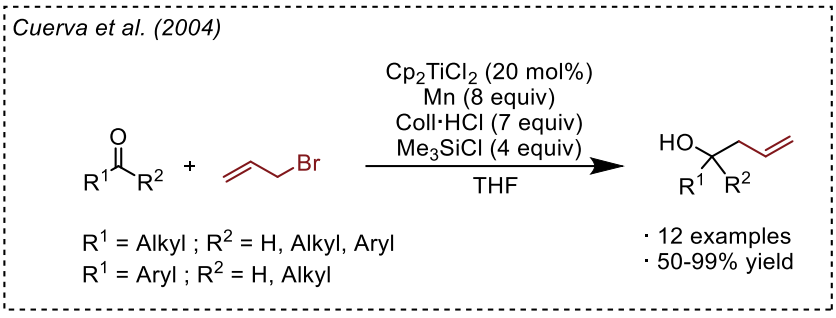

Figure 6.1 First titanium-catalyzed allylation of carbonyls reported by the Cuerva group.

The reaction was found to be tolerant to aromatic and aliphatic aldehydes and ketones and it was proved to be chemoselective, as esters did not react. Furthermore, even though acetophenone and benzaldehyde tend to undergo pinacol coupling reactions in the presence of single-electron-transfer reagents, they reacted smoothly as electrophilic partners. Allyl chloride was also briefly tested as an alternative activated allyl precursor, giving the same yield as the model allyl bromide. In the same work, the authors reported few examples of Ti(III)-mediated propargylation and benzylation of decanal. In the case of the propargylation, only the homopropargyl alcohol was detected. Finally, few attempts were made to induce enantioselectivity using Brintzinger's and Kagan's complex with modest enantioselectivity (20-30% *ee*) but proving for the first time that it is possible to induce asymmetric reactions with titanocene complexes under Barbier-type conditions.

Based on these preliminary results, the same group reported in 2009 a more detailed propargylation protocol,[352] while the Oltra group reported a regiodivergent propargylation/allenylation protocol using various substituted propargyl halides.[353]

Extending the allylation protocol to more substituted allyl moieties, in 2011 the same group reported a Ti(III)-mediated crotylation of aliphatic aldehydes and ketones (*Figure 6.2*).[354]

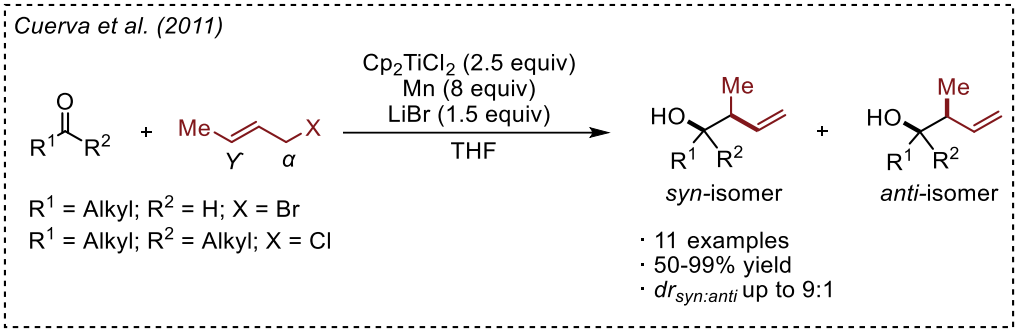

Figure 6.2 Titanium-mediated crotylation of aliphatic aldehydes and ketones reported by the Cuerva group.

The study was first carried out with a stoichiometric amount of Cp_2TiCl_2 and, operating at 0°C, the reaction gave an exclusive Y- selectivity in good yield and diastereocontrol in favor of the *syn*-isomer, as expected from a Zimmerman-Traxler transition state.

In the case of aldehydes, crotyl bromide was chosen, while in the case of ketones, crotyl chloride was preferred to ensure a better reaction outcome. The explanation given by the authors is that, when aldehydes are used as starting materials, a more reactive allyl bromide (BDE = 56.7 kcal/mol)[349] is preferred to avoid the Ti-mediated pinacolization reaction. On the other hand, when ketones are used as starting materials, the addition reaction of the allenyl-titanium intermediate is slower and undesirable side-reactions occur. In this case propargyl chloride (BDE = 71.3 kcal/mol)[349], which slowly generates the initial allyl radical, gave better results.

To make the process more attractive on both laboratory and industrial scales, the authors also reported a catalytic version. In this case a system to restore the titanium catalytic cycle, was mandatory. A mixture of 2,4,6-collidine and Me_3SiCl was used in a similar manner as before.(*Figure 6.3*).

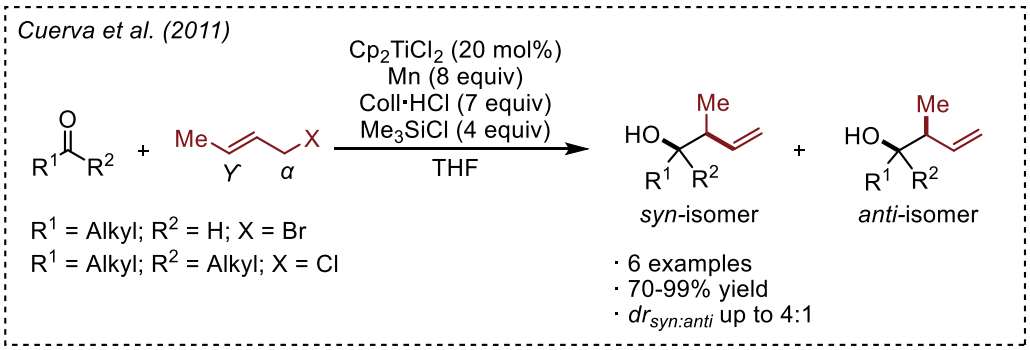

Figure 6.3 Catalytic version of the crotylation protocol in Figure 6.2 reported by the Cuerva group.

The mechanism of the Ti(III)-mediated allylation and crotylation is shown in *Figure 6.4*. Reduction of Cp_2TiCl_2 by elemental Mn(0) results in the active Cp_2TiCl complex. Two molecules of Cp_2TiCl are required to form the $Cp_2Ti(\pi\text{-allyl})Cl$ species: the first reduces the allyl halide derivative, forming an allyl radical and regenerating a Cp_2TiCl_2, while the second can capture the allyl radical forming the nucleophilic organometallic $Cp_2Ti(\pi\text{-allyl})Cl$. Addition to the carbonyl leads to the homoallyl product as

titanium alkoxide. Finally, the Ti-O bond is cleaved by (Coll-$SiMe_3$)$^+Cl^-$, releasing the product as TMS-protected alcohol and restoring the metal catalytic cycle.

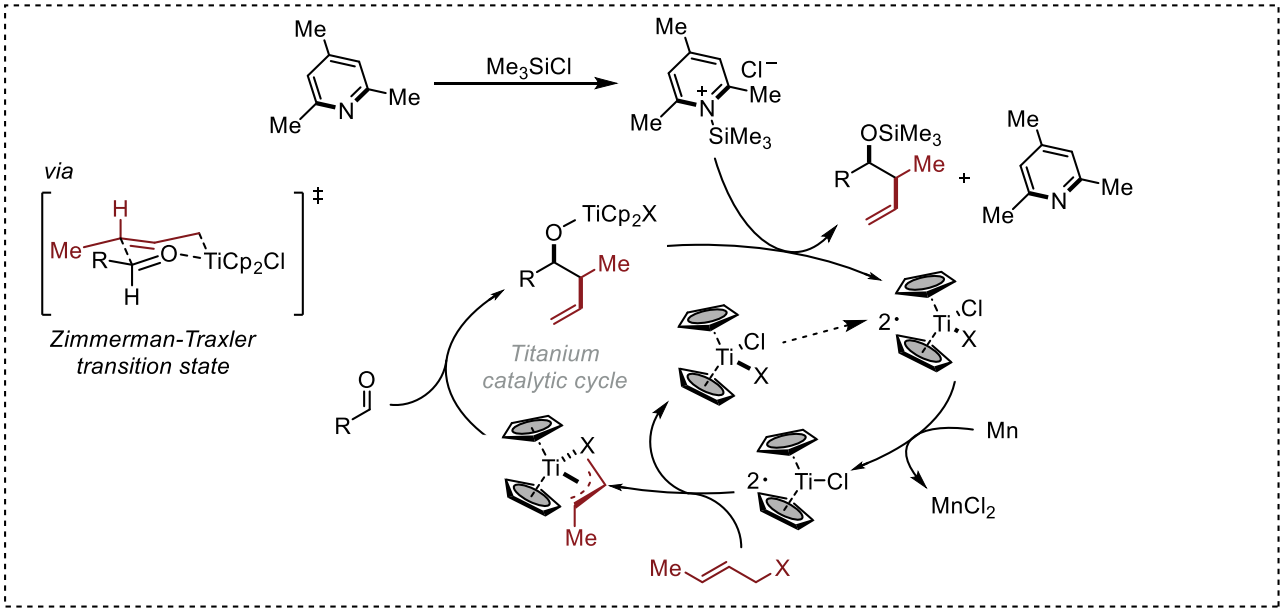

Figure 6.4 Mechanism of the titanium-catalyzed crotylation of carbonyls.

The Y-selectivity observed for the Ti-mediated allylation is strongly dependent on the titanium source. Indeed, the Gansäuer group reported in 2014 the Ti-mediated prenylation of carbonyls[355] with exclusive α-selectivity using a titanocene carboxylate complex (*Figure 6.5*).[356] The clear superiority of this titanium complex over Cp_2TiCl_2 was observed, even in the case of α,β-unsaturated aldehydes, both in the regioselectivity, with exclusive α-selectivity, and in the chemoselectivity in the presence of aromatic aldehydes and epoxides, as neither pinacol coupling products nor the epoxide ring opening were observed.

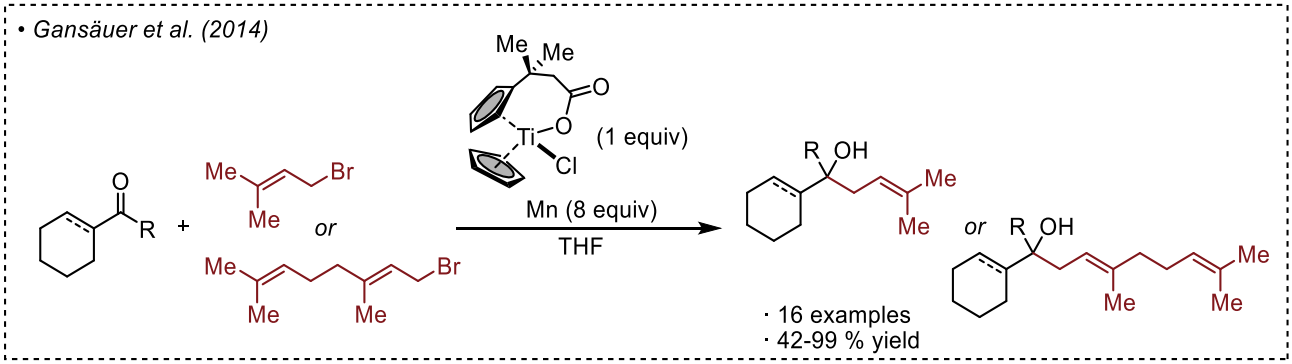

Figure 6.5 Ti-mediated α-prenylation of carbonyls reported by the Gansäuer group.

Although these examples from the literature represent a milestone of the enormous potential of titanium, the need for stoichiometric amounts of metal reductants or Ti complexes remains the main drawback of these reactions. As emphasized in the previous chapters, photoredox catalysis offers the possibility to replace the reductive behavior of a metal with a milder photocatalytic cycle.

For example, in recent years our group has developed a dual photoredox- and titanium-catalyzed allylation (*Figure 6.6*)[232] and propargylation[236] of aldehydes using a catalytic amount of Cp_2TiCl_2 as a Ti(IV) source, 3DPAFIPN as the organic photocatalyst and Hantzsch esters (methyl- and ethyl-ester respectively) as the final organic reductant under blue light irradiation.

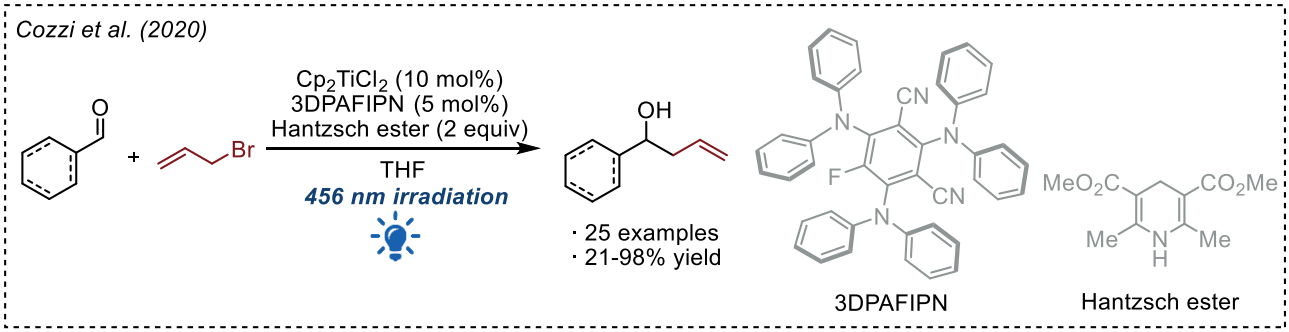

Figure 6.6 Dual photoredox- and Cp_2TiCl_2-mediated allylation of aldehydes reported by the Cozzi group.

The protocol was found to be suitable for both aromatic and aliphatic aldehydes with generally high yields and functional group tolerance. Substituted allyl bromides were briefly tested. Yields, regioselectivities and diastereoselectivities were found to be highly dependent on the substitution of the allylic source. In fact, crotyl bromide, which is even less reactive than the unsubstituted allyl bromide, was found to be moderately reactive and gave the Y-allylated product in decent yields and with good regio- and diastereocontrol, while the more steric-demanding cinnamyl bromide gave less regiocontrol in favor of the Y-isomer and lower yields, as did the prenyl bromide (*Figure 6.7*).

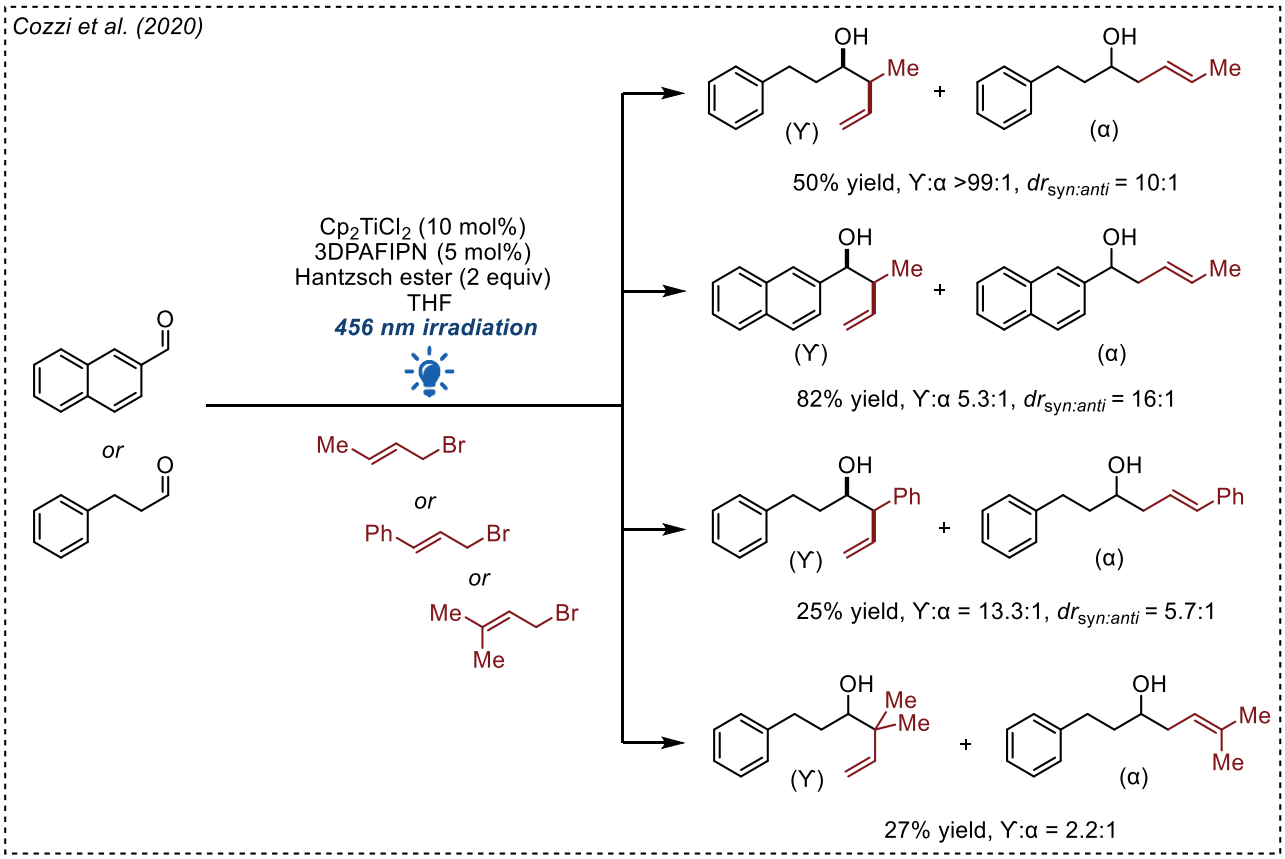

Figure 6.7 Dual photoredox- and Cp_2TiCl_2-mediated allylation of aldehydes using substituted allyl sources reported by the Cozzi group.

Later, the Shi group reported a very similar protocol using 4CzIPN as the photocatalyst, Cp_2TiCl_2 as the Ti(IV) source and THF as the solvent (*Figure 6.8*).[357] The protocol, compared to Cozzi's work, gave similar results with aromatic aldehydes, while aliphatic aldehydes were superficially investigated (2 examples). On the other hand, the latter conditions were found to be more suitable for aliphatic ketones and with substituted allyl sources giving better yields, regio- and diastereocontrol.

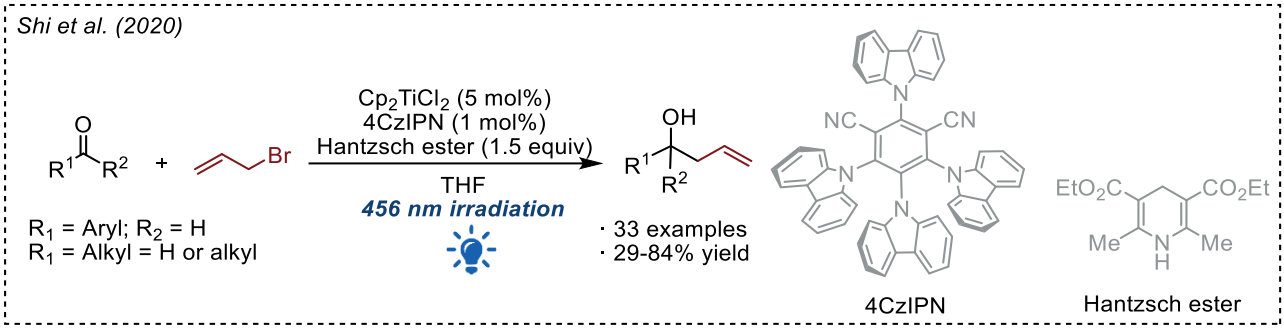

Figure 6.8 Dual photoredox- and Cp_2TiCl_2-mediated allylation of aldehydes reported by the Shi group.

In conclusion, as can be seen from these examples and also from others recently reported[358,359] the installation of a multi-decorated allyl moiety on carbonyl groups represents a highly valuable transformation. In particular, α-vinyl-β-hydroxy esters are a class of molecules with a high synthetic potential in the construction of natural product scaffolds, as well as synthons for pharmacologically active lactones.[360] Despite their high value, only a few examples can be found in the literature, following two main strategies: 1. vinylic aldol/Mukaiyama reactions in the presence of dienolates, or 2. formation of transient nucleophilic allyl species under Barbier conditions starting from suitable halocrotonates.

1. The vinylogous approach is a well-established principle and consists on the transmission of the electronic effects of a functional group in a molecule to a distal position through interposed conjugated multiple bonds.[361] This principle has been exploited by the Kalesse group in the allylation of aldehydes using *Z*-vinylogous silyl ketene acetals in a vinylogous aldol/Mukaiyama reaction with exclusive Y-selectivity (*Figure 6.9*).[362] An enantioselective version has also been reported by the Denmark group.[363]

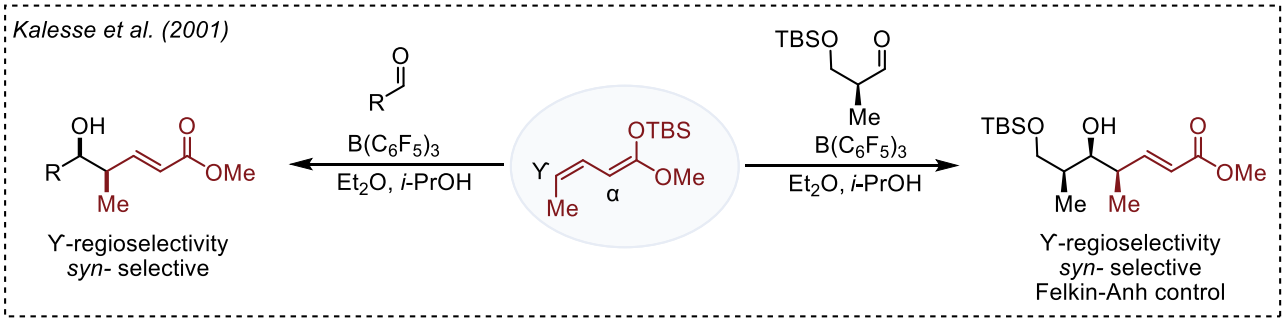

Figure 6.9 Vinylogous aldol/Mukaiyama allylation reaction reported by the Kalesse group.

In addition to silicon-based nucleophilic species, the Kim group reported the use of borinate derivatives as allyl source.[364] In contrast to the previous protocol, complete α-selectivity was observed, providing the *syn*- or the *anti*-diastereoisomer using *Z*- and *E*-dienes respectively (*Figure 6.10*). An enantioselective variant using a chiral dienolborinate has also been reported.[365]

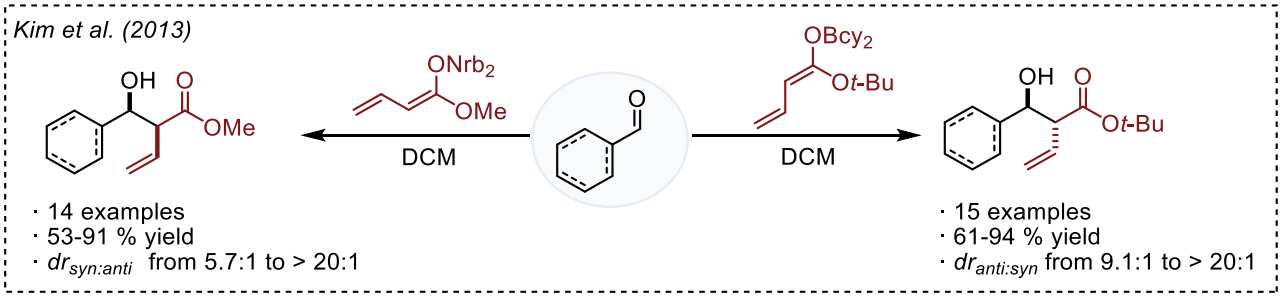

Figure 6.10 Vinylogous aldol allylation reaction with E/Z dienolborinates reported by the Kim group.

These examples provide a cornerstone for the synthesis of diastereo- and enantiodefined α-vinyl-β-hydroxy esters, but they still remain limited to the use of a stoichiometric amount of preformed boron-based nucleophiles.

2. The preparation of α-vinyl-β-hydroxy esters using halocrotonates under Barbier conditions is known as the *α-selective vinylogous Reformatsky reaction* and has been reported in the literature with several transition metals in low oxidation state, among which zinc plays an important role.[366–368] The reactivity of zinc-dienolates under Barbier/Reformatsky conditions has been studied both in the presence of simple carbonyl compounds, such as aldehydes and ketones, and with unsaturated α,β-carbonyls. The choice of the polarity of the solvent, as well as the metal reducing agent, was found to be critical for the regioselectivity (*α*- vs *γ*-competition), as reported by the Hudlicky group (*Figure 6.11*).[369]

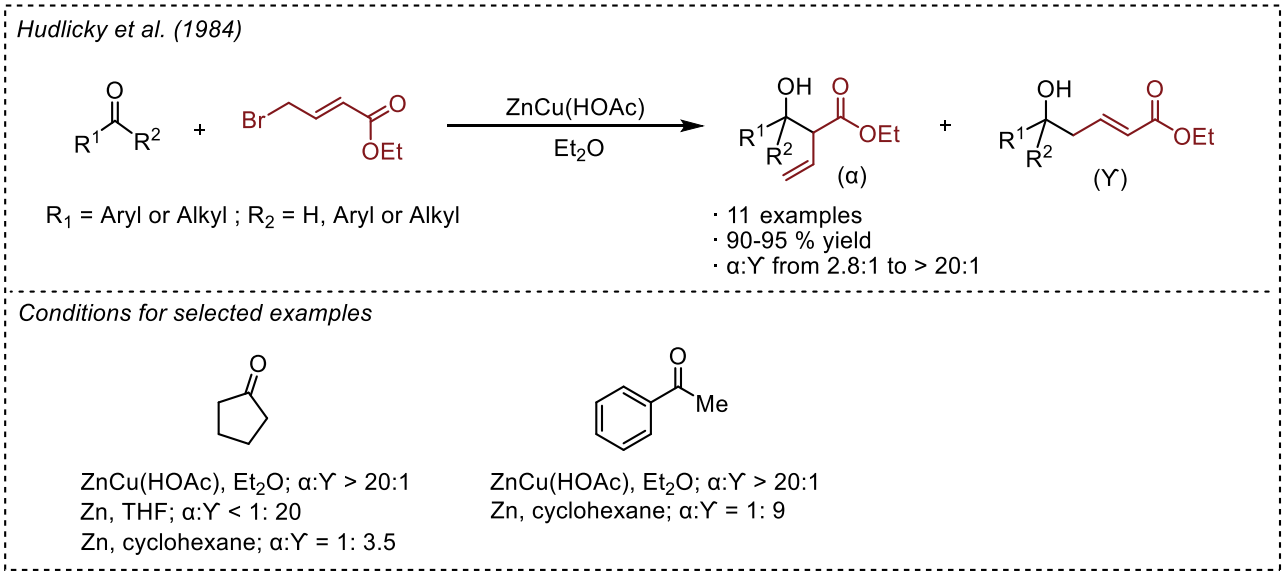

Figure 6.11 Regiodivergent conditions for the synthesis of α-vinyl-β-hydroxy esters reported by the Hudlicky group.

Beyond the well-established stoichiometric zinc chemistry, the development of similar Barbier-type methodologies with different metals was rarely been investigated. Stoichiometric amounts of Ga(0),[370] Sn(0),[371] In(0),[372] or Bi(0) [373] have been reported in aqueous conditions with 4-halocrotonates, in the presence of selected aldehydes. Interestingly, the Barrett group used this methodology with a stoichiometric amount of indium for a highly diastereoselective transformation in the total synthesis of viridiofungin derivatives.[374] Finally, stoichiometric Cr(II) has been reported in an allylation protocol using also unprotected 4-halo-crotonic acids with both aldehydes and ketones.[375] In these protocols a six-membered ring Zimmerman-Traxler transition state is proposed to explain the preferential formation of the *syn*-diastereomer.

6.2 Presented work

At the present time, the α-selective vinylogous Reformatsky-type reaction remains a rather underdeveloped transformation. Except for a few examples,[376–378] the use of catalytic amounts of active metal complexes has not been fully realized. Access to a Cp_2TiCl species, both in stoichiometric and catalytic form, opens a wide range of useful transformations, many of which for brevity, are not discussed in the introduction. The replacement of a stoichiometric amount of metal reductant with a catalytic photoredox cycle in the dual photoredox- and titanium-mediated allylation of carbonyls represents a step forward in the sustainability of this chemical process.[379] To broaden its applicability and introduce a multi-decorated allyl moiety to carbonyl groups, in the following paragraphs a novel

dual photoredox- and Cp_2TiCl_2-allylation protocol using 4-bromocrotonates as the allyl source is reported (*Figure 6.12*). The protocol introduces for the first time multi-decorated halocrotonates with exclusive α-regioselectivity and moderate diastereoselectivity under photoredox conditions avoiding the use of overstoichiometric amounts of preformed metal-based allyl nucleophiles.

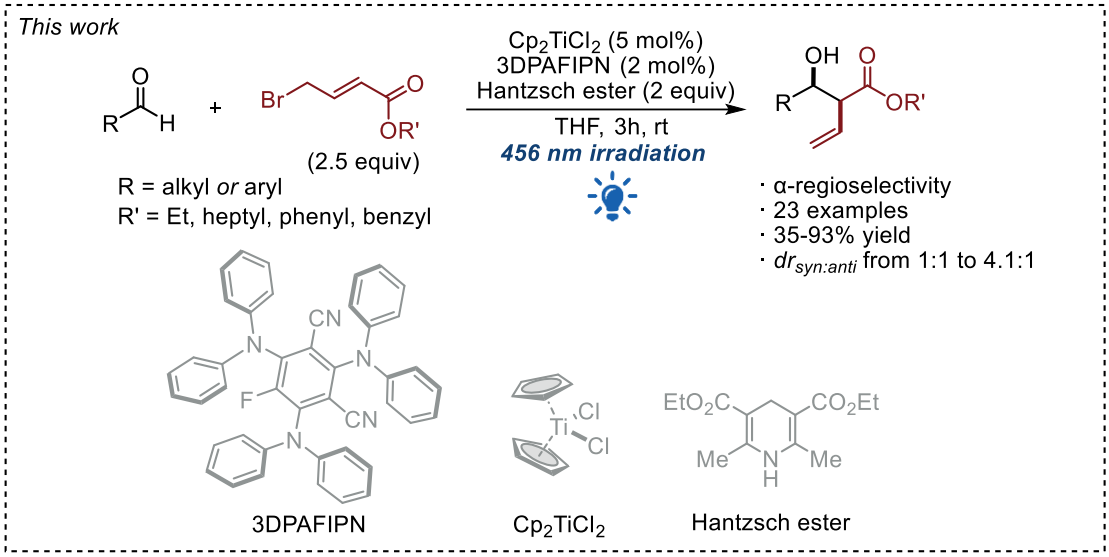

Figure 6.12 Presented work

6.3 Optimization

In order to optimize the reaction and in view of the knowledge gained during the study of the previously presented dual photoredox- and titanium-catalyzed methodologies,[83,232,236] we started the study of this new transformation using 4-chlorobenzaldehyde as the model substrate. Considering our previous work on titanium chemistry, we initially chose THF as the solvent. Since the previous dual photoredox- and titanium-catalyzed protocols reported by our group demonstrated the efficient formation of titanium in low oxidation state promoted by 3DPAFIPN as the photocatalyst in the presence of Hantzsch ester as the organic sacrificial reductant under blue light irradiation, we postulated that an effective allylation reaction could also be achieved in this system (*Table 6.1*). Under the preliminary conditions using 10 mol% of Cp_2TiCl_2 as Ti(IV) precatalyst, 5 mol% of 3DPAFIPN and 2.0 equivalents of Hantzsch ester (HE) in THF (0.05 M) under blue light irradiation (456 nm) for 16h (entry 1), we observed complete conversion of the aldehyde into the α-vinyl-β-hydroxy ester with a discrete *dr* of 2.8:1 in favor of the *syn*-diastereoisomer but with exclusive α-regiocontrol. In general, traces of the non-diastereoselective pinacol coupling are observed as the main side-product in all the optimization tests, along with the dimerization of the allylic source **2a**, as expected from the literature.[355] The reaction was immediately tested at gradually reduced irradiation times and complete conversion was observed after 6 hours (entry 2) and 3 hours of irradiation (entry 3). To increase the diastereoselectivity, the reaction was tested at 0°C under irradiation for 5h (entry 4), but only a reduced conversion and no increase in *dr* was observed. Under these preliminary conditions, the effect of the concentration was evaluated. Because Cp_2TiCl_2 absorbs light in the blue region, a more diluted solution (0.05 M versus the usual 0.1 M) is usually required in order to suppress parasitic reactions mediated by the excited titanocene.[232,380] As expected, increasing the concentration to 0.1 M (entry 5) reaction gave full conversion of **1a** and the α-vinyl-β-hydroxy ester as the main product, but with a non-negligible formation of undefined side-products, while at 0.2 M (entry 6) the pinacol product was observed as the main product. Other solvents were then investigated. Toluene (entry 7) gave better results compared to MeCN (entry 8) and DCM (entry 9) but

THF provided the best results in terms of both yield and diastereoselectivity. Diethyl ether (entry 10) was found to be ineffective due to the low solubility of the reactants.

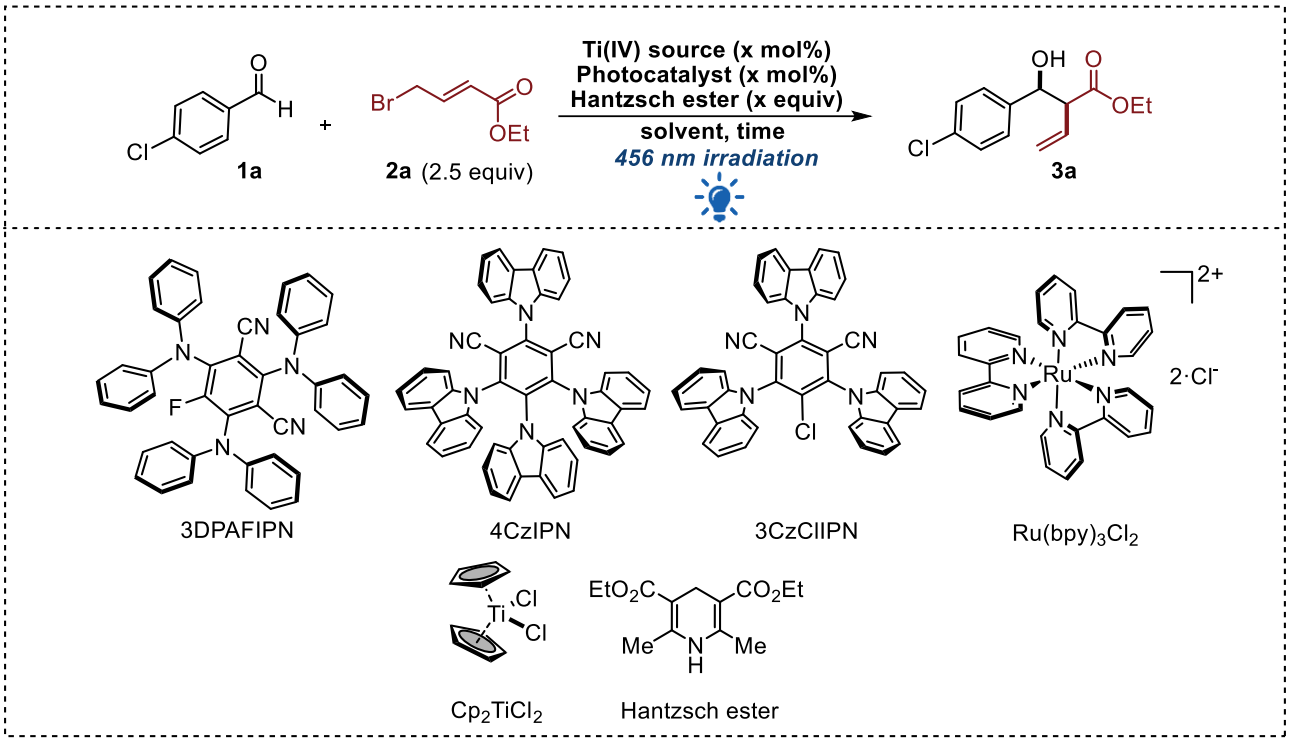

Entry	Time (h)	Ti source (mol%)	PC (mol%)	HE (equiv.)	Solvent (M)	Conversion(%)[a]	*dr*[b]
1	16	Cp_2TiCl_2 (10)	3DPAFIPN (5)	2.0	THF (0.05)	99	2.8:1
2	6	Cp_2TiCl_2 (10)	3DPAFIPN (5)	2.0	THF (0.05)	99 (91)	3.7:1
3	3	Cp_2TiCl_2 (10)	3DPAFIPN (5)	2.0	THF (0.05)	98 (91)	2.8:1
4[c]	5	Cp_2TiCl_2 (10)	3DPAFIPN (5)	2.0	THF (0.05)	89 (84)	3.7:1
5	3	Cp_2TiCl_2 (10)	3DPAFIPN (5)	2.0	THF (0.1)	99 (69)[d]	2.9:1
6	3	Cp_2TiCl_2 (10)	3DPAFIPN (5)	2.0	THF (0.2)	75 (0)[e]	-
7	3	Cp_2TiCl_2 (10)	3DPAFIPN (5)	2.0	Toluene (0.05)	88 (80)	3.0:1
8	3	Cp_2TiCl_2 (10)	3DPAFIPN (5)	2.0	MeCN (0.05)	71 (63)	2.8:1
9	3	Cp_2TiCl_2 (10)	3DPAFIPN (5)	2.0	DCM (0.05)	50 (32)	2.0:1
10	3	Cp_2TiCl_2 (10)	3DPAFIPN (5)	2.0	Et_2O (0.05)	99 (0)[e]	-
11	3	Cp_2TiCl_2 (5)	3DPAFIPN (5)	2.0	THF (0.1)	98 (90)	3.2:1
12	**3**	**Cp_2TiCl_2 (5)**	**3DPAFIPN (2)**	**2.0**	**THF (0.1)**	**98 (90)**	**3.2:1**
13	3	Cp_2TiCl_2 (10)	3DPAFIPN (5)	1.5	THF (0.05)	88 (85)	3.2:1
14	3	Cp_2TiCl_2 (5)	3DPAFIPN (2)	1.8	THF (0.1)	88 (83)	3.2:1
15	3	Cp_2TiCl_2 (5)	3CzClIPN (2)	2.0	THF (0.1)	93 (87)	3.0:1
16	3	Cp_2TiCl_2 (5)	4CzIPN (2)	2.0	THF (0.1)	93 (88)	3.0:1
17	3	Cp_2TiCl_2 (5)	$Ru(bpy)_3Cl_2$ (1)	2.0	THF (0.1)	NR	
18	3	$TiCl_4$ (5)	3DPAFIPN (2)	2.0	THF (0.1)	99 (0)[e]	-

*Table 6.1 [a] Determined by ^{1}H NMR analysis on the reaction crude. Isolated yields are reported in brackets.[b] drs reported as syn:anti and determined by ^{1}H NMR analysis on the reaction crude by integration of the vinylic C-H signals at H_{syn}= 5.88 ppm and H_{anti}= 5.62 ppm.[c] Reaction performed at 0°C.[d] Product **3a** formed as major product. Non-negligible undefined parasitic side-products detected.[e] No product detected. Pinacolization of **1a** as major side-product with $dr_{d/l:meso}$ = 1:1. NR = No reaction.*

Because the promising results under 3 hours of irradiation, we tried to reduce the amount of Cp_2TiCl_2, 3DPAFIPN and Hantzsch ester. We were able to reduce the amount of the titanium source to 5 mol%

(entry 11) and then the photocatalyst to 2 mol% (entry 12) without any significant decrease in the yield and in the stereoselectivity of the protocol. On the other hand, decreasing the amount of Hantzsch ester led to a drop of the conversion, even when using both 10 mol% of Cp_2TiCl_2 and 5 mol% of 3DPAFIPN (entry 13), or 5 mol% of Cp_2TiCl_2 and 2 mol% of 3DPAFIPN (entry 14).

Other TADF-emitter photocatalysts, i.e. 3CzClIPN (entry 15) and 4CzIPN (entry 16), were tested and they gave similar results, while the Ru-based photocatalyst $[Ru(bpy)_3]Cl_2$ (entry 17), although it should be suitable for the reduction of titanium,[381] was completely unable to catalyze the reaction.

Finally, other Ti(IV) sources were evaluated. Although the use of $TiCl_4$ in dual photoredox reactions was recently reported by Kanai,[382] under our conditions (entry 18) only the non-diastereoselective pinacolization of the aldehyde was observed.

Once we had the optimized conditions in hand, all the necessary control experiments were performed to find further confirmation about the reaction mechanism (*Table 6.2*). As expected, photoexcitation of the photocatalyst (entry 1) is mandatory for the reaction. Even though titanium itself could absorb light radiation at 456 nm (see the section 6.5 dedicated to the Photophysical studies for more details), the photocatalyst is the only species capable of undergoing productive SET events (entry 2). The Hantzsch ester is essential to sustain the catalytic cycle as the reducing agent (entry 3). Finally, the presence of Cp_2TiCl_2 is necessary (entry 4) since the photocatalyst is able to reduce the aldehyde in the presence of the pyridinium ion of the Hantzsch ester, as shown in the previous chapters, leading to the non-diastereoselective pinacol coupling.

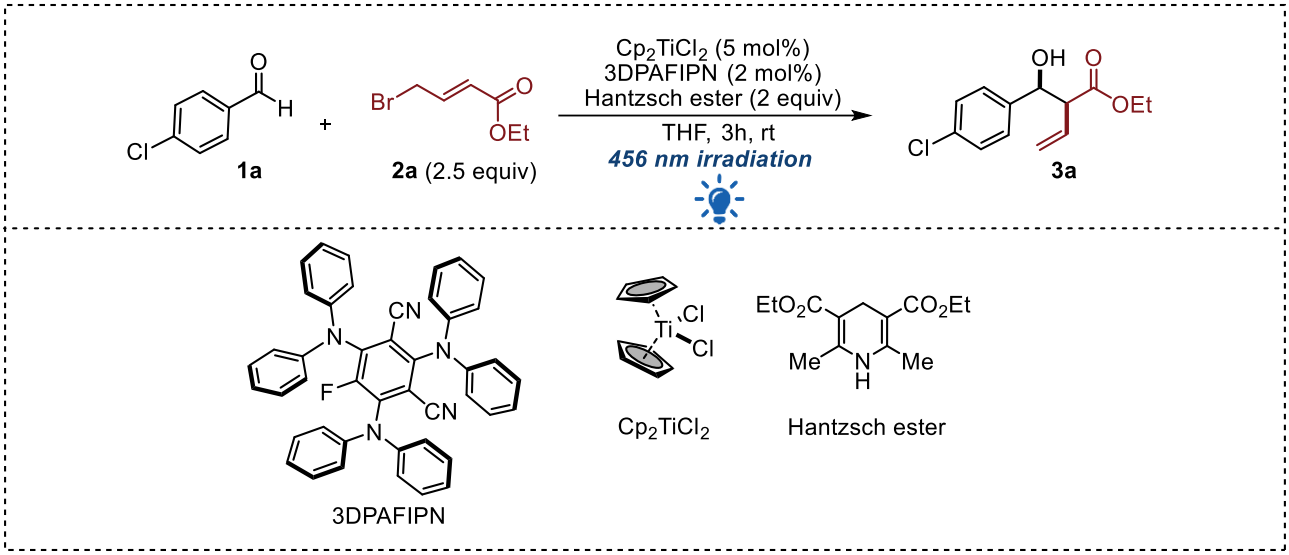

Entry	Deviation from standard conditions	Conversion(%)[a]	*dr*[b]
0	**none**	**98 (90)**	**3.2:1**
1	No light irradiation	NR	
2	No photocatalyst	NR	
3	No Hantzsch ester	NR	
4	No Cp_2TiCl_2	99 (0)[c]	-

*Table 6.2 [a] Determined by ^{1}H NMR analysis on the reaction crude. Isolated yields are reported in brackets.[b] drs reported as syn:anti and determined by ^{1}H NMR analysis on the reaction crude by integration of the vinylic C-H signals at H_{syn}= 5.88 ppm and H_{anti}= 5.62 ppm.[c] No product detected. Pinacolization of **1a** as major side-product with $dr_{d/l:meso}$ = 1:1. NR = No reaction.*

After a systematic evaluation of all reaction parameters, we were able to reveal the optimized conditions, shown in *Figure 6.12* obtaining the product **3a** in 90% of isolated yield, with a *dr* of 3.2:1 in favor of the *syn*-isomer and complete regiocontrol in favor of the branched-substituted homoallyl alcohol.

6.4 Scope evaluation

The optimized conditions were applied to a library of substituted aromatic aldehydes shown in *Figure 6.13*. All the reactions were carried on a 0.2 mmol scale.

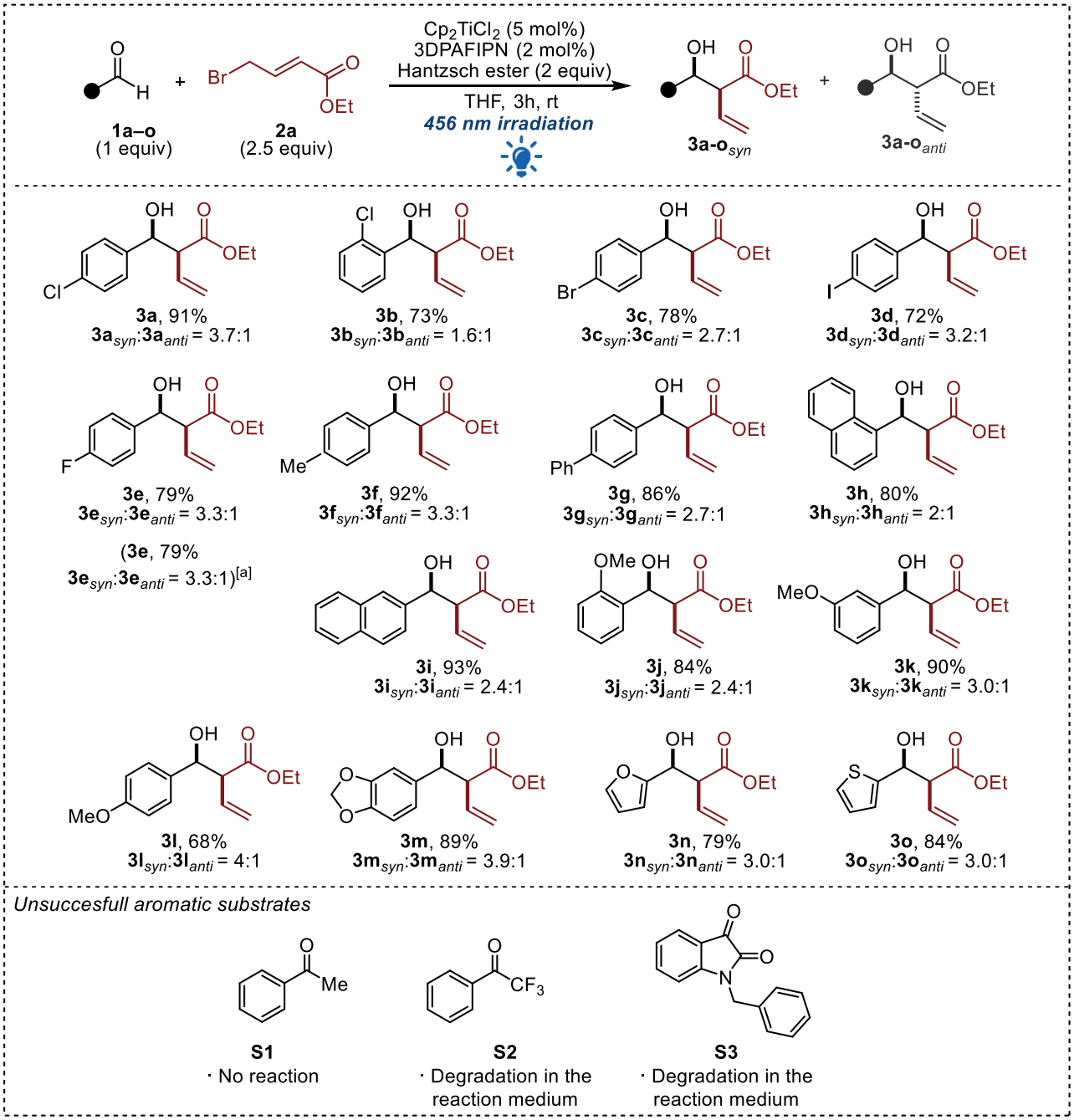

Figure 6.13 Scope of the aromatic aldehydes.[a] 1 mmol scale. Irradiation time extended to 16h.

In all cases the presence of the γ-allylation product was not detected. In general, we observed moderate *dr* ratios in the range of 1.6:1 to 4:1 in favor of the *syn*-diastereoisomer with a strong influence of the steric and the electronic properties of the aldehydes. The presence of steric hindrance near the carbonyl group, as in the case of 2-chlorobenzaldehyde (**1b**) and 2-methoxybenzaldehyde (**1j**), did not affect the yield of the transformation but led to a decrease in the diastereoselectivity (**3b**$_{syn}$:**3b**$_{anti}$ = 1.6:1 and **3j**$_{syn}$:**3j**$_{anti}$ = 2.4:1). On the other hand, the presence of electron donating groups in other positions of the aromatic ring had a positive effect on the diastereoselectivity, as in the case of 4-methoxybenzaldehyde (**3l**) (**3l**$_{syn}$:**3l**$_{anti}$ = 4.0:1). This could be due to a higher electronic density on the aldehydes which coordinates the titanium center more tightly in the cyclic transition state.

In contrast, the reactivity of the protocol was found to be independent from both electronic and steric effects. Electron-deficient 4-bromobenzaldehyde (**1c**), 4-iodobenzaldehyde (**1d**) and 4-fluorobenzaldehyde (**1e**), electron-neutral aromatic aldehydes (**1f-i**), as well as electron-rich **1j**, **1k** and **1m** were found to be suitable substrates under the optimal conditions leading to the formation of the corresponding α-vinyl-β-hydroxy esters with yields ranging between 78% and 93%. Remarkably, although the oxidation of the Hantzsch ester produces a strong Brønsted acid, sensitive substrates such as furfural (**1n**) were found to be suitable under the reaction conditions and no side-products were detected.

Substrate **1e** was chosen to test the scalability of the method on a 1 mmol scale. To ensure complete conversion of the starting material, the irradiation time was extended from 3 to 16 hours and the same results were obtained as for the 0.2 mmol scale.

Unfortunately, aromatic ketones were found not to be suitable substrates. While the simple acetophenone (**S1**) was not found to be reactive and was detected unreacted from ^{1}H NMR after the work-up of the reaction, activated ketones (**S2** and **S3**) gave unknown degradation side-products, detected by ^{1}H NMR.

The protocol was also applied to a few selected aliphatic aldehydes (*Figure 6.14*). Even when the irradiation time was extended to 16 hours keeping the other reaction parameters constant, a moderate reactivity and a lower diastereomeric control was observed. Since aliphatic aldehydes have a more negative reduction potential than their aromatic counterparts, the lower yields observed do not depend on the reductive dimerization of the carbonyl. On the contrary, from the analysis of the crude reaction mixture, the main parasitic reaction affecting the yield of the reaction has been attributed to the self-condensation of the aldehydes by aldol reactions: the presence of the acidic pyridinium salt, derived from the oxidation of the Hantzsch ester, probably favors this undesirable process by facilitating the formation of enols. Substituted hydrocinnamic aldehydes (**1p-t**) were tolerated under these conditions as well as aliphatic substrates bearing differently protected hydroxy groups (**1s** and **1t**). Furthermore, our protocol was found to be suitable in the presence of secondary aliphatic aldehydes, i.e. cyclohexane carboxaldehyde (**1u**) and linear unsubstituted aldehydes (**1v** and **1z)**. Unfortunately, after several attempts, we were unable to separate these products from undefined side-products derived from the degradation of **2a**. Moreover, only in the case of the linear aliphatic dodecanal (**1z**) both the regioisomers (**3z** and **3z'**) were detected. All the attempts to isolate **3z'** from the same unknown impurities derived from **2a** were unsuccessful.

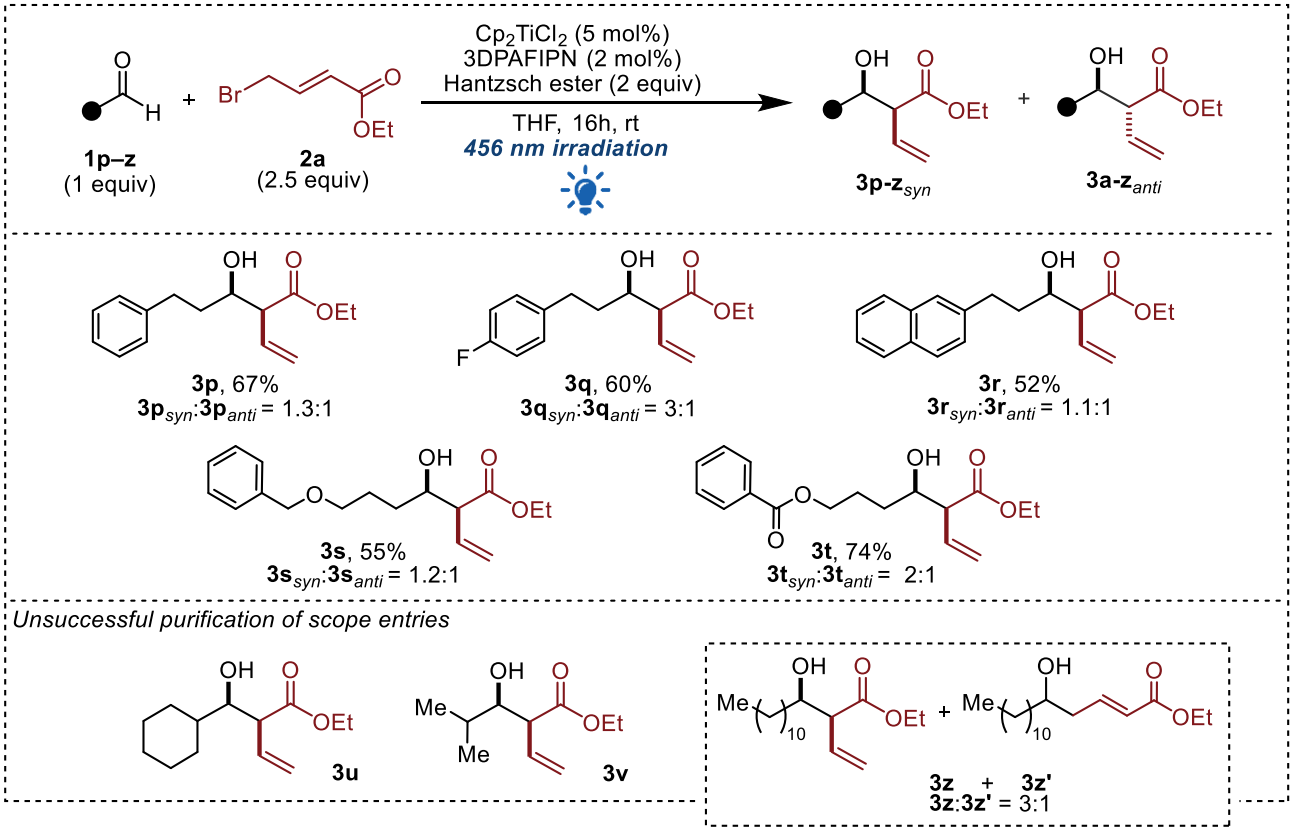

Figure 6.14 Scope of the aliphatic aldehydes.

We also extend the applicability of the protocol to other non-commercial 4-halocrotonate esters (*Figure 6.15*).

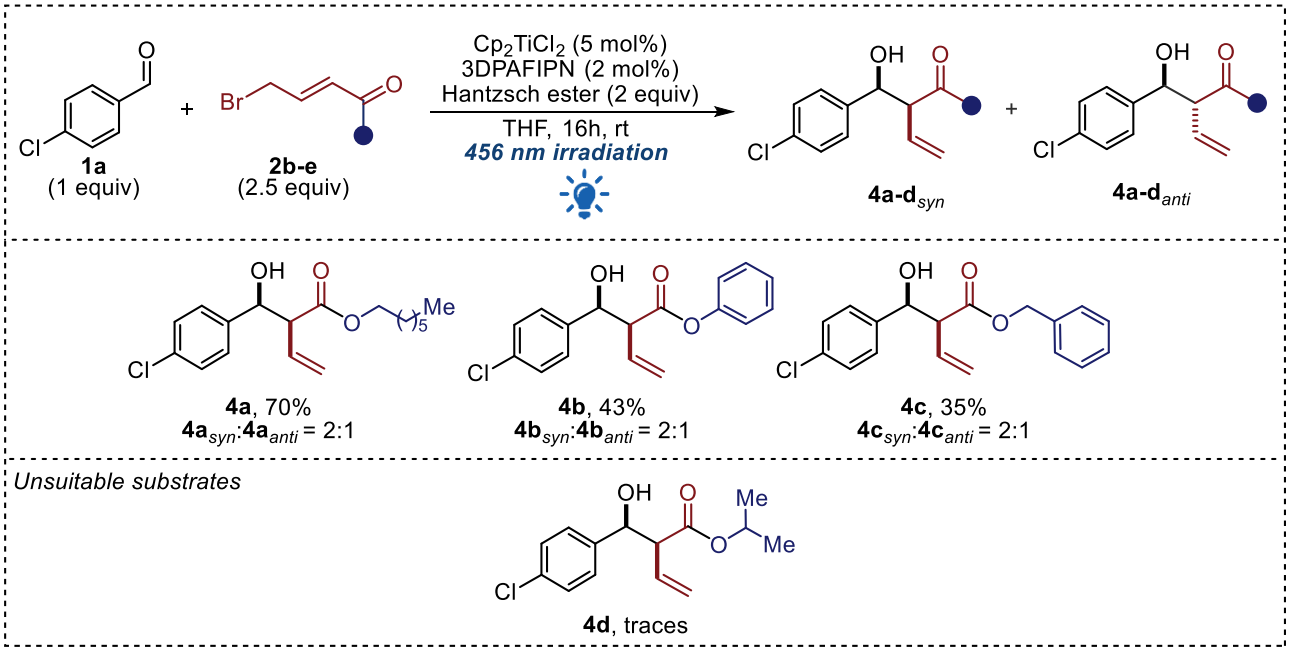

Figure 6.15 Scope of different esters of the 4-bromocrotonic acid.

However, when moving from the ethyl ester derivatives to the more sterically demanding heptyl (**4a**), phenyl (**4b**) or benzyl esters (**4c**), we observed a reduced reactivity, so the irradiation time was extended to 16h. At the same time, lower *dr* ratios were found. If a longer alkyl ester chain resulted in a slight

decrease in the yield, the use of a phenyl or benzyl ester produced a drastic decrease in the reactivity, while the more sterically demanding isopropyl ester (**4d**) caused a complete shutdown of the catalytic system.

Other pronucleophiles were also explored but unsaturated bromoketones or amides were found not suitable under the reported reaction conditions (*Figure 6.16*).

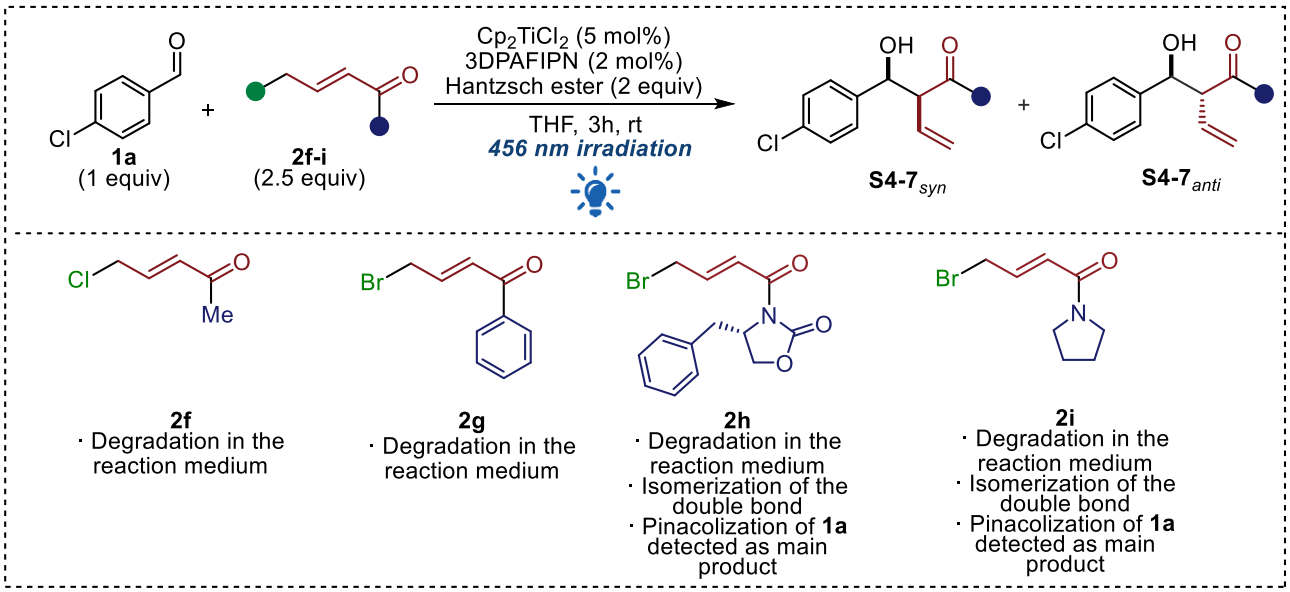

Figure 6.16 Unsuccessful attempts to use different pronucleophile allyl sources.

Finally, after having explored the generality of the protocol, we have briefly investigated the reactivity and the synthetic utility of α-vinyl-β-hydroxy esters by performing some further functionalization of **3e**, as shown in *Figure 6.17*.

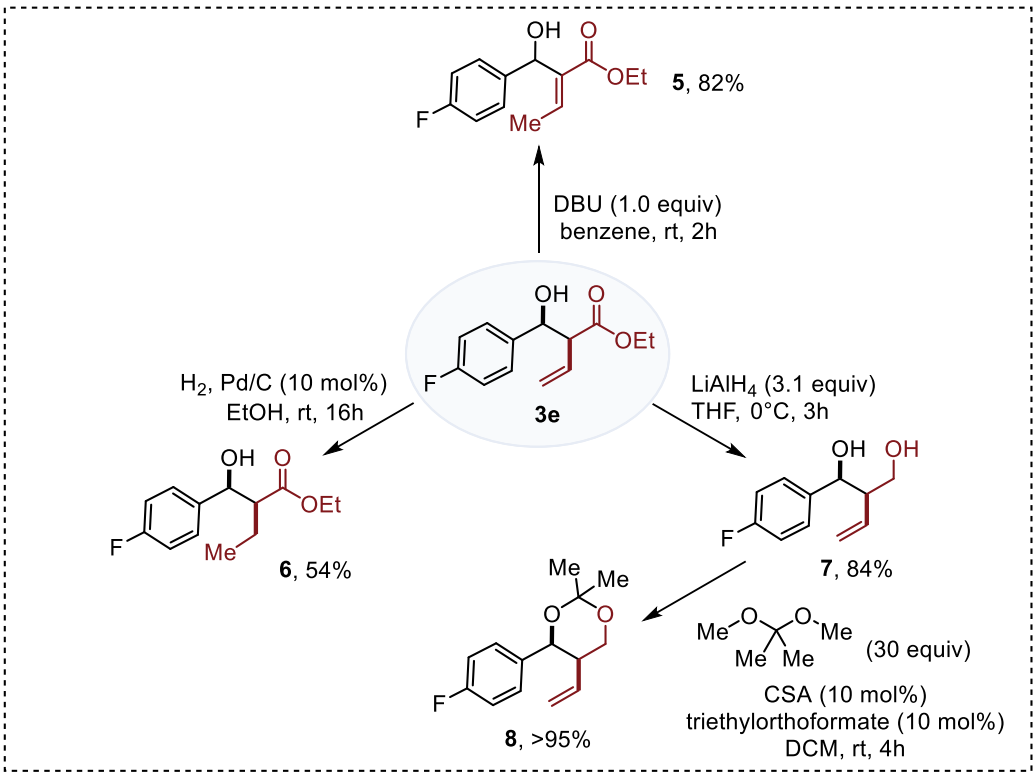

*Figure 6.17 Post functionalization of the substrate **3e**.*

First, from a diastereoisomeric mixture of **3e** (**3e**$_{syn}$:**3e**$_{anti}$ = 2.6:1) the terminal double bond was subjected to isomerization to approach the (*E*)-β-methyl Baylis–Hillman adduct.[383] Using a stoichiometric amount of 1,5-diazabicyclo(5.4.0)undec-7-ene (DBU) in benzene at room temperature, the thermodynamically favored α,β-unsaturated ester **5** was obtained in 82% yield with an *E/Z* ratio of 17:1. Starting from the diastereomerically pure **3e** (**3e**$_{syn}$:**3e**$_{anti}$ >20:1), the reduction of the double bond was accomplished in a diastereoselective manner and in a moderate yield using a catalytic amount of palladium on carbon (10 mol% w/w) under hydrogen atmosphere (1 atm) affording product **6**. Finally, to highlight the synthetic utility of the electron withdrawing ester moiety, diastereomerically pure **3e** (**3e**$_{syn}$:**3e**$_{anti}$ >20:1), was first reduced in the presence of lithium aluminium hydride ($LiAlH_4$) to give the corresponding 2-vinyl-1,3-diol **7**. The diol was further treated in the presence of an excess of 2,2-dimethoxypropane and a catalytic amount of camphorsulfonic acid (CSA, 10 mol%) and triethylorthoformate, giving access to the *syn*-1,3-acetonide **8** in quantitative yield. A slight erosion of the diastereomeric ratio was observed during the transformation from **3e** to **8.**

6.5 Photophysical studies and reaction mechanism

The analysis of the photophysical behavior of 3DPAFIPN in the presence of the different components of the reaction mixture shed light on the key aspects of the photoredox catalytic cycle. As shown in a previous publication by a combined photophysical and computational study,[237] catalytic 3DPAFIPN in the presence of an overstoichiometric amount of Hantzsch ester (HE) at concentrations near to its solubility limit in THF (0.1 M), is expected to quantitatively form with the HE the photoactive complex [3DPAFIPN · HE] (*Figure 6.18*).

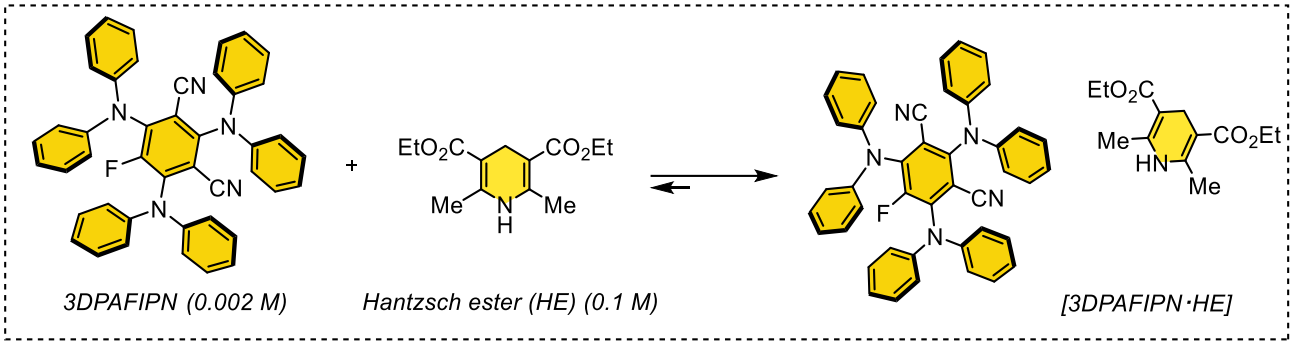

Figure 6.18 Formation of the photoactive complex [3DPAFIPN · HE] in the reaction conditions.

The complex thus formed still possesses suitable redox potentials for the efficient photoinduced electron transfer to the reactants involved in the transformation. As previously reported in a deaerated, stabilizer-free THF solution, it exhibits an absorption band in the visible range (ε = 14900 $M^{-1}cm^{-1}$ at λ = 370 nm) with an absorption onset at 470 nm, and an emission band centered at 520 nm, attributed to prompt fluorescence (τ = 3.6 ns) and delayed fluorescence (τ = 110 μs).

In particular, a quenching constant (k_q) of 2.1×10^8 M^{-1} s^{-1} was measured in the presence of an excess of Hantzsch ester (HE), which can effectively quench the excited state of the [3DPAFIPN · HE] complex at concentrations above 130 μM. In addition, aldehyde **1a**[237] and the pronucleophilic species **2a** do not significantly affect the luminescence lifetime ($k_q < 1.0\times10^6$ M^{-1} s^{-1}) (*Figure 6.19*)

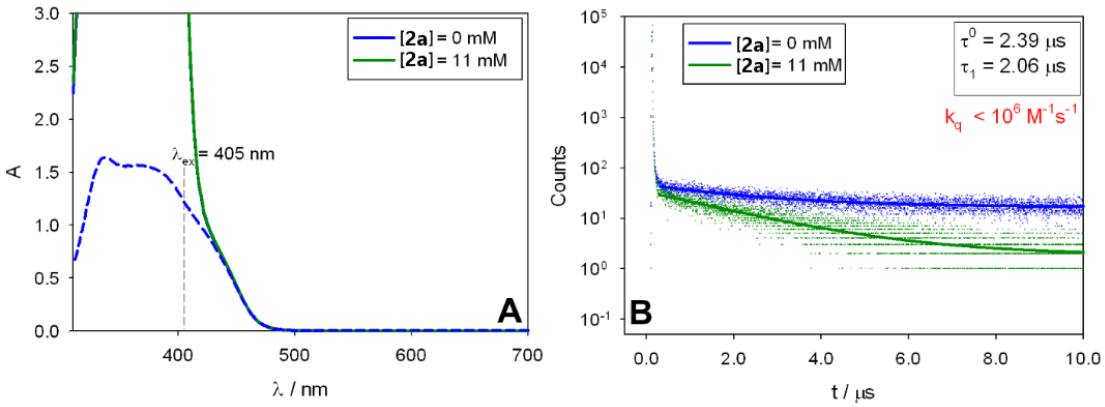

Figure 6.19 ***A****) Absorption spectra for a solution of 3DPAFIPN in THF (0.11 mM, dashed blue line), following the addition of HE (2.1 mM, solid blue line) and subsequent addition of* ***2a*** *(11.0 mM, green line).* ***B****) Corresponding emission intensity decays of 3DPAFIPN (λ_{ex} = 405 nm; λ_{em} = 530 nm) upon addition of HE (2.1 mM, blue dots) and subsequent addition of* ***2a*** *(11.0 mM, green dots). The corresponding monoexponential fitting are showed as the solid blue and green lines, respectively.*

On the contrary, for Cp_2TiCl_2 an efficient quenching of the luminescence lifetime of the [3DPAFIPN · HE] complex was determined (k_q = 1.1×10^9 M^{-1}s^{-1}) (*Figure 6.20*). Although Hantzsch ester has a lower quenching constant compared to that determined for Cp_2TiCl_2 (k_q = 2.1×10^8 M^{-1}s^{-1} *vs* 1.1×10^9 M^{-1}s^{-1}, respectively), considering the difference in concentration between Cp_2TiCl_2 and Hantzsch ester in the reaction mixture, the corresponding quenching efficiency for HE is higher compared to Cp_2TiCl_2 (78% *vs* 20%, respectively).

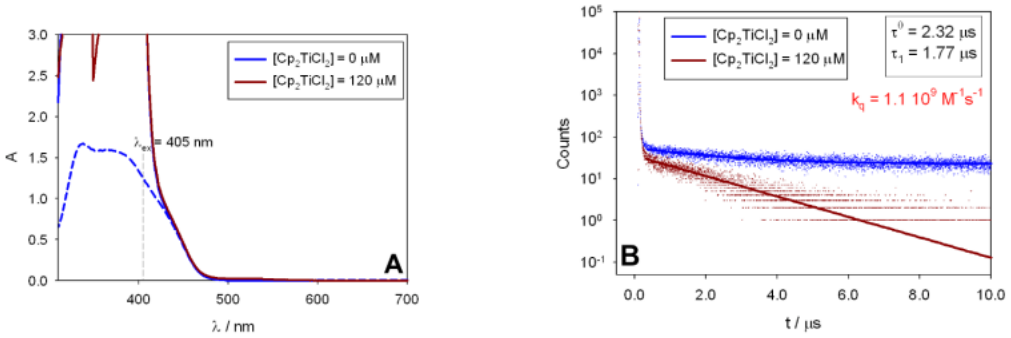

Figure 6.20 ***A****) Absorption spectra for a solution of 3DPAFIPN in THF (0.11 mM, dashed blue line), following the addition of HE (2.1 mM, solid blue line) and subsequent addition of Cp_2TiCl_2 (0.12 mM, brown line).* ***B****) Corresponding emission intensity decays of 3DPAFIPN (λ_{ex} = 405 nm; λ_{em} = 530 nm) upon addition of HE (2.1 mM, blue dots) and subsequent addition of Cp_2TiCl_2 (0.12 mM, brown lines). The corresponding monoexponential fitting are showed as the solid blue and brown lines, respectively.*

From the evidence obtained from the photophysical study we were able to propose a mechanistic cycle for the presented protocol (*Figure 6.21*). The process is initiated by the absorption of visible radiation by the photocatalyst. The Hantzsch ester can act as an efficient reductant (E_{ox}(HE$^{\bullet+}$/HE) = +1.0 V *vs* SCE) of the excited photoactive complex *[3DPAFIPN·HE] (*E_{red}(*[3DPAFIPN·HE]/[3DPAFIPN·HE]$^{\bullet-}$) = +0.58 V *vs* SCE) leading to the formation of [3DPAFIPN · HE]$^{\bullet-}$ and the concomitant formation of HE$^{\bullet+}$. The former, in a second step, can reduce (E_{red}([3DPAFIPN·HE]/[3DPAFIPN·HE]$^{\bullet-}$)= –1.59 V *vs* SCE) the Cp_2TiCl_2 (E_{red}(Ti^{IV}/Ti^{III}) = –0.75 V *vs* SCE in THF) triggering its redox activity towards the 4-bromocrotonate and simultaneously restoring the photoredox catalytic cycle.

Two molecules of Cp_2TiCl are necessary for the formation of the transient nucleophilic (π-allyl)-titanium organometallic species: the first one reduces the allyl halide derivative generating an allyl radical and restoring the titanium catalytic cycle, while the second one can trap the allyl radical, generating the nucleophilic organometallic $Cp_2Ti(\pi\text{-allyl})Cl$. Since the mechanism formally requires two molecules of Barbier-active transition metal for the generation of one transient nucleophilic organometallic reagent, it is not possible to exclude a possible role of the strong reductant $HE^{\bullet+}$ in further reductive events, leading to a short radical chain, that is light-independent.[3] Addition to the carbonyl leads to the homoallyl product as titanium alkoxide. During the approach, to rationalize the exclusive formation of the *syn*-products, a Zimmerman-Traxler transition state is plausible. Finally, the Ti-O bond is broken by the scavenging effect of the protons arising from the oxidative pathway of the Hantzsch ester, restoring the metal catalyst and releasing the desired product.

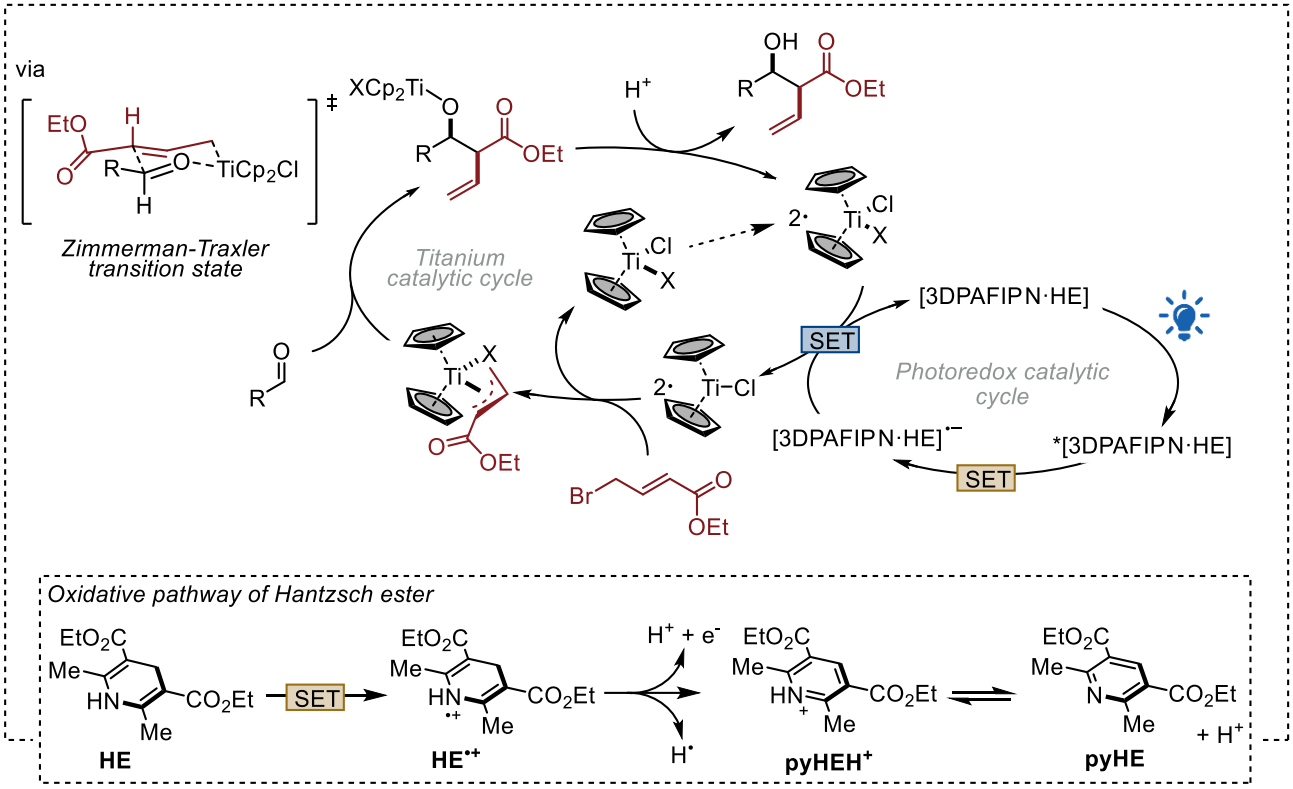

Figure 6.21 Proposed mechanism.

6.6 Conclusions

In conclusion, we have described a novel dual photoredox- and Cp_2TiCl_2-mediated allylation of aldehydes for the direct access to α-vinyl-β-hydroxy esters. The main advantages of this protocol compared to other routes already reported in the literature are the low titanium and photocatalyst loading, the fast, reproducible, robust and regioselective methodology and the wide compatibility of substrates. Although the protocol is suitable only for 4-halocrotonic esters and cannot be extended to other functional groups such as ketones or amides, and the moderate diastereoselectivity, the protocol avoids the use of metal reducing agents, expensive rare metals such as indium, or boron-based preformed nucleophilic allyl species, making it a valid and attractive alternative to get access to a multi-decorated homoallylic moiety. The presence of different functional groups has been exploited in different post-functionalization reactions, demonstrating the versatility of the substrate. Further

studies, directed towards a general Reformatsky reaction promoted by titanium or other metals are in progress in our research group.

Full account and description of the content of the chapter have been published in: E. Pinosa, A. Gualandi, A. Fermi, P. Ceroni, F. Calogero, P. G. Cozzi, *J. Org. Chem.* **2023**, *26*, e202300421.

6.7 Experimental section

General Methods

^{1}H NMR spectra were recorded on Varian Mercury 400 and on Bruker 600 spectrometer. Chemical shifts are reported in ppm from TMS with the solvent resonance as the internal standard ($CHCl_3$, δ = 7.26 ppm). Data are reported as follows: chemical shift, multiplicity (s = singlet, d = doublet, t = triplet, q = quartet, dd = doublet of doublets, ddd = doublet of doublet of doublets, dt = doublet of triplets, dq = doublet of quartets, dddd = doublet of doublet of doublet of doublets, ddt = doublet of doublet of triplets, dtd = doublet of triplet of doublets, tdd = triplet of doublet of doublets, td = triplet of doublets, tt = triplet of triplets, qd = quartet of doublets, m = multiplet), coupling constants (Hz), number of protons. ^{13}C NMR spectra were recorded on Varian Mercury 400 spectrometer. Chemical shifts are reported in ppm from TMS with the solvent as the internal standard ($CDCl_3$, δ = 77.0 ppm, C_6D_6, δ = 127.7 ppm). ^{19}F NMR spectra were recorded on Varian Mercury 400 spectrometer. Chemical shifts are reported in ppm. All the reagents were purchased from commercial sources (Sigma-Aldrich, Alfa Aesar, Fluorochem, Strem Chemicals, TCI) and used without further purification unless specified. Liquid aldehydes were purified by distillation prior to use. Starting materials (**1p-t**) were prepared according to a reported procedure.[237] Ethyl 4-bromobut-2-enoate was purchased by Fluorochem (*E/Z* ratio > 20:1 calculated from ^{1}H NMR). HRMS was performed on a Waters Xevo G2-XS QTof, ESI+, cone voltage 40 V, Capillary 3KV, with a source temperature of 120°C. All reactions requiring inert atmosphere were set up under an argon atmosphere in heat gun-dried glassware using standard Schlenk techniques. Anhydrous solvents were supplied by Aldrich in Sureseal® bottles and, unless specified, were used without further treatment. Anhydrous tetrahydrofuran (THF) was obtained by standard sodium/benzophenone distillation starting from reagent grade THF, supplied by TCIR or Sigma Aldrich®. Freshly distilled THF was stored under argon atmosphere in a dry Schlenk tube, equipped with a Rotaflo® stopcock with activated 3Å molecular sieves (ca. 5 g of MS for 100 mL of solvent). 3Å molecular sieves were supplied by Sigma-Aldrich®. Activation of the MS was performed through 5 x 6-minute cycles in microwave (750 W). Once the cycles are completed the MS are rapidly inserted in a heat gun- dried dry Schlenk tube, equipped with a Rotaflo® stopcock and then flame-dried for 5 minutes under vacuum before starting the distillation. Kessil® PR160L@456 nm were used as light source for the photocatalytic reactions (see *Figure 6.22* for the emission profile). 2,4,6-tri(diphenylamino)-5-fluoroisophthalonitrile (3DPAFIPN), 2,4,6-tri(9H-carbazol-9-yl)-5-chloro-isophthalonitrile (3CzClIPN) and 2,4,5,6-tetrakis(carbazol-9-yl)-isophthalonitrile (4CzIPN), were prepared according to published literature procedures.[90] Synthesis of Hantzsch ethyl ester was achieved following the reported literature procedure.[244]

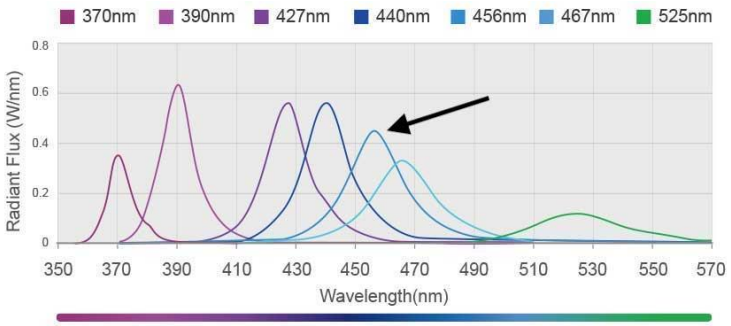

Figure 6.22 Emission profile of the Kessil® PR160L@456 nm used to irradiate the solutions (from Kessil® website: https://www.kessil.com/science/PR160L.php)

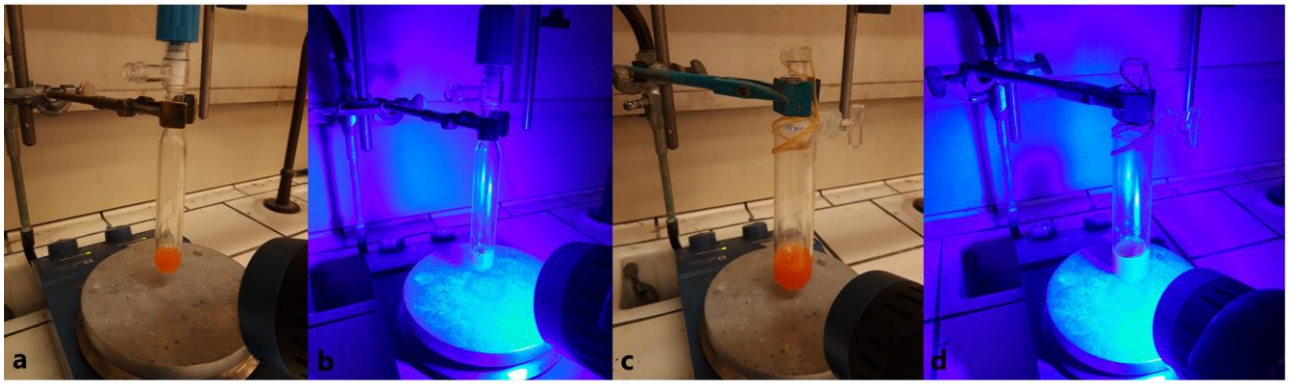

*Figure 6.23 (**a**) Model reaction set-up before and (**b**) during irradiation with Kessil® PR160L@456 nm lamp. (**c**) 1 mmol scale before and (**d**) during irradiation with Kessil® PR160L@456 nm lamp. The reaction flasks were positioned approximatively at 15 cm from the light source and Kessil® PR160. The reaction temperature was close to room temperature (25-28°C) during the irradiation.*

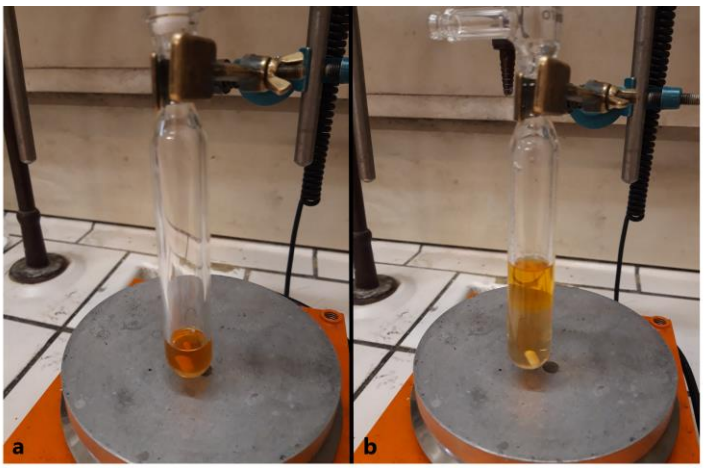

*Figure 6.24 (**a**) Model reaction before and (**b**) after quenching with 2M HCl.*

Photophysical analyses

General Methods

All the photophysical analyses were carried out in deoxygenated, stabilizer-free tetrahydrofuran (THF) at 298 K, unless otherwise specified. Experiments in absence of oxygen were carried out in a nitrogen-filled glovebox in a custom-made quartz cuvette. UV–vis absorption spectra were recorded with a PerkinElmer λ40 spectrophotometer using quartz cells with 1.0 cm optical path. Luminescence spectra were performed with an Edinburgh FS5 spectrofluorometer equipped with a Hamamatsu

Photomultiplier R928P phototube. Lifetimes shorter than 10 μs were measured by an Edinburgh FLS920 spectrofluorometer by time-correlated single-photon counting (TCSPC) technique. Lifetimes longer than 10 μs were measured by the above-mentioned Edinburgh FS5 spectrofluorometer or by a Varian Cary Eclipse fluorescence spectrophotometer. The estimated experimental errors are 2 nm on the band maximum, 5% on the molar absorption coefficient and luminescence lifetimes.

General procedure for dual photoredox Barbier titanium-catalyzed vinylogous aldol reaction with a 4-bromocrotonate.

All the reactions were performed on 0.2 mmol scale. A heat-gun dried 10 mL Schlenk tube, equipped with a Rotaflo stopcock, magnetic stirring bar and an argon supply tube, was first charged under argon with the substrate **1** if solid or not volatile (0.2 mmol), photocatalyst 3DPAFIPN (2.6 mg, 0.004 mmol, 2 mol%), Cp_2TiCl_2 (2.5 mg, 0.01 mmol, 5 mol%) and diethyl 1,4-dihydro-2,6-dimethyl-3,5-pyridinedicarboxylate (Hantzsch ester, 101 mg, 0.4 mmol, 2 equiv.). THF (2 mL to obtain a 0.1 M substrate solution) was then added, and the reaction mixture was further subjected to a freeze-pump-thaw procedure (three cycles) and the vessel was refilled with argon. Then, (*E*)-ethyl 4-bromobut-2-enoate **2a** (69 μL, 0.5 mmol, 2.5 equiv.) and **1** (if volatile, 0.2 mmol) were added. The reaction was irradiated under vigorous stirring for the desired time (3h for aromatic substrates **1a-o** or 16h for aliphatic substrates **1p-t**). After that the reaction mixture was quenched with HCl 2M (ca. 5 mL) and extracted with AcOEt (3 x 10 mL). The reaction crude was analyzed by ^{1}H NMR for the evaluation of the diastereomeric ratio. The NMR sample was carefully recovered, and the solvent was removed under reduced pressure. The title compounds were isolated by flash column chromatography (SiO_2). In most of the cases, unless otherwise noted, two consecutive flash chromatography purifications were needed. (1st with DCM/Hexane as eluent, 2nd with AcOEt/Hexane as eluent).

General procedure for the 1 mmol scale reaction

A dry 50 mL Schlenk tube, equipped with a Rotaflo stopcock, magnetic stirring bar, and an argon supply tube, was first charged under argon with photocatalyst 3DPAFIPN (13 mg, 0.02 mmol, 2 mol%), Cp_2TiCl_2 (12.5 mg, 0.05 mmol, 5 mol%) and diethyl 1,4-dihydro-2,6-dimethyl-3,5-pyridinedicarboxylate (Hantzsch ester, 506 mg, 2 mmol, 2 equiv.). THF (20 mL to obtain a 0.1 M substrate solution) was then added, and the reaction mixture was further subjected to a freeze-pump-thaw procedure (three cycles) and the vessel refilled with argon. Then, freshly distilled 4-fluorobenzaldeyde **1e** (107 μL, 1 mmol, 1 equiv.) and (*E*)-ethyl 4-bromobut-2-enoate **2a** (344 μL, 2.5 mmol, 2.5 equiv.) were added. The reaction was irradiated under vigorous stirring for 16h. After that the reaction mixture were quenched with HCl 2M (ca. 20 mL) and extracted with AcOEt (3 x 15 mL). The reaction crude was analyzed by ^{1}H NMR for the evaluation of the diastereomeric ratio. The NMR sample was carefully recovered, the solvent was removed under reduced pressure and purified by two consecutive flash chromatography (SiO_2, 1st 9:1 DCM/Hexane to 100% DCM, 2nd 7:1 Hexane/AcOEt). After purification, product **3e** was obtained in 79% yield. In detail, 134 mg (56% yield) of **3e** were isolated as a single *syn*– diastereoisomer. 54 mg (23% yield) of **3e** were isolated as a mixture 5:1 *anti:syn*.

Synthesis of heptyl (*E*)-but-2-enoate (S9)

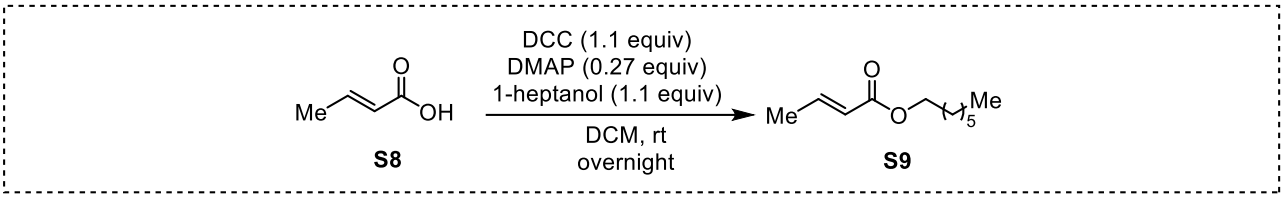

A flame-dried three neck bottom flask under nitrogen atmosphere was charged with **S8** (672 mg, 7 mmol, 1 equiv.), 4-dimethylaminopyridine (DMAP, 196 mg, 1.9 mmol, 0.27 equiv.) and 16 mL of DCM, then a solution of 1-heptanol (1.1 mL, 7.7 mmol, 1.1 equiv.), *N,N'*-dicyclohexylcarbodiimide (DCC, 1.59 g, 7.7 mmol, 1.1 equiv.) in 16 mL of DCM was added dropwise. The reaction mixture was stirred for 16h at room temperature. After the consumption of the starting material the solvent was removed *in vacuo*. The reaction crude was dissolved in diethyl ether and the solid precipitated was filtered off and rinsed with diethyl ether. The crude product was purified by flash chromatography (SiO_2, 100% Petroleum ether to 20:1 Petroleum ether/AcOEt) to afford **S9** as a colorless oil in 74% yield (1.0 g, 5.18 mmol). Spectroscopic data are in agreement with those reported in the literature.[384]

Synthesis of phenyl (*E*)-but-2-enoate (S10)

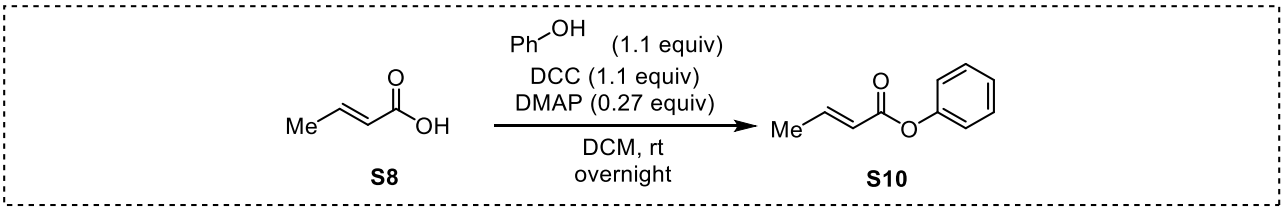

A flame-dried three neck bottom flask under nitrogen atmosphere was charged with **S8** (672 mg, 7 mmol, 1 equiv.), 4-dimethylaminopyridine (DMPA, 196 mg, 1.9 mmol, 0.27 equiv.) and 16 mL of DCM, then a solution of 1-heptanol (1.1 mL, 7.7 mmol, 1.1 equiv.), *N,N'*-dicyclohexylcarbodiimide (DCC, 1.59 g, 7.7 mmol, 1.1 equiv.) in 16 mL of DCM was added dropwise. The reaction mixture was stirred for 16h at room temperature. After the consumption of the starting material the solvent was removed *in vacuo*. The reaction crude was dissolved in diethyl ether and the solid precipitated was filtered off and rinsed with diethyl ether. The crude product was purified by flash chromatography (SiO_2, 100% Petroleum ether to 20:1 Petroleum ether/AcOEt) to afford **S10** as a colorless oil in 44% yield (500 mg, 3.08 mmol). Spectroscopic data are in agreement with those reported in the literature.[385]

Synthesis of (*E*)-4-bromobut-2-enoic acid (S11)

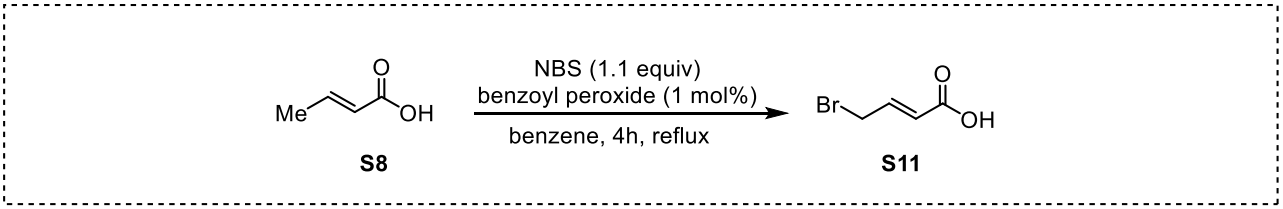

Adapted from literature.[386] A flame-dried two neck bottom flask under nitrogen atmosphere was charged with **S8** (288 mg, 3 mmol, 1 equiv.) and 5mL of benzene. Then *N*-bromosuccinimide (NBS, 587 mg, 3.3 mmol, 1.1 equiv.) and benzoyl peroxide (7.3 mg, 0.03 mmol, 1 mol%) were added. The reaction mixture was refluxed under vigorous stirring for 4h. After the consumption of the starting material the solvent was removed *in vacuo*. The reaction crude was dissolved in diethyl ether and the solid precipitated was filtered off and rinsed with diethyl ether. The crude product was washed with water to remove the remaining succinimide. The organic phase was dried over Na_2SO_4 and the solvent was

removed *in vacuo*. The crude product **S11** was used without further purification in the next step. Spectroscopic data are in agreement with those reported in the literature.[387]

Synthesis of heptyl (*E*)-4-bromobut-2-enoate (2b)

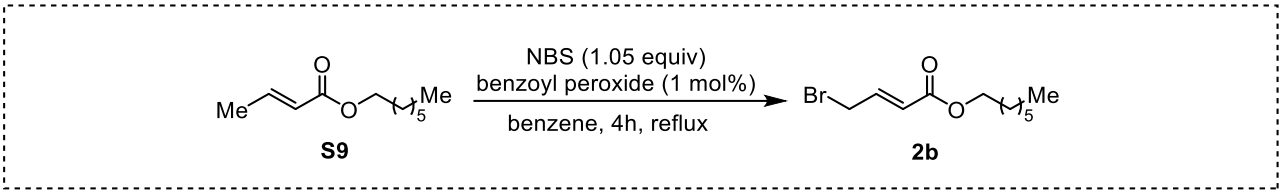

Adapted from literature.[386] A flame-dried two neck bottom flask under nitrogen atmosphere was charged with **S9** (552 mg, 3 mmol, 1 equiv.) and 6 mL of benzene. Then *N*-bromosuccinimide (NBS, 561 mg, 3.15 mmol, 1.05 equiv.) and benzoyl peroxide (7.3 mg, 0.03 mmol, 1 mol%) were added. The reaction mixture was refluxed under vigorous stirring for 4h. After the consumption of the starting material the solvent was removed *in vacuo*. The reaction crude was dissolved in diethyl ether and the solid precipitated was filtered off and rinsed with diethyl ether. The crude product was washed with water to remove the remaining succinimide. The organic phase was dried over Na_2SO_4 and the solvent was removed in vacuo. The crude product was purified by flash chromatography (SiO_2, 60:1 Petroleum ether/Et_2O) to afford **2b** as a colorless oil in 43% yield (337 mg, containing approximatively 10% of starting ester).

^{1}H NMR (600 MHz, $CDCl_3$) δ = 7.03 – 6.97 (m, 1H), 6.03 (dt, *J* = 15.3, 1.3 Hz, 1H), 4.15 (t, *J* = 6.7 Hz, 2H), 4.01 (dd, *J* = 7.3, 1.3 Hz, 2H), 1.68 – 1.64 (m, 2H), 1.37 – 1.27 (m, 8H), 0.89 (t, *J* = 7.0 Hz, 3H). ^{13}C NMR (150 MHz, $CDCl_3$) δ = 165.7, 141.7, 124.8, 65.1, 31.8, 29.3, 29.0, 28.7, 26.0, 22.7, 14.2.

Synthesis of phenyl (*E*)-4-bromobut-2-enoate (2c)

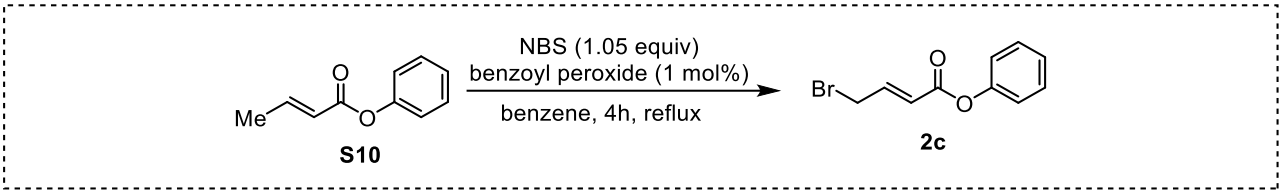

Adapted from literature.[386] A flame-dried two neck bottom flask under nitrogen atmosphere was charged with **S10** (500 mg, 3.1 mmol, 1 equiv.) and 10 mL of benzene. Then *N*-bromosuccinimide (579 mg, 3.26 mmol, 1.05 equiv.) and benzoyl peroxide (7.3 mg, 0.03 mmol, 1 mol%) were added. The reaction mixture was refluxed under vigorous stirring for 4 hours. After the consumption of the starting material the solvent was removed in vacuo. The reaction crude was dissolved in diethyl ether and the solid precipitated was filtered off and rinsed with diethyl ether. The crude product was washed with water to remove the remaining succinimide. The organic phase was dried over sodium sulphate and the solvent was removed *in vacuo*. The crude product was purified by flash chromatography (SiO_2, 30:1 Petroleum ether/Et_2O) to afford **2c** as a colorless oil in 26% yield (191 mg, 0.81 mmol). Spectroscopic data are in agreement with those reported in the literature.[388]

Synthesis of benzyl (*E*)-4-bromobut-2-enoate (2d)

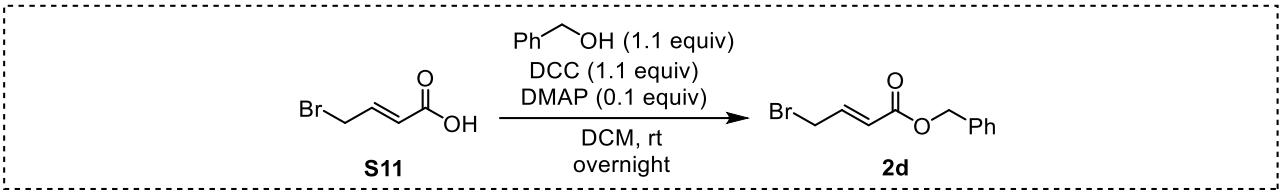

A flame-dried three neck bottom flask under nitrogen atmosphere was charged with **S11** (330 mg, 2 mmol, 1 equiv.), 4-dimethylaminopyridine (DMAP, 66 mg, 0.54 mmol, 0.27 equiv.) and 4 mL of DCM, then a solution of 1-heptanol (0.23 mL, 2.2 mmol, 1.1 equiv.), *N,N'*-dicyclohexylcarbodiimide (DCC, 433 mg, 2.1 mmol, 1.05 equiv.) in 4 mL of DCM was added dropwise. The reaction mixture was stirred for 3h at room temperature. After the consumption of the starting material the solvent was removed *in vacuo*. The reaction crude was dissolved in diethyl ether and the solid precipitated was filtered off and rinsed with diethyl ether. The crude product was purified by flash chromatography (SiO_2, 40:1 Petroleum ether/Et_2O) to afford **2d** as a colorless oil in 47% yield (240 mg, 0.94 mmol). Spectroscopic data are in agreement with those reported in the literature.[388]

Characterization of the products

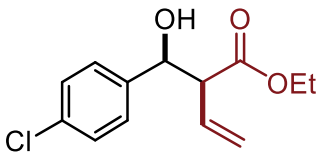

Ethyl 2-((4-chlorophenyl)(hydroxy)methyl)but-3-enoate (3a). Yield 91% (46 mg, 0.181 mmol). Pale yellow oil. $dr_{syn:anti}$ = 3.2:1 calculated considering the ^{1}H NMR spectrum of the reaction crude and comparing the integral of the signal at 5.90 ppm for the *syn*-diastereoisomer and at 5.66 ppm for the *anti*-diastereoisomer. **3a** was obtained following the general procedure as stated above employing 0.2 mmol (28 mg, 1 equiv.) of **1a** and 0.5 mmol (69 µL, 2.5 equiv.) of **2a**. The title compound was isolated by two consecutive flash column chromatography (SiO_2, 1st 100% DCM, 2nd 9:1 Hexane/AcOEt) and it was obtained as a 2.6:1 *syn*:*anti* mixture.

***Syn*-diastereoisomer** ^{1}H NMR (600 MHz, $CDCl_3$) δ = 7.29 – 7.21 (m, 4H, overlapped with the residual peak of the NMR solvent, *syn*+*anti*), 5.90 (ddd, J = 17.3, 10.2, 8.9 Hz, 1H), 5.25 (dd, J = 10.3, 1.2 Hz, 1H,), 5.13 (d, J = 17.3 Hz, 1H), 4.97 (d, J = 5.9 Hz, 1H), 4.05 (q, J = 7.1 Hz, 2H), 3.25 (dd, J = 8.9, 5.8 Hz, 1H), 3.09 – 3.02 (m, 1H), 1.13 (t, J = 7.1 Hz, 3H). ^{13}C NMR (101 MHz, $CDCl_3$) δ = 172.4, 139.2, 133.5, 131.4, 128.3 (2C), 127.8 (2C), 120.9, 73.2, 61.1, 58.1, 14.0.

***Anti*-diastereoisomer** ^{1}H NMR (600 MHz, $CDCl_3$) δ = 7.29 – 7.21 (m, 4H, overlapped with the residual peak of the NMR solvent, *syn*+*anti*), 5.66 (ddd, J = 17.3, 10.3, 8.6 Hz, 1H), 5.08 (d, J = 10.4 Hz, 1H), 5.04 – 4.99 (m, 1H), 4.90 – 4.85 (m, 1H), 4.16 (q, J = 7.1 Hz, 2H), 3.34 (t, J = 8.3 Hz, 1H), 3.11 (d, J = 5.2 Hz, 1H), 1.22 (t, J = 7.1 Hz, 3H).^{13}C NMR (101 MHz, $CDCl_3$) δ = 172.7, 139.7, 133.6, 131.9, 128.4 (2C), 128.0 (2C), 119.8, 74.5, 61.1, 57.8, 14.1.

HRMS (ESI/Q-TOF) m/z: $[M+Na]^+$ calcd for $C_{13}H_{15}ClNaO_3$ 277.0602, found 277.0595.

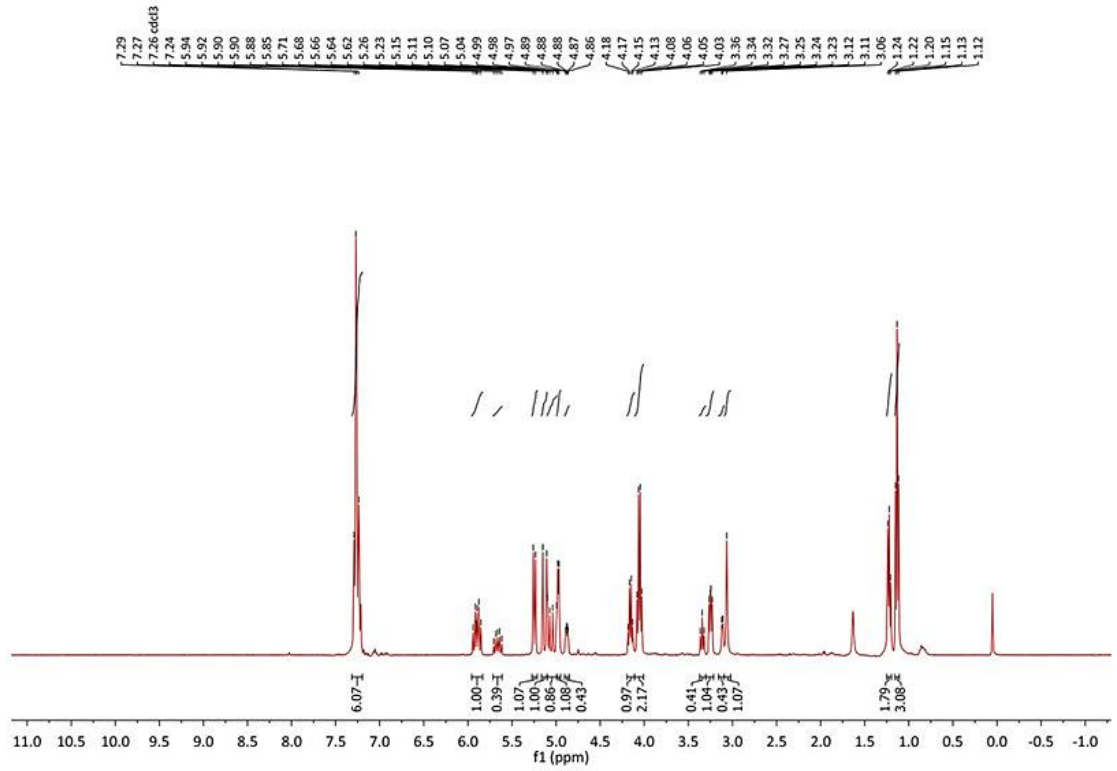

*Figure 6.25 ^{1}H NMR of **3a** ($dr_{syn:anti}$ = 2.6:1).*

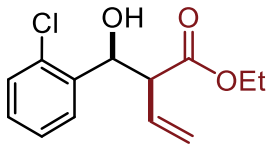

Ethyl 2-((2-chlorophenyl)(hydroxy)methyl)but-3-enoate (3b). Yield 73% (37 mg, 0.146 mmol). Pale yellow oil. $dr_{syn:anti}$ = 1.6:1 calculated considering the ^{1}H NMR spectrum of the reaction crude and comparing the integral of the signal at 5.52 ppm for the *syn*-diastereoisomer and at 5.38 ppm for the *anti*-diastereoisomer. **3b** was obtained following the general procedure as stated above employing 0.2 mmol (28 mg, 23 µL, 1 equiv.) of freshly distilled **1b** and 0.5 mmol (69 µL, 2.5 equiv.) of **2a**. The title compound was isolated by two consecutive flash column chromatography (SiO^{2}, 1st 4:1 DCM/Hexane to 100% DCM, 2nd 9:1 Hexane/AcOEt). 18 mg (36% yield) of **3b** were isolated as a single *syn*-diastereoisomer. 7 mg (14% yield) of **3b** were isolated as a single *anti*-diastereoisomer. 12 mg (23% yield) of **3b** were isolated a mixture 1:1.5 *anti*:*syn* diastereoisomers.

***Syn*-diastereoisomer** ^{1}H NMR (400 MHz, $CDCl_3$) δ = 7.53 (dd, J = 7.7, 1.8 Hz, 1H), 7.32 (dd, J = 7.8, 1.4 Hz, 1H), 7.27 (td, J = 7.5, 1.5 Hz, 1H, overlapped with the residual peak of the NMR solvent), 7.20 (td, J = 7.6, 1.8 Hz, 1H), 5.90 (ddd, J = 17.2, 10.3, 8.7 Hz, 1H), 5.52 (d, J = 3.4 Hz, 1H), 5.16 (dd, J = 10.3, 1.3 Hz, 1H), 4.95 (dt, J = 17.2, 1.1 Hz, 1H), 4.20 (q, J = 7.1 Hz, 2H), 3.52 (dd, J = 8.8, 3.4 Hz, 1H), 1.25 (t, J = 7.4 Hz, 3H). ^{13}C NMR (101 MHz, $CDCl_3$) δ = 173.5, 137.8, 131.4, 130.2, 129.2, 128.7, 128.7, 126.6, 120.7, 70.1, 61.3, 53.9, 14.0.

***Anti*-diastereoisomer** ^{1}H NMR (400 MHz, $CDCl_3$) δ = 7.48 (dd, J = 7.7, 1.7 Hz, 1H), 7.34 – 7.31 (m, 1H), 7.31 – 7.27 (m, 1H), 7.24 – 7.19 (m, 1H), 5.91 (ddd, J = 16.9, 10.3, 8.5 Hz, 1H), 5.38 (t, J = 6.6 Hz, 1H), 5.18 – 5.09 (m, 2H), 4.16 – 4.11 (m, 2H), 3.57 – 3.54 (m, 1H), 3.53 (d, J = 6.7 Hz, 1H), 1.19 (t, J = 7.1 Hz, 3H). ^{13}C NMR (101 MHz, $CDCl_3$) δ = 172.9, 138.8, 132.4, 132.1, 129.4, 128.9, 127.8, 127.0, 119.4, 71.8, 61.1, 56.1, 14.0.

HRMS (ESI/Q-TOF) m/z: $[M + Na]^{+}$ calcd for $C_{13}H_{15}ClNaO_3$ 277.0602, found 277.0594.

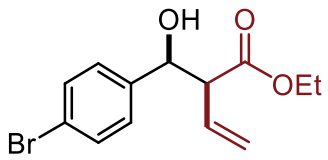

Ethyl 2-((4-bromophenyl)(hydroxy)methyl)but-3-enoate (3c). Yield 78% (47 mg, 0.156 mmol). Pale yellow oil. $dr_{syn:anti}$ = 2.7:1 calculated considering the ^{1}H NMR spectrum of the reaction crude and comparing the integral of the signal at 3.26 ppm for the *syn*-diastereoisomer and at 3.33 ppm for the *anti*-diastereoisomer. **3c** was obtained following the general procedure as stated above employing 0.2 mmol (37 mg, 1 equiv.) of **1c** and 0.5 mmol (69 µL, 2.5 equiv.) of **2a**. The title compound was isolated by two consecutive flash column chromatography (SiO_2, 1st 100% DCM, 2nd 9:1 Hexane/AcOEt). 20 mg (33% yield) of **3c** were isolated as a single *syn*-diastereoisomer. 27 mg (45% yield) of **3c** were isolated as a mixture 2.1:1 *anti:syn* diastereoisomers.

***Syn*-diastereoisomer** ^{1}H NMR (400 MHz, $CDCl_3$) δ = 7.48 – 7.42 (m, 2H), 7.24 – 7.18 (m, 2H), 5.91 (ddd, J = 17.2, 10.2, 8.9 Hz, 1H), 5.27 (dd, J = 10.1, 1.3 Hz, 1H), 5.15 (dt, J = 17.2, 1.1 Hz, 1H), 4.99 (dd, J = 5.7, 2.1 Hz, 1H), 4.08 (q, J = 7.1 Hz, 2H), 3.26 (dd, J = 8.9, 5.7 Hz, 1H), 3.08 (d, J = 2.4 Hz, 1H), 1.16 (t, J = 7.1 Hz, 3H). ^{13}C NMR (101 MHz, $CDCl_3$) δ = δ 172.4, 139.6, 131.3 (2C), 131.2, 128.1 (2C), 121.7, 121.0, 73.2, 61.1, 58.0, 14.0.
***Anti*-diastereoisomer**. Selected signals. ^{1}H NMR (400 MHz, $CDCl_3$) δ = 5.65 (ddd, J = 17.1, 10.3, 8.6 Hz, 1H), 5.07–4.98 (m, 2H), 4.88–4.84 (m, 1H), 4.19 – 4.12 (q, J = 7.1 Hz, 2H), 3.33 (t, J = 8.3 Hz, 1H), 3.16 (d, J = 5.4 Hz, 1H), 1.22 (t, J = 7.1 Hz, 3H). ^{13}C NMR (101 MHz, $CDCl_3$) δ = 172.7, 140.2, 131.8, 131.3 (2C), 128.3 (2C), 121.8, 119.9, 74.6, 61.2, 57.7, 14.1.

HRMS (ESI/Q-TOF) m/z: $[M+Na]^+$ calcd for $C_{13}H_{15}BrNaO_3$ 321.0097, found 321.0089.

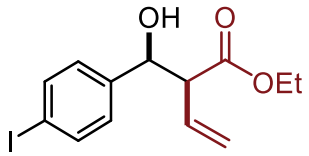

Ethyl 2-(hydroxy(4-iodophenyl)methyl)but-3-enoate (3d). Yield 72% (50 mg, 0.147 mmol). White solid. $dr_{syn:anti}$ = 3.2:1 calculated considering the ^{1}H NMR spectrum of the reaction crude and comparing the integral of the signal at 5.89 ppm for the *syn*-diastereoisomer and at 5.67 ppm for the *anti*-diastereoisomer. **3d** was obtained following the general procedure as stated above employing 0.2 mmol (47 mg, 1 equiv.) of **1d** and 0.5 mmol (69 µL, 2.5 equiv.) of **2a**. The title compound was isolated by flash column chromatography (SiO_2, 100% DCM). 38 mg (55% yield) of **3d** were isolated as a single *syn*-diastereoisomer. 12 mg (17% yield) of **3d** were isolated as a single *anti*-diastereoisomer.

***Syn*-diastereoisomer** ^{1}H NMR (400 MHz, $CDCl_3$) δ = 7.65 – 7.61 (m, 2H), 7.09 – 7.05 (m, 2H), 5.89 (ddd, J = 17.2, 10.2, 8.9 Hz, 1H), 5.25 (dd, J = 10.3, 1.2 Hz, 1H), 5.13 (dt, J = 17.1, 1.1 Hz, 1H), 4.95 (m, 1H), 4.11 (q, J = 7.1 Hz, 2H) 3.24 (m, 1H), 3.06 (br , 1H), 1.14 (t, J = 7.1 Hz, 3H). ^{13}C NMR (101 MHz, $CDCl_3$) δ = 172.4, 140.3, 137.2 (2C), 131.2, 128.4 (2C), 121.0, 93.3, 73.2, 61.1, 57.9, 14.0.
***Anti*-diastereoisomer** ^{1}H NMR (400 MHz, $CDCl_3$) δ = 7.67 – 7.63 (m, 2H), 7.05 (m, 2H), 5.67 (ddd, J = 17.1, 10.2, 8.4, 1H), 5.10 (dd, J = 10.3, 1.0 Hz, 1H), 5.03 (dd, J = 17.3, 1.1 Hz, 1H), 4.86 (m, 1H), 4.16 (q, J = 7.0, 1.3 Hz, 2H), 3.38 – 3.32 (m, 1H), 1.22 (t, J = 7.1 Hz, 3H). ^{13}C NMR (101 MHz, $CDCl_3$) δ = 172.7, 140.8, 137.4 (2C), 131.8, 128.5 (2C), 119.8, 93.4, 74.7, 61.1, 57.6, 14.0.

HRMS (ESI/Q-TOF) m/z: $[M+Na]^+$ calcd for $C_{13}H_{15}INaO_3$ 368.9958; found 368.9949.

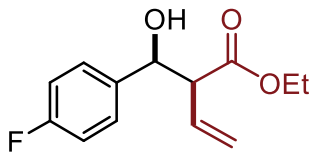

Ethyl 2-((4-fluorophenyl)(hydroxy)methyl)but-3-enoate (3e). Yield 79 % (37 mg, 0.158 mmol). Pale yellow oil. $dr_{syn:anti}$ = 3.3:1 calculated considering the ^{1}H NMR spectrum of the reaction crude and comparing the integral of the signal at 5.87 ppm for the *syn*-diastereoisomer and at 5.67 ppm for the *anti*-diastereoisomer. **3e** was obtained following the general procedure as stated above employing 0.2 mmol (25 mg, 22 µL, 1 equiv.) of freshly distilled **1e** and 0.5 mmol (69 µL, 2.5 equiv.) of **2a**. The title compound was isolated by two consecutive flash column chromatography (SiO_2, 1st 100% DCM, 2nd 7:1 Hexane/AcOEt). 26.1 mg (70% yield) of **3e** were isolated as a single *syn*-diastereoisomer. 11.4 mg (9% yield) of **3e** were isolated as a mixture 10:1 *anti:syn* diastereoisomers.

***Syn*-diastereoisomer** ^{1}H NMR (400 MHz, $CDCl_3$) δ = 7.24 (m, 2H), 6.94 (m, 2H), 5.87 (ddd, J = 17.1, 10.2, 9.0 Hz, 1H), 5.21 (dd, J = 10.2, 1.2 Hz, 1H), 5.10 (dt, J = 17.2, 1.0 Hz, 1H), 4.91 (d, J = 6.1 Hz, 1H), 3.98 (q, J = 7.1 Hz, 2H), 3.20 (m, 1H), 2.95 (s, 1H), 1.06 (t, J = 7.1 Hz, 3H). ^{13}C NMR (101 MHz, $CDCl_3$) δ = 172.5, 162.5 (d, J = 246.0 Hz), 136.5 (d, J = 3.2 Hz), 131.8, 128.3 (d, J = 8.1 Hz, 2C), 121.0, 115.2 (d, J = 21.5 Hz, 2C), 73.4, 61.1, 58.5, 14.1. ^{19}F NMR (377 MHz, $CDCl_3$) δ = -114.58 (m, 1F).
***Anti*-diastereoisomer** ^{1}H NMR (400 MHz, $CDCl_3$) δ = 7.30 – 7.25 (m, 2H), 7.03 – 6.98 (m, 2H), 5.67 (ddd, J = 17.2, 10.3, 8.6 Hz, 1H), 5.10 –5.02 (m, 2H), 4.90 (dd, J = 8.2, 4.0 Hz, 1H), 4.17 (q, J = 7.1 Hz, 2H), 3.36 (t, J = 8.3 Hz, 1H), 2.99 (d, J = 4.9 Hz, 1H), 1.23 (t, J = 7.1 Hz, 3H). ^{13}C NMR (101 MHz, $CDCl_3$) δ = 172.8, 162.3 (d, J = 246.1 Hz), 136.9 (d, J = 3.1 Hz), 132.0, 128.3 (d, J = 8.1 Hz, 2C), 119.7, 115.2 (d, J = 21.4 Hz, 2C), 74.5, 61.1, 57.9, 14.1. ^{19}F NMR (377 MHz, $CDCl_3$) δ = -114.41 (m, 1F).

HRMS (ESI/Q-TOF) m/z: $[M+Na]^+$ calcd for $C_{13}H_{15}FNaO_3$ 261.0897; found 261.0896.

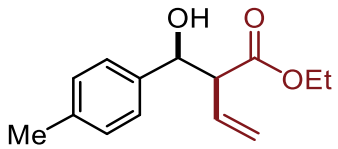

Ethyl 2-(hydroxy(p-tolyl)methyl)but-3-enoate (3f). Yield 92% (43 mg, 0.184 mmol). Pale yellow oil. $dr_{syn:anti}$ = 3.3:1 calculated considering the ^{1}H NMR spectrum of the reaction crude and comparing the integral of the signal at 3.30 ppm for the *syn*-diastereoisomer and at 3.41 ppm for the *anti*-diastereoisomer. **3f** was obtained following the general procedure as stated above employing 0.2 mmol (24 mg, 24 µL, 1 equiv.) of freshly distilled **1f** and 0.5 mmol (69 µL, 2.5 equiv.) of **2a**. The title compound was isolated by flash column chromatography (SiO_2, 100% DCM). 27.6 mg (60% yield) of **3f** were isolated as a single *syn*-diastereoisomer. 15.4 mg (32% yield) of **3f** were isolated a mixture 3.7:1 *anti:syn* diastereoisomers.

***Syn*-diastereoisomer** ^{1}H NMR (400 MHz, $CDCl_3$) δ = 7.21 (d, J = 8.0 Hz, 2H), 7.11 (d, J = 7.8 Hz, 2H), 5.95 (ddd, J = 17.1, 10.3, 8.9 Hz, 1H), 5.27 – 5.23 (m, 1H), 5.16 (dt, J = 17.2, 1.1 Hz, 1H), 4.95 (dd, J = 6.3, 2.0 Hz, 1H), 4.03 (q, J = 7.1 Hz, 2H), 3.30 (dd, J = 8.8, 6.2 Hz, 1H), 2.86 (d, J = 2.5 Hz, 1H), 2.31 (s, 3H), 1.11 (t, J = 7.1 Hz, 3H). ^{13}C NMR (101 MHz, $CDCl_3$) δ = 172.4, 137.7, 137.5, 132.1, 128.9 (2), 126.3 (2C), 120.4, 73.8, 60.8, 58.3, 21.1, 13.9.
***Anti*-diastereoisomer** Selected signals. ^{1}H NMR (400 MHz, $CDCl_3$) δ = 5.72 – 5.62 (m, 1H), 4.18 (qd, J = 7.1, 0.8 Hz, 2H), 3.41 (td, J = 8.4, 1.0 Hz, 1H), 1.25 (t, J = 7.2 Hz, 3H). ^{13}C NMR (101 MHz, $CDCl_3$) δ = 172.9, 138.1, 137.7, 132.3, 129.0 (2C), 126.5 (2C), 119.2, 75.1, 61.0, 57.8, 22.3, 14.1.

HRMS (ESI/Q-TOF) m/z: $[M+Na]^+$ calcd for $C_{14}H_{18}NaO_3$ 257.1148, found 257.1142.

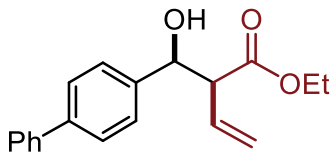

Ethyl 2-([1,1'-biphenyl]-4-yl(hydroxy)methyl)but-3-enoate (3g). Yield 86% (51 mg, 0.172 mmol). Pale yellow solid. $dr_{syn:anti}$ = 2.7:1 calculated considering the ^{1}H NMR spectrum of the reaction crude and comparing the integral of the signal at 3.38 ppm for the *syn*-diastereoisomer and at 3.46 ppm for the *anti*-diastereoisomer. **3g** was obtained following the general procedure as stated above employing 0.2 mmol (37 mg, 1 equiv.) of **1g** and 0.5 mmol (69 µL, 2.5 equiv.) of **2a**. The title compound was isolated by flash column chromatography (SiO_2, 7:3 DCM/Hexane). 33 mg (56% yield) of **3g** were isolated as a single *syn*-diastereoisomer. 9 mg (15% yield) of **3g** were isolated as a single *anti*-diastereoisomer. 9 mg (15% yield) of **3g** were isolated a mixture 1:1.2 *anti:syn*.

***Syn*-diastereoisomer** ^{1}H NMR (400 MHz, $CDCl_3$) δ = 7.58 (m, 4H), 7.46 – 7.41 (m, 4H), 7.37 – 7.33 (m, 1H), 6.00 (ddd, J = 17.2, 10.3, 8.8 Hz, 1H), 5.31 (dd, J = 10.2, 1.3 Hz, 1H), 5.22 (d, J = 17.2 Hz, 1H), 5.06 (d, J = 6.1 Hz, 1H), 4.08 (qd, J = 7.1, 2.0 Hz, 2H), 3.38 (dd, J = 8.9, 6.1 Hz, 1H), 3.01 (s, 1H), 1.14 (t, J = 7.1 Hz, 3H). ^{13}C NMR (101 MHz, $CDCl_3$) δ = 172.4, 140.7, 140.7, 139.7, 131.9, 128.7 (2C), 127.3, 127.0 (2C), 126.9 (2C), 126.9 (2C), 120.7, 73.7, 61.0, 58.3, 14.0.
***Anti*-diastereoisomer** ^{1}H NMR (400 MHz, $CDCl_3$) δ = 7.59 – 7.54 (m, 4H), 7.44 – 7.36 (m, 4H), 7.35 – 7.31 (m, 1H), 5.74 (ddd, J = 17.2, 10.3, 8.5 Hz, 1H), 5.14 – 5.04 (m, 2H), 4.97 (d, J = 8.1 Hz, 1H), 4.19 (q, J = 7.1 Hz, 2H), 3.46 (t, J = 8.3 Hz, 1H), 3.01 (s, 1H), 1.24 (t, J = 7.2 Hz, 3H). ^{13}C NMR (101 MHz, $CDCl_3$) δ = 172.9, 140.8, 140.6, 140.1, 132.1, 128.8 (2C), 127.3, 127.0 (4C), 127.0 (2C), 119.6, 75.0, 61.1, 57.7, 14.1.

HRMS (ESI/Q-TOF) m/z: $[M+Na]^+$ calcd for $C_{19}H_{20}NaO_3$ 319.1305, found 319.1297.

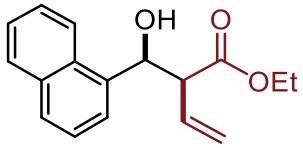

Ethyl 2-(hydroxy(naphthalen-1-yl)methyl)but-3-enoate (3h). Yield 80% (43 mg, 0.159 mmol). Pale yellow oil. $dr_{syn:anti}$ = 2:1 calculated considering the ^{1}H NMR spectrum of the reaction crude and comparing the integral of the signal at 3.60 ppm for the *syn*-diastereoisomer and at 3.77 ppm for the *anti*-diastereoisomer. **3h** was obtained following the general procedure as stated above employing 0.2 mmol (31 mg, 27 µL, 1 equiv.) of **1h** and 0.5 mmol (69 µL, 2.5 equiv.) of **2a**. The title compound was isolated by flash column chromatography (SiO_2, 9:1 DCM/Hexane) and it was obtained as a 2.3:1 *syn:anti* diastereoisomers mixture.

***Syn*-diastereoisomer** ^{1}H NMR (600 MHz, $CDCl_3$) δ = 8.06 – 8.03 (m, 1H), 7.88 (dd, J = 8.0, 1.5 Hz, 1H), 7.79 (dd, J = 8.3, 3.6 Hz, 2H, *syn+anti*), 7.66 (dt, J = 7.2, 1.0 Hz, 1H), 7.58 – 7.43 (m, 5H, *syn+anti*), 6.02 (ddd, J = 17.2, 10.2, 8.7 Hz, 1H), 5.90 (d, J = 4.5 Hz, 1H), 5.20 (dt, J = 10.3, 0.9 Hz, 1H), 4.94 (dt, J = 17.3, 1.1 Hz, 1H), 4.14 – 4.07 (m, 2H), 3.60 (ddt, J = 8.7, 4.5, 0.8 Hz, 1H), 1.14 (t, J = 7.1 Hz, 3H).
***Anti*-diastereoisomer** ^{1}H NMR (600 MHz, $CDCl_3$) δ = 8.18 – 8.14 (m, 1H), 7.79 (dd, J = 8.3, 3.6 Hz, 2H, *syn+anti*), 7.58 – 7.43 (m, 5H, *syn+anti*), 5.85 – 5.75 (m, 1H), 5.70 (d, J = 7.5 Hz, 1H), 5.09 – 5.01 (m, 2H), 4.18 (q, J = 7.2, 2H), 3.77 (ddd, J = 8.4, 7.5, 0.9 Hz, 1H), 1.21 (t, J = 7.1 Hz, 3H).
***Syn+Anti*-diastereoisomer** (peaks are given without assignment) ^{13}C NMR (150 MHz, $CDCl_3$) δ = 173.3, 173.3, 137.0, 136.1, 134.0, 133.8, 132.6, 131.4, 130.9, 130.2, 129.2, 129.1, 128.7, 128.4, 126.3, 125.7, 125.6, 125.3, 124.7, 124.6, 123.5, 122.8, 120.6, 119.2, 72.7, 70.5, 61.3, 61.2, 57.0, 56.3, 14.2, 14.1.

HRMS (ESI/Q-TOF) m/z: $[M+Na]^+$ calcd for $C_{17}H_{18}NaO_3$ 293.1148, found 293.1142.

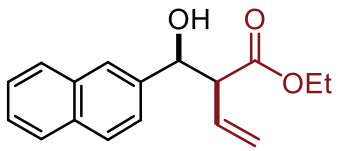

Ethyl 2-(hydroxy(naphthalen-2-yl)methyl)but-3-enoate (3i) Yield 93% (50 mg, 0.185 mmol). Pale yellow oil. $dr_{syn:anti}$ = 2.4:1 calculated considering the ^{1}H NMR spectrum of the reaction crude and comparing the integral of the signal at 3.45 ppm for the *syn*-diastereoisomer and at 3.53 ppm for the *anti*-diastereoisomer. **3i** was obtained following the general procedure as stated above employing 0.2 mmol (31 mg, 1 equiv.) of **1i** and 0.5 mmol (69 µL, 2.5 equiv.) of **2a**. The title compound was isolated by two consecutive flash column chromatography (SiO_2, 1st 9:1 DCM/Hexane, 2nd 10:1 Hexane/AcOEt). 43 mg (79% yield) of **3i** were isolated as a single *syn*-diastereoisomer. 7 mg (14% yield) of **3i** were isolated a mixture 2:1 *anti:syn* diastereoisomers.

***Syn*-diastereoisomer** ^{1}H NMR (400 MHz, $CDCl_3$) δ = 7.82 (m, 4H), 7.49 – 7.44 (m, 3H), 6.00 (ddd, J = 17.2, 10.3, 8.8 Hz, 1H), 5.26 (dd, J = 10.3, 1.2 Hz, 1H), 5.21 – 5.14 (m, 2H), 4.05 (q, J = 7.1 Hz, 2H), 3.45 (dd, J = 8.8, 5.8 Hz, 1H), 3.12 (s, 1H), 1.09 (t, J = 7.1 Hz, 3H). ^{13}C NMR (101 MHz, $CDCl_3$) δ = 172.6, 138.1, 133.1, 133.0, 131.7, 128.0, 128.0, 127.6, 126.1, 125.9, 125.5, 124.2, 120.6, 73.9, 61.0, 58.0, 13.9.
***Anti*-diastereoisomer** selected signals. ^{1}H NMR (400 MHz, $CDCl_3$) 5.73 = (ddd, J = 17.1, 10.4, 8.5 Hz, 1H), 5.12 – 5.00 (m, 3H), 4.17 (q, J = 7.1 Hz, 2H), 3.53 (t, J = 8.3 Hz, 1H), 1.22 (t, J = 7.1 Hz, 3H). ^{13}C NMR (101 MHz, $CDCl_3$) 172.9, 75.4, 61.1, 57.7, 14.1.

HRMS (ESI/Q-TOF) m/z: $[M+Na]^+$ calcd for $C_{17}H_{18}NaO_3$ 293.1148, found 293.1141.

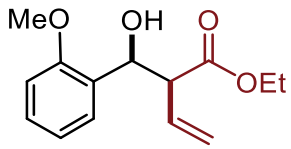

Ethyl 2-(hydroxy(2-methoxyphenyl)methyl)but-3-enoate (3j). Yield 84% (42 mg, 0.168 mmol). Pale yellow oil. $dr_{syn:anti}$ = 2.2:1 calculated considering the ^{1}H NMR spectrum of the reaction crude and comparing the integral of the signal at 5.95 ppm for the *syn*-diastereoisomer and at 5.75 ppm for the *anti*-diastereoisomer. **3j** was obtained following the general procedure as stated above employing 0.2 mmol (27 mg, 1 equiv.) of freshly distilled **1j** and 0.5 mmol (69 µL, 2.5 equiv.) of **2a**. The title compound was isolated by flash column chromatography (SiO_2, 100% DCM). 29 mg (58% yield) of **3j** were isolated as a single *syn*–diastereoisomer. 9 mg (16% yield) of **3j** were isolated as a single *anti*-diastereoisomer. 4 mg (8% yield) of **3j** were isolated as a mixture 1.7:1 *anti:syn* diastereoisomers.

***Syn*-diastereoisomer** ^{1}H NMR (400 MHz, $CDCl_3$) δ = 7.33 (dd, J = 7.5, 1.7 Hz, 1H), 7.27 – 7.22 (m, 1H, overlapped with the residual peak of the NMR solvent), 6.93 (td, J = 7.5, 1.0 Hz, 1H), 6.86 (dd, J = 8.2, 1.0 Hz, 1H), 5.95 (ddd, J = 17.1, 10.2, 8.7 Hz, 1H), 5.23 (t, J = 5.2 Hz, 1H), 5.20 – 5.17 (m, 1H), 5.06 (dt, J = 17.2, 1.2 Hz, 1H), 4.08 (q, J = 7.1 Hz, 2H), 3.86 (s, 3H), 3.56 (dd, J = 8.6, 5.5 Hz, 1H), 3.46 (d, J = 5.3 Hz, 1H), 1.16 (t, J = 7.4 Hz, 3H). ^{13}C NMR (101 MHz, $CDCl_3$) δ = 173.2, 156.1, 132.1, 128.6, 128.5, 128.1, 120.5, 119.6, 110.2, 70.7, 60.8, 55.3, 55.3, 14.0.
***Anti*-diastereoisomer** ^{1}H NMR (400 MHz, $CDCl_3$) δ = 7.26 – 7.20 (m, 3H, overlapped with the residual peak of the NMR solvent), 6.92 (td, J = 7.5, 1.0 Hz, 1H), 6.86 (d, J = 8.1 Hz, 1H), 5.75 (ddd, J = 16.8, 10.5, 8.6 Hz, 1H), 5.12 – 5.06 (m, 1H), 5.04 – 4.96 (m, 2H), 4.15 (q, J = 7.1 Hz, 2H), 3.85 (s, 3H), 3.60 (t, J = 8.3 Hz, 1H), 3.47 (d, J = 8.2 Hz, 1H), 1.21 (t, J = 7.1 Hz, 3H). ^{13}C NMR (101 MHz, $CDCl_3$) δ = 173.2, 156.8, 133.1, 129.0, 129.0, 128.4, 120.7, 118.7, 110.6, 72.9, 61.0, 56.8, 55.4, 14.3.

HRMS (ESI/Q-TOF) m/z: $[M+Na]^+$ calcd for $C_{14}H_{18}NaO_4$ 273.1097, found 273.1090.

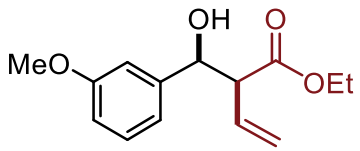

Ethyl 2-(hydroxy(3-methoxyphenyl)methyl)but-3-enoate (3k). Yield 90% (45 mg, 0.180 mmol). Pale yellow oil. $dr_{syn:anti}$ = 3:1 calculated considering the ^{1}H NMR spectrum of the reaction crude and comparing the integral of the signal at 5.94 ppm for the *syn*-diastereoisomer and at 5.69 ppm for the *anti*-diastereoisomer. **3k** was obtained following the general procedure as stated above employing 0.2 mmol (27 mg, 24 µL, 1 equiv.) of freshly distilled **1k** and 0.5 mmol (69 µL, 2.5 equiv.) of **2a**. The title compound was isolated by two consecutive flash column chromatography (SiO_2, 1st 100% DCM, 2nd 10:1 Hexane/AcOEt). 30.1 mg (60% yield) of **3k** were isolated as a mixture 1:19 *anti:syn* diastereoisomers.15 mg (30% yield) of **3k** were isolated as a mixture 3:1 *anti:syn* diastereoisomers.

***Syn*-diastereoisomer** ^{1}H NMR (400 MHz, $CDCl_3$) δ = 7.26 – 7.18 (m, 1H, overlapped with the residual peak of the NMR solvent), 6.91 – 6.87 (m, 2H), 6.82 – 6.77 (m, 1H), 5.94 (ddd, J = 17.2, 10.3, 8.8 Hz, 1H), 5.25 (ddd, J = 10.3, 1.3, 0.6 Hz, 1H), 5.15 (dt, J = 17.2, 1.1 Hz, 1H), 5.00 – 4.95 (m, 1H), 4.06 (q, J = 7.1, 2H), 3.78 (s, 3H), 3.30 (ddt, J = 8.8, 6.0 Hz, 1H), 2.95 (d, J = 2.6 Hz, 1H), 1.13 (t, J = 7.1 Hz, 3H). ^{13}C NMR (101 MHz, $CDCl_3$) δ = 173.2, 156.8, 133.1, 129.0, 129.0, 128.4, 120.7, 118.7, 110.6, 72.9, 61.0, 56.8, 55.4, 14.3.
***Anti*-diastereoisomer** ^{1}H NMR (400 MHz, $CDCl_3$) δ = 7.26 – 7.18 (m, 1H, overlapped with the residual peak of the NMR solvent), 6.92 – 6.85 (m, 2H), 6.84 – 6.77 (m, 1H), 5.69 (ddd, J = 17.1, 10.3, 8.5 Hz, 1H), 5.10 – 5.01 (m, 2H), 4.88 (dd, J = 8.2, 4.6 Hz, 1H), 4.20 – 4.14 (m, 2H), 3.79 (d, J = 0.8 Hz, 3H), 3.45 – 3.36 (m, 1H), 2.96 (d, J = 5.4 Hz, 1H), 1.25 – 1.21 (m, 3H). ^{13}C NMR (101 MHz, $CDCl_3$) δ = 172.8, 159.6, 142.8, 132.2, 129.3, 119.3, 119.0, 113.5, 112.1, 75.2, 61.0, 57.7, 55.2, 14.1.

HRMS (ESI/Q-TOF) m/z: $[M+Na]^+$ calcd for $C_{14}H_{18}NaO_4$ 273.1097, found 273.1091.

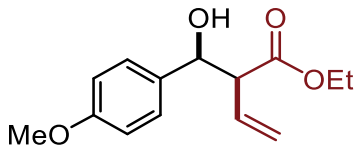

Ethyl 2-(hydroxy(4-methoxyphenyl)methyl)but-3-enoate (3l). Yield 68% (34.1 mg, 0.136 mmol). Colorless solid. $dr_{syn:anti}$ = 4:1 calculated considering the ^{1}H NMR spectrum of the reaction crude and comparing the integral of the signal at 3.29 ppm for the *syn*-diastereoisomer and at 3.39 ppm for the *anti*-diastereoisomer. **3l** was obtained following the general procedure as stated above employing 0.2 mmol (27 mg, 24 µL, 1 equiv.) of freshly distilled **1l** and 0.5 mmol (69 µL, 2.5 equiv.) of **2a**. The title compound was isolated by two consecutive flash column chromatography (SiO_2, 1st 100% DCM, 2nd 6:1 Hexane/AcOEt). 7.9 mg (14% yield) of **3l** were isolated as a single *syn*–diastereoisomer. 26.2 mg (54% yield) of **3l** were isolated a mixture 1:5.3 *anti:syn* diastereoisomers.

***Syn*-diastereoisomer** ^{1}H NMR (400 MHz, $CDCl_3$) δ = 7.25 (d, J = 8.9 Hz, 2H, overlapped with the residual peak of the NMR solvent), 6.87 – 6.82 (m, 2H), 5.95 (ddd, J = 17.1, 10.2, 8.9 Hz, 1H), 5.28 – 5.15 (m, 2H), 4.93 (dd, J = 6.5, 2.2 Hz, 1H), 4.03 (q, J = 7.1 Hz, 2H), 3.78 (s, 3H), 3.29 (dd, J = 8.9, 6.4 Hz, 1H), 2.78 (d, J = 2.5 Hz, 1H), 1.11 (t, J = 7.1 Hz, 3H). ^{13}C NMR (101 MHz, $CDCl_3$) δ = 172.3, 159.2, 132.8, 132.2, 127.7 (2C), 120.4, 113.6 (2C), 73.6, 60.8, 58.5, 55.2, 14.0.
***Anti*-diastereoisomer** ^{1}H NMR (400 MHz, $CDCl_3$) δ = 7.27 – 7.20 (m, 2H, *syn*+*anti*, overlapped with the residual peak of the NMR solvent), 6.86 – 6.81 (m, 2H, *anti* + *syn*), 5.65 (ddd, J = 17.2, 10.3, 8.5 Hz, 1H), 5.07 – 4.98 (m, 2H), 4.87 (d, J = 8.4 Hz, 1H), 4.18 (q, J = 7.1 Hz, 2H), 3.39 (t, J = 8.5 Hz, 1H), 1.24 (t, J = 7.1

Hz, 2H). ^{13}C NMR (101 MHz, $CDCl_3$) δ = 172.9, 159.3, 133.3, 132.3, 127.8, 119.2, 113.7, 74.8, 61.0, 57.9, 55.2, 14.1.

HRMS (ESI/Q-TOF) m/z: $[M+Na]^+$ calcd for $C_{14}H_{18}NaO_4$ 273.1097, found 273.1090.

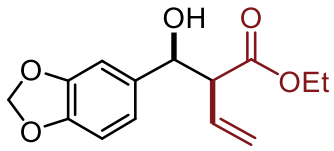

Ethyl 2-(benzo[d][1,3]dioxol-5-yl(hydroxy)methyl)but-3-enoate (3m). Yield 89% (47 mg, 0.177 mmol). Pale yellow oil. $dr_{syn:anti}$ = 3.9:1 calculated considering the ^{1}H NMR spectrum of the reaction crude and comparing the integral of the signal at 3.24 ppm for the *syn*-diastereoisomer and at 3.37 ppm for the *anti*-diastereoisomer. **3m** was obtained following the general procedure as stated above employing 0.2 mmol (30 mg, 1 equiv.) of **1m** and 0.5 mmol (69 µL, 2.5 equiv.) of **2a**. The title compound was isolated by two consecutive flash column chromatography (SiO_2, 1st 100% DCM, 2nd 4:1 Hexane/AcOEt). 45 mg (85% yield) of **3m** were isolated as a single *syn*–diastereoisomer. 2 mg (4% yield) of **3m** were isolated a mixture 1:1 diastereoisomers.

***Syn*-diastereoisomer** ^{1}H NMR (400 MHz, $CDCl_3$) δ = 6.84 (m, 1H), 6.78 – 6.70 (m, 2H), 6.00-5.89 (m, 3H), 5.26 (dd, J = 10.2, 1.4 Hz, 1H), 5.18 (m, 1H), 4.88 (d, J = 6.4 Hz, 1H), 4.05 (q, J = 7.1, 2H), 3.24 (dd, J = 8.9, 6.4 Hz, 1H), 2.91 (s, 1H), 1.12 (t, J = 7.1, 1.1 Hz, 3H). ^{13}C NMR (101 MHz, $CDCl_3$) δ = 172.3, 147.5, 147.1, 134.7, 132.0, 120.6, 119.9, 107.9, 107.0, 101.0, 73.7, 60.9, 58.6, 14.0.
***Anti*-diastereoisomer** selected signals. ^{1}H NMR (400 MHz, $CDCl_3$) 5.67 (ddd, J = 17.1, 10.3, 8.6 Hz, 1H), 4.20 (q, J = 7.1 Hz, 2H), 3.37 (t = 8.5 Hz, 1H), 1.16 (d, J = 7.2 Hz, 3H).

HRMS (ESI/Q-TOF) m/z: $[M+Na]^+$ calcd for $C_{14}H_{16}NaO_5$ 287.0890, found 287.0883.

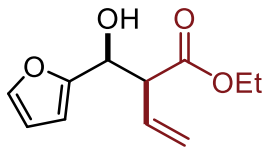

Ethyl 2-(furan-2-yl(hydroxy)methyl)but-3-enoate (3n). Yield 79% (33 mg, 0.157 mmol). Pale yellow oil. $dr_{syn:anti}$ = 3:1 calculated considering the ^{1}H NMR spectrum of the reaction crude and comparing the integral of the signal at 3.57 ppm for the *syn*-diastereoisomer and at 3.71 ppm for the *anti*-diastereoisomer. **3n** was obtained following the general procedure as stated above employing 0.2 mmol (19 mg, 17 µL, 1 equiv.) of freshly distilled **1n** and 0.5 mmol (69 µL, 2.5 equiv.) of **2a**. The title compound was isolated by flash column chromatography (SiO_2, 100% DCM). Spectroscopic data were in agreement with those reported in literature.[365] 33 mg (79% yield) of **3n** were isolated as a mixture 1:3 *anti:syn* diastereoisomers.

***Syn*-diastereoisomer** ^{1}H NMR (400 MHz, C_6D_6) δ = 7.14 (dd, J = 1.8, 0.9 Hz, 1H), 6.35 (dt, J = 3.3, 0.9 Hz, 1H), 6.16 – 6.07 (m, 4H, *syn*+*anti*), 5.19 – 5.12 (m, 4H, *syn*+*anti*), 3.96 – 3.90 (m, 2H), 3.67 (ddt, J = 8.7, 6.2, 0.8 Hz, 1H), 2.80 (d, J = 4.8 Hz, 1H), 0.92 (t, J = 7.1 Hz, 3H). ^{13}C NMR (101 MHz, C_6D_6) δ = 171.6, 154.5, 141.7, 132.2, 119.5, 110.1, 107.0, 68.5, 60.5, 55.4, 13.6.
***Anti*-diastereoisomer** ^{1}H NMR (400 MHz, C_6D_6) δ = 7.11 (dd, J = 1.8, 0.9 Hz, 1H), 6.16 – 6.07 (m, 4H, *syn*+*anti*), 5.88 (ddd, J = 17.2, 10.2, 8.5 Hz, 1H), 5.19 – 5.12 (m, 4H, *syn*+*anti*), 5.07 (t, J = 7.2 Hz, 1H), 5.02 (ddd, J = 10.3, 1.4, 0.7 Hz, 1H), 4.03 (qd, J = 7.1, 4.2 Hz, 2H), 3.81 (ddt, J = 8.7, 7.8, 0.9 Hz, 1H), 2.94 (d, J = 7.1 Hz, 1H), 0.99 (t, J = 7.1 Hz, 3H). ^{13}C NMR (101 MHz, C_6D_6) δ = 172.0, 154.7, 141.9, 132.3, 118.9, 110.0, 107.4, 69.0, 60.6, 55.5, 13.7.

HRMS (ESI/Q-TOF) m/z: $[M+Na]^+$ calcd for $C_{11}H_{14}NaO_4$ 233.0784, found 233.0778.

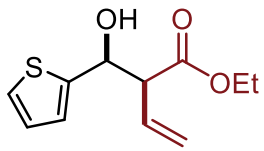

Ethyl 2-(hydroxy(thiophen-2-yl)methyl)but-3-enoate (3o). Yield 84% (38 mg, 0.168 mmol). Pale yellow oil. $dr_{syn:anti}$ = 3:1 calculated considering the ^{1}H NMR spectrum of the reaction crude and comparing the integral of the signal at 3.42 ppm for the *syn*-diastereoisomer and at 3.48 ppm for the *anti*-diastereoisomer. **3o** was obtained following the general procedure as stated above employing 0.2 mmol (22 mg, 18 µL, 1 equiv.) of freshly distilled **1o** and 0.5 mmol (69 µL, 2.5 equiv.) of **2a**. The title compound was isolated by two consecutive flash column chromatography (SiO_2, 1st 100% DCM, 2nd 10:1 Hexane/AcOEt). Were obtained 9 mg of *syn*-diastereoisomer (40% yield) and 29 mg of a mixture 3.3:1 *syn:anti* diastereoisomers. 9 mg (20% yield) of **3o** were isolated as a single *syn*-diastereoisomer. 29 mg (64% yield) of **3o** were isolated as a mixture 1:3.1 *anti:syn* diastereoisomers.

***Syn*-diastereoisomer** ^{1}H NMR (400 MHz, $CDCl_3$) δ = 7.25 (d, J = 1.3 Hz, 1H), 6.99 – 6.94 (m, 2H), 5.99 (ddd, J = 17.1, 10.3, 8.8 Hz, 1H), 5.39 – 5.26 (m, 3H), 4.10 (qd, J = 7.1, 1.6 Hz, 2H), 3.42 (dd, J = 8.8, 6.2 Hz, 1H), 3.06 (d, J = 3.2 Hz, 1H), 1.18 (t, J = 7.1 Hz, 3H). ^{13}C NMR (101 MHz, $CDCl_3$) δ = 172.1, 144.3, 131.6, 126.5, 124.9, 124.5, 121.0, 70.4, 61.1, 58.4, 14.0.
***Anti*-diastereoisomer.** Selected signals. ^{1}H NMR (400 MHz, $CDCl_3$) δ = 5.75 (ddd, J = 17.4, 9.9, 8.5 Hz, 1H), 4.18 (qd, J = 7.2, 1.0 Hz, 2H), 3.50 – 3.45 (t, J = 7.8 Hz, 1H), 3.21 (d, J = 6 .0 Hz, 1H), 1.24 (t, J = 7.1 Hz, 3H). ^{13}C NMR (101 MHz, $CDCl_3$) δ = 172.6, 145.2, 131.8, 126.5, 125.2, 124.8, 119.9, 71.2, 61.2, 57.8, 14.1.

HRMS (ESI/Q-TOF) m/z: $[M+Na]^+$ calcd for $C_{11}H_{14}NaO_3S$ 249.0556, found 249.0551.

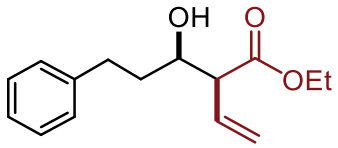

Ethyl 3-hydroxy-5-phenyl-2-vinylpentanoate (3p). Yield 67% (33 mg, 0.133 mmol). Pale yellow oil. $dr_{syn:anti}$ = 1.3:1 calculated considering the ^{1}H NMR spectrum of the reaction crude and comparing the integral of the signal at 3.94 ppm for the *syn*-diastereoisomer and at 3.84 ppm for the *anti*-diastereoisomer. **3p** was obtained following the general procedure as stated above employing 0.2 mmol (27 mg, 26 µL, 1 equiv.) of freshly distilled **1p** and 0.5 mmol (69 µL, 2.5 equiv.) of **2a**. The title compound was isolated by two consecutive flash column chromatography (SiO_2, 1st 9:1 DCM/Hexane, 2nd 8:1 to 4:1 AcOEt/Hexane). Spectroscopic data were in agreement with those reported in literature.[365] 24 mg (49% yield) of **3p** were isolated as a single *syn*-diastereoisomer. 9 mg (18% yield) of **3p** were isolated as a mixture 1.1:1 *anti:syn* diastereoisomers.

***Syn*-diastereoisomer.** ^{1}H NMR (400 MHz, $CDCl_3$) δ = 7.31 – 7.26 (m, 2H), 7.20 (m, 3H), 5.94 (ddd, J = 17.2, 10.2, 9.2 Hz, 1H), 5.31 (dd, J = 10.3, 1.5 Hz, 1H), 5.24 (dt, J = 17.4, 1.2 Hz, 1H), 4.17 (q, J = 7.1 Hz, 2H), 3.94 (dd, J = 9.2, 3.7 Hz, 1H), 3.06 (dd, J = 9.2, 4.3 Hz, 1H), 2.85 (ddd, J = 14.7, 9.9, 5.2 Hz, 1H), 2.78 (d, J = 3.2 Hz, 1H), 2.67 (ddd, J = 13.7, 9.6, 6.8 Hz, 1H), 1.81 (ddt, J = 14.5, 9.5, 4.7 Hz, 1H), 1.68 (dddd, J = 13.8, 10.3, 6.9, 3.8 Hz, 1H), 1.26 (t, J = 7.13 Hz, 3H). ^{13}C NMR (101 MHz, $CDCl_3$) δ = 173.3, 141.8, 131.6, 128.4 (2C), 128.4 (2C), 125.8, 120.5, 70.5, 61.0, 55.8, 35.8, 31.9, 14.1.
***Anti*-diastereoisomer**. Selected signals. ^{1}H NMR (400 MHz, $CDCl_3$) δ = 5.78 (ddd, J = 17.4, 10.0, 8.9 Hz, 1H), 3.84 (m, 1H), 3.13 – 3.07 (d, J = 8.4 Hz, 1H). ^{13}C NMR (101 MHz, $CDCl_3$) δ = 173.1, 141.8, 132.7, 128.4 (2C), 128.4 (2C), 125.8, 119.5, 71.6, 61.0, 56.7, 36.3, 31.8, 14.1.

HRMS (ESI/Q-TOF) m/z: $[M+Na]^+$ calcd for $C_{15}H_{20}NaO_3$ 271.1305, found 271.1298.

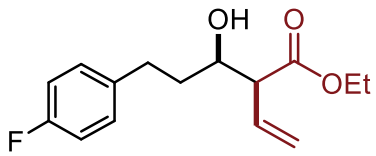

Ethyl 5-(4-fluorophenyl)-3-hydroxy-2-vinylpentanoate (3q). Yield 60% (32 mg, 0.120 mmol). Pale yellow oil. $dr_{syn:anti}$ = 3:1 calculated considering the ^{1}H NMR spectrum of the reaction crude and comparing the integral of the signal at 3.91 ppm for the *syn*-diastereoisomer and at 3.80 ppm for the *anti*-diastereoisomer. **3q** was obtained following the general procedure as stated above employing 0.2 mmol (30 mg, 1 equiv.) of **1q** and 0.5 mmol (69 µL, 2.5 equiv.) of **2a**. The title compound was isolated by two consecutive flash column chromatography (SiO_2, 1st 100% DCM, 2nd 10:1 Hexane/AcOEt). 15 mg (28% yield) of **3q** were isolated as a single *syn*-diastereoisomer. 17 mg (32% yield) of **3q** were isolated as a mixture 1:6.3 *anti:syn* diastereoisomers.

***Syn*-diastereoisomer**. ^{1}H NMR (400 MHz, $CDCl_3$) δ = 7.19 – 7.09 (m, 2H), 6.99 – 6.93 (m, 2H), 5.94 (ddd, J = 17.2, 10.2, 9.2 Hz, 1H), 5.31 (dd, J = 10.3, 1.5 Hz, 1H), 5.24 (ddd, J = 17.1, 1.5, 0.8 Hz, 1H), 4.17 (q, J = 7.1 Hz, 2H), 3.95 – 3.87 (m, 1H), 3.05 (dd, J = 9.2, 4.4 Hz, 1H), 2.86 – 2.75 (m, 2H), 2.65 (ddd, J = 13.9, 9.5, 7.0 Hz, 1H), 1.76 (dtd, J = 14.4, 9.4, 5.1 Hz, 1H), 1.64 (dddd, J = 13.6, 10.1, 6.9, 3.6 Hz, 1H), 1.26 (t, J = 7.1 Hz, 3H). ^{13}C NMR (101 MHz, $CDCl_3$) δ = 173.23, 161.2 (d, J = 243.4 Hz), 137.3 (d, J = 3.3 Hz), 131.5, 129.7 (d, J = 7.8 Hz, 2C), 120.6, 115.1 (d, J = 21.1 Hz, 2C), 70.3, 61.0, 55.8, 35.9, 31.0, 14.1. ^{19}F NMR (377 MHz, $CDCl_3$) δ = -117.76 (ddd, J = 14.4, 8.7, 5.4 Hz, 1F).
***Anti*-diastereoisomer** selected signals. ^{1}H NMR (400 MHz, $CDCl_3$) δ = 5.83 – 5.70 (m, 1H), 3.80 (m, 1H), 3.08 (dd, J = 8.9, 7.6 Hz, 1H). ^{13}C NMR (101 MHz, $CDCl_3$) δ = 132.7, 122.3, 119.5, 115.1 (d, J = 83.4 Hz), 71.4, 61.0, 56.7, 36.4, 30.9, 14.2. ^{19}F NMR (377 MHz, $CDCl_3$) δ = -116.99 (m, 1F).

HRMS (ESI/Q-TOF) m/z: $[M+Na]^+$ calcd for $C_{15}H_{19}FNaO_3$ 289.1210, found 289.1203.

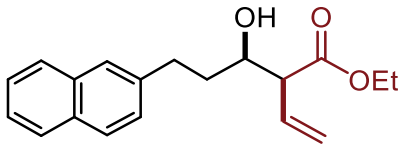

Ethyl 3-hydroxy-5-(naphthalen-2-yl)-2-vinylpentanoate (3r). Yield 52% (31 mg, 0.110 mmol). Pale yellow oil. $dr_{syn:anti}$ = 1:1:1 calculated considering the ^{1}H NMR spectrum of the reaction crude and comparing the integral of the signal at 3.98 ppm for the *syn*-diastereoisomer and at 3.86 ppm for the *anti*-diastereoisomer. **3r** was obtained following the general procedure as stated above employing 0.2 mmol (37 mg, 1 equiv.) of **1r** and 0.5 mmol (69 µL, 2.5 equiv.) of **2a**. The title compound was isolated by two consecutive flash column chromatography (SiO_2, 1st 100% DCM, 2nd 10:1 AcOEt/Hexane). 27 mg (45% yield) of **3r** were isolated as a mixture 1:13 *anti:syn* diastereoisomers. 4 mg (7% yield) of **3r** were isolated as a mixture 4.5:1 *anti:syn* diastereoisomers.

***Syn*-diastereoisomer**. ^{1}H NMR (400 MHz, $CDCl_3$) δ = 7.82 – 7.76 (m, 3H), 7.64 (s, 1H), 7.48 – 7.39 (m, 2H), 7.35 (dd, J = 8.4, 1.8 Hz, 1H), 5.96 (ddd, J = 17.2, 10.2, 9.2 Hz, 1H), 5.32 (dd, J = 10.2, 1.5 Hz, 1H), 5.26 (dt, J = 17.1, 1.1 Hz, 1H), 4.17 (q, J = 7.1 Hz, 2H), 3.98 (dq, J = 7.3, 3.7 Hz, 1H), 3.08 (dd, J = 9.3, 4.3 Hz, 1H), 3.02 (ddd, J = 14.4, 9.6, 5.2 Hz, 1H), 2.90 – 2.80 (m, 2H), 1.96 – 1.85 (m, 1H), 1.78 (dddd, J = 13.6, 9.7, 7.1, 3.7 Hz, 1H), 1.25 (t, J = 7.1 Hz, 3H). ^{13}C NMR (101 MHz, $CDCl_3$) δ = 173.3, 139.3, 133.6, 132.0, 131.6, 127.9, 127.6, 127.4, 127.3, 126.5, 125.9, 125.1, 120.5, 70.5, 61.0, 55.9, 35.7, 32.0, 14.1.
***Anti*-diastereoisomer**. Selected signals. ^{1}H NMR (400 MHz, $CDCl_3$) δ = 5.79 (dt, J = 18.2, 9.5 Hz, 1H), 3.86 (m, 1H).

HRMS (ESI/Q-TOF) m/z: $[M+Na]^+$ calcd for $C_{19}H_{22}NaO_3$ 321.1461, found, 321.1460.

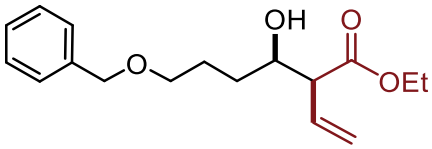

Ethyl 6-(benzyloxy)-3-hydroxy-2-vinylhexanoate (3s). Yield 55% (32 mg, 0.110 mmol). Yellow oil. $dr_{syn:anti}$ = 1.2:1 calculated considering the ^{1}H NMR spectrum of the reaction crude and comparing the integral of the signal at 3.92 ppm for the *syn*-diastereoisomer and at 3.85 ppm for the *anti*-diastereoisomer. **3s** was obtained following the general procedure as stated above employing 0.2 mmol (36 mg, 1 equiv.) of **1s** and 0.5 mmol (69 µL, 2.5 equiv.) of **2a**. The title compound was isolated by flash column chromatography (SiO_2, 1st 100% DCM, then 100% AcOEt). 32 mg (55% yield) of **3s** were isolated as a mixture 1:4.2 *anti:syn* diastereoisomers.

***Syn*-diastereoisomer** ^{1}H NMR (600 MHz, $CDCl_3$) δ = 7.37 – 7.24 (m, 10H, *syn+anti*), 5.95 (ddd, J = 17.0, 10.2, 9.1 Hz, 1H), 5.29 (dd, J = 10.3, 1.5 Hz, 1H), 5.26 – 5.19 (m, 3H, *syn+anti*), 4.50 (s, 2H), 4.21 – 4.14 (m, 4H, *syn+anti*), 3.94 (dt, J = 7.9, 4.6 Hz, 1H), 3.49 (m, 4H, *syn+anti*), 3.06 (dd, J = 9.1, 4.7 Hz, 1H), 1.86 – 1.69 (m, 4H, *syn+anti*), 1.63 – 1.49 (m, 4H, *syn+anti*), 1.29 – 1.24 (m, 6H, *syn+anti*). ^{13}C NMR (150 MHz, $CDCl_3$) δ = 173.4 138.5, 132.2, 128.5, 127.8, 127.7, 120.2, 73.1, 71.4, 70.3, 61.1, 56.1, 31.5, 26.2, 14.3.
***Anti*-diastereoisomer** ^{1}H NMR (600 MHz, $CDCl_3$) δ = 7.37 – 7.24 (m, 10H, *syn+anti*), 5.82 (ddd, J = 17.0, 10.2, 9.0 Hz, 1H), 5.26 – 5.19 (m, 3H, *syn+anti*), 5.17 – 5.09 (m, 1H), 4.49 (s, 2H), 4.21 – 4.14 (m, 4H, *syn+anti*), 3.87 (ddt, J = 7.4, 5.4, 2.3 Hz, 1H), 3.49 (m, 4H, *syn+anti*), 3.10 (d, J = 8.5 Hz, 1H), 1.86 – 1.69 (m, 4H, *syn+anti*), 1.63 – 1.49 (m, 4H, *syn+anti*), 1.29 – 1.24 (m, 6H, *syn+anti*). ^{13}C NMR (150 MHz, $CDCl_3$) δ = 173.2, 138.4, 133.2, 128.5, 127.8, 127.8, 119.4, 73.1, 72.3, 70.3, 61.0, 57.3, 31.9, 26.1, 14.3.

HRMS (ESI/Q-TOF) m/z: $[M+Na]^+$ calcd for $C_{17}H_{24}NaO_4$ 315.1567, found 315.1561.

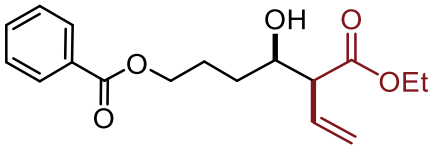

5-(ethoxycarbonyl)-4-hydroxyhept-6-en-1-yl benzoate (3t). Yield 74% (45 mg, 0.147 mmol). Orange oil. $dr_{syn:anti}$ = 2:1 calculated considering the ^{1}H NMR spectrum of the reaction crude and comparing the integral of the signal at 5.93 ppm for the *syn*-diastereoisomer and at 5.80 ppm for the *anti*-diastereoisomer. **3t** was obtained following the general procedure as stated above employing 0.2 mmol (38 mg, 1 equiv.) of **1t** and 0.5 mmol (69 µL, 2.5 equiv.) of **2a**. The title compound was isolated by flash column chromatography (SiO_2, 1st 100% DCM, then 100% AcOEt). 45 mg (74% yield) of **3t** were isolated as a mixture 1:4.3 *anti:syn* diastereoisomers.

***Syn*-diastereoisomer**. ^{1}H NMR (400 MHz, $CDCl_3$) δ = 8.04 – 8.01 (m, 4H, *syn+anti*), 7.56 – 7.52 (m, 2H, *syn+anti*), 7.45 – 7.40 (m, 4H, *syn+anti*), 5.94 (ddd, J = 17.2, 10.3, 9.2 Hz, 1H), 5.31 (dd, J = 10.3, 1.5 Hz, 1H), 5.28 – 5.18 (m, 3H, *syn+anti*), 4.39 – 4.32 (m, 4H, *syn+anti*), 4.16 (q, J = 7.1 Hz, 4H, *syn+anti*), 3.99 (dt, J = 8.7, 4.5 Hz, 1H), 3.07 (dd, J = 9.2, 4.5 Hz, 1H), 2.15 – 1.55 (m, 8H, *syn+anti*), 1.27 – 1.23 (m, 6H, *syn+anti*). ^{13}C NMR (101 MHz, $CDCl_3$) δ = 173.2, 166.6, 132.8, 131.5, 130.3, 129.5 (2C), 128.3 (2C), 120.6, 70.9, 64.7, 61.0, 55.9, 30.5, 25.0, 14.1.
***Anti*-diastereoisomer** ^{1}H NMR (400 MHz, $CDCl_3$) δ = 8.04 – 8.01 (m, 4H, *syn+anti*), 7.56 – 7.52 (m, 2H, *syn+anti*), 7.45 – 7.40 (m, 4H, *syn+anti*), 5.82 (ddd, J = 17.2, 10.2, 9.0 Hz, 1H), 5.28 – 5.18 (m, 3H, *syn+anti*), 4.39 – 4.32 (m, 4H, *syn+anti*), 4.16 (q, J = 7.1 Hz, 4H, *syn+anti*), 3.95 – 3.89 (m, 1H), 3.12 (dd, J = 8.8, 7.5 Hz, 1H), 2.15 – 1.55 (m, 8H, *syn+anti*), 1.27 – 1.23 (m, 6H, *syn+anti*). ^{13}C NMR (101 MHz, $CDCl_3$) δ = 177.3, 166.4, 132.9, 132.7, 130.1, 129.5 (2C), 128.3 (2C), 119.6, 71.8, 63.8, 61.0, 56.8, 30.9, 24.9, 14.1.

HRMS (ESI/Q-TOF) m/z: $[M+Na]^+$ calcd for $C_{17}H_{22}NaO_5$ 329.1359, found 329.1351.

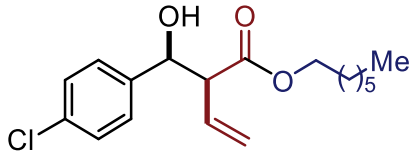

Heptyl 2-((4-chlorophenyl)(hydroxy)methyl)but-3-enoate (4a). Yield 70% (45 mg, 0.139 mmol). Pale yellow oil. $dr_{syn:anti}$ = 2:1 calculated considering the ^{1}H NMR spectrum of the reaction crude and comparing the integral of the signal at 3.25 ppm for the *syn*-diasteroisomer and at 3.34 ppm for the *anti*-diastereoisomer. **4a** was obtained following the general procedure as stated above employing 0.2 mmol (28 mg, 1 equiv.) of **1a** and 0.5 mmol (132 mg, 2.5 equiv.) of **2b**. The title compound was isolated by two consecutive flash column chromatography (SiO_2, 1st 9:1 DCM/Hexane, then 2nd 10:1 Hexane/AcOEt). 45 mg (70% yield) of **4a** were isolated as a mixture 1:2.2 *anti:syn* diastereoisomers.

***Syn*-diastereoisomer** ^{1}H NMR (600 MHz, $CDCl_3$) δ =7.24 (m, 8H, *syn+anti*, overlapped with the residual peak of the NMR solvent), 5.89 (dt, J = 17.9, 9.6 Hz, 1H), 5.24 (d, J = 10.2 Hz, 1H), 5.13 (d, J = 17.2 Hz, 1H), 4.95 (d, J = 5.9 Hz, 1H), 3.97 (t, J = 6.7 Hz, 2H), 3.25 (dd, J = 8.8, 6.1 Hz, 1H), 3.03 (d, J = 2.5 Hz, 1H), 1.49 – 1.44 (m, 2H), 1.22 (m, 16H, *syn+anti*), 0.86 (t, J = 7.1 Hz, 6H, *syn+anti*). ^{13}C NMR (151 MHz, $CDCl_3$) δ =172.6, 139.3, 133.7, 131.7, 128.5 (2C), 128.0 (2C), 121.1, 73.4, 65.4, 58.4, 31.8, 29.0, 28.5, 25.8, 22.7, 14.2.
***Anti*-diastereoisomer** ^{1}H NMR (600 MHz, $CDCl_3$) δ = 7.24 (m, 8H, *syn+anti*, overlapped with the residual peak of the NMR solvent), 5.67 (dt, J = 17.8, 9.4 Hz, 1H), 5.08 (d, J = 10.2 Hz, 1H), 5.02 (d, J = 17.2 Hz, 1H), 4.87 (dd, J = 7.7, 5.2 Hz, 1H), 4.07 (t, J = 6.8 Hz, 2H), 3.34 (t, J = 8.2 Hz, 1H), 3.14 (d, J = 5.5 Hz, 1H), 1.56 (m, 2H), 1.22 (m, 16H, *syn+anti*), 0.86 (t, J = 7.1 Hz, 6H, *syn+anti*). ^{13}C NMR (150 MHz, $CDCl_3$) δ = 173.0, 139.9, 133.8, 132.1, 128.6 (2C), 128.1 (2C), 119.9, 74.7, 65.5, 57.9, 31.8, 29.0, 28.6, 25.9, 22.7, 14.2.

HRMS (ESI/Q-TOF) m/z: $[M+Na]^+$ calcd for $C_{18}H_{25}ClNaO_3$ 347.1384, found 347.1376.

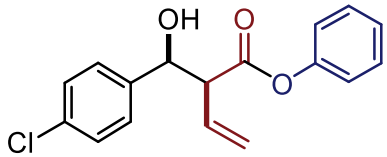

Phenyl 2-((4-chlorophenyl)(hydroxy)methyl)but-3-enoate (4b). Yield 43% (26 mg, 0.086 mmol). Pale yellow oil. $dr_{syn:anti}$ = 5:1 calculated considering the ^{1}H NMR spectrum of the isolated product and comparing the integral of the signal at 3.54 ppm for the *syn*-diastereoisomer and at 3.63 ppm for the *anti*-diastereoisomer. **4b** was obtained following the general procedure as stated above employing 0.2 mmol (28 mg, 1 equiv.) of **1a** and 0.5 mmol (121 mg, 2.5 equiv.) of **2c**. The title compound was isolated by two consecutive flash column chromatography (SiO_2, 1st 100% DCM, then 2nd 15:1 Hexane/AcOEt). 26 mg (43% yield) of **4b** were isolated as a mixture 1:5 *anti:syn* mixture.

***Syn*-diastereoisomer** ^{1}H NMR (600 MHz, $CDCl_3$) δ = 7.39 – 7.31 (m, 12H, *syn+anti*), 7.25 – 7.20 (m, 2H, *syn+anti*), 6.88 – 6.82 (m, 2H), 6.06 (ddd, J = 17.2, 10.2, 8.9 Hz, 1H), 5.40 (dd, J = 10.2, 1.1 Hz, 1H), 5.36 – 5.32 (m, 1H), 5.10 (dd, J = 6.5, 1.8 Hz, 1H), 3.54 (dd, J = 8.9, 6.4 Hz, 1H), 2.86 (d, J = 2.7 Hz, 1H). ^{13}C NMR (151 MHz, $CDCl_3$) δ = 169.7, 149.2, 138.0, 132.9, 130.2, 128.5 (2C), 127.6 (2C), 127.1 (2C), 125.1, 120.7, 120.2 (2C), 72.4, 57.4.
***Anti*-diastereoisomer** ^{1}H NMR (600 MHz, $CDCl_3$) δ = 7.39 – 7.31 (m, 12H, *syn+anti*), 7.25 – 7.20 (m, 2H, *syn+anti*), 7.06 – 7.03 (m, 2H), 5.79 (ddd, J = 17.2, 10.3, 8.6 Hz, 1H), 5.23 – 5.17 (m, 2H), 5.03 (dd, J = 8.5,

4.2 Hz, 1H), 3.63 (t, J = 8.5 Hz, 1H), 2.93 (d, J = 5.1 Hz, 1H). ^{13}C NMR (151 MHz, $CDCl_3$) δ = 170.2, 149.4, 138.4, 132.9, 130.3, 128.5 (2C), 127.6 (2C), 127.1 (2C), 125.1, 120.4, 119.6, 73.7, 56.9.

HRMS (ESI/Q-TOF) m/z: $[M+Na]^+$ calcd for $C_{17}H_{15}ClNaO_3$ 325.0602, found 325.0595.

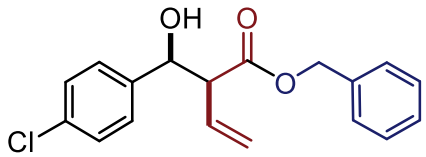

Benzyl 2-((4-chlorophenyl)(hydroxy)methyl)but-3-enoate (4c). Yield 35% (22 mg, 0.070 mmol). Pale yellow oil. $dr_{syn:anti}$ = 2:1 calculated from the isolated product considering the ^{1}H NMR spectrum and comparing the integral of the signal at 3.36 ppm for the *syn*-diastereoisomer and at 3.47 ppm for the *anti*-diastereoisomer. **4c** was obtained following the general procedure as stated above employing 0.2 mmol (28 mg, 1 equiv.) of **1a** and 0.5 mmol (128 mg, 2.5 equiv.) of **2d**. The title compound was isolated by two consecutive flash column chromatography (SiO_2, 1st 100% DCM, 2nd 12:1 Hexane/AcOEt). 22 mg (35% yield) of **4c** were isolated as a mixture 1:2 *anti:syn* diastereoisomers.

***Syn*-diastereoisomer** ^{1}H NMR (600 MHz, $CDCl_3$) δ = 7.38 – 7.17 (m, 18H, *syn+anti*, overlapped with the residual peak of the NMR solvent), 5.95 (ddd, J = 17.1, 10.2, 8.9 Hz, 1H), 5.30 (dd, J = 10.2, 1.1 Hz, 1H), 5.20 - 4.97 (m, 8H, *syn+anti*), 3.34 (dd, J = 9.0, 6.2 Hz, 1H), 2.89 (d, J = 2.5 Hz, 1H).
***Anti*-diastereoisomer** ^{1}H NMR (600 MHz, $CDCl_3$) δ = 7.38 – 7.17 (m, 18H, *syn+anti*, overlapped with the residual peak of the NMR solvent), 5.72 (ddd, J = 17.2, 10.3, 8.6 Hz, 1H), 5.20 - 4.97 (m, 8H, *syn+anti*), 4.93 (dd, J = 7.7, 4.6 Hz, 1H), 3.45 (t, J = 8.2 Hz, 1H), 3.02 (d, J = 5.5 Hz, 1H).
***Syn+Anti*-diastereoisomer** (peaks are given without assignment) ^{13}C NMR (150 MHz, $CDCl_3$) δ = 171.5, 171.0, 138.5, 138.0, 134.4, 134.2, 132.7, 132.6, 130.7, 130.4, 127.6, 127.5, 127.4, 127.4, 127.3, 127.3, 127.2, 127.1, 126.9, 126.9, 120.2, 119.1, 73.5, 72.3, 65.8, 65.8, 57.4, 56.7.

HRMS (ESI/Q-TOF) m/z: $[M+Na]^+$ calcd for $C_{18}H_{17}ClNaO_3$ 339.0758, found 339.0751.

Functionalizations of α-vinyl-β-hydroxy esters

Synthesis of Ethyl (*E*)-2-((4-fluorophenyl)(hydroxy)methyl)but-2-enoate (5)

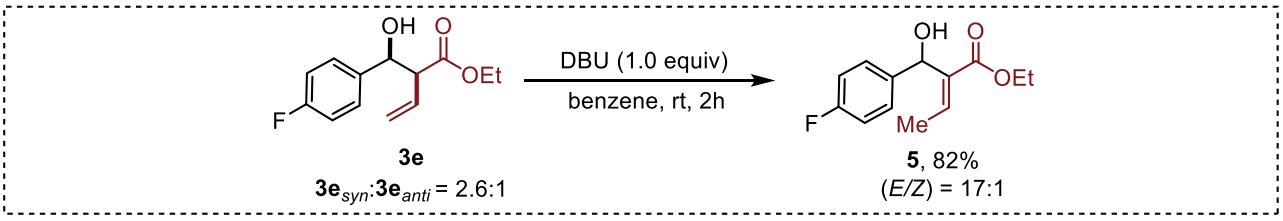

3e
3e$_{syn}$:**3e**$_{anti}$ = 2.6:1

5, 82%
(*E*/*Z*) = 17:1

Adapted from literature.[383] A flame-dried two neck bottom flask under nitrogen atmosphere was charged with **3e** (mixture *anti:syn* = 2.6:1, 32 mg, 0.133 mmol, 1 equiv.) and 1.5 mL benzene, then 1,5-diazabiciclo(5.4.0)undec-7-ene (DBU, 20 µL, 0.138 mmol, 1 equiv.) was added. The reaction mixture was vigorously stirred at room temperature and the conversion was monitored by ^{1}H NMR. After the consumption of the starting material, the solvent was removed *in vacuo* and the product was purified by flash chromatography (SiO_2, 10:1 Hexane/AcOEt) to afford **5** as a colorless oil in 82% yield (26 mg, 0.109 mmol).

^{1}H NMR (400 MHz, $CDCl_3$) δ = 7.33 (dd, J = 8.5, 5.4 Hz, 2H), 7.08 (q, J = 7.3 Hz, 1H), 7.01 (t, J = 8.7 Hz, 2H), 5.68 (d, J = 10.8 Hz, 1H), 4.23 (d, J = 11.1 Hz, 1H), 4.19 – 4.08 (m, 2H), 1.97 (d, J = 7.2 Hz, 3H), 1.22 (t, J =

7.1 Hz, 3H). ^{13}C NMR (101 MHz, $CDCl_3$) δ = 167.1, 161.9 (d, J = 245.0 Hz), 139.8, 138.6 (d, J = 3.1 Hz), 133.4, 126.9 (d, J = 8.0 Hz, 2H), 115.0 (d, J = 21.4 Hz, 2H), 68.8, 60.8, 14.2, 14.0. ^{19}F NMR (377 MHz, $CDCl_3$) δ = -116.05 (m, 1F, *Z*-isomer), -116.43 (td, J = 8.9, 4.6 Hz, 1F, *E*-isomer).

Synthesis of Ethyl 2-((4-fluorophenyl)(hydroxy)methyl)butanoate (6)

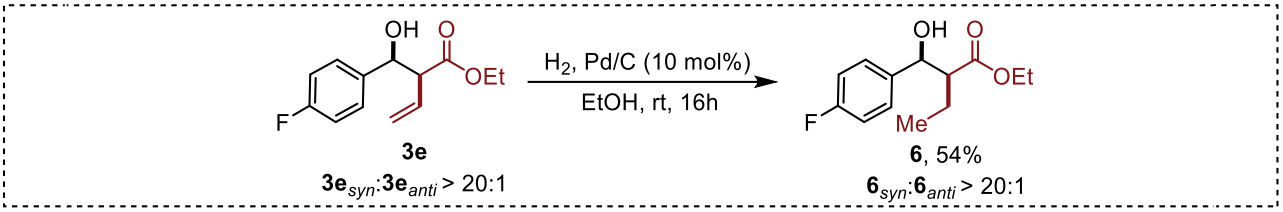

3e
3e$_{syn}$:**3e**$_{anti}$ > 20:1

6, 54%
6$_{syn}$:**6**$_{anti}$ > 20:1

A flame-dried two neck bottom flask under nitrogen atmosphere was charged with *syn*-**3e** (24 mg, 0.1 mmol, 1 equiv.) and 1 mL ethanol, then palladium on activated carbon (Pd/C 10 wt. % loading, 2.1 mg, 10% w/w) was added. The flask was evacuated and then refilled with hydrogen (balloon, ca. 1 atm), and the reaction mixture was vigorously stirred at room temperature for 16h and monitored by GC-MS. After the consumption of the starting material the reaction mixture was filtered over a Celite® pad washing with EtOH. The solvent was removed in vacuo and the crude product was further purified by flash chromatography (SiO_2, 10:1 Hexane:AcOEt) to afford *syn*-**6** as a colorless oil in 54% yield (13 mg).

^{1}H NMR (400 MHz, $CDCl_3$) δ = 7.35 – 7.29 (m, 2H), 7.06 – 6.98 (m, 2H), 4.92 (d, J = 5.7 Hz, 1H), 4.07 (qd, J = 7.1, 2.8 Hz, 2H), 2.87 (d, J = 2.5 Hz, 1H), 2.59 (ddd, J = 10.1, 5.8, 4.3 Hz, 1H), 1.78 – 1.65 (m, 2H), 1.15 (t, J = 7.1 Hz, 3H), 0.88 (t, J = 7.5 Hz, 3H). ^{13}C NMR (101 MHz, $CDCl_3$) δ = 175.0, 162.4 (d, J = 245.6 Hz), 137.6 (d, J = 3.2 Hz), 128.0 (d, J = 8.1 Hz, 2C), 115.2 (d, J = 21.4 Hz, 2C), 73.7, 60.7, 54.7, 20.5, 14.3, 12.1. ^{19}F NMR (377 MHz, $CDCl_3$) δ = –114.88 - –114.98 (m, 1F).

Synthesis of 1-(4-fluorophenyl)-2-vinylpropane-1,3-diol (7)

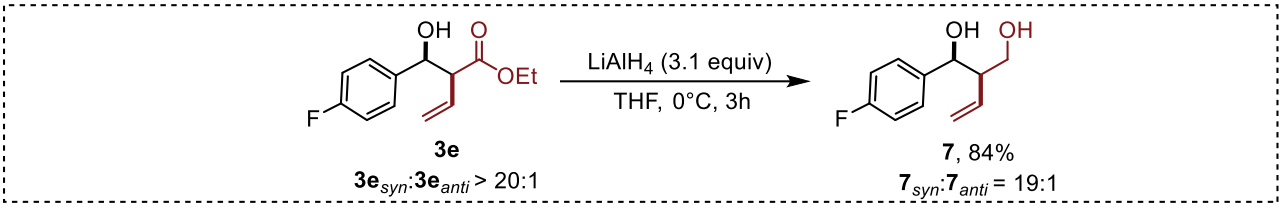

3e
3e$_{syn}$:**3e**$_{anti}$ > 20:1

7, 84%
7$_{syn}$:**7**$_{anti}$ = 19:1

In a flame-dried two neck bottom flask under nitrogen atmosphere, to a suspension of $LiAlH_4$ (15 mg, 0.395 mmol, 3.1 equiv.) in 1 mL of dry THF at 0°C a solution of *syn*-**3e** (30 mg, 0.133 mmol, 1 equiv.) in 0.5 mL of dry THF was added dropwise. The reaction mixture was allowed to slowly warm to room temperature and vigorously stirred under N_2. Reaction progress was monitored with TLC. After consumption of the starting material the reaction mixture was cooled to 0°C and water (15 µL), NaOH (15 µL, 15% aq.) and water (45 µL) were consecutively added. Reaction mixture was then allowed to warm to room temperature, and it was stirred for 30 minutes. Insoluble salts were filtered over a Celite® pad washing with Et_2O. The solvent was removed in vacuo to afford *syn*-**7** as a colorless oil in 84% yield (21 mg, 0.112 mmol, *dr* = 19:1).

^{1}H NMR (400 MHz, $CDCl_3$) δ = 7.34 – 7.27 (m, 2H), 7.06 – 7.00 (m, 2H), 5.79 (ddd, J = 17.4, 10.4, 8.7 Hz, 1H), 5.25 (dd, J = 10.5, 1.7 Hz, 1H), 5.14 (dt, J = 17.4, 1.3 Hz, 1H), 4.83 (d, J = 5.6 Hz, 1H), 4.65 (s, 1H), 3.69 – 3.56 (m, 2H), 2.60 – 2.49 (m, 1H), 1.98 (s, 1H). ^{13}C NMR (101 MHz, $CDCl_3$) δ = 162.2 (d, J = 245.6

Hz), 137.8 (d, J = 3.3 Hz), 134.9, 128.0 (d, J = 8.2 Hz, 2C), 119.8, 115.1 (d, J = 21.3 Hz, 2C), 74.3, 63.8, 53.5. ^{19}F NMR (377 MHz, $CDCl_3$) δ = -115.06 (tt, J = 8.8, 5.3 Hz, 1F).

Synthesis of 4-(4-fluorophenyl)-2,2-dimethyl-5-vinyl-1,3-dioxane (8)

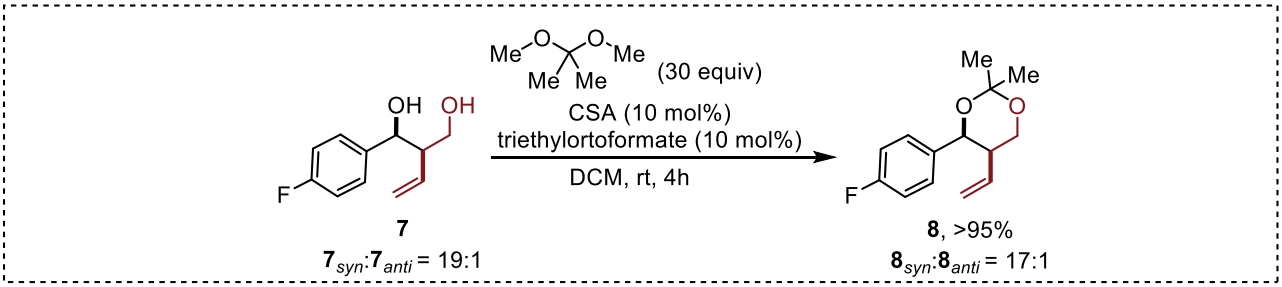

7
$\mathbf{7}_{syn}$:$\mathbf{7}_{anti}$ = 19:1

8, >95%
$\mathbf{8}_{syn}$:$\mathbf{8}_{anti}$ = 17:1

A flame-dried two neck bottom flask under nitrogen atmosphere was charged with *syn*-**7** (21 mg, 0.11 mmol, 1 equiv.) and 1 mL of anhydrous DCM, then 2,2-dimethoxypropane (0.4 mL, 3.27 mmol, 30 equiv.), camphor sulfonic acid (CSA, 3 mg, 11 µmol, 0.1 equiv.) and triethyl orthoformate (3 drops) were added. Reaction mixture was vigorously stirred at room temperature and monitored with TLC. After the consumption of the starting material the solvent was removed *in vacuo* and the product was purified by flash chromatography (Al_2O_3, 30:1 Hexane:AcOEt) to afford **8** as a colorless oil in quantitative yield (25.5 mg, 0.10 mmol, *dr* = 17:1).

^{1}H NMR (400 MHz, $CDCl_3$) δ = 7.25 – 7.21 (m, 2H), 7.02 – 6.98 (m, 2H), 6.04 (ddd, J = 17.4, 10.5, 9.0 Hz, 1H), 5.16 (d, J = 2.8 Hz, 1H), 4.95 (dd, J = 10.5, 1.9 Hz, 1H), 4.80 (ddd, J = 17.4, 1.9, 0.8 Hz, 1H), 4.35 (dd, J = 11.5, 2.8 Hz, 1H), 3.86 (dd, J = 11.4, 1.8 Hz, 1H), 2.29 – 2.25 (m, 1H), 1.57 (s, 3H), 1.54 (s, 3H). ^{13}C NMR (101 MHz, $CDCl_3$) δ = 161.7 (d, J = 244.5 Hz), 136.3, 135.0, 127.3 (d, J = 7.8 Hz, 2C), 117.3, 114.7 (d, J = 21.3 Hz, 2C), 99.3, 72.6, 65.6, 44.8, 29.7, 19.0. ^{19}F NMR (377 MHz, $CDCl_3$) δ = -114.47 (m, 1F, *anti*-diastereoisomer), -115.92 (m, J = 8.8, 5.4 Hz, 1F, *syn*-diastereoisomer).

6.8 Bibliography

[348] I. Marek, *Titanium and Zirconium in Organic Synthesis*, Wiley-VCH Verlag GmbH & Co, **2002**.
[349] R. E. Estévez, J. Justicia, B. Bazdi, N. Fuentes, M. Paradas, D. Choquesillo-Lazarte, J. M. García-Ruiz, R. Robles, A. Gansäuer, J. M. Cuerva, J. E. Oltra, *Chem. Eur. J.* **2009**, *15*, 2774–2791.
[350] H. A. Martin, F. Jellinek, *J. Organomet. Chem.* **1966**, *6*, 293–296.
[351] A. Rosales, J. L. Oller-López, J. Justicia, A. Gansäuer, J. E. Oltra, J. M. Cuerva, *Chem Commun* **2004**, 2628–2629.
[352] J. Justicia, I. Sancho-Sanz, E. Álvarez-Manzaneda, J. E. Oltra, J. M. Cuerva, *Adv. Synth. Catal.* **2009**, *351*, 2295–2300.
[353] J. Muñoz-Bascón, I. Sancho-Sanz, E. Álvarez-Manzaneda, A. Rosales, J. E. Oltra, *Chem. Eur. J.* **2012**, *18*, 14479–14486.
[354] I. Sancho-Sanz, D. Miguel, A. Millán, R. E. Estévez, J. L. Oller-López, E. Álvarez-Manzaneda, R. Robles, J. M. Cuerva, J. Justicia, *J. Org. Chem.* **2011**, *76*, 732–735.
[355] S. P. Morcillo, Á. Martínez-Peragón, V. Jakoby, A. J. Mota, C. Kube, J. Justicia, J. M. Cuerva, A. Gansäuer, *Chem. Commun.* **2014**, *50*, 2211–2213.
[356] A. Gansäuer, D. Franke, T. Lauterbach, M. Nieger, *J. Am. Chem. Soc.* **2005**, 127, *33*, 11622–11623.
[357] F. Li, Y. Chen, S. Lin, C. Shi, X. Li, Y. Sun, Z. Guo, L. Shi, *Org. Chem. Front.* **2020**, *7*, 3434–3438.
[358] E. Hao, B. Lu, Y. Liu, T. Yang, H. Yan, X. Ding, Y. Jin, L. Shi, *Org. Lett.* **2023**, *25*, 5094–5099.
[359] H. Yan, Q. Liao, Y. Chen, G. G. Gurzadyan, B. Lu, C. Wu, L. Shi, *Angew. Chem. Int. Ed.* **2023**, *62*, e202302483.
[360] J. Hur, J. Jang, J. Sim, *Int. J. Mol. Sci.* **2021**, *22*, 2769.
[361] C. Curti, L. Battistini, A. Sartori, F. Zanardi, *Chem. Rev.* **2020**, *120*, 2448–2612.
[362] J. Hassfeld, M. Christmann, M. Kalesse, *Org. Lett.* **2001**, 3, *22*, 3561–3564.
[363] J. R. Heemstra Jr., G. L. Beutner, S. E. Denmark, *Angew. Chem. Int. Ed.* **2005**, *44*, 4682–4698.
[364] P. V. Ramachandran, D. Nicponski, B. Kim, *Org. Lett.* **2013**, *15*, 1398–1401.
[365] J. Kister, D. H. Ess, W. R. Roush, *Org. Lett.* **2013**, *15*, 5436–5439.
[366] T. Hudlicky, R. P. Short, *J. Org. Chem.* **1982**, 47, *8*, 1522–1527.
[367] M. Bellassoued, F. Dardoize, Y. Frangin, M. Gaudemar, *J. Organomet. Chem.* **1981**, *219*, C1–C4.
[368] R. P. Short, J. M. Revol, B. C. Ranu, T. Hudlicky, *J. Org. Chem.* **1983**, *48*, 4453–4461.
[369] L. E. Rice, M. C. Boston, H. O. Finklea, B. J. Suder, J. O. Frazier, T. Hudlicky, *J. Org. Chem.* **1984**, 49, *10*, 1845–1848.
[370] S. Yuana, C.-J. Lib, Z. Wang, *Tetrahedron Lett.* **2002**, *43*, 5097–5099.
[371] Z. Zha, S. Qiao, J. Jiang, Y. Wang, Q. Miao, Z. Wang, *Tetrahedron* **2005**, *61*, 2521–2527.
[372] B. Prabhudas, F. A. Khan, *Tetrahedron* **2000**, *56*, 7595–7599.
[373] X.-Y. Liu, B.-Q. Cheng, Y.-C. Guo, X.-Q. Chu, Y.-X. Li, T.-P. Loh, Z.-L. Shen, *Adv. Synth. Catal.* **2019**, *361*, 542–549.
[374] S. M. Goldup, C. J. Pilkington, A. J. P. White, A. Burton, A. G. M. Barrett, *J. Org. Chem.* **2006**, 71, *16*, 6185–6191; *J. Org. Chem.* **2019**, 84, *10*, 6546.
[375] L. A. Wessjohann, H. Wild, L. A. Ferreira, H. S. Schrekker, *Appl. Organometal. Chem.* **2016**, *30*, 674–679.
[376] P. B. Kisanga, J. G. Verkade, *J. Org. Chem.* **2002**, 67, *2*, 426–430.
[377] S. T. Nguyen, S. M. Sephton, Z. D. Matesich, S. E. Denmark, *J. Org. Chem.* **2018**, *83*, 23−48.
[378] A. M. Jadhav, V. V. Pagar, D. B. Huple, R.-S. Liu, *Angew. Chem. Int. Ed.* **2015**, *54*, 3812–3816.
[379] https://www.acs.org/greenchemistry/principles/12-principles-of-green-chemistry.html.
[380] Z. Zhang, T. Hilche, D. Slak, N. R. Rietdijk, U. N. Oloyede, R. A. Flowers II, A. Gansäuer, *Angew. Chem. Int. Ed.* **2020**, *59*, 9355–9359.
[381] https://macmillan.princeton.edu/wp-content/uploads/Merck-Photocatalysis-Chart.pdf.
[382] M. Yamane, Y. Kanzaki, H. Mitsunuma, M. Kanai, *Org. Lett.* **2022**, *24*, 1486–1490.
[383] J. H. Cha, A. N. Pae, K. I. I. Choi, Y. S. Cho, H. Y. Koh, E. Lee, *J. Chem. Soc. Perkin 1* **2001**, 2079–2081.
[384] Y.-C. Xin, S.-H. Shi, D.-D. Xie, X.-P. Hui, P.-F. Xu, *Eur. J. Org. Chem.* **2011**, *2011*, 6527–6531.

[385] L. Meng, Y. Kamada, K. Muto, J. Yamaguchi, K. Itami, *Angew. Chem. Int. Ed.* **2013**, *52*, 10048–10051.
[386] H. Gershon, L. Shanks, D. E. Gawiak, *J. Med. Chem.* **1976**, *19*, 1069–1072.
[387] T. den Hartog, B. Maciá, A. J. Minnaard, B. L. Feringa, *Adv. Synth. Catal.* **2010**, *352*, 999–1013.
[388] A. D. Gammack Yamagata, S. Datta, K. E. Jackson, L. Stegbauer, R. S. Paton, D. J. Dixon, *Angew. Chem. Int. Ed.* **2015**, *54*, 4899–4903.

ACKNOWLEDGEMENTS

I would like first to thank my advisor, Prof. Pier Giorgio Cozzi for the opportunity to work in his group as a PhD student. His deep and wide knowledge of chemistry has always impressed me and been an inspiration. During these three years I learnt a lot and I grew professionally under his leadership and advice. I want to thank the whole group and, in particular, my co-advisor Prof. Andrea Gualandi for his advice in the everyday work in the laboratory, Dr. Simone Potenti (Simo) for introducing me into the group and for his essential tips and tricks during my first few months in the lab. Finally, among all the former students that spent some time in our lab, I want to thank Yuri, who shared with me the challenges of the vanadium work in its early days, Matteo (Matte), who worked at the end of the same project, Ayoub and Davide (Jeppy) who brought good cheer into the lab and with whom I shared my last days of work. I wish them all the best for their future!

Between 2023 and 2024 I had the opportunity to spend six amazing months in Bristol. I am deeply grateful to Prof. Varinder K. Aggarwal for his warm hospitality, professionalism and charismatic personality. Thanks to Prof. Adam Noble for his advice in the everyday work in the laboratory and for all the constructive discussions during group meetings. I want to thank also the whole research group. I felt part of this international and stimulating environment since day one and I had the pleasure of meeting talented chemists working on fascinating projects. In particular Kevin, a colleague and friend, with whom I worked side by side sharing both disappointments and satisfactions of the project we worked together on. I want also to thank the whole crew with whom I shared most of the time inside and outside the university between one, or more, pints at the pub and a game of pool: Marghe, Josh, Hetty, Chris, Tom and Jay. Special thanks go to Malcolm and Sarah, who hosted me for a week last December for a reunion (not the first, not the last!), and Kris and Rosa, I had the pleasure to see them again last June here in Bologna. Finally, I want to thank Tim and Sue, my ''English family'', for hosting me in their homes, for their kindness and for always being very helpful and supportive when I needed.

Over these years I had the opportunity to meet many people and to make new friends with whom I shared the day life in university (and the hand-pong matches!). The list is too long so I want to thank in particular Tommi, Robi, Vale, Ama, Riri, Paolone, Passo, Grigo, Passo F., La Monda, Leo, Fabia, Giu, Mag, Samu, Patty, Glenn, the ''Team Gargnano'' made by Chia, Carbo and Nunzio for the unforgettable week we spent together in Gargnano in 2023 between lakeside breakfasts, late nights and even a boat trip, and the SCI2024 team made by Dem, Lucia, Dario, Junior and Andre for the memorable trip in Milan between French breakfasts, CityLife-style meals, fancy dinners, aperitifs on the Navigli and late night "cultural tv shows".

Many thanks to Chia and Federico (Fede), Nunzio and Federica (Fede) and my friends since master's degree Ange', Leo and Alessia (Ale) for all the good times we had, and for those we are having, outside the uni.

Special thanks go to my friend Chia, an extraordinary person with whom I shared passions, ideas, great adventures and memories in Gargnano, Bristol, Oxford, London, Bologna, etc etc. Thank you for all the laughs, the support and the quality time we spent together.

During the doctorate I made a lot of new friends, but I wouldn't have got where I am today without my long-standing friends.

First, I want to thank Ale, my best friend and girlfriend. We have known each other for 14 years and been together for 10. We spent all our most important moments together, as well as we shared all our achievements. I want to especially thank her for being always by my side, for sharing our daily life (even though I am not always the easiest person to stand) and being a person I can always count on.

I want to thank Barni, my craziest friend, with whom I have been having incredible, sometimes unexpected, unpredictable adventures for more than a decade, ranging from questionable night hikes in the mountains to sleepless nights clubbing in Rome. Looking forward to the next one!

On the same page I thank Chiappo, Ajitha, Elia, Silvia e Agnul, I am always certain that when I come back home you are always there to have memorable nights, even at short notice, but also Dario, Nico, Ila and Luca, we have known each other for more than ten years and it is always a pleasure to meet each other again and have great time together.

L'ultimo ringraziamento, ma non per importanza, va fatto in italiano. Se sono arrivato alla fine anche di questo percorso lo devo alla mia famiglia. È impossibile ringraziarli come si deve in poche righe per tutti gli insegnamenti e per il supporto incondizionato che mi dànno da sempre. Mi hanno permesso di lasciare casa presto per studiare in diverse città, fare esperienze che sono state fondamentali per la mia crescita personale e professionale e mi hanno assecondato e sostenuto nelle mie passioni, dallo sport al Conservatorio. A loro va tutta la mia gratitudine.